

# CHEMICAL KINETICS OF CYCLIC ETHERS IN COMBUSTION

Luc-Sy Tran<sup>1,\*</sup>, Olivier Herbinet<sup>2</sup>, Hans-Heinrich Carstensen<sup>3,4</sup>, Frédérique Battin-Leclerc<sup>2</sup>

<sup>1</sup> Univ. Lille, CNRS, UMR 8522 - PC2A - Physicochimie des Processus de Combustion et de l'Atmosphère, F-59000 Lille, France

<sup>2</sup> Univ. Lorraine, CNRS, UMR 7274 - LRGP - Laboratoire Réactions et Génie des Procédés, F-54000, Nancy, France

<sup>3</sup> Fundación Agencia Aragonesa para la Investigación y Desarrollo (ARAID), Zaragoza, Spain,

<sup>4</sup> Department of Chemical and Environmental Engineering, University of Zaragoza, Spain

\* Corresponding author:

Dr. Luc-Sy Tran.

Univ. Lille, CNRS, UMR 8522 - PC2A - Physicochimie des Processus de Combustion et de l'Atmosphère, F-59000 Lille, France.

E-mail: luc-sy.tran@univ-lille.fr

**Full-length review article**

## **ABSTRACT**

Cyclic Ethers (CEs) belong to a class of compounds of importance to understand the chemistry of both the engine auto-ignition of hydrocarbon fuels and the combustion of oxygenated biofuels. This article, divided in six parts, aims at systematically analyzing how up-to-date experimental and theoretical methods were applied to unveil the gas-phase oxidation chemistry of these compounds. The first part gives a brief overview on the significance of CEs as intermediates formed during alkane low-temperature oxidation summarizing its generally accepted chemical mechanism. This part also addresses the role of CEs as potential biofuels derived from lignocellulosic biomass and discusses the production methods of these molecules and their combustion performances in engine. The second part presents the different theoretical methods dedicated to calculate the electronic structure, thermochemical and kinetic data of CEs. The third part introduces the experimental methods used in studies related to CEs with a special focus on mass spectrometry and gas chromatography. The fourth part reviews the experimental and modeling studies related to CE formation during the low-temperature oxidation of linear, branched, cyclic alkanes, alkylbenzenes, olefins, and oxygenated fuels. The fifth part analyses the published work concerning the CE degradation chemistry and highlights the dominant involved reactions. To finish, the sixth part concludes and proposes future research directions.

**Keywords:** Cyclic ethers, gas phase kinetics, hydrocarbon oxidation, lignocellulosic biofuels, furan derivatives.

## CONTENTS LIST

Abstract.....	2
Contents list .....	3
List of abbreviations.....	5
1. Introduction.....	6
1.1. Cyclic ethers in the context of low-temperature oxidation chemistry .....	8
1.1.1. Summary of alkane low-temperature oxidation mechanism .....	8
1.1.2. Significance of cyclic ether production during alkane low-temperature ignition.....	10
1.2. Cyclic ethers in the context of renewable energy.....	12
1.2.1. The interest of cyclic ethers as biofuels.....	13
1.2.2. Cyclic ether production from lignocellulosic biomass through catalytic processes .....	16
1.2.3. Cyclic ethers considered as fuels in internal combustion engines.....	20
1.2.3.1. Combustion performances of cyclic ethers as internal combustion engine fuels .....	20
1.2.3.2. Potential of cyclic ether combustion processes to yield toxic products.....	24
1.3. Scope and structure of the paper .....	26
2. Names, structures, thermochemical properties, and theoretical methods.....	28
2.1. Overview of the theoretical methods used to calculate the cyclic ether related thermochemical data .....	28
2.1.1. Electronic structure calculations.....	30
2.1.2. Thermodynamic data and thermal rate coefficients.....	37
2.1.2.1. Enthalpies of formation .....	37
2.1.2.2. Internal rotations .....	38
2.1.2.3. Symmetry factors and optical isomers.....	39
2.1.2.4. Calculation of rate expressions for thermalized reactions .....	41
2.1.3. Pressure-dependent reactions .....	43
2.1.4. Optimization of the reaction network.....	45
2.2. Names, structures, and thermodynamic data.....	47
3. Experimental methods used in cyclic ether kinetic studies .....	65
3.1. Main experimental devices used to investigate the gas-phase reactions involving cyclic ethers... 65	
3.1.1. Initiation through photolysis.....	65
3.1.2. Initiation through flame propagation.....	65
3.1.3. Initiation by heating a reactive mixture .....	67
3.1.3.1. Heating by mechanical compression .....	68
3.1.3.2. Heating through contact with hot walls.....	69
3.2. Main analytical techniques used to measure cyclic ethers during their gas-phase reactions..... 70	
3.2.1. Mass spectrometry.....	71
3.2.1.1. Sampling strategy and ionization sources .....	72
3.2.1.2. Determination of the ionization energies of cyclic ether isomers.....	74
3.2.1.3. Cyclic ether identification during thermally induced fuel oxidation .....	77
3.2.1.4. Cyclic ether isomer identification during photolytically induced fuel oxidation .....	79
3.2.1.5. Cyclic ether quantification .....	81
3.2.2. Gas chromatography.....	84
3.2.2.1. Sampling strategies and analytical procedures .....	84
3.2.2.2. Identification by electron-impact mass spectrometry coupled to gas chromatography .....	87
3.2.2.3. Quantification using flame ionization detectors .....	89
4. Experimental and modeling work related to the gas-phase formation chemistry of cyclic ethers .....	92
4.1. Cyclic ether formation from the low-temperature oxidation of linear and branched alkanes .....	93
4.1.1. Experimental quantification of cyclic ethers from linear and branched alkanes .....	93
4.1.2. Possible cyclic ether hydroperoxide formation .....	102
4.1.3. Progress in modelling cyclic ether formation.....	105
4.1.3.1. General remarks on low-temperature oxidation .....	106
4.1.3.2. Generic rate expressions for cyclic ether formation during the oxidation of alkanes.....	108
4.1.3.3. Modeling of cyclic ether formation during the oxidation of n-alkanes .....	116
4.2. Formation of cyclic ethers during the low-temperature oxidation of cyclic and unsaturated hydrocarbons .....	121
4.2.1. Cyclic ethers from cyclic alkanes.....	121
4.2.1.1. Cyclic ethers from cyclohexane .....	124
4.2.1.2. Cyclic ethers from alkylcyclohexanes.....	126
4.2.2. Cyclic ethers from alkylbenzenes.....	130
4.2.2.1. n-Butylbenzene.....	130

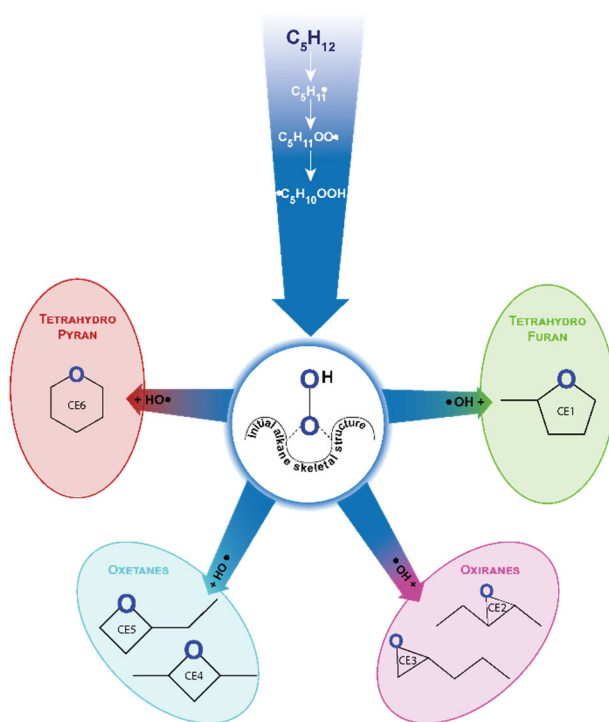
4.2.2.2. Di-alkylbenzenes .....	131
4.2.3. Cyclic ethers from olefins and dienes .....	132
4.3. Formation of cyclic ethers during the low-temperature oxidation of oxygenated molecules.....	140
4.3.1. Methyl esters .....	140
4.3.2. Aldehydes.....	145
4.3.3. Saturated and unsaturated alcohols .....	146
4.3.4. Linear, branched and cyclic ethers .....	148
4.4. Conclusion .....	153
5. Kinetics of the degradation of cyclic ethers .....	156
5.1. General overview of cyclic ether reaction kinetics .....	156
5.1.1. Saturated cyclic ethers.....	156
5.1.1.1. H-abstraction reactions.....	156
5.1.1.2. Unimolecular reactions of saturated cyclic ethers .....	159
5.1.1.3. Unimolecular reactions of radicals of saturated cyclic ethers .....	162
5.1.1.4. O <sub>2</sub> addition to cyclic ether radicals.....	166
5.1.2. Unsaturated cyclic ethers.....	169
5.2. Experimental and modelling studies on the combustion chemistry of saturated cyclic ethers.....	172
5.2.1. Non-substituted saturated cyclic ethers .....	176
5.2.1.1. Tetrahydrofuran.....	176
5.2.1.2. Other non-substituted saturated cyclic ethers .....	181
5.2.1.3. Comparison of the behavior of the non-substituted saturated cyclic ethers .....	188
5.2.1.4. Detailed kinetic models of non-substituted saturated cyclic ethers .....	192
5.2.2. Substituted saturated cyclic ethers.....	197
5.2.2.1. Oxirane rings substituted by alkyl chains.....	198
5.2.2.2. THF substituted by alkyl chains .....	200
5.2.2.3. THF substituted by an oxygenated group.....	203
5.2.2.4. Detailed kinetic models of substituted saturated cyclic ethers .....	205
5.3. Experimental and modelling studies on the chemistry of unsaturated cyclic ethers .....	210
5.3.1. Furan, 2-MF and 2,5-DMF .....	214
5.3.2. Influence of the degree of unsaturation and of C <sub>1+</sub> alkyl substitutions.....	220
5.3.3. Influence of oxygenated substituents .....	221
5.3.4. Performance of kinetic models.....	224
5.3.4.1. Furan, 2-MF, 2,5-DMF.....	225
5.3.4.2. Other furan derivatives .....	227
5.4. Conclusion .....	229
6. Conclusion and perspectives .....	232
6.1. Experimental kinetic studies related to cyclic ethers .....	234
6.2. Theoretical calculation procedures in cyclic ether kinetic studies .....	238
6.3. Ways cyclic ethers are considered in kinetic modelling .....	240
Acknowledgements.....	242
References.....	243

## LIST OF ABBREVIATIONS

Chemical species names:	Non-chemical name abbreviations:
<p><b>CE</b> cyclic ether  <b>EFFE</b> ethylfurfurylether  <b>GVL</b> <math>\gamma</math>-valerolactone  <b>HO<math>\dot{O}</math></b> hydroperoxy radical  <b>KHP</b> ketohydroperoxide  <b><math>\dot{O}H</math></b> hydroxyl radical  <b><math>\dot{O}OQOOH</math></b> hydroperoxyalkyl peroxy radical  <b><math>\dot{P}(OOH)_2</math></b> dihydroperoxy alkyl radical  <b><math>\dot{Q}OOH</math></b> hydroperoxyalkyl radical  <b><math>\dot{R}</math></b> alkyl radical  <b>RH</b> fuel (alkanes)  <b>RO<math>\dot{O}</math></b> alkylperoxy radical  <b>THF</b> tetrahydrofuran  <b>THP</b> tetrahydropyran  <b>2-AF</b> 2-acetylfuran  <b>2-BF</b> 2-<i>n</i>-butylfuran  <b>2-BTHF</b> 2-<i>n</i>-butyltetrahydrofuran  <b>2-BOTHP</b> 2-Butoxytetrahydropyran  <b>2-EF</b> 2-ethylfuran  <b>2-ETHF</b> 2-ethyltetrahydrofuran  <b>2-EOMTHP</b> 2-ethoxymethyltetrahydropyran  <b>2-FFOH</b> 2-furfurylalcohol  <b>2-MF</b> 2-methylfuran  <b>2-MTHF</b> 2-methyltetrahydrofuran  <b>2-MOF</b> Methyl furan-2-carboxylate  <b>2-PTHF</b> 2-propyltetrahydrofuran  <b>2-THFFEE</b>: 2-tetrahydrofurfurylethylether  <b>2-THFFBE</b>: 2-tetrahydrofurfurylbutylether  <b>2-THFFOH</b> 2-tetrahydrofurfurylalcohol  <b>2-THFFPE</b>: 2-tetrahydrofurfurylpropylether  <b>2,3-DHF</b> 2,3-dihydrofuran  <b>2,3-DMTHF</b> 2,3-dimethyltetrahydrofuran  <b>2,5-DHF</b> 2,5-dihydrofuran  <b>2,5-DMF</b> 2,5-dimethylfuran  <b>2,5-DMTHF</b> 2,5-dimethyltetrahydrofuran  <b>3-MTHF</b> 3-methyltetrahydrofuran  <b>5-HMF</b> 5-hydroxymethyl-2-furaldehyde</p>	<p><b>BDE</b> bond dissociation energy  <b>BP</b> boiling point  <b>BAC</b> bond additive correction  <b>CAS</b> complete active space  <b>CASPT2</b> complete active space second order perturbation theory  <b>CBS</b> complete basis set  <b>CC</b> coupled cluster  <b>CCSD(T)</b> coupled cluster method with single, double and perturbative triple excitations  <b>CI</b> configuration interactions  <b>CN</b> cetane number  <b>CVB</b> constant volume bomb  <b>CFR</b> cooperative fuel research  <b>DCN</b> derived cetane number  <b>DFT</b> density functional theory  <b>ECN</b> effective carbon number  <b>FR</b> flow reactor  <b>EI</b> electron-ionization  <b>FID</b> flame ionization detector  <b>GA</b> group additivity  <b>GAV</b> group additive value  <b>GC</b> gas chromatography  <b>GC-MS</b> gas chromatography mass spectrometry  <b>HF</b> Hartree Fock  <b>IDT</b> ignition delay time  <b>IE</b> ionization energy  <b>JSR</b> jet-stirred reactor  <i>k</i> rate coefficient  <i>k<math>_{\infty}</math></i> high-pressure limit rate coefficient  <b>L</b> reaction path degeneracy  <b>LBV</b> laminar burning velocity  <b>LHV</b> lower heating values  <b>MB</b> molecular beam  <b>ME</b> master equation  <b>MS</b> mass spectrometry  <b>MP</b> Møller Plesset  <b>P</b> pressure  <b>PEPICO</b> photoelectron photoion coincidence  <b>PES</b> potential energy surface  <b>PI</b> photo-ionization  <b>PIMS</b> photo-ionization mass spectrometry  <b>PIE</b> photo-ionization efficiency  <b>PLF</b> premixed laminar flame  <b>PM</b> particulate matter  <b>QCI</b> quadratic configuration interaction  <b>RCM</b> rapid compression machine  <b>RON</b> research octane number  <b>ST</b> shock tube  <b>SVUV</b> synchrotron vacuum ultra-violet  <b>TS</b> transition state  <i>T</i> temperature  <b>TOF</b> time-of-flight  <b>Y<sub>CE</sub></b> CE yield</p> <p><b>Greek symbols:</b></p> <p><math>\phi</math> equivalence ratio  <math>\tau</math> residence time</p>

## 1. INTRODUCTION

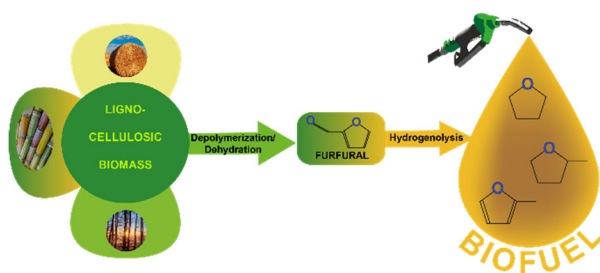
In the last decades, the need to develop new technologies for mitigating global warming has placed a double focus on Cyclic Ethers (CEs) with one or more ring oxygen atoms. On the one hand, the development of newly proposed types of internal combustion engines, homogeneous charge compression ignition or low-temperature combustion diesel engines, as it was described by Dec [1], Musculus *et al.* [2] or Saxena and Bedoya [3], has made it crucial to better understand the chemistry involved during the low-temperature gas-phase oxidation of fuel components. This chemistry occurs from 500 to about 900 K and CEs have been known since the 1970's as important products of it [4]. The main reactions are comprised of addition of alkyl radicals to oxygen followed by isomerizations and decompositions yielding  $\dot{\text{O}}\text{H}$  radicals [5] as shown in Fig. 1. These reactions are detailed in Part 1.1.



**Fig. 1.** Conceptual model of the formation of cyclic ethers during the low-temperature gas-phase oxidation of *n*-pentane.

On the other hand, the need to produce chemicals and fuels from non-fossil sources has triggered the development of strategies to utilize biomass, an abundantly available resource [6].

Of particular interest are new generation biofuels that do not compete with the food chain. One class of such biofuels is that of CEs, which has gained more and more interest during the past 10 years. This is evidenced by the growing number of studies devoted to chemical synthesis of furan derivatives to be used as potential biofuels [7–9]. Indeed, CEs can be produced from lignocellulosic biomass through catalytic reaction pathways schematized in Fig. 2, which shows an example of such pathways going through furfural as described in Part 1.2.



**Fig. 2.** Schematic presentation of chemical processes producing biofuel from lignocellulosic biomass.

In the context of combustion chemistry, CEs are organic compounds including a ring composed of at least one oxygen atom and several carbon atoms. The fully saturated CEs with two, three, four or five carbon atoms are named, respectively, oxiranes, oxetanes, oxolanes (more commonly tetrahydrofurans), and oxanes (more commonly tetrahydropyrans). In CEs, the numbering of the ring starts with the oxygen atom and proceeds around the ring to give substituents the lowest numbered positions. Therefore, in Fig. 1, CE1 is 2-methyltetrahydrofuran (2-MTHF), CE2 is 2-ethyl-3-methyloxirane, CE3 is propyloxirane, CE4 is 2,4-dimethyloxetane, CE5 is 2-ethyloxetane; finally, the non-substituted CE6 is simply tetrahydropyran (THP).

Lactones are not ethers but esters. Because they are similar in structure to cyclic ethers, *e.g.* they contain C–O–C group in the ring, because they can be formed in low-temperature oxidation of fuels/biofuels and because they are also proposed as biofuels, their combustion chemistry is also discussed in the present paper. Thus, “CE” nomenclature used in this paper includes lactones.

The two following parts describe the importance of CEs in the context of low-temperature oxidation chemistry and of biofuels, respectively.

### **1.1. Cyclic ethers in the context of low-temperature oxidation chemistry**

The two parts below illustrate how CE production can be significant during alkane low-temperature oxidation and afterwards summarizes the chemical mechanism, which is commonly accepted to explain this formation.

#### ***1.1.1. Summary of alkane low-temperature oxidation mechanism***

Due to its importance for understanding the phenomena occurring in internal combustion engines, hydrocarbon low-temperature oxidation has been the subject of many studies described in recent review papers. Battin-Leclerc [10], Curran [11] and Westbrook *et al.* [12] were interested in the main features of this chemistry and its kinetics. The paper by Zádor *et al.* [13] provided more details on the related elementary steps. Sarathy *et al.* [14] and Glaude *et al.* [15] described how combustion mechanisms could be extended to alcohols and methyl esters, respectively. In 2021, Rotavera and Taatjes [16] pointed out the influence of oxygenated functional groups (alcohols, esters, ketones, acyclic and cyclic ethers) on this chemistry.

In brief, the low-temperature oxidation chemistry of alkanes (RH) occurs through a well-accepted mechanism and may involve two, in some cases, three [17] additions to oxygen molecules starting from alkylic radicals ( $\dot{R}$ ). Fig. 1 presents the reactions, which are involved in the propagation cycle involving the addition of an alkyl radical to oxygen (forming alkylperoxy radical;  $RO\dot{O}$ ) when fuel is *n*-pentane. The chain carriers in this propagation cycle are  $\dot{O}H$  radicals. This cycle goes through the formation of a hydroperoxyalkyl radical,  $C_5H_{10}OO\dot{H}$ , via an intramolecular H-abstraction. This type of radical, usually named  $\dot{Q}OOH$ , easily decomposes to produce aldehydes, ketones or CEs (see Fig. 1) with the same carbon atom skeleton as the reactant. Experimental evidence for the  $\dot{Q}OOH$  radicals has recently been



reported in the literature, such as by Savee *et al.* [18] who detected a resonance-stabilized  $\dot{Q}OOH$  radical formed during oxidation of 1,3-cycloheptadiene or by Hansen *et al.* [19] who measured the unimolecular decomposition of a carbon-centered  $\dot{Q}OOH$  radical, namely 2-hydroperoxy-2-methylprop-1-yl. In parallel, the  $\dot{Q}OOH$  radical may add to a second molecule of oxygen. The adduct forms after intramolecular H-abstraction the corresponding dihydroperoxyalkyl radical ( $\dot{P}(OOH)_2$ ). (Note that  $\dot{P}(OOH)_2$  radicals with a radical site on a HOO group carrying carbon are not stable and in such a case, a ketohydroperoxide and  $\dot{O}H$  radical are formed instead.)  $\dot{P}(OOH)_2$  formation leads to the second propagation cycle including a branching step. While the occurrence of a third oxygen addition step has recently been proven by Wang *et al.* [20], the main fate of the  $\dot{P}(OOH)_2$  radical is thermal decomposition yielding an  $\dot{O}H$  radical and a ketohydroperoxide or hydroperoxyCE molecule. Hydroperoxy molecules contain a fragile RO–OH bond (the bond energy is between 42 and 44 kcal/mol for alkylhydroperoxides [21]), which easily breaks at low temperatures to produce two new reactive radicals, amongst which is a  $\dot{O}H$  radical. Ketohydroperoxides, the formation of which in a propagation step explains the high reactivity of fuel components even at temperature as low as 500 K (see for instance diethylether oxidation [22]), have been the subject of a recent review paper by Wang *et al.* [23].

The existence of two competing propagation cycles, the first one leading to stable products, such as CEs, and the second one going through the formation of the branching agents, ketohydroperoxides, assigns a particular importance to CE formation. The pathways leading to CEs have an important impact on fuel ignition and they explain the particular behavior observed during fuel low-temperature oxidation, such as the presence of a negative temperature coefficient zone and related cool flames as described by Ju *et al.* [24,25]. The paper by Rotavera and Taatjes [16] clearly demonstrated how the presence of certain functional groups directs the reaction flow towards ketohydroperoxides with a significant effect on fuel reactivity.

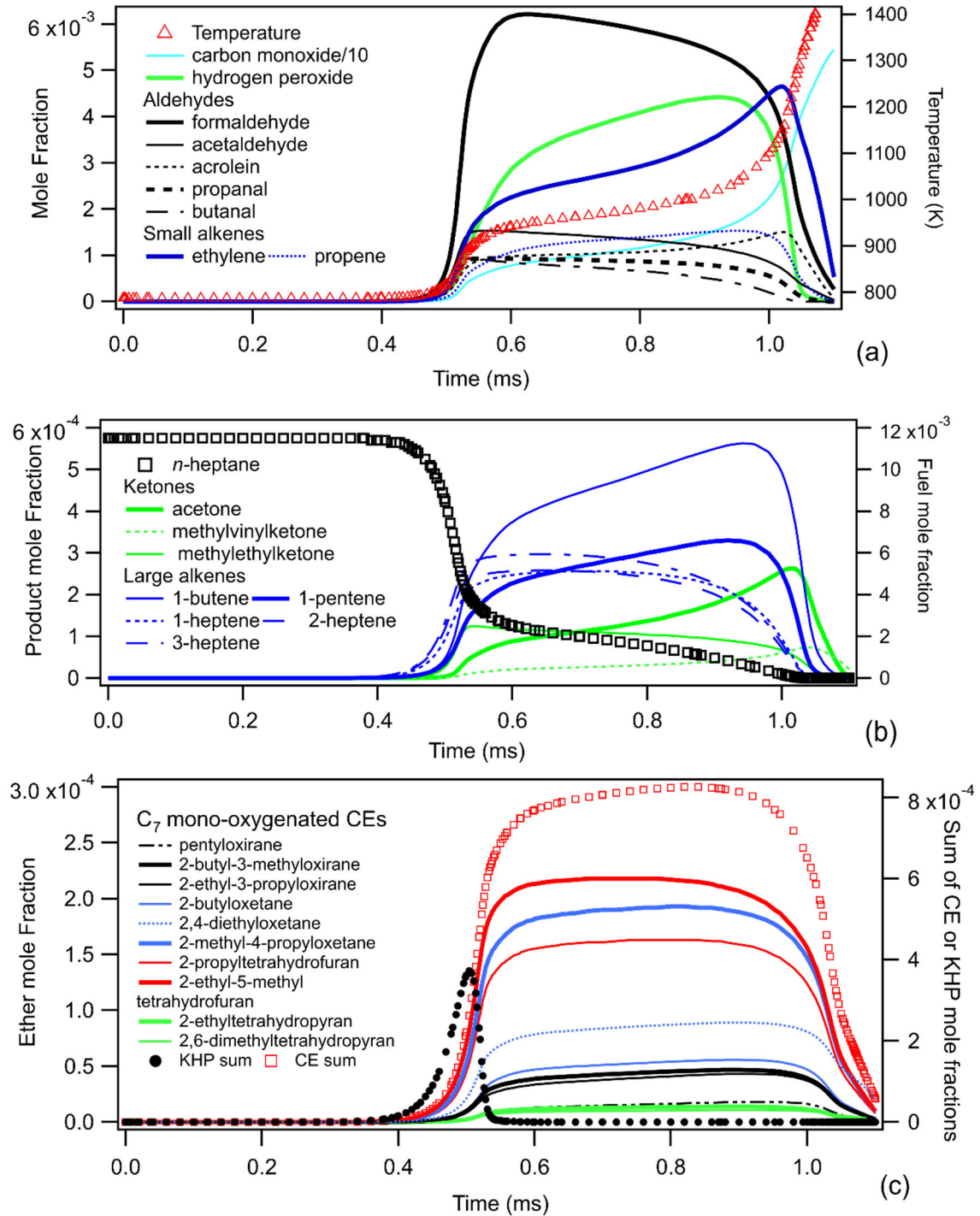
### ***1.1.2. Significance of cyclic ether production during alkane low-temperature ignition***

Low-temperature oxidation precedes auto-ignition and its chemistry controls the time when auto-ignition occurs. Fig. 3 displays a simulation of the time dependence of species (CO, H<sub>2</sub>O<sub>2</sub>, aldehydes, ketones, alkenes, CEs) mole fractions that are representative for the large variety of products formed during *n*-heptane ignition under engine-related conditions.

These species mole fractions have been plotted in order to cover the period in which the temperature approaches a plateau level at around 1000 K corresponding to a cool flame, as is described hereafter. While CO, formaldehyde, acetaldehyde and ethylene are the major products (with plateau mole fractions above  $1 \times 10^{-3}$ , Fig. 3a), this figure clearly demonstrates that the formation of CEs (the plateau mole fractions of CEs sum up to  $8 \times 10^{-4}$ , Fig. 3c), occurs with the same order of magnitude as those of several other significant products. While low-temperature oxidation alkane models can still be questionable concerning CE predictions, as it is discussed further in the text, the predicted plateau of cool flame products agree with experimental quantifications previously reported in rapid compression machines for several fuels (*e.g.* *n*-propylcyclohexane in Lille [26] or *iso*-octane/ethanol blends in Ann Arbor [27]).

In Fig. 3, slow oxidation occurs in the zone between 0 ms and 0.5 ms. It is followed by the cool flame in the interval between 0.5 ms and 1 ms. At 0.5 ms, a sharp decline of the ketohydroperoxide concentration (Fig. 3c) caused by its thermal decomposition is observed. This marks the start of chain branching, which leads to a significant reactivity increase indicated by the rise in temperature and in mole fraction of reaction products, aldehydes (Fig. 3a), alkenes (Fig. 3b), and CEs (Fig. 3c). Even though the ketohydroperoxide concentration is declining, their rate of production remains important as long as the temperature is still lower than 930 K (*i.e.* at the end of the first temperature increase shown in Fig. 3), as indicated by the high concentration of aldehydes, their derived products. Ketohydroperoxides could also be precursors of species with two carbonyl groups, diones, and carboxylic acids (not shown in Fig.

3) as reported in previous studies [28–30]. Tentative mechanisms responsible for their formation have been proposed (*e.g.* [31,32] for carboxylic acids and [29,33,34] for diones.



**Fig. 3.** Simulated formation of cool flame products during *n*-heptane ignition in an adiabatic closed homogeneous batch reactor under engine-related conditions (initial temperature of 787 K, equivalence ratio of 1.0, pressure of 5 bar, initial composition: 1.15% *n*-heptane / 12.7%  $O_2$  / 86.15%  $N_2$ ) using the model of Zhang *et al.* [33]. The time dependence of the temperature and of the mole fractions of the fuel *n*-heptane, the sum of  $C_7$  ketohydroperoxides (KHP sum) and the sum of CEs (CE sum) are also displayed.

With increasing temperature, ketohydroperoxide production is reduced because of the enhanced reversibility of the additions of  $\dot{R}$  and  $\dot{QOOH}$  radicals to  $O_2$  together with the increased competition with other channels, such as the formation of conjugated alkenes and relatively unreactive  $HO\dot{O}$  radical (from  $\dot{R}$ ) or the CE formation (from  $\dot{QOOH}$ ). Consequently, the reactivity is severely reduced. At 0.6 ms, the temperature, fuel consumption, and product concentration profiles reach plateau values and the temperature reaches around 1000 K. Fig. 3 indicates that, according to the kinetic model, the CE concentrations remain stable from 0.6 to 1 ms, while those of aldehydes, which are products of ketohydroperoxides decomposition, slowly decrease. The reason for that the competition for  $\dot{QOOH}$  radical consumption turns in favor of CE formation instead of  $2^{nd}$   $O_2$  addition when increasing temperature.

Despite the low reactivity, the high exothermicity of the slow oxidation chemistry causes the temperature to steadily increase. At the same time, the concentration of  $HO\dot{O}$  radicals formed along with the production of conjugated alkenes increases, which leads to an accumulation of  $H_2O_2$  mainly yielded by self-reaction of  $HO\dot{O}$  radicals. The end of the plateau is reached when the temperature is high enough to allow the occurrence of a new branching step: thermal decomposition of  $H_2O_2$  produces two  $\dot{O}H$  radicals. This is the point of auto-ignition. The fuel is completely oxidized and the temperature quickly increases to values up to 2000 K.

The first objective of this paper is to review the experimental, theoretical and modelling foundations, which support the current understanding of CE formation during fuel or biofuel oxidation.

## **1.2. Cyclic ethers in the context of renewable energy**

The high energy density of liquid fuels is an important advantage compared to the electrical storage of energy and in the foreseeable future engines of heavy-duty vehicles, ships and planes

will continue to run on liquid fuels [35,36]. Amongst liquid fuels, biofuels produced from the vast and renewable resources of biomass represent a growing fraction compared to hydrocarbons produced from depleting petroleum reserves. Oxygenated chemicals with a variety of molecular structures have been proposed as biofuels: alcohols, methyl esters, acyclic ethers, and CEs [37–39]. It has been reported that the presence of oxygen has a positive impact on pollutant emissions, especially by reducing the formation of Particulate Matter (PM) [40].

We describe hereafter why CEs have been considered as biofuels, how they are produced from lignocellulosic biomass using catalytic strategies, and finally how they are expected to perform when used in internal combustion engines.

### ***1.2.1. The interest of cyclic ethers as biofuels***

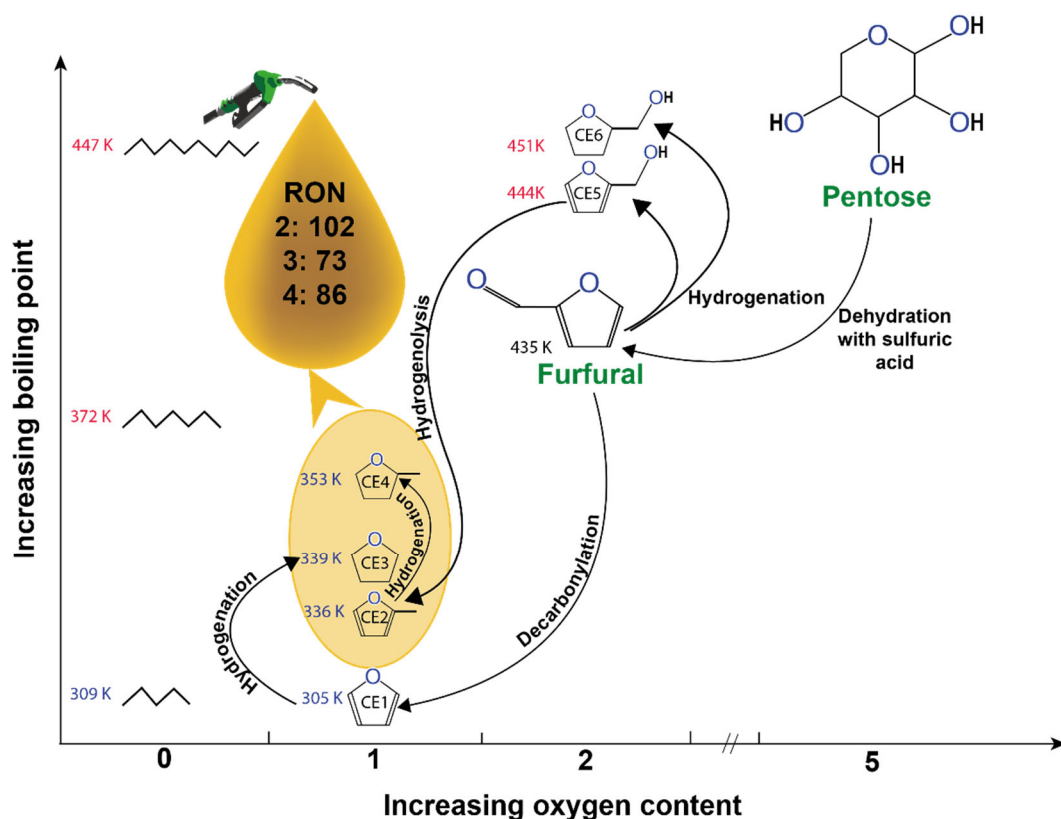
As mentioned by Grad [41], the first practical internal combustion engine - patented by Nikolaus Otto in 1877 - ran on alcohols (gasoline was not even known yet). Alcoholic biofuels, mostly ethanol, and with a lower importance butanol [42], can easily be produced by fermentation from starches and sugary plant parts. They can be used in internal combustion engines either as pure component or blended with gasolines [43] and their addition in petroleum fuel was shown to reduce the emissions of pollutants. For instance, 10 and 15% of ethanol in Diesel blends potentially reduce soot particulate emission by 20-27% and 30-41%, respectively [44]. Studies on alcohol combustion chemistry were exhaustively reviewed by Sarathy *et al.* [14] in 2014.

As reviewed by Knothe and Razon [45], the second type of biofuels used nowadays in transportation is obtained from vegetable oils, animal fats or other materials consisting mainly of triglycerides. It is known as biodiesel and its composition depends on the type of fatty acid source (mainly rapeseed, palm and soybean oils, and increasingly yellow grease coming from filtered cooking oil wastes [46]) used in biodiesel production. Biodiesel is composed of a blend of mostly unsaturated C<sub>16</sub>-C<sub>18</sub> methyl esters produced by catalytic transesterification of fatty

acids with monohydric alcohols, most commonly methanol, yielding glycerol as by-product [47].

The possible competition for the production of these 1<sup>st</sup> generation biofuels with that of edible resources has made it crucial to find ways to use other biomass types to produce biofuels. From this point of view, lignocellulosic biomass is of particular interest because of its high-volume availability and of its non-competitiveness with food.

As described by Tran *et al.* [39], after adequate biomass pretreatments [48], lignocellulosic biomass can be transformed in several ways to produce biofuels. The molecular composition of the components of lignocellulosic biomass, mainly cellulose, hemicellulose and lignin, is characterized by a high content in oxygen atoms. As exemplified in Fig. 4, biofuel synthesis from lignocellulosic biomass comprises oxygen removal steps to obtain fuels with boiling points in the range of the alkanes present in current transportation fuels. The reduction to form a variety of platform chemicals can be done via high-temperature thermochemical conversion processes, such as gasification, hydrothermal liquefaction, or pyrolysis, or via mild temperature liquid-phase catalytic processes, such as hydrolysis followed by dehydration.



**Fig. 4.** Example of pathways from carbohydrates to cyclic ether candidates to be used as biofuels via furfural as platform chemical according to [49,50]. CE1 is furan, CE2 2-methylfuran, CE3 tetrahydrofuran, CE4 2-methyltetrahydrofuran, CE5 2-furfuryl alcohol and CE6 2-tetrahydrofurfuryl alcohol. The temperature next to each cyclic structure is its boiling point; those of *n*-pentane, *n*-heptane and *n*-decane are shown for comparison. RON is the Research Octane Number and the values are taken from [51–53].

Fixed-bed or fluidized bed gasifiers can be used to produce syngas, a mixture of mainly H<sub>2</sub> and CO, from biomass partial oxidation at temperatures around 1200 K [37,54]. After careful cleaning, syngas can be transformed via the catalytic Fischer-Tropsch synthesis to hydrocarbons of excellent transportation fuel quality [55]. This is of particular interest when the presence of oxygen atoms in fuel molecules has to be avoided, such as for aviation purpose due to weight limitation [56]. In addition to hydrocarbons, syngas can be used to produce other compounds of interest as other fuels for internal combustion engines, *e.g.* methanol [57], ethanol and heavier alcohols [58], or dimethylether [59].

Liquid bio-oils can be directly obtained from lignocellulosic biomass by the two following processes [60]: hydrothermal liquefaction, in the presence of a solvent (often water)

at moderate to high temperature (520-820 K) and pressure (50-250 bar) [61,62], and fast pyrolysis under atmospheric pressure [63]. The fast or flash pyrolysis process involves reaching high-temperatures (from 750 K to 1400 K) with a high heating-rate and a short residence time (heating rate up to  $10^4$  K/s for a residence time below 1 s for flash pyrolysis) in the absence of oxygen [64]. The higher the heating rate, the higher the bio-oil yield. Flash pyrolysis typically requires small feed particle sizes (<200  $\mu$ m) and the highest temperatures, but may produce bio-oil yields of up to 75wt%, together with gas and char formation. Beside the high water content (15-40 wt%), bio-oils are complex mixtures of hundreds of oxygenated species, including furan derivatives [37], with a lower amount of nitrogen-containing compounds. The bio-oil composition is not easy to characterize [65,66]. The corrosivity caused by its high acidity, its high water content, and its poor thermal stability provide severe challenges for their use as fuel components in transportation without further upgrading [67].

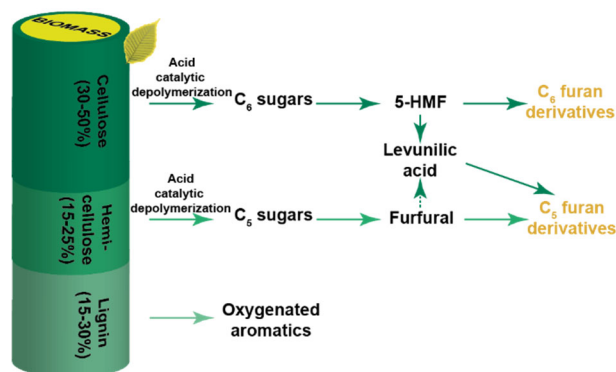
In addition to the thermal production of syngas, which is a highly energy consuming process, and of complex bio-oils, which are not directly usable in fuel blends, suitable fuel candidates, *e.g.* cyclic ethers, can be produced from lignocellulosic biomass via catalytic processes.

### ***1.2.2. Cyclic ether production from lignocellulosic biomass through catalytic processes***

Fig. 5 displays the principle of current catalytic concepts used to produce furan derivatives, the group of cyclic ethers that are regarded to be the most promising biofuel candidates, as it was described by Luterbacher *et al.* [9]. These strategies start with the depolymerization of the constituents of lignocellulosic biomass (usually at temperatures between 298 to 400 K in water in the presence of acid (HCl)) to produce sugars and further dehydration products, such as furfural, levulinic acid and 5-hydroxymethyl-2-furaldehyde (5-HMF), the main platform chemicals for the synthesis of furan derivatives; for more details about lignin valorization see

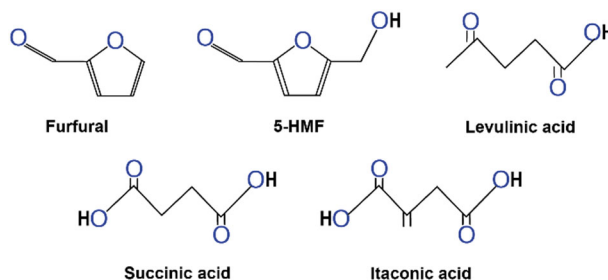


[68]. Only cellulose and hemicellulose, which are a source of sugars, can be converted into furan derivatives. The catalytic transformation of lignin yields various oxygenated compounds, however no CEs [69].



**Fig. 5.** Lignocellulosic biomass upgrading according to the strategy described by [9]. Full line arrows correspond to a single-step catalytic reaction, the dotted one to a two-step process.

Leitner *et al.* [8] recently reviewed several platform chemicals, which have been proposed for cyclic ether synthesis and which are shown in Fig. 6. These authors have detailed the industrial processes leading to these molecules and how furan derivatives can be obtained from them.



**Fig. 6.** Platform chemicals proposed for cyclic ether synthesis [8].

In the following, the major reaction pathways towards furan derivatives starting from the three main platform chemicals, furfural, 5-HMF, and levulinic acid are summarized.

**Furfural** is one of the few chemicals that has been produced commercially for a long time from lignocellulosic biomass [8]. It is obtained from C<sub>5</sub> sugars (pentoses), xylose or arabinose, which arise from the degradation of the hemicellulosic fraction of agricultural wastes

(corncoobs or bagasse). Fig. 4 shows how furan derivatives can be produced from C<sub>5</sub> sugars derived from hemicellulose using furfural as platform chemical. Sugar dehydration leading to furfural takes place in water at around 550 K and is favored by the presence of strong acids, *e.g.* sulfuric acid [7,9]. Furfural can be converted into furan derivatives in a few catalytic steps [7]. Its decarbonylation yields furan, which can be hydrogenated to tetrahydrofuran (THF). A second pathway involves furfural hydrogenation to produce 2-furfuryl alcohol (2-FFOH) and 2-tetrahydrofurfuryl alcohol (2-THFFOH). The hydrogenolysis of 2-FFOH is the common source of 2-methylfuran (2-MF), whose hydrogenation yields 2-methyltetrahydrofuran (2-MTHF) [49,50]. Amongst the species drawn in Fig. 4, Research Octane Number (RON) values can only be found for CE2 (2-MF), CE3 (THF), and CE4 (2-MTHF). The formation of further potential biofuel candidates derived from furfural was also considered [8,70,71], such as 2-*n*-butylfuran (2-BF) and 2-*n*-butyltetrahydrofuran (2-BTHF) via a reaction of furfural with acetone followed by selective hydrogenations/dehydration, 2-ethyltetrahydrofuran (2-ETHF) via furan Friedel–Crafts acylation as proposed by Leitner *et al.* [8], ethylfurfuryl ether (EFFE) by etherification of 2-FFOH with ethanol as proposed by Tian *et al.* [70] or additives for biodiesel from acetalization of furfural with glycerol [71]. Dahmen and Marquardt [72] have also proposed the formation of dioxygenated molecules such as 2-tetrahydrofurfuryl ether (2-THFFEE), 2-tetrahydrofurfuryl propyl ether (2-THFFPE), 2-tetrahydrofurfuryl butyl ether (2-THFFBE), and 2-ethoxymethyltetrahydropyran (2-EOMTHP), by etherification of furfural derivatives with alcohols.

**5-hydroxymethyl-2-furaldehyde** is obtained from the dehydration of C<sub>6</sub> sugars (hexoses), such as fructose and glucose, derived from cellulose, the most abundant component of lignocellulosic biomass. 5-HMF can easily be converted to C<sub>6</sub> furan derivatives. This platform chemical, which contains three oxygen atoms, has a high boiling point (564 K, solid at room temperature) that prevents it from being considered as a potential biofuel. As described

by Román-Leshkov *et al.* [73], 5-HMF can be converted catalytically to 2,5-dimethylfuran (2,5-DMF) via a hydrogenation (to form 2,5-dihydroxymethylfuran) and a subsequent hydrogenolysis (to yield 2-hydroxymethyl,5-methylfuran). De Jong and Gruter from Avantium [74] proposed liquid 5-HMF ethers (5-(methoxymethyl)furfural, 5-(ethoxymethyl)furfural or 5-(tert-butoxymethyl)furfural) as biofuel candidates, but without providing information about the possible performances of these molecules in engines. 5-HMF can also be converted to 2,5-dimethyltetrahydrofuran (2,5-DMTHF) [71,75].

**Levulinic acid** is produced by dehydration of 5-HMF. Luterbacher *et al.* have noted that co-production of furfural and levulinic acid is a target when working with lignocellulosic biomass and producing dehydration products [9]. A pathway from furfural to levulinic acid via 2-FFOH has also been proposed [71]. The catalytic hydrogenation of levulinic acid is the most efficient way to produce 2-MTHF, with better yields than from furfural. Levulinic acid can also be converted into  $\gamma$ -valerolactone (GVL), a proposed biofuel and a polar aprotic molecule proposed as solvent in sugar dehydration processes [76]. GVL is an additional source of 2-MF [71].

**Succinic and itaconic acids** were also mentioned as potential platform chemicals by Leitner *et al.* [8]. The first acid offers an additional way to produce THF and itaconic acids could be an efficient source of 3-methyltetrahydrofuran (3-MTHF) [77].

More references about the possible routes to formation of furan derivatives can be found in [16]. Below are a few other CEs considered as potential biofuels: 2-ethylfuran (2-EF) obtained from glucose hydrogenolysis [78], 2,3-dimethyltetrahydrofuran (2,3-DMTHF) and 2-propyltetrahydrofuran (2-PTHF) considered by Dahmen and Marquardt [72], 2,3-dihydrofuran (2,3-DHF) and 2,5-dihydrofuran (2,5-DHF) derived from alcohols produced from biomass fermentation [79,80], and tetrahydropyran (THP), the core structure of glucose [81], whose combustion properties have been investigated since 1991 [82]. Recently light has

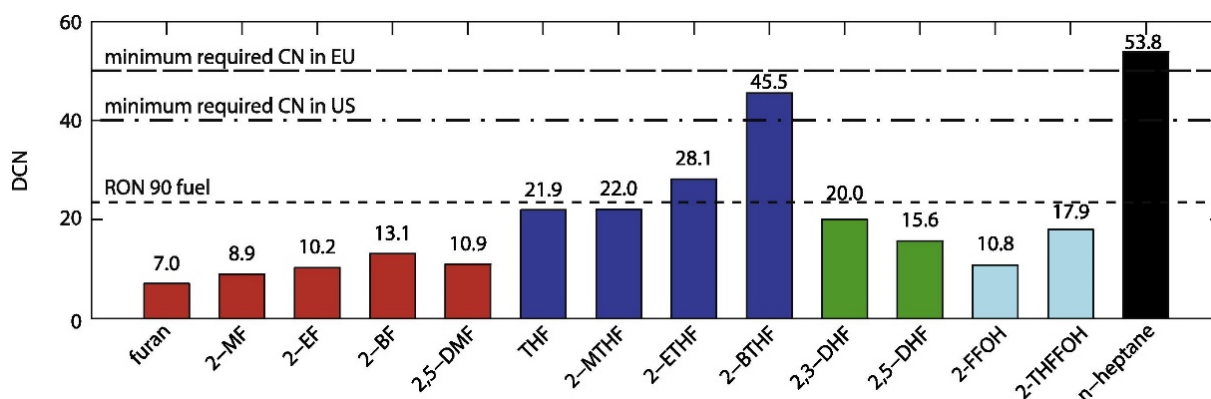
also been shed on the possibility to use the diethers, 1,3 dioxolane (5-membered ring) and 1,3-dioxane (6-membered ring) as biofuels. Both contain two oxygen atoms in their ring. 1,3-Dioxolane and 1,3-dioxane can both be produced catalytically from glycerol, a by-product of biodiesel production [71]. 1,3-Dioxane can also be synthesized from ethylene glycol produced from cellulose [83,84]. 1,4-Dioxane, a solvent widely used in chemical synthesis [85], has been proposed as a potential biodiesel fuel additive [86].

### ***1.2.3. Cyclic ethers considered as fuels in internal combustion engines***

To decide if CEs are realistic candidates to be used in internal combustion engines, it is important to examine data about their combustion performances and their potential to create toxic pollutants during the combustion process.

#### ***1.2.3.1. Combustion performances of cyclic ethers as internal combustion engine fuels***

Two numbers have been proposed to characterize the fuel auto-ignition performances: the octane number (often Research Octane Number (RON)), which rates the fuel resistance to auto-ignition [51], and the Cetane Number (CN), which in contrast rates the fuel ignitibility; the lower RON and the higher CN, the more ignitable the fuel. Fig. 7, taken from Sudholt *et al.* [87], presents the cetane rating of several furan derivatives proposed as potential biofuel according to the above-described catalytic chemical processes. As described in [87], the plotted Derived Cetane Numbers (DCN) were calculated from ignition delay times experimentally measured under engine relevant conditions in an ignition quality tester. Biofuels were purchased when possible, or synthesized following pathways proposed in [88]. Fig. 7 shows that all these furan derivatives, except for 2-ETHF and 2-BTHF, have DCN below that of RON 90 fuel indicating that these fuels have a good resistance to auto-ignition and might be used in gasoline engines.



**Fig. 7.** Derived Cetane Number (DCN) for furan derivatives proposed as potential biofuels. For comparison, this figure plots also the *n*-heptane CN (*n*-C<sub>16</sub>H<sub>34</sub> CN is 100), the minimum CN values required in Diesel fuels in Europe and United states and the CN value of a fuel with RON equal to 90, which is the maximum CN value for a fuel to be used in Spark-Ignited engines. Reproduced from Ref. [87] with permission of Elsevier.

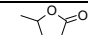
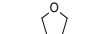
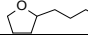
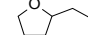

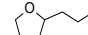
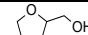
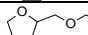
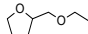
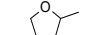
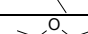
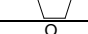
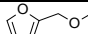
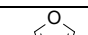
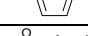
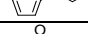
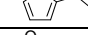
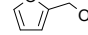
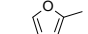
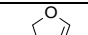
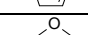
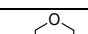
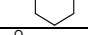
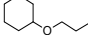
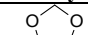
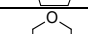
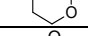
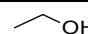
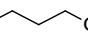
More generally, Table 1 gathers the available values of density, Boiling Point (BP) and performance indicators related to combustion in engines (heating values, RON and DCN) of all CEs here-before mentioned as potential biofuels according to literature. For the sake of comparison, the corresponding data is also provided for gasolines, Diesel fuels, and two well-studied alcohols, ethanol and *n*-butanol.

Concerning physico-chemical properties, the density of all the CEs listed in Table 1 (liquid under standard conditions) are above those of conventional fuels and alcohols, except that of 2,5-DMTHF. The BPs of all CEs listed in Table 1 except for GVL, which strictly speaking is a cyclic ester, (491 K) are in the same range as the values of the compounds included in gasoline. Despite its high resistance to auto-ignition (RON = 100), GVL's low volatility strongly limits its use as gasoline blend. According to Table 1, the presence of an alcohol function or of a C<sub>3</sub>-C<sub>4</sub> alkyl or ether chain significantly lowers the CE volatility (BP above 400 K).

Concerning combustion performance indicators, the Lower Heating Values (LHV) by volume, which is of interest for ground transportation, and on mass basis (important for aviation) are given in Table 1. The LHV per mass of all the CEs listed in Table 1 are above that

of *n*-butanol except that of GVL. Amongst all these CEs, 2-MF and 2,5-DMF (in bold in Table 1) have a BP below 370 K, a mass LHV above that of *n*-butanol (26.8), and a RON above 100, which makes these two CE particularly interesting as potential octane boosting additives in gasoline blends. The RON of 2,5-DMF (119) is very close to that of ethanol (120) indicating similar resistance to auto-ignition. In addition, it was recently shown that 2-MF exhibits an exceptional synergetic anti-knock blending effect in mixture with alkanes [89].

**Table 1.** Physico-chemical properties (standard conditions) and combustion performances of CEs proposed as biofuel candidates, conventional fuels, and two alcohols [39,51,70,72,73,86,87,90–97].

Name <sup>a</sup>	Formula	Structure	Density (kg/L)	BP <sup>b</sup> (K)	LHV <sup>b</sup>	RON <sup>b</sup>	DCN <sup>b</sup>
					MJ/L(MJ/kg)		
<b>Cyclic ethers</b>							
<b>Tetrahydrofuran derivatives</b>							
GVL	C <sub>5</sub> H <sub>8</sub> O <sub>2</sub>		1.05	491	26.2 (25.0)	100	--
THF	C <sub>4</sub> H <sub>8</sub> O		0.89	339	29.1 (32.7)	73	21.9
2-BTHF	C <sub>8</sub> H <sub>16</sub> O		0.85	432	31.5 (37.0)	--	45.5
2-ETHF	C <sub>6</sub> H <sub>12</sub> O		0.86	382	--	--	28.1
2-MTHF	C <sub>5</sub> H <sub>10</sub> O		0.85	353	28.5 (33.5)	86	22.0
2-PTHF	C <sub>7</sub> H <sub>14</sub> O		0.87	406	31.3 (36.2)	--	42.9
2-THFFOH	C <sub>5</sub> H <sub>10</sub> O <sub>2</sub>		1.05	451	27.5 (26.2)	--	17.9
2-THFFEE	C <sub>7</sub> H <sub>16</sub> O <sub>2</sub>		0.91	429	28.0 (30.4)	--	78.9
2-THFFBE	C <sub>8</sub> H <sub>16</sub> O <sub>2</sub>		0.92	451	29.6 (32.0)	--	63.8
2,3-DMTHF	C <sub>6</sub> H <sub>12</sub> O		0.87	378	30.4 (34.9)	--	24.5
2,5-DMTHF	C <sub>6</sub> H <sub>12</sub> O		0.83	364	29.5 (35.5)	82	24.5
3-MTHF	C <sub>5</sub> H <sub>10</sub> O		0.86	362	29.1 (33.6)	--	24.9
<b>Furan derivatives</b>							
EFFE	C <sub>7</sub> H <sub>10</sub> O <sub>2</sub>		0.99 <sup>d</sup>	423	30.5 (28.8)	--	18.4
Furan	C <sub>4</sub> H <sub>4</sub> O		0.94	305	--	--	7.0
2-BF	C <sub>8</sub> H <sub>12</sub> O		0.90	413	31.3 (34.8)	--	13.1
2-EF	C <sub>6</sub> H <sub>8</sub> O		0.91	366	--	--	10.2
2-FFOH	C <sub>5</sub> H <sub>6</sub> O <sub>2</sub>		1.13	443	--	--	10.8
2-MF	C <sub>5</sub> H <sub>6</sub> O		0.91	336	27.7 (30.4)	102	8.9
2,3-DHF	C <sub>4</sub> H <sub>6</sub> O		0.93	328	--	--	20.0
2,5-DHF	C <sub>4</sub> H <sub>6</sub> O		0.93	340	--	--	15.6
2,5-DMF	C <sub>6</sub> H <sub>8</sub> O		0.90	367	30.0 (33.7)	119	10.9
<b>Tetrahydropyran derivatives</b>							
THP	C <sub>5</sub> H <sub>10</sub> O		0.88	361	--	--	--
2-BOTHP	C <sub>9</sub> H <sub>18</sub> O <sub>2</sub>		0.91	473	29.9 (32.9)	--	76
2-EOMTHP	C <sub>8</sub> H <sub>16</sub> O <sub>2</sub>		0.94	452	30.4 (32.2)	--	63.8
<b>Cyclic ethers containing two ring oxygen atoms</b>							
1,3-dioxolane	C <sub>3</sub> H <sub>6</sub> O <sub>2</sub>		1.06	351	37.1 (35)	--	30
1,3-dioxane	C <sub>4</sub> H <sub>8</sub> O <sub>2</sub>		1.03	376	--	--	--
1,4-dioxane	C <sub>4</sub> H <sub>8</sub> O <sub>2</sub>		1.03	374	--	--	58
<b>Conventional fuels</b>							
Gasolines <sup>c</sup>	C <sub>4</sub> -C <sub>14</sub> HC		0.74	303-473	31.6 (42.7)	95	~23
Diesels <sup>c</sup>	C <sub>8</sub> -C <sub>25</sub> HC		0.84	443-633	36.1 (43.0)	--	40-55
<b>Alcoholic fuels</b>							
Ethanol	C <sub>2</sub> H <sub>5</sub> OH		0.80	352	21.3 (26.8)	120	8
n-Butanol	C <sub>4</sub> H <sub>9</sub> OH		0.81	356	26.8 (33.1)	96	15.9

<sup>a</sup> See full name in Table 4. <sup>b</sup> BP: Boiling Point; LHV: Lower Heating Value; RON: Research Octane Number; DCN: Derived Cetane Number. <sup>c</sup> Fuel standard. <sup>d</sup> at 15 °C. "--": unavailable.

### ***1.2.3.2. Potential of cyclic ether combustion processes to yield toxic products***

To access the potential sources of toxic products amongst the species present in the exhaust gas of automobile engines, one should examine the emission of unburned fuel, NO<sub>x</sub>, carbonyl compounds and hydrocarbons, especially those identified as potential soot precursors.

Concerning the impact of possible emission of unburned fuels, furan derivatives are not considered as particularly toxic compounds, except for furan and 1,4-dioxane, for which possible carcinogenic effects on humans were reported [8,98]. However, the impacts of CEs on human health and atmosphere should be better characterized. Because furan derivatives contain double bonds which allow OH addition reactions, they can degrade rapidly in the atmosphere and be a source of by-products, such as butanedial [99].

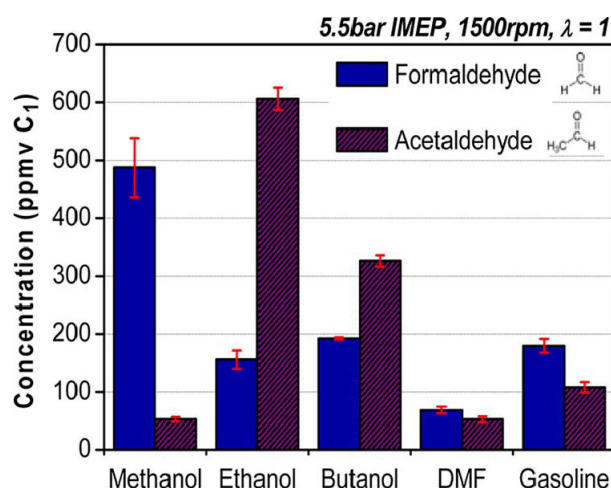
Following regulated gaseous pollutants in a spark-ignited engine, Wang *et al.* [100] demonstrated that fueling with 2-MF or 2,5-DMF instead of gasoline leads to lower emissions of unburned hydrocarbons, but to higher ones of CO and NO<sub>x</sub>. Due to the high in-cylinder temperature 2-MF and 2,5-DMF generate up to 82% and 33% more NO<sub>x</sub> emissions than gasoline, respectively.

Carbonyl compounds present in the exhaust gas of a spark-ignited engine fueled either with gasoline or with different potential biofuels, including 2,5-DMF, were quantified by Daniel *et al.* [101] using Gas Chromatography Mass Spectrometry (GC-MS). The conclusion drawn by the authors was that 2,5-DMF produced the lowest overall carbonyl emissions compared to gasolines and C<sub>1</sub>-C<sub>4</sub> alcohols. More specifically, as shown in Fig. 8, 2,5-DMF led to the lowest formaldehyde emission amongst the tested fuels. A possible reason for the low emission of carbonyl products is its aromatic structure, which leads to specific decomposition reactions discussed in Part 5. On the other hand, alcohols and regular ethers are known to produce aldehydes as intermediate during their combustion (Part 4). A similar study carried out



by Wang *et al.* [100] indicates that formaldehyde emissions are even lower, with similar acetaldehyde emissions, when using 2-MF instead of 2,5-DMF.

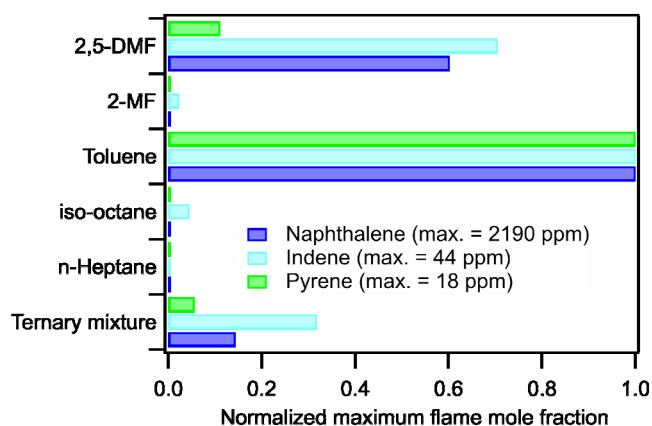
Monitoring pollutant emissions from a diesel engine fueled with biodiesel and its blend with 2-MF, Xiao *et al.* [102] reported a decrease of the emissions of CO, 1,3-butadiene, benzene and acetaldehyde with increasing CE mass fraction, but in contrast NO<sub>x</sub> emissions increased.



**Fig. 8.** Emissions of formaldehyde and acetaldehyde from a spark-ignited engine fueled with methanol, ethanol, *n*-butanol, 2,5-DMF (noted DMF in the figure), and gasoline. Given concentrations are in C<sub>1</sub>-equivalent, *i.e.* quantification is performed by comparing the areas between the standard and the sample on a C<sub>1</sub> (formaldehyde) basis. Reproduced from Ref. [101] with permission of ACS.

Concerning soot production in SI engines, Wang *et al.* [100] noted that 2-MF produced significantly less PM in number and in mass compared to gasoline. Daniel *et al.* [101] identified a notable presence of 1,3-cyclopentadiene and aromatics in the emission of a SI engine fueled with 2,5-DMF, which is in agreement with detailed kinetic modeling performed by Tran *et al.* [103]. From their measurements of emissions in a practical diesel engine, Song *et al.* [96] concluded that, when added to a base Diesel fuel, 1,3-dioxolane was by far less efficient in soot reduction than linear C<sub>4</sub>H<sub>10</sub>O<sub>2</sub> and C<sub>6</sub>H<sub>14</sub>O<sub>3</sub> ethers.

Fig. 9 presents simulated mole fractions of compounds, commonly considered as soot precursors (naphthalene, indene and pyrene), computed for laminar premixed flames fed with 2,5-DMF, 2-MF, toluene, *n*-heptane, *iso*-octane, and a ternary gasoline mixture made using the three previous molecules (13.7% (vol.) *n*-heptane, 42.9% *iso*-octane, 43.4% toluene).



**Fig. 9.** Fuel influence on the normalized maximum flame mole fraction of soot precursors (normalization is done using the value in the toluene flame) according to the detailed kinetic modelling of Tran *et al.* [103].

The model of Tran *et al.* [101] predicts that the 2,5-DMF flame produces significantly higher quantities of the three soot precursors than gasoline surrogate (“ternary mixture” shown in Fig. 9), although less than toluene, a common octane boosting additive. In contrast, the 2-MF flame produces very low levels of soot precursors, close to those of the alkanes. Experimental studies would be helpful to verify these model predictions.

In line with these results on soot precursor formation from furan derivatives, the second objective of this review is to show how experimental and modeling kinetic studies have helped to improve the understanding of the combustion and oxidation chemistry of CEs as potential biofuels.

### 1.3. Scope and structure of the paper

This paper aims at describing the current understanding of the chemistry and kinetics related to gas-phase CE oxidation and the experimental, theoretical and modelling studies, which have been performed to achieve it. This paper includes an analysis of the pathways by which CEs are formed during the low-temperature oxidation of organic compounds, including alkanes, but also unsaturated hydrocarbons and oxygenated molecules. This paper also reviews studies in which CE act as fuel. These investigations deal with the consumption pathways of CE in

combustion (including pyrolysis and low-/high-temperature oxidation) and are thus complementary to the CE formation chemistry studies.

Besides Part 1 explaining why studies of the CEs gas-phase kinetics are needed, the core of the present paper consists of the following parts:

- Part 2 discusses the theoretical methods, which have been used to investigate CE chemistry, and presents the naming, structure and thermochemical properties of the CEs mentioned in this paper.
- Part 3 introduces the experimental tools in terms of equipment and analytical techniques used in the studies reviewed in Parts 4 and 5.
- Part 4 summarizes the previous experimental, theoretical and modeling work related to the CE formation during combustion chemistry of hydrocarbons and oxygenated compounds.
- Part 5 has the same objective as Part 4, but deals with the consumption of CEs.
- In Part 6, the main conclusions are presented and perspectives for future work are provided.

It is well known that notable amounts of dioxins and benzofurans are produced during combustion processes [104,105]. However, these CEs including an aromatic ring are not considered in this paper because the involved chemistry is significantly different from what is attempted to be described here.

The combination of Parts 4 and 5 is of interest in understanding how CE detailed kinetic models can help to improve the combustion in ICE engines. Part 4 concerns CE formation from hydrocarbons and biofuels, which is of interest for improving engine efficiency due to the competition of this pathway with KHP formation during low-temperature oxidation. Part 5 reviews the current understanding of CE consumption reactions with an eye on the formation of pollutants from furan derivatives. Such an understanding is needed to evaluate their potential as biofuels to replace fossil fuels with the goal to contribute to the reduction of greenhouse gas emissions.

## **2. NAMES, STRUCTURES, THERMOCHEMICAL PROPERTIES, AND THEORETICAL METHODS**

Before reviewing the combustion kinetics studies related to the formation and consumption of CEs in Parts 4 and 5, this part aims at presenting the names, structures and the thermochemical data of all CEs mentioned in this paper. Before that, a description of the methods used to theoretically calculate the related kinetic and thermochemical data is given.

### **2.1. Overview of the theoretical methods used to calculate the cyclic ether related thermochemical data**

Theoretical investigations contribute significantly towards the understanding of CE chemistry. They provide Potential Energy Surfaces (PESs) that allow identification of energetically possible pathways, thermodynamic data for equilibrium considerations, reaction barriers and structural details of transition states for the calculation of thermal rate coefficients and the description of pressure effects for non-thermalized reactions. This review is concerned with two aspects of CE chemistry: first, their formation as products in low-temperature oxidation of other fuels (Part 4) and second, the combustion chemistry of CEs themselves (Part 5). Given this focus, the theoretical methods used to describe CE chemistry are essentially the same as those used for low-temperature oxidation in general. In 2009, Pilling [106] presented an overview of the state of the art of mechanism development for low-temperature oxidation based on elementary reactions, and Zádor *et al.* [107] provided an excellent discussion on a strategy to develop rate expressions involving close interaction between theory and experiment.

The calculation of rate coefficients may be considered as a stepwise process starting from first principles to determine electronic energies and structural parameters of reactants, Transition States (TSs) and products. This leads to PESs, on which reactants, addition products, their isomers, and bi- (or tri-) molecular product channels are connected with each other through TSs. The molecular information is used to calculate thermodynamic properties of individual

species based on statistical mechanics and to calculate their high-pressure limit rate coefficient ( $k_{\infty}$ ) using statistical rate theory. In non-thermal processes, the population of the energy states in species changes with time due to collisional energy transfer and chemical transformation. The solution of the representative Master Equation (ME) describes the fluxes between these states and those can be converted to rate expressions to be used in kinetic mechanisms. Comparison of predictions with reliable experimental data allows, if necessary, an adjustment of critical parameters within their uncertainty range to improve the mechanism until satisfactory results are achieved. Fig. 10 illustrates such a stepwise approach for kinetic calculations and some details are discussed in the following paragraphs.

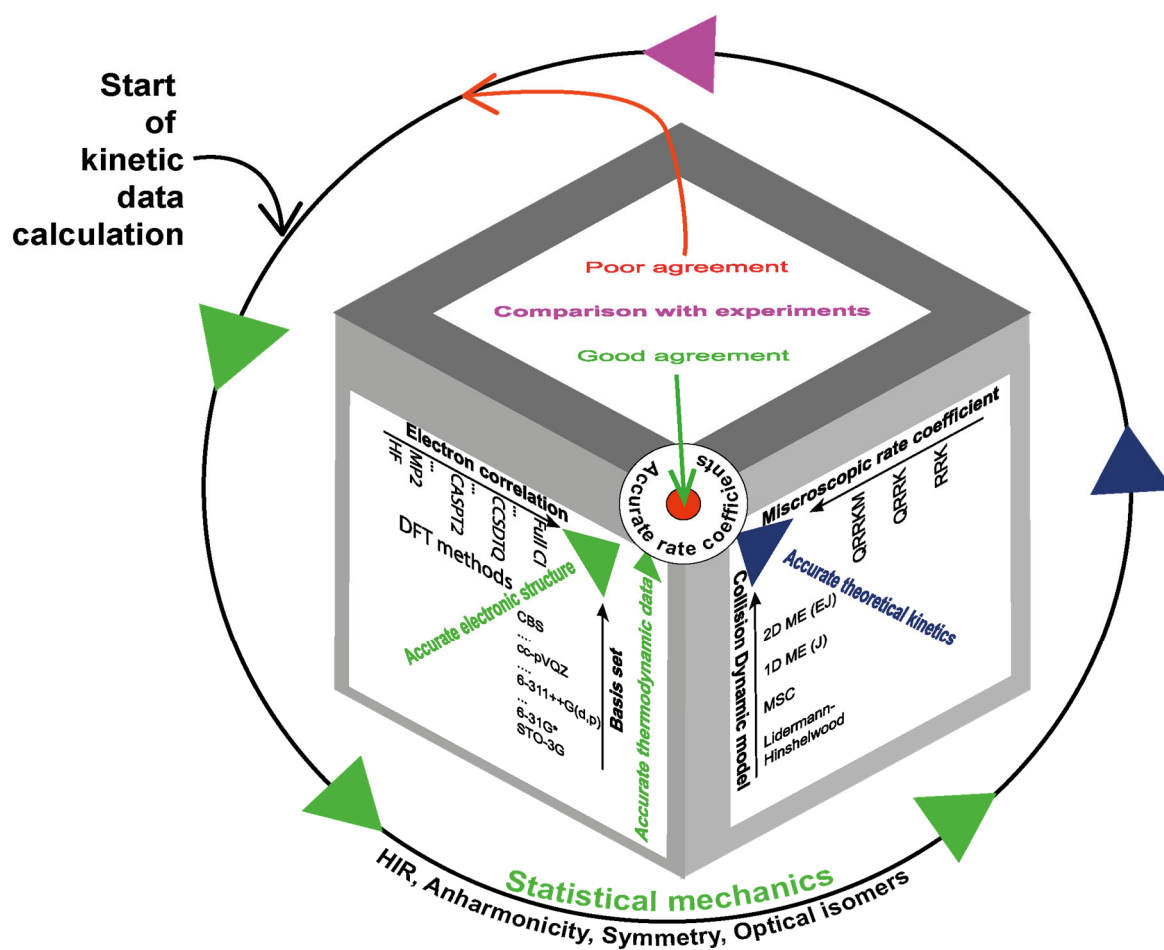


Fig. 10. Toolbox for the calculation of rate expressions.

### *2.1.1. Electronic structure calculations*

The electronic Schrodinger equation for chemical species is nowadays routinely solved with user-friendly first principles software packages to establish their optimized geometries, (an)harmonic frequency spectra and absolute electronic energies. The results of these electronic structure calculations strongly depend on the method and basis set chosen. The method essentially describes the accuracy with which the interactions between electrons are treated while the size and structure of the basis set determines the flexibility to optimize the wavefunction when solving the eigenvalue (electronic energy) – eigenvector (wavefunction) problem.

At the Hartree Fock (HF) level, a given electron interacts with all other electrons only through an average field (mean field assumption) meaning without individual electron-electron correlations. Any post-HF method adds electron correlation either through Møller Plesset perturbation theory (MP), Complete Active Space (CAS) configuration interaction, various Quadratic Configuration Interaction (QCI) and similar Coupled Cluster (CC) theories or by Full Configuration Interactions (Full-CI). The horizontal axis of Fig. 10 lists exemplarily some methods: MP2 ([108]), CASPT2 (Complete Active Space second order Perturbation Theory [109]), CCSD(T) (CC with Single, Double and Perturbative Triple excitations [110]) and Full-CI [111]. They are ordered with respect to increasing accuracy, which correlates with the demand in computational power. Full-CI completely recovers the electron correlation and is exact in this sense.

Density Functional Theory (DFT) also addresses electron correlation through empirical so-called exchange and correlation functionals. A large number of DFT methods exist which are often parametrized for special purposes. Since DFT methods are not post-HF methods, they are shown separated in Fig. 10. DFT methods are generally faster than most post-HF methods but they are often not as accurate as some affordable post-HF methods. Nevertheless, they play

an important role in quantum chemical studies as they are dominantly used in geometry and frequency calculations.

The vertical axis shows examples of basis sets starting from the STO-3G (Slater Type Orbitals approximated by 3 Gaussian functions) basis set, followed by examples of Pople's Gaussian-type basis sets [112], a Dunning correlation consistent *polarized valence* basis set and ends with the Complete Basis Set (CBS) limit. The Pople *split-valence zeta* Gaussian basis sets [112] are named X-YZ...+G(d,...) with X,Y,Z, ... being integer numbers indicating how many Gaussian functions are used to describe core shell (X) and valence (Y,Z,...) electron orbitals. "6-311+G(d)" for example means that the core orbitals are described by a set of six Gaussian functions and the valence orbital functions are built from three sets of basis functions, the first set comprises of three Gaussian functions and the other two consist each of one Gaussian function. The radial sizes of the three sets are different, hence by optimizing the contributions of these three sets, the location of the valence orbitals can be varied. "+" indicates the addition of an extra *diffuse* basis function describing a large s-orbital for non-hydrogen atoms and (d) indicates that extra *polarized* d-orbital is added for non-hydrogen atoms which as the name suggests allows for charge separation. The basis set 6-311++G(d,p) contains more functions than the 6-31G(d) basis set (3 split valence functions versus two; ++: diffuse functions also for hydrogen and not just for non-hydrogen atoms; d,p: a polarizing p-orbital for hydrogen atoms next to the polarized d function for non-hydrogens), which leads to more parameters for the wavefunctions to be optimized and thus more accurate but also more time-consuming calculations. Another popular type of basis sets is that developed by Dunning *et al.* [113]: the Dunning correlation consistent *polarized valence* basis sets (aug-cc-pVNZ, with 'Z' saying that the basis set is built from several basis functions of increasing shell size, and N=D, T, Q, 5 indicates the largest shell included (double, triple, ...)). The 'aug' prefix means that extra

'diffuse' orbitals are added. The Dunning basis sets are specially suitable to allow extrapolation to the complete basis set.

The perfect solution of the electronic Schroedinger equation is 'theoretically' achieved with a Full-CI / CBS calculation, but this is not achievable. In reality, the methodology and basis set size are chosen such that the calculations provide sufficiently accurate results with the available computational resources. Studies of the CE chemistry of small molecules can be performed at higher levels than those involving large molecules, which leads to the strategy to study small *model* systems in great detail with the highest levels of theory and transfer the results to larger systems. This leads to the rate rules and Group Additivity (GA) concepts used to build kinetic models for CE chemistry.

Post-HF levels are only reliable for single-reference problems meaning that the lowest energy electron configuration is well described by a single determinant (Hartree Fock) wavefunction. If the lowest energy state is (nearly) degenerate, then a multi-reference treatment is needed. The methods CASPT2 and Full-CI shown in Fig. 10 contain multi-reference contributions and are used for such cases. The T1 diagnostic by Lee [114] introduces a criterion to identify multi-reference behavior: If the dimensionless T1 value is larger than 0.02, then treating the species with single-reference methods *might* lead to severe errors, but often values up to 0.03 or 0.04 are considered to be safely treatable by single reference methods. As can be seen from Table 2, which presents T1 values for important species on the  $C_2H_5+O_2$  PES, the T1 values of most species exceeds this crucial threshold. The T1 value for the TS for CE formation is the second highest reported value suggesting that results obtained with single reference methods without additional corrections might be highly inaccurate. Nevertheless, many if not almost all reported theoretical results for low-temperature oxidation reactions are based on single-reference methods.



Harding *et al.* [115] explored the accuracy of CCSD(T) and CASPT2 among other methods for ten test reactions, including four radical-radical reactions, three abstraction reactions, one H-addition to a triple bond and two molecular elimination reactions. The main conclusions for these small systems were that CCSD(T) is very reliable for single-reference problems, *e.g.* CH<sub>4</sub> elimination from CH<sub>3</sub>CHO through a tight high energy transition state, and CASPT2 is a good choice for multi-reference problems, such as radical-radical reactions. They also recommend the use of CASPT2 for geometry and frequency calculations in *a priori* studies.

As will be discussed in part 4, reported rate expressions for CE formation show significant variations, both in barriers and pre-exponential factors. Those are largely calculated with single-reference techniques or DFT. The relatively high T1 value in Table 2 for the CE channel together with the conclusion by Harding *et al.* [115] suggest that CASPT2 theory could be applied to improve the kinetics. In this context, however, it should be noted that the choice of the active space, *e.g.* the identification of the electrons and orbitals to be included, can be a challenging task [115–118], while single-reference calculations do not require the user to make such choices, even though the stability of the guessed initial wavefunction should be checked with the *ab initio* software.

**Table 2.** T1 values calculated at CCSD(T1Diag)/CBSB7 for important stationary points on the C<sub>2</sub>H<sub>5</sub> + O<sub>2</sub> PES. Transition states are named TS(reactant→product) and the transition state for CE formation is highlighted in blue.

Species	T1 value	Species	T1 value
C <sub>2</sub> H <sub>5</sub> O $\dot{O}$	0.025	TS( $\dot{C}COOH \rightarrow$ oxirane + $\dot{O}H$ )	0.041
$\dot{C}COOH$	0.012		
TS(C <sub>2</sub> H <sub>5</sub> O $\dot{O} \rightarrow$ C <sub>2</sub> H <sub>4</sub> + HO $\dot{O}$ )	0.034	TS( $\dot{C}COOH \rightarrow$ C <sub>2</sub> H <sub>4</sub> + HO $\dot{O}$ )	0.032
TS(C <sub>2</sub> H <sub>5</sub> O $\dot{O} \rightarrow$ $\dot{C}COOH$ )	0.025	TS( $\dot{C}COOH \rightarrow$ CH <sub>3</sub> CHO + $\dot{O}H$ )	0.052

Determination of the lowest energy geometry (structure) of a species is a prerequisite of a high-level electronic energy calculation, since the final energy result depends on this geometry. These optimizations and the corresponding (harmonic oscillator) frequencies are generally done at a lower level of theory, often invoking DFT methods, because geometry

optimization is an iterative procedure that requires many energy calculations. Furthermore, the frequency calculation has to be done with the same method as that used to optimize the geometry. The most widely used method is B3LYP [119]. It is an integral part of several composite methods to be discussed below. Besides B3LYP, the highly parameterized Minnesota functional M06-2x [120] combined with a large basis set has gained popularity as method for geometry and frequency calculations. It is nowadays common to combine these methods with rather large split valence basis sets that include diffuse and polarized functions. The importance of diffuse functions is illustrated in Table 3, which contains the energy differences between the two conformers of ethanol calculated at various levels of theory and with different basis sets. Since the *trans* conformer is known to be more stable, negative entries in Table 3 indicate a wrong energy order of the conformers. This problem has been reported by Sun and Bozzelli [121] at the B3LYP/6-31G(d,p) level. As can be seen from Table 3, even CC methods lead to incorrect predictions when used with unsuitable basis sets. On the other hand, all calculations done with diffuse functions containing basis sets lead to the correct answer. Note that the CBS-QB3 and G4 composite methods contain energy calculation steps that employ diffuse functions.

**Table 3.** Calculated 0 K energy (kcal/mol) differences between the *gauche* and *trans* conformers of ethanol. Results in blue suggest that the *gauche* conformer is more stable.

Method	Basis set	E( <i>gauche</i> ) – E( <i>trans</i> )
HF	6-31+G(d)	0.31
	6-311G(d,p)	0.14
	6-311++G(d,p)	0.33
MP2	6-31+G(d)	0.26
	6-311G(d,p)	-0.10
	6-311++G(d,p)	0.31
B3LYP	6-31G(d)	-0.24
	6-31+G(d)	0.10
	6-311G(d,p)	-0.17
	6-311++G(d,p)	0.17
M06-2X	6-31G(d)	-0.20
	6-31+G(d)	0.12
	6-311G(d,p)	-0.20
	6-311++G(d,p)	0.05
CCSD(T)	cc-VTZ	-0.02
	aug-cc-VTZ	0.12
	cc-VQZ	0.10
CBS-QB3		0.22
G4		0.24

Accurate electronic energies for low-temperature oxidation chemistry that includes CE forming and consuming reactions are generally obtained with either composite methods or CBS extrapolated coupled cluster calculations. Composite methods are multi-step calculations that include geometry optimization and frequency calculations as well as several energy calculation steps at different levels of theory. The results combined with additional empirical corrections are used to estimate the energy at a high level. The step-wise well-defined procedures provide estimates of accurate energies at reduced computational cost by combining high-level electron correlation methods with small basis sets with lower level calculations but large basis sets. The final energy is calculated from a well-chosen series of energy calculations taking advantage of the assumption that increases of the basis set and level of theory lead to additive improvements of the energy. The most prominent families of composite methods are the Gaussian-x methods developed by Pople and coworkers, of which Gaussian-3 or G3 [122] and Gaussian-4 or G4 [123] are widely used, the complete basis set methods developed by the group of Petersson (*e.g.* the highly successful CBS-QB3 method [124,125] and CBS-APNO [126]), the series of Weizman methods  $W_n$  by Martin and de Oliveira of which the less computational intensive W1 and W2 theories are more suitable for low-temperature oxidation systems [127] and the correlation consistent composite approach (ccCA) by Wilson and coworkers [128]. More highly accurate composite methods such as HEAT [129] or the ANL0 and ANL1 [130] procedures are known but their applicability is currently restricted to small species. In particular, the CBS-QB3 and G4 methods have been and are still popular choices for the development of combustion models. Their average accuracy is on the order of 1 kcal/mol based on comparison with test sets [123–125], however, as pointed out by Ruscic, the uncertainty based on a 95% confidence interval is 2.5-3.5 times higher [131]. Higher uncertainties of the CBS-QB3 method based on 2 sigma errors rather than average accuracies have also been reported, *e.g.*, by Simmie and

Somers [132]. In Klippenstein *et al.* [130], substantial differences between the CBS-QB3 results and the Active Thermochemical Tables (ATcT [133]) are noted. The main advantage of composite methods is that they provide generally a good compromise between accuracy and demand of computational resources, but in light of abovementioned uncertainties, the results need to be handled with caution.

Due to enormous advances in computer power and improvements in *ab initio* software packages, coupled cluster calculations with single, double and perturbative triple excitations (CCSD(T)) and sufficiently large basis sets are nowadays feasible for medium sized species (10 or more heavy atoms, see *e.g.* [134]). This allows their use for low-temperature oxidation models of small fuel molecules. Using Dunning's correlation consistent basis sets discussed above,  $E_{l_{max}}$ , which is the electronic energy from a CCSD(T)//cc-pVNZ calculation with  $N=l_{max}$  can be extrapolated to the complete basis set ( $E_{\infty}$ ), *e.g.* using the scheme suggested by Martin [135] and Feller and Dixon [136],

$$E_{\infty} = E_{l_{max}} - B/(l_{max} + 1)^4 \quad (1)$$

where  $B$  is a constant and  $l_{max}$  is the maximum component of angular momentum in the cc-pVNZ basis set. For example, if the cc-pVQZ basis set is used,  $l_{max}=4$ . Feller and Franz [137], who study the heats of formation of furan, THF and THF radicals, nicely demonstrate how well the CCSD(T) results converge with increasing basis set.

In contrast to many composite methods, the CBS extrapolation of coupled cluster calculations does not require empirical corrections. Therefore, CCSD(T)/CBS calculations are considered to be reliable for all species as long as the electronic ground state is not degenerated or mixed with higher electronic states. Species, for which this is the case, should be treated with multi-reference methods (*e.g.* CASPT2) as discussed above.

### **2.1.2. Thermodynamic data and thermal rate coefficients**

Besides rate expressions, kinetic models, require thermodynamic properties such as the Gibbs free energy for all species considered. They are needed, *e.g.*, to solve the energy balance of adiabatic reactors or to calculate rate coefficients of reverse reactions. Thermodynamic properties can be calculated from the fundamental results from electronic structure calculations, which are the electronic energy, the geometry and internal modes of a species through well-established standard methods of statistical mechanics [138]. At this stage, only a few selected aspects of the procedure are briefly discussed, which are (a) the conversion of electronic energies into enthalpies of formation (b) the handling of internal rotations and (c) the role of symmetry and optical isomers. Finally, the calculation of the rate coefficients of thermalized reactions are described. It should be noted that a recent paper discussed in detail an automated strategy for thermochemistry calculations [139] including ways to handle the aspects mentioned above.

#### **2.1.2.1. Enthalpies of formation**

Two strategies are employed to calculate the enthalpies of formation from the *ab initio* results: the use of isodesmic (or similar) reactions and the atomization method. In isodesmic reactions [140], the reactants and products contain the same number of bonds of a given type. If in addition the groups (substructures consisting of a multivalent atom and its ligands) are also conserved, the reaction is called homodesmotic. According to the assumption of additivity of thermochemical properties (Benson's GA method [141]) homodesmotic reactions should be thermoneutral. The *ab initio* calculated enthalpy of reaction should be very accurate because any systematic weaknesses of the calculation method would cancel out. If the enthalpies of formation for all but one species of an isodesmic reaction are known with high accuracy, the missing value can be calculated. Bozzelli and coworkers have extensively used isodesmic

reactions for species related to low-temperature oxidation [142–144] and showed that even DFT level calculations yield very accurate results [145]. This indicates that the errors in low level calculations are dominantly of systematic nature that cancel out. The accuracy of isodesmic reactions depends on the availability of well-known experimental enthalpies of formation. This presents a drawback, which has been partly overcome by using highly accurate theoretical data instead for the reference species. The need to choose the representative reactions introduces some subjectivity, which has been a point of criticism [146]. Furthermore, confusion about the correct definition of such reactions have lead to inconsistent results [147].

The atomization method [148] is the more widely used approach to convert electronic energies into enthalpies of formation. The energy for complete dissociation of a species to its atoms, *e.g.*  $C_xH_yO_z \rightarrow xC + yH + zO$ , is calculated *ab initio* at 0 K. Using experimentally known energies to convert the atoms from 0 K to the standard states of the elements at 298 K and the *ab initio* calculated thermal energy of the species, the enthalpy of formation can be calculated. The calculation of atomization energies does not require any reference species besides the atoms. Unlike isodesmic reactions, atomization energies are in principle independent of user input, hence unbiased. However, in practice this is not necessarily the case because *ab initio* methods optimized for small species often contain systematic errors, which become more severe with increasing molecule size. This leads to the need to improve results by applying corrections, *e.g.* specific to chemical bonds (BAC or bond additive correction) [149,150]. The correction parameters are obtained from comparisons to selected experimental data, which introduces subjectivity. Paraskevas *et al.* successfully applied bond additive corrections to CBS-QB3 results of oxygenated hydrocarbons [151].

#### **2.1.2.2. Internal rotations**

It is nowadays common practice to treat internal modes that resemble rotations of moieties within the species as hindered rotors and not as harmonic oscillators to improve the predictions

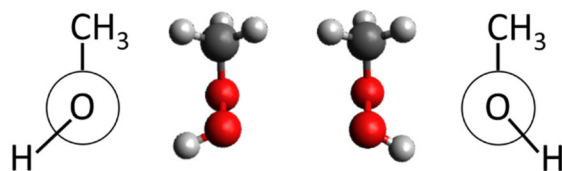
of entropy, heat capacity and thermal energy contributions. If those internal rotations are independent from other modes, they can be described by 1-D rotors. The hindrance potentials are calculated *ab initio* and represented as Fourier series and the effective moment of inertia is calculated based on work by Pitzer and coworkers [152–154] or East and Radom [155]. The solutions of the corresponding Schroedinger equation obtained with free rotor basis functions are the energy levels of the rotation, which are numerically included in the partition functions used to calculate thermal energy, entropy and heat capacities via statistical mechanics [138]. Coupled internal rotors are generally also approximated as 1-D rotors and only few publications explicitly address the coupling [156]. The explicit treatment of internal modes improves the results in particular of the entropies, but even for small molecules substantial deviations between calculated and experimental entropies may exist [155]. There is no real consensus established for the choice of the level of theory for the hindrance potential calculations. In addition, different research teams apply different thresholds (barrier heights) for the identification of internal modes as rotors. Another source of uncertainty arises from conformers. Commonly the lowest energy conformer is used but if only 1-D internal rotors are considered, it is not clear if the lowest energy geometry is always found (see also the previous discussion on the basis set dependence of relative conformer energies). The work by Simmie and Somers [132] provides an example, in which the contributions of different conformers are accounted for, and the work by Sharma *et al.* [156] also puts an emphasis on properly treating coupled internal rotations. Furthermore, Zheng *et al.* describe a computer program that automatically addresses torsional anharmonicity [157].

### **2.1.2.3. Symmetry factors and optical isomers**

Entropies also depend on the correct assignment of symmetry factors and a consistent handling of optical isomers (or more general entropy of mixing). The correction for the existence of optical isomers depends partly on the internal rotor treatment discussed above. Taking ROOH

as example, the rotation around the RO–OH bond has a significant barrier of about 6-7 kcal/mol for methylhydroperoxide. If such a barrier is considered too high for a hindered rotation, and the harmonic oscillator assumption is applied, then two optical isomers exist, as is shown in Fig. 11. The optical isomers cause the entropy of the racemic mixture to increase by  $R \cdot \ln(2)$ . On the other hand, if the barrier is considered low enough to treat the mode as internal rotation then these optical isomers are no longer distinguishable. This is a judgement call as no established guidelines for the classification exist (in the particular example of ROOH, the best option would be to treat the double-well potential as anharmonic oscillator, since both optical isomers are separated by just a small barrier, but routine application do not provide such an option).

In 2001, Sumathi *et al.* [158] compared for *n*-butane the entropy calculated either with internal rotation of the CC–CC bond or without internal rotation but instead accounting for mixing of all conformers. They obtained very similar results for 298K entropies and thermal energy contributions. Of course, this is not true for the heat capacity. For instance, at high temperature fully activated rotors contribute only  $R/2$  to the heat capacity while harmonic oscillators contribute  $R$  ( $R$  = gas constant). The lack of a general accepted protocol creates uncertainty in *ab initio* derived thermodynamic data, which might explain why studies using reportedly the same method of theory obtain different results for thermodynamic properties, but also for rate expressions (see next paragraph).



**Fig. 11.** Optical isomers of methylhydroperoxide if the harmonic oscillator assumption is applied.



#### 2.1.2.4. Calculation of rate expressions for thermalized reactions

Canonical high-pressure limit rate coefficients ( $k_\infty$ ) can be calculated with transition state theory (TST) [159,160].

$$k(T) = L \cdot \chi(T) \cdot \frac{k_B T}{h} \cdot \frac{q_{TS}^\ddagger}{\prod_i q_i} \cdot e^{-E/(RT)} \quad (2)$$

or

$$k(T) = L \cdot \chi(T) \cdot \frac{k_B T}{h} \cdot (V_{mol})^{m-1} \cdot e^{-\Delta G^\ddagger/RT} \quad (3)$$

Both equations are equivalent.  $\chi(T)$  is the tunneling correction factor,  $q_{TS}^\ddagger$  and  $q_i$  are the partition functions for the transition state and reactants, respectively,  $E$  is the zero-point corrected barrier height,  $V_{mol}$  the molar volume at standard condition,  $m$  is the molecularity of the reaction and  $\Delta G^\ddagger$  the Gibbs free energy difference between transition state and reactants. The  $\ddagger$  mark indicates that the transitional mode is omitted.  $L$  is the reaction path degeneracy, which only needs to be applied if the partition functions or  $\Delta G^\ddagger$  do not yet account for symmetry and optical isomer contributions. All other symbols have their usual meaning.  $L$  is given by

$$L = \frac{OI^{TS} \cdot \sigma^{reactants}}{OI^{reactants} \cdot \sigma^{TS}} \quad (4)$$

with  $OI$  specifying the correction for the presence of optical isomers and  $\sigma$  presents the total symmetry contribution due to (external) molecular symmetry and the symmetry of internal rotors [161,162].  $\chi(T)$  is usually estimated using asymmetric Eckart barriers [163,164] or the small-curvature approximation [165]. All input data is available from *ab initio* calculations after evaluation with statistical mechanics.

The *ab initio* results also allow calculation of the microcanonical rate coefficient  $k(E)$  with (Rice–Ramsperger–Kassel–Marcus) RRKM theory [166].

$$k(E) = \frac{W^\ddagger(E)}{h \cdot \rho(E)} \quad (5)$$

with

$$W^\ddagger(E) = \int_0^{E-E_0} \rho^\ddagger(E_\ddagger) dE_\ddagger. \quad (6)$$

Here,  $W^\ddagger(E)$  symbolizes the sum of states of the active complex (transition state) with energies up to  $E$ ,  $E_0$  is the barrier height meaning that  $E - E_0$  is the energy in the transition state ( $E \geq E_0$ ).  $\rho(E)$  is the density of states of the reacting molecule and  $\rho^\ddagger(E_\ddagger)$  that of the activated complex. If symmetry and optical isomer effects play a role,  $k(E)$  has to be multiplied with the reaction path degeneracy  $L$  given above.

For thermalized reactions,  $k(T)$  can be calculated from  $k(E)$  through integration over all  $E$

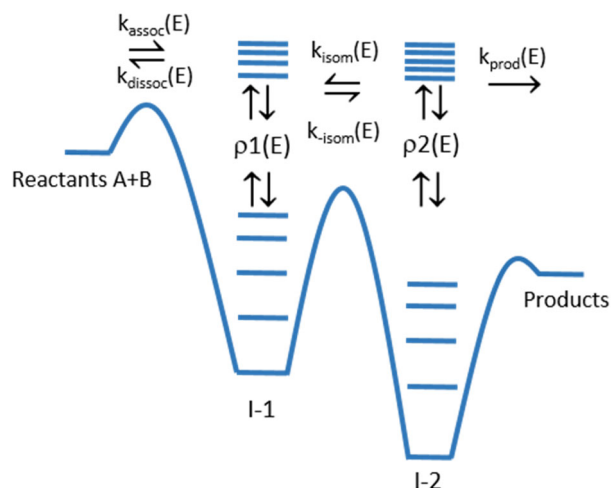
$$k(T) = \int_{all E} k(E) \varrho(E) dE \quad (7)$$

because the energy distribution function  $\varrho(E)$  is the Boltzmann distribution. The importance of the microcanonical rate coefficient is that it is required in the analysis of non-thermalized reactions, for which  $\varrho(E)$  needs to be replaced by the non-thermal energy distribution function  $f(E)$ . The sum and density of states can easily be calculated from the *ab initio* results with the Beyer-Swinehart algorithm [167,168].

Rate coefficients for reactions proceeding through transition states without distinct barrier are calculated with variational transition state theory (vTST). In canonical vTST the location of the transition state is systematically varied for a given temperature to find the smallest rate coefficient for that temperature. A more accurate procedure is to variationally calculate the microcanonical rate coefficients  $k(E,J)$ . The most important method used in the combustion community is that developed by Klippenstein and coworkers [169,170], in which not only the relative position of reacting groups is optimized but also the pivot positions in these groups. Prerequisite for reliable results is a proper description of the potential energy surface for barrierless reactions, which requires the use of methods that can handle multi-reference states. Therefore, CASPT2 is generally used for these studies.

### 2.1.3. Pressure-dependent reactions

The rate coefficients of the reactions of species, which are not thermalized (the energy states are not populated according to the Boltzmann distribution), depend on pressure because non-reactive collisions with the bath gas will change the energy state populations and therefore the overall reactivity. Miller and Klippenstein [171] and Robertson *et al.* [172] provide detailed descriptions of how the related ME are solved and how the results need to be interpreted. An update of the state of the art is discussed by Jasper *et al.* [173]. Here only a very brief overview is given. Fig. 12 shows a two-well system as an example, in which the reaction is initiated by the reactants A and B. The initial population of isomer one (I-1) is determined by the energy distributions of these reactants and the barrier height; subsequent non-reactive collisions alter this distribution by transferring energy to or from the states of I-1. Isomerization populates I-2 and dissociation reproduces the reactants. I-2 may react to yield the products, isomerize to I-1 or change the population of states through energy transferring collisions. The complete set of all possible processes leads to the ME, which is an eigenvalue-eigenvector problem. Its solution yields the populations of all states as a function of time (eigenvector) as well as the flux coefficients (eigenvalues). One may distinguish between two types of eigenvalues: those describing the energy flux among different energy states (internal energy relaxation eigenvalues (IEREs)) and those that lead to chemical changes (chemically significant eigenvalues (CSEs)). If energy transfer among the states is fast compared to all chemical transformations, then these eigenvalues are clearly separated and the CSE can be converted to rate expressions. On the other hand, if energy relaxations and chemical transformations occur on similar time scales, then the rate expressions are time dependent and typical constant rate expression can only be approximated.



**Fig. 12.** Schematic illustration of a pressure-dependent two-well systems (adapted from Glowacki *et al.* [174]).

Given that realistic reaction systems contain many isomers and that they require large arrays of energy grains to properly describe the energy distribution on vastly different timescales, solving the ME poses a severe numerical problem. Codes like MESMER [174] or MESS [175] use quadruple precision variables to obtain converged numerical solutions. MultiWell [176] is another ME package, which uses a stochastic formulation of the ME problem. The accuracy of any solution – taking numerical problems aside – depends on the accuracy of the features of the PES as well as on a proper description of the chemistry and energy transfer during collisions. Fig. 10 symbolizes this in the right-hand box: the historic Lindeman theory [177], which assumes each collision to be completely activating or deactivating, can be improved by Troe’s modified strong collision (MSC) approach [178], which assumes that a fraction of the collisions transfer the full amount of excess energy. Significantly more accurate and physically sound state-resolved collision models are used in modern ME solving programs with the exponential down model being the most popular one. Collision models describing energy and angular momentum transfer would yield the most accurate ME solutions but the 2-D ME can currently only be solved for special cases. Microcanonical  $k(E)$  expressions are nowadays almost exclusively calculated with RRKM

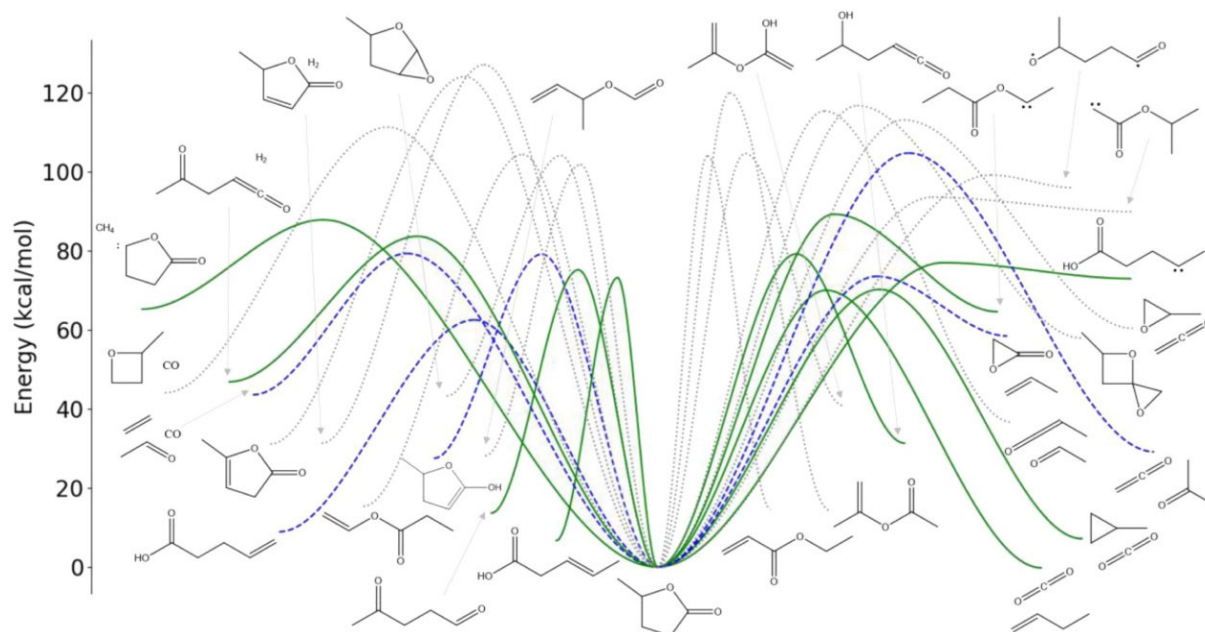
theory because the required input parameters are readily available from *ab initio* calculations. Newer implementations of QRRK [179], which preceded the RRKM theory, are interesting for automated mechanism generation because QRRK does not require detailed species information (frequencies and geometries) but works with input parameters that are available from GA. Furthermore, software is being developed to simplify the translation of ME results to lumped phenomenological rate expressions for implementation into kinetic models [180].

#### **2.1.4. Optimization of the reaction network**

Many input values for kinetic models contain uncertainties that may jeopardize the agreement with accurate experiments. By adjusting the input data within the limits of uncertainty the performance of kinetic models can be improved [107]. Refinements can be made to energies of the underlying potential energy surface, treatments of internal modes or energy transfer of pressure-dependent reactions, depending on which parameters are the most uncertain ones and have an impact on the predictions. As an example, in DeSain *et al.* [181] minor adjustments to energies of stationary points of the PES are made to improve the predictions of  $\dot{\text{O}}\text{H}$  and  $\text{HO}\dot{\text{O}}$  profiles measured in the photochemically initiated reaction of ethyl and propyl radicals with molecular oxygen. These adjustments lead to accurate predictions of the  $\text{HO}\dot{\text{O}}$  time profiles and supported the interpretation that this radical is partially produced by a direct formation channel. Burke *et al.* [182,183] term this optimization approach “Multiscale informatics” and Welz *et al.* have applied this approach recently to further deepen the understanding of propane oxidation at low temperatures [184]. In Fig. 10, the iterative adjustment process is shown to emphasize the importance of feedback between theory and experiment.

Besides the adjustment of parameters, uncertainties can also originate from an incomplete description of the chemistry. A ME analysis can only provide accurate rate expressions for a reaction system if all relevant reaction pathways are included in the analysis. Recent work demonstrated that important reaction pathways can easily be missed [185]. PES exploring

algorithms such as KINBOT [186] have been developed to address this problem by automatically scanning a PES. As an example, Fig. 13 shows a PES for  $\gamma$ -valerolactone decomposition. Compared to the previously published PES, KINBOT finds substantially more reaction pathways, some of which are of low energy and thus potentially kinetically relevant.



**Fig. 13.** PES for the decomposition of  $\gamma$ -valerolactone, automatically generated by KINBOT. Only the pathways in dotted blue lines were previously reported in the literature, all others are reported for the first time. The green lines represent reactions with barriers below the lowest bond dissociation energy, those in gray have higher energies. Reproduced from Ref. [186] with permission of Elsevier.

Automated thermochemical data [139] and mechanism generators such as RMG [187,188] and Genesys [189] contain tools for ‘on-the-fly’ calculation of rate coefficients for reaction pathways that can be identified but for which accurate kinetic parameters are not available in databases. It is foreseeable that in the future, theoretical studies of low-temperature chemistry including those involving CEs will take advantage of automated procedures that ensure completeness of the chemical network [11]. There are also other mechanism generators available, such as REACTION [190,191], MAMOX ++ [192], and EXGAS [193,194]. REACTION uses the concept of pathways instead of an exhaustive application of reaction

classes. MAMOX ++ distinguishes itself by generating a hierarchy of lumped mechanisms. The main specificity of EXGAS is the use of the most complete reaction class database and the wide choice offered to the user for the customization of the mechanism. This latter system was applied for combustion of some CEs, such as THF [195] and THP [196], but with complement of theoretical calculations for taking into account the specificity of CE reactivity. The reader is referred to the corresponding references for the details of each generator. In addition, the mechanisms generators mentioned were synthesized in a chapter of a book by Blurock *et al.* [197] and in a review by Van de Vijver *et al.* [198].

## **2.2. Names, structures, and thermodynamic data**

Table 4 presents IUPAC names (full and abbreviated), formula, 2-D structure, enthalpy of formation and entropy under standard conditions for all the CE molecules mentioned in this review. Since this paper is related to combustion, only gas phase values are given. The IUPAC names reflect IUPAC rules applicable for CE, such as the alphabetic order of detachable prefixes (*e.g.* ethyl appear before methyl), the priority of functional groups (*e.g.* the ether group has lower priority than an alcohol which is lower in priority than an ester group) and that the numbers should be as small as possible. These names have automatically been generated with ChemSketch software from Advanced Chemistry Development, Inc. (ACD/Labs) [199].

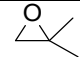
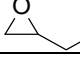
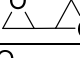

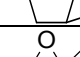


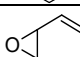

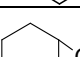
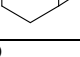
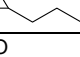
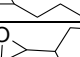
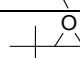
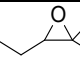
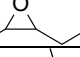
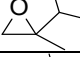
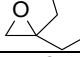
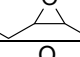

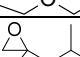
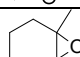
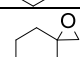
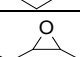
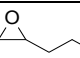
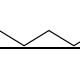
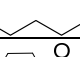
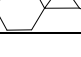


The heterocyclic nature of CEs leads to characteristic thermodynamic properties, in particular for furanic species. In Table 4, the enthalpy and entropy entries are divided into three groups: those based on experiments, those calculated with theoretical methods and finally those obtained using GA (Group Additivity). A quick glance at Table 4 shows that experimental and calculated data are very limited, but the GA method as implemented in the RMG program [187] is able to provide thermodynamic data for all species of interest. In the GA method, a molecule is divided into functional groups and the contribution of each functional group to the overall thermochemistry, the Group Additivity Value (GAVs), are added. These GAVs as well as any

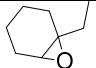
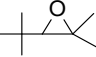
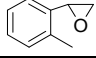

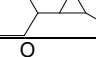

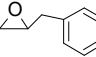
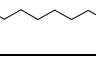
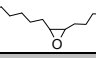
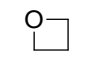
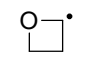
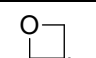
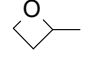
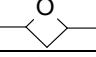
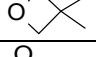

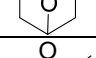
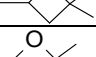
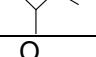

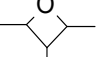
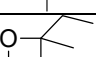

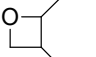
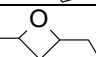
additional corrections for non-nearest neighbor interactions such as ring strains are developed from theoretical calculations and experimental data found in the literature. For example, thermodynamic properties for THF are calculated as follow with GA:  $group(C-O-C) + 2 \times group(O-CH_2-C) + 2 \times group(C-CH_2-C) + ring(Tetrahydrofuran)$ . The nomenclature are taken from RMG [187]. The thermodynamic properties for the  $group(C-O-C)$  and the  $group(O-CH_2-C)$  were calculated by Paraskevas *et al.* [151] at the CBS-QB3 level, while those for the  $group(C-CH_2-C)$  and ring (THF) were taken from [200]. For thermodynamic properties of radicals, the hydrogen bond increment method is used [187,201]. A brief discussion on the performance of GA is given at the end of this part.

**Table 4.** Full (and abbreviated) name, formula/structure and gas-phase thermochemistry data ( $\Delta H^\circ$ ,  $S^\circ$ ) of CEs considered in the review, together with a few representative radicals. Names in blue are those used in this review. When several names are given, the first name is the IUPAC one; names are separated by “;”. **Bold font:** experimental data including reviews of those (often found in the NIST WebBook [202]), regular font: theoretical calculations, *italic font:* group additivity (from RMG [187], unless otherwise noted). Some original data that are reported in kJ/mol have been converted to kcal/mol. Data precision is restricted to one decimal (rounded). The entries are ordered with respect to (i) cyclic ether ring size/type, (ii) type of molecule (e.g. aromatic, unsaturated saturated) and (iii) sum formula. Radicals, for which experimental or calculated thermodynamic data is available, are listed together with the parent molecules ( $\Delta H^\circ$ ,  $S^\circ$ ).

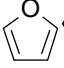

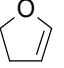
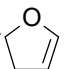
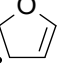

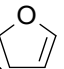
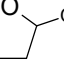
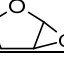
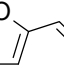
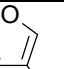
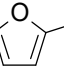
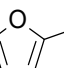
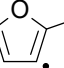
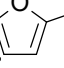
Species	Formula	Structure	$\Delta H^\circ$ (kcal/mol)	$S^\circ$ (cal/mol/K)
3-Membered cyclic ethers (oxiranes)				
Oxirane; Ethylene oxide	C <sub>2</sub> H <sub>4</sub> O		-12.6 [203] -12.6 [204] <b>-16.8</b> [205] -12.4 ± 0.6 [206] -12.2 to -13.3 [132] -9.6 [133] -13.2 [207] -12.7 [208] <i>-13.1</i>	<b>58.1</b> [203] <b>58.1</b> [209] <b>58.0</b> [210] 57.9 ± 0.5 [206] 58.0 [207] <i>57.0</i>
			Radicals	
	C <sub>2</sub> H <sub>3</sub> O Oxiran-2-yl; Oxiranyl		40.0 ± 0.9 [206] 39.7 [208] <i>30.8</i>	60.4 ± 0.5 [206] <i>59.3</i>
2-Methyloxirane; Propylene oxide; Methyloxirane	C <sub>3</sub> H <sub>6</sub> O		-22.6 ± 0.2 [211] <b>-22.2 ± 0.3</b> [212] <b>-28.0</b> [205] -22.3 ± 0.9 [206] -23.3 [207] -23.6 [213] <i>-21.1</i>	<b>68.9 ± 0.2</b> [209] <sup>a</sup> <b>68.7 ± 0.2</b> [214] <b>68.2 ± 2.0</b> [215] 68.5 ± 1.1 [206] 68.5 [207] <i>65.2</i>
			Radicals	
	C <sub>3</sub> H <sub>5</sub> O (Oxiran-2-yl)methyl		26.0 ± 0.9 [206] <i>29.5</i>	69.9 ± 1.2 [206] <i>67.5</i>
2-Ethenyloxirane; Ethenyloxirane	C <sub>4</sub> H <sub>6</sub> O		3.9	73.9
2,3-Dimethyloxirane	C <sub>4</sub> H <sub>8</sub> O		-30.2/-32.6 <sup>b</sup> [216] -32.8 [213] <i>-29.1</i>	70.6

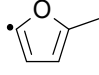
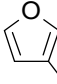
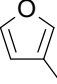
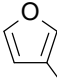
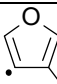
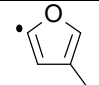
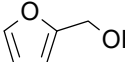
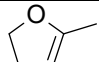
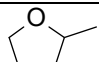
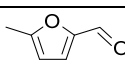
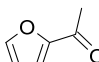
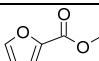
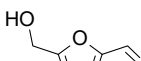
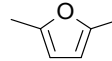
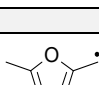
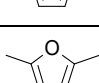
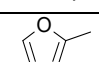
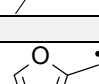
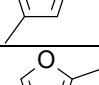
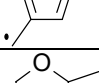


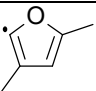
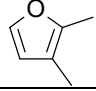
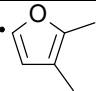
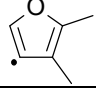

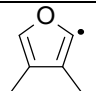
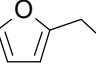
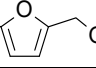
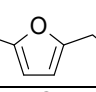
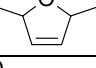
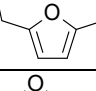

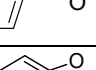
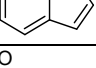
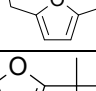
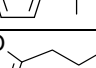
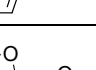
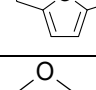
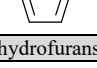
2,2-Dimethyloxirane; Isobutylene epoxide	C <sub>4</sub> H <sub>8</sub> O		-30.2	71.4
2-Ethyloxirane; Ethyloxirane	C <sub>4</sub> H <sub>8</sub> O		-26.1	77.4 [209] 74.6
Bioxirane	C <sub>4</sub> H <sub>6</sub> O <sub>2</sub>		-21.9	72.6
2-(Methoxymethyl)oxirane	C <sub>4</sub> H <sub>8</sub> O <sub>2</sub>		-53.0	83.4
6-Oxabicyclo[3.1.0]hexan-3-one	C <sub>5</sub> H <sub>6</sub> O <sub>2</sub>		-44.9	82.2
2,2,3-Trimethyloxirane; Trimethyloxirane	C <sub>5</sub> H <sub>10</sub> O		-41.9 [213] -38.2	78.1
2-Ethyl-3-methyloxirane	C <sub>5</sub> H <sub>10</sub> O		-34.1	81.4
2-Propyloxirane; Propyloxirane	C <sub>5</sub> H <sub>10</sub> O		-31.0	84.0
7-Oxabicyclo[4.1.0]hept-2-ene; 3,4-Epoxy cyclohex-1-ene	C <sub>6</sub> H <sub>8</sub> O		-0.1 [217] 2.4	75.4 [217] 75.6
7-Oxabicyclo[4.1.0]hept-3-ene; 4,5-Epoxy cyclohex-1-ene	C <sub>6</sub> H <sub>8</sub> O		3.0	73.2
7-Oxabicyclo[4.1.0]heptane; 1,2-Epoxy cyclohexane	C <sub>6</sub> H <sub>10</sub> O		-29.0 ± 0.5 [218] -30.0 ± 0.3 [219] -30.3 [220] -18.3	77.2 [220] 77.2
2-(But-3-en-1-yl)oxirane; But-3-enyloxirane	C <sub>6</sub> H <sub>10</sub> O		-5.8	91.8
2-Butyloxirane; Butyloxirane	C <sub>6</sub> H <sub>12</sub> O		-35.9	93.5
2-(Butan-2-yl)oxirane	C <sub>6</sub> H <sub>12</sub> O		-37.4	92.1
2-tert-Butyloxirane; tert-Butyloxirane	C <sub>6</sub> H <sub>12</sub> O		-41.0	84.4
3-Ethyl-2,2-dimethyloxirane	C <sub>6</sub> H <sub>12</sub> O		-43.1	87.6
2-Methyl-3-propyloxirane	C <sub>6</sub> H <sub>12</sub> O		-39.0	90.8
2-Methyl-2-(propan-2-yl)oxirane; 2-Methyl-2-isopropyloxirane	C <sub>6</sub> H <sub>12</sub> O		-42.3	87.5
2,2-Diethyloxirane	C <sub>6</sub> H <sub>12</sub> O		-40.1	90.2
2,3-Diethyloxirane	C <sub>6</sub> H <sub>12</sub> O		-39.0	89.4
Tetramethyloxirane	C <sub>6</sub> H <sub>12</sub> O		-47.3	82.9
2-(Propoxymethyl)oxirane	C <sub>6</sub> H <sub>12</sub> O <sub>2</sub>		-66.0	101.8
2-Methyl-2-[(propan-2-yl)oxy]oxirane	C <sub>6</sub> H <sub>12</sub> O <sub>2</sub>		-81.2	91.7
1-Methyl-7-oxabicyclo [4.1.0]heptane	C <sub>7</sub> H <sub>12</sub> O		-27.4	84.7
1-Oxaspiro[2,5]octane	C <sub>7</sub> H <sub>12</sub> O		-31.2	82.9
2-Ethyl-3-propyloxirane	C <sub>7</sub> H <sub>14</sub> O		-43.9	98.9
2-Butyl-3-methyloxirane	C <sub>7</sub> H <sub>14</sub> O		-43.9	100.2
2-Pentyloxirane; Pentyloxirane	C <sub>7</sub> H <sub>14</sub> O		-40.9	102.9
2-Hexyloxirane; Hexyloxirane	C <sub>8</sub> H <sub>16</sub> O		-45.8	112.3
2-Methyl-1-oxaspiro[2.5]octane	C <sub>8</sub> H <sub>14</sub> O		-39.2	89.7

1-Ethyl-7-oxabicyclo[4.1.0]heptane	C <sub>8</sub> H <sub>14</sub> O		-32.3	94.1
3- <i>tert</i> -Butyl-2,2-dimethyloxirane	C <sub>8</sub> H <sub>16</sub> O		-58.1	97.3
2-(2-Methylphenyl)oxirane; 2-Methylphenyloxirane	C <sub>9</sub> H <sub>10</sub> O		3.08	97.27
2-Ethyl-1-oxaspiro[2.5]octane	C <sub>9</sub> H <sub>16</sub> O		-44.1	99.1
2-Cyclohexyl-3-methyloxirane	C <sub>9</sub> H <sub>16</sub> O		-45.4	96.9
2-Ethyl-3-phenyloxirane	C <sub>10</sub> H <sub>12</sub> O		-1.9	103.1
2-Benzyl-3-methyloxirane	C <sub>10</sub> H <sub>12</sub> O		-1.8	101.7
Methyl 9-(oxiran-2-yl)nonanoate	C <sub>12</sub> H <sub>22</sub> O <sub>3</sub>		-138.3	162.1
Methyl 8-(3-octyloxiran-2-yl)octanoate	C <sub>19</sub> H <sub>36</sub> O <sub>3</sub>		-175.9	224.0
4-Membered cyclic ethers (oxetanes)				
Oxetane	C <sub>3</sub> H <sub>6</sub> O		-19.3 [221] -19.3 ± 0.2 [204] -19.0 ± 0.9 [206] -19.7 [207] -19.2 [208] -19.8	64.9 [210] 65.6 ± 0.9 [206] 65.1 [207] 63.8
	Radicals			
	C <sub>3</sub> H <sub>5</sub> O 2-Oxetanyl		24.4 ± 0.9 [206] 24.6 [208] 23.5	67.6 ± 0.9 [206] 65.5
C <sub>3</sub> H <sub>5</sub> O 3-Oxetanyl		30.6 ± 0.9 [206] 30.9 [208] 27.7	66.8 ± 1.0 [206] 67.1	
2-Methyloxetane	C <sub>4</sub> H <sub>8</sub> O		-30.7 [207] -29.5 [213] -27.8	74.6 [207] 72.0
2,4-Dimethyloxetane	C <sub>5</sub> H <sub>10</sub> O		-35.8	77.4
3,3-Dimethyloxetane	C <sub>5</sub> H <sub>10</sub> O		-35.4 [222] -34.8	81.2 [222] 75.8
2-Ethyloxetane	C <sub>5</sub> H <sub>10</sub> O		-32.7	81.4
6-Oxabicyclo[3.1.1]heptane; 1,3-Epoxycyclohexane	C <sub>6</sub> H <sub>10</sub> O		-25.6 [220] -17.5	75.7 [220] 73.3
2,2,4-Trimethyloxetane	C <sub>6</sub> H <sub>12</sub> O		-44.9	84.9
2,2,3-Trimethyloxetane	C <sub>6</sub> H <sub>12</sub> O		-44.0	84.9
2,3,3-Trimethyloxetane	C <sub>6</sub> H <sub>12</sub> O		-42.8	83.9
2,3,4-Trimethyloxetane	C <sub>6</sub> H <sub>12</sub> O		-43.0	84.1
2-Ethyl-2-methyloxetane	C <sub>6</sub> H <sub>12</sub> O		-41.8	87.6
3-Ethyl-3-methyloxetane	C <sub>6</sub> H <sub>12</sub> O		-39.7	85.2
3-Ethyl-2-methyloxetane	C <sub>6</sub> H <sub>12</sub> O		-39.9	88.1
2-Ethyl-4-methyloxetane	C <sub>6</sub> H <sub>12</sub> O		-40.7	88.2

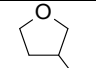
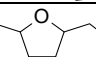
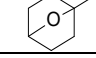
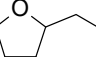
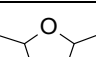
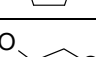
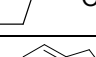
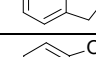
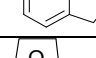
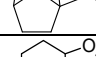
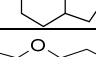
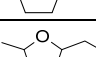
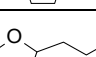
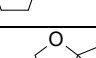
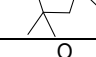
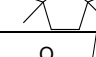
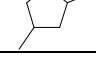
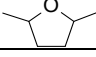
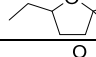
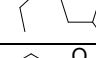
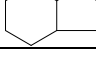
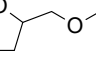
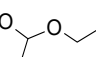
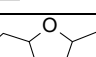
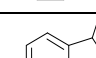
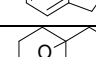
2-Propyloxetane	C <sub>6</sub> H <sub>12</sub> O		-37.7	90.8
3-Propyloxetane	C <sub>6</sub> H <sub>12</sub> O		-36.8	89.4
2-(Propan-2-yl)oxetane; 2-Isopropyloxetane	C <sub>6</sub> H <sub>12</sub> O		-39.9	88.1
3-(Propan-2-yl)oxetane; 3-Isopropyloxetane	C <sub>6</sub> H <sub>12</sub> O		-39.1	86.7
2-Propoxyoxetane	C <sub>6</sub> H <sub>12</sub> O <sub>2</sub>		-74.5	100.0
2-Butyloxetane	C <sub>7</sub> H <sub>14</sub> O		-42.6	100.2
2-Methyl-4-propyloxetane	C <sub>7</sub> H <sub>14</sub> O		-45.7	97.6
2,4-Diethyloxetane	C <sub>7</sub> H <sub>14</sub> O		-45.7	96.2
2-tert-Butyl-3-methyloxetane	C <sub>8</sub> H <sub>16</sub> O		-54.9	97.9
3,3-Dimethyl-2-(propan-2-yl)oxetane; 2-Isopropyl-3,3-dimethyloxetane	C <sub>8</sub> H <sub>16</sub> O		-54.9	100.1
2,2-Dimethyl-4-(propan-2-yl)oxetane	C <sub>8</sub> H <sub>16</sub> O		-57.0	101.1
3-Methyl-2-(2-methylpropyl)oxetane	C <sub>8</sub> H <sub>16</sub> O		-51.2	104.3
8-Ethyl-7-oxabicyclo[4.2.0]octane	C <sub>9</sub> H <sub>16</sub> O		-38.4	96.6
2-Methyl-1-oxaspiro[3.5]nonane	C <sub>9</sub> H <sub>16</sub> O		-42.9	94.5
2-Heptyloxetane	C <sub>10</sub> H <sub>20</sub> O		-57.4	128.5
2-Hexyl-4-methyloxetane	C <sub>10</sub> H <sub>20</sub> O		-60.5	125.9
2-Ethyl-4-pentyloxetane	C <sub>10</sub> H <sub>20</sub> O		-60.5	124.5
2-Butyl-4-propyloxetane	C <sub>10</sub> H <sub>20</sub> O		-60.5	124.5
2-Methyl-4-phenyloxetane	C <sub>10</sub> H <sub>12</sub> O		-3.6	100.5
2-Benzyloxetane	C <sub>10</sub> H <sub>12</sub> O		-0.5	101.7
Methyl 7-[4-(hydroxymethyl)oxetan-2-yl]heptanoate	C <sub>12</sub> H <sub>22</sub> O <sub>4</sub>		-180.6	167.5
4-Membered cyclic ethers (dioxetanes)				
1,3-Dioxetane	C <sub>2</sub> H <sub>4</sub> O <sub>2</sub>		-53.2	54.1
2-Methoxy-1,3-dioxetane	C <sub>3</sub> H <sub>5</sub> O <sub>3</sub>		-92.1	77.9
2,2,4,4-Tetramethyl-1,3-dioxetane	C <sub>6</sub> H <sub>12</sub> O <sub>2</sub>		-94.8	80.1
5-Membered cyclic ethers (furans and dihydrofurans)				
Furan	C <sub>4</sub> H <sub>4</sub> O		-6.6 [223] -7.1 [224] -8.3 [225] -8.2 [226] -8.3 ± 0.7 [227] -7.7 ± 0.5 [137]	<b>63.9</b> [209] <b>63.9</b> [210] 65.2 [226] 65.5

			-7.5 [144] -8.6 ± 0.1 [228] -8.2 [133] -8.6 [229] -8.9 [230] -8.3	
	Radicals			
	C <sub>4</sub> H <sub>3</sub> O Furan-2-yl		59.0 [226] 60.2 ± 1.3 [231] 61.7 ± 1.3 [232] <sup>e</sup> 60.9 ± 1.3 [232] <sup>d</sup> 48.9	66.5 [226] 73.3
	C <sub>4</sub> H <sub>3</sub> O Furan-3-yl		59.2 [226] 60.3 +/- 1.3 [231] 61.8 ± 1.3 [232] <sup>e</sup> 61.0 ± 1.3 [232] <sup>d</sup> 39.4	66.3 [226] 67.6
2,3-Dihydrofuran; 2,3-DHF	C <sub>4</sub> H <sub>6</sub> O		-17.3 ± 0.1 [233] -18.2 [195] -21.8 [226] -27.4 <sup>e</sup>	69.9 [210] 70.9 [195] 67.0 [226] 61.3
	Radicals			
	C <sub>4</sub> H <sub>5</sub> O 2,3-Dihydrofuran-2-yl		18.1 [226] 19.2	68.2 [226] 62.3
	C <sub>4</sub> H <sub>5</sub> O 2,3-Dihydrofuran-3-yl		8.5 [226] 0.7	68.1 [226] 56.6
2,5-Dihydrofuran; 2,5-DHF	C <sub>4</sub> H <sub>6</sub> O		-15.2 [195] -14.2 [226] -15.7	67.9 ± 0.2 [209] 67.9 [210] 68.0 [195] 65.1 [226] 68.5
	Radicals			
	C <sub>4</sub> H <sub>5</sub> O 2,3-Dihydrofuran-3-yl		8.5 [226] 0.7	68.1 [226] 56.6
2,3-Dihydrofuran-2-ol	C <sub>4</sub> H <sub>6</sub> O <sub>2</sub>		-74.7	70.2
2,6-Dioxabicyclo[3.1.0]hexane	C <sub>4</sub> H <sub>6</sub> O <sub>2</sub>		-45.0	72.0
Furan-2-carbaldehyde; Furfural	C <sub>5</sub> H <sub>4</sub> O <sub>2</sub>		-34.5 [234] -35.8 [235] -36.1 [236] -36.2 [224] -36.1 ± 1.1 [237] -37.6 ± 0.4 [238] -36.1	79.5
Furan-3-carbaldehyde; 3-Furaldehyde	C <sub>5</sub> H <sub>4</sub> O <sub>2</sub>		-36.3 ± 0.3 [239] -36.8 ± 0.3 [238] -34.4 [1]	77.4
2-Methylfuran; 2-MF	C <sub>5</sub> H <sub>6</sub> O		-18.3 ± 0.3 [240] -18.9 [226] -19.2 ± 1.2 [227] -18.8 to -18.0 [144] -19.3 ± 0.1 [231] -17.5	73.8 [226] 76.6
	Radicals			
	C <sub>5</sub> H <sub>5</sub> O (Furan-2-yl)methyl		14.4 [226] 14.8 ± 1.2 [231] 25.3 ± 2.9 [241] <sup>f</sup> 19.4	72.6 [226] 70.3
	C <sub>5</sub> H <sub>5</sub> O 2-Methylfuran-3-yl		49.2 ± 1.3 [231] 30.2	77.3
	C <sub>5</sub> H <sub>5</sub> O 5-Methylfuran-3-yl		49.0 ± 1.4 [231] 30.2	77.3

	C <sub>5</sub> H <sub>5</sub> O 5-Methylfuran-2-yl		49.0 ± 1.4 [231] 39.7	83.0
3-Methylfuran; 3-MF	C <sub>5</sub> H <sub>6</sub> O		-16.1 to -15.2 [144] -16.6 ± 0.1 [231] -16.4	74.1
	Radicals			
	C <sub>5</sub> H <sub>5</sub> O (Furan-3-yl)methyl		21.6 ± 1.3 [231] 19.7	73.7
	C <sub>5</sub> H <sub>5</sub> O 3-Methylfuran-2-yl		51.9 ± 1.4 [231] 40.8	80.5
	C <sub>5</sub> H <sub>5</sub> O4- Methylfuran-3-yl		51.7 ± 1.4 [231] 31.3	74.8
	C <sub>5</sub> H <sub>5</sub> O 4-Methylfuran-2-yl		51.4 ± 1.4 [231] 40.8	80.5
(Furan-2-yl)methanol; 2-Furfuryl alcohol; 2-FFOH	C <sub>5</sub> H <sub>6</sub> O <sub>2</sub>		-50.6 ± 0.5 [212,224] -50.7 [242] -50.8 [234] -52.6 ± 0.4 [238] -53.5	88.1
5-Methyl-2,3-dihydrofuran; 5-Methyl-2,3-DHF	C <sub>5</sub> H <sub>8</sub> O		-36.6	71
2-Methyl-2,5-dihydrofuran; 2-Methyl-2,5-DHF	C <sub>5</sub> H <sub>8</sub> O		-25.1	77.3
5-Methylfuran-2-carbaldehyde; 5-Methylfurfural	C <sub>6</sub> H <sub>6</sub> O <sub>2</sub>		-45.3	89.2
1-(Furan-2-yl)ethan-1-one; 2-Acetylfuran 2-AF	C <sub>6</sub> H <sub>6</sub> O <sub>2</sub>		-46.3	88.9
Methyl furan-2-carboxylate; 2-MOF	C <sub>6</sub> H <sub>6</sub> O <sub>3</sub>		-72.0	100.0
5-(Hydroxymethyl)furan-2-carbaldehyde; 5-Hydroxymethyl-2-furaldehyde; 5-HMF	C <sub>6</sub> H <sub>6</sub> O <sub>3</sub>		-81.3	100.7
2,5-Dimethylfuran; 2,5-DMF	C <sub>6</sub> H <sub>8</sub> O		-30.6 ± 0.2 [243] -29.8 ± 1.4 [227] -30.0 [244] -26.7	80.9 [244] 84.9
	Radicals			
	C <sub>6</sub> H <sub>7</sub> O (5-Methylfuran-2-yl)methyl		2.8 ± 1.4 [231] 2.7 [244] 11.3	81.2 [244] 87.5
C <sub>6</sub> H <sub>7</sub> O 2,5-Dimethylfuran-3-yl		37.6 ± 1.3 [231] 21.0	87.0	
2,4-Dimethylfuran	C <sub>6</sub> H <sub>8</sub> O		-28.1 ± 0.2 [231] -27.5 [244] -23.4	82.3 [244] 80.4
	Radicals			
	C <sub>6</sub> H <sub>7</sub> O (4-Methylfuran-2-yl)methyl		5.7 [244] 5.8 ± 1.4 [231] 11.0	81.4 [244] 77.8
	C <sub>6</sub> H <sub>7</sub> O (5-Methylfuran-3-yl)methyl		9.6 [244] 9.6 ± 1.5 [231] 10.5	80.3 [244] 83.5
C <sub>6</sub> H <sub>7</sub> O 2,4-dimethylfuran-3-yl		40.1 +/- 1.3 [231] 22.1	84.5	

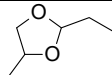
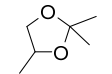
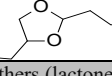
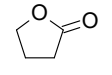
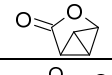
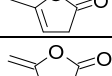
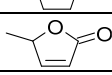
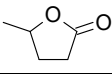
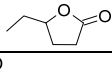
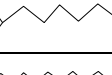
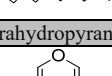
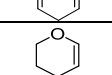
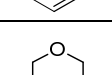
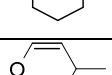
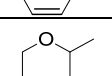
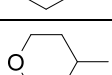
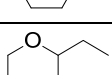
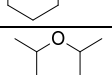
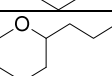
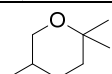
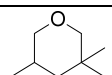



	C <sub>6</sub> H <sub>7</sub> O 3,5-dimethylfuran-2-yl		40.3 +/- 1.4 [231] 31.6	90.2
2,3-Dimethylfuran	C <sub>6</sub> H <sub>8</sub> O		-27.8 ± 0.3 [231] -25.6	83.8
	Radicals			
	C <sub>6</sub> H <sub>7</sub> O 4,5-dimethylfuran-2-yl		40.1 +/- 1.4 [231] 31.6	90.2
	C <sub>6</sub> H <sub>7</sub> O 4,5-dimethylfuran-3-yl		40.2 +/- 1.3 [231] 22.1	84.5
3,4-Dimethylfuran	C <sub>6</sub> H <sub>8</sub> O		-25.7 ± 0.2 [231] -25.1 [244] -24.5	80.9 [244] 80.0
	Radicals			
	C <sub>6</sub> H <sub>7</sub> O 3,4-dimethylfuran-2-yl		42.4 +/- 1.4 [231] 32.7	87.8
2-Ethylfuran; 2-EF	C <sub>6</sub> H <sub>8</sub> O		-24.2 ± 0.2 [231] -22.3	86.4
(5-Methylfuran-2-yl) methanol; 2-Hydroxymethyl,5-methylfuran	C <sub>6</sub> H <sub>8</sub> O <sub>2</sub>		-62.7	97.8
(Furan-2,5-diyl)dimethanol; 2,5-Dihydroxymethylfuran	C <sub>6</sub> H <sub>8</sub> O <sub>3</sub>		-98.8	108.0
2,5-Dimethyl-2,5-dihydrofuran; 2,5-Dimethyl-2,5DHF	C <sub>6</sub> H <sub>10</sub> O		-34.6	83.2
5-(Methoxymethyl)furan-2-carbaldehyde; 5-(Methoxymethyl)furfural	C <sub>7</sub> H <sub>8</sub> O <sub>3</sub>		-75.7	108.2
2-Ethyl-5-methylfuran	C <sub>7</sub> H <sub>10</sub> O		-31.5	96.1
2-(Ethoxymethyl)furan; Ethylfurfuryl ether; EFFE	C <sub>7</sub> H <sub>10</sub> O <sub>2</sub>		-56.0	104.6
1-Benzofuran; Benzofuran	C <sub>8</sub> H <sub>6</sub> O		3.3 ± 0.2 [245] 12.9	75.9
5-(Ethoxymethyl)furan-2-carbaldehyde; 5-(Ethoxymethyl)furfural	C <sub>8</sub> H <sub>10</sub> O <sub>3</sub>		-83.8	117.2
2-tert-Butylfuran	C <sub>8</sub> H <sub>12</sub> O		-39.1 ± 0.2 [243] -36.2	96.1
2-n-Butylfuran; 2-BF	C <sub>8</sub> H <sub>12</sub> O		-32.1	105.2
5-(tert-Butoxymethyl)furan-2-carbaldehyde; 5-(tert-Butoxymethyl)furfural	C <sub>10</sub> H <sub>14</sub> O <sub>3</sub>		-99.9	128.0
2,5-Di-tert-butylfuran	C <sub>12</sub> H <sub>20</sub> O		-70.2 ± 0.3 [243] -64.1	124.0
5-Membered cyclic ethers (tetrahydrofurans / oxolanes)				

Oxolan-3-one; 3-THFone	C <sub>4</sub> H <sub>6</sub> O <sub>2</sub>		-66.9	77.5	
Oxolane; Tetrahydrofuran; THF	C <sub>4</sub> H <sub>8</sub> O		-44.0 ± 0.2 [204] -44.0 ± 0.2 [237] <sup>g</sup> -44.0 ± 0.7 [137] -44.1 [195] -44.6 [207] -44.0 [208] -44.1 [226] -43.9	72.3 ± 0.7 [209] 72.3 [210] 72.1 ± 0.4 [246] 68.8 ± 0.1 [247] 72.4 [195] 71.1 [207] 69.3 [226] 65.9	
	Radicals				
	C <sub>4</sub> H <sub>7</sub> O Oxolan-2-yl; THF-yl-2		-0.2 [248] -2.9 [249] <sup>h</sup> -0.5 ± 1.0 [137] -2.2 [195] -2.0 [208] -4.1 [226] -0.6	73.1 [195] 71.9 [226] 67.6	
C <sub>4</sub> H <sub>7</sub> O Oxolan-3-yl; THF-yl-3		1.5 to 2.5 [237] -4.0 ± 1.6 [250] <sup>f</sup> 3.6 ± 1.0 [137] 2.1 [195] 2.5 [208] -1.6 [226] 3.7	74.0 [195] 71.9 [226] 70.5		
Oxolan-3-ol; 3-Hydroxytetrahydrofuran	C <sub>4</sub> H <sub>8</sub> O <sub>2</sub>		-84.4	75.3	
2-Methyloxolan-3-one; 2-Methyltetrahydrofuran-3-one	C <sub>5</sub> H <sub>8</sub> O <sub>2</sub>		-78.4	87.1	
2-Methyloxolane; 2-Methyltetrahydrofuran; 2-MTHF	C <sub>5</sub> H <sub>10</sub> O		-54.6 [207] -54.0 [90] -53.6 [213] -51.9	80.9 [207] 74.0	
3-Methyloxolane; 3-Methyltetrahydrofuran; 3-MTHF	C <sub>5</sub> H <sub>10</sub> O		-51.8 [207] -50.6 [213] -51.0	79.2 [207] 74.0	
(Oxolan-2-ylidene)methanol	C <sub>5</sub> H <sub>8</sub> O <sub>2</sub>		-61.0 ( <i>trans</i> ) [251] -64.7 ( <i>cis</i> ) [251] -81.1	83.6 ( <i>trans</i> ) [251] 81.7 ( <i>cis</i> ) [251] 79.3	
(Oxolan-2-yl)methanol; 2-Tetrahydrofurfuryl alcohol; 2-THFFOH	C <sub>5</sub> H <sub>10</sub> O <sub>2</sub>		-88.2 ± 1.5 [224] -89.2 [251] -88.2	85.5 [251] 89.2	
7-Oxabicyclo[2.2.1]hept-2-ene; 1,4-Epoxy cyclohex-2-ene	C <sub>6</sub> H <sub>8</sub> O		-5.8 [217] -10.3	71.3 [217] 72.6	
7-Oxabicyclo[2.2.1]heptane; 1,4-Epoxy cyclohexane	C <sub>6</sub> H <sub>10</sub> O		-43.8 [220] -33.4	74.9 [220] 70.0	
2,3-Dimethyloxolane; 2,3-Dimethyltetrahydrofuran; 2,3-DMTHF	C <sub>6</sub> H <sub>12</sub> O		-59.0	80.8	
2,4-Dimethyloxolane; 2,4-Dimethyltetrahydrofuran; 2,4-DimethylTHF	C <sub>6</sub> H <sub>12</sub> O		-59.0	80.8	
2,5-dimethyloxolane; 2,5-dimethyltetrahydrofuran; 2,5-dimethylTHF; 2,5-DMTHF	C <sub>6</sub> H <sub>12</sub> O		-59.9	79.4	
3,3-Dimethyloxolane; 3,3-DimethylTHF	C <sub>6</sub> H <sub>12</sub> O		-58.8	79.2	
2-Ethyloxolane; 2-Ethyltetrahydrofuran; 2-ETHF	C <sub>6</sub> H <sub>12</sub> O		-56.8	83.4	

3-Ethylloxolane; 3-EthylTHF	C <sub>6</sub> H <sub>12</sub> O		-56.0	83.4
(5-Methyloxolan-2-yl)methanol; 2-Methyl-5-hydroxymethylTHF	C <sub>6</sub> H <sub>12</sub> O <sub>2</sub>		-97.4	91.5
1-Methyl-7-oxabicyclo[2.2.1]heptane	C <sub>7</sub> H <sub>12</sub> O		-42.5	78.9
2-Propyloxolane; 2-Propyltetrahydrofuran; 2-PTHF	C <sub>7</sub> H <sub>14</sub> O		-61.7	92.9
2-Ethyl-5-methyloxolane; 2-Ethyl-5-methyltetrahydrofuran; 2-Ethyl-5-methylTHF	C <sub>7</sub> H <sub>14</sub> O		-64.8	90.2
2-(ethoxymethyl)oxolane; 2-Tetrahydrofurfurylethylether; 2-THFFEE	C <sub>7</sub> H <sub>16</sub> O <sub>2</sub>		-91.8	101.2
1,3-Dihydro-2-benzofuran	C <sub>8</sub> H <sub>8</sub> O		-10.15	80.50
2,3-Dihydro-1-benzofuran	C <sub>8</sub> H <sub>8</sub> O		-15.13	78.58
1-Ethyl-7-oxabicyclo[2.2.1]heptane	C <sub>8</sub> H <sub>14</sub> O		-47.4	88.3
Octahydro-1-benzofuran	C <sub>8</sub> H <sub>14</sub> O		-49.5	86.7
2-Methyl-5-(prop-2-en-1-yl)oxolane	C <sub>8</sub> H <sub>14</sub> O		-39.6	98.0
2-Methyl-5-propyloxolane; 2-Methyl-5-propylTHF	C <sub>8</sub> H <sub>16</sub> O		-69.7	99.6
2-Butyloxolane; 2-n-Butyltetrahydrofuran; 2-BTHF;	C <sub>8</sub> H <sub>16</sub> O		-66.7	102.3
2,2,4,4-Tetramethyloxolane; 2,2,4,4-TetramethylTHF	C <sub>8</sub> H <sub>16</sub> O		-75.9	92.1
2,2,5,5-Tetramethyloxolane; 2,2,5,5-TetramethylTHF	C <sub>8</sub> H <sub>16</sub> O		-78.0	91.8
4-Methyl-2-(propan-2-yl)oxolane	C <sub>8</sub> H <sub>16</sub> O		-71.1	96.9
2-Methyl-5-(propan-2-yl)oxolane; 2-Isopropyl-5-methylTHF	C <sub>8</sub> H <sub>16</sub> O		-72.0	97.0
5-Ethyl-2,2-dimethyloxolane; 2,2-Dimethyl-5-ethylTHF	C <sub>8</sub> H <sub>16</sub> O		-73.9	96.4
4-Methyl-2-propyloxolane; 3-Methyl-5-propylTHF	C <sub>8</sub> H <sub>16</sub> O		-68.9	99.6
2-Methyloctahydro-1-benzofuran	C <sub>8</sub> H <sub>16</sub> O		-57.5	93.4
2-(Propoxymethyl)oxane; 2-Tetrahydrofurfurylpropylether; 2-THFFPE	C <sub>8</sub> H <sub>16</sub> O <sub>2</sub>		-96.8	110.7
2-Butoxyoxolane; 2-Tetrahydrofurfurylbutylether; 2-THFFBE	C <sub>8</sub> H <sub>16</sub> O <sub>2</sub>		-103.5	111.5
(5-Propyloxolan-2-yl)methanol; 2-Propyl-5-hydroxymethylTHF	C <sub>8</sub> H <sub>16</sub> O <sub>2</sub>		-107.2	110.4
1-Methyl-1,3-dihydro-2-benzofuran	C <sub>9</sub> H <sub>10</sub> O		-19.59	89.20
1-Propyl-7-oxabicyclo[2.2.1]heptane	C <sub>9</sub> H <sub>16</sub> O		-52.3	97.7
7-Ethyl-6-oxabicyclo[3.2.1]octane	C <sub>9</sub> H <sub>16</sub> O		-56.2	94.5



2-Phenylloxolane; 2-PhenylTHF	C <sub>10</sub> H <sub>12</sub> O		-19.7	95.7
2-Hexylloxolane; 2-HexylTHF	C <sub>10</sub> H <sub>20</sub> O		-76.5	121.1
2-Methyl-5-pentylloxolane; 2-Methyl-5-pentylTHF	C <sub>10</sub> H <sub>20</sub> O		-79.6	118.5
2-Butyl-5-ethylloxolane; 2-Butyl-5-ethylTHF	C <sub>10</sub> H <sub>20</sub> O		-79.6	117.1
2,5-Dipropylloxolane; 2,5-DipropylTHF	C <sub>10</sub> H <sub>20</sub> O		-79.6	117.1
Methyl 6-(oxolan-2-yl)hexanoate; 2-MethylhexanoateTHF	C <sub>11</sub> H <sub>20</sub> O <sub>3</sub>		-154.3	142.6
Methyl 5-(5-methyloxolan-2-yl)pentanoate; 2-Methyl-5-methylpentanoateTHF	C <sub>11</sub> H <sub>20</sub> O <sub>3</sub>		-157.3	140.0
Methyl 4-(5-ethylloxolan-2-yl)butanoate; 2-Ethyl-5-methylbutanoateTHF	C <sub>11</sub> H <sub>20</sub> O <sub>3</sub>		-157.3	138.6
Methyl 3-(5-propylloxolan-2-yl)propanoate; 2-Propyl-5-methylpropanoateTHF	C <sub>11</sub> H <sub>20</sub> O <sub>3</sub>		-157.3	138.6
Methyl (5-butyloxolan-2-yl)acetate; 2-Butyl-5-methylethanoateTHF	C <sub>11</sub> H <sub>20</sub> O <sub>3</sub>		-157.3	140.0
Methyl 5-pentylloxolane-2-carboxylate; 2-Pentyl-5-methylmethanoateTHF	C <sub>11</sub> H <sub>20</sub> O <sub>3</sub>		-157.1	141.1
Methyl 3-[5-(but-3-en-1-yl)oxolan-2-yl]propanoate; Methyl 2-[5-but-3-en-1-yl-THF-2-yl]propanoate	C <sub>12</sub> H <sub>20</sub> O <sub>3</sub>		-132.1	146.4
Methyl 6-(5-methyloxolan-2-yl)hexanoate; Methyl 6-(5-methylTHF-2-yl)hexanoate	C <sub>12</sub> H <sub>22</sub> O <sub>3</sub>		-162.3	149.4
Methyl 6-[5-(hydroxymethyl)oxolan-2-yl]hexanoate; Methyl 6-[5-(hydroxymethyl)THF-2-yl]hexanoate	C <sub>12</sub> H <sub>22</sub> O <sub>4</sub>		-199.7	160.1
2-Dodecylloxolane; 2-DodecylTHF	C <sub>16</sub> H <sub>32</sub> O		106.1	177.6
2-Methyl-5-undecylloxolane; 2-Methyl-5-undecylTHF	C <sub>16</sub> H <sub>32</sub> O		-109.2	175.0
2-R-5-R'oxolane <sup>k</sup> ; 2-R-5-R'THF	C <sub>16</sub> H <sub>32</sub> O	$\text{CH}_3(\text{CH}_2)_{10n} \text{O} \text{C}(\text{CH}_2)_{2n} \text{CH}_3$ l	-109.2	173.6
2-R-5-(MeOOCR')oxolane <sup>k</sup> ; 2-R-5-(MeOOCR')THF	C <sub>17</sub> H <sub>32</sub> O <sub>3</sub>	$\text{CH}_3(\text{CH}_2)_{2n} \text{O} \text{C}(\text{CH}_2)_{10n} \text{C}(\text{O})\text{OCH}_3$ m	-186.9	195.1
Methyl-9-(5-undecylloxolan-2-yl)formate	C <sub>17</sub> H <sub>32</sub> O <sub>3</sub>		-186.7	197.6
Methyl-11-(oxolan-2-yl)dodecanoate	C <sub>17</sub> H <sub>32</sub> O <sub>3</sub>		-183.8	199.2
Methyl 11-(5-methyloxolan-2-yl)undecanoate	C <sub>17</sub> H <sub>32</sub> O <sub>3</sub>		-186.9	196.5
<b>5-Membered cyclic ethers (dioxolones)</b>				
1,3-Dioxolane	C <sub>3</sub> H <sub>6</sub> O <sub>2</sub>		-72.1±0.5 [252] -74.5	74.2±1 [253] 59.8
2-Methyl-1,3-dioxolane	C <sub>4</sub> H <sub>8</sub> O <sub>2</sub>		-83.7 ± 0.8 [254] -84.6	73.0
4,5-dimethylidene-1,3-dioxolane; 1,3-Dioxolane,4,5-bis(methylene)-	C <sub>5</sub> H <sub>6</sub> O <sub>2</sub>		-53.5	62.9

2-Ethyl-4-methyl-1,3-dioxolane	C <sub>6</sub> H <sub>12</sub> O <sub>2</sub>		-97.5	89.2
2,2,4-Trimethyl-1,3-dioxolane	C <sub>6</sub> H <sub>12</sub> O <sub>2</sub>		-103.3	81.0
4-Ethyl-2-propyl-1,3-dioxolane	C <sub>8</sub> H <sub>16</sub> O <sub>2</sub>		-107.4	108.1
5-Membered cyclic ethers (lactones)				
Oxolan-2-one; $\gamma$ -Butyrolactone	C <sub>4</sub> H <sub>6</sub> O <sub>2</sub>		-87.4 $\pm$ 0.1 [233] -87.0 $\pm$ 0.8 [255] -87.6 $\pm$ 0.2 [256] -90.3 [257] -88.1 [258] -90.6	73.1
3-Oxatricyclo[3.1.0.0 <sup>2,6</sup> ]hexan-4-one	C <sub>5</sub> H <sub>4</sub> O <sub>2</sub>		-11.7	74.6
5-Methylfuran-2(3H)-one; $\alpha$ -Angelicalactone	C <sub>5</sub> H <sub>6</sub> O <sub>2</sub>		-73.2	77.1
5-Methylideneoxolan-2-one; $\gamma$ -Methylene- $\gamma$ -butyrolactone	C <sub>5</sub> H <sub>6</sub> O <sub>2</sub>		-71.4	80.2
5-Methylfuran-2(5H)-one	C <sub>5</sub> H <sub>6</sub> O <sub>2</sub>		-57.8	78.1
5-Methyloxolan-2-one; $\gamma$ -Valerolactone; GVL	C <sub>5</sub> H <sub>8</sub> O <sub>2</sub>		-97.2 $\pm$ 0.3 [256] -98.2 $\pm$ 0.3 [259] -95.8	83.6
5-Ethylloxolan-2-one; 5-Ethyl-dihydrofuranone	C <sub>6</sub> H <sub>10</sub> O <sub>2</sub>		-100.8	93.0
5-Octyl-1,3-dioxolan-4-one	C <sub>11</sub> H <sub>20</sub> O <sub>3</sub>		-161.6	145.2
5-Tetradecyl-1,3 dioxolan-4-one	C <sub>17</sub> H <sub>32</sub> O <sub>3</sub>		-191.2	201.7
6-Membered cyclic ethers (tetrahydropyrans / oxanes)				
4H-pyran	C <sub>5</sub> H <sub>6</sub> O		-2.1	72.6
3,4-Dihydro-2H-pyran	C <sub>5</sub> H <sub>8</sub> O		-32.9	68.9
3,6-Dihydro-2H-pyran	C <sub>5</sub> H <sub>8</sub> O		-24.7	73.0
Oxane; Tetrahydropyran; THP	C <sub>5</sub> H <sub>10</sub> O		-53.5 $\pm$ 0.2 [204] -53.4 $\pm$ 0.4 [212,260] -52.6 $\pm$ 0.6 [261] -54.1	73.7 [262] 72.9
4-Methyl-4H-pyran	C <sub>6</sub> H <sub>8</sub> O		-9.2	77.5
2-Methyloxane; 2-Methyltetrahydropyran; 2-MethylTHP	C <sub>6</sub> H <sub>12</sub> O		-62.1	81.1
4-Methyloxane; 4-Methyltetrahydropyran; 4-MethylTHP	C <sub>6</sub> H <sub>12</sub> O		-61.2	79.6
2-Ethyloxane; 2-Ethyltetrahydropyran; 2-EthylTHP	C <sub>7</sub> H <sub>14</sub> O		-67.0	90.5
2,6-Dimethyloxane; 2,6-Methyltetrahydropyran	C <sub>7</sub> H <sub>14</sub> O		-70.1	86.5
2-Propyloxane; 2-Propyltetrahydropyran	C <sub>8</sub> H <sub>16</sub> O		-71.9	99.9
2,2,5-Trimethyloxane; 2,2,5-Trimethyl-tetrahydropyran; 2,2,5-TrimethylTHP	C <sub>8</sub> H <sub>16</sub> O		-78.3	94.0
3,3,5-Trimethyloxane; 3,3,5-Trimethyl-tetrahydropyran	C <sub>8</sub> H <sub>16</sub> O		-76.2	93.0

2-(Ethoxymethyl)oxane; 2-Ethoxymethyltetrahydropyran; 2-EOMTHP	C <sub>8</sub> H <sub>16</sub> O <sub>2</sub>		-102.0	108.3
3,4-Dihydro-1H-2-benzopyran	C <sub>9</sub> H <sub>10</sub> O		-19.38	86.69
2-Butoxyoxane; 2-Butoxytetrahydropyran; 2-BOTHP	C <sub>9</sub> H <sub>18</sub> O <sub>2</sub>		-113.7	118.5
3-Butoxyoxane; 3-Butoxytetrahydropyran; 3-BOTHP	C <sub>9</sub> H <sub>18</sub> O <sub>2</sub>		-106.9	117.7
2-Butyl-6-methyloxane; 2-Butyl-6-methylTHP	C <sub>10</sub> H <sub>20</sub> O		-84.8	116.1
2-Ethyl-6-propyloxane; 2-Ethyl,6-propyl-tetrahydropyran; 2-Ethyl-6-propylTHP	C <sub>10</sub> H <sub>20</sub> O		-84.8	114.7
2-Pentyloxane; 2-Pentyl-tetrahydropyran; 2-PentylTHP	C <sub>10</sub> H <sub>20</sub> O		-81.8	118.8
6-Membered cyclic ethers (non-tetrahydropyrans) and larger rings				
1,3,5-Trioxane	C <sub>3</sub> H <sub>6</sub> O <sub>3</sub>		-115.0	53.2
2,3-Dihydro-1,4-dioxin; 1,4-Dioxene	C <sub>4</sub> H <sub>6</sub> O <sub>2</sub>		-57.4 (est.) [262] -63.7	72.1 (est.) [262] 57.4
1,2-Dioxane	C <sub>4</sub> H <sub>8</sub> O <sub>2</sub>		-33.2	72.2
1,4-Dioxane	C <sub>4</sub> H <sub>8</sub> O <sub>2</sub>		-76.5	69.5
2H-Pyran-2-one; $\alpha$ -Pyrone	C <sub>5</sub> H <sub>4</sub> O <sub>2</sub>		-48.4 [263] -35.3	70.6
Oxan-4-one; Tetrahydro-4H-pyran-4-one	C <sub>5</sub> H <sub>8</sub> O <sub>2</sub>		-80.6	79.0
6-Methyloxan-2-one 6-Methyl-tetrahydropyranone	C <sub>6</sub> H <sub>10</sub> O <sub>2</sub>		-107.4	84.7
4-Methyl-2-propyl-1,3-dioxane	C <sub>8</sub> H <sub>16</sub> O <sub>2</sub>		-110.6	103.9
2H-1,3-dioxepin; 1,3-Dioxepin	C <sub>5</sub> H <sub>6</sub> O <sub>2</sub>		-51.3	53.0
4,7-dihydro-2H-1,3-dioxepin ; 4,7-Dihydro-1,3-dioxepin	C <sub>5</sub> H <sub>8</sub> O <sub>2</sub>		-53.2	72.8

<sup>a</sup> 68.6 kcal/mol according to the original paper

<sup>b</sup> For *cis/trans* respectively.

<sup>c</sup> B3LYP/6-311G(d,p) level

<sup>d</sup> G3MP2B3/B3LYP6-31G(d,p) level

<sup>e</sup> The GAV for Cds-CdsOsH (2.03 kcal/mol) differs significantly from that proposed by Benson 8.6 kcal/mol

<sup>f</sup> Value is based on an assumed BDE, which is likely overestimated by 11 kcal/mol

<sup>g</sup> As cited in Ref. [224]

<sup>h</sup> Bond dissociation energy of 93.2 kcal/mol is converted to  $\Delta H$  using 44.0 kcal/mol for THF and 52.1 kcal/mol for hydrogen.

<sup>i</sup> Bond dissociation energy of 92.1 kcal/mol is converted to  $\Delta H$  using 44.0 kcal/mol for THF and 52.1 kcal/mol for hydrogen.

<sup>j</sup> The higher entropy value compared to 2-propyl-5-methylpropanoateTHF is surprising.

<sup>k</sup> Describes a family of CEs discussed in Part 4 of this review, R and R' being alkyl groups.

<sup>l</sup> CH<sub>3</sub>[CH<sub>2</sub>]<sub>10-n</sub> and [CH<sub>2</sub>]<sub>n</sub>CH<sub>3</sub> correspond to R and R' in the molecule name, respectively.

<sup>m</sup> CH<sub>3</sub>[CH<sub>2</sub>]<sub>n</sub> corresponds to R in the molecule name.

In the following, some thermodynamic properties of species are discussed in general terms. Experimental thermodynamic data are only available for a limited number of CEs, *e.g.* oxirane, methyloxirane, 1,2-epoxycyclohexane, oxetane, furan, several substituted furans, tetrahydrofuran, 2-tetrahydrofurfuryl alcohol, 2-methyl-1,3-dioxolane,  $\gamma$ -butyrolactone,  $\gamma$ -valerolactone, and tetrahydropyran. In addition, Table 4 lists experimentally based entropies for 1,5-dihydrofuran and 1,4-dioxene. With the exception of oxirane, for which the oldest enthalpy value by Moureu and Dode [205] differs by more than 4 kcal/mol from later results, the experimental data are in good agreement with each other. This can in part be explained by the fact that some entries are just re-evaluations of previous data hence the data are not independent from each other. Most enthalpy results are from calorimetric measurements of the heat of formation of the liquid, which after correcting for the enthalpy of vaporization yield the gas phase enthalpies of formation. Most entropies are calculated from spectroscopic data.

Only a few research teams have specifically studied the thermodynamic properties of CEs theoretically, although many more studies are available in which thermodynamic data have been created as a side-product of kinetic calculations. The latter data are not necessarily included in Table 4. Goldsmith *et al.* [206] employed B3LYP/6-311++G(d,p) for geometry calculations to the lowest energy conformer of a species identified with CBS-QB3. The QCISD(T) method extrapolated to the CBS limit was used to calculate the electronic energy and BAC corrections were applied for further improvements. As part of a larger study, Goldsmith *et al.* calculated thermodynamic properties for oxirane, methyloxirane and oxetane and the radicals of these CEs. All results agree very well with the available experimental data. Simmie and coworkers [90,132,227,231,238] made substantial contributions to the thermochemistry of CEs. In a systematic study Simmie and Curran [231] used the composite methods G3, CBS-QB3 and CBS-APNO in connection with isodesmic reactions to calculate the enthalpies of formation of alkylfurans and their radicals. They reported bond strengths,

resonance stabilization effects and showed that the experimental data of 2,5-dimethyl-, 2-tert-butyl-, and 2,5-di-tert-butylfurans appeared to be self-consistent. More substituent effects of furans were reported in [238] using the same levels of theory. Simmie and Somers calculated as part of a benchmark study the enthalpy of formation of oxirane using five different composite methods. All results agree within 1.1 kcal/mol with each other and also with experimental data and the value recommended by the ATcT [133]. Feller and Simmie [227] calculated the enthalpies of formation of furan, 2-methylfuran and 2,5-dimethylfuran using the CCSD(T)-F12 method with Dunning basis sets and extrapolation to the CBS limit. Very good agreement with experimental data is achieved.

Tian *et al.* [226] provide enthalpies and entropies calculated at CBS-QB3 level of theory for furan, methyl furan, dihydrofurans and THF as well as for derived radicals of those. Most reported data, however, were obtained with THERGAS software [264] and for those that are calculated with the CBS-QB3 method via isodesmic reactions, details of the calculations are missing. In some cases, substantial differences can be seen between the values reported by Tian and others listed in Table 4. For example, the entropy for furan-2-yl of 66.5 cal/mol-K is 6.8 cal/mol-K lower than that calculated with the RMG GA tool. For 2,3-dihydrofuran, the enthalpy value of -21.8 kcal/mol reported by Tian *et al.* is 5.6 kcal/mol higher than the GA value. The entropy for the same species is 67.0 cal/mol-K compared to 61.3 cal/mol-K obtained with GA. For the radical 2,3-dihydro-furan-3-yl, the differences are also severe (enthalpy: 8.5 kcal/mol [226] versus 0.7 kcal/mol calculated with GA, entropy (cal/mol-K): 68.1 versus 56.6). Since Tian and GA are the only data available for these species more studies are needed to resolve these discrepancies.

Feller and Franz [137] studied the heats of formation of furan, THF and the two THF radicals. They used the couple cluster method CCSD(T) with several Dunning aug-cc-pVxZ basis sets which allowed extrapolation to the CBS limit. The results for furan and THF are in

very good agreement with experimental data, while the enthalpies of the radicals are somewhat higher than those reported by other studies. They are, however, in good agreement with the GA data.

Hudzik and Bozzelli [144] use isodesmic reactions to calculate the enthalpies of formation for furan, 2-methylfuran and 3-methylfuran. The electronic energies were calculated with the B3LYP and M06-2x DFT methods and CBS-QB3 and CBS-APNO composite methods. Other studies from the Bozzelli group [208,213] provide thermochemical properties (enthalpies and entropies) of methyl-substituted CE (oxiranes, oxetanes and oxolans) using the same methodology as above. The CBS-QB3 values are generally recommended. All results agree well with other studies if available.

Using high level coupled cluster calculations Mai *et al.* [228] confirmed the lowest enthalpy of formation values reported for furan.

Isodesmic reactions were used by Sebbar *et al.* [232] with G3MP2B3 and B3LYP/6-311g(d,p) calculations to determine the enthalpies of formation of the two furan radicals. As it can be seen from the entries in Table 4, the results compare well to those by Tian *et al.* [226] and Simmie and Curran [231] and casts doubts that the GA calculated values for these species are correct.

As part of a chemical kinetics study of the thermal decomposition of 2,5-DMF, Sirjean and Fournet [244] reported enthalpies of formation and entropy values for various methyl substituted furans and their corresponding radicals. The calculations were done with CBS-QB3 and three to four not further specified isodesmic reactions were used to derive the final enthalpies. The authors pointed out that the C–H bond strength of the methyl group depends on its ring position and it is higher if the methyl group is in the  $\beta$ -position to the ring oxygen.

CBS-QB3 was also used by Tran and coworkers [195] to calculate enthalpy, entropy and heat capacity data for dihydrofurans and tetrahydrofurans. The THERMO module of the master

equation software MultiWell was used for the conversion of the quantum calculation results. As can be seen from Table 4, the results are in line with other studies, *e.g.* that of Feller and Franz [137] discussed earlier and the work of Wijaya *et al.* [207]. The latter work also utilized the CBS-QB3 method, although with an earlier and less reliable implementation in the Gaussian program package. One outcome of this study, which besides oxolanes also calculated thermodynamic properties for oxetanes and oxiranes, was the definition to ring strain corrections to be used in GA applications.

Morais [263] studied the enthalpy of formation of  $\alpha$ - and  $\gamma$ -pyrone using various isodesmic and homodesmotic reaction schemes and several composite methods (G3 and its G3(MP2) variation, G4, CBS-QB3, CBS-APNO). The required reference data are either from experiments or from accurate calculations. For  $\alpha$ -pyrone, which is included in Table 4, the heats of formation averaged for each method separately agree very well (clearly within less than 1.0 kcal/mol) and a value of -48.4 kcal/mol is obtained by averaging the results from all methods. The authors performed further consistency tests to demonstrate the reliability of this result.  $\gamma$ -pyrone was found to be less stable by about 9 kcal/mol. Interestingly, the GA result of -35.3 kcal/mol deviates significantly from Morais result. For  $\gamma$ -pyrone (not reported in Table 4) the difference is smaller, -39.0 kcal/mol (Morais) versus -32.3 kcal/mol (GA), but still quite large. A possible explanation is that the reported GA value is calculated without contributions from a missing group.

In summary, in most cases theoretically determined thermodynamic properties obtained with various methodologies agree well with available experimental values. However, for many CE species, such calculations are not available or hidden within kinetic studies. Group additivity as implemented in the RMG website is able to fill all gaps. In many cases, these GA data are very close to either experimental or calculated values, which allows CE thermochemistry to be calculated reliably by automated mechanism generating software.

However, some exceptions exist for enthalpies and entropies. For example, GA predicts the enthalpy of 2,3-DHF to be about 10 kcal/mol more stable than experimentally found, while GA performs well for 2,5-DHF. As indicated in Table 4, a wrongly assigned GA value might be causing this issue. For  $\alpha$ -pyrone, the difference between the theoretically calculated and GA predicted enthalpies is about 13 kcal/mol (in this case the GA value is less exotherm), which is presumably caused by ignoring the contributions of a missing group. Clear enthalpy and entropy deviations also exist for CE radicals, *e.g.* 2,3-dihydro-furan-3-yl. In this specific case, the applied Hydrogen Bond Increment correction term might be a poor choice, because it likely does not include the stabilizing effect of the CE oxygen.

While the above mentioned examples seem special cases, systematic problems are visible for furanic radicals. In these cases, the GA implementation does not reflect the extraordinarily strong C–H bonds in furan and its derivatives as well as the degree of resonance stabilization the furan ring provides to furanylalkyl radicals. Revised Hydrogen Bond Increment for these radicals should fix this problem.



### 3. EXPERIMENTAL METHODS USED IN CYCLIC ETHER KINETIC STUDIES

Before discussing the current understanding of CE chemistry in detail, this part describes in more general terms the experimental devices and analytical techniques used in these studies.

#### 3.1. Main experimental devices used to investigate the gas-phase reactions involving cyclic ethers

The experimental devices used to study gas-phase reactions involving CEs as products or as reactants can be classified according to the methods used to initiate the reactions. In the context of CE chemistry, three main initiation methods are in use, which are photolysis, flame propagation and thermal activation of a reactive mixture.

##### 3.1.1. Initiation through photolysis

The main characteristic of this method is that **radicals are created by laser photolysis**, which starts the low-temperature oxidation process. This method has only been used in a few studies concerning CEs. It is often employed in measurements of rate constants of elementary reactions. The review of Rotavera and Taatjes [16] recently described the kinetics studies of the reactions of CEs with radicals ( $\dot{\text{O}}\text{H}$ ,  $\text{HO}\dot{\text{O}}$ ). The experimental setups consist of quartz reactors operating at temperatures between 400 and 700 K, at pressures from 9 Torr to 2 atm and slow gas flows [265,266]. The oxidation reactions are initiated through reactions of the radicals or atoms with fuel molecules in the presence of  $\text{O}_2$  and oxidation products are sampled via a pinhole in the reactor wall made in order to create a molecular beam.

##### 3.1.2. Initiation through flame propagation

The method, in which reactions are **initiated by the propagation of an ignited laminar premixed flame**, is the most widely used for CE studies. Only very few CE studies involve diffusion flames, mainly for soot formation investigation (*e.g.* [267]). While not specifically

focusing on CEs, two review papers will describe the experimental devices commonly used for flame studies. The review paper by Konnov *et al.* [268] focuses on the experimental devices that are used for measuring Laminar Burning Velocities (LBVs). LBV is a global parameter of interest for representing combustion properties, which is also widely used as a target for testing detailed kinetic models. The work by Egolfopoulos *et al.* [269] pays more attention to the experimental devices used for chemical speciation in flames.

Concerning CEs, two types of studies of Premixed Laminar Flames (PLFs) are performed. The first one consists of the measurement of adiabatic LBVs at pressures at or above atmospheric pressure using either a Constant Volume Bomb (CVB), in which a flame is spark-ignited and LBVs are obtained after data processing to correct for stretch [270], or a flat flame burner based on the heat-flux method [271]. The second type aims at measuring the profiles of temperature and product mole fractions as a function of height above burner in a flat PLF stabilized at a pressure below atmospheric pressure [272]. Fig. 14 displays the burner used in Nancy for this kind of studies for furan derivatives.



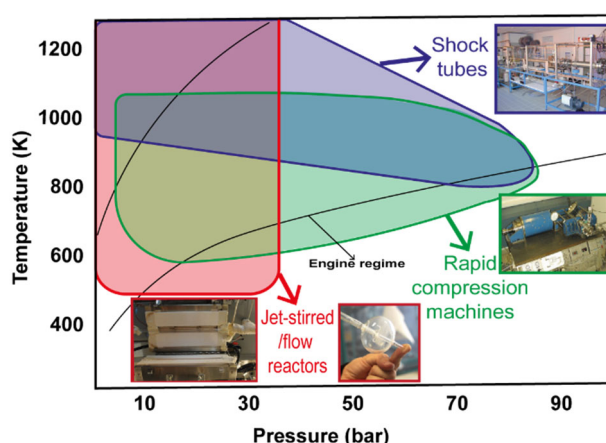
**Fig. 14.** Photography of the McKenna flat flame burner with its thermocouple and sampling probe used at Nancy during speciation studies in flames of furan derivatives [103,273–275].

In the speciation studies of low-pressure flat flames, the temperature profiles are either deduced from pressure measurements in the first pumping stage of the used mass spectrometer [273] or measured with a coated thermocouple taking into account radiative heat loss corrections [276]. Products are sampled with a quartz probe located inside the flame. The shapes

of the quartz probes differ according to the used detection method: a quartz cone is used for mass spectrometry and a sonic probe for gas chromatography. Fig. 14 shows the PtRh (6%)-PtRh (30%) type B thermocouple (diameter 100  $\mu\text{m}$ ) and the sonic quartz probe used for sampling for gas chromatography analysis in the Nancy device. Tran *et al.* [103] discussed the effect of probes on temperature measurement for the case of 2,5-DMF flames.

### 3.1.3. Initiation by heating a reactive mixture

In most studies that investigate CE production during low-temperature oxidation, the reactions are **initiated thermally by heating the reactive mixture** using mechanical compression in a motored engine, a rapid compression machine or a shock tube, or by heat transfer from the external wall of static (closed), flow or jet-stirred reactors. While in the 70s, adiabatic static reactors were largely used to demonstrate CE formation during fuel slow oxidation (reaction occurring with no temperature rise) and cool-flames (reaction occurring with a temperature rise by at most a few dozens of K) [4,277], static reactors and motored engines are less frequently used for combustion studies related to CEs since the 90s. As is shown in Fig. 15, the four other types of devices involving reactive mixture heating cover a large part of engine relevant conditions.

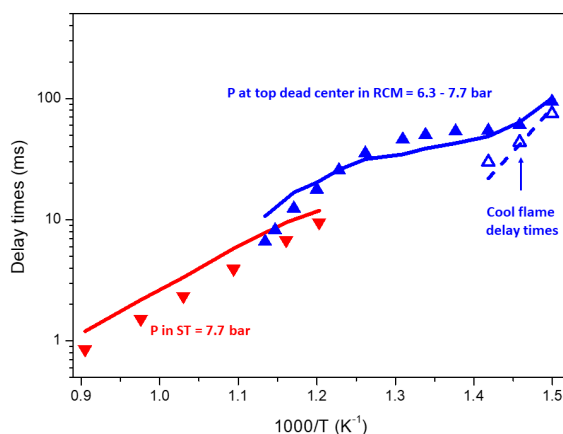


**Fig. 15.** Temperature-pressure diagram of typical operating conditions for the experimental devices based on reaction initiation by heating (adapted from [278]). The inserted photographs provide examples of the types of the most currently used devices: a flow reactor at Colorado School of Mines (not actually used for CE studies), USA (by courtesy of A. Dean), a jet-stirred reactor at CNRS-Nancy, France, the rapid compression machine of CNRS-Lille, France (by courtesy of G. Vanhove), the shock tube installation of CNRS-Nancy, France.

### ***3.1.3.1. Heating by mechanical compression***

In a Shock Tube (ST) the reactive mixture is heated by compressing it by a pressure (or shock) wave that propagates along a usually few meters long closed tube. This wave is created by the sudden expansion of a high-pressure gas into the reactive gas mixture maintained at low pressure. To investigate CE combustion, STs have been operated in single pulse (the incident shock wave is used for the measurements with reflections being avoided) or in reflected mode. This latter mode uses the wave front after it is reflected from the end plate. The reflection leads to further compression and higher temperatures. In the case of CE studies, single pulse STs are used to produce speciation concentration data at the end of the shock heating in order to study pyrolysis reactions [279]. STs operating in reflected mode are used to measure ignition delay times [280]. The ST used to investigate THF auto-ignition in Nancy is shown as insert in Fig. 15.

As comprehensively reviewed by [278], the heating process of a gas mixture by mechanical compression in a Rapid Compression Machine (RCM) is similar to that occurring during a single cycle of an internal combustion engine. Temperatures can be varied by changing the composition of the inert gas mixture and can reach from 550 to about 1300 K. Together with STs, RCMs are commonly used to study the Ignition Delay Time (IDT) of reactive mixtures as shown in Fig. 16 for the case of THF. The RCM installation in Lille used in this study is shown as an insert in Fig. 15. Both figures illustrate that the operating conditions reachable in STs and RCMs are complementary. However, in a RCM, as it can be seen in Fig. 16, the delay time of the cool flame that precedes ignition can also be accessed.



**Fig. 16.** Experimental IDTs for THF measured in a ST [281] (red) and in a RCM [282] (blue). Symbols represent the experimental data ( $\phi=1$ , values derived using the experimentally determined correlation in ST) and lines show simulation results using the model of [283]. Reproduced from Ref. [283] with permission of Elsevier.

### 3.1.3.2. Heating through contact with hot walls

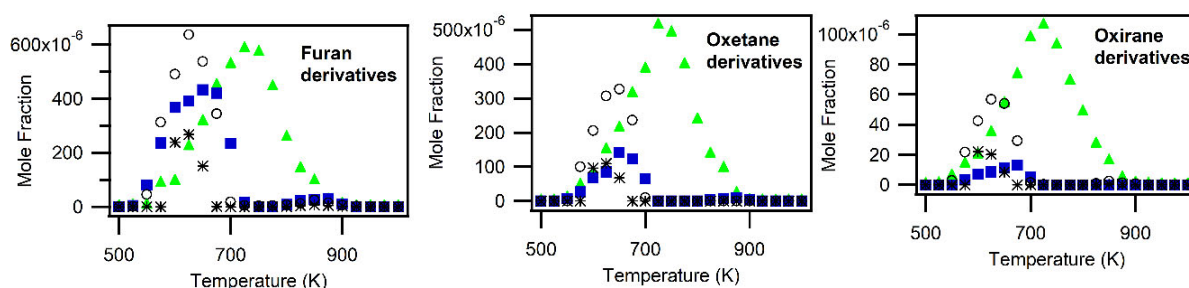
Continuous reactors are characterized by a steady gas stream that flows through a heated zone. Since they allow for easy gas sample collection and analysis, these reactors are frequently used in speciation experiments. Furnaces or electrical resistance wires or tapes are used for heating and temperature measurement is achieved with thermocouples.

A flow reactor (FR) is simply a tube through which the reactive gas is flowing [284]. As an example, the FR used in Colorado School of Mines is shown as an insert of Fig. 15. For CE studies, FRs have been used below or at atmospheric pressure.

The main type of Jet-Stirred Reactors (JSRs), which has been used for CE studies, consists of a sphere, in which four turbulent jets created from a cross-shaped inlet located at its center ensure the stirring [285]. The JSR used in Nancy for investigating THF low-temperature oxidation is displayed as an insert in Fig. 15. JSR are generally operated at isothermal conditions achieved by highly diluting the reactive mixture with an inert gas (He or N<sub>2</sub>) to avoid temperature increases caused by the chemical reactions. Using such reactors, the research groups at Orléans and Nancy were able to identify a large number of CEs in the low-temperature

oxidation of hydrocarbons at conditions similar to those observed during cool flames. JSRs for CE related studies have been used at pressures from 1 to 40 bar.

More recently, the group of Ju at Princeton developed a supercritical JSR that can be utilized to investigate oxidation chemistry at supercritical conditions 100-200 bar [286]. In addition, a system of an atmospheric pressure JSR coupled simultaneously with GC and SVUV-PIMS of high mass resolution ( $\sim 5000$ ) was developed in Hefei group [287]. Fig. 17 displays an example of temperature dependent CE mole fractions measured in a JSR study in the low-temperature oxidation of *n*-heptane. It can be observed that CEs start to be produced at temperatures as low as 550 K. In agreement with the predictions shown in Fig. 3 in Part 1, furan and oxetane derivatives are produced in higher amounts than other CEs. Note also the peak broadening in lean mixtures.



**Fig. 17.** Temperature dependence of the cyclic ethers produced in the low-temperature oxidation of *n*-heptane (pressure of 800 Torr, residence time of 2 s, initial fuel mole fraction of 0.005 with He dilution, green triangles:  $\phi = 0.25$ , blue squares:  $\phi = 1$ , black empty circles:  $\phi = 2$ , stars:  $\phi = 4$  [288]).

The methods used for the identification and the quantification of the CE isomers in Fig. 17 are described in the following part.

### 3.2. Main analytical techniques used to measure cyclic ethers during their gas-phase reactions

The two major techniques used for the CE analysis are mass spectrometry (MS) and gas chromatography (GC). Note that the methods used to measure CEs also allow the detection of most of the products formed during their decomposition (unsaturated and oxygenated

hydrocarbons). A third promising technique is molecular absorption spectroscopy, which allows probing a large variety of species during combustion experiments [23]. Although to the best of knowledge of the authors, this technique has not yet been used to detect CE in oxidation processes, Rotavera and coworkers [289] recently published measurements of absorption cross-sections in the vacuum ultraviolet (5.17 - 9.92 eV) using differential absorption spectroscopy for five- and six-membered cyclic species including CEs.

### ***3.2.1. Mass spectrometry***

Mass Spectrometry (MS) consists in the transformation of all components in a sample into ions, their acceleration by an electric field, and the separation of ions with different mass to charge ( $m/z$ ) ratios by means of a magnetic or electric field [290]. Since Thomson's experiments, which led to the award of the Nobel prize in 1906, a large number of systems have been developed for ion separation, *e.g.* Time-Of-Flight (TOF), quadrupole, ion trap [291]. Single component samples are preferentially ionized at high-energy (*e.g.* electron impact at 70 eV). The high energy impact leads to compound fragmentation and the features of the resulting mass spectrum are a kind of fingerprint of the molecule to be analyzed. This spectrum can be deciphered either using known molecule fragmentation rules [291] or by comparison to spectra taken at the same conditions stored in databases.

If gas mixtures need to be analyzed, the use of low Ionization Energy (IE) is preferred to minimize the fragmentation and to avoid getting an indecipherable mass spectrum [292]. Low energy MS is most frequently used together with TOF ion separation. In MS studies at low energy with strongly reduced fragmentation the observed  $m/z$  ratios in most cases equal the molecular weight of the molecules present in the gas mixture. Mass spectrometers with sufficient resolution allow one to distinguish between hydrocarbon and oxygenate ions with similar but not equal  $m/z$  ratio, which reduces the uncertainty in species identification (as an example one can cite the unambiguous separation of ketene,  $^{12}\text{C}_2\text{H}_2^{16}\text{O}$ , at mass 42.0106 from

propene,  $^{12}\text{C}_3\text{H}_6$ , at mass 42.0470 [293]). Note also that the natural occurrence of isotopes and the use of isotope labeled reactants can be used to identify products and reaction mechanisms because these isotope distributions are directly reflected in the mass spectra.

The text hereafter describes how CEs can be identified and quantified by MS operated at lower IEs, detailing the sampling strategies and ionizations sources, CE isomer ionization energy determination, CE isomer identification during fuel oxidation induced in thermally heated reactors or by photolysis, and CE isomer quantification during flame and JSR experiments.

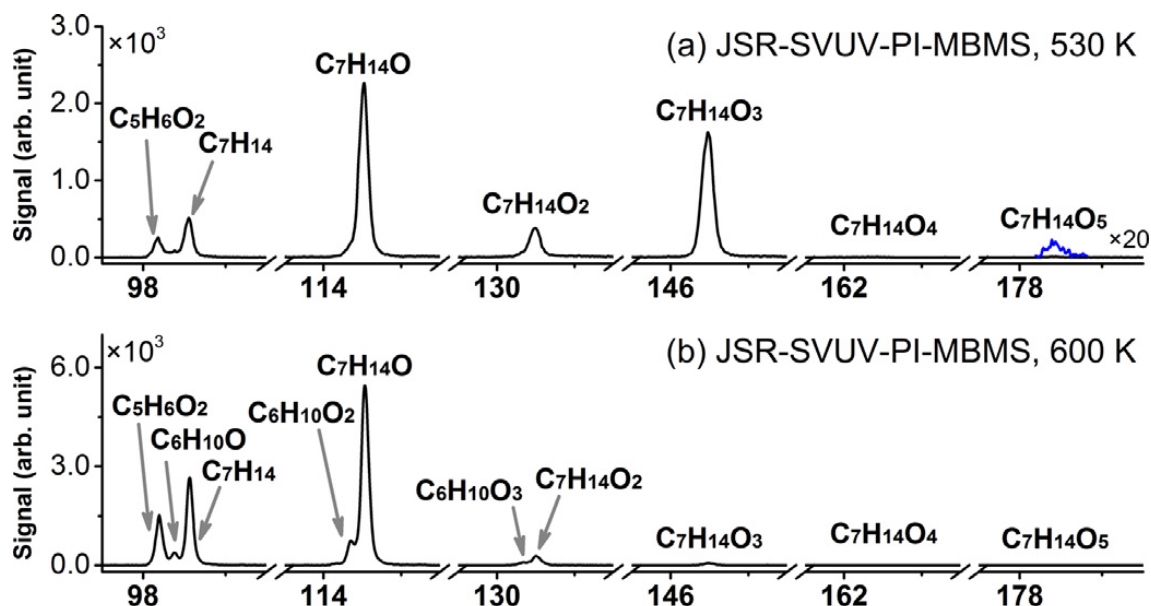
### ***3.2.1.1. Sampling strategy and ionization sources***

Mass spectrometry uses Electron-Ionization (EI) or Photo-Ionization (PI). When using sampling by Molecular Beam (MB) supersonic expansion [294], MS enables the detection of both stable and reactive species. In the group of Kohse-Höinghaus in Bielefeld, EI is used to investigate the high-temperature reactions of CEs in PLF [273] using a quartz cone to create the MB. Samples are extracted from flames fueled with furan derivative using a quartz cone with a 320  $\mu\text{m}$  diameter orifice at the tip and an angle of 25°. These are ionized using five different nominal IEs (10.5, 11.25, 12, 16.5, and 17 eV) [273]. In the CE decomposition studies in a 1 mm SiC FR, the group of Ellison in Boulder directly expands the effluent gases from the reactor into vacuum and uses PIMS or Resonance-Enhanced MultiPhoton Ionization (REMPI)/MS for analysis.

During low-temperature fuel oxidation experiments in a JSR, gas samples are extracted with a cone to create a MB or through a capillary tube [23]. The obtained PI mass spectra commonly include a large signal at the  $m/z$  ratio corresponding to CEs with the same carbon number as the reactant. This is illustrated by Fig. 18 taken from the work of Wang *et al.* [28] concerning the JSR low-temperature oxidation of *n*-heptane, who detected a significant signal for  $m/z$  114 attributed to  $\text{C}_7\text{H}_{14}\text{O}$  species. Note that the relative importance of this signal



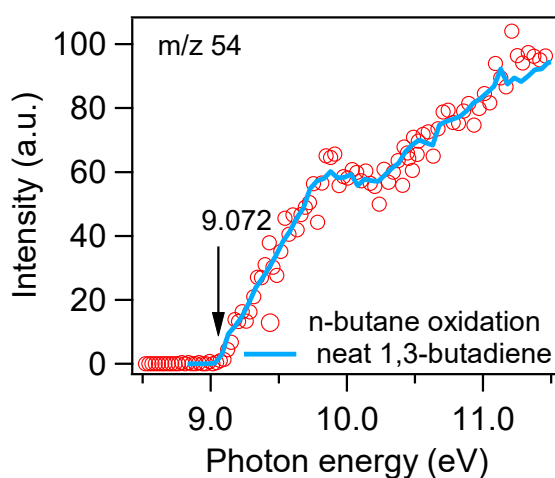
compared to those of other low-temperature oxidation products (e.g.  $C_7H_{14}O_3$  (KHPs)) increases with temperature as expected according to the reactions described in Part 1. Taking advantage of previous literature on *n*-heptane oxidation studies [32,33,295], Wang *et al.* attributed the  $m/z$  114 signal mainly to *trans*- and *cis*-2-ethyl-5-methylTHF.



**Fig. 18.** SVUV-PIMS mass spectra (IE =9.6 eV) of intermediates with  $C_7H_{14}O_x$  ( $x = 0-5$ ) molecular formula obtained during *n*-heptane JSR low-temperature oxidation carried out at the Advanced Light Source at the Lawrence Berkeley National Laboratory. Reproduced from [28] with Elsevier permission.

In recent years, MS has also been used with devices involving heating by compression during CE related studies. In the RCM of Orléans [296] a sampling orifice located at the end wall is opened, in each run, at a preset time and the gas of the combustion chamber is evacuated and stored inside a pre-vacuumed sampling tank, which is then kept inside a freezer at a temperature of 243 K before it is solved in a solvent (acetonitrile) and analyzed. This type of MS analysis allowed the identification of hydroperoxidic species. The gas in the ST of Karlsruhe [297] is sampled continuously and analyzed at intervals of 50 or 100  $\mu s$  [298] by a TOF-MS allowing after calibration with pure substances, the measurement of the time evolution of species concentrations.

For PIMS experiments, different light sources for low IE in the 8-20 eV range can be used, *e.g.* lamps, lasers or synchrotron radiation. The advantage of synchrotron vacuum ultraviolet (SVUV) radiation is the availability of a wide range of well-defined narrow linewidth tunable wavelengths. In SVUV-PIMS analyses, species are usually identified by comparing their Photo-Ionization Efficiency (PIE) spectrum recorded at a specific  $m/z$  ratio with threshold ionization energies of potential candidates. A confirmation can be obtained by comparing the PIE curve obtained for a given  $m/z$  ratio to that of a standard. A helpful PIE spectrum database [299] is established by NSRL in Hefei. As an example, Fig. 19 displays the PIE curve for  $m/z$  54 recorded during the oxidation of *n*-butane [300]. The IE of 1,3-butadiene (9.072 eV [202]) matches the PIE onset in the spectrum. This comparison works well for single species but it is less straightforward if the recorded PIE spectrum at a given  $m/z$  involves contributions of several isomers.



**Fig. 19.** Comparison of the PIE curve for  $m/z$  54 [300] and PIE spectrum of 1,3-butadiene [301]. 9.072 eV is the ionization energy of 1,3-butadiene [202].

### 3.2.1.2. Determination of the ionization energies of cyclic ether isomers

The identification of CE isomers during PIMS experiments relies on an accurate knowledge of their IE. However, only a few experimental IEs for CEs are available in the literature. For small species, IE data is available as can be seen in Table 5, which lists the experimentally measured IEs for cyclic ethers found in the literature.

**Table 5.** Experimentally measured IEs for CEs available in the literature.

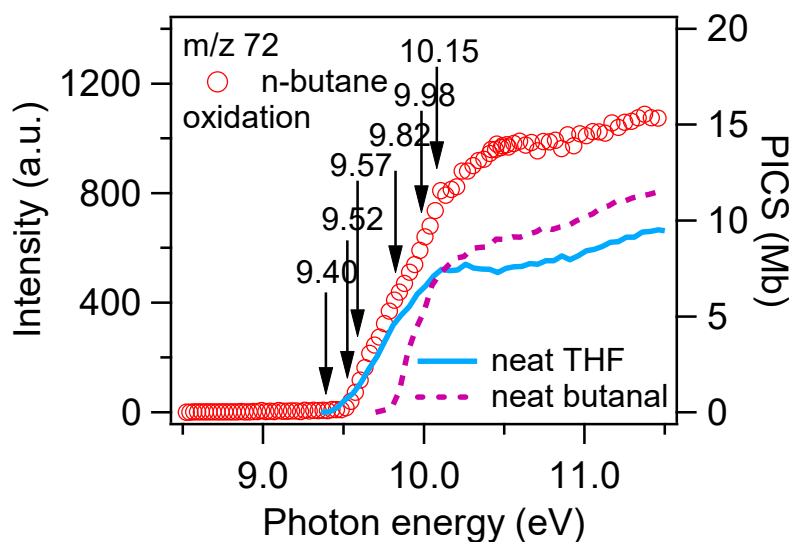
Formula	MW	Species	IEs (eV)	References
C <sub>2</sub> H <sub>4</sub> O	44	Oxirane	10.56 ± 0.01	Data evaluated by NIST [202] from 15 literature data [302–315]
C <sub>3</sub> H <sub>6</sub> O	58	Methyloxirane	10.22 ± 0.02	Data evaluated by NIST [202] from 4 literature data [304,310,314,316]
		Oxetane	9.65 ± 0.01	Data evaluated by NIST [202] from 6 literature data [302,304,315,317–319]
C <sub>4</sub> H <sub>4</sub> O	68	Furan	8.88 ± 0.01	Data evaluated by NIST [202] from 23 literature data [313,314,320–340]
			8.86 ± 0.03	[341]
			8.86 ± 0.05	[342]
C <sub>4</sub> H <sub>6</sub> O	70	2,3-DHF	8.38	[301]
			9.16	[343]
			9.16	[344]
		2,5-DHF	9.14 ± 0.02	[345]
			9.16	[301]
		Ethenyloxirane	9.52	[346] in [202]
			9.7 ± 0.3	[347]
9.94	[316]			
C <sub>4</sub> H <sub>8</sub> O	72	THF	9.40 ± 0.02	Data evaluated by NIST [202] from 10 literature data [344,345,348–350]
		Ethyloxirane	10.15	Only one data point in NIST [202] from [316]
		<i>trans</i> -2,3-Dimethyloxirane	9.98	Only one data point in NIST [202] from [316]
		2,2-Dimethyloxirane	10.00	[316]
C <sub>5</sub> H <sub>6</sub> O	82	2-MF	8.38 ± 0.01	Data evaluated by NIST [202] from 9 literature data [310,321,337,339,351–355]
			8.38 ± 0.03	[341]
			8.38 ± 0.05	[342]
		3-MF	8.64	[351]
			8.58	[329]
		4H-Pyran	8.70	[354]
			8.40	[351]
8.38 ± 0.02	[356]			
C <sub>5</sub> H <sub>8</sub> O	84	3,4-Dihydro-2H-pyran	8.35 ± 0.01	Data evaluated by NIST [202] from 4 literature data [310,356–358]
C <sub>4</sub> H <sub>6</sub> O <sub>2</sub>	86	$\gamma$ -Butyrolactone	10.06 ± 0.03	[359]
			10.10 ± 0.05	[342]
		1,4-Dioxene	8.07 ± 0.02	[356]
C <sub>5</sub> H <sub>10</sub> O	86	THP	9.25 ± 0.01	Data evaluated by NIST [202] from 8 literature data [302,310,314,319,357,360–362]
		2-MTHF	9.22 ± 0.05	Only one data point in NIST [202] from [302]
		1,4-Dioxane	9.19 ± 0.01	Data evaluated by NIST [202] from 7 literature data [310,313,314,361–364]
C <sub>4</sub> H <sub>8</sub> O <sub>2</sub>	88	1,3-Dioxane	10.33, 10.12, 10.12, 10.1	Four data in NIST [202] from [361,362,365,366]
			10.0	Only one data point in NIST [202] from [367]
		1,2-Dioxane	10.0	Only one data point in NIST [202] from [367]
		2-(Methoxymethyl)oxirane	9.5, 10.08	[368]
		3-Hydroxytetrahydrofuran	9.77	[369]
C <sub>3</sub> H <sub>6</sub> O <sub>3</sub>	90	1,3,5-Trioxane	10.3, 10.59 ± 0.05, ~10.8	Three data in NIST [202] from [362,370]
			9.22 ± 0.01	Data evaluated by NIST [202] from 5 literature data [310,320,331,371]
C <sub>5</sub> H <sub>4</sub> O <sub>2</sub>	96	Furfural	9.22 ± 0.05	[372]
			9.35 ± 0.05	[373]
		3-Oxatricyclo[3.1.0.0 <sup>2,6</sup> ]hexan-4-one	10.05	[374]
C <sub>6</sub> H <sub>8</sub> O	96	2,5-DMF	7.8	[321]
			8.25 ± 0.10	[375]
			8.03	[321]
			7.95 ± 0.03	[341]
			7.95 ± 0.05	[342]

		2,4-Dimethylfuran	8.39 ± 0.10	[375]
		2,3-Dimethylfuran	8.25 ± 0.10	[375]
			8.0	[353]
		2-EF	8.45 ± 0.05	[331]
			8.43 ± 0.05	[372]
		4-Methyl-4H-pyran	8.51	[351]
		1,4-Epoxy-cyclohex-2-ene	9.44 ± 0.02	[345]
		$\alpha$ -Angelicalactone	9.62 ± 0.05	[376]
			8.97 ± 0.05	[342]
		$\gamma$ -Methylene- $\gamma$ -butyrolactone	9.05 ± 0.05	[342]
C <sub>5</sub> H <sub>6</sub> O <sub>2</sub>	98	1,3-Dioxepin	8.0, 8.3	[377]
		1,3-Dioxolane,4,5-bis(methylene)-	8.62	[378]
		5-Methylfuran-2(5H)-one	10.12 ± 0.05	[376]
C <sub>5</sub> H <sub>8</sub> O <sub>2</sub>	100	GVL	9.98 ± 0.05	[342]
		4,7-Dihydro-1,3-dioxepin	9.0, 9.54	[379]
			9.02	[320]
C <sub>6</sub> H <sub>6</sub> O <sub>2</sub>	110	2-Acetylfuran	9.27 ± 0.05	[331]
			9.01 ± 0.05	[372]
C <sub>8</sub> H <sub>16</sub> O	128	2,2,5,5-TetramethylTHF	8.8	[380]

The difficulty in the experimental determination of the IEs of CEs can be partially overcome by the means of theoretical calculations. As an example, in the *n*-butane oxidation study by Herbinet *et al.* [300], the ionization energy of 2-methyl-oxetane was calculated with the composite CBS-QB3 method [124] using the Gaussian software package [381] with a typical uncertainty of 0.1 eV. These calculations require finding the lower energy conformer, which can be a complex task for large species. Rayne and Forest [382] tested data computed at the G4 and W1BD levels of theory for 17 small organic compounds (belonging to a wide range of chemical families) having well-constrained NIST evaluated experimental adiabatic IEs. They obtained an excellent agreement between theoretical and experimental values with mean absolute deviation of 0.03 and 0.04 eV at the G4 and W1BD levels of theory, respectively. El-Nahas *et al.* [383] calculated ionization potentials of selected C<sub>1</sub>–C<sub>5</sub> oxygenates and showed that long-range corrected (LC- $\omega$ PBE, LC-BOP, LCgau-BOP, LC-BOP12, LCgau-B97) density functionals gave good results compared with other density functional theory methods (BHandHLYP, B3LYP, MPW3LYP, MPW1B95, BMK, MPW1K, MPWB1K, BB1K) with a maximum deviation of 0.4 eV. The precision might be poorer for larger species.

### 3.2.1.3. Cyclic ether identification during thermally induced fuel oxidation

Mass spectrometry with photo-ionization has been used to detect CEs formed during the JSR low-temperature oxidation of many fuels (*e.g.*, [28,300,384,385]). However, the MS identification of the CEs produced during thermally induced low-temperature fuel oxidation can rapidly become a complex problem even for small reactants, as shown by Herbinet *et al.* [300] during the low-temperature oxidation of *n*-butane. The authors coupled a JSR to SVUV-PIMS. They detected a signal at  $m/z$  72 that corresponded to the expected  $C_4H_8O$  isomers. As shown in Fig. 20, the threshold in the PIE spectrum recorded for  $m/z$  72 is around 9.5 eV and could correspond to two species with close IEs: butanone and 2-methyloxetane (IEs of 9.52 and 9.57, respectively). THF has an IE of 9.40 eV. Other candidates (butanal, ethyloxirane and 2,3-dimethyloxirane) have higher IEs (9.82, 10.15 and 9.98 eV, respectively) but no obvious change in the PIE curve was observed at these energies. The comparison of the PIE spectrum with the literature cross section of THF [386] demonstrated that the contribution of this species was minor and that the large signal increase around 9.5 eV is likely due to contributions of butanone and 2-methyloxetane.



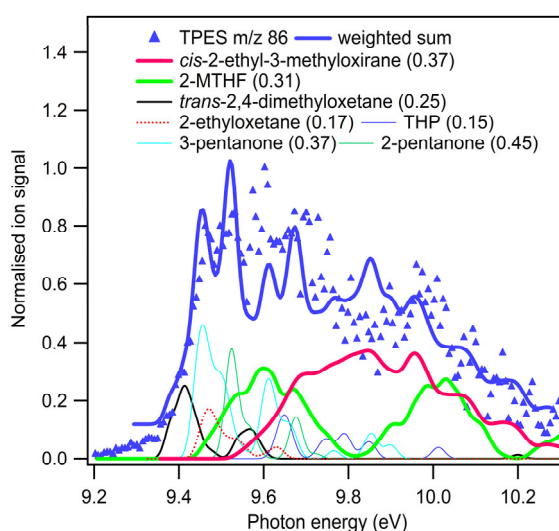
**Fig. 20.** PIE curves for  $m/z$  72 [300] (left axis), PI cross section for  $m/z$  72 for neat THF [386] and for neat butanal [301] (right axis). IEs of 9.40, 9.52, 9.57, 9.82, 9.98 and 10.15 eV are for THF, butanone, 2-methyloxetane, butanal, 2,3-dimethyloxirane and ethyloxirane, respectively.

Complementary GC analyses highlighted the presence of seven  $C_4H_8O$  isomers: butanone, butanal, ethyloxirane, 2,3-dimethyloxirane (*cis* and *trans* isomers were separated), 2-methyloxetane, THF, and butenol. Butenol and oxiranes were present in smaller amounts than the other species. This study, which combined two diagnostics shows that the identification of isomers using solely time-of-flight mass spectrometry with photo-ionization is extremely difficult, even for a small hydrocarbon, such as *n*-butane and that GC performs better for this type of species.

To overcome this CE isomer identification problem, an attempt to use PhotoElectron PhotoIon COincidence (PEPICO) spectroscopy has been made. MS with PEPICO spectroscopy is a technique in which PIMS and photoelectron spectra are simultaneously measured (double imaging) [387–389]. In line with previous gas phase kinetic studies [390,391], Bourgalais *et al.* [392] recently studied the JSR low-temperature oxidation of *n*-pentane using this advanced diagnostics at the synchrotron Soleil, France. The goal of this study was to investigate how the identification of reaction products can be improved by the analysis of the coincident mass-tagged threshold photoelectron spectra in comparison to the sole analysis of the PIE spectra obtained by SVUV-PIMS. Experimental threshold photoelectron spectra were compared with the combination of spectra of potential candidates obtained from first principle computations of the adiabatic ionization energies. Such a spectrum offers a better sensitivity and selectivity because each electronic/vibronic state of the ion appears as a distinct peak rather than a change of the slope in a PIE spectrum (the PIE curve of a species is the result of the integration of its PhotoElectron Spectra).

However, for mixtures including a large number of isomers, as it is the case for low-temperature oxidation products, even with the PEPICO technique the isomer identification is not straightforward. Fig. 21 presents a tentative identification of the CE isomers corresponding to  $m/z$  ratio 86 during JSR *n*-pentane oxidation [392]. The sum in Fig. 21 was obtained by

summing the weighted (best-fit procedure) photoelectron spectra calculated for the seven major C<sub>5</sub>H<sub>10</sub>O species, which were detected in previous GC studies. Fig. 21 confirms the significant formations of 2-ethyl-3-methyloxirane and 2-MTHF as was shown by GC. However, according to the authors, the relative contribution of the different isomers needed to be interpreted with care because of the noise level and because the photoelectron spectra of the isomers overlap in a narrow energy region. By GC analysis, the 2-MTHF mole fraction is about four times that of 2-ethyl-3-methyloxirane.

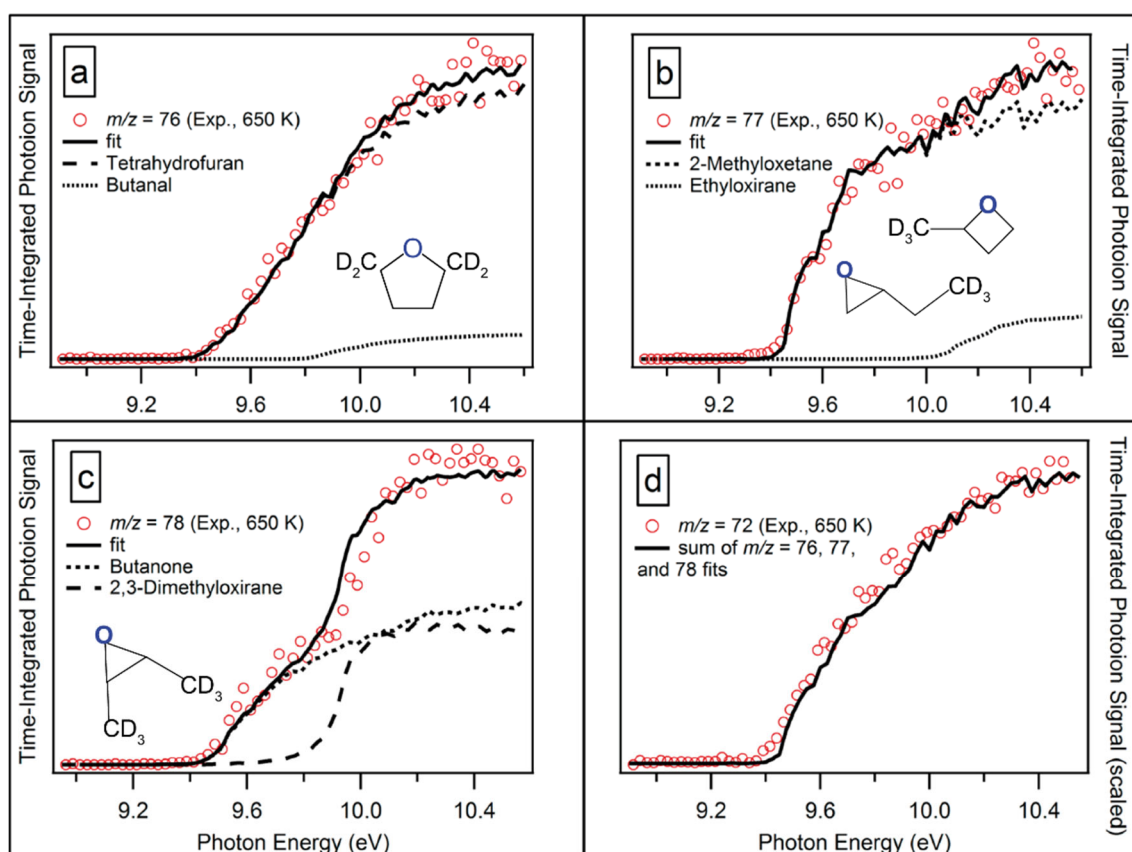


**Fig. 21.** Comparison of the measured threshold photoelectron spectra (TPES) obtained by scanning the photon energy and detecting only so-called threshold photoelectrons at  $m/z$  86 (symbols) obtained during JSR oxidation of  $n$ -pentane at 585 K ( $\phi = 0.5$ ) to the weighted sum of the envelopes from convolution of the calculated Franck–Condon factors for potential candidates. Figure redrawn from the data of [392].

#### 3.2.1.4. Cyclic ether isomer identification during photolytically induced fuel oxidation

One of the main advantages of PI-TOF-MS is its ability to follow fast changes in species concentration on a short time. This is particularly valuable for reactions induced by photolysis, because this allows the monitoring of temporal species profiles on short time scales, *e.g.* just after a laser pulse [265]. In order to circumvent the poor ability of PIMS to identify CE isomers during their photolysis studies, Eskola *et al.* [390] proposed the use of *partially deuterated* reactants. To illustrate how this method helps in the identification of C<sub>4</sub>H<sub>8</sub>O isomers during the

laser-initiated low-temperature (575–700 K) oxidation of *n*-butane, Fig. 22 presents the PIE spectra obtained when 1,1,1,4,4,4-hexadeuterobutane ( $\text{CD}_3\text{CH}_2\text{CH}_2\text{CD}_3$ ) was used as reactant instead of the non-deuterated *n*-butane. Based on the assumed mechanism, the only expected product with  $m/z$  76 in Fig. 22a is THF, with another possible  $\text{C}_4\text{H}_8\text{O}$  product, butanal, starting to appear at IEs above 9.8 eV. In Fig. 22b, the signal at the lowest photon energies,  $m/z$  77 corresponds to 2-methyloxetane, and ethyloxirane starts to appear above 10 eV. The only CE expected to be produced from  $\text{CD}_3\text{CH}_2\text{CH}_2\text{CD}_3$  and corresponding to  $m/z$  78 in Fig. 22c is 2,3-dimethyloxirane, which appears at a photon energy about 1 eV higher than butanone. Note that because of the close similarity of the *cis*- and *trans*-2,3-dimethyloxirane spectra, these two isomers were not separated. Overall, in Fig. 22d, the sum of the  $m/z$  76, 77 and 78 fits well with the PI spectrum recorded at  $m/z$  72 for *n*-butane.



**Fig. 22.** Experimental time-integrated photoion signal vs. photon energy (symbols), measured PI cross-section spectra of the pure compounds (broken or dotted lines) and applicable fits obtained (full lines) during the Cl-initiated oxidation of partially deuterated *n*-butane ( $\text{CD}_3\text{CH}_2\text{CH}_2\text{CD}_3$ ) at 650 K (a–c). Plot (d) displays the non-deuterated results with the spectrum constructed from the fittings at  $m/z$  76, 77 and 78. Reproduced from Ref. [390] with permission of ACS.



### 3.2.1.5. Cyclic ether quantification

The quantification of the species detected by MS does not necessarily require an external calibration with a standard as this can be performed using a reference species (an internal standard) if the EI or PI ionization cross sections of both species are known [23]. In this case,  $x_i(T)$ , the mole fraction of the targeted species  $i$  at a given temperature, is related to that of a reference species  $x_{ref}(T)$ , by the following equation [393]:

$$\frac{x_i(T)}{x_{ref}(T)} = \frac{S_i(T,E)}{S_{ref}(T,E)} \cdot \frac{MDF_{ref}}{MDF_i} \cdot \frac{\int \sigma_{ref}(E) \cdot f(E-\tau) d\tau}{\int \sigma_i(E) \cdot f(E-\tau) d\tau} \quad (8)$$

where,  $S_i(T,E)$  and  $S_{ref}(T,E)$  are, respectively, the integrated ion signal of species  $i$  and reference species at the energy  $E$  and the temperature  $T$ ;  $\sigma_i(E)$  and  $\sigma_{ref}(E)$  are the EI or PI cross sections of species  $i$  and that of species  $ref$ , respectively;  $MDF_i$  and  $MDF_{ref}$  are their mass discrimination factors;  $f(E-\tau)$  is the energy distribution of the ionizing particles with  $\tau$  being the mathematical integration variable (*i.e.* the convolution of two functions of electron energy distribution and cross section). Note that for the photo-ionization approach, due to a narrow energy distribution, the integral simplifies to  $\sigma_{ref}(E)/\sigma_i(E)$  [394].

Unfortunately, the recent literature is scarce when it comes to the PI cross sections of CEs (Table 6). Data are available for some cyclic ethers deriving from the low-temperature oxidation of alkanes, such as THF, THP and 2-MTHF, and for cyclic ethers, which can be found in bio-oils processed from ligno-cellulosic biomass. Some data include the individual contribution of the main fragment ions to the total ion cross section, which is a useful information for confirming species identification and the origin of fragments detected during the analysis.

**Table 6.** Literature PI cross sections of CEs

Formula	MW	CE	Photon energy range (eV)	Recorded $m/z$	References	
C <sub>2</sub> H <sub>4</sub> O	44	Oxirane	20	44	Estimated [299]	
C <sub>3</sub> H <sub>6</sub> O	58	Methyloxirane	11-12	58	Estimated [299]	
C <sub>4</sub> H <sub>4</sub> O	68	Furan	8.7-11.7	68	[301]	
			8.73-11.48	68	[341]	
			7.988-11.188	68	[342]	
C <sub>4</sub> H <sub>6</sub> O	70	Ethenyloxirane	9.0402-11.0402	70	[395]	
		2,3-DHF	8.23-11.78	42, 69 & 70	[301]	
		2,5-DHF	8.98-11.78	42, 69 & 70	[301]	
C <sub>4</sub> H <sub>8</sub> O	72	THF	9.36-11.71	72, 71 & 42	[299]	
			10.5	72	[396]	
C <sub>5</sub> H <sub>6</sub> O	82	2-MF	8.30-11.51	81 & 82	[341]	
			7.988-11.188	81 & 82	[342]	
C <sub>5</sub> H <sub>8</sub> O	84	3,4-Dihydro-2H-pyran	7.988-10.188	84	[397,398]	
		3,6-Dihydro-2H-pyran	9.01-11.01	84	[397,398]	
C <sub>4</sub> H <sub>6</sub> O <sub>2</sub>	86	$\gamma$ -Butyrolactone	9.613-11.013	42 & 86	[342]	
		Bioxirane	9.040-11.040	86	[395]	
C <sub>5</sub> H <sub>10</sub> O	86	THP	9.20-11.75	86, 85, 71, 56 & 45	[301]	
			9.015-11.015	86	[397,398]	
			2-MTHF	9.25-11.70	86, 85, 71, 56, 45, 43 & 42	[301]
C <sub>6</sub> H <sub>8</sub> O	96		7.83-11.51	81, 95 & 96	[341]	
			7.988-11.188	81, 95 & 96	[342]	
			2-EF	8.1-11.0	81, 95 & 96	[372]
			3,4-Epoxy-cyclohex-1-ene	8.502-11.002	96	[399]
			4,5-Epoxy-cyclohex-1-ene	9.002-11.002	96	[399]
C <sub>5</sub> H <sub>4</sub> O <sub>2</sub>	96	Furfural	9.0-11.0	95 & 96	[372]	
C <sub>5</sub> H <sub>6</sub> O <sub>2</sub>	98	$\alpha$ -Angelicalactone	8.841-11.041	98	[342]	
		$\gamma$ -Methylene- $\gamma$ -butyrolactone	8.841-11.041	70 & 98	[342]	
C <sub>5</sub> H <sub>8</sub> O <sub>2</sub>	100	GVL	9.613-11.013	56, 85 & 100	[342]	
C <sub>6</sub> H <sub>6</sub> O <sub>2</sub>	110	2-Acetylfuran	8.9-11.0	95 & 110	[372]	
C <sub>8</sub> H <sub>16</sub> O	128	2,2,5,5-TetramethylTHF	8.5-11.0	128	[380]	

The Ar signal is usually used as internal calibration standard in flame and JSR experiments (IE = 15.8 eV). In the experiments at Bielefeld with MB-EIMS [273,400,401], the species-related terms can be condensed into a calibration factor  $k_{i/Ar}$ . The Eq. (8) becomes:

$$x_i(T)/x_{Ar}(T) = S_i(T, E)/S_{Ar}(T, E) \times 1/k_{i/Ar}(E) \quad (9)$$

The data evaluation proceeds in two steps. The first step is to determine the mole fractions of the major species, namely the fuels, O<sub>2</sub>, H<sub>2</sub>, H<sub>2</sub>O, CO, CO<sub>2</sub>, and the inert diluent gas (usually Ar). The calibration factors for these species, referenced to argon as internal calibration standard, are determined based on the elemental C, H, and O balances derived from the exhaust gas and the inlet conditions. The second step consists in determining the mole fractions of intermediate species. In the MB-EIMS experiments, the broad energy distribution of the ionizing electrons allows the detection of argon even at very low nominal ionization energies,

for example at 10-13 eV [401]. Calibration factors for intermediate species were obtained, with argon still as the reference, by cold-gas calibration measurements of known gas compositions (direct), by estimation using the relative ionization cross section method (RICS) [402], or by convolution of the known ionization cross section with the measured energy distribution of the ionizing electrons as detailed in [400].

In MB-PIMS flame experiments, particularly in the system in Hefei [292,403,404], the mole fraction determination for major species relies upon a similar procedure as for MB-EIMS described above. However, for intermediate species a different approach is used for quantification because of differences in the characteristics of the two ionization methods. SVUV-PI provides a very narrow and accurate ionization energy distribution, and scans for intermediates are performed at energies lower than that of argon (15.8 eV). Therefore, the Ar signal is not present in these spectra. Mole fractions at a given flame sampling position (*i.e.* a given temperature) are still calculated from Eq. (8), however, using reference species other than Ar. Using the same methodology during JSR low-temperature oxidation studies, reference species having a low IE are also used to quantify CEs from PIMS measurements. For example, propene, which can reliably be quantified by GC (see Part 3.2), is often used as a reference [300].

No study was specifically performed to investigate the uncertainties in the quantification of CEs. But in general, as declared by the teams where MB-EI/PIMS are used, the estimated error is below 50% for directly calibrated species or for species with known ionization cross sections [400,404,405]. If the EI/PI cross section is estimated, mole fraction uncertainties of a factor of 2-4 can be expected [400,404,405]. Note that when the isomeric composition is complex, such as for fuel-specific CEs produced from  $C_{>5}$  fuels, the identification of these species is ambiguous, which increases further the uncertainties in CE quantification.

### **3.2.2. Gas chromatography**

In Gas Chromatography (GC) analytics [406], a gas mixture is injected into a column coated or filled with an adsorbent. A carrier gas carries the species along this stationary phase toward a detector, *e.g.* MS, Flame Ionization Detector (FID), Thermal Conductivity Detector (TCD). (The TCD is not actually used for CE detection.) The compounds to be analyzed are separated according to the time needed to reach the detector (retention time), which depends on their affinity to the stationary column material. At a given GC condition, the retention time of a molecule is constant and can be used as one criterion for its identification using a standard. Concerning CE analysis, the main GC advantage is the straightforward non-destructive separation of their numerous isomers.

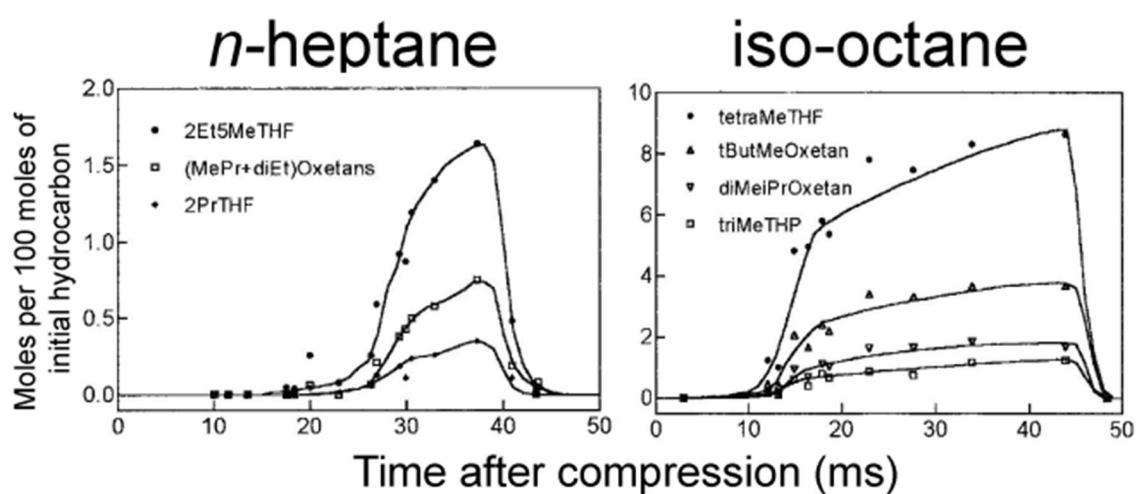
Reviewing early experimental results, Griffiths [277] demonstrated how the development of GC methods from the late 1950s to 1995 allowed the first qualitative and quantitative understanding of the chemistry involved during the low-temperature oxidation of hydrocarbons, with significant progress especially with respect to understanding of the CE formation channels. Since then, GCs equipped with FID or MS detection have been used in numerous oxidation studies for the identification and the quantification of CEs, as will be discussed in Parts 4 and 5. The following discussion describes sampling strategies and analytical procedures used, as well the methods available for CE identification and quantification.

#### **3.2.2.1. Sampling strategies and analytical procedures**

Back in the 90's, the teams of Minetti in Lille [407–411] and Cathonnet in Orléans [295,412–414] focused on the GC identification and the quantification of CEs formed during the low-temperature combustion of alkanes.

In Lille, experiments were performed in a RCM [407–411]. The gaseous mixtures were sampled just before auto-ignition and quenched by rapid adiabatic expansion into a vacuum

chamber [408]. Samples were then injected into a gas chromatograph equipped with a Poraplot Q capillary column and coupled to a mass spectrometer (GC-MS) for the identification of the species. The quantification was performed using gas chromatograph fitted with a Porapak Q column and a FID. Fig. 23 shows the results of successive experiments with sampling at different times after compression [410]. This allowed to study the time dependence of the product formation occurring during cool flame in the RCM. The data compare well to the plateau shape exhibited in Fig. 3.



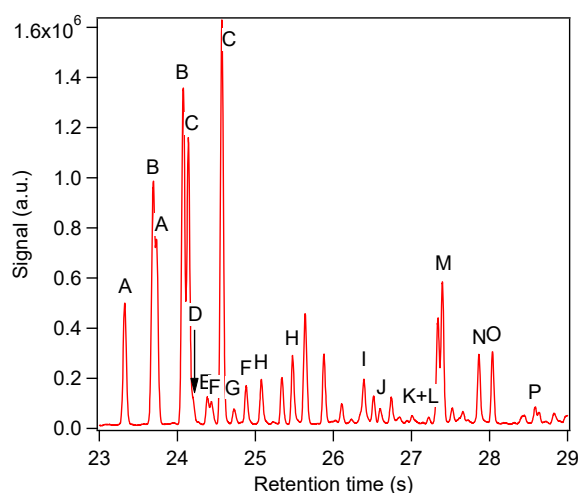
**Fig. 23.** Experimental profiles of the products in a two-stage auto-ignition of a stoichiometric mixture of *n*-heptane ( $T = 667$  K,  $P = 3.4$  bar) or *iso*-octane ( $T = 708$  K,  $P = 13.4$  bar) in air (2Et5MeTHF is 2-ethyl-5-methylTHF, (MePr+diEt)Oxetans is the sum of 2-methyl-4-propyloxetane and 2,4-diethyloxetane, 2PrTHF is 2-PTHF, tButMeOxetan is 2-*tert*-butyl-3-methyloxetane, diMeiPrOxetan is 2-*isopropyl*-3,3-dimethyloxetane and tetraMeTHF is 2,2,4,4-tetramethylTHF) - extracted from Fig. 4 of Ref. [410].

In Orléans, experiments were conducted in a JSR operated at a high pressure [295,412–414]. Sampling was performed using a sonic probe and the obtained sample was stored in a bulb at low pressure ( $\leq 30$  Torr). Gas samples were then pressurized in a temperature-controlled piston and injected into several gas chromatographs. Oxygenated species were analyzed on a Poraplot U column connected to a FID preceded by a methanizer, or on a CPSii 5B column with FID detection [412].

From 2009 onwards, CEs were observed in JSR studies in Nancy. These investigations were dedicated to the low-temperature oxidation of different fuel families (*n*-alkanes, cyclo-

alkanes, olefins, methyl esters, aldehydes and ethers) [15,32,33,293,415–424]. Sampling was usually performed online using a heated transfer line connecting the reactor outlet to a sampling loop mounted on the six-port sampling valve connected to a gas chromatograph. Detection was carried out with a FID. Depending on the species size, separation was achieved on PLOT-Q, HP1 or HP5 capillary columns. In the case of heavy fuels such as the long chain alkanes present in diesel fuels or methyl esters [415] present in biodiesel fuels, condensation in the transfer line may occur. In this case, an offline sampling strategy was applied: 1) trapping at liquid nitrogen temperature in a glass trap connected to the reactor outlet, 2) progressive warming up to ambient temperature, 3) addition of solvent and internal standard, 4) injection of the obtained liquid sample into a gas chromatograph.

The GC ability to separate the large number of CE isomers (some of them being present as *cis* and *trans* isomers) produced during heavy fuel oxidation was found to be sufficient for species containing up to 10 carbon atoms. For heavier species, limitations were encountered. Even for *n*-decane, the chromatogram reported by Hakka *et al.* [415] (see Fig. 24) shows that several molecules corresponding to C<sub>10</sub>H<sub>20</sub>O isomers (cyclic ethers, ketones and the aldehyde) could be distinguished but were nevertheless co-eluted. Due to the low volatility of these CEs, a HP-1 column was used for separation.



**Fig. 24.** Chromatogram (HP-1 capillary column, FID) obtained during *n*-decane oxidation (650 K) of (A: *cis*- & *trans*-2,5-dipropylTHF – B: *cis*- & *trans*-2-butyl-5-ethylTHF – C: *cis*- & *trans*-2-methyl-5-pentylTHF – D: 2-ethyl-6-propylTHP – E: 2-hexyl-4-methyloxetane – F: *cis*- & *trans*-2-ethyl-4-

pentylloxetane – G: 2-butyl-6-methylTHP – H: *cis*- & *trans*-2-butyl-4-propylloxetane – I: 2-heptyloxetane – J: 2-pentylTHP – K: 4-decanone – L: 5-decanone – M: 2-hexylTHF – N: 3-decanone – O: 2-decanone – P: decanal) redrawn from the data in [415].

GC was also used in Nancy to investigate the species profiles in low-pressure PLFs fueled with some CEs that are potential biofuel candidates [103,273–275]. Sampling was facilitated with a quartz probe located inside the flame and connected through a heated (at 423 K) online connection to a chromatograph fitted with a HP-Plot Q column. The probe was a 6 mm tube tipped by a small cone with a 100  $\mu\text{m}$  diameter orifice and a tip angle to the vertical of 20° [273].

### 3.2.2.2. Identification by electron-impact mass spectrometry coupled to gas chromatography

Species formed during gas-phase reactions are commonly identified through GC-MS, in which the GC enables species separation and the coupled MS operating at 70eV EI provides their characteristic mass spectra. The comparison with mass spectra found in databases [425] enables the identification of species. Reference mass spectra are available for many oxiranes, but the databases are less complete as far as 4-, 5- and 6-membered cyclic ethers are concerned. Authentic samples of the expected species can also be used to verify species assignments.

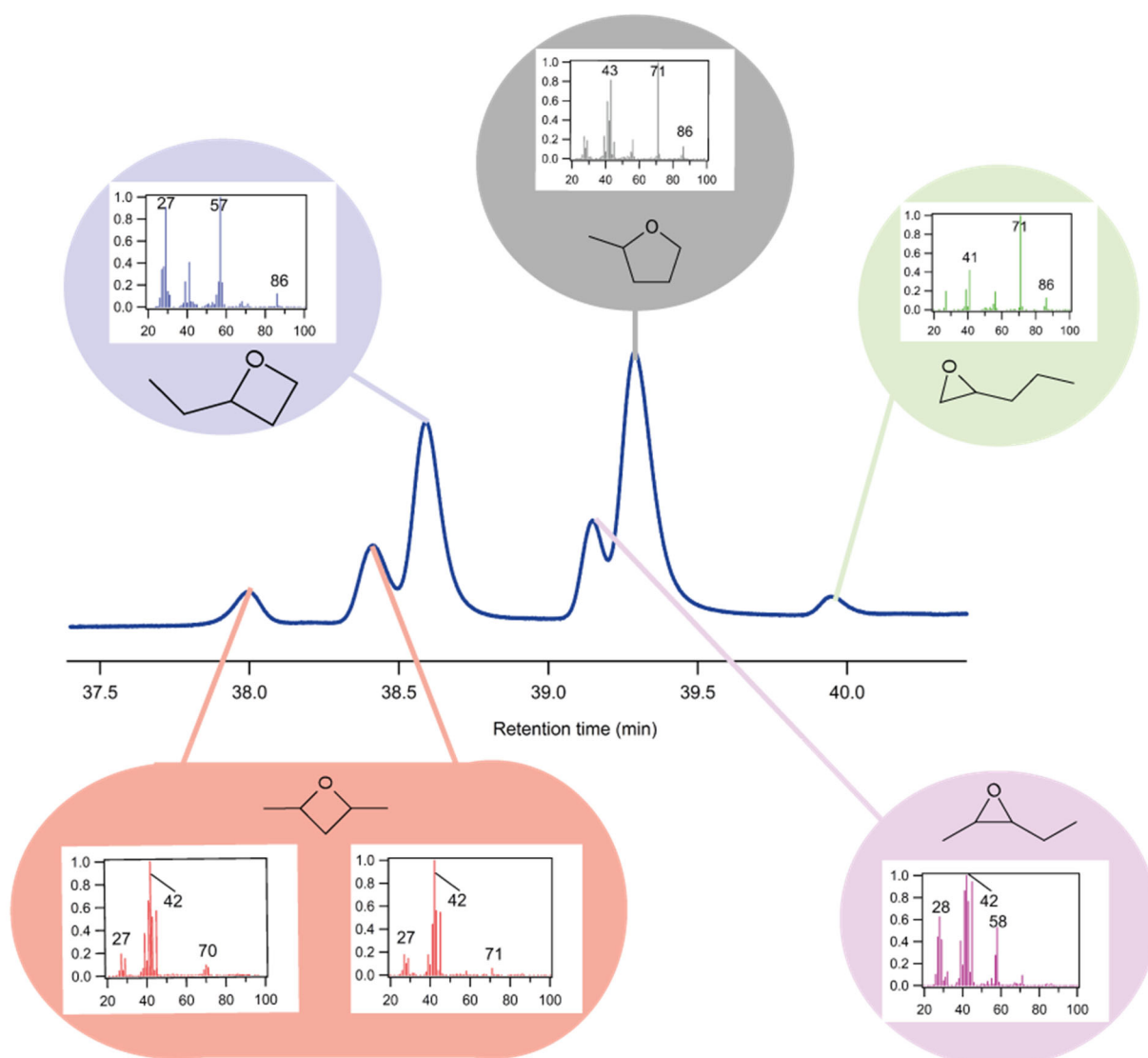
Past research on fuel low-temperature oxidation contributed substantially to enlarge aforementioned databases by reporting mass spectra of cyclic ethers. Dagaut *et al.* [426] reported for the first time mass spectra for some CEs formed during the low-temperature oxidation of *n*-heptane (2-methyl-4-propylloxetane, 2,4-diethylloxetane), *iso*-octane (2,2,4,4-tetramethylTHF, 2-*tert*butyl-3-methylloxetane, 2-*isopropyl*-3,3-dimethylloxetane), and *n*-decane (2-methyl-5-pentylTHF, and 2-butyl-5-ethylTHF).

Herbinet *et al.* [427] also analyzed cyclic ethers in the exit gas stream of a JSR, in which the low-temperature oxidation of a series of *n*-alkanes (from *n*-pentane (see Fig. 25) to *n*-octane, *n*-decane, *n*-dodecane and *n*-hexadecane) was carried out. Analyzes were performed by GC-

MS and mass spectra for 17 CEs were reported. Herbinet *et al.* [427] also proposed rules for the fragmentation of CEs in electron impact mass spectrometry to allow their identification when their mass spectra are not available. More recently, Koritzke *et al.* [428] performed a similar work and reported mass spectra for 10 CEs. The authors considered four conventional mechanisms to analyze fragmentation patterns in the mass spectra:  $\alpha$ -cleavage, inductive effect, hydrogen rearrangement and transannular cleavage. Rules were proposed to explain the main fragments observed in the CE mass spectra [427,428]. The analysis of mass spectra for a series of 5- and 6-membered ring cyclic ethers that are formed in *n*-alkane oxidation (with one alkyl group in position 2 or two alkyl groups in positions 2 and 5) showed that the molecular ions are quite unstable and likely decompose through the loss of one of the alkyl chains. For species with two alkyl groups in positions 2 and 5, water elimination is possible from the ion fragment obtained from the molecular ion after losing one of the two alkyl chains. 4-Membered ring CEs (oxetane derivatives) with a single alkyl chain seem to lose the alkyl chain similar to 5- and 6-membered CEs. The peak at  $m/z$  57 in the mass spectrum of 2-ethyloxetane likely results from the loss of the ethyl group. The mass spectra obtained by Koritzke *et al.* [428] showed that the fragmentation of oxirane type cyclic ethers is even more complex.

To conclude this discussion, the analysis of mass spectra shows that simple fragmentation rules can be derived for 5- and 6- membered rings, whereas the fragmentation rules of CEs with a smaller ring, such as oxetane and oxirane derivatives, are more complex.





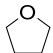
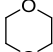
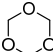
**Fig. 25.** GC-MS chromatogram [429] of the CEs obtained during *n*-pentane oxidation ( $T = 650$  K). The inserts show normalized MS signals as function of the  $m/z$  ratio. For 2,4-dimethyloxetane, the two mass spectra correspond to *cis* and *trans* isomers.

### 3.2.2.3. Quantification using flame ionization detectors

Because its calibration might be obtained without available standards, FID has been proven to be a particularly efficient tool for the quantification of carbon containing species, especially CEs [407,412,415]. This detector relies on the formation of  $CH_x$  ions from the solute in a hydrogen-air flame [430] and measurement of the resulting current. For CEs, the FID detection threshold is about 1 ppm.

When available, the calibration is usually performed by injecting known amounts of standards. However, as most cyclic ethers formed during the low-temperature oxidation of fuels are not commercially available, the Effective Carbon Number (ECN) method [431,432] is often used to estimate the response of a particular cyclic ether. The ECN method is based on the FID response of the carbon atoms present in the molecule to analyze. Each carbon atom contributes additively to the response, which may be affected by the atomic composition and structure of the molecule. This is the case for cyclic ethers. As an example, for cyclic ethers ( $C_nH_{2n}O$ ) formed during the low-temperature oxidation of  $n$ -alkanes, it was observed that the response was similar to that of a  $C_{n-1}$  alkane (for example methyloxirane has a response similar to that of ethane) [431,432]. This means that the presence of the oxygen atom reduces the response by that equivalent of one carbon atom in the molecule, probably because of the formation of CO instead of a  $CH_x$  ion. The ECN method is not straightforward for CEs including more than one oxygen atom. Therefore, the calibration of those species may require the injection of a standard. Table 7 contains ECN values for some CEs found in the literature. As shown in Table 7, the ECN experimental value of 1,3,5-trioxane [432], which includes three atoms of oxygen separated by three methylene groups, is 0.45 and not 0.

**Table 7.** Literature effective carbon number for CEs.

Name	Formula	Structure	ECN	Reference
THF	$C_4H_8O$		3.000	[432]
1,4-Dioxane	$C_4H_8O_2$		2.124	[432]
1,3,5-Trioxane	$C_3H_6O_3$		0.450 0.46	[432] [433]

Data obtained using GC-FID have uncertainties of ~5% when species are calibrated using a standard, while those by the ECN method have uncertainties of ~10%. The latter method shows reliable results even in the case of CEs containing two or three ether-O atoms as demonstrated for poly(oxyethylene) dimethyl ethers [432]. However, uncertainties for multi-functional oxygenated species (*i.e.* containing additional functions other than ether) are not well

known and need to be better characterized. The use of a methanizer (nickel catalyst for hydrogenation) preceding a flame ionization detector [434] improves CE quantification because CE belong to the types of molecule, which can completely catalytically reduced by hydrogen to the corresponding alkane. Thus, considering methyloxirane again as example, its response after passing through a methanizer is that of propane instead of that of ethane [435].

Despite its high ability to separate many types of molecules, GC cannot be used to analyze all species produced during fuel low-temperature oxidation. For example, GC analysis fails for species with a hydroperoxide function due to the instability of this functional group. Hydroperoxide CEs may be formed as products of the third addition to O<sub>2</sub> pathway [436] as it will be discussed in Part 4.1.2. Because the nominal mass of hydroperoxide CEs is the same as that of KHP, both types of species cannot be easily differentiated in usual SVUV-PIMS. For example, *n*-pentane oxidation would produce C<sub>5</sub>H<sub>10</sub>O<sub>3</sub> that could correspond to KHPs, *e.g.* 4-hydroperoxypentan-2-one, or hydroperoxide CEs, *e.g.* 1-(oxiran-2-yl)propane-2-peroxol. The PEPICO technique [437–440] might be able to help with this identification task.

#### 4. EXPERIMENTAL AND MODELING WORK RELATED TO THE GAS-PHASE FORMATION CHEMISTRY OF CYCLIC ETHERS

As comprehensively reviewed by Pollard [4] and Griffiths [277], CEs were frequently detected products in the experimental studies using GC analysis of the slow oxidation or cool flames of O<sub>2</sub>/alkane mixtures in static or flow reactors, rapid compression machines or engines. At this time, it was already understood that CEs were formed following QOOH radical formation. The fact that small alkanes initially produce significant amounts of alkenes led first to the hypothesis that CEs are formed from their “conjugated alkenes”. This idea stated that alkenes react with HO $\dot{O}$  radicals to produce QOOH radicals, which further react to aldehydes or oxiranes together with one  $\dot{O}H$  radical that is needed for chain propagation [441]. Since this mechanism did not predict the large amounts of 3,3-dimethyloxetane formed during *neo*-pentane low-temperature oxidation [442], this explanation was challenged by Fish and coworkers by proposing an alkylperoxy radical isomerization mechanism [443]. Numerous studies demonstrated that low-temperature oxidation of any large alkanes yields CEs of various ring sizes belonging to the oxirane, oxetane, tetrahydrofuran and tetrahydropyran families. This led Pollard [4] to conclude that the formation of derivatives of oxetane, furan and pyran was diagnostic of alkylperoxy radical isomerizations and subsequent decompositions.

Even though the basic mechanistic understanding of low-temperature oxidation was largely developed some 50 years ago, detailed kinetic modeling reproducing CE formation with acceptable rate parameters had to wait until the team of Pilling in Leeds developed a more detailed understanding of QOOH radical formation in 1992 [444]. This followed the experimental determination of the rate parameters for the isomerization of peroxy radicals 10 years earlier by the team of Walker in Hull [445]. The rate parameters proposed by Hughes *et al.* [444] allowed models to be proposed by research groups in Livermore [446], Milano [447], and Nancy [448], which were able to reproduce both, the NTC behavior and the formation of

THF derivatives that were measured by the group of Cathonnet in Orléans [412] in 1993 during JSR *n*-heptane oxidation.

Following this pioneering work, oxirane, oxetane and THP derivatives have been quantified next to THF derivatives in many alkane oxidation studies performed in continuous reactors and in RCMs. Focusing on the low-temperature oxidation of linear and branched alkanes, experimental results obtained after 1994 are described in Part 4.1.1, while Part 4.1.2 considers also the possibility of producing hydroperoxidic CEs. The results presented in Part 4.1.1 combined with theoretical calculations have greatly improved CE detailed kinetic modelling capabilities. Currently in many cases, satisfactory although not always perfect agreement of model predictions with experiments is achieved. The progress made in theoretical understanding of CE chemistry is the topic of Part 4.1.3. To give a full view on CE formation, Part 4.2 focuses on the oxidation of cyclic alkanes, alkylbenzenes, olefins, and Part 4.3 on that of oxygenated hydrocarbons; CE formation from these fuels are discussed, both from experimental and theoretical points of view.

#### **4.1. Cyclic ether formation from the low-temperature oxidation of linear and branched alkanes**

The following part is interested in how CEs are formed during the low-temperature oxidation of linear and branched alkanes. In the low-temperature oxidation of alkanes (except methane and ethane), NTC behavior and CE formation may always be observed, which demonstrates well that NTC behavior, CE formation and QOOH radical chemistry are tightly linked together.

##### ***4.1.1. Experimental quantification of cyclic ethers from linear and branched alkanes***

Tables 8 and 9 list the studies published since 1994, in which CEs formed during the thermally activated (as opposed to photolytic initiated) low-temperature oxidation of linear and branched alkanes were quantified, including mole fraction profiles (time or temperature dependences).

As it was already mentioned in Part 1 and will be more detailed in Part 4.1.3, the formation of the CEs listed in Tables 8 and 9 from linear and branched alkanes occurs through a series of reactions involving H-abstraction from the fuel, the addition of alkyl radicals to oxygen, isomerization and  $\dot{\text{O}}\text{H}$  radical elimination. All the studies listed in Tables 8 and 9 report pronounced NTC behaviors. To provide an idea of the amounts of CEs produced, we mention in this part the peak CE mole fractions ( $X_{\text{CE}}$ ) or, for comparison purpose, CE yields ( $Y_{\text{CE}}$ ), which is  $X_{\text{CE}}$  divided by the initial fuel mole fraction ( $X^{\circ}_{\text{fuel}}$ ) used in the related study.

Table 8 shows that the first CE quantifications reported since 1994 were carried out in continuous reactors operated by the groups of Cernansky in Drexel [449] and Cathonnet in Orléans [295,413], as well as by the team of Minetti in Lille using a RCM [407].

In Drexel a peak  $Y_{\text{CE}}$  of methyloxirane  $\sim 0.2\%$  was quantified during propane oxidation in a flow reactor close to 730 K at 15 bar [449]. To the authors' best knowledge, the only other CE quantification published by the group of Cernansky is that describing the low-temperature oxidation of *neo*-pentane (Wang *et al.* [450]). In this flow reactor study, the temperature dependence of the mole fraction of 3,3-dimethyloxetane was measured and a maximum  $Y_{\text{CE}}$  of  $\sim 6\%$  close to 780 K was found. Recently, Bourgalais *et al.* [451] again measured this CE (with peak  $Y_{\text{ce}} \sim 10 \pm 1\%$  at 730K) during the low-temperature oxidation of *neo*-pentane in a JSR using GC and PEPICO-PIMS.

While not explicitly mentioned in Table 8 and Table 9 for  $\text{C}_4$  and larger fuel molecules, oxirane and methyloxirane have been detected and quantified in almost all listed studies. This is because, as stated before, these light CEs are easily formed by the addition of  $\text{HO}\dot{\text{O}}$  radicals to ethylene and propene (see Part 4.2.3), which are common primary products of alkane low-temperature oxidation.

**Table 8.** Oxidation studies of C<sub>3</sub>-C<sub>6</sub> alkanes performed from 1994, in which CE isomer profiles have been quantified.

Fuel		<i>T</i> (K)	<i>P</i> (bar)/ diluent	$\tau$ (s)	X <sup>o</sup> <sub>fuel</sub> (%)	$\phi$	Quantified CE isomers <sup>a</sup>	Year & Ref.
Propane	FR	600-900	10-15 /N <sub>2</sub> of air	0.2	1.07, 1.59, 2.15	0.4	methyloxirane	1994 [449]
	JSR	530-730	1.07/He	6	12	1	methyloxirane, oxetane	2012 [384]
	RCM <sup>b</sup>	747, 765	30, 50 /N <sub>2</sub> -Ar-CO <sub>2</sub>	-	4.03	1	methyloxirane	2020 [452]
<i>n</i> -Butane	JSR	550-800	1.07 /He (Ar)	6	4	1	2,3-dimethyloxirane <sup>c</sup> , ethyloxirane, 2-methyloxetane, THF	2011 [300]
	RCM <sup>b</sup>	700-900	9-11 /N <sub>2</sub> of air	-	3.13	0.8, 1.2	2,3-dimethyloxirane, 2-ethyloxirane, 2-methyloxetane, THF	1994 [407]
<i>n</i> -Pentane		550-1100	1.07/He	2	1	0.5, 1, 2	propyloxirane, 2-ethyl-3-methyloxirane, 2-ethyloxetane, 2,4-dimethyloxetane, 2-MTHF, THP	2017 [429]
	JSR	550-1100	10/N <sub>2</sub>	0.7	0.1	0.3, 0.5, 1, 2	2-ethyl-3-methyloxirane, 2,4-dimethyloxetane, 2-MTHF	2017 [429]
		500-1100	5, 10/He	2	0.5	1	propyloxirane, 2-ethyl-3-methyloxirane, 2-ethyloxetane, 2,4-dimethyloxetane, 2-MTHF, THP	2020 [453]
	RCM <sup>b</sup>	733	6.9/N <sub>2</sub> -Ar-CO <sub>2</sub>	-	2.56	1	propyloxirane, 2-ethyl-3-methyloxirane, 2-ethyloxetane, 2,4-dimethyloxetane, 2-MTHF	1998 [411]
<i>neo</i> -Pentane	FR	620-810	8/N <sub>2</sub>	0.2	0.12, 0.2	0.3	3,3-dimethyloxetane	1999 [450]
	JSR	500-850	1.07/He-Ar	3	1.5	0.5, $\infty$	3,3-dimethyloxetane	2021 [451]
<i>n</i> -Hexane		530-1160	10/N <sub>2</sub>	0.7	0.95 <sup>d</sup>	0.5, 1, 2	2-ethyl-4-methyloxetane, 2,5-DMTHF, 2-ethylTHF	2015 [454]
	JSR	550-1000	1.07/He	2	2	1	2,3-diethyloxirane, 2-methyl-3-propyloxirane, 2-butyloxirane, 2-propyloxetane, 2-ethyl-4-methyloxetane, 2,5-DMTHF, 2-ethylTHF, 2-methylTHP	2014 [419]
2-Methyl pentane							3-ethyl-2,2-dimethyloxirane, 2,2,4-trimethyloxetane, 2- <i>isopropyl</i> oxetane, 3-propyloxetane, 2,3-dimethylTHF, 2,4-dimethylTHF	
3-Methyl pentane							2,2,4-trimethyloxetane, 2-ethyl-2-methyloxetane, 2,3-dimethylTHF, 3-ethylTHF, 4-methylTHP	
2,2-Dimethyl butane	JSR	550-1000	1.07/He	2	2	1	<i>tert</i> butyloxirane, 3-ethyl-2,2-dimethyloxirane, 2,3,3-trimethyloxetane, 3,3-dimethylTHF	2014 [419]
2,3-Dimethyl butane							2-methyl-2- <i>isopropyl</i> oxirane, tetramethyloxirane, 2,2,3-trimethyloxetane, 3- <i>isopropyl</i> oxetane, 2,4-dimethylTHF	

<sup>a</sup> Only the saturated CEs with the same carbon number as the fuel are listed, <sup>b</sup> *T* and *P* in all RCM studies are those after compression, <sup>c</sup> *cis* and *trans*, <sup>d</sup> + 0.005% 3-methylpentane as impurity.

**Table 9.** Oxidation studies of C<sub>7</sub>-C<sub>16</sub> alkanes performed after 1990, in which CE isomers have been quantified.

Fuel	<i>T</i> (K)	<i>P</i> (bar)/ diluent	$\tau$ (s)	X <sup>o</sup> <sub>fuel</sub> (%)	$\phi$	Quantified CE isomers <sup>a</sup>	Year & Ref.	
<i>n</i> -Heptane	JSR	550-1150	10/N <sub>2</sub>	1	0.1	0.3, 0.5, 1, 1.5	2-ethyl-5-methylTHF <sup>b,c</sup> , 2-propylTHF <sup>c</sup>	1993 [412]
		550-1150	10,40/N <sub>2</sub>	0.1, 0.5, 2	0.1, 0.05	1	2-methyl-4-propyloxetane <sup>b</sup> , 2-propylTHF, 2-ethyl-5-methylTHF <sup>b</sup>	1995 [295]
	RCM <sup>d</sup>	500-1100	1.07/He	2	0.5	0.25, 1, 2, 4	2-ethyl-3-propyloxirane <sup>b</sup> , 2-butyl-3-methyloxirane, 2-methyl-4-propyloxetane, 2,4-diethyloxetane, 2-propylTHF, 2-ethyl-5-methylTHF	2012, 16 [32,33]
		500-1100	1.07/He	1, 2	0.1, 0.5	3	2-ethyl-5-methylTHF <sup>b</sup> , 2-propylTHF	2015 [455]
		500-1100	10/He	2	0.1	1	2-ethyl-5-methylTHF <sup>b</sup> , 2-propylTHF	2020 [456]
	667	3.3/N <sub>2</sub> -Ar-CO <sub>2</sub>	0-0.05	1.87	1	2-methyl-4-propyloxetane, 2,4-diethyloxetane, 2-propylTHF, 2-ethyl-5-methylTHF	1995, 96 [408,410]	
2-Methyl heptane	JSR	500-1200	10/N <sub>2</sub>	0.7	0.1	0.5, 1, 2	2-isopropyl-5-methylTHF, 2,2-dimethyl-5-ethylTHF, 3-methyl-5-propylTHF	2014 [457]
2,5-Dimethyl hexane	JSR	550-1150	10/N <sub>2</sub>	0.7	0.1	0.5, 1, 2	2,2,5,5-tetramethylTHF	2011 [458]
<i>iso</i> -Octane	JSR	550-1150	10/N <sub>2</sub>	1	0.1	0.3, 0.5, 1, 1.5	2,2,4,4-tetramethylTHF (below 1ppm)	1993 [412]
		500-1100	1.07/He	2.0	0.5, 1	0.25, 1, 2, 0.25	3- <i>tert</i> butyl-2,2-dimethyloxirane, 2-isopropyl-3,3-dimethyloxetane, 2,2,4,4-tetramethylTHF	2016 [288]
	RCM <sup>d</sup>	708	13.4/N <sub>2</sub> -Ar-CO <sub>2</sub>	0-0.05	1.65	1	2- <i>tert</i> butyl-3-methyloxetane, 2-isopropyl-3,3-dimethyloxetane, 2,2,4,4-tetramethylTHF, 2,2,5-trimethylTHP	1996 [410]
<i>iso</i> -Octane + anisole	RCM <sup>d</sup>	684	20/N <sub>2</sub> -Ar-CO <sub>2</sub>	0-0.05	1.86 <sup>e</sup>	1	2- <i>tert</i> butyl-3-methyloxetane, 2- <i>iso</i> propyl-3,3-dimethyloxetane, 2,2,4,4-tetramethylTHF	2021 [459]
<i>iso</i> -Octane + <i>n</i> -heptane <sup>f</sup>	JSR	550-1150	10/N <sub>2</sub>	1	0.1	1	2- <i>iso</i> propyl-3,3-dimethyloxetane, 2- <i>tert</i> butyl-3-methyloxetane, 2,2,4,4-tetramethylTHF, + 2-ethyl-3-propyloxirane, <i>cis</i> -2-butyl-3-methyloxirane, 2-methyl-4-propyloxetane <sup>b</sup> , 2-propylTHF, 2-ethyl-5-methylTHF <sup>b</sup> , 2-ethylTHP	1994 [413]
		550-1150	10/N <sub>2</sub>	1	0.1	1	2,5-dipropylTHF <sup>b</sup> , 2-ethyl-5-butylTHF <sup>b</sup> , 2-methyl-5-pentylTHF <sup>b</sup> , 2-hexylTHF	1994 [414]
<i>n</i> -Decane	JSR	550-1100	1.07/He	1.5	0.23	1	2,5-dipropylTHF + sum of (2-hexyl-4-methyloxetane, 2-ethyl-4-pentyloxetane, 2-butyl-4-propyloxetane, 2-heptyloxetane, 2,5-dipropylTHF, 2-ethyl-5-butylTHF, 2-methyl-5-pentylTHF, 2-hexylTHF, 2-ethyl-6-propylTHP, 2-methyl-6-butylTHP, 2-pentylTHP)	2009, 16, 17 [288,415, 460]
		550-1100	1.07/He	1.5	0.2 <sup>h</sup>	1	2-methyl-5-undecylTHF + sum of (2-dodecylTHF, 2-ethyl-5-decylTHF, 2-propyl-5-nonylTHF, 2-butyl-5-octylTHF, 2-pentyl-5-heptylTHF, 2,5-dihexylTHF)	2009 [415]

<sup>a</sup> only CEs with the same number of carbon atoms as the reactant are listed, <sup>b</sup> *cis* and *trans*, <sup>c</sup> only maximum mole fractions are reported, <sup>d</sup> *T* and *P* in all RCM studies are those after compression, <sup>e</sup> 1.12% of *iso*-octane + 0.74% for anisole, <sup>f</sup> only relative CE amount was shown, <sup>g</sup> in Table 4, except 2-dodecylTHF and 2-methyl-5-undecylTHF, C<sub>16</sub> CEs are shown under the lumped name “2-R-5-R’THF”, <sup>h</sup> 75% of *n*-decane + 25% of *n*-hexadecane.

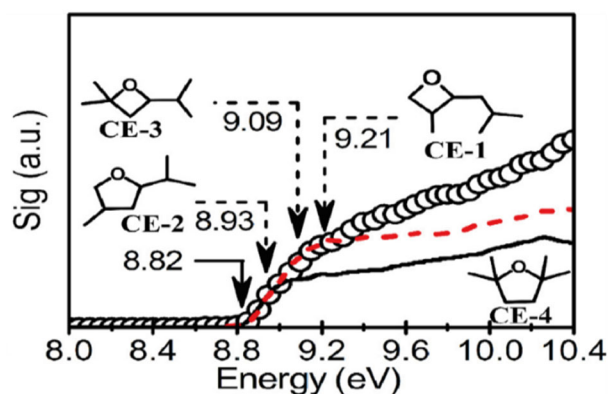


Progress made on CE identification by GC-MS [426] allowed the Orléans team of Cathonnet to report in 1994-1995 several quantitative JSR oxidation studies: *n*-heptane [295,412], *iso*-octane [412], *n*-decane [414] and mixture of the two reference fuels [413]; the latter two molecules serve as primary reference fuels for RON rating. The largest number of CE isomers was identified for the fuel mixture of *n*-heptane and *iso*-octane. Instead of temperature dependent absolute mole fractions, only relative CE isomer yields were reported. In the *n*-heptane oxidation experiment at 10 bar, the peak concentration of 2-ethyl-5-methylTHF was measured to be  $Y_{CE} \sim 7.5\%$  at 700 K [295], while for *iso*-octane oxidation at 10 bar, a  $Y_{CE}$  value below 0.1% was reported for 2,2,4,4-tetramethylTHF. Both studies do not provide information on CEs other than THF derivatives.

From 2011 to 2015, the Orléans group reported CE quantifications for *n*-hexane [454], 2-methylheptane [457] and 2,5-dimethylhexane [458] oxidation at three equivalence ratios ( $\phi = 0.5, 1$  and  $2$ ), showing that the maximum obtained  $Y_{CE}$  sum is rather equivalence ratio ( $\phi$ ) independent ( $\sim 8 \pm 1.2\%$  for *n*-hexane and for 2-methylheptane,  $\sim 10 \pm 1.5\%$  for 2,5-dimethylhexane). However, in agreement with *n*-pentane results, a decrease of  $\phi$  significantly enlarges the NTC zone, which is found between 700 and 900 K. In the NTC zone, the measured concentrations of products including CEs are very low well demonstrating the reactivity decrease, as is described in Part 1. In the three studies, the model developed by the authors nicely reproduces this behavior. In the *n*-hexane oxidation study only three CE isomers were quantified while eight CEs could be expected, and for 2,5-dimethylhexane only 2,2,5,5-tetramethylTHF was reported. The only other CE quantification made in Orléans for alkane JSR oxidation dates from 2017 and concerns *n*-pentane at 10 bar [429] as described later.

While not reporting CE mole fractions, Rotavera *et al.* [380] investigated CE formation during the oxidation of 2,5-dimethylhexane initiated by Cl-atom in a FR and followed by SVUV-PIMS. Based on calculated adiabatic IEs for all possible CE isomers (the IEs are in the

range 8.45-9.88 eV), the authors indicated that the largest contribution to the MS signal at  $m/z$  128 (which corresponds to  $C_8$ -CEs) arises from 2,2,5,5-tetramethylTHF (CE-4 in Fig. 26 with an IE = 8.82 eV). Later, as is shown in Fig. 26, Wang *et al.* [20] also reported 2,2,5,5-tetramethylTHF formation during their JSR study using SVUV-PIMS. These measurements are in good agreement with those of Rotavera *et al.* [380]. At photon energies above 9.0 eV, the difference between the experimental signal for the reactive mixture and that with only 2,2,5,5-tetramethylTHF indicates that other CE isomers (e.g. CE-2, CE-3 or CE-1 in Fig. 26) may be present as well.



**Fig. 26.** 2,5-Dimethylhexane oxidation: measured PI energy scan at  $m/z$  128 (white circles by Wang *et al.* [20] in JSR at 510 K overlaid with their absolute PI spectrum of 2,2,5,5-tetramethylTHF (black line) scaled to align with the slope at the onset energy (8.8 eV) of the  $m/z$  128 signal. This figure also displays the PI spectrum of 2,2,5,5-tetramethylTHF previously measured by Rotavera *et al.* [380] in a FR at 650 K (broken red line) - reproduced from Ref. [20] with permission of Elsevier.

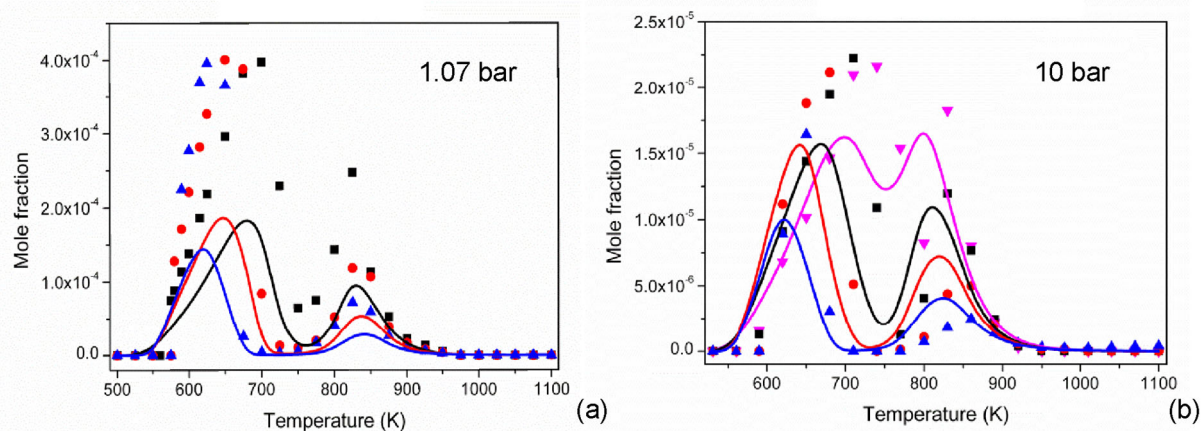
Building on the methods developed in Orléans, in 2011, the group of Battin-Leclerc in Nancy began with quantitative studies of CE formation using JSR experiments (mostly at 1 bar, except in [33,453]). The low-temperature oxidation of propane [384], *n*-butane [300], *n*-pentane [429,453], *neo*-pentane [451], the five isomers of hexane [419], *n*-heptane [32,33,455,456], *iso*-octane [288,461], *n*-decane [415] and *n*-hexadecane [415] were examined, using various equivalence ratios for *n*-pentane, *n*-heptane and *iso*-octane. For *n*-hexane, for which the total yield of the listed CEs reached a maximum of 29% ( $\phi=1$ ), and for lighter *n*-alkanes, all expected CE isomers were identified. For branched hexanes and  $C_7$  alkanes, as they were produced in too

low amounts, not all expected CEs could be identified, but THF derivatives were the CEs detected in highest amounts. While CEs with several ring sizes were obtained at 5 and 10 bar for *n*-pentane [453] (in agreement with results by the group of Dagaut [429]), for *n*-heptane in JSR at 10 bar only THF derivatives could be detected [412,456].

As already mentioned in Part 3, the GC separation of CE isomers is difficult for very heavy reactants, such as *n*-decane and *n*-hexadecane. For those reactants, due to overcrowded chromatograms, often only the sum of THF derivatives could be quantified. The obtained CE mole fraction profiles were reproduced in a reasonable way by detailed kinetic models developed either by the Nancy group or by other groups, *e.g.* [462] for propane and *n*-butane, [463] for *n*-pentane, [449] for neo-pentane, [454] for *n*-hexane, [34] for *n*-heptane, and [461] for *iso*-octane. The temperature dependence of the mole fraction of the measured CE sums was simulated using a model generated by EXGAS by [464] for the *n*-decane and for *n*-decane/*n*-hexadecane mixture [465]. Since no suitable model was available at the time of publication, simulation of CEs produced from branched isomer of hexanes cannot be reported.

The oxidation of *n*-pentane was investigated both in Orléans at 10 bar and in Nancy at 1.07 bar under otherwise similar conditions during a joint study [429] performed in order to provide JSR data for the validation of kinetic models developed in the group of Curran at the National University of Ireland - Galway based on revisited rate rules for alkane oxidation chemistry [466]. Overall, the predicted CE mole fractions agree reasonably well with the experiments, however the degree of agreement varies for the various CEs detected. Fig. 27 shows measured and predicted 2-MTHF profiles as a function of temperature and both pressures. 2-MTHF is the dominant CE in *n*-pentane oxidation under these conditions. Fig. 27 shows that low pressure favors CE formation because at the lowest pressure (1.07 bar) the highest peak  $Y_{2\text{-MTHF}}$ , ~4%, is obtained compared to ~2.2% at 10 bar. Such a pressure effect is

less obvious in the Nancy *n*-heptane oxidation data obtained at 1.07 and 10 bar, where  $Y_{CE}$  for 2-ethyl-5-methylTHF is highest at 10 bar while more 2-propylTHF [33] is produced at 1.07 bar.



**Fig. 27.** Temperature dependence of the mole fraction of 2-MTHF during the oxidation of *n*-pentane at **(a)** 1.07 bar in Nancy and **(b)** 10 bar in Orléans (see initial conditions in Table 8). Symbols are experimental data, lines simulations, pink color for  $\phi = 0.3$ , black for  $\phi = 0.5$ , red for  $\phi = 1$ , and blue for  $\phi = 2$ ; reproduced from the supplementary material of [429].

The double-peak structures seen in Fig. 27 are caused by NTC behavior. This clearly shows that CEs are already formed at low temperatures when the equilibrium of the alkyl+O<sub>2</sub> reaction favors alkylperoxy radical formation. Over this temperature range, CEs are produced in parallel with KHPs and other products from QOOH radicals. Further temperature increase leads to the NTC zone, in which the overall reactivity including the CE formation declines. Although at even higher temperature, the alkyl+O<sub>2</sub> reaction shifts even more towards the reactants, new radical forming reactions, such as H<sub>2</sub>O<sub>2</sub> decomposition, increase the alkyl radical concentration drastically and therefore accelerate the RO $\dot{O}$  chemistry again. This leads to the second CE peak. At these higher temperatures, according to kinetic analysis, alkyl radical decomposition to smaller species becomes more and more competitive and at even higher temperatures these decomposition reactions become dominant resulting in a decline of the CE yield.

Concerning the effect of equivalence ratio in open flow reactors, as it was already noted from the Orléans results on *n*-hexane and 2,5-dimethylhexane, Fig. 27 well shows that  $\phi$  has little effect on the experimental peak mole fraction obtained below 800 K, except at  $\phi$  equal 2 and 10 bar. However, an increase of  $\phi$  while keeping the fuel mole fraction unchanged enlarges the NTC zone between 700 and 900 K in which very low CE amounts are observed for stoichiometric and rich mixtures. This NTC enlargement is well reproduced by the model, but the maximum mole fractions below 800 K are notably underpredicted.

Full sets of CEs were quantified during the RCM experiments of several alkane/air mixtures by the Lille group from 1994 to 1999.  $Y_{CE}$  were quantified for *n*-butane, *n*-pentane, *n*-heptane and *iso*-octane. These studies also report ignition and cool flame delay times. Except for *n*-butane, only stoichiometric conditions were investigated. Examples of temporal profiles of CE mole fractions obtained for *n*-heptane (maximum  $Y_{CE}$  of 1.6% for 2-ethyl-5-methylTHF, the major measured CE ( $P = 3.3$  bar)) and *iso*-octane (maximum  $Y_{CE}$  of 8.5% for 2,2,4,4-tetramethylTHF, the major detected CE ( $P = 13.4$  bar)) are given in Fig. 23 in Part 3. For pure *iso*-octane, at a pressure of 13.3 bar after compression, five CE isomers (two oxetane, two THF and one THP derivatives) were quantified. In contrast, the JSR study at 10 bar performed in Orléans reported only the detection of 2,2,4,4-tetramethylTHF in very low amounts. The CE identification for *iso*-octane oxidation in RCM was confirmed in 2021 using the same device with an *iso*-octane/anisole mixture, in which the pre-ignition temporal profiles of CE mole fractions were reported [459]. The THF derivative is found to be the CE produced in highest amounts. These data were simulated using a model based on the *iso*-octane sub-mechanism recently developed at Livermore [467].

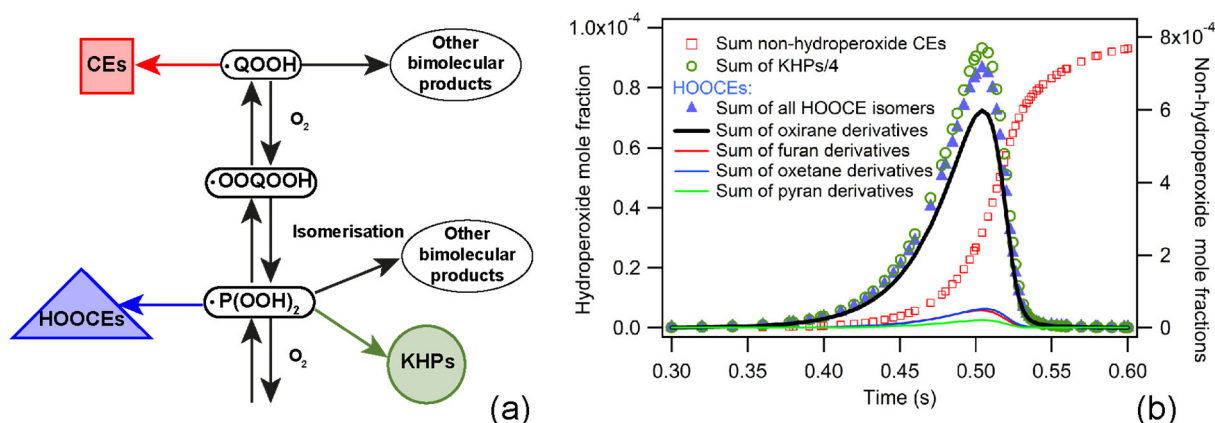
The group of Heufer *et al.* in Aachen also reported CE quantification in RCM experiments in 2020 [452], together with pressure profiles indicating the occurrence of a cool flame. These experiments using propane were performed at pressures, after compression, as high as 50 bar.

Methyloxirane mole fractions were measured through GC-FID analysis and temporal evolution was reported for times before auto-ignition. A peak value of ~185 ppm was determined at 30 bar and about 90% of IDT.

To finish the discussion about CE formation during alkane low-temperature oxidation, the recent detection of CEs during *n*-heptane and *iso*-octane plasma-assisted oxidation in a flow reactor at room temperature and low pressure of 40 mbar by EI-MS should be mentioned [468]. Even though no detailed quantifications were provided, global CE mole fractions around ~200 ppm and ~500 ppm were reported for *n*-heptane and *iso*-octane, respectively, with a high sensitivity to plasma voltage.

#### **4.1.2. Possible cyclic ether hydroperoxide formation**

The demonstration of the occurrence of a third oxygen addition step by Wang *et al.* [20] during 2,5-dimethylhexane oxidation through high-resolution MS detection of species containing 4 or 5 oxygen atoms has given a new importance to the reactions of  $\dot{P}(\text{OOH})_2$  radicals.  $\dot{P}(\text{OOH})_2$  radicals are the products of the second oxygen addition, followed by intramolecular H-abstraction. In line with what was proposed in 1998 by [469], Wang *et al.* [20] underlined the possible formation of hydroperoxide CEs (HOOCEs) from  $\dot{P}(\text{OOH})_2$ , in addition to the previously proposed production of KHPs and olefinic hydroperoxides (through  $\text{HO}\dot{\text{O}}$  radical elimination). Based on model predictions intended to demonstrate the feasibility to detect species originating from a third oxygen addition step during 2-methylhexane auto-ignition at low temperatures, Wang *et al.* [436] noted that the most abundant predicted HOOCEs were oxirane derivatives. Fig. 28a summarizes the channels that yield CEs and HOOCEs starting from a  $\dot{\text{Q}}\text{OOH}$  radical.

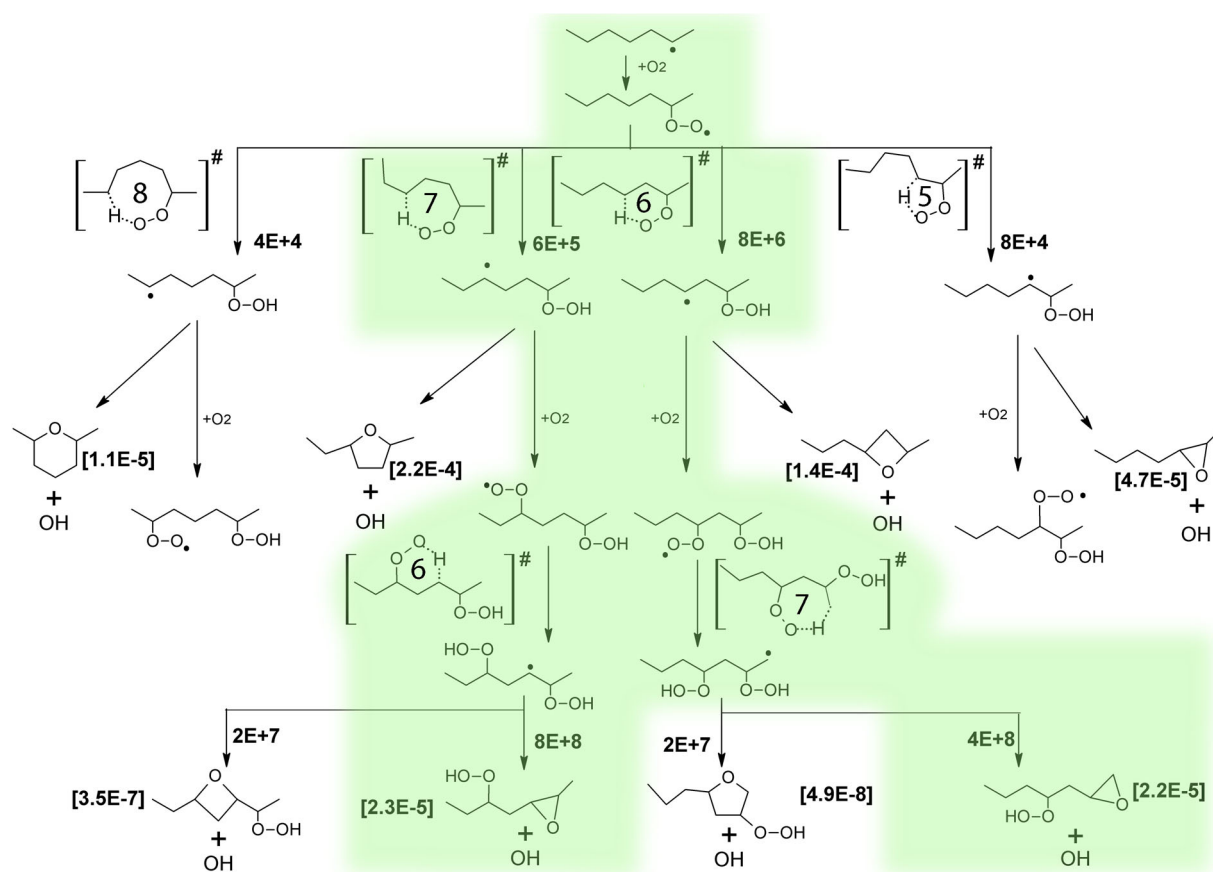


**Fig. 28.** Formation of hydroperoxide CEs: **(a)** lumped reaction scheme from  $\dot{Q}OOH$  radicals inspired by Warth *et al.* [469], **(b)** simulated formation of HOOCEs for the conditions given in Fig. 3 in Part 1 using the model of Zhang *et al.* [33].

Since the work by Wang *et al.* [436], alkane oxidation models such as that for *n*-heptane proposed by the group of Curran [33] include HOOCE chemistry. Fig. 28b displays the predicted HOOCEs using the model of Zhang *et al.* [33]. It shows that according to the kinetic model these species are formed in significant amounts, since the sum of their mole fractions represents about a quarter of the sum of KHP mole fractions. Contrary to non-hydroperoxide CEs, which are mainly THF derivatives for alkanes from  $C_7$  (see Table 9 and Fig. 3 in Part 1), the majority of hydroperoxidic CEs are oxirane derivatives. To understand the favored formation of oxirane derivatives after the second  $O_2$  addition, Fig. 29 presents a flow rate analysis (using 2-hydroperoxyheptyl radical as initial radical), in which the pathways leading to the major hydroperoxyoxirane derivatives are highlighted. In the model of Zhang *et al.* [33], the rate constants for the peroxyalkyl radical isomerizations and the decompositions of hydroperoxyalkyl radicals to cyclic ethers and  $\dot{O}H$  radicals are those proposed, respectively, by Sharma *et al.* [156] and Villano *et al.* [470], which are in agreement with the new theoretical calculations by Duan *et al.* [471]. The same rate coefficients are also used for analogous isomerization and decomposition reactions of  $\dot{P}(OOH)_2$  radicals.

As was observed during the experiments listed in Table 9 and is numerically confirmed in Fig. 29, the isomerization reactions of alkylperoxy radicals ( $RO\dot{O} \rightarrow \dot{Q}OOH$ ) proceeding

through 6-membered or 7-membered ring TSs are favored. This is caused by the low energy barriers for these reactions [471] and explains the preferential formation of THF derivatives (through 7-membered ring TS) and oxetane derivatives (through 6-membered ring TS). The  $\dot{Q}OOH$  radicals from these routes are abundant and available for the second  $O_2$  addition forming the  $\dot{O}OQOOH$  radicals. These latter radicals isomerize also preferentially through 6- or one 7-membered ring TSs to form  $\dot{P}(OOH)_2$  ( $\dot{O}OQOOH = \dot{P}(OOH)_2$ ), which in turn form hydroperoxyCE by release of OH. As can be seen in Fig. 29, each  $\dot{P}(OOH)_2$  radical may produce two different hydroperoxyCEs, but the reactions leading to hydroperoxyoxirane derivatives have rate coefficients more than an order of magnitude larger than those for the alternative pathways.



**Fig. 29.** Flow-rate analysis for 2-heptyl oxidation with focus on hydroperoxide CEs formation. The conditions are the same as in Fig. 3. The green area highlights formation pathways of hydroperoxyoxirane derivatives. Numbers near the arrows are the rates (in mole/cm<sup>3</sup>/s unit) of the corresponding reaction averaged from 700 K to 1000 K, and numbers in square brackets near molecules are the peak mole fractions of the corresponding molecules. The numbers inserted in the transition states belong to the ring size. For clarity reasons, several important pathways, such as KHP formation, are omitted.

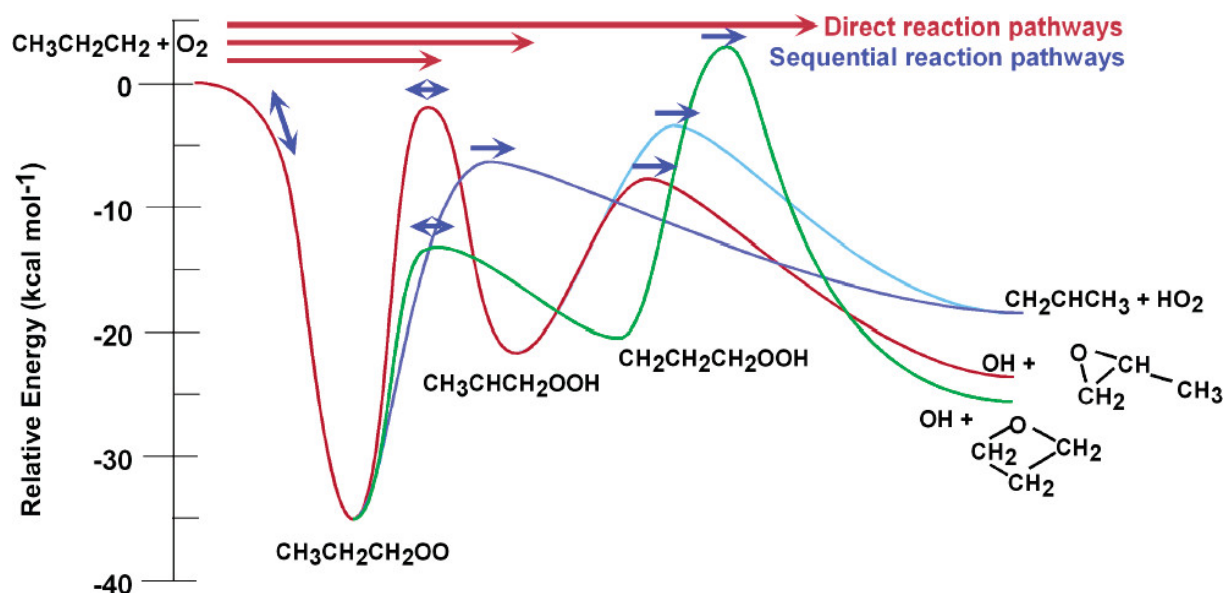


Note that standalone MS analysis cannot distinguish between hydroperoxide CEs and KHPs if their spectra do not contain characteristic fragmentation patterns as their parent ions have the same  $m/z$  ratio. In their SVUV-PIMS investigation of *n*-butane JSR oxidation, Battin-Leclerc *et al.* [472] calculated the IEs of several species corresponding to  $m/z$  104. The calculated IEs of both C<sub>4</sub> KHPs (between 9.36 and 9.39 eV) and 3-hydroperoxyTHF (9.37 eV) were found compatible with the observed signal rise at  $m/z$  104 (at 9.29 eV). Further investigation based on the PEPICO technique or using deuterated isotopes might be able to provide evidence that hydroperoxide CEs are indeed formed.

#### **4.1.3. Progress in modelling cyclic ether formation**

The double peak structure of the 2-MTHF profile in *n*-pentane oxidation nicely demonstrates the close link between CE yields and NTC behavior or low-temperature oxidation chemistry including the role of peroxides, which due to their weak O-O bond, become an additional source of radicals. While the oxidation of short alkanes mainly yields oxiranes via hydroperoxy (HO $\dot{O}$ ) radical addition to alkenes – the latter are formed via the concerted HO $\dot{O}$  elimination from alkylperoxy radicals (RO $\dot{O}$ ) or  $\beta$ -scission of alkyl or hydroperoxyalkyl radicals – larger alkanes follow the more typical alkane oxidation sequence (Fig. 28). As presented in Fig. 28, CEs are produced together with the chain propagating  $\dot{O}H$  radical as one of the bimolecular product channels of hydroperoxyalkyl radicals ( $\dot{Q}OOH$ ). An exact treatment of the competition between CE formations with alternate reaction channels requires a full and detailed analysis of the underlying PES and the corresponding Master Equation (ME) because the RO $\dot{O}$  radical is formed as a chemically activated species, which contains excess energy comparable to the barriers on the PES. Similarly, isomerization steps may produce energized species that continue to further react prior to being thermalized [473,474]. In Fig. 30 the PES for *n*-propyl radicals reacting with O<sub>2</sub> demonstrates this point. Several barriers are below the entrance channel and

the flux through different reaction pathways notably depends on the energy distribution (hence competition between chemical transformations and energy transfer). Consequently, a number of recent reviews on low-temperature oxidation strongly emphasize the importance of solving the underlying ME *e.g.* [106,475–477].



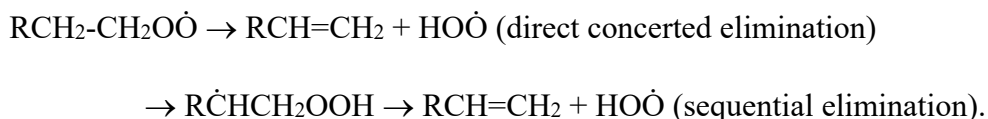
**Fig. 30.** Schematic PES of the *n*-propyl+O<sub>2</sub> PES. The red arrows demonstrate well-skipping reactions of chemically excited species, while the blue arrows follow step-wise transformations that can be described by high-pressure limited rate expressions - reproduced from Ref. [473] with permission of ACS.

It is not the focus of this review paper to further discuss ME analyses because they depend on the details of each PES. Instead, the main focus is on generalized high pressure rate expressions for the elementary reactions leading directly to CEs. Before this, a brief summary on some selected theoretical studies that lead to the current general understanding of low-temperature oxidation is given, since CE formation is a part of this.

#### 4.1.3.1. General remarks on low-temperature oxidation

As mentioned in the introduction to Part 4, the importance of radical chemistry involving the reaction of alkyl radicals with O<sub>2</sub> and subsequent chemistry of RO $\dot{O}$  was already recognized more than 40 years ago by Pollard [4]. However, a detailed understanding of the involved individual steps had to wait for reliable quantum mechanical methods to become available.

Pioneering work on  $C_2H_5+O_2$  by Schaefer III and coworkers [478–481] and Miller and Klippenstein [482] established that direct  $HO\dot{O}$  concerted elimination from a  $RCH_2O\dot{O}$  radical (R is an a H-atom or an alkyl group) is a feasible alternative to the indirect sequential pathway involving prior isomerization to  $\dot{Q}OOH$  radical:



By directly monitoring  $HO\dot{O}$  profiles via infrared absorption spectroscopy, Clifford *et al.* [483] demonstrated experimentally the relevance of the direct (‘prompt’)  $HO\dot{O}$  channel for the ethyl +  $O_2$  reaction resulting from chemically activated  $RO\dot{O}$  radicals, and Carstensen *et al.* [484] and DeSain *et al.* [181,485] presented modeling studies confirming the important role of the chemical activated  $C_2H_5O\dot{O}$  radical for the correct prediction of time-dependent product yields in the  $C_2H_5+O_2$  reaction. Conclusions drawn for ethyl +  $O_2$  also largely hold for  $C_3H_7+O_2$  (see Fig. 30 “direct reaction pathways”) [473]. More recent calculations, *e.g.* by Launder *et al.* [486] or Klippenstein [476] further improved the accuracy of the  $C_2H_5+O_2$  PES, but the main features remained unchanged.

Routinely solving the ME for the oxidation chemistry of large alkanes is not practical and it would significantly slow down the automated and/or systematic development process of low-temperature mechanisms. Fortunately, the importance of chemically activated reactions diminishes with increasing molecule size, increasing pressure and decreasing temperature, which justifies the use of high-pressure rate expressions as a good approximation of the exact kinetics [487,488]. This allows kinetic models for the low-temperature oxidation of alkanes to be based on reactions classes with assigned high-pressure rate expressions for each reaction class or family. A review by Battin-Leclerc [10] emphasizes the systematic way, in which large kinetic models by the Ranzi group (Milano) [489,490], the Westbrook and Pitz group (Lawrence Livermore National Laboratory) [491] and the Nancy group [193,194] were

constructed up to 2008, but this is also true for models from other research groups, *e.g.* that of the group of Warnatz [492]. Since the time of that review (2008), thermochemical data have been refined and missing reaction classes have been added, *e.g.* the Korcek reaction [31] or more detailed 2<sup>nd</sup> and 3<sup>rd</sup> O<sub>2</sub> addition chemistry [493], but the general kinetic model development approach remains the same.

In order to further improve earlier low-temperature oxidation models, theoretical studies have been conducted to extract or confirm systematic trends in rate expressions for the various reaction pathways related to this chemistry [156,470,487,488,494,495]. Especially, the ring-size and substitution patterns of the hydroperoxyalkyl carrying carbon and radical site alter the pre-exponential factors and barrier heights of several reaction classes relevant to low-temperature oxidation. Studies specifically addressing CE forming reactions will be discussed in detail below. The availability of generic rate expressions is essential to extend basic oxidation mechanisms for small species such as the validated AramcoMech 3.0 model [496] to larger regular alkanes. These models can further be augmented with *ab initio* calculated oxidation kinetics to address subtle deviations from the generic rate expressions for specific fuels.

#### ***4.1.3.2. Generic rate expressions for cyclic ether formation during the oxidation of alkanes***

Several systematic studies on the formation of CEs at low-temperature oxidation conditions are available and these are listed in Table 10. The investigations of individual reaction systems are not included.

Chan *et al.* [497], Wijaya *et al.* [207] and Miyoshi [494] calculated the rate coefficient for the simplest member of a reaction class, which was then used as the representative rate expression for the reaction class. For example,  $\dot{\text{C}}\text{H}_2\text{CH}_2\text{OOH} \rightarrow \text{cy}(\text{CH}_2\text{OCH}_2) + \dot{\text{O}}\text{H}$  is the simplest oxirane forming reaction that involves a primary radical site, while the corresponding

2,2-dimethyloxirane forming reaction  $(\text{CH}_3)_2\dot{\text{C}}\text{CH}_2\text{OOH} \rightarrow \text{cy}(\text{C}(\text{CH}_3)_2\text{OCH}_2) + \dot{\text{O}}\text{H}$  is the simplest reaction that involves a tertiary radical site. Each reaction class is defined by the CE formed and radical type involved. The above-mentioned examples belong to the oxirane forming reaction classes from either p- or t-type radicals.

**Table 10.** *Ab initio* based development of generic rate expressions for CE forming reactions. p,s,t refer to primary, secondary and tertiary sites and CE-x specifies the CE type: x=3,4,5,6 are oxiranes, oxetanes, oxolanes and oxanes, respectively.

Authors & Ref.	Year	Method	Number of calculated reactions	Target
Chan <i>et al.</i> [497]	1999	DFT BHandHLYP/6-311G**	10	CE-3,4: p,s,t (radical sites) CE-5: p,s (radical sites) CE-6: p (radical site)
Wijaya <i>et al.</i> [207]	2003	CBS-QB3 <sup>a</sup>	9	CE-3,4,5: p,s,t (radical sites)
Miyoshi [494]	2011	CBS-QB3	73	CE-3,4,5,6: p,s,t (QOOH + radical sites) CE-7: p-p and s-s sites Ring substitution effects
Villano <i>et al.</i> [487]	2012	CBS-QB3	51	CE-3,4,5: p,s,t (most QOOH + radical site combinations) CE-6: only (p,p), (p,s), (s,p)
Cord <i>et al.</i> [498]	2012	CBS-QB3	9	CE-3,4,5: p,s,t (radical sites)
Bugler <i>et al.</i> [499]	2017	CCSD(T)/CBS// M06-2X/6-311++ G(d,p)	43	CE-3,4,5,6: example reactions for (most QOOH + radical site combinations), no explicit rate rules

<sup>a</sup> preferred method, others used: DFT, CBS-Q

Miyoshi [494] showed that the *ab initio* reaction barriers for CE formation correlate with the enthalpies of reaction (Evans-Polanyi relationship), which is used to estimate the activation energies of the rate expressions. Villano *et al.* [487] averaged the *ab initio*/TST results from a larger set of reactions by determining a common A factor and providing Evans-Polanyi parameters to calculate the barriers from the reaction enthalpies. Bugler *et al.* [499] did not derive generic rate expressions but a large set of individually calculated rate coefficients was provided, from which such rules can be deduced. The studies mentioned in Table 10 are discussed in more detail below.

Table 11 compares the CE rate expressions from the studies mentioned in Table 10 at 700 K. These were calculated either directly using the reported rate rules, if available, or they were deduced from rate coefficients found in these studies. In the latter case, *e.g.* applicable to

the work by Bugler *et al.* [499], the reported rate expressions have been generalized in terms of rate rules in order to calculate the entries in Table 11.

The main conclusion one might draw from this compilation is that the CBS-QB3 based rate expressions are generally higher than those obtained by the study of Bugler *et al.* [499]. It should also be noted that different studies using the same CBS-QB3 method clearly report different rate expressions for the same reaction class (or even reaction). Some possible causes for this were already discussed in Part 2, *e.g.* the discussion of the treatment of internal rotations in 2.1.2.2. In addition, Wijaya *et al.* [207] have corrected the CBS-QB3 energies to account for excessive higher order corrections, while such corrections have not been applied by Miyoshi [494] nor by Villano *et al.* [487].

Prior to 2011, only a few systematic theoretical studies were available. Limited CPU resources and restrictions in the levels of theory led to results with large uncertainties and significant differences between different groups [497]. In 2003, Wijaya *et al.* [207] calculated barrier heights for CE formation that were generally found to be consistent with the earlier studies by Chan *et al.* [497] and [500] but the A-factors differed substantially. The authors pointed out that internal rotors play an important role as they may freeze in transition states. Consequently, an accurate treatment of these internal rotations is required to obtain reliable pre-exponential factors.

**Table 11.** Rate expressions calculated with rate rules for CE forming reactions at 700 K. p,s,t refer to primary, secondary and tertiary carbons. CE ring sizes 3,4,5,6 refer to oxiranes, oxetanes, oxolanes and oxanes, respectively. For keeping a reasonable size to this table, reaction classes, for which rate rules were only reported by Miyoshi, were omitted. The number in parenthesis in the entries for Villano *et al.* and Bugler *et al.* indicates how many reactions were evaluated to derive this rate coefficient. All other rate constants are based on a single reaction.

CE ring size	HOO carrying carbon type	Nature of radical site	k(700 K) [s <sup>-1</sup> ]					
			Chan <i>et al.</i> <sup>a</sup> [497]	Wijaya <i>et al.</i> [207]	Miyoshi [494]	Villano <i>et al.</i> <sup>d</sup> [487]	Cord <i>et al.</i> [498]	Bugler <i>et al.</i> <sup>d</sup> [463]
3	p	p	6.9×10 <sup>8</sup>	2.0×10 <sup>7</sup>	2.1×10 <sup>8</sup>	1.4×10 <sup>8</sup> (1)	1.7×10 <sup>8</sup>	6.5×10 <sup>7</sup> (1)
	p	s	8.3×10 <sup>8</sup>	1.5×10 <sup>7</sup>	4.4×10 <sup>8</sup>	1.0×10 <sup>9</sup> (6)	2.3×10 <sup>8</sup>	6.0×10 <sup>7</sup> (3) <sup>e</sup>
	p	t	2.3×10 <sup>9</sup>	2.0×10 <sup>8</sup>	1.0×10 <sup>9</sup>	1.6×10 <sup>9</sup> (1)	1.5×10 <sup>9</sup>	2.6×10 <sup>8</sup> (2)
	s	p			7.3×10 <sup>8</sup>	7.0×10 <sup>8</sup> (4)		3.8×10 <sup>8</sup> (4)
	s	s			6.0×10 <sup>8</sup>	9.7×10 <sup>8</sup> (6)		4.6×10 <sup>8</sup> (7)
	s	t			1.1×10 <sup>9</sup>	3.1×10 <sup>9</sup> (1)		
	t	p			1.5×10 <sup>9</sup>	2.3×10 <sup>9</sup> (2)		3.7×10 <sup>8</sup> (2)
	t	s			3.4×10 <sup>9</sup>	2.3×10 <sup>9</sup> (1)		4.1×10 <sup>8</sup> (1)
4	p	p	3.0×10 <sup>5</sup> 6.3×10 <sup>6b</sup>	6.5×10 <sup>4</sup>	3.6×10 <sup>5</sup> 1.2×10 <sup>6b</sup> , 3.6×10 <sup>6c</sup>	1.4×10 <sup>6</sup> (4)	1.9×10 <sup>5</sup>	3.0×10 <sup>5</sup> (4)
	p	s	6.3×10 <sup>5</sup>	1.7×10 <sup>5</sup>	3.3×10 <sup>6</sup> 7.9×10 <sup>6b</sup> , 1.8×10 <sup>7c</sup>	3.0×10 <sup>6</sup> (4)	3.8×10 <sup>5</sup>	1.5×10 <sup>5</sup> (4)
	p	t	1.3×10 <sup>6</sup>	1.2×10 <sup>6</sup>	1.0×10 <sup>7</sup> 5.5×10 <sup>7b</sup> , 4.3×10 <sup>7c</sup>	7.7×10 <sup>6</sup> (1)	3.8×10 <sup>6</sup>	3.8×10 <sup>5</sup> (1)
	s	p			2.4×10 <sup>6</sup> 3.8×10 <sup>7b</sup> , 1.5×10 <sup>7c</sup>	2.5×10 <sup>6</sup> (4)		9.8×10 <sup>5</sup> (4)
	s	s			9.8×10 <sup>6</sup> 1.7×10 <sup>7b</sup> , 9.8×10 <sup>7c</sup>	2.0×10 <sup>6</sup> (2)		3.9×10 <sup>5</sup> (2)
	s	t			6.9×10 <sup>7</sup> 6.5×10 <sup>8b</sup> , 1.5×10 <sup>8c</sup>	1.7×10 <sup>7</sup> (1)		
	t	p			6.7×10 <sup>6</sup> 2.4×10 <sup>7b</sup> , 6.6×10 <sup>7c</sup>	3.3×10 <sup>6</sup> (1)		2.7×10 <sup>5</sup> (1)
5	p	p	7.5×10 <sup>6</sup>	1.2×10 <sup>6</sup>	7.3×10 <sup>6</sup> 1.4×10 <sup>8c1</sup> , 7.6×10 <sup>7c2</sup>	1.4×10 <sup>7</sup> (2)	3.1×10 <sup>6</sup>	2.2×10 <sup>6</sup> (3)
	p	s	1.0×10 <sup>7</sup>	3.2×10 <sup>6</sup>	6.8×10 <sup>7</sup> 4.0×10 <sup>8c1</sup> , 1.4×10 <sup>8c2</sup>	4.1×10 <sup>7</sup> (2)	3.0×10 <sup>6</sup>	4.6×10 <sup>6</sup> (1)
	p	t	N/A	6.6×10 <sup>6</sup>	2.2×10 <sup>8</sup> 5.8×10 <sup>8c1</sup> , 7.3×10 <sup>8c2</sup>	1.8×10 <sup>8</sup> (1)	1.8×10 <sup>7</sup>	
	s	p			4.1×10 <sup>6</sup> 4.2×10 <sup>3c1</sup> , 8.5×10 <sup>7c2</sup>	7.8×10 <sup>6</sup> (1)		1.1×10 <sup>6</sup> (1)
6	p	p	1.5×10 <sup>6</sup>	N/A	1.1×10 <sup>6</sup>	2.3×10 <sup>6</sup> (4)		2.6×10 <sup>5</sup> (1)
	p	s			3.6×10 <sup>6</sup>	1.3×10 <sup>7</sup> (1)		
	s	p			1.1×10 <sup>5</sup>	5.5×10 <sup>5</sup> (1)		

<sup>a</sup> rate rules for reverse reactions are also reported but not compared here.

<sup>b</sup> methyl substitution on non-reacting ring carbon.

<sup>c</sup> double methyl substitution on non-reacting ring carbon; <sup>c1</sup>: vicinal to OOH, <sup>c2</sup>: vicinal to radical site.

<sup>d</sup> reevaluated based on the rate coefficients given in the study.

<sup>e</sup> one entry is ignored (outlier).

The studies by Chan *et al.* and by Wijaya *et al.* are the first systematic investigations of the effect of ring size and substituent on CE formation, but they are based on limited sets of reactions – three each for oxirane, oxetane and oxolane. Nevertheless, a clear trend towards lower activation energy when going from primary to secondary and tertiary radicals was observed. Another outcome was that oxetane formation is slower than oxirane or oxolane

formation for the same radical type. CBS-QB3 was found to be a reliable method (except for implementation problems in the Gaussian software package used), although Wijaya *et al.* [207] raised concerns about contributions of higher order corrections, which might lead to unrealistic low barriers for some reactions. In those cases, Wijaya *et al.* [207] corrected the *ab initio* results by 2.5 kcal/mol.

In 2011, Miyoshi [494] conducted a very detailed and comprehensive CBS-QB3 study on all important low-temperature oxidation reactions including CE formation. The impact of the radical structure on barrier heights, reaction energies and pre-exponential factors was identified. Those can largely be related to ring strain effects in the cyclic transition states. While for most reaction classes, only the substitution of the radical carrying site (primary, secondary, tertiary) alters the reactivity notably, the CE formation rate coefficient is also affected by the type of carbon that carries the hydroperoxy group. High-pressure rate coefficients were calculated for the simplest reactions of a given substitution pattern with Eckart tunneling corrected transition state theory and the results were generalized in form of rate rules. Internal rotations were accounted for, but only at an approximate Pitzer-Gwinn level. Next to RO $\dot{O}$ /QOOH reactions, Miyoshi also analyzed CE formation reactions following the addition of a second O<sub>2</sub> to QOOH and concluded that the rate expressions for these reactions were largely in line with those of the first O<sub>2</sub> addition. The work by Miyoshi provides the most detailed and complete set of rate rules for CE forming reactions known as of today.

Villano *et al.* [487] also used the CBS-QB3 method to study alkyl + O<sub>2</sub> reactions including CE formation. This study is very similar to that of Miyoshi but not as comprehensive in terms of detailed rate rules. One difference between the two studies is that Villano *et al.* treated every internal rotation separately as 1-D rotor with effective reduced moments of inertia that largely decoupled this rotation from the external modes. The explicit calculation and evaluation of hindrance potentials might have allowed Villano *et al.* to find lower energy



conformers, which are sometimes difficult to locate. The rate rules by Villano *et al.*, who also observed that the rate coefficients for CE formation depended on the degree of substitution of both the hydroperoxy group carrying site and the radical site, are overall in good agreement with those developed by Miyoshi. One notable difference was seen for the CE formation from tertiary  $\beta$ - $\dot{Q}OOH$ , for which Villano *et al.* found a lower activation energy than Miyoshi but in line with that found by Cord *et al.* [498]. Villano *et al.* also carried out a steady state ME analysis for the reactions on the  $n$ - $C_4H_7+O_2$  PES and calculated the pressure-dependent rate expressions for this system. They showed that the predictions of a kinetic model using high-pressure rate expressions agree at 500 K and 750 K excellently with the one that explicitly accounts for pressure-dependence. Even at 1000 K, the differences were found to be small.

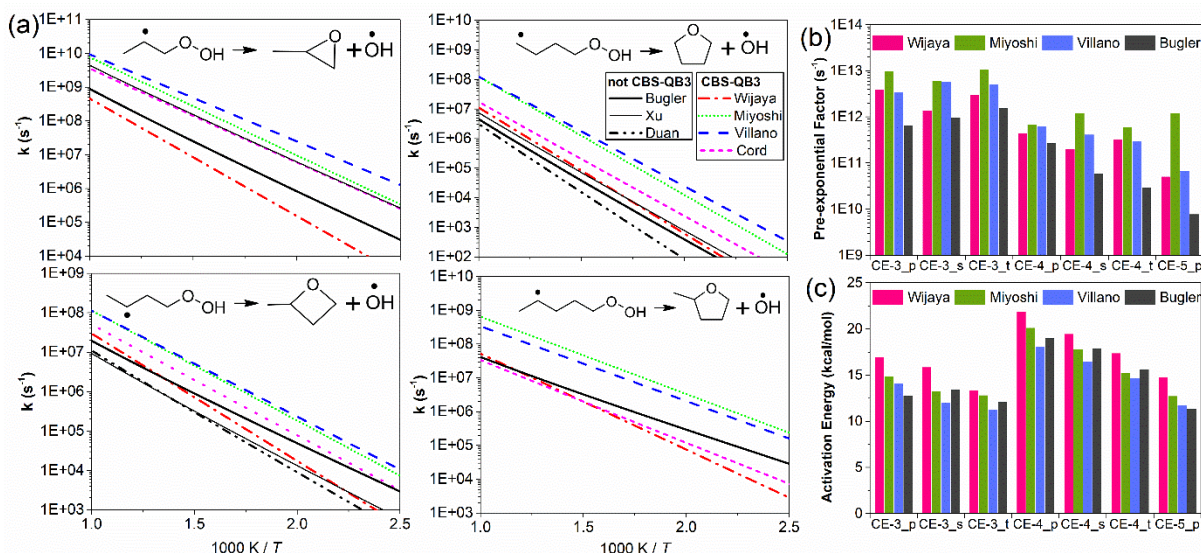
Cord *et al.* [498], also applying the CBS-QB3 method, calculated rate coefficients for nine CE producing reactions from primary, secondary and tertiary hydroperoxyalkyl radicals forming oxirane, oxetane and tetrahydrofuran  $C_4$  products. The results were compared to generic expressions used in the EXGAS software and substantial differences were observed. The authors point out that their results deviate clearly from those by Miyoshi [494] and suggest that differences in the hindered rotor treatment and the application of tunneling correction factors could be reasons.

Bugler and coworkers [463] presented their own study on this subject. While an earlier publication by Bugler *et al.* [499] recommended rate expressions based on the studies by Miyoshi [494] and Villano *et al.* [487] for CE formation reactions with rather large uncertainty assignments, two years later, they investigated 43 CE formation reactions involving alkyl chains from  $C_2$  to  $C_5$  with the M06-2X/6-311++G(d,p) method to calculate geometries and frequencies and CCSD(T)/CBS for energies. The different methodology provides an alternative evaluation of these reactions compared to the CBS-QB3 investigations by Miyoshi [494] and Villano *et al.* [487]. The re-evaluation was motivated by the suspicion that CBS-QB3 predicted barriers

were potentially systematically too low. This would lead to an overestimation of CE formation and too high CE yields. The newly calculated rate expressions are generally lower than those obtained with CBS-QB3 (see Table 11).

Several other studies reporting on rate coefficients for individual CE forming reactions seem to support Bugler's analysis that the prior CBS-QB3 based rate rules might overestimate the CE formation step. Sheng *et al.* employed CBS-Q/B3LYP/6-31G(d,g) level of theory to calculate the rate coefficient for hydroxyethyl reacting to give oxirane and OH radical [501] and basically reproduced the result by Wijaya *et al.* [207]. Oakley *et al.* [502] studied the formation of oxiranes from various hydroperoxyalkyl radicals using G4 theory. They concluded in agreement with Bugler that the CBS-QB3 method underpredicts the barrier for this reaction by about 2.5 kcal/mol. The barriers were expressed in terms of an Evans-Polanyi relationship but no generic rate expression was provided. Hashemi *et al.* [503] used in their high pressure ethane oxidation model a rate coefficient for oxirane formation from hydroperoxyethyl radical, which was very close to that of Bugler *et al.* and lower than those calculated by Villano *et al.* and Miyoshi. This rate coefficient was extracted from a ME analysis by Klippenstein [476] based on a PES at the ANL0 level of theory, which, as mentioned in Part 2.1.1, is a high level coupled cluster composite approach that includes CCSDT(Q) corrections. Xu *et al.* [504] recalculated the PES for alkyl+O<sub>2</sub> (ethyl, propyl, butyl) at various coupled cluster type levels of theory and concluded that CCSD(T)-F12a/cc-pVDZ-F12 was the best method for ethyl+O<sub>2</sub>. The activation energy for this reaction is higher than those obtained by Bugler *et al.* [463] or Villano *et al.* [487], but similar to that of Miyoshi [494]. Nevertheless, the rate coefficient is predicted to be lower than those obtained with CBS-QB3 by Miyoshi and Villano *et al.* supporting the idea that the CBS-QB3 rate rule for this reaction overestimates the reactivity. The same is true for the study by Duan *et al.* [505], which calculated high-pressure and pressure-dependent rate expressions for CE forming reaction from the oxidation of *n*-butyl radicals.

Fig. 31a compares the generic rate expressions for several CE forming reactions. Similar but more extended comparisons can be found in the supporting material of Bugler *et al.* [499]. Unlike one would expect from the previous discussion on activation energies, the Arrhenius plots are rather parallel but the pre-exponential factors differ substantially (Fig. 31b) with those calculated by Bugler *et al.* being systematically smaller than those from the CBS-QB3 studies by Miyoshi [494] and Villano *et al.* [487]. As can be seen in Fig. 31c, the activation energies at 700 K calculated by Bugler *et al.* at the CCSD(T) level are not always higher than the corresponding CBS-QB3 values. This does not necessarily contradict statements about 0 K barriers since the 700 K data contain thermal contributions. However, most importantly, Fig. 31b demonstrates the importance of the pre-exponential factors, which goes back to proper treatments of internal rotors and symmetries. Given the importance of these rate expressions not only for accurate CE yield predictions but also to describe the competition between chain propagation and chain branching correctly (and therefore ignition behavior), the observed large spreads in the rate expressions, which has also been noted by Atef *et al.* [467], is not satisfactory. More studies are needed to improve this situation. For example, the G4 composite method, which does not apply the often questioned [498,506] empirical spin contamination correction used by CBSQB3 and has been shown by Simmie to perform better than CBS-QB3 [132] could be tested. If successful it would provide a computationally affordable method to study large fuel molecules. Alternatively, systematic coupled cluster and CASPT2 studies that account for multi-reference character in the transition state as shown in Table 2 and discussed in Section 2.1.1 would be helpful.



**Fig. 31.** Comparison of rate expressions for selected CE formation reactions. **(a):** Arrhenius plots of rate expressions for QOOH cyclization forming methyl oxirane, methyl oxetane, furan and methyl furan, respectively. **(b):** Comparison of pre-exponential factors ( $A$ ) at 700 K of different rate rule studies. **(c):** Comparison of activation energies ( $E_a$ ) at 700 K of different rate rule studies. The Arrhenius  $A$  and  $E_a$  are either directly taken from the rate expression or calculated as  $A = A_{\text{modArrh}} \times T^n \times e^n$  and  $E_a = E + nRT$  from modified Arrhenius rate expressions. References: Wijaya *et al.* [207], Miyoshi [494], Villano *et al.* [487], Cord *et al.* [498], Bugler *et al.* [499], Xu *et al.* [504] and Duan *et al.* [505]. In the CE- $n_x$  label, the  $n$  value refers to the ring size and  $x$  denotes the type of radical (primary, secondary, tertiary) as defined in Table 11 for a primary HO $\dot{O}$  carrying C-atom. In (a) all color lines are CBS-QB3 based while the black lines indicate coupled cluster type calculations.

#### 4.1.3.3. Modeling of cyclic ether formation during the oxidation of $n$ -alkanes

In the last three decades, many models considering the CE formation from alkanes were developed, see for instance those by [384,462,496] for propane, by [462,469,498,505,507] for  $n$ -butane, by [411,429] for pentanes, by [454] for  $n$ -hexane, by [33,34,194,408,446,447] for  $n$ -heptane, by Wang *et al.* [20] for 2,5-dimethylhexane, by [459,467,508] for *iso*-octane, by [509] for *iso*-dodecane, by [464,491,510] for C<sub>8</sub>-C<sub>16</sub> $n$ -alkanes and by [457] for 2-methylalkanes from C<sub>7</sub> to C<sub>20</sub>. This list is by far not exhaustive, but it aims at including the major models having allowed progress in modelling alkane oxidation at low-temperature. In addition, although all these models include reaction channels leading to CEs, only a part of them were tested against CE quantifications, which are available in a limited number of studies.

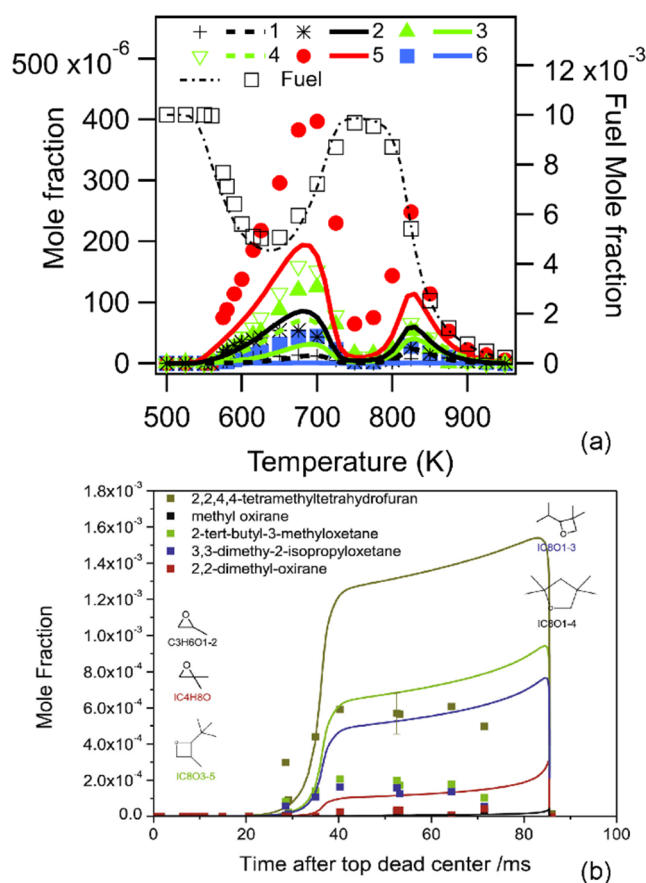
In their earliest attempt of modelling their *n*-butane RCM experiments, Minetti *et al.* [407] used the model by Wilk *et al.* [507]. Simulations using this previously developed model well predicted the fuel consumption, and the yields of the reported products (CO, ethylene, propene, butenes, methanol, propanal) were also well reproduced (within a factor of 2). However, the model overestimated by up to a factor of about 10 the reported yields for all CEs (2,3-dimethyloxirane, 2-ethyloxirane, 2-methyloxetane and THF). Amongst the data listed in Tables 8 and 9, various levels of agreement were reported using the before-listed models with still significant deviations observed even after the theoretical effort described in Part 4.1.3.2. A few examples of the recently obtained best agreements using theoretically calculated kinetics are discussed below.

In order to model their propane RCM data, Ramalingam *et al.* [452] used the model independently developed in Galway [496]. Their simulations reproduced the methyloxirane yields very well at 50 bar and quite well (slight overprediction) at 30 bar.

For heavier linear alkanes, Bugler *et al.* [429] in Galway used an updated version of their 2016 model [466] and showed improved predictions of 2-MTHF and 2,4-dimethyloxetane mole fractions from JSR measurements at 1.07 bar and  $\phi = 1$  (see Table 8). Bugler *et al.* point out that the use of pressure-dependent rate expressions makes a difference in the predictions, which contrasts the previously discussed analysis by Villano *et al.* for *n*-butane [487]. However, as is shown by Fig. 32a, in JSR ( $P = 1$  bar,  $\phi = 0.5$ ), while the agreement is excellent for the fuel consumption, as it was also the case for RCM IDTs in the work of Bugler *et al.* (see Ref. [429]), significant deviations can be seen in the prediction of the mole fractions of all the observed types of CEs. Oxirane derivatives are predicted best, but THF- and oxetane-derivatives are underestimated below 700 K by more than a factor of two and THP by a factor of around 50. In the model of Bugler *et al.* [429], THP formation in *n*-pentane oxidation proceeds mainly through the typical low-temperature oxidation pathways. The underprediction of THP and its

cause were not discussed by Burgler *et al.*. Note that, while different rate constants were calculated for the formation of *cis*- and *trans*-isomers, they were not considered in the pressure-dependent rate expressions included in the model used for simulations. Although the model prediction for absolute values of CE mole fractions still needs to be improved, the model predicts the peak positions of all CEs shown in Fig. 32a very well. It is also noted that the first peak of CEs occurs in the NTC zone, which indicates the close connection of CE formation to the NTC causing chemistry.

Again in Galway, Zhang *et al.* [33] developed a model for the low-temperature oxidation of *n*-heptane. The rate constants used for the low-temperature oxidation chemistry were based on the calculation by Sharma *et al.* [156] for RO $\dot{O}$  isomerizations and by Villano *et al.* [487] for CE formations. Despite small adjustments of the calculated rate rules to improve the agreement, significant deviations between experimental and simulated results are observed in lean mixtures for fuel consumption. Nevertheless, the distribution between the four oxirane-, oxetane- and THF-derivatives that were experimentally observed [33] (see Table 9) is well predicted within the studied temperature range and for  $\phi$  from 0.25 to 4. However, the formation of 2-ethyl-3-propyloxirane is overestimated by more than a factor of five and no simulated profile for 2-ethyl-3-propyloxirane is reported. A possible cause for the observed deviations might lie in the oversimplified consumption chemistry of these CEs used in the model. In the models developed in Galway, each CE is considered to react with  $\dot{O}H$  and  $HO\dot{O}$  to give two sets of products including a radical, an unsaturated hydrocarbon, a ketone or an aldehyde (*e.g.*  $C_2H_5CO\dot{C}H_2$  and propene in one set and  $CH_3CO\dot{C}H_2$  and 1-butene in the second set for H-abstraction from 2-ethyl-5-methylTHF in the *n*-heptane oxidation model of [33]).



**Fig. 32.** Example of CE mole fraction predictions in alkane oxidation using recent models: **(a)** *n*-pentane in a JSR in Nancy along with fuel mole fraction (1: propyloxirane, 2: 2-ethyl-3-methyloxirane, 3: 2-ethyloxetane, 4: *cis+trans* 2,4-dimethyloxetane, 5: 2-MTHF, 6: THP) (see Table 8,  $\phi = 0.5$ ) vs. predictions with the Galway model (both, the model used for the simulations and the experimental data were taken from [429]), **(b)** *iso*-octane (in presence of anisole) in the Lille RCM (see Table 8) vs. predictions by a model developed based on that of Livermore - reproduced from Ref. [459] with permission of Elsevier.

Concerning  $C_{7+}$  alkanes, Cai *et al.* [510] proposed optimized reaction rate rules for the low-temperature oxidation of  $C_7$ – $C_{11}$  *n*-alkanes. As a starting point for their optimization they used a Livermore model [457], in which the low-temperature oxidation kinetics was updated according to the work by Bugler *et al.* [429]. The optimization was done with experimental IDTs from the literature for  $C_7$ – $C_{11}$  *n*-alkanes. The obtained rate rules were then applied to develop a model for *n*-dodecane giving satisfactory IDT prediction. Unfortunately, while these rate rules involve CEs, the accuracy of the obtained models towards the predictions of CE could not be tested because experimental data are not available.

Concerning branched alkanes, two models using theoretically calculated kinetics were developed in the group of Pitz and Westbrook in Livermore, one for *iso*-octane [467] and one [509] for *iso*-dodecane. The rate constants used for the low-temperature oxidation chemistry were updated from Villano *et al.* [487] for RO $\dot{O}$  isomerizations and from Miyoshi [494] (with  $A \times 2$ ) for CE formations. For this last reaction class, Atef *et al.* [467] noted in the case of *iso*-octane significant differences between the rate constants obtained with the rate rules of Villano *et al.* [487] and with those of Miyoshi [494]. The reason for this is in the thermochemistry, because Villano *et al.* formulate their rate rules as function of the enthalpy of reaction. Atef *et al.* [467] and Fang *et al.* [509] did not report simulated CE formation; however, the first model was later embedded in that of Mergulhão *et al.* [459] for an *iso*-octane/anisole mixture. Fig. 32b presents a comparison between the CE yields simulated using this model and those experimentally measured in the RCM of Lille (see Table 9). Taking into account that the model notably overestimates the fuel consumption (see Fig. 3 in [459]), the distribution of C<sub>8</sub> oxetane- and THF-derivatives is reasonably well reproduced.

Observed deviations in the predictions of CE mole fractions can be explained by uncertainties in the kinetics of the reactions yielding them, but also by inaccurate mechanisms for their consumption. As further discussed in Part 5, the recent work of Rotavera group [395,511] points out that reactions that consume CEs are often too simplified in kinetic models. Moreover, these studies point out that there are mechanistic connections between CEs and products that were thought previously to derive primarily from KHPs. The need to properly account for secondary reactions of CEs has been realized for a long time (*e.g.* [469]), but in the past the lack of accurate kinetics made a proper inclusion of such chemistry impossible and chemical analogy principles had to be used [464]. Given the availability of fast *ab initio* methods, Rotavera and coworkers [395,511] argue that detailed kinetic information needs to be implemented in order to account for the complexity of CE consumption pathways.



## 4.2. Formation of cyclic ethers during the low-temperature oxidation of cyclic and unsaturated hydrocarbons

When looking at CE creation during the low-temperature oxidation of gasoline and Diesel fuel components, not only their production from linear and branched alkanes should be examined but also their formation from cyclic alkanes, alkylbenzenes, linear and branched alkenes, as well as from linear and cyclic dienes. Table 12 lists the studies published since 1994, which present quantifications, including mole fraction profiles (time or temperature dependences), of the CEs produced during the low-temperature oxidation of these cyclic or unsaturated reactants.

### 4.2.1. Cyclic ethers from cyclic alkanes

Although the reactivity of  $C_{\geq 5}$  cycloalkanes during low-temperature oxidation is lower than that of the similar alkanes with the same number of carbon atoms, a marked NTC behavior is always observed, for example for cyclopentane [512–514] and cyclohexane [418,515]. Similar to the low-temperature oxidation chemistry of alkanes, the formation of the CEs listed in Table 12 from cyclic alkanes occurs through a series of reactions involving an H-abstraction from the fuel, a first addition of alkyl radicals to oxygen, an isomerization and an  $\dot{O}H$  radical elimination. However, the isomerization is in most cases hindered by the necessity to go through bicyclic transition states, which increases the ring strain compared to open chain alkanes [516].

As is shown in Table 12 for cyclic alkane oxidation, quantitative CE information is available from JSR experiments at Nancy and Shanghai, and from RCM tests at Lille. The oxidation of cyclic alkanes was also studied in JSR in Orléans but no CE formation was reported in their cyclohexane studies [517,518] at temperatures starting from 750 K nor in the experiments of Ristori *et al.* [519] on *n*-propylcyclohexane oxidation at temperatures starting from 950 K, *i.e.* above the low-temperature reaction zone. While qualitative information is available [520], no quantification for CEs during cyclopentane oxidation was reported in the

literature. Below, first the results for cyclohexane oxidation are discussed and afterwards those for alkylcyclohexane oxidation.

**Table 12.** Studies of the oxidation of cyclic alkanes and alkylbenzenes, in which CE isomers have been quantified.

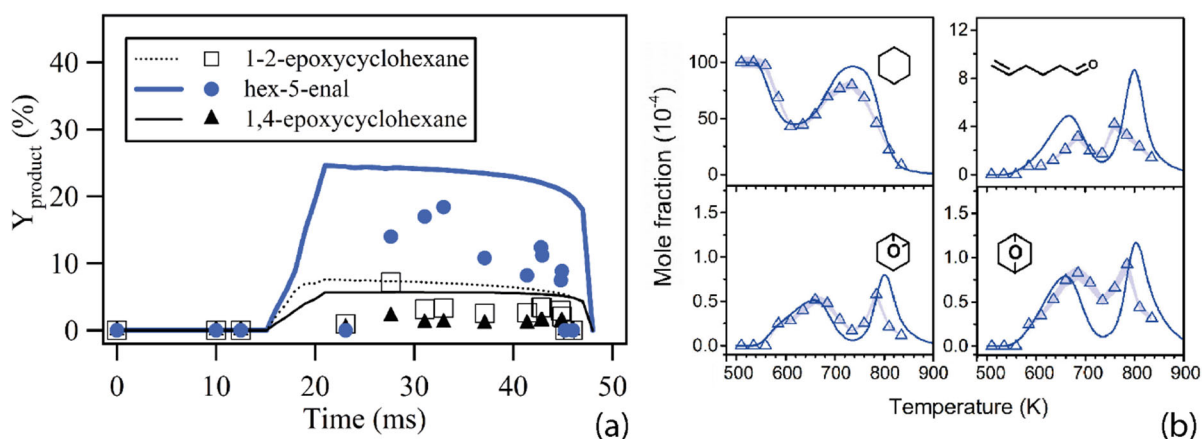
Fuel		<i>T</i> (K)	<i>P</i> (bar)/ diluent	$\tau$ (s)	$X^{\circ}_{\text{fuel}}$ (%)	$\phi$	Quantified CE isomers <sup>a,b</sup>	Year & Ref.
Cyclohexane	RCM <sup>c</sup>	600-900	7-14 /N <sub>2</sub> -Ar-CO <sub>2</sub>	0-0.05	2.31	1	1,2-epoxycyclohexane, 1,3-epoxycyclohexane, <b>1,4-epoxycyclohexane</b>	2001 [521]
	JSR	500-1100	1.07/ He	2.0	0.67	0.5, 1, 2	1,2-epoxycyclohexane, <b>1,4-epoxycyclohexane</b>	2013 [418]
		500-840	1.04/ Ar	4.0	1	0.25	1,2-epoxycyclohexane, <b>1,4-epoxycyclohexane</b>	2021 [522]
Methyl cyclohexane	JSR	500-1100	1.07/ He	2.0	0.57	0.25, 1, 2	1-oxaspiro[2,5]octane, 1-methyl-7-oxabicyclo [4.1.0]heptane, 1-methyl-7-oxabicyclo[2.2.1]heptane	2019 [424]
Ethyl cyclohexane	JSR	500-1100	1.07/ He	2.0	0.5	0.25, 1, 2	2-methyl-1-oxaspiro[2.5]octane, 1-ethyl-7-oxabicyclo[4.1.0]heptane, <b>1-ethyl-7-oxabicyclo[2.2.1]heptane, octahydro-1-benzofuran</b>	2012 [417]
<i>n</i> -Propyl cyclohexane	RCM <sup>c</sup>	620-930	4.5-13.4 /N <sub>2</sub> -Ar-CO <sub>2</sub>	0-0.03	0.46, 0.62, 0.77	0.3, 0.4, 0.5	2-cyclohexyl-3-methyloxirane, 2-ethyl-1-oxaspiro[2.5]octane, 8-ethyl-7-oxabicyclo[4.2.0]octane, 2-methyl-1-oxaspiro[3.5]nonane, <b>1-propyl-7-oxabicyclo[2.2.1]heptane, 7-ethyl-6-oxabicyclo[3.2.1]octane, 2-methyloctahydro-1-benzofuran</b>	2010 [26]
<i>o</i> -Xylene	RCM <sup>c</sup>	704	15.6/N <sub>2</sub> -Ar- CO <sub>2</sub>	0.35	2.51	1	<b>1,3-dihydro-2-benzofuran</b>	2000 [523]
<i>o</i> -Ethyl toluene	RCM <sup>c</sup>	694	15.3/N <sub>2</sub> -Ar- CO <sub>2</sub>	0.37	2.20	1	2-methylphenyloxirane, <b>1-methyl-1,3-dihydro-2-benzofuran</b> , 3,4-dihydro-1H-2-benzopyran	2000 [523]
<i>n</i> -Butyl benzene	RCM	640-840	15.4 /N <sub>2</sub> -Ar-CO <sub>2</sub>	0-0.05	1.55	1	2-benzyl-3-methyloxirane, 2-ethyl-3-phenyloxirane, 2-methyl-4-phenyloxetane, 2-benzyloxetane, <b>2-phenylTHF</b>	2000 [523,524]
	JSR	550-1100	1.07/ He	2.0	0.4	0.25, 1, 2	<b>2-phenylTHF</b>	2012 [525]

<sup>a</sup> only CEs with the same number of carbon atoms as the reactant are listed, <sup>b</sup> oxetane derivatives are in *italics* and THF ones in **bold** (others are oxirane or THP derivatives), <sup>c</sup> *T* and *P* in all RCM studies are those after compression.

#### 4.2.1.1. Cyclic ethers from cyclohexane

Since 1994, the low-temperature oxidation of cyclohexane was first studied by Lemaire *et al.* [521] in a RCM with ignition and cool flame delay time recording, as well as product quantification. The measured CEs were assigned as 1,2-epoxycyclohexane, 1,3-epoxycyclohexane, 1,4-epoxycyclohexane. These results, together with the related IDTs, are well predicted by models such as those developed in Milano [526], Nancy [516], and Livermore [515]. However, as first explained by Gulati and Walker [527] based on their GC quantification of the CEs produced during the addition of cyclohexane to slowly reacting H<sub>2</sub>-O<sub>2</sub> mixtures in a static reactor at 753 K, although the cyclohexane chair form permits the formation of the relatively strain-free six-membered ring of the transition state leading to 1,3-epoxycyclohexane, the rigidity of the chair imposes too much strain for the formation of the oxetane ring and its rupture to form hex-5-enal is energetically more favorable [527]. This hypothesis was considered in the modelling approaches of Milano [526], Nancy [516], Livermore [515], and Shanghai [522]. The three first modelling approaches were mostly based on corrections due to the change in the strain energies in the transition states of the RO<sub>2</sub> isomerizations; the fourth one on theoretical calculations. Fig. 33a presents a comparison of the experimental results of Lemaire *et al.* [521] with the predictions obtained using the model of [516] for the yields of 1,2-epoxycyclohexane, 1,4-epoxycyclohexane and hex-5-enal ( $Y_{\text{product}}$  in Fig. 33a).

1,2-Epoxycyclohexane, 1,4-epoxycyclohexane and hex-5-enal were also quantified during the JSR study of the low-temperature oxidation of cyclohexane of Serinyel *et al.* [418]. These authors studied three equivalence ratios, 0.5, 1 and 2, and demonstrated that a decrease of the equivalence ratio notably increases the CE yields. These authors proposed a kinetic model based on theoretically calculated rate constants for the reactions of cycloalkylperoxy radicals [220], with overall good predictions of IDTs and product formations, but significant deviation for the amounts of C<sub>6</sub> oxygenated species.



**Fig. 33.** Oxidation of cyclohexane (see conditions in Table 12): **(a)** RCM selectivity of the CEs measured by Lemaire *et al.* [521] (symbols) and kinetic modelling by Buda *et al.* [516] assuming that 1,3-epoxycyclohexane is decomposed to hex-5-enal; **(b)** JSR experimental (symbols) and predicted (lines) mole fractions by Zou *et al.* (reproduced from Ref. [522] with permission of Elsevier).

Two recent JSR studies at Shanghai [522,528] with SVUV-PIMS analysis present mole fraction profiles as a function of temperature of a lumped  $C_6H_{10}O$  species assumed to include the three molecules of Fig. 33a (1,2-epoxycyclohexane, 1,4-epoxycyclohexane, hex-5-enal) together with cyclohexanone. The most recent paper [522] also presents results using GC-FID to quantify these three molecules (the sum of  $Y_{CE}$  peak is  $\sim 1.6 \pm 0.16\%$ ) during the JSR study of the low-temperature oxidation of cyclohexane, as is shown in Fig. 33b. The studies of Zou *et al.* [522] and Serinyel *et al.* [418], both detected hex-5-enal, which was presumed to form from 1,3-epoxycyclohexane, in significantly higher yields than those of the two bicyclic CEs. As is also shown in Fig. 33b, CE formation below 800 K is well predicted by the last model proposed by the Shanghai group [522]; the obtained prediction of the data of Serinyel *et al.* [418] is also overall satisfactory. The cyclohexane model of Zou *et al.* [522] was based on a theoretical study performed by the same group [529], in which pressure- and temperature-dependent rate constants and branching ratios were determined from solutions of the RRKM/master-equation for the major reaction channels in the first and second oxygen additions. The authors noted that rapid inversion-topomerization processes facilitate fast equilibrium between axial and

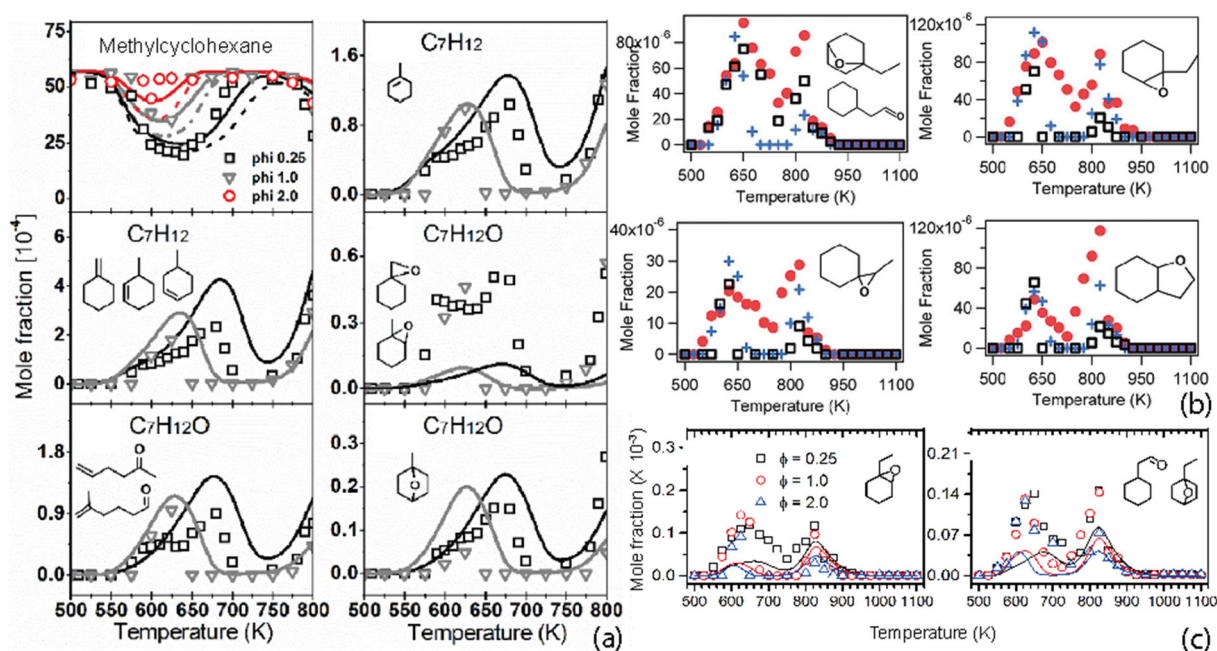
equatorial conformers, which can greatly counterbalance the influence of initial positions of side-chain peroxy and hydroperoxy groups on low-temperature oxidation process. For example, the equatorial-RO $\dot{O}$  radicals preferably switch the peroxy group from equatorial to axial position by inversion-topomerization and form the axial-RO $\dot{O}$  radicals with an overall energy barrier of 11.08 kcal/mol that is much lower than the barrier of intramolecular hydrogen transfer ( $\geq 31.8$  kcal/mol) and concerted elimination (32.0 kcal/mol). The  $\gamma$ -QOOH radical could react to form the corresponding oxetane and  $\dot{O}H$  radical, or alternatively by ring-opening to yield the unstable [C=CCCCOOH] species, which instantaneously decomposes to 5-hexenal and  $\dot{O}H$ . At CBS-QB3 level, the energy for the corresponding transition state is about 3 kcal/mol higher than that for the oxetane formation. The entropy on the other hand favors ring-opening. Several studies [418,515,528,530,531] have shown that the ring-opening step is fast, which would explain why 5-hexenal is detected in high quantities. As shown in [528], the calculated or estimated rate expressions of five studies [418,515,528,530,531] deviate by several orders of magnitude, which in part might be caused by different methodologies used and partly by the existences of several conformers. Given this severe uncertainty in the rate expressions, the overprediction of the 5-hexenal yield by only a factor of two seen in Fig. 33a is quite reasonable.

#### **4.2.1.2. Cyclic ethers from alkylcyclohexanes**

Methylcyclohexane is a simple alkylcycloalkane frequently suggested as a potential surrogate to represent the naphthenic content in transportation fuels [532]. Its low-temperature oxidation chemistry with a notable NTC behavior was studied in the first decade of this millennium in RCM experiments but without product formation measurements [533–535]. Methylcyclohexane oxidation was also investigated in a CFR (Cooperative Fuel Research) engine by Yang *et al.* [536] who report only CO measurements. This study analyzed the impact of steric cyclic structure on the low-temperature oxidation. For the RCM studies, reasonable detailed kinetic models were proposed in each of the three papers; the latest one by Weber *et*

*al.* [535] being based on theoretical calculations, especially those from the work of Yang *et al.* [536].

In 2019, Bissoonauth *et al.* [424] reported CE measurements for methylcyclohexane from a JSR study by the Nancy group together with modelling by the group of Sarathy at KAUST. This was done in order to validate their detailed kinetic model based on an update of that of Weber *et al.* [535]. Fig. 34a displays the observed CE mole fractions, showing that the highest  $Y_{CE}$  was found for two oxirane derivatives (1-oxaspiro[2,5]octane and 1-methyl-7-oxabicyclo[4.1.0]heptane), which could not be separated by GC analysis, while a product with THF structure (1-methyl-7-oxabicyclo[2.2.1]heptane) was detected in lower amounts. The maximum sum of  $Y_{CE}$  is  $\sim 2.5 \pm 0.25\%$ . Note that the two oxiranes originate from the tertiary ROO radical. Fig. 34a also displays results from the simulations, showing that while the predictions are very satisfactory for the reactant and for unsaturated hydrocarbons and aldehydes, they deteriorate for CEs, especially the oxirane derivatives. This led Bissoonauth *et al.* [424] to conclude that more work on the CE sub-mechanism is necessary.



**Fig. 34.** Experimental (symbols) and predicted (lines) mole fractions during  $C_7$ - $C_8$  alkylcyclohexane oxidation in a JSR (see conditions in Table 12): **(a)** reactant and initial oxidation products in methylcyclohexane [424]; **(b)** all CEs quantified in ethylcyclohexane oxidation [417] ( $\bullet$ )  $\phi = 0.25$ ;

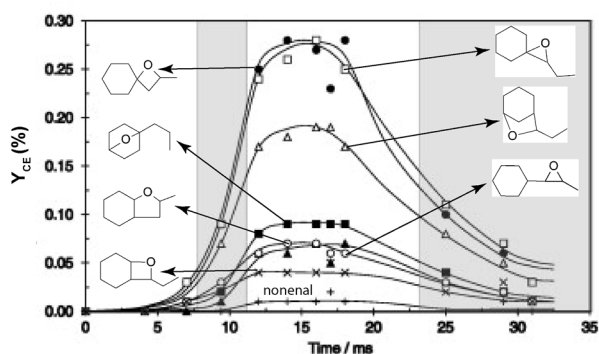
(+)  $\phi = 1$ ; ( $\square$ )  $\phi = 2$ ); **(c)** comparison between simulations by [537] and experimental results of [417] for ethylcyclohexane oxidation. When several molecules are shown in a figure, the experimental profile represents the summed mole fractions of the displayed molecules, while the simulated profile is the sum of all the isomers with similar structures. Reproduced from Ref. [424] with permission of Elsevier, from Ref. [417] with the permission of ACS, and from the supplementary material of [537].

Quantification of CEs during the low-temperature oxidation of ethylcyclohexane was first reported in 2012 by Husson *et al.* [417] using a JSR coupled to a GC. These results are displayed in Fig. 34b, which shows the four quantified CEs. Those include 2 sets of products: one set of two CEs (1-ethyl-7-oxabicyclo[4.1.0]heptane, 1-ethyl-7-oxabicyclo[2.2.1]heptane) in which the newly formed CE ring is fused to the cyclohexane ring, and a second set of two CEs (2-methyl-1-oxaspiro[2.5]octane, octahydro-1-benzofuran) in which the new CE ring is formed on the side chain. The largest experimental  $Y_{CE}$  was obtained for these last two CEs (peak value above  $2 \pm 0.2\%$  for each of them). In line with their previous methylcyclohexane model, Wang *et al.* [538] reported the first simulations of the data of [417], together with an experimental study performed in a JSR at atmospheric pressure with SVUV-PIMS analysis and made in order to identify highly oxygenated products, thus without individual CE quantification nor simulations. In their recent experimental and modelling study of ethylcyclohexane oxidation, Zou *et al.* [537] reported measured and simulated temperature dependent mole fractions (peak  $Y_{CE} \sim 10\%$  at 650 K,  $\tau = 2$  s) of a lumped  $C_8H_{14}O$  species, which presumably consists mainly of the CEs octahydro-1-benzofuran and 1-ethyl-7-oxabicyclo[4.1.0]heptane, but also of 2-ethylhex-5-enal and 2-ethylcyclohexan-1-one. The total mole fraction profiles of these species were well predicted by the model of Zou *et al.* [537] for the three equivalence ratios studied ( $\phi = 0.5, 1$  and  $2$ ). Zou *et al.* [537] also used their model to simulate the data of Husson *et al.* [417]. However, the mole fraction profiles of only two of  $C_8H_{14}O$  CEs (1-ethyl-7-oxabicyclo[4.1.0]heptane, 1-ethyl-7-oxabicyclo[2.2.1]heptane) were presented and show a significant under-prediction as seen in Fig. 34c. Fig. 34 clearly demonstrates that most of the bicyclic CEs observed during ethylcyclohexane oxidation result from reaction sequences that



presumably include the abstraction of the tertiary H-atom, either by metathesis or through internal isomerization.

Continuing with increasing alkyl chain, CE quantifications were reported in 2010 during *n*-propylcyclohexane oxidation experiments performed in the Lille RCM in the group of Minetti [26]. This work reports on measurements of cool flame delay times and IDT, as well as on product quantification. The time dependence of the mole fractions of seven CEs was measured as shown in Fig. 35, under lean conditions ( $\phi$  from 0.3 to 0.5). These include oxirane, oxetane and THF derivatives, with 2-ethyl-1-oxaspiro[2,5]octane and 2-methyl-1-oxaspiro[2,5]nonane having the highest  $Y_{CE}$ .



**Fig. 35.**  $Y_{CE}$  during *n*-propylcyclohexane RCM two-stage ignition ( $T$  and  $P$  after compression were 669 K and 7 bar, respectively,  $\phi = 0.5$  (see Table 12)). The cool flame and ignition regions are indicated as grey zones. Experimental results were connected by a line to guide the eye. Reproduced from Ref. [26] with permission of Elsevier.

Fig. 35 shows that the two bicyclic ethers produced in the highest quantities are those formed through reactions involving tertiary H-atoms. To the authors' best knowledge, no modelling attempt of these RCM results has been made. Note that Ristori *et al.* [519] also reported an experimental and modelling study on the JSR oxidation of *n*-propylcyclohexane. This study was performed at temperatures above 950 K. CE formation was not discussed.

To finish the discussion on alkylcyclohexanes, the Nancy group detected a large number of species with a molar mass of 154 g/mol during their JSR study of *n*-butylcyclohexane oxidation. These correspond to cyclic ethers, ketones and aldehydes with the same carbon

number as the reactant. However, contrary to the previously described ethylcyclohexane work, these important products could not be identified accurately due to too crowded chromatograms.

#### **4.2.2. Cyclic ethers from alkylbenzenes**

The reactions involved in CE formation from alkylbenzenes are very similar to those playing a role in alkane oxidation: H-abstraction from the fuel, first addition of alkyl radical to oxygen, isomerization and  $\dot{\text{O}}\text{H}$  radical elimination. Contrary to cycloalkanes, the phenyl ring itself is unreactive at low temperatures but affects the reactivity of the alkyl chain by induced resonance stabilization. As is shown in Table 12, CEs were observed in *n*-butylbenzene and C<sub>8</sub>-C<sub>9</sub> di-alkylbenzene oxidation, by the research groups in Lille and in Nancy. CE formation was only reported for those alkylbenzenes that displayed a marked NTC behavior. Traces of THF derivatives across the alkyl chain were reported during a JSR study of *n*-hexylbenzene oxidation performed by the Nancy group [539,540].

##### **4.2.2.1. *n*-Butylbenzene**

As is shown in Table 12, the first authors to mention CE formation from *n*-butylbenzene oxidation were Ribaucour *et al.* [524] in 2000 using the RCM of the group of Minetti in Lille. In addition to ignition and cool flame delay times, they reported  $Y_{\text{CE}}$  of five CEs, two oxirane, two oxetane and one THF derivatives. This last compound, 2-phenylTHF, is produced with a  $Y_{\text{CE}}$  (10%) at least five times higher than those of the other CEs. Ribaucour *et al.* [524] presented a detailed kinetic model reproducing their data with overall acceptable agreement for delay times, benzaldehyde and styrene selectivity, but significant deviations for  $Y_{\text{CE}}$ .

Only 2,3-dihydro-1-benzofuran, a CE with one carbon atom less than the reactant, was quantified during JSR experiments on *n*-butylbenzene oxidation performed in Nancy close to atmospheric pressure [525]. Due to the fact that *n*-butylbenzene is not very reactive at low-temperature under the conditions of this study, only traces (amounts < 0.1 ppm) of

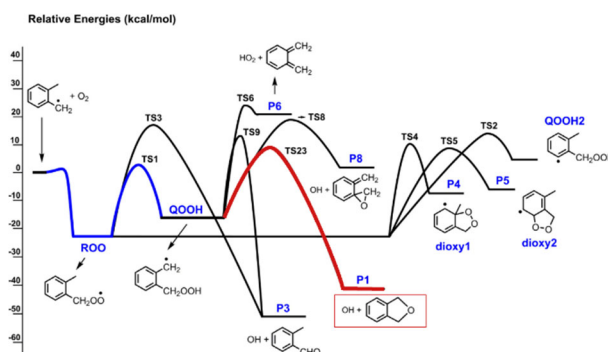
2-phenylTHF, 2-ethyl-3-phenyloxirane, and 2-benzyl-3-methyloxirane were observed. No CE formation was observed in the JSR experiments at 10 bar by Diévar *et al.* [541] in Orléans despite investigating the 500-1150 temperature range and observing a notable NTC behavior for the lean mixture. Husson *et al.* [525] proposed a detailed kinetic model which overall satisfactorily predicted the JSR data as well as IDTs measured in ST and RCM. However, CE predictions using this model under RCM conditions at  $\phi=0.5$  predicted 2-ethyl-3-phenyloxirane to be the CE with the highest yield, while 2-phenylTHF was experimentally found to be the major CE in the study of Ribaucour *et al.* [524] at similar conditions but at  $\phi=1$ .

#### 4.2.2.2. Di-alkylbenzenes

In the RCM in Lille, CE quantifications were reported from *o*-xylene and *o*-ethyltoluene oxidation studies. To the author's best knowledge, these results have never been modelled. In *o*-xylene oxidation, a THF derivative (1,3-dihydro-2-benzofuran) can be formed by bridging both alkyl chains [523]; this bridging is not possible for *m*- and *p*-xylenes, explaining their lower reactivity and why neither cool flame, NTC nor CE were detected for these last two reactants [542]. The 1,3-dihydro-2-benzofuran (13%) yield in *o*-xylene oxidation is higher than that of 2-methylbenzaldehyde (9%) [523] that is formed from the same  $\dot{Q}OOH$  radical. As illustrated in Fig. 36, the theoretical study of Ye *et al.* [543] explains how the classical low-temperature scheme described in Part 1 is also valid for *o*-xylene. The peroxy radical formed by  $O_2$  addition to the benzylic radical site abstracts a H-atom from the ortho-methyl chain, which facilitates the isomerization  $RO\dot{O} \rightleftharpoons \dot{Q}OOH$ .

The alkyl chain bridging is also observed for *o*-ethyltoluene, for which a THF (1-methyl-1,3-dihydro-2-benzofuran) and a THP (3,4-dihydro-1H-2-benzopyran) derivative can be produced. 2-methylphenyloxirane was also observed in *o*-ethyltoluene oxidation experiments. With a  $Y_{CE}$  of about 15%, 1-methyl-1,3-dihydro-2-benzofuran, which originates

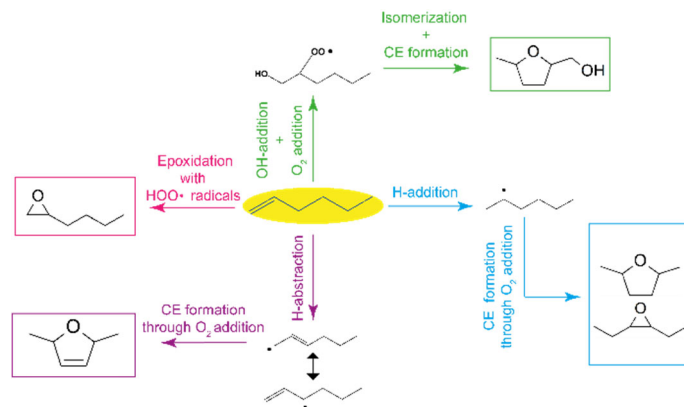
from the benzylic radical, is more abundant than 3,4-dihydro-1H-2-benzopyran, which is produced from the less stable 2-phenylethyl radical [523].



**Fig. 36.** Relative energies of major reaction pathways on PES of *o*-xylyl + O<sub>2</sub> at 0 K in kcal/mol (the initial bimolecular reactants are set to energy zero)– reproduced from Ye *et al.* [543] with permission of Elsevier.

#### 4.2.3. Cyclic ethers from olefins and dienes

The need for a thorough understanding of alkene low-temperature oxidation arises from the fact that these unsaturated compounds are the most abundant products of alkane oxidation. The combustion chemistry of alkenes and alkadienes is synthesized and discussed in a recent review paper of Zhou *et al.* [544]. While all reactions classes are discussed in [544], we focus in the present review on the formation of CEs. As is shown in Fig. 37 for the case of 1-hexene, the number of reaction pathways leading to CEs starting from alkenes is larger than from alkanes. Alkenyl radicals obtained from H-abstractions from the fuel can lead to unsaturated CEs by the same reaction series as described for alkanes, an addition to oxygen followed by an isomerization and an OH radical elimination. However, resonance stabilization in allylic alkenyl radicals, which is the most likely formed type of radicals, leads to a low stability of the ROO radicals. Furthermore, the barriers for isomerization reactions across a double bond are higher than for corresponding C-H bonds in alkanes. For these reasons, alkene oxidation is slower than the oxidation of the corresponding alkane.



**Fig. 37.** CE formation pathways from 1-hexene (according to [420]). Only reactions leading to CEs are displayed.

As also shown in Fig. 37, radical additions to the fuel double bond are important CE sources:

- as proposed by the teams of Walker in Hull [545] and Stark in York [546,547], the single-step epoxidation of alkenes by peroxy radicals, especially  $\text{HO}\ddot{\text{O}}$  radicals, which starts with radical addition to the double bond followed by cyclization forming the CE formation and hydroxyl radicals as bimolecular products.
- H-addition and  $\text{CH}_3$  radical addition reactions (less often considered in modelling, since no  $\text{C}_{n+1}$  products are usually detected) provide a source of alkyl radicals, which lead to CE formation by the series of reactions previously described for alkyl radicals.
- $\ddot{\text{O}}\text{H}$  radical addition to the alkene double bond produces a hydroxyalkyl radical, which adds to oxygen and after isomerization and  $\ddot{\text{O}}\text{H}$  radical elimination yields a CE bearing an alcohol function

As is shown in Table 13, quantitative CE data were obtained during the oxidation of linear  $\text{C}_{5+}$  alkenes, but also for a linear  $\text{C}_6$  diene, 1,5-hexadiene, as well as for two cyclic unsaturated  $\text{C}_6$  molecules, cyclohexene and cyclo-1,3-hexadiene. CE quantifications are only available from RCM experiments in Lille and JSR studies in Nancy. Fig. 37 presents all CEs identified using GC-MS by Meng *et al.* [548] during 1-hexene JSR, as listed in Table 13.

**Table 13.** Studies of the oxidation of linear and cyclic alkenes and dienes, in which CE isomers have been quantified.

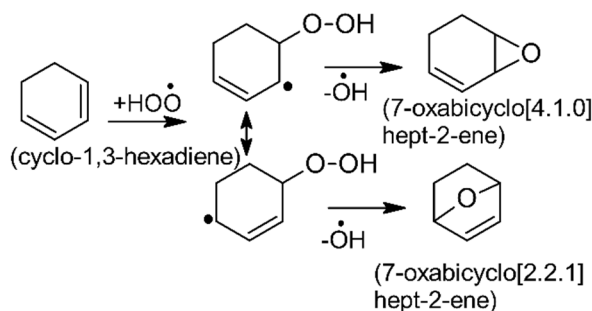
Fuel		<i>T</i> (K)	<i>P</i> (bar)/ diluent	$\tau$ (s)	$X^{\circ}_{\text{fuel}}$ (%)		Quantified CE isomers <sup>a,b</sup>	Year & Ref.
Propene	JSR	800- 1000	1.07 /He	2.0	1.1, 1.65	0.64, 1.68, 2.19	<i>methyloxirane</i>	2014 [549]
1-Pentene	RCM <sup>c</sup>	733	6.9 /N <sub>2</sub> -Ar-CO <sub>2</sub>	-	2.56	1	<i>2-propyloxirane, 2-ethyl-3-methyloxirane,</i> <i>2-ethyloxetane, 2,4-dimethyloxetane, 2-MTHF</i>	1998 [411]
2-Methyl-2-butene	JSR	600- 1150	1.067 /He	1.5	1	1	<i>2,2,3-trimethyloxirane</i>	2015 [550]
1-Hexene	JSR	500- 1100	1.067/He	2.0	0.95	0.5, 1, 2	<i>butyloxirane, 2,3-diethyloxirane, 2,5-dimethylTHF,</i> <b>2-methyl-5-hydroxymethylTHF, 2,5-dimethyl-2,5-dihydrofuran<sup>d</sup></b>	2017 [548]
1-Octene	JSR	500- 1100	1.067/He	2.0	0.5	0.25, 0.5, 1, 2	<i>hexyloxirane,</i> <b>2-propyl-5-hydroxymethylTHF<sup>d</sup></b>	2017 [421]
1,5-Hexadiene	JSR	500- 1100	1.067/He	2.0	0.8	1, 2	<i>but-3-enyloxirane</i>	2017 [551]
Cyclohexene	RCM <sup>c</sup>	600-900	7-14 /N <sub>2</sub> -Ar-CO <sub>2</sub>	0-0.05	2.44	1	<i>1,2-epoxycyclohexane, 7-oxabicyclo[4.1.0]hept-2-ene,</i> <b>7-oxabicyclo[2.2.1]hept-2-ene</b>	2001 [521]
Cyclo-1,3-hexadiene	RCM <sup>c</sup>	600-900	7-14 /N <sub>2</sub> -Ar-CO <sub>2</sub>	0-0.05	2.59	1	<i>7-oxabicyclo[4.1.0]hept-2-ene,</i> <b>7-oxabicyclo[2.2.1]hept-2-ene</b>	2001 [521]

<sup>a</sup> only CEs with the same number of carbon atoms as the reactant are listed; <sup>b</sup> oxirane derivatives are in *italics* and THF ones in **bold**; <sup>c</sup> *T* and *P* in all RCM studies are those after compression; <sup>d</sup> *cis* and *trans*.

Except for the special case of the oxidation of cyclo-1,3-hexadiene (see further discussion), the behavior of the unsaturated hydrocarbons in Table 13 can be divided into those showing no NTC behavior (CEs (oxirane derivatives) are only produced through HO $\dot{O}$  radical epoxidation) and those displaying NTC behavior. The oxidation of the latter group of molecules produces CEs through O<sub>2</sub> addition pathways. Amongst the molecules in Table 13, which produce CEs only through HO $\dot{O}$  radical addition to the double bond, are propene, 2-methyl-2-butene, 1,5-hexadiene and cyclo-1,3-hexadiene. The first three molecules were studied in a JSR close to atmospheric pressure [549–551] and only oxirane derivatives were quantified as CE. The peak Y<sub>CE</sub> of methyloxirane (0.2±0.01%) formed in propene oxidation was observed at 925 K ( $\phi = 1$ ), that of 2,3,3-trimethyloxirane (2.7±0.27%) in 2-methyl-2-butene oxidation was recorded at 800 K ( $\phi = 1$ ), and that of but-3-enyloxirane (1.4±0.14%) in 1,5-hexadiene oxidation at 785 K ( $\phi = 1$ ). These experimental results were reproduced by simulations using kinetic models developed by the same authors with good agreements for propene and 1,5-hexadiene, but the CE from branched 2-methyl-2-butene was overpredicted by a factor of about two. The lack of NTC and the sole production of oxiranic CEs from these molecules can be explained by HO $\dot{O}$  addition being the only CE formation process, meaning that RO $\dot{O}$ /QOOH chemistry plays no role for these molecules.

During cyclo-1,3-hexadiene RCM oxidation by Lemaire *et al.* [521], the oxirane derivative 7-oxabicyclo[4.1.0]hept-2-ene was quantified with a peak Y<sub>CE</sub> of 1%, but also, despite the lack of NTC behavior, a dihydrofuran derivative, 7-oxabicyclo[2.2.1]hept-2-ene with a peak Y<sub>CE</sub> of 2.7%. Both CEs may be assumed to be formed by addition of an HO $\dot{O}$  radical to the end of one of the double bonds forming a resonantly stabilized QOOH intermediate [521], as summarized in Fig. 38. The electron delocalization in the QOOH radical intermediate allows it produce either the oxirane or the THF derivative. The THF derivative is formed with the highest yield (maximum Y<sub>CE</sub> above 2.7%). Cyclo-1,3-hexadiene RCM

oxidation has been modeled by Schönborn *et al.* [217] using a manually constructed mechanism based on the rules of the EXGAS generation algorithm [194]. This model reproduced the results obtained by Lemaire *et al.* [521] for 7-oxabicyclo[4.1.0]hept-2-ene well but postulated 7-oxabicyclo[2.2.1]hept-2-ene to further decompose in furan and ethylene. Schönborn *et al.* [217] assumed this second CE observed by Lemaire *et al.* [521] to rather be the sum of co-eluted 6-oxabicyclo[3.1.1]hept-2-ene (an oxetane derivative obtained from the reaction series starting by H-addition to the double bond and involving O<sub>2</sub> addition) and hexa-3,5-dienal, obtained by pericyclic decomposition of this oxetane derivative. Note that the absence of NTC behavior would make an O<sub>2</sub> addition reaction sequence quite unlikely.



**Fig. 38.** Possible formation pathways of CEs from cyclo-1,3-hexadiene oxidation based on the study of [521].

Among the molecules of Table 13, 1-pentene [411], 1-hexene [548], 1-octene [421], and cyclohexene [521] display NTC behavior in their oxidation and produce CEs also from pathways starting by O<sub>2</sub> addition. 1-Pentene is the smallest alkene, for which NTC behavior has been reported. The RCM results of Ribaucour *et al.* [411] indicate that cool flames are visible only between 700 and 800 K and that the not very intense NTC zone is restricted to the narrow temperature region 760–800 K. The CEs found in 1-pentene oxidation are the same as those reported in *n*-pentane oxidation, with propyloxirane, the CE obtained from HO• radical epoxidation of 1-pentene being observed in the clearly highest amount (maximum Y<sub>CE</sub> of 2.7%). Other CEs are derived from the pentyl radicals that are formed through H-atom addition

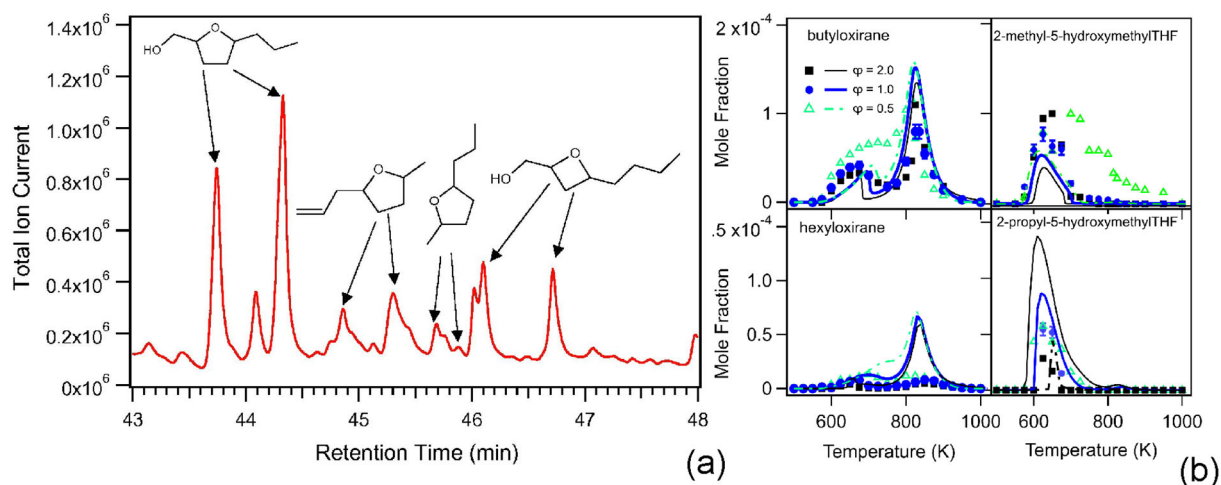


to the double bond. The model proposed by [411] predicts these experimental results reasonably well.

Measurements of IDTs during cyclohexene RCM oxidation indicate a narrow NTC range limited to 20 K. The presence of three CEs were reported, 1,2-epoxycyclohexane, a CE also produced from cyclohexane, which is the CE with the highest yield (maximum  $Y_{CE}$  of 0.6%), and the two CEs also formed in cyclo-1,3-hexadiene oxidation, which are 7-oxabicyclo[4.1.0]hept-2-ene and 7-oxabicyclo[2.2.1]hept-2-ene. The CE results were modeled by Ribaucour *et al.* [552], who showed that the most abundantly produced 1,2-epoxycyclohexane was formed via  $HO\dot{O}$  radical addition to the fuel molecule, while both unsaturated bicyclic ethers were formed by reaction series involving the abstraction of the allylic H-atom, followed by  $O_2$  addition, isomerization, and  $\dot{O}H$  elimination.

1-Hexene and 1-octene display significant reactivity during low-temperature oxidation in a JSR [421,548], with maximum observed fuel conversions below 800 K of 40% and 50% ( $\phi = 0.5$  at conditions given in Table 13), respectively. For 1-hexene, all CEs displayed in Fig. 39a were quantified. For 1-octene, quantitative data were only reported for hexyloxirane and for 2-propyl-5-hydroxymethylTHF. Other cyclic ethers were also detected but could not be quantified due to co-elution and relatively small concentrations [421]. Fig. 39a shows the chromatogram corresponding to *cis*- and *trans*-2-propyl-5-hydroxymethylTHF, together with not quantified CEs with similar retention times. Fig. 39b displays the temperature dependence of  $X_{CE}$  for the alkyloxiranes and hydroxyTHF derivatives obtained from 1-hexene and 1-octene. Detailed kinetic models, in which the kinetics of the most important reactions was updated based on theoretical calculations (*e.g.* [553–555]), were proposed for both fuels by [421,548]. However, while an overall acceptable agreement between experiments and simulations was obtained for the main products produced in the oxidation of both fuels, and for propyloxirane

and 5-methyl-5-hydroxymethylTHF in 1-hexene oxidation, CE predictions for 1-octene oxidation deviated substantially.



**Fig. 39.** CEs in C<sub>6</sub>-C<sub>8</sub> alkene JSR oxidation: **(a)** chromatogram of the CEs from 1-octene with retention times close to that of 2-propyl-5-hydroxymethylTHF (reproduced from [421] – with the permission of Elsevier); **(b)** experimental and simulated temperature dependence of the mole fractions of the alkyloxirane and hydroxy cyclic ether of the same size as the fuel under conditions given in Table 13 (drawn from the data of [421,548]). In **(b)**, *top panel*: 1-hexene oxidation, *bottom panel*: 1-octene oxidation.

The group of Qi in Hefei studied the oxidation of 1-heptene in a JSR coupled to a SVUV-PIMS detector [556]. They reported the detection of C<sub>7</sub> hydroxyCEs and unsaturated oxirane and THF derivatives. However, SVUV-PIMS does not allow to distinguish between hydroxyCEs and alkenylhydroperoxides of the same size, as was previously noted by Battin-Leclerc *et al.* [420] during their investigation of the JSR oxidation of 1-hexene also using the SVUV-PIMS setup in Hefei.

Unlike the situation for alkanes, comprehensive systematic studies of CE formation in alkene oxidation are not known. As shown in Fig. 37 and as pointed out by Battin-Leclerc *et al.* [420], three reaction types lead to CE formation: (1) HO $\dot{O}$  radicals addition to the double bond forming QOOH, which ring-closes to the corresponding oxirane derivative while releasing an  $\dot{O}H$  radical. (2) Alkenyl radical addition to O<sub>2</sub> forming a RO $\dot{O}$  radical, which isomerizes to QOOH and subsequently produces CE and  $\dot{O}H$ . In a related reaction sequence,

HO $\dot{O}$  addition to the alkenyl radical forms the corresponding hydroperoxide, which upon H-abstraction could form the  $\dot{Q}OOH$  radical. (3) Radical (or atom) addition to the double bond leading to a (substituted) alkyl radical, which proceeds through the O<sub>2</sub> addition pathway to CE. Despite the larger number of pathways to CE, the low-temperature oxidation reactivity of alkenes is lower than that of alkanes. Since the reaction types (2) and (3) are not specific to CE formation from alkenes, they will not be discussed in detail except for pointing out that the most stable radicals formed from alkenes are the resonantly stabilized allylic radicals, which form only weakly bound RO $\dot{O}$  radicals and thus subsequent reactions are hindered by barriers higher than the energy needed for redissociation [557,558]. This is one reason for the low reactivity of alkenes. Radical addition to the double bond has been discussed, *e.g.*, by Burke [549] in propene oxidation, however, their rate analysis suggests that HO $\dot{O}$  addition to the double bond is the only important CE formation pathway.

Concerning reaction type (1), Villano *et al.* [488] used the CBS-QB3 level of theory to develop rate rules for HO $\dot{O}$  addition to double bonds, which either produces  $\dot{Q}OOH$  or, as a concerted reaction, RO $\dot{O}$  radicals.  $Y_{CE}$  thus depends on the competition between these channels, although Villano *et al.* show that the concerted addition only plays a role for alkenes with a terminal double bond. The activation energies for HO $\dot{O}$  addition to double bonds follow an Evans-Polanyi relationship with a steep slope of  $> 0.9$ . This indicates a late TS, meaning that the stability of the formed products determines largely the reaction barrier. A comparison to individual rate coefficients calculated in other studies [107,142,494] shows significant uncertainty in the rate expressions for  $\dot{Q}OOH$  formation, while those for the competing concerted addition agree well. The CBS-QB3 rate coefficients of Villano *et al.* are found to be generally faster than the experimental rate coefficients measured by Baldwin *et al.* [559], even though they agree within the error limits. This calls for calculations at higher levels of theory to validate or improve the rate expressions for epoxidation. Finally, it should be noted, that

pressure-dependence is important for this reaction class [107,142,488,494,560], because the quick release of an OH radical by the chemically activated adduct forming a CE competes with collision stabilization (however only at very high pressures), and with redissociation at low pressures as shown for 1-butene in Figure 8 in the paper of Villano *et al.* [488].

### **4.3. Formation of cyclic ethers during the low-temperature oxidation of oxygenated molecules**

In addition to hydrocarbons, CEs were also quantified in the oxidation of methyl esters, ethers, alcohols and aldehydes. This will be described in the following paragraphs. Table 14 and Table 15 list the studies published since 1994 in which CE yields have been quantified. For all oxygenated compounds listed in Table 14 and Table 15, CE quantifications were obtained in JSR experiments in Nancy using GC detection, except for 2-methyl-1-butanol, diethyl and *n*-propyl ethers, which were studied in Orléans using the same method.

#### **4.3.1. Methyl esters**

Since methyl esters are considered suitable surrogates for biodiesel, their low-temperature oxidation has been thoroughly investigated in the last two decades [561]. However, only few studies address the low-temperature oxidation of methyl esters with a size comparable to those present in actual fuels (from 16 carbon atoms [47]). As is shown in Table 14, CEs were quantified in the oxidation of saturated (methyl decanoate and methyl palmitate,  $Y_{CE}$  of  $\sim 7 \pm 0.7\%$  for both fuels under stoichiometric conditions) and unsaturated (methyl-10-undecenoate and methyl oleate,  $Y_{CE}$  of  $\sim 0.7 \pm 0.07\%$  and  $\sim 0.6 \pm 0.06\%$ , respectively, under stoichiometric conditions) methyl esters. These four esters display considerable low-temperature oxidation activity including NTC behavior. In the studies listed in Table 14, no species indicating the occurrence of H- or OH- or HOO-additions on the C=O bond was found. The data obtained for the total CE yield from methyl decanoate was satisfactorily reproduced

using kinetic models developed either by the Nancy group [15] or by the Livermore group [562]. These detailed kinetic models indicate that the measured THF derivatives are formed in very similar ways as alkanes (see Part 4.1.3). This being said, it is surprising that no quantitative CE data have been reported in oxidation studies of middle sized methyl esters below 800 K, *e.g.*, methyl hexanoate oxidation in a FR [563] or methyl octanoate oxidation by Togbé *et al.* [564] and methyl heptanoate oxidation by Dayma *et al.* [565] in a JSR. No CE measurement can be found in this last paper, but it is noted that their simulation predicted 67% of the fuel to be consumed by pathways yielding CEs. In their recent study of ozone-initiated oxidation of methyl hexanoate in a JSR with SVUV-PIMS, Rousso *et al.* [566] reported at temperatures starting from 450 K a signal at  $m/z$  value that corresponds to CEs. This signal was not observed in the absence of ozone. However, this signal might also be due to carbonyl products, the formation of which might be favored at these low temperatures through disproportionation of ROO radicals.

In their recent JSR study of methyl heptanoate oxidation using SVUV-PIMS, Zhai *et al.* [567] did not mention any MS signal at  $m/z$  corresponding to CEs, but only reported the mole fractions of unsaturated C<sub>4</sub>-C<sub>6</sub> methyl esters pointing out that they derived from CE decomposition.

Molecules including both THF and ester groups were quantified by the Nancy group [15] during the JSR oxidation of methyl decanoate. The temperature dependence of their mole fraction was predicted with acceptable accuracy by their model, which included a rather detailed sub-mechanism of ester group substituted CE consumption reactions via H-abstractions with taking into account the ester function location (inside and outside the CE ring).

Table 14. Studies of the oxidation of saturated and unsaturated methyl esters and aldehydes, during which CE isomers have been quantified.

Fuel		$T$ (K)	$P$ (bar)/ diluent	$\tau$ (s)	$X^{\circ}_{\text{fuel}}$ (%)	$\phi$	Quantified CE isomers <sup>a,b</sup>	Year & Ref.
<b>Methyl decanoate</b>	JSR	500-1000	1.07 /He	1.5	0.21	1	2-methylhexanoateTHF, 2-methyl-5-methylpentanoateTHF, 2-ethyl-5-methylbutanoateTHF, 2-propyl-5-methylpropanoateTHF, 2-butyl-5-methylethanoateTHF, 2-pentyl-5-methylmethanoateTHF, 5-octyl-1,3-dioxolan-4-one	2010 [15]
<b>Methyl palmitate + <i>n</i>-decane<sup>c</sup></b>	JSR	550-1100	1.07 /He	1.5	0.2 <sup>d</sup>	1	methyl 4-(5-methyloxolan-2-yl)undecanoate + + sum of (methyl-11-(5-methyloxolan-2-yl)undecanoate, methyl-10-(5-ethyloxolan-2-yl)decanoate, methyl-9-(5-propyloxolan-2-yl)nonanoate, methyl-9-(5-butyloxolan-2-yl)octanoate, methyl-9-(5-pentyloxolan-2-yl)heptanoate, methyl-9-(5-hexyloxolan-2-yl)hexanoate, methyl-9-(5-heptyloxolan-2-yl)pentanoate methyl-9-(5-octyloxolan-2-yl)butanoate methyl-9-(5-nonyloxolan-2-yl)propanoate methyl-9-(5-decyloxolan-2-yl)acetate methyl-9-(5-undecyloxolan-2-yl)formate methyl-11-(oxolan-2-yl)dodecanoate 5-tetradecyl-1,3,dioxolan-4-one2-yl)formate)	2009 [415]
<b>Methyl-10-undecenoate</b>	JSR	500-1100	1.07 /He	1.5	0.21	0.5, 1, 2	methyl 9-(oxiran-2-yl)nonanoate, <b>methyl 7-[4-(hydroxymethyl)oxetan-2-yl]heptanoate</b> , methyl 2-[5-but-3-en-1-yl-THF-2-yl]propanoate, methyl 6-(5-methylTHF-2-yl)hexanoate, <b>methyl 6-[5-(hydroxymethyl)THF-2-yl]hexanoate</b>	2017 [568]
<b>Methyl oleate+ <i>n</i>-decane</b>	JSR	500-1100	1.07 /He	1.5	0.2 <sup>d</sup>	1	methyl 8-(3-octyloxiran-2-yl)octanoate	2010 [416]
<b><i>n</i>-Butanal</b>	JSR	500-1100	1.067 /He	2.0	0.5	0.25, 1, 2	<i>methyloxirane</i>	2019 [569]
<b><i>n</i>-Pentanal</b>	JSR	500-1100	1.067 /He	2.0	0.5	0.25, 1, 2	<i>THF, ethyloxirane, 2,3-dimethyloxirane</i>	2019 [569]
<b><i>n</i>-Hexanal</b>	JSR	475-1100	1.067 /He	2.0	0.5	0.25, 1, 2	<i>2-MTHF</i> , 6-methyl-tetrahydropyranone, 5-ethyl-dihydrofuranone	2017 [293]

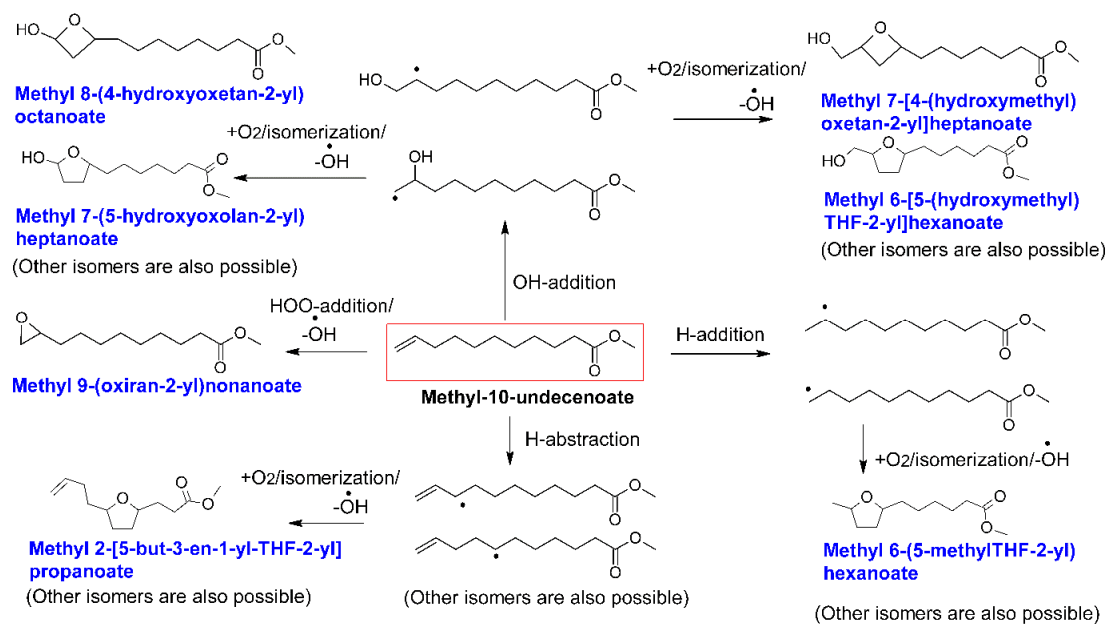
<sup>a</sup> only CEs including a saturated alkyl chain, with the same number of carbon atoms (n) as the reactant or with n-1 atoms of carbon (in *italics* in the list) are listed, <sup>b</sup> hydroxy CEs in **bold**, <sup>c</sup> in Table 4, except methyl-9-(5-undecyloxolan-2-yl)formate, methyl-11-(oxolan-2-yl)dodecanoate and methyl 11-(5-methyloxolan-2-yl)undecanoate, C<sub>17</sub> CEs are shown under the lumped name “2-R-5-(MeOOCR’)THF”, <sup>d</sup> 74% *n*-decane/26% ester.

**Table 15.** Studies of the oxidation of linear mono- and di-oxygenated ethers and saturated and unsaturated alcohols, during which CE isomers have been quantified.

Fuel		$T$ (K)	$P$ (bar)/ diluent	$\tau$ (s)	$X^{\circ}\text{fuel}$ (%)	$\phi$	Quantified CE isomers <sup>a</sup>	Year & Ref.
Diethylether	JSR	450-1250	1, 10 /N <sub>2</sub>	0.07 - 0.7	0.1	0.5, 1, 2	2-methyl-1,3-dioxolane	2018 [570]
		400-1100	1.07 /He	2.0	1	1	2-methyl-1,3-dioxolane	2019 [22]
		400-1100	2.5-10 <sup>b</sup> /He	2.0	0.5	1	2-methyl-1,3-dioxolane	2020 [453]
Di- <i>n</i> -propyl ether	JSR	450-950	10 /N <sub>2</sub>	0.7	0.1	0.5	2-(propoxymethyl)oxirane, 2-ethyl-4-methyl-1,3-dioxolane <sup>c,d</sup>	2021 [571]
Di- <i>n</i> -butyl ether	JSR	435-1100	1.07 /He	2.0	1	1	oxirane, methyloxirane, 2-THFFBE, 4-ethyl-2-propyl-1,3-dioxolane <sup>d</sup> , 4-methyl-2-propyl-1,3-dioxane	2019 [422]
Dimethoxy methane	JSR	500-1100	1.07 /He	2.0	1	0.25, 1, 2	2-methoxy-1,3-dioxetane	2018 [433]
<i>n</i> -Butanol	JSR	500-1100	1.07 /He	2.0	0.5	0.5, 1.0, 2.0	THF	2020 [572]
<i>n</i> -Pentanol	JSR	500-1100	1.07 /He	2.0	0.5	0.5, 1.0, 2.0	<i>oxirane, methyloxirane</i>	2020 [572]
<i>n</i> -Hexanol	JSR	500-1100	1.07 /He	2.0	0.5	0.5, 1.0, 2.0	5-ethyl-dihydrofuranone	2020 [572]
2-Methyl-1-butanol	JSR	700-1200	10 /N <sub>2</sub>	0.7	0.1	0.5, 1.0, 2.0, 4.0	2,3-dimethyloxirane	2016 [573]
3-Methyl-2-buten-1-ol	JSR	500-1100	1.07 /He	2.0	0.8	0.5, 1, 2	3-methylfuran	2016 [573]

<sup>a</sup> When they are present, only the saturated CEs with the same carbon number as the fuel are listed (other CEs are in *italics*), <sup>b</sup> at 5 bar: neat DEE, at other pressures: DEE blended with *n*-pentane (equimolar mixture), <sup>c</sup> only maximum mole fractions are reported; <sup>d</sup> *cis* and *trans*.

While there is not yet any modeling study to support this assumption, CE formation chemistry in the oxidation of unsaturated methyl esters appears experimentally to be similar to that proposed for alkenes (see Part 4.2.3), meaning that oxirane formation starts with HO $\dot{O}$  radical addition to the double bond in the fuel and subsequent cyclization and  $\dot{O}H$  radical release. This proposed mechanism is supported by the presence of methyl 9-(oxiran-2-yl)nonanoate and methyl 8-(3-octyloxiran-2-yl)octanoate in the JSR oxidation of methyl-10-undecenoate and methyl oleate, respectively. In methyl-10-undecenoate oxidation, the formation of methyl 7-[4-(hydroxymethyl)oxetan-2-yl]heptanoate and methyl 6-[5-(hydroxymethyl)THF-2-yl]hexanoate was assumed by Meng *et al.* [568] to be initiated by  $\dot{O}H$  addition to the double bond, the formation of methyl 6-(5-methylTHF-2-yl)hexanoate starts with H addition, and the formation of methyl 2-[5-but-3-en-1-yl-THF-2-yl]propanoate is initiated by an H-abstraction reaction. These formation pathways are summarized in Fig. 40.

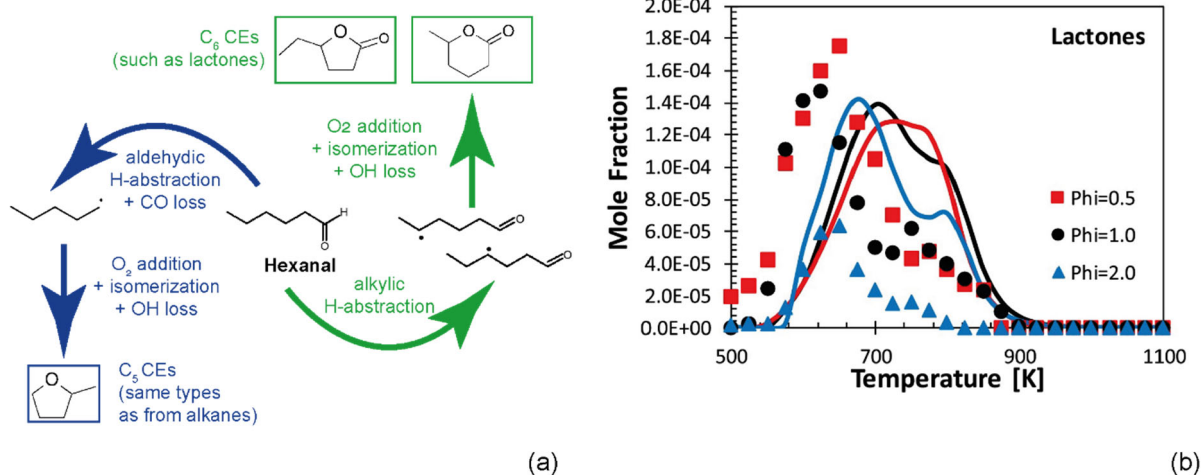


**Fig. 40.** Examples of possible formation pathways of CEs during the low-temperature oxidation of methyl-10-undecenoate.



### 4.3.2. Aldehydes

Aldehydes are not part of automotive fuels, but they are notable products of alkane and alkene oxidation. As is shown in Table 14, CEs were quantified during the oxidation of the three linear C<sub>4</sub>-C<sub>6</sub> aldehydes. During their JSR low-temperature oxidation, these three compounds display a higher reactivity than the corresponding alkanes with the same number of carbon atoms. The oxidation of all three aldehydes exhibits strong NTC behavior [293,569]. The CEs detected contain one carbon atom less than the aldehyde. As illustrated in Fig. 41a, these CEs are formed from the alkyl radical obtained after abstraction of the aldehydic H-atom followed by CO loss. The activation energy in the rate expressions for H-abstraction of the aldehydic H-atom is estimated to be 4.5 kcal/mol lower than that for the analogous H-abstraction reaction from a primary H-atom of alkanes [574]. In the case of *n*-hexanal, lactones (see mole fractions in Fig. 41b) can also be produced by O<sub>2</sub> addition to the radicals yielded by abstraction of a non-aldehydic H-atom. In the case of *n*-pentanal, 2,3-DHF and furan, obtained by dehydrogenation of the THF product were also detected, however in yields below 1% [575]. The peak Y<sub>CE</sub> was observed at 800 K for *n*-butanal (methyloxirane, 0.5±0.05%,  $\phi = 0.5$ ), 725 K for *n*-pentanal with THF being the major CE (4.5±0.45%,  $\phi = 0.5$ ), and at 700 K for *n*-hexanal with 2-MTHF being the major CE (5.7±0.9%,  $\phi = 0.5$ ) followed by 5-ethyl-dihydrofuranone with about half the yield of 2-MTHF. CE formation is favored under stoichiometric and lean mixtures.



**Fig. 41.** CE formation from aldehydes: **(a)** pathways from the aldehyde fuel (CEs in insert are those quantified for *n*-hexanal by [293], only reactions leading to CEs are displayed), **(b)** experimental (of [293]) and simulated (Milano model [569]) temperature dependence of lactone mole fraction (sum of both lactone isomers) during the JSR oxidation of *n*-hexanal – reproduced from Ref. [569].

Together with their experimental study, Rodriguez *et al.* [293] proposed a detailed kinetic model for *n*-hexanal oxidation mainly generated by the EXGAS generation algorithm [194], considering a virtual blend of *n*-hexanal and *n*-pentane to better account for the chemistry of the *n*-pentyl radical, and predicting well the formation of the three observed CE isomers. Based on their experience with smaller aldehydes [574], Pelucchi *et al.* [569] proposed kinetic models for the JSR oxidation of the three linear aldehydes based on the lumping approach developed in Milano [576]. Overall reasonable predictions of the CEs of the same type as from alkanes were obtained for the three fuels, as well as for the lactones yields in *n*-hexanal oxidation, as is shown in Fig. 41b, which presents the comparison experiments/simulations for the total sum of lactones using the lumped model.

#### 4.3.3. Saturated and unsaturated alcohols

The interest in studying the low-temperature oxidation of large saturated alcohols lies in the fact that they are amongst the newly proposed biofuels with LHV's higher than ethanol [14]. No low-temperature reactivity was observed during the JSR oxidation of the *n*-alcohols listed in

Table 15 [573] at 1 bar, even though about 40% maximum conversion was obtained during that of *n*-hexanol at 10 bar in Orléans ( $T = 650$  K,  $\phi = 0.5$ ,  $t = 0.7$  s, 0.1% initial fuel) [577]. Except for oxirane and methyloxirane, which originated from the abundantly produced ethylene and propene, respectively, and which were observed during the JSR oxidation of the three listed *n*-alcohols by Pelucchi *et al.* [572], only low amounts of CE formation were reported in the literature on alcohol oxidation. Specifically, no fuel-specific CE (containing fuel's OH group) were experimentally quantified even though CE pathways with low energy barriers exist. Hydroxy CEs (*e.g.* 2-hydroxy-3-ethyloxirane), the formation of which was postulated by Welz *et al.* [578] during their study of *n*-butanol oxidation, could not be detected in a JSR experiment [572]. Due to possibly important fragmentation of hydroxyCEs, only a weak signal was recorded at  $m/z$  88 ( $C_4H_8O_2$ ) during the chlorine atom-initiated reaction investigated in FRs using SVUV-PIMS by [578]. In recent modeling studies, some fuel-specific CEs were predicted to form in non-negligible mole fractions (up to a magnitude of  $10^{-4}$ ) during the oxidation of *n*-butanol or *n*-pentanol [572,579]. Rotavera and coworkers [16,579] recently demonstrated a profound influence of the branching ratio of H-abstractions from *n*-butanol by OH on the formation of 2-hydroxytetrahydrofuran. However, this CE has not been experimentally detected from *n*-butanol oxidation. Further experiments on alcohol oxidation are needed to resolve this question [16,579].

Amongst the CEs formed from *n*-alcohols listed in Table 15, THF was experimentally quantified in *n*-butanol oxidation and 5-ethyl-dihydrofuranone in *n*-hexanol oxidation. Since alcohol oxidation produces the corresponding aldehydes as major products, it is possible that the two observed CEs are actually products of these aldehydes and not of the alcohols. This interpretation is supported by the fact that the kinetic model for alcohol oxidation of Milano [572] did not predict these CEs but otherwise performed well in simulating most other oxidation products including oxirane and methyl oxirane. No CE formation was reported in the oxidation

of *n*-hexanol in a JSR at 10 bar studied at Orléans [577]. Even for *n*-octanol oxidation, which exhibits strong low-temperature reactivity and notable NTC behavior, no CE formation was reported either in ST (20 bar, with similar ignition performance as *n*-octane) nor in JSR (10 bar with a start of reactivity at 550 K) experiments. Instead, high amounts of C<sub>2</sub>-C<sub>7</sub> aldehydes [580] were formed.

Looking at branched saturated alcohols, 2,3-dimethyloxirane was quantified as the sole CE in the JSR study of the oxidation of 2-methyl-1-butanol in Orléans [581]. No NTC behavior was reported for this fuel and CE formation was assumed to be caused by HO $\dot{O}$  epoxidation of 2-methyl-1-butene, a product obtained in large quantities under the conditions of that study. The model proposed by [581] underestimates the formation of 2-methyl-1-butene by a factor of about two.

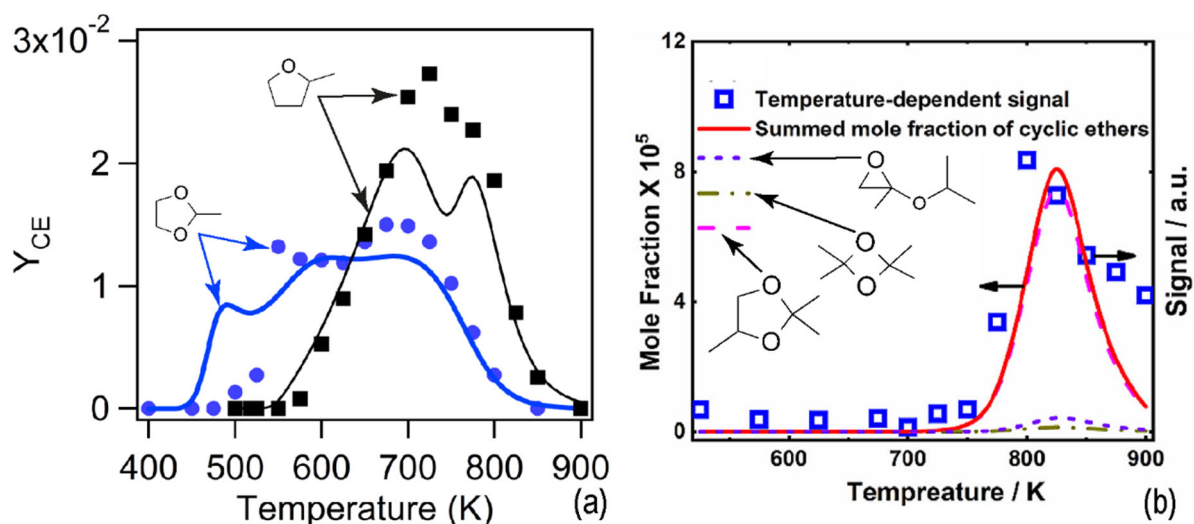
Concerning unsaturated alcohols, 3-methylfuran (peak Y<sub>CE</sub> of 1.4% at 850 K,  $\phi = 1$ ) was quantified in the JSR oxidation of 3-methyl-2-buten-1-ol (commonly named prenil) above 800 K by De Bruycker *et al.* [573]. A small NTC zone was observed for this fuel under lean conditions. This unsaturated CE, the formation of which is well predicted by the model developed by [573], is formed through 3-methyl-2-butenal, a major product of prenil oxidation, by abstraction of a primary H-atom followed by cyclization. During the study of the chlorine atom-initiated low-temperature oxidation of prenil in a FR (550 K, 8 Torr) using SVUV-PIMS, Welz *et al.* [582] recorded a strong signal at *m/z* 82 (C<sub>5</sub>H<sub>6</sub>O) and tentatively assigned it as 3-methylfuran. The slow rise of the 3-methylfuran signal suggests that it was formed as a secondary product.

#### ***4.3.4. Linear, branched and cyclic ethers***

As reviewed by Cai *et al.* [583], acyclic ethers have recently attracted considerable attention as potential diesel fuel substitutes or additives in CI engines. Table 15 shows that CE isomers were

quantified in the JSR oxidation of C<sub>4</sub>, C<sub>6</sub>, C<sub>8</sub> linear symmetrical mono-oxygenated ethers, as well as of dimethoxymethane, a di-oxygenated ether. The low-temperature oxidation of mono-oxygenated ethers is remarkable because the reactivity starts at temperatures as low as 450 K and displays under some conditions a double NTC region [22,433,584]. Some of the observed CEs contain two ring oxygens, *e.g.* dioxetane derivatives, dioxolane derivatives or dioxane derivatives.

The low-temperature oxidation of *diethyl ether* was studied as a neat compound at 1 bar [22,570], 5 bar [453] and 10 bar [570], and in a mixture with *n*-pentane between 2.5 and 10 bar. Only 2-methyl-1,3-dioxolane was reported as CE product. Fig. 42a shows that 2-methyl-1,3-dioxolane is formed at lower temperature (about 100 K) than 2-MTHF. This coincides with the fact that diethyl ether oxidation occurs at lower temperature than *n*-pentane oxidation. Above 600 K, the conversion of  $\dot{Q}OOH$  radical to CE competes with the formation of carbonyl compounds. Note that the latter are not only formed through the typical  $[RR'C\cdot OOH] \rightarrow RR'C=O + \dot{O}H$  decomposition mechanism but also through fast  $\beta$ -scission of the  $C\cdot OR$  moiety ( $\rightarrow C=O + R\cdot$ ). The high tendency of carbonyl compound production leads to lower CE yields. In diethyl ether oxidation (for 2-methyl-1,3-dioxolane, the peak  $Y_{CE}$  is  $1.5 \pm 0.2\%$ ) the maximum CE yield is clearly lower than in *n*-pentane oxidation (peak  $Y_{2-MTHF}$  is  $2.7 \pm 0.4\%$ ).



**Fig. 42.** CE formation during ether JSR oxidation: **(a)** diethyl ether: temperature dependence of the  $Y_{CE}$  of 2-methyl-1,3-dioxolane and that of 2-MTHF during *n*-pentane oxidation in JSR at 5 bar (drawn from data taken in [453]). The relative uncertainties of the  $Y_{CE}$  are 15%; **(b)** diisopropyl ether: experimental MS signal and simulations of corresponding CE mole fractions (Reproduced from Ref. [585] with permission of Elsevier).

Serinyel *et al.* [586] in Orléans were the first to study *di-n-propyl ether* oxidation in a JSR over a temperature range from 450 to 1250 K and pressures of 1 and 10 bar, with an initial fuel mole fraction of 0.1% ( $\phi = 0.5, 1, 2$  and 4) and constant residence times (70 and 700 ms, respectively). While they observed very strong low-temperature reactivity even below 500 K coupled with strong NTC behavior, CEs were only detectable in trace amounts. A subsequent study by the same group [571] focused more on hydroperoxide characterization using high-resolution MS (orbitrap) or liquid chromatography coupling. Nevertheless Belhadj *et al.* [571] also quantified CEs in GC spectra and report a maximum  $Y_{CE}$  of  $0.4 \pm 0.06\%$  for 2-(propoxymethyl)oxirane and of  $\sim 6 \pm 0.9\%$  for 2-ethyl-4-methyl-1,3-dioxolane. For comparison, the maximum  $Y_{CE}$  of 2-ethyl-5-methylTHF obtained from *n*-heptane under similar conditions was  $\sim 7.5 \pm 0.8\%$  [295]. Belhadj *et al.* [571] also observed a signal at  $m/z$  116 in their mass spectra, which is thought to arise from a CE with the same number of carbon atoms as the fuel. No comparisons between experimental data and model predictions were presented for the detected CE mole fractions. Finally, Fan *et al.* [587] investigated *di-n-propyl ether* oxidation in

a JSR at near-atmospheric pressure using PI-MBMS at Lawrence Berkeley National Laboratory and also observed a signal at  $m/z$  116 that was identified to be mainly 2-ethyl-4-methyl-1,3-dioxolane and 2-propoxyoxetane according to the recording PIE curves; no quantification was performed.

Four CE isomers containing 8 carbon atoms were quantified in the di-*n*-butyl ether JSR oxidation study in Nancy. These are 2-THFFBE, *cis* and *trans* 4-ethyl-2-propyl-1,3-dioxolane (separated but with MS not allowing to distinguish them), and 4-methyl-2-propyl-1,3-dioxane [422]. In the same paper, the  $m/z$  144 signal, which is assigned to the sum of CEs, was followed by MS in a FR at Bielefeld. Comparisons between experimental results for CEs in both reactors and simulation using the models developed by Cai *et al.* [588] and by Thion *et al.* [584] indicate a better performance of the model by Cai *et al.* [588] that was developed to reproduce ignition and flame speed data. Thion *et al.* [584] studied the di-*n*-butyl ether low-temperature oxidation in a JSR study at Orléans at 1 and 10 bar. They reported the formation of 2,3-DHF but did not mention any CEs with 8 carbon atoms amongst the observed products. However, using the same experimental methodology as in their work on di-*n*-propyl ether [571], the group of Dagaut [296] reported a signal at  $m/z$  144 related to C<sub>8</sub> CEs not only in the effluent of a JSR (560 K and 10 bar), but also in gas samples from a RCM (570 K and 7 bar).

No CE isomers were quantified in the studies of the oxidation of branched ethers. However, the temperature dependence of the signal at  $m/z$  116 corresponding to CEs or ketones with the same number of carbon atoms as the fuel was reported in the JSR study of diisopropyl ether oxidation using SVUV-PIMS [585]. No NTC region was observed for this fuel. From comparison between measured and calculated PIEs, the  $m/z$  116 signal was attributed mainly to 2-methyl-2-[(propan-2-yl)oxy]oxirane, 2,2,4,4-tetramethyl-1,3-dioxetane, and 2,2,4-trimethyl-1,3-dioxolane. Ketone formation was not considered. The shape of the temperature dependence of the  $m/z$  signal at 116 agrees well with the sum of the mole fractions

of these three CEs predicted using a kinetic model developed by the authors, with 2,2,4-trimethyl-1,3-dioxolane being the major product as is shown in Fig. 42b.

Concerning dioxygenated ethers, a low yield of *2-methoxy-1,3-dioxetane* (peak  $Y_{CE}$  of  $0.8 \pm 0.08\%$  at 510 K,  $\phi = 0.25$ ) was reported by Vermeire *et al.* [433] in the JSR oxidation of 1,2-dimethoxymethane, which started to react around 650 K and displayed weak NTC behavior. CE formation was simulated with a kinetic model developed by the authors based on theoretical calculations. The reaction path analysis indicates the importance of the competition of the CE formation and the CO bond breaking reactions in the consumption of the QOOH radical. Both reactions proceed through transition states with an energy barrier of 125 kJ/mol (29.9 kcal/mol). The oxidation of dimethoxymethane was also studied by Marrodán *et al.* [589] in a FR (at temperatures from 373 to 1073 K at 20, 40, 60 bar) but CEs were not detected.

In their JSR study of *1,2-diethoxyethane* oxidation at 10 bar with GC-FID diagnostics at Orléans, Sun *et al.* [385] reported no CE detection. However, when using SVUV-PIMS at 1 bar at Berkeley, the signal at  $m/z$  104.05 ( $C_4H_8O_3$ ) was assigned to 4-methoxy-1,3-dioxolane based on the calculated IE (9.68 eV) which agreed with the measured value. Also, the measured  $m/z$  104 signal profile shape agrees well with the predicted profile for 4-methoxy-1,3-dioxolane calculated using the kinetic model developed by the authors.

Cyclic ethers as fuels are discussed in detail in Part 5. CEs as products of cyclic ether oxidation were only quantified in *THF* oxidation; those are 2,3-DHF and 2,5-DHF, which were quantified by GC during JSR experiments in Nancy [282] and detected in RCM in Lille. The formations of both CEs was reasonably well reproduced using the model of Fenard *et al.* [283]. They were formed through HO $\dot{O}$  elimination from the two possible THF-yl peroxy radicals. In their study of THF oxidation in a JSR combined with high-resolution MS analytics, Belhadj *et al.* [590] recorded signals at the  $m/z$  corresponding to 2,3-DHF and 2,5-DHF, but also to 2-hydroperoxyTHF, to 2-hydroperoxy-3,4-DHF and to the KHP isomers deriving from THF.



THF low-temperature oxidation can also yield bicyclic ethers. However, for  $\alpha$ - $\dot{Q}OOH$  (which is a hydroperoxyfuryl radical in which the hydroperoxy group is attached to the carbon ( $C_\alpha$ ) next to the ether oxygen), ring-opening proceeds through lower barriers than oxirane (or oxetane) ring formation, which effectively prevents bicyclic ethers to be formed. Very little  $\beta$ - $\dot{Q}OOH$  (which is a hydroperoxyfuryl radical in which the hydroperoxy group is attached to the carbon next to  $C_\alpha$ ) is formed due to the preferred H-abstraction from the  $\alpha$  site. According to the PES presented by Fenard *et al.* [283] bicyclic diether formation starting from the  $\beta$ - $\dot{Q}OOH$  radical proceeds through energetically competitive channels suggesting that they could be formed and should be looked for in future experiments.

#### 4.4. Conclusion

The review on CE formation during the low-temperature oxidation of a large range of fuels presented in Part 4 has allowed us to emphasize the enormous progress made since 1994 in establishing quantitative experimental data for these products. JSRs and RCMs coupled with GC have been the most commonly used tools for these measurements, surpassing, except when hydroperoxides were to be considered, MS for discriminating the generally large number of obtained isomers. While CEs were frequently detected from RCM experiments fueled with hydrocarbons, they were, except for THF, rarely mentioned in studies of oxygenated fuels in compression devices. In JSRs, CEs were experimentally quantified not only from alkanes, but also from a wide range of unsaturated, cyclic or oxygenated fuels. CEs were mainly observed from fuels displaying a significant low-temperature reactivity and a notable NTC zone. However, due to  $HO\dot{O}$  epoxidation (oxirane derivative formation), CEs are also formed in the oxidation of dienes, such as 1,3-hexadiene or cyclo-1,3-hexadiene, or from 2-methyl-1-butanol, which do not react via the peroxy radical pathway. Concerning biofuel molecules, CE are notable primary products of the oxidation of methyl esters, aldehydes and linear ethers. Surprisingly, attempts to find fuel-specific CEs, which would still contain the alcohol group, in

the low-temperature oxidation of alcohols have not been successful. The currently experimentally detected CEs in alcohol oxidation originate from secondary chemistry. Both, for hydrocarbon and oxygenated fuels, significantly more CE formation data are available for linear molecules than for branched ones. Only a limited numbers of studies exist that deal with fuels containing more than 8 carbon atoms.

This review shows that CEs are usually present in relatively small amounts. The maximum total  $Y_{CE}$  of  $\sim 29 \pm 2.9\%$  reported for *n*-hexane JSR oxidation [419] is an exception, but generally the  $Y_{CE}$  is below 10% for most studied cases. This can be explained by the fact that CE are faster consumed through H-abstraction reactions than most fuel molecules due to the low C–H bond strength in  $\alpha$ -position to the ether oxygen, as will be discussed in Part 5. Flow rate analyses below 800 K mostly show a dominant contribution of fuel consumption via CE formation in competition with KHP production. Therefore, the measurement and the prediction of the distribution of CE isomers is of crucial importance for the accurate simulation of fuel auto-ignition.

The possible formation of several types of CEs, which are postulated by models, needs to be more thoroughly investigated. This is the case of hydroperoxyCEs, especially oxirane derivatives, or of hydroxyCEs which are predicted to be formed in notable amounts during the oxidation of alkanes and of alkenes, respectively. Regular MS analysis cannot discriminate hydroperoxyCEs from KHPs, or hydroxyCEs from alkenyl hydroperoxides. It is also difficult to identify the unique products from hydroperoxyCEs because the most important consumption pathway for hydroperoxyCE consumption could be the O–OH scission followed by  $\beta$ -scission leading to the formation of an aldehyde and a radical (hydroperoxyCE  $\rightarrow$  OH+aldehyde+radical). However, the same aldehydes can be also formed from the corresponding KHPs.

Although the CE formation reactions in low-temperature oxidation of alkanes have been systematically studied at several levels of theory and it is agreed that the rate expressions depend both on the nature of the radical site and that of the hydroperoxy group carrying carbon site, there is still severe uncertainty on the exact values of the rate coefficients. Comparisons of various proposed rate rules show substantial variations in the pre-exponential factors and in the reaction barriers, leading - as can be seen in Fig. 31 - to uncertainties of one order of magnitude or more. In order to avoid commonly practiced adjustments of these rate expressions in model development, new studies at high levels of theory are needed to propose improved rate expressions with high accuracy. This need is even greater when fuels other than alkanes are concerned.

The progress in the theoretical calculations related to low-temperature oxidation channels has allowed a noticeable refinement of the CE related rate constants, however the performances of the recent models in predicting the reviewed experimental data concerning CEs are still significantly poorer than for other products (*e.g.* alkenes or aldehydes). Moreover, because these are steady-state measurements, the mole fractions reported for CEs in the studies listed in Part 4 reflect a balance between formation and consumption rates. A good understanding of CE consumption reactions is crucial for an accurate assessment for their formation kinetics. Therefore, Part 5 reports on the studies related to CE consumption.

## 5. KINETICS OF THE DEGRADATION OF CYCLIC ETHERS

Whether formed in low-temperature oxidation or used as biofuels, a good understanding of the chemistry leading to CE consumption is essential and needs to be incorporated into sophisticated combustion models for fuels and biofuels. In this part, experimental, theoretical and kinetic modeling studies related to the degradation chemistry of CEs are reviewed. A recent paper by Leitner *et al.* [8] reviewed different aspects of the combustion chemistry of potential biofuels (see Table 1 in Part 1), *e.g.* IDTs or pollutant formation in flames, with the objective to identify appropriate candidates. The aim of Part 5 is broader and provides a more comprehensive analysis of the consumption chemistry of all CE families.

### 5.1. General overview of cyclic ether reaction kinetics

The basic reactions of CEs are discussed in this part. Given that unsaturated CEs and in particular aromatic ones differ substantially in their reactivity from saturated CEs, both groups are discussed separately starting with saturated CEs.

#### 5.1.1. Saturated cyclic ethers

Saturated CEs either decompose via unimolecular reactions such as ring-opening caused by bond scissions similar to those of cycloalkanes, or via bimolecular H-abstraction reactions forming the corresponding CE radicals, which might react by  $\beta$ -scission – possibly preceded by isomerization steps –, or bimolecularly, *e.g.*, by adding to molecular oxygen. For the sake of keeping this part short, all these reactions will be discussed only briefly using examples rather than attempting to provide a complete account of all relevant studies.

##### 5.1.1.1. H-abstraction reactions

In the low-temperature oxidation regime below 900 K, in which CE yields can reach high levels, CEs are mainly consumed by H-abstraction reactions. At the lowest temperatures the

H-abstraction reactions by  $\dot{\text{O}}\text{H}$  and  $\text{HO}\dot{\text{O}}$  radicals dominate. The importance of  $\dot{\text{O}}\text{H}$  as an abstracting radical results from (a) low activation energies and (b) the unique role of this radical in the chain propagating and branching chemistry of low-temperature oxidation.  $\text{HO}\dot{\text{O}}$  radicals are also primary products formed in rather high concentrations, which explains that H-abstraction reactions by  $\text{HO}\dot{\text{O}}$  are relevant. For example, according to the THF model by Fenard *et al.* [283], in a JSR at atmospheric pressure and 600 K 90% of THF is consumed by  $\dot{\text{O}}\text{H}$  radicals and about 10% by  $\text{HO}\dot{\text{O}}$  radicals. At higher temperatures, H atoms,  $\dot{\text{C}}\text{H}_3$  and other radicals become more abundant and their H-abstraction reactions gain importance.

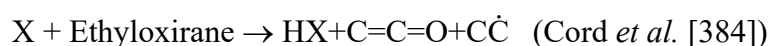
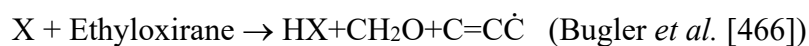
Even though H-abstraction reactions from CEs appear in every newer kinetic model dealing with low-temperature oxidation chemistry, these reactions are not as thoroughly studied as one would think. Most experimental studies date back to before 2000, *e.g.* [591–601], while rather few recent experimental studies are known [602–607]. A few examples of theoretical studies of specific molecules are H-abstractions from substituted THF by, *e.g.*, Simmie [90], Chakravarty and Fernandes [608] and Illés *et al.* [607], from THP by Tran *et al.* [196], from 1,4-dioxane and 1,3,5-trioxane by Saheb and Bahadori [609], and from lactones by Barnes *et al.* [604] and De Bruycker *et al.* [259].

Often in kinetic modeling the rate coefficients of these reactions are estimated with generic rate rules [195,466,498,508,610]. Even in recent models, the rules used are surprisingly simple, *e.g.* Bugler *et al.* [466] assign the same rate coefficients to H-abstraction reactions from ethyloxirane by H-atom, O-atom and  $\dot{\text{O}}\text{H}$  radical. Other models account for chemical and structural differences, *e.g.* C–H bond strength variations in CE (discussed later), which are caused by the presence of the ether oxygen. C–H moieties in an  $\alpha$ -position to the ether oxygen atom are particularly weak due to resonance stabilization of the corresponding radical by the oxygen, while C–H sites farther away are “regular”, meaning that those sites in CE have bond strengths comparable to those of their cycloalkane counterparts (see later). Simmie [90],

studying reactions of THF, 2-MTHF and 2,5-DMTHF, found a good correlation between activation energies for H-abstractions by H-atoms and CH<sub>3</sub> radicals and the enthalpies of reaction (Evans-Polanyi relationship), which provides an easy way to incorporate the reactivity differences into rate expressions.

The ring size also affects the C–H stability because the ring strains of the parent and radical differ and this difference translates to variations in the H-abstraction rate coefficients. Furthermore, the ether oxygen atom may act as acceptor of a hydrogen bond facilitating formation of a pre-complex prior to the abstraction process. For example, Rotavera and Taatjes [16] showed that at low-temperature the H-abstraction reaction by  $\dot{\text{O}}\text{H}$  radical from THF is faster than that from cyclopentane, which was explained by the formation of such a complex.

Some CE radicals produced by H-abstraction reactions are inherently unstable and rapidly decompose to open-chain isomers or bimolecular products. This fact was used by Cord *et al.* [384] and Bugler *et al.* [466] to reduce the model by lumping the H-abstraction with the decomposition step to a single reaction. For example (X=abstracting species),



In addition to the different products assumed in both models for this specific reaction, lumping may lead to a general problem of “mechanism truncation error” as the group of Rotavera pointed out [395,511]. This is particularly true if larger CE radicals with less ring strain are produced, *e.g.* THF radicals, but *e.g.* Lopez *et al.* [611] even treat H-abstraction from the smallest CE, oxirane, as a two-step process with subsequent chemistry of the oxiranyl radical. The latter implementation of H-abstraction reactions from CEs allows for the possibility that the CE radical might be able to add to oxygen at high oxygen concentrations.

Surprisingly, several recent kinetic model, *e.g.* [384,466] contain lumped H-abstraction reactions even for large CEs such as THF, meaning that no THF-yl radical is considered

(THF-yl includes both the THF-yl-2 and THF-yl-3 radicals). The discussion of THF chemistry (given in Part 5.1.1.4) demonstrates the importance of THF-yl radical oxidation chemistry and therefore the need to include CE radical species into kinetic models. At this stage, it should only be mentioned that uncertainties in H-abstraction reactions from THF are considered a likely cause for the failure to correctly predict  $\beta$ -KHP yields in the low-temperature THF oxidation [612].

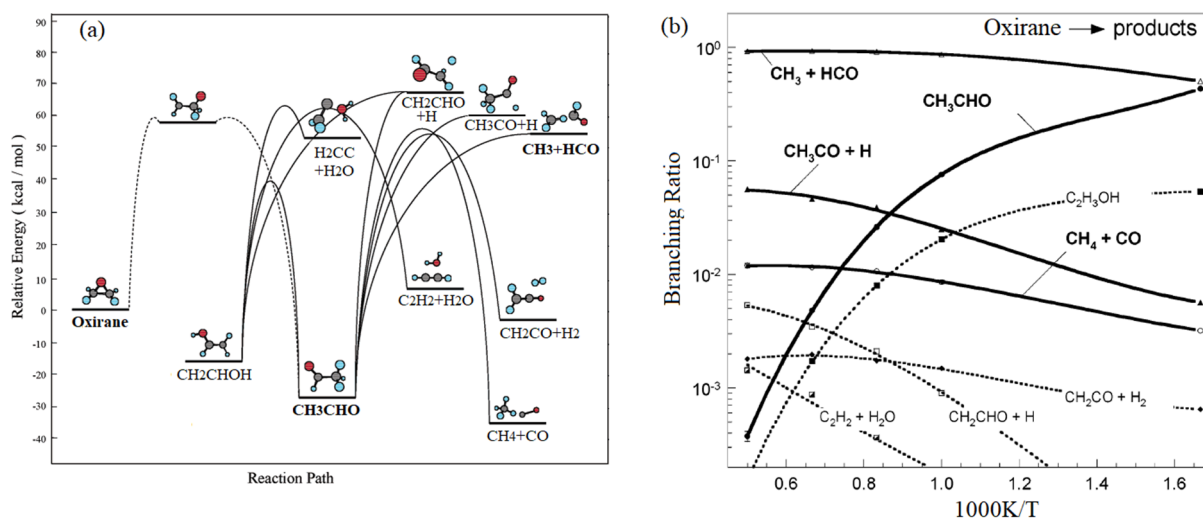
In summary, H-abstraction reactions from CE are currently not as well understood as necessary to reliably describe CE consumption reactions.

#### **5.1.1.2. Unimolecular reactions of saturated cyclic ethers**

Experiments by [594,610,613–616] and theoretical results by, *e.g.*, [617–619] show that unimolecular reactions may contribute substantially to CE decomposition. For example, in oxirane pyrolysis and combustion, acetaldehyde has been detected in high amounts. Joshi *et al.* [617] proposed the PES shown in Fig. 43a for this reaction.

The isomerization starts with C–O bond scission followed by an intramolecular H atom transfer. Subsequent isomerization, bond scission and elimination steps lead to experimentally observed products. Caused by the high 59 kcal/mol barrier, the initial reaction step produces chemically activated acetaldehyde, which may be stabilized by collisions or directly decompose to bimolecular products. The Master equation analysis results for 2 atm in the bath of Ar, shown in Fig. 43b, clearly demonstrates the importance of the chemically activated channel. Even at temperatures below 625 K ( $1000\text{K}/T = 1.6$ ) the formation of the radicals  $\dot{\text{C}}\text{H}_3$  and  $\text{H}\dot{\text{C}}\text{O}$  dominates the acetaldehyde production and higher temperatures substantially increase the importance of the radical formation channel. It should be noted that Joshi *et al.* [617] also reported on the rate expression for a H atom catalyzed decomposition mechanism. This reaction

has, according to a rate analysis at shock tube conditions, some impact on the predictions, but the unimolecular chemistry is more important.



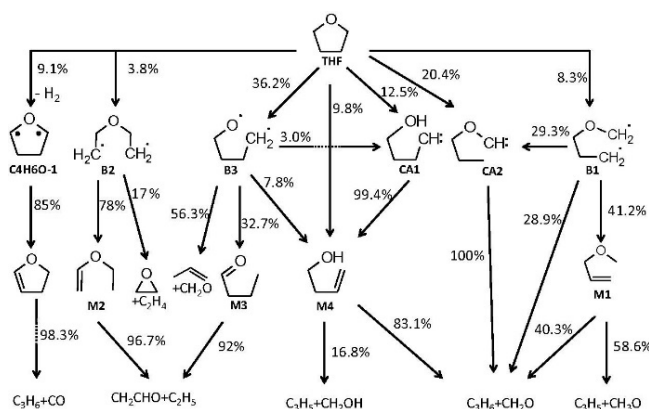
**Fig. 43.** Oxirane unimolecular decomposition: *left panel* - PES determined at the G3B3 level of theory, *right panel* - branching ratios computed in Ar bath gas at 2 atm. Reproduced from Ref. [617] with permission of ACS.

While not considered in oxirane decomposition, Dubnikova and Lifshitz [620] suggested C–C bond scission to be responsible for methyl vinyl ether formation from methyloxirane. The barrier for this reaction is with about 59 kcal/mol higher than those of the two possible C–O bond scissions (54–55 kcal/mol). The latter reactions were interpreted as concerted reactions in which the biradical transition state directly connects methyloxirane to the isomerization products (acetone and propanal). The methyloxirane study by Dubnikova and Lifshitz [620] also considered carbene chemistry but found it not to be competitive.

Shiroudi *et al.* [619] calculated concerted decomposition pathways for oxetane and the methyl and 2,2-dimethyl substituted analogues, which however lead to bimolecular products instead of isomers. They found that the barrier decreases by about 4 kcal/mol for each methyl substitution. The total barriers are with 53 to 61 kcal/mol similar to those found for (substituted) oxiranes.



Verdicchio *et al.* [618], using a modified CBS-QB3 methods adapted to describe bi-radical species and CASPT2 calculations to verify the reliability of their study, argued that in THF decomposition next to the biradical mechanism a carbene mechanism also plays a role. This leads to a highly complex decomposition chemistry as shown in the reaction path analysis for 1200 K pyrolysis in Fig. 44. The carbene pathway distinguishes CE decomposition from that of cycloalkanes because it relies on the free electrons located on the oxygen atom in the ring.



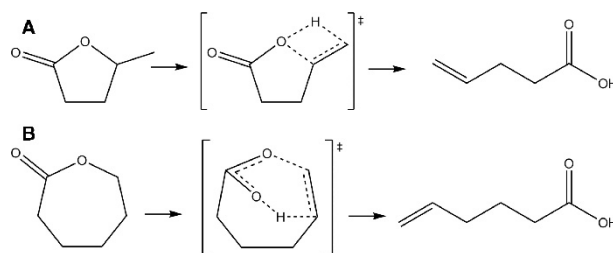
**Fig. 44.** Reaction path analysis for THF pyrolysis at 1200 K, 3 bar and a residence time of 2 ms corresponding to 0.65% THF conversion [618]. The numbers near the arrows indicate relative fluxes. The initial consumption fluxes of THF are normalized by the sum of only unimolecular decomposition fluxes. Reproduced from Ref. [618] with permission of Elsevier.

Related to the carbene pathway are pericyclic ring-opening reactions, which have been studied by Lizardo-Huerta *et al.* [621]. The barriers for pericyclic reactions involving the side chain in  $\alpha$ -position are low making these reactions competitive at low temperatures. For example, De Bruycker *et al.* [259] observed that GVL decomposition is initiated by isomerization to pentenoic acid. An example of this pathway is presented in Fig. 45 for two lactones (GVL and  $\epsilon$ -caprolactone). Verdicchio [618] report on an H<sub>2</sub> elimination path from THF, which also proceeds through a concerted reaction.

Lizardo-Huerta *et al.* [621] investigated concerted reactions in THP and concluded that those should be of similar importance as in THF, for which 20% of the total unimolecular

decomposition flux is attributed to concerted pathways. According to Lizardo-Huerta [621], 4-penten-1-ol is the main product in THP decomposition and alkyl substitution in the  $\alpha$ -position increases the dominance of the alcohol formation channel over the alternative H<sub>2</sub> elimination pathway .

In summary, CE including substituted derivatives display a rich unimolecular decomposition chemistry ranging from simple bond scission reactions similar to those found in cycloalkanes to concerted pericyclic reactions that involve lone pair electrons of the ether oxygen in the transition state. Since different pathways compete, the detailed features of the PES of a CE are important and unimolecular CE reactions are best evaluated individually using high level QM calculations and kinetic theory.

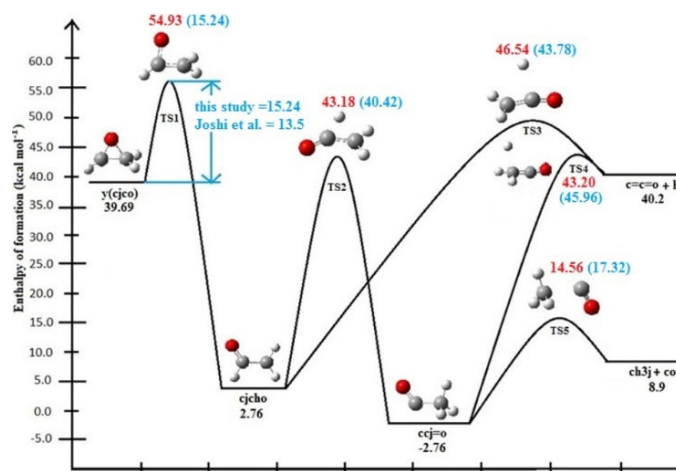


**Fig. 45.** Formation of unsaturated acids from lactones, GVL (A) and  $\epsilon$ -caprolactone (B), through unimolecular reactions. Reproduced from Ref. [259] with permission of Elsevier.

### 5.1.1.3. Unimolecular reactions of radicals of saturated cyclic ethers

As mentioned in Part 5.1.1.1, CE radicals may either rapidly decompose or, if long-lived, serve as target for oxygen addition. Nevertheless, even if the CE radical is not stable, its decomposition chemistry needs to be understood in order to reliably assign the decomposition products as a function of time (see the above discussion in Part 5.1.1.1 about differences in the Cord and Bugler mechanisms). Here only some studies will be highlighted without the claim of being comprehensive. The fate of the *oxiranyl* radical has been analyzed by Joshi *et al.* [617] and later by Wang and Bozzelli [622]. The PES reported by Wang and Bozzelli is reproduced

in Fig. 46. It nicely demonstrates that the barrier for oxiranyl (named  $\gamma(\text{cjco})$  in Fig. 46) decomposition is with about 15 kcal/mol very small and thus the thermal energy available at low-temperature oxidation is sufficient for this radical to quickly decompose. The comparison between Joshi *et al.* and Wang and Bozzelli provides an idea of the uncertainty of the barrier energies but also demonstrates that despite differences in the details, the barriers for bimolecular product formation are all lower than that of the initial ring-opening step. The highest barriers for the two product channels are quite similar (*e.g.*, 43.18 kcal/mol versus 46.54 kcal/mol using the Wang and Bozzelli data), which means that both channels should contribute. This raises the question if Bugler's [466] and Cord's [384] treatment of H-abstractions for oxiranes considering solely one product channel is adequate. Finally, the PES features suggest that pressure-dependence of the product distribution needs to be taken into account as has been done by both, Joshi *et al.* [617] and Wang and Bozzelli [622].

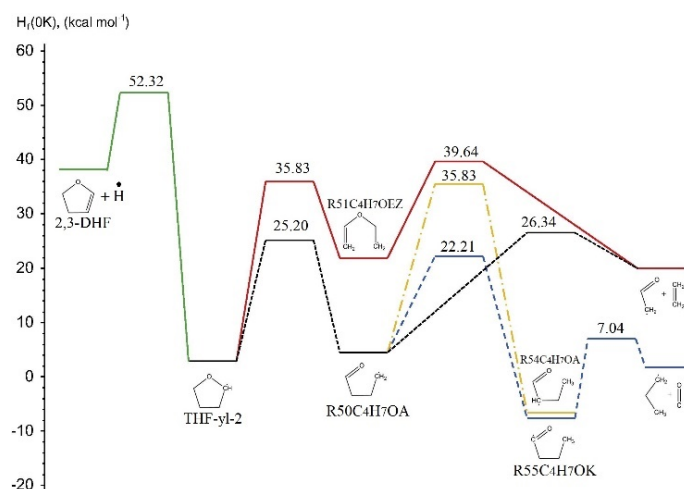


**Fig. 46.** *Ab initio* calculated PES for unimolecular isomerization and decomposition pathways of the oxiranyl radical (named  $\gamma(\text{cjco})$  in the figure). Reproduced from [622] with permission of John Wiley and Sons.

To the best of our knowledge, the *oxetanyl* radicals have not been studied but given the high ring strain, ring-opening to  $\text{C}_2\text{H}_4$  and  $\text{H}\dot{\text{C}}\text{O}$  is likely the only important pathway. This is reflected in most kinetic models. However, Dagaut *et al.* [623] considers in his 1997 model also

reactions of oxetanyl with methyl radicals to produce ethylene and acetaldehyde or propene and formaldehyde, using estimated rate expressions.

The situation is more complex when it comes to radicals of THF and substituted THFs. Fig. 47 clearly shows that the barriers for the decomposition of THF-yl-2 are higher than those of oxiranyl, which causes THF-yl-2 to be rather long-lived and to be able to participate in oxygen addition reactions and to start low-temperature oxidation chemistry [283,612,624]. Since THF-yl-2 is preferentially formed in H-abstraction reactions due to the weaker C–H bond, oxidation products originate mainly from this radical. The detection of significant amounts of  $\alpha$ -KHP confirms this interpretation [624,625]. THF-yl-3 (PES not shown) is even more stable with respect to ring-opening which allows H elimination producing 2,5-DHF to become competitive with the second bimolecular decomposition channel, the formation of allyl and formaldehyde [90,283]. However, according to the available models [283], at low temperatures this radical is formed in lower yields compared to THF-yl-2, and consequently low-temperature oxidation products from this radical, *e.g.*  $\beta$ -KHP, are detected in lower concentrations [625]. Note that, as demonstrated by Giri *et al.* [606], the formation of THF-yl-3 becomes important in higher temperatures because the branching ratio for H-abstractions from THF by OH leading to THF-yl-2 and THF-yl-3 (*i.e.* THF-yl-2:THF-yl-3) was found to be 68.8:31.2 (at 800 K) and 42.8:57.2 (at 1350 K).



**Fig. 47.** PES of THF-yl-2 (values are 0 K energies in kcal/mol) calculated by [195]. Reproduced from Ref. [195] with permission of Elsevier.

Interestingly, according to Fenard *et al.*, the increased stability of THF radicals allows also abstraction reactions with oxygen to play a role and these reactions are found to be the most effective way to form 2,3-DHF. The oxidation chemistry of THF will be discussed more thoroughly in Part 5.2.1.1.

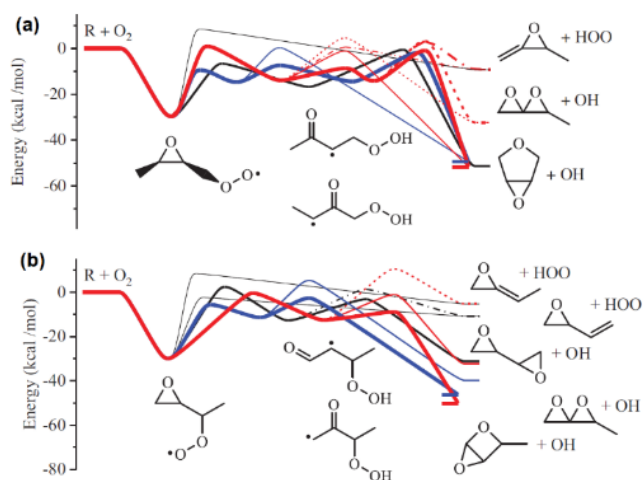
Methyl (or more general alkyl) substitution alters the ring-opening chemistry of THF radicals in several ways [90]: (1) a larger number of products can be formed, (2) the barriers are reduced because the methyl group stabilizes the transition state via hyperconjugation, (3) ring-opening can be initiated by the side chain radical (furylmethyl radical), (4) alkyl side chains also provide the possibility for ring enlargement as has been shown by Tran *et al.* [251] in the case of tetrahydrofurfuryl alcohol.

Regarding radicals of THP, the few THP models [196,626,627] consider mainly ring-opening reactions as well as H elimination to form dihydropyran. Since three THP radicals exist, a large variety of reactions are possible, however, H-abstraction reactions preferentially produce the  $\alpha$ -radical (*i.e.* which has the radical site on the carbon atom connected to the ether oxygen) and those reactions dominate. Based on the analysis by Rotavera *et al.* [398], this  $\alpha$ -radical is especially prone to ring-opening due to its very low C–O bond energy (3.7

kcal/mol). So far, only high-temperature THP models have been developed, however, some THP radicals should be stable enough to allow oxygen addition. While substituted THF radicals can undergo ring enlargement reactions (ring-opening followed by closing to a THP ring), the opposite, ring contraction, is possible for THP radicals.

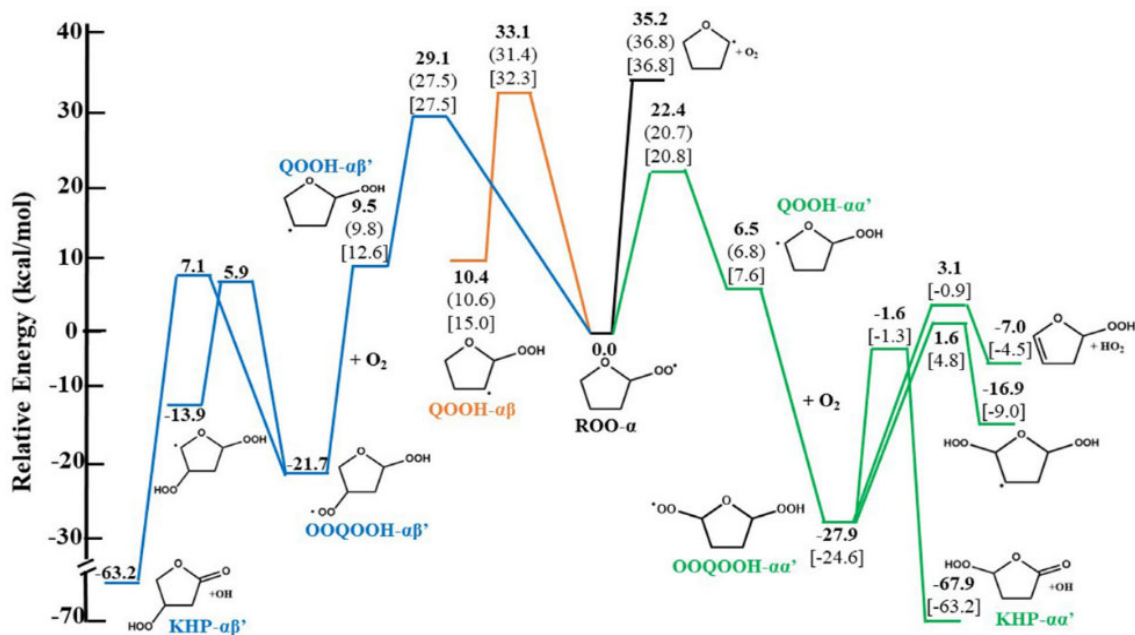
#### **5.1.1.4. $O_2$ addition to cyclic ether radicals**

As mentioned earlier, the barriers for ring-opening of oxiranyl and oxetanyl radicals are low and thus decomposition is fast.  $O_2$  addition reaction is too slow to play a notable role. The situation changes if radicals of substituted CE are taken into account, which carry the radical site on the substituent group. These radicals may undergo low-temperature oxidation chemistry as, *e.g.*, the PESs for 2,3-dimethyloxiranyl and 2-ethyloxirane-3-yl show in Fig. 48. The reaction steps are essentially the same as in alkane oxidation, however the ring structure affects some reaction products. For example, in Fig. 48a, intramolecular H-abstraction of the  $RO\dot{O}$  forming  $\dot{Q}OOH$  leads simultaneously to ring-opening (keto radical) if the abstracted H atom originates from the ring. The PES in Fig. 48a is certainly not complete as it does not contain a pathway to keto oxirane and  $\dot{O}H$  but only considers formation of the epoxyTHF. Similarly, Fig. 48b demonstrates only energetically accessible reaction pathways that start with ring-opening followed in a later step by ring closure, which effectively reproduces the oxirane structure lost in the initial ring-opening step. A main point of this PES is to show that similar products can be formed from the two CE isomer radicals.



**Fig. 48.** PES of  $\beta$ -*cis*-2,3-dimethyloxiranyl (R) + O<sub>2</sub> (a) and 2-ethyloxirane-3-yl (R) + O<sub>2</sub> (b) determined at ccCA-PS3 level of theory. Reproduced from Refs. [395,511] with permission of John Wiley and Sons

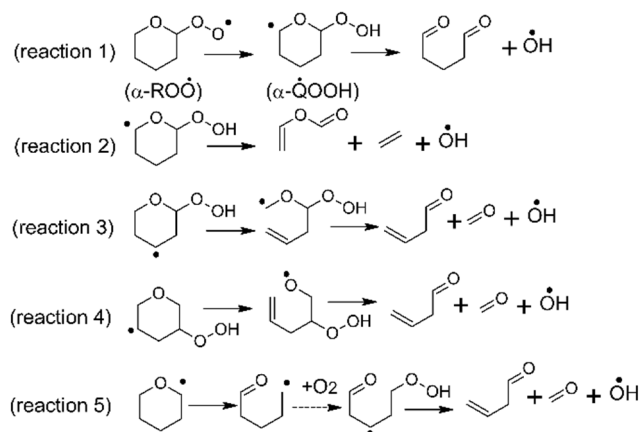
Given that the ring strain is much lower in THF-yl radicals compared to oxiranyl and oxetanyl radicals, the oxidation of THF at low temperature allows typical second oxygen addition chemistry similar to that of alkane oxidation to be important. This can be seen from the partial THF-yl-2 PES reported by Lockwood and Labbe [612], which is shown in Fig. 49. Intramolecular H-abstraction by RO $\dot{O}$  forms the corresponding  $\dot{Q}OOH$  radical. Since the ring radical is relatively stable, addition of a second O<sub>2</sub> molecule favorably competes with ring-opening which paves the way for KHP formation. It should be noted that this PES misses CE forming, ring-opening, and HO $\dot{O}$  elimination channels since the focus of this particular study was on KHP chemistry. A more complete PES for this reaction can be found in the studies by Antonov *et al.* [624] and Fenard *et al.* [283].



**Fig. 49.** PES of THF-2-peroxy radical (noted ROO- $\alpha$  in the figure) (values are 0 K, energies in kcal/mol relative to ROO- $\alpha$ ) from Lockwood and Labbe [612] (in bold), Fenard *et al.* [283] (in parentheses), and Antonov *et al.* [624] (in brackets). Reproduced from [612] with permission of Elsevier.

For THP, only little is known about its low-temperature oxidation chemistry, but the THP-peroxy radical (ROO $\dot{O}$ ) has been detected [628]. Chen *et al.* [629] report on Cl-initiated oxidation of THP and detect  $\dot{O}H$  and HO $\dot{O}$  radicals, which further indicates that the oxidation of THP at low temperatures follows the typical reaction sequences. The observed fast formation of HO $\dot{O}$  and  $\dot{O}H$  radicals points to an important role of direct decomposition of the chemically activated ROO $\dot{O}$ . This is supported by the low barrier found for HO $\dot{O}$  elimination from the most likely formed  $\alpha$ -ROO $\dot{O}$  (see structure in Fig. 50) [398,629]. Another important feature is the low C–O bond energy of the  $\alpha$ -ROO $\dot{O}$  radical which enables ring-opening to compete at elevated temperatures. The ring-opening reaction of the  $\alpha$ -QOOH radical (see structure in Fig. 50) forming pentanedial and  $\dot{O}H$  (reaction 1 in Fig. 50) is used to explain the increasing  $\dot{O}H$  yield with increasing temperature [629], but Davis *et al.* [397] provide evidence that other ring-opening channels (reactions 2-5 in Fig. 50) also play a role.





**Fig. 50.** Some  $\cdot\text{OH}$  formation paths in THP oxidation mechanism. Redrawn from [397,629].

In summary, THF and THP undergo characteristic low-temperature oxidation chemistries due to special features of the corresponding PESs of the fuel radical and  $\text{ROO}\cdot$ . The high ring strain prevents such chemistry for unsubstituted oxiranes and oxetanes, while side groups enable low-temperature oxidation chemistry.

### 5.1.2. Unsaturated cyclic ethers

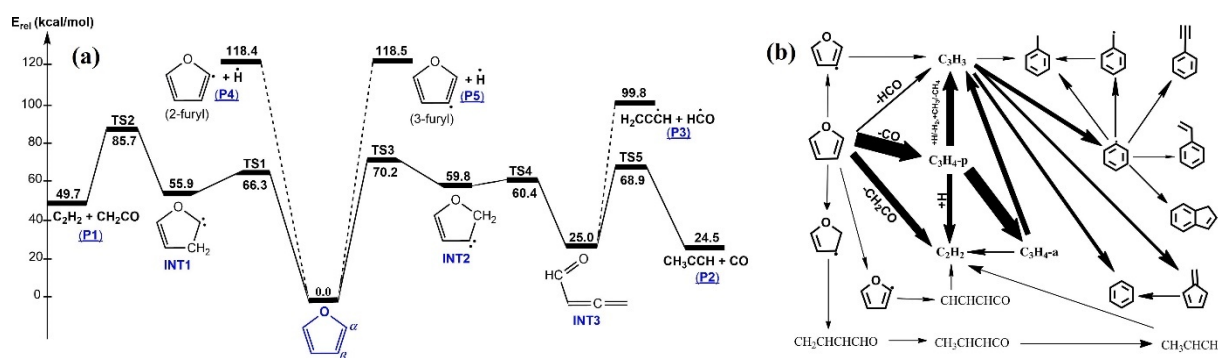
The most important representatives of non-aromatic unsaturated CEs are 2,3-DHF and 2,5-DHF and their pyran analogues. Besides typical H-abstraction and radical addition to the double bond, which resemble reactions discussed in Part 5.1.1 or in Part 4.2, unimolecular rearrangement of 2,3-DHF to either cyclopropanecarboxaldehyde or propenylaldehyde plays an important role [630]. The barriers for these reactions are above 50 kcal/mol, meaning that these reactions will only be important at temperatures above 1000 K. A similar rearrangement mechanism was also identified for 5-methyl-2,3-DHF. In contrast, for 2,5-DHF and 2-methyl-2,5-DHF, the concerted  $\text{H}_2$  elimination pathway forming (2-methyl) furan dominates. Since such a pathway is not available for 2,3-DHF, both DHF isomers display distinctly different pyrolysis product spectra observed in shock tube experiments [631,632]. According to Fan *et al.* [633], the decomposition chemistry of 2,3-DHF and 2,5-DHF at 1600 K is more complicated

but dominated by ring-opening steps. In the high-temperature model for furan, Tian *et al.* [226] consider mainly bimolecular reactions of 2,3-DHF.

Dubnikova and Lifshitz [634] identified a low energy H<sub>2</sub> elimination pathway for 2,5-DHF which is also available for 2-methyl-2,5-DHF but not for 2,3-DHF. 2,3-DHF may eliminate H<sub>2</sub> only through a high energy 4-centered transition state or a carbene intermediate, which are both not competitive with the ring opening reactions mentioned above. Consequently H<sub>2</sub> elimination has only be observed experimentally for 2,5-DHF and its methyl derivative.

Due to the unsaturated 6-membered ring structure, Tran *et al.* [196] include, next to H-abstraction reactions, retro-Diels-Alder reactions for the dihydro-pyrans in their THP model, while H<sub>2</sub> elimination reactions were not considered. Since the model reproduced the experimental dihydro-pyran yields around 1000 K quite well, it seems that these reactions are of most importance for dihydro-pyrans.

In a recent review, Westbrook and Curran [635] nicely characterized the specific reactivity of furans, the most prominent example of unsaturated aromatic CE. The special character of unsubstituted furan is easily recognized by inspecting its PES [228,636,637] shown in Fig. 51a.



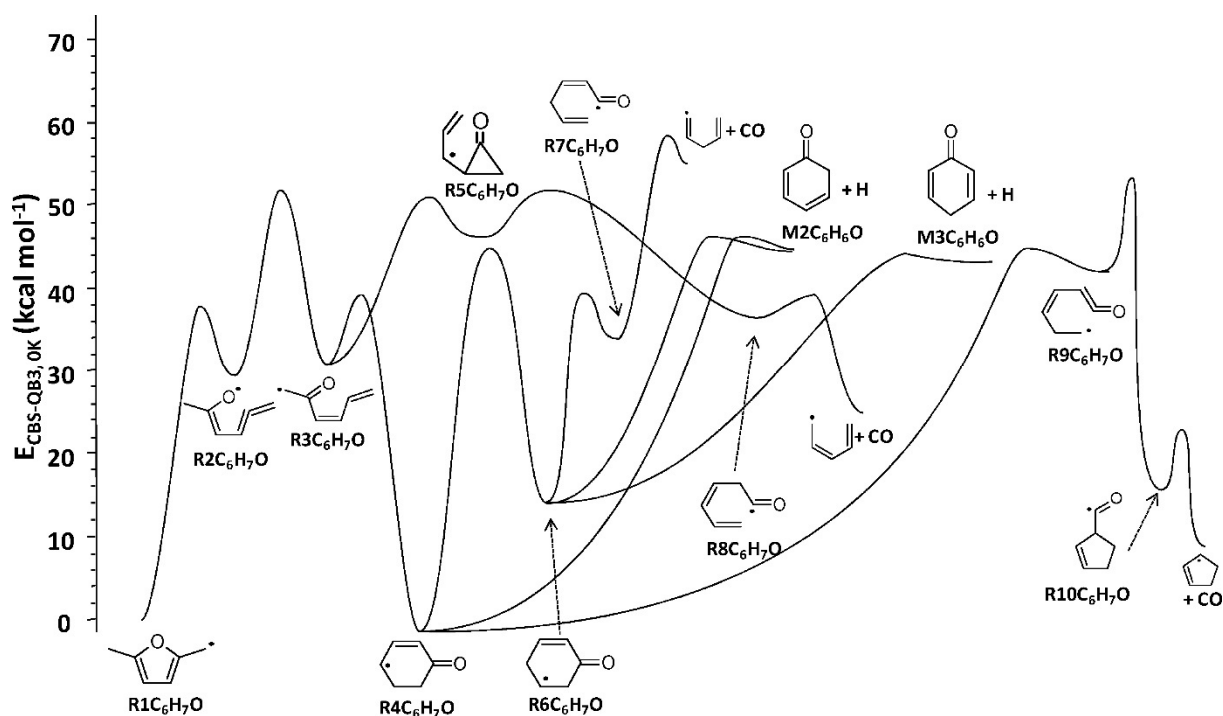
**Fig. 51.** (a) PES of unimolecular dissociation of furan taken from [228]; 2-furyl is furan-2-yl, 3-furyl furan-3-yl. (b) Reaction flux analysis for furan decomposition at 1575 K using the model by Cheng *et al.* [638]. Reproduced from [228,638] with permission of Elsevier

The unimolecular decomposition of furan mechanism is initiated by intramolecular H migration forming one of two possible carbenes. These intermediates upon  $\beta$ -scission produce

stable molecular products, except for very high temperatures at which bond scission to propargyl ( $\text{HC}\equiv\text{C}-\dot{\text{C}}\text{H}_2$ ) and  $\text{H}\dot{\text{C}}\text{O}$  is feasible [637]. In substituted furans, the migrating H atom can be replaced by a group such as formyl, which provides a mechanism for isomerization (see *e.g.* [423]). Fig. 51b clearly shows the dominance of this carbene ring-opening mechanism. The extraordinarily strong C–H bonds in furan ( $\sim 120.5$  kcal/mol) [231,637] prevents H-abstraction reactions to play a significant role except at high temperatures and the aromatic character of furan creates higher barriers for H atom or radical addition reactions to the ring. However, as will be discussed later, ring-opening reactions initiated by radical addition to the furan ring play a role at elevated temperatures.

The carbene mechanism is also important in substituted furans, *e.g.* 2,5-DMF [639], 2-THFFOH [640] and furfurals [423,640], but the alkyl side chain allows additional reaction channels such as H-abstraction from the substituent, to compete. In the case of 2,5-DMF, H-abstraction leads to the (5-methylfuran-2-yl)methyl radical, which PES is shown in Fig. 52. One important feature of this PES is the rather low barrier (just above 50 kcal/mol) to enlarge the 5-membered ring to a 6-membered keto species which may ultimately produce phenol or cyclopentadienyl and CO. This explains the tendency of 2,5-DMF to produce larger aromatic species [275,641]. H-atom addition followed by  $\dot{\text{C}}\text{H}_3$  elimination explains the production of furan and 2-MF from 2,5-DMF or in general from substituted furans.

In summary, unsaturated CEs are characterized by specific decomposition chemistries, which require the study of the corresponding PESs and detailed kinetic analyses. Rate rules are not applicable for these molecules [635] but for the most prominent members of this family, furan, 2-MF and 2,5-DMF, numerous theoretical studies are available and well-tested models exist.



**Fig. 52.** PES of the unimolecular decomposition of the (5-methylfuran-2-yl)methyl radical ( $R1C_6H_7O$ ) calculated by Sirjean *et al.* [642]. Values are 0 K, energies in kcal/mol relative to  $R1C_6H_7O$ .  
 Reproduced from [642] with permission of Elsevier.


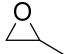
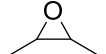
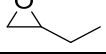


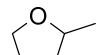
## 5.2. Experimental and modelling studies on the combustion chemistry of saturated cyclic ethers

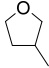
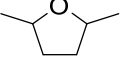
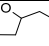
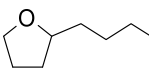
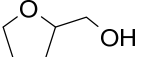
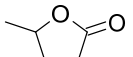
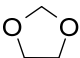
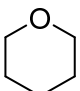
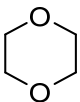
Table 16 lists about 90 experimental studies related to the consumption of saturated CEs, which will be discussed in detail in this part. Each study contains different datasets that include several data points. These studies were mainly performed using RCMs, JSRs and FRs, in the same way as the low-temperature experiments described in Part 4, but also in ST, constant volume bomb (CVB) and PLF, which are more suitable for high-temperature work. The listed studies report oxidation and pyrolysis chemistry concerning global combustion parameters (about 40 studies), *e.g.* laminar burning velocity (LBV) or IDT, and chemical species formation (about 50 studies), with a high interest in low-temperature chemistry.

The gas-phase reactions of saturated CEs have been studied from 1990, *e.g.* for oxirane and THF. Several CEs have been investigated intensively and for those, comprehensive databases containing measurements over large ranges of temperatures, pressures, and

equivalence ratios are available. This is the case for THF with about 20 reported studies at temperatures from 400 K to 2300 K (because of its different nature, the initial temperatures of LBV or engine experiments are not considered), pressures from 0.01 to 40 bar, equivalence ratios from 0.36 to  $\infty$  and for 2-MTHF with 16 reported studies at temperature from 639 to 2240 K, pressure from 0.04 to 40 bar,  $\phi$  from 0.5 to  $\infty$ . Investigations of other CEs begun only recently, *e.g.* alkyl-substituted oxiranes and alkyl-substituted THFs. No flame speciation data is available for oxirane derivatives except for methyloxirane, oxetane derivatives, and alkyl-substituted THFs heavier than 2-MTHF. Studies involving diffusion flames are also unavailable. Part 5.2.1 describes the available studies on unsubstituted saturated CEs, starting with THF, and Part 5.2.2 presents those related to substituted ones.

**Table 16.** The main experimental studies for the combustion chemistry of saturated CEs from 1980. The studies are sorted by the experimental target, *i.e.* LBV, IDT, speciation data (spec. data). "--" indicates that the information is not available

Fuel	Exp. Target	Reactor	Operating conditions				Year, first author, ref.
			<i>T</i> (K)	<i>P</i> (bar)	$\phi$	Fuel % (diluent)	
Oxirane 	IDT	ST	1067-1328	5-15	0.4-3.2	3-9 (N <sub>2</sub> )	1980 Burcat [643]
			875-1513	-- <sup>a</sup>	0.7-1.7	2.3-14.3 (Ar)	1993, 1996, Kang [644,645]
			910-1200	2.5-7	0.5-1	1-4 (Ar)	1994, Lifshitz [646]
			1050-1400	2-5	0.5-2	0.5-2 (Ar)	1996, Würmel [647]
	Spec. data	ST	830-1200	1.5-10	$\infty$	0.25-1 (Ar),	1983 Lifshitz [594]
	JSR	800-1150	1-10	0.5-2	0.15 (N <sub>2</sub> )	1996 Dagaut [610]	
	FR	753	0.08-0.7	$\infty$ ,	1.7-4 (N <sub>2</sub> )	1984 Baldwin [616]	
				0.2-3.2 <sup>b</sup>	1 <sup>c</sup> (N <sub>2</sub> )		
Methyloxirane 	LBV	CVB	298 <sup>d</sup>	1	0.7-2.1	3.6-10 (N <sub>2</sub> )	2010 Burluka [648]
	IDT	ST	960-1300	2.5-7	0.5-1	2-4 (Ar)	1994 Lifshitz [646]
			962-1127	10-40	0.5-2	2.6-9.5 (IM <sup>f</sup> )	2021, Ramalingam [649]
		RCM	870-980	10-20	0.5-2	1.7-5 (IM <sup>f</sup> )	2021 Ramalingam [649]
	Spec. data	ST	850-1250	2	$\infty$	0.1-1 (Ar)	1994 Lifshitz [614]
900-1450			40	$\infty$	0.5 (Ar)	2021 Ramalingam [649]	
	PLF	up to 1600	1	1.0-1.6	2.8-3.9 (Ar)	2021 Knyazkov [650]	
2,3-Dimethyloxirane 	IDT	ST	980-1250	2.5-7	1-2	1.45-2.9 (Ar)	1994 Lifshitz [646]
	Spec. data	ST	900-1150	2	$\infty$	1 (Ar)	1995 Lifshitz [651]
		FR <sub>photolysis</sub>	650-800	0.01	-- <sup>n</sup>	-- (He) <sup>n</sup>	2021 Doner [511]
Ethyloxirane 	IDT	ST	980-1250	2.5-7	1-2	1.45-2.9 (Ar)	1994 Lifshitz [646]
	Spec. data	FR <sub>photolysis</sub>	650-800	0.01	-- <sup>n</sup>	-- (He) <sup>n</sup>	2021 Christianson [395]
Oxetane 	IDT	ST	1050-1780	1.7-5.3	0.5-2	0.5-2 (Ar)	1997 Dagaut [623]
	Spec. data	JSR	800-1150	1-10	0.5-2	0.1 (N <sub>2</sub> )	1997 Dagaut [623]
THF 	LBV	PLF	298-398 <sup>d</sup>	1	0.55-1.6	2.1-5.8 (N <sub>2</sub> )	2015 Tran [195]
		CVB	373-453 <sup>d</sup>	1-4	0.7-1.6	2.2-5.8 (N <sub>2</sub> )	2020 Wang [652]
	IDT	ST	1000-1800	2-5	0.5-2	0.5-2 (Ar)	1998 Dagaut [653]
			691-1100	20-40	1	3.6 (N <sub>2</sub> )	2014 Uygun [281]
			1300-1700	8.1-9.3	0.5-2	0.25-1 (Ar)	2015 Tran [195]
			640-900	5-10	1	3.7 (IM <sup>e</sup> )	2015 Vanhove [282]
		RCM	640-770	20	1	3.68 (IM <sup>f</sup> )	2016 Sudholt [654]
	650-900		18	1	1 (IM <sup>f</sup> )	2020 Wu [655]	
	Spec. data		ST	1070-1530	2-10	$\infty$	0.25-1 (Ar)
		PLF	up to 2300	0.02-0.03	1.0-1.75	11.5-18 (Ar)	2011 Kasper [656]
			up to 2300	0.07	0.7-1.3	2.7-4.9 (Ar)	2015 Tran [195]
		JSR	800-1100	10	0.5-1	0.1 (N <sub>2</sub> )	1998 Dagaut [653]
			500-1100	1.07	0.5-2	1 (He)	2015 Vanhove [282]
	500-700		0.9	0.36	1 (Ar)	2019 Hansen [625]	
	550-620		10	0.5	0.5 (N <sub>2</sub> )	2021 Belhadj [590]	
	Static reactor	493	0.2	2.75	33.3 <sup>g</sup>	1988 Molera [657]	
		CFR engine	400 <sup>h</sup> , 827 <sup>i</sup>	0.8 <sup>h</sup> , 12 <sup>i</sup>	0.95-1	3.7 (N <sub>2</sub> )	1991 Leppard [82]
		RCM	710	7.7	1	3.7 (IM <sup>e</sup> )	2015 Vanhove [282]
	FR <sub>photolysis</sub>	400-700	0.01-2.7	-- <sup>n</sup>	-- (He) <sup>n</sup>	2016 Antonov [624]	
2-MTHF 	LBV	PLF	298-398 <sup>d</sup>	1	0.6-1.6	1.79-4.63 (N <sub>2</sub> )	2017 De Bruycker [658]
		CVB	373-453 <sup>d</sup>	1-4	0.7-1.6	2.08-4.63 (N <sub>2</sub> ) <sup>j</sup>	2018, 2020 Wang [652,659]
			423 <sup>d</sup>	1-10	0.7-1.5	2.08-4.36 (N <sub>2</sub> , He)	2021 Li [660]
	IDT	ST	1050-1800	1.2-10.1	0.5-2	0.25-1 (Ar)	2015, 2016 Wang [661,662]
			753-1349	10-20	0.5-2	1.46-5.83 (N <sub>2</sub> )	2017 Tripathi [663]
			1034-1515	3-12.1	0.5-3	3 (Ar)	2016, 2019 Jouzdani [664,665]
				RCM	640-770	20	1
			640-900	3-21	1	2.91 (IM <sup>e</sup> )	2017 Fenard [666]
		639-878	10-40	0.5-2	1.4-5.83 (IM <sup>f</sup> )	2017 Tripathi [663]	
Spec. data	ST	1325-1648	3.3-11	$\infty$	3 (Ar)	2019 Jouzdani [664]	

		FR	900-1100	1.7	$\infty$	9.1 (N <sub>2</sub> )	2017 De Bruycker [658]	
		PLF	up to 2100	0.04	1.7	14.5 (Ar)	2013 Moshammer [667]	
			up to 2240	0.07	0.7-1.3	2.7-5 (Ar)	2017 De Bruycker [658]	
			up to 1634	0.05	1	1.4 <sup>k</sup> (N <sub>2</sub> )	2021 Tran [668]	
		CFR engine	400 <sup>h</sup>	0.8 <sup>h</sup>	0.95-1	3 (N <sub>2</sub> )	1991 Leppard [82]	
		RCM	719	7.6	1	2.91 (IM <sup>e</sup> )	2017 Fenard [666]	
3-MTHF 	IDT	ST	715-1250	10-40	0.5-2	1.5-5.7 (N <sub>2</sub> )	2019 Tripathi [669]	
		RCM	615-900	10-40	0.5-2	1.5-5.7 (N <sub>2</sub> )	2019 Tripathi [669]	
			630-715	20	1	2.91 (IM <sup>f</sup> )	2016 Sudholt [654]	
2,5-DMTHF 	LBV	CVB	373-453 <sup>d</sup>	1-4	0.7-1.6	1.72-3.85 (N <sub>2</sub> )	2020 Wang [652]	
		ST	860-1320	10-40	1	2.41 (N <sub>2</sub> )	2019 Fenard [670]	
	IDT	RCM	660-880	10-20	1	2.41 (IM <sup>e</sup> )	2019 Fenard [670]	
		Spec. data	RCM	712	10	1	2.41 (IM <sup>e</sup> )	2019 Fenard [670]
		FR	948-1198	0.04	$\infty$	--	2019 Wang [671]	
2-ETHF 	IDT	RCM	650-714	20	1	2.41 (IM <sup>f</sup> )	2016 Sudholt [654]	
2-BTHF 	LBV	CVB	448 <sup>d</sup>	1-3	0.7-1.35	1.28-2.43 (N <sub>2</sub> )	2017 Cai [672]	
		ST	705-1210	20	1	1.82 (N <sub>2</sub> )	2017 Cai [672]	
	IDT	RCM	650-900	10.1	0.5-1	0.9-1.8 (IM <sup>f</sup> )	2017 Cai [672]	
2-THFFOH 	Spec. data	PLF	up to 1735	0.05	1	1.5 <sup>k</sup> (N <sub>2</sub> )	2021 Tran [251]	
			up to 1668	0.05	1	0.8 <sup>k</sup> (N <sub>2</sub> )	2021 Tran [668]	
GVL 	Spec. data	FR	873-1113	1.7	$\infty$	9.1 (N <sub>2</sub> )	2015, 2016 De Bruycker [259,673]	
		PLF	up to 2250	0.07	1	1.4 <sup>l</sup> (Ar)	2017 Sudholt [674]	
1,3-dioxolane 	IDT	ST	1032-1289	20-40	1	2 (Ar)	2021 Wildenberg [675]	
		RCM	662-911	20-40	1	3 (IM <sup>f</sup> )	2021 Wildenberg [675]	
	Spec. data	FR	963-1093	1	$\infty$	~1 (H <sub>2</sub> O)	1987 Cutler [676]	
		Static reactor	373-575	0.04	$\infty$	67 ( <sup>m</sup> )	1991 Fernández [677]	
		JSR	700-1180	10	1	0.1 (N <sub>2</sub> )	2021 Wildenberg [675]	
THP 	LBV	PLF	298-398 <sup>d</sup>	1	0.55-1.5	2-5.5 (N <sub>2</sub> )	2015 Tran [196]	
		IDT	1000-1700	2-5	0.5-2	0.5-2 (Ar)	1997 Dagaut [627]	
	Spec. data	PLF		1350-1613	8.8-9.1	0.5-2	0.5-1 (Ar)	2015 Tran [196]
				up to 2250	0.03	1.75	15 (Ar)	2013 Labbe [626]
				up to 2240	0.07	1.0-1.3	3-3.9 (Ar)	2015 Tran [196]
			CFR engine	358 <sup>h</sup>	0.6 <sup>h</sup>	0.95-1	3 (N <sub>2</sub> )	1991 Leppard [82]
			JSR	800-1100	10	0.5-2	0.1 (N <sub>2</sub> )	1997 Dagaut [627]
			FR	913-1133	1.7	$\infty$	3.9-9.2 (N <sub>2</sub> )	2015 Tran [196]
				500-700	0.01-2	-- <sup>n</sup>	-- (He) <sup>n</sup>	2017 Rotavera [398]
			500-700	0.01-2	-- <sup>n</sup>	--(He) <sup>n</sup>	2019 Davis [397]	
1,4-dioxane 	Spec. data	Static reactor	473, 783-823	0.4, 0.025	5, $\infty$	50, 100	1989, 1991 Battin [678,679]	
				1550-2100	0.07-0.16	$\infty$	1-4 (Kr)	2011 Yang [680]
				--	0.04	1.8	13.2 (Ar)	2009 Lin [681]

<sup>a</sup> Initial pressure ( $P_1$ ) of 0.13 bar, but the final pressure ( $P_3$ ) was not provided in the original paper.

<sup>b</sup> In oxidation, mixtures are made of oxirane, O<sub>2</sub>, H<sub>2</sub> and N<sub>2</sub>.

<sup>c</sup> 1% of oxirane in the mixtures of oxirane, O<sub>2</sub>, H<sub>2</sub> and N<sub>2</sub>.

<sup>d</sup> Initial temperature.

<sup>e</sup> Inert mixture of N<sub>2</sub>, Ar, and CO<sub>2</sub>

<sup>f</sup> Inert mixture of N<sub>2</sub> and Ar

<sup>g</sup> Undiluted.

<sup>h</sup> In the intake manifold.

<sup>i</sup> Maximum value in the cylinder at a compression ratio of 8.7.

<sup>j</sup> Data for 2-MTHF and *iso*-octane mixtures are also available in [659].

<sup>k</sup> CH<sub>4</sub> is added to stabilize the flame.

<sup>l</sup> 6.25% CH<sub>4</sub> is added to stabilize the flame.

<sup>m</sup> Mixed with acetone in a 2 : 1 ratio, and using the photolysis of acetone

<sup>n</sup> Mixture of O<sub>2</sub>, CE, He, and Cl radical produced via photolysis of oxalyl chloride (COCl)<sub>2</sub>.

### 5.2.1. Non-substituted saturated cyclic ethers

Among non-substituted CEs, oxirane, THF, and THP have been frequently investigated, while only a limited number of studies are known for oxetane [623], as is shown in Table 16. A few studies were also found for CEs containing 2 O-atoms in the ring, e.g. 1,3-dioxolane and 1,4-dioxane. The experimental studies for THF will be detailed in Part 5.2.1.1 and those of other non-substituted saturated CEs will be discussed in Part 5.2.1.2. Finally, the chemistry of these CEs will be compared in Part 5.2.1.3 and a description of their detailed kinetic models follows in Part 5.2.1.4.

#### 5.2.1.1. Tetrahydrofuran

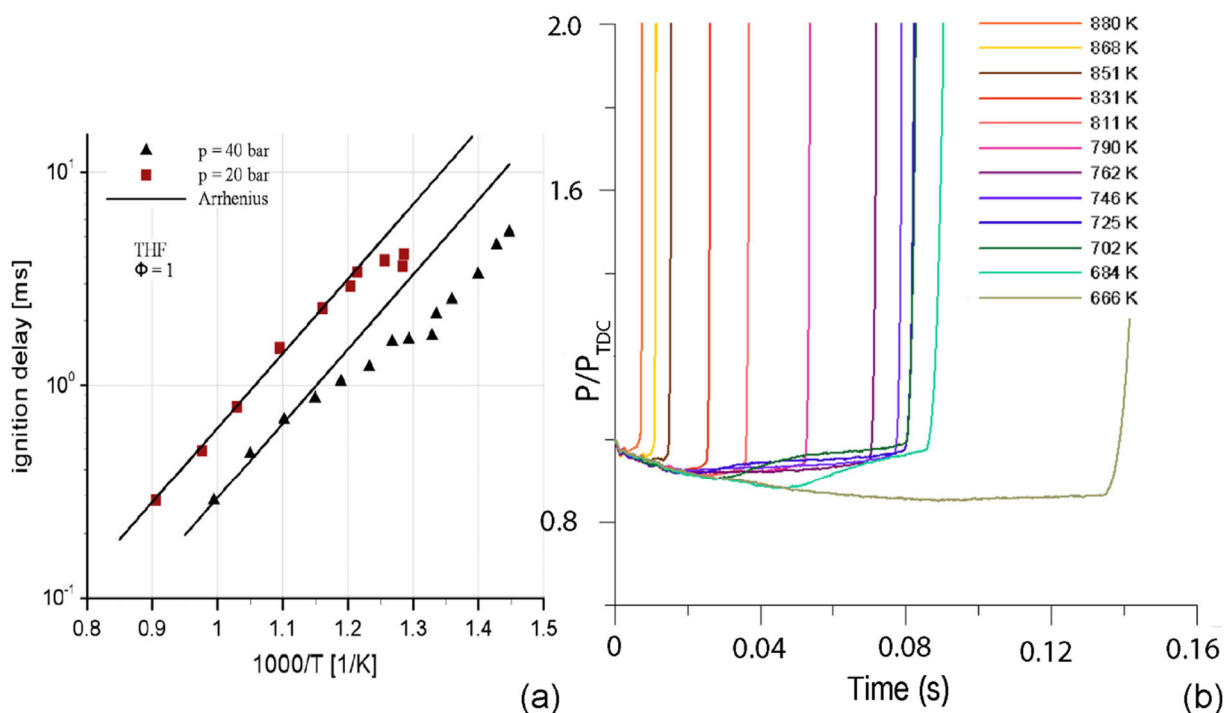
THF is the core structure of the tetrahydrofuranic biofuels, such as itself, 2-MTHF, 2,5-DMTHF, 2-THFFOH, etc., as discussed in Part 1. Numerous experimental datasets are available for THF, including measurements of its global parameters (LBV and IDT) and detailed product detections and quantifications.

*Laminar burning velocities* of THF were recently measured by [195,652] using CVB or PLF at 1-4 bar and a range of equivalence ratios of 0.55-1.6. The results obtained with different experimental methods show good consistency. As usual for CEs, the peak LBV for THF is observed around  $\phi=1.1$  and it decreases with increasing initial pressure. At 1 bar, 298K, and  $\phi=1.1$ , the LBV of THF was determined to be  $43\pm 1.7$  cm/s [195,652].

The *ignition* behavior of THF was investigated from 640 K to 1800 K in RCMs by [282,654,655] and in STs by [195,281,653]. High-temperature ignition delay times follow classical Arrhenius behavior as is shown in the ST work of Uygun *et al.* [281] (see Fig. 16 of Part 3, above 1000 K) and of Dagaut *et al.* [653]. The latter authors reported a decrease of reactivity with increasing  $\phi$  and an increase of reactivity with increasing pressure. A study in the high-pressure shock tube of Aachen at 20 and 40 bar was able to investigate the ignition behavior below 1000 K and to demonstrate a clear inflection in the Arrhenius slope [281] (see



Fig. 53a). This agrees with the observation by Vanhove *et al.* [282] from their RCM experiments that two-stage ignition (cool flame) was visible up to 810 K as is illustrated in Fig. 53b.



**Fig. 53.** THF auto-ignition at low-temperature: (a) ignition delay times in a ST (THF/air mixtures), (b) normalized pressure profiles during auto-ignition at different core gas temperatures (stoichiometric THF/O<sub>2</sub>/inert mixture). Reproduced from Refs. [281] and [282] with permission of Elsevier and of American Chemical Society, respectively.

*Product speciation data* were measured during THF pyrolysis and oxidation in different reactor types, as well as in two PLFs, as is shown in Table 16. Based on their pyrolysis results obtained behind reflected shock wave in a single-pulse ST with GC analysis, Lifshitz *et al.* [613] suggested two initiation steps for THF pyrolysis, with the first one ( $\text{THF} \rightarrow \text{C}_2\text{H}_4 + \text{CH}_3\text{CHO}$ ) being four times faster than the second one ( $\text{THF} \rightarrow \text{C}_3\text{H}_6 + \text{CH}_2\text{O}$ ). The experimental data of [613] were later used by Verdicchio *et al.* [618] to compare with their model developed using quantum-mechanical calculations, showing the importance of both, carbene and biradical reactions that are discussed in Part 5.1.

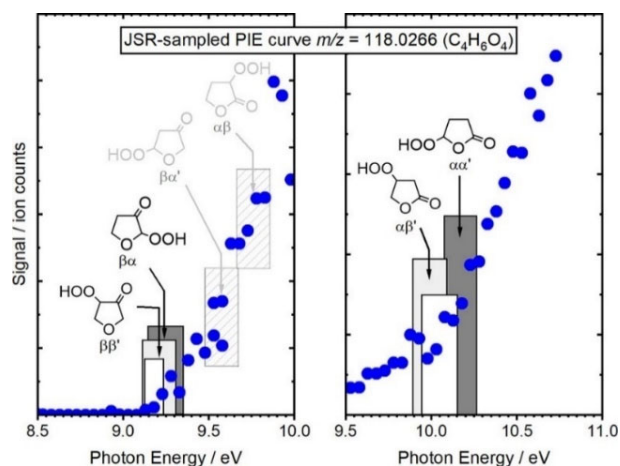
Data were reported on THF oxidation products above 800 K by Dagaut *et al.* [653] using a JSR (800-1100 K, 10 bar) with GC, as well as by Kasper *et al.* [656] and by Tran *et al.* [195] using PLFs with EI/PI-MBMS and GC. These data suggest that THF decomposition occurs mainly through a ring cleavage (after H-abstractions) into ethylene and oxygenated intermediates, which finally yield carbon monoxide. Hydrogen release of the initial radicals, *i.e.* THF-yl-2 and THF-yl-3, result in the formation of 2,3-DHF and 2,5-DHF. Both products were observed in trace amounts in JSR [653] but in more notable quantities in PLFs [195,656]. In the PLF, mole fraction profiles of more than 60 chemical species with molar masses ranging from 2 (H<sub>2</sub>) to 86 (2-MTHF) were measured as a function of the height above the burner. C<sub>2</sub>H<sub>4</sub> was identified as the most abundant intermediate.

Products yields during THF oxidation below 800 K were first reported by Molera *et al.* [657] and by Leppard [82] in a static reactor and a CFR engine, respectively. Besides CO, formaldehyde and acetaldehyde, the intermediate species 2,3-DHF, tetrahydrofuran-3-one, succinic dialdehyde (butanedial), and succinic acid were detected in significant concentrations. The formation of the three latter species was explained by O<sub>2</sub> addition to the THF-yl-2 or THF-yl-3 radicals [82,657].

Vanhove *et al.* [282] reported GC measurements during THF oxidation in a JSR from 500 K to 1100K and in a RCM at 710 K. These datasets confirmed the presence of the NTC behavior in lean and stoichiometric mixtures. The main products observed below 800 K in the JSR are CO, CH<sub>4</sub>, C<sub>2</sub>H<sub>4</sub>, formaldehyde, acetaldehyde, 2,3-DHF and 2,5-DHF, which is consistent with the observations made in earlier studies [82,657]. No bicyclic ethers were detected. Similarly to Leppard [82], butanedial was also detected under RCM conditions (7.7 bar, 710 K) and explained to be produced through the route of the first O<sub>2</sub> addition to the THF-yl-2 radical. Vanhove *et al.* [282] also quantified several other C<sub>2+</sub> oxygenated species, *e.g.* oxirane,

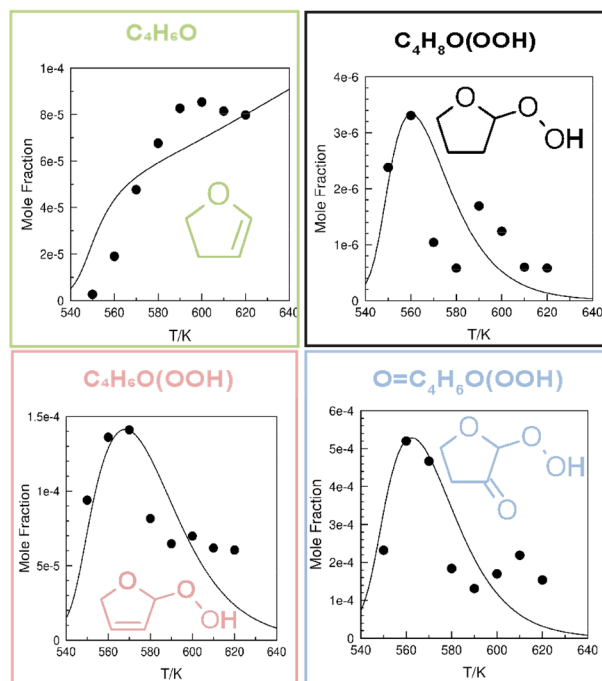
acrolein, propanal, and 1,4-dioxene establishing a database used by Fenard *et al.* [283] for testing their model.

Three recent studies focusing mainly on hydroperoxide formation have presented product speciations of THF oxidation in JSR and FR. In Antonov *et al.* [624], transient intermediates and products were probed using SVUV-MBMS during THF oxidation initiated by chlorine radical attack in a flow reactor (0.01-2.7 bar, 400-700 K). The experimental data were interpreted based upon the calculations of the PES of THF-yl + O<sub>2</sub> and QOOH + O<sub>2</sub>. The main features of these PES were confirmed by Fenard *et al.* [283] as presented in Part 5.1. The experiments revealed a key reaction sequence consisting in the conversion of THF-yl peroxy (ROO<sup>•</sup>) to hydroperoxy-THF-yl radicals (QOOH<sup>•</sup>), followed by a second O<sub>2</sub> addition and subsequent decomposition to dihydrofuranyl hydroperoxide + HO<sup>•</sup>O or to  $\gamma$ -butyrolactone hydroperoxide (a KHP obtained from THF) + OH<sup>•</sup>. THF has later been used as a prototype fuel for studying hydroperoxide formation from cyclic bio-molecules. Hansen *et al.* [625] used a JSR (0.9 bar, 500-700 K) with SVUV-MBMS diagnostics and presented the partially isomer-resolved detection and quantification of the KHPs obtained during THF oxidation. Fig. 54 presents the experimentally observed PIE curve at  $m/z$  118 corresponding to KHPs (C<sub>4</sub>H<sub>6</sub>O<sub>4</sub>) together with theoretically predicted ionization energies. Quantification was attempted (peak mole fractions of  $8 \times 10^{-6}$  -  $6 \times 10^{-4}$ ) with uncertainties optimistically estimated within a factor of 2 despite possible uncertainties due to possible KHP fragmentation after ionization. Even though Hansen *et al.* [625] were unable to separate KHP- $\beta\beta'$  from KHP- $\beta\alpha$  experimentally, the observed KHPs seem to be predominantly KHP- $\beta\alpha$  (see Fig. 54 for the KHP structures) as recently suggested by the theoretical study of Lockwood and Labbe [612].



**Fig. 54.** Experimental PIE curve of  $m/z$  118 ( $C_4H_6O_4$ ) (symbols) obtained during THF oxidation in a JSR from 8.5 to 10.0 eV (left panel) and 9.5 to 11.0 eV (right panel). The experimentally observed ionization thresholds are indicated with white boxes and are compared with theoretically predicted ionization energies (marked in gray) of the six conceivable KHP isomers. Reproduced from Ref. [625] with permission of American Chemical Society.

Very recently, Belhadj *et al.* [590] investigated THF oxidation in a JSR under fuel-lean conditions ( $\phi=0.5$ ), 10 bar and 550–620 K, using high-resolution MS (orbitrap) and liquid chromatography. They detected KHPs ( $C_4H_6O_4$ ) and other highly oxygenated molecules (*e.g.*  $C_4H_4O_5$ ,  $C_4H_8O_5$ ,  $C_4H_6O_6$ , and  $C_4H_8O_7$ ), which were assumed to result from the addition of up to three  $O_2$  molecules to radicals of the fuel. Fig. 55 shows the scaled signal profiles of selected products, as they were not quantified.



**Fig. 55.** Profiles of selected species during THF oxidation in a JSR ( $\phi=0.5$ , 0.5% THF, 10 bar, residence time of 2 s): experimental signal profiles (*dots*) [590] scaled to the maximum computed mole fraction using the model of Fenard *et al.* [283]. (*lines*). Reproduced from Ref. [590] with permission of American Chemical Society.

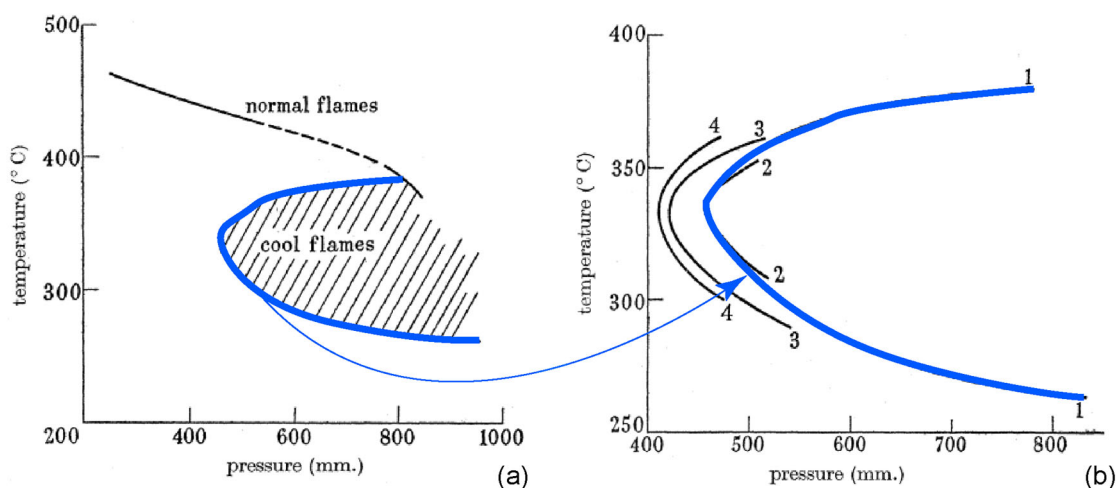
### 5.2.1.2. Other non-substituted saturated cyclic ethers

While THF is the non-substituted saturated CE, for which the largest number of studies can be found, the degradation chemistries of oxirane, oxetane and THP were also investigated.

#### Oxirane:

Although oxirane has never been proposed as a biofuel it was detected as an intermediate during the oxidation of many hydrocarbons and oxygenated reactants (see Part 4). Most of the experimental studies concerning the reactivity of this CE were performed before 1996 (see Table 16). No published study is available on oxirane chemistry in flames.

*Concerning ignition behavior*, Burden and Burgoyne [684] showed that cool flames can be initiated in oxirane-air mixtures at atmospheric pressure in a silica vessel. An increase of the oxirane proportion substantially lowered the minimum pressure for cool-flame initiation (Fig. 56).



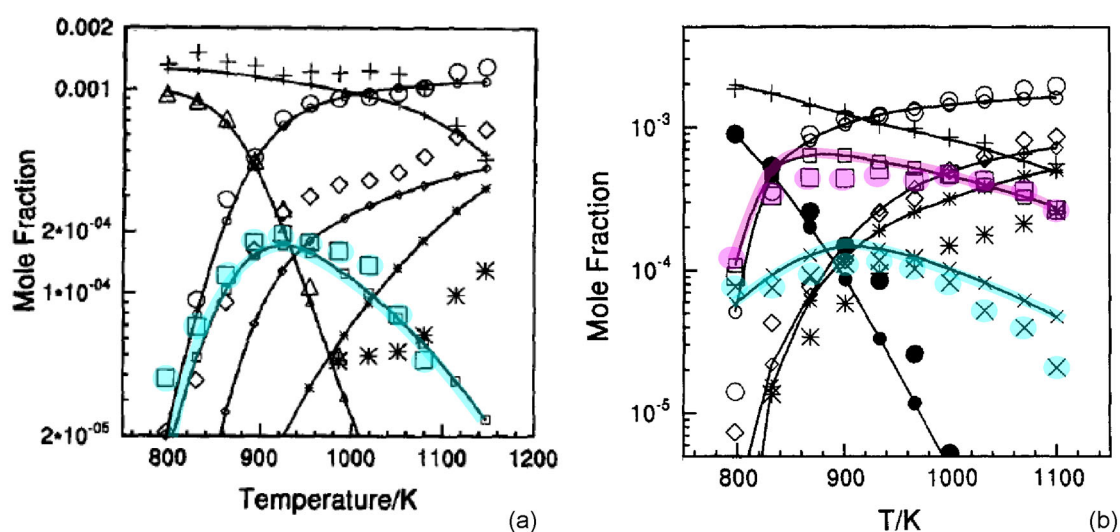
**Fig. 56.** Ignition temperature-pressure limits for oxirane-oxygen mixtures in a quartz explosion vessel. **(a)** Equimolecular fuel-O<sub>2</sub> mixture. **(b)** Effect of fuel-O<sub>2</sub> mixture composition on the cool flame pressure-temperature limit. Curves: 1, oxirane + O<sub>2</sub>; 2, oxirane + 2×O<sub>2</sub>; 3, 2×oxirane + O<sub>2</sub>; 4, 4×oxirane + O<sub>2</sub>. Reproduced from Ref. [684] with permission of the Royal Society.

Later, IDTs of oxirane were measured in STs by Burcat [643], Würmel *et al.* [647], Kang *et al.* [644,645], and Lifshitz *et al.* [646]. The experiments of [645] show the activation energy in Ar to be almost half of that measured in N<sub>2</sub>, due to the higher heat capacity of N<sub>2</sub> (7.8 cal/mol/K at 1000 K) compared to Ar (4.9 cal/mol/K at 1000 K) causing the temperature increase with N<sub>2</sub> to be smaller than with Ar. The IDTs of oxirane are markedly reduced compared to those of its isomer acetaldehyde [645,647].

*Oxirane pyrolysis* was studied by Lifshitz and Ben-Hamou [594] in a ST (1.5-10 bar, 830-1200 K) and by Baldwin *et al.* [616] in a FR (0.08-0.7 bar, 753 K). CO, CH<sub>4</sub>, C<sub>2</sub>H<sub>6</sub>, and acetaldehyde were the major products. The former study [594] suggested that the main initiation step in the pyrolysis of oxirane is its isomerization to yield acetaldehyde, which decomposes to form smaller products. This reaction was later theoretically investigated [617] showing that it proceeds through a C–O rupture to form the  $\dot{\text{C}}\text{H}_2\text{CH}_2\dot{\text{O}}$  biradical, followed by 1,2-H shift in the biradical to form chemically activated CH<sub>3</sub>CHO, which can either be stabilized by collisions or directly dissociate to radical products [617,685], as shown in Fig. 43 (Part 5.1). The oxirane-

acetaldehyde isomerization was found to play also a very important role under ST ignition [644,647] or JSR oxidation [610] conditions.

Concerning oxidation product quantification, an early study was performed by Burgoyne and Kapur in 1951 [686] in a silica vessel at temperatures of 693 K and 571 K, being, respectively, above and below the optimum conditions for cool-flame formation. They measured the profiles of reactants, CO, CO<sub>2</sub>, CH<sub>2</sub>O, the sum of acids, and the sum of other aldehydes as a function of time. Later, Baldwin *et al.* [616] studied oxirane oxidation at 753 K in a slowly reacting mixture of H<sub>2</sub> + O<sub>2</sub> and confirmed that OH attack was more important than H attack. In 1996, following their pioneering work concerning hydrocarbon oxidation, which is described in Part 4, the group of Cathonnet in Orléans [610] studied oxirane oxidation in a JSR (1-10 bar, 800-1150 K). Using GC analysis, they showed that this CE rapidly produces CO, H<sub>2</sub>, CH<sub>2</sub>O, and CH<sub>3</sub>CHO. Fig. 57a presents an example of the mole fraction profiles of the detected species. The peak mole fraction of CH<sub>3</sub>CHO, the experimentally detected most abundant oxygenated intermediate, occurs around 900 K. During its JSR oxidation studied by [610], oxirane was found to be consumed largely (> 60%) *via* unimolecular reactions, *e.g.* the isomerization to yield acetaldehyde.



**Fig. 57.** Mole fraction profiles of species produced during the oxidation of oxirane (a) and oxetane (b) in a JSR (10 bar,  $\phi=2$ ,  $\tau=1$  s, 0.1-0.15% fuel). Symbols: experiment, lines with small symbols: model (in (a): O<sub>2</sub>, +; CO, o; CO<sub>2</sub>, \*; oxirane,  $\Delta$ ; CH<sub>3</sub>CHO,  $\square$ ; H<sub>2</sub>,  $\diamond$ ; in (b): O<sub>2</sub>, +; CO, o; CO<sub>2</sub>, \*; CH<sub>2</sub>O,  $\times$ ; oxetane,  $\bullet$ ; C<sub>2</sub>H<sub>4</sub>,  $\square$ ; H<sub>2</sub>,  $\diamond$ ). Reproduced from Refs. [610,623] with permission of Elsevier.

### **Oxetane:**

While, as mentioned in Part 5.1, several theoretical studies addressed the kinetics of oxetane decomposition [615,619,687,688], only one experimental study was found concerning its oxidation [623] (see Table 16) above 800 K.

*Ignition delay times* of oxetane were measured in a ST (1050-1780 K, 1.7-5.3 bar) by Dagaut *et al.* [623] in 1997. They express the ignition delay time in terms of the concentrations of each component in the gas phase as  $\tau=10^{-13.5} \exp(13389/T_5)[\text{oxetane}]^{-0.36}[\text{O}_2]^{-0.59}[\text{Ar}]^{0.088}$  (units: s, mole, cm<sup>3</sup>, K). The negative order for the fuel is similar to that found for oxirane (-0.4) [645]. Such an ignition enhancing effect is usually not observed for hydrocarbons [623] and larger CE as the values for THF (0.3) [653] and ~0 for THP [627] show.

*The mole fraction profiles of the species* formed during the oxidation of oxetane in JSR were measured at 1 bar and 10 bar over the temperature range 800-1150 K by Dagaut *et al.* [623]. CO, CO<sub>2</sub>, CH<sub>4</sub>, CH<sub>2</sub>O, C<sub>2</sub>H<sub>6</sub>, C<sub>2</sub>H<sub>4</sub>, C<sub>2</sub>H<sub>2</sub>, CH<sub>3</sub>CHO, C<sub>3</sub>H<sub>8</sub>, C<sub>3</sub>H<sub>6</sub>, propyne, and 1,3-C<sub>4</sub>H<sub>6</sub> were detected, but no propanal. The lack of propanal indicates a possible difference in the unimolecular initiation mechanism of oxetane compared to that of oxirane. Formaldehyde and ethylene (Fig. 57b) were the major intermediates, which was explained with the reaction  $\text{oxetane} \rightarrow \text{CH}_2\text{O} + \text{C}_2\text{H}_4$ . This pathway accounts for around 50% of oxetane consumption under the JSR oxidation conditions and it was also found to be very important under thermal decomposition conditions in the theoretical study of [619].

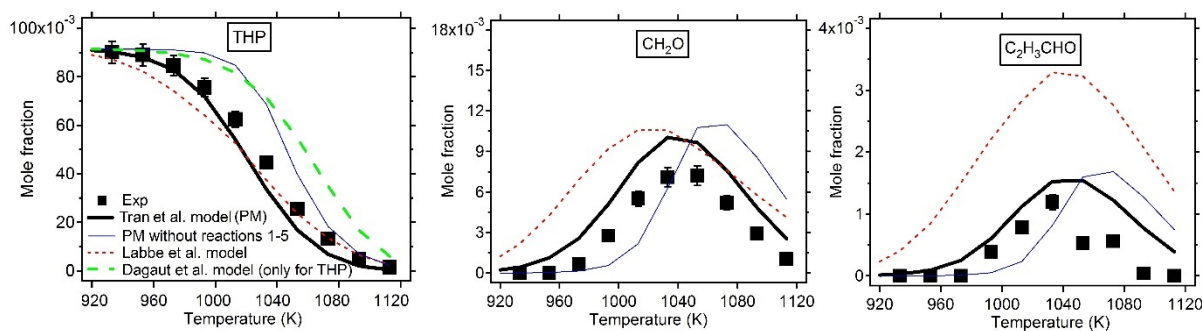
### **THP:**

*Laminar burning velocities* of THP were measured by Tran *et al.* [196] at atmospheric pressure. No high-pressure data is reported in the literature. At 1 bar, 298K, and  $\phi=1.1$ , the LBV is around  $44 \pm 1.8$  cm/s, *i.e.* very close to that of THF. No data was found for oxirane and oxetane for comparison.



High-temperature IDTs were measured in ST by Dagaut *et al.* [627] in the 90s (2-5 bar, 1000-1700 K) and by Tran *et al.* [196] in 2015 over a complementary pressure range (8.8-9.1 bar).

Speciation data measured in pyrolysis and in flames are available from studies in FRs and in flames [82,196,626,627] (see Table 16). Tran *et al.* [196] measured the species formed during the THP pyrolysis in a FR and reported the mole fraction profiles of more than twenty products with up to ten heavy atoms (naphthalene). Several of them were identified as primary products of THP thermal decomposition, such as CO, C<sub>2</sub>H<sub>4</sub>, CH<sub>2</sub>O, C<sub>2</sub>H<sub>3</sub>CHO, C<sub>3</sub>H<sub>6</sub>, and 1,3-C<sub>4</sub>H<sub>6</sub>. Fig. 58 presents the temperature dependence of the mole fractions of THP and of two important aldehydes, CH<sub>2</sub>O and C<sub>2</sub>H<sub>3</sub>CHO. These data were used to test the kinetic models developed by [196,626,627]. The mole fraction profiles of more than thirty C<sub>0</sub>-C<sub>6</sub> species were measured in PLFs fueled with THP by Labbe *et al.* [626] and Tran *et al.* [196] using PI-MBMS and GC, respectively. CH<sub>2</sub>O, C<sub>2</sub>H<sub>4</sub>, 1,3-C<sub>4</sub>H<sub>6</sub>, and C<sub>2</sub>H<sub>3</sub>CHO were detected as the important intermediates.



**Fig. 58.** Mole fraction profiles of THP, CH<sub>2</sub>O, and C<sub>2</sub>H<sub>3</sub>CHO measured during FR pyrolysis at 1.7 bar. Symbols: experiments [196]; lines: simulations with the models of Tran *et al.* [196], Labbe *et al.* [626], Dagaut *et al.* [627]. “PM without reactions 1-5”: Tran *et al.* model without the five unimolecular initiations involving C–C and C–O (see text in Part 5.2.1.4). Reproduced from Ref. [196] with permission of Elsevier.

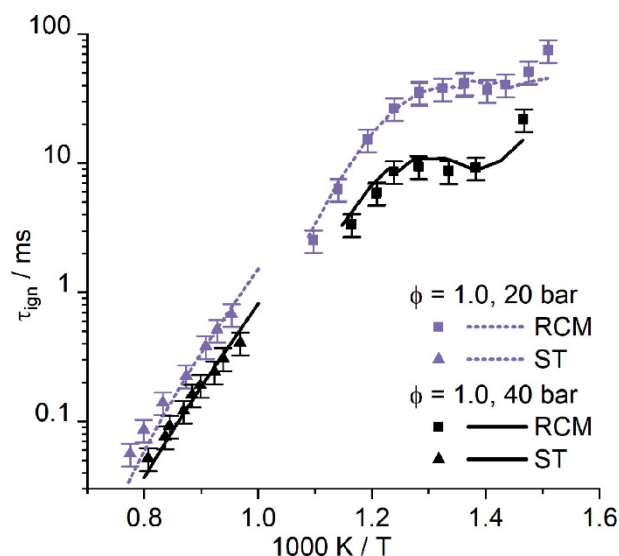
Concerning products formed during THP oxidation, early studies were performed in the 90s by Leppard [82] in a CFR engine and by Dagaut *et al.* [627] in a JSR (800-1100 K, 10 bar). Similar to what was observed for pyrolysis and flame, these oxidation studies showed that CO,

$C_2H_4$ ,  $CH_2O$ , and  $C_3H_6$  were formed in high concentrations. Leppard [82] detected  $C_2H_3CHO$ , dihydropyrans, tetrahydro-4H-pyran-4-one, and 1,5-pentanedial in non-negligible amounts under the CFR engine conditions. The presence of the three latter species indicates an effective role of THP low-temperature oxidation chemistry under these conditions.

Following a previous study of their group on the yields of conjugate alkene plus  $HO_2$  formation [398], Davis *et al.* [397] studied the Cl-initiated oxidation of THP and of its cycloalkane counterpart, cyclohexane, in a FR (500-700 K, 0.01 and 2 bar) using multiplexed PIMS. For both fuels, they observed time-resolved ion signals corresponding to fuel-specific cyclic KHP, at  $m/z$  132 ( $C_5H_8O_4$ ) for THP and  $m/z$  130 ( $C_6H_{10}O_3$ ) for cyclohexane. These KHPs were produced in lower concentration from THP than from cyclohexane, as inferred from ion signal intensity. This depletion was explained by the ease of ring-opening of the THP related  $\dot{Q}OOH$  radicals yielding 1,5-pentanedial, which leads to a reduced importance of second  $O_2$  addition reactions necessary for KHP formation in THP.

### **1,3-Dioxolane ( $C_3H_6O_2$ ):**

The *IDTs* of 1,3-dioxolane were recently measured in a ST and in a RCM [675] over the temperature range 630-1300 K. As is shown in Fig. 59, the group of Heufer in Aachen was able to measure *IDTs* at 20 and 40 bar using both types of devices. A very weak NTC zone was observed under the RCM conditions.



**Fig. 59.** Simulated (lines) and measured (symbols) ignition delay times at 20 and 40 bar (2% and 3.2% fuel in ST and RCM experiments, respectively). Reproduced from Ref. [675] with permission of Elsevier

Regarding product formation, the earliest studies [676,677,689,690] indicate  $\text{H}_2$ ,  $\text{CO}$ ,  $\text{CO}_2$ ,  $\text{CH}_2\text{O}$ ,  $\text{CH}_4$ ,  $\text{C}_2\text{H}_4$ , and  $\text{C}_2\text{H}_6$  as the main products of 1,3-dioxolane pyrolysis or photodecomposition. Wildenberg *et al.* [675] measured these species plus water in abundant amounts during the oxidation of this CE in a JSR at 10 bar above 700 K, with no reactivity observed below. Note, however, that a study of Molera *et al.* [691] in 1971 detected some specific low-temperature species, *e.g.* 1,3-dioxolan-2-one, 1,3-dioxolan-4-one, 1,3-dioxolan-2-hydroperoxides in a static reactor at temperatures below 613 K with initial fuel mole fractions up to 50%.

#### **1,4-Dioxane ( $\text{C}_4\text{H}_8\text{O}_2$ ):**

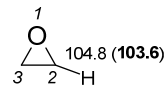
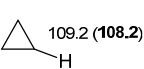
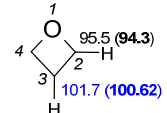
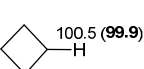
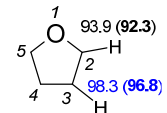
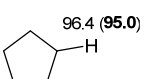
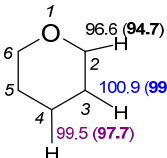
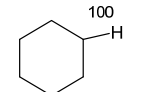
The studies for 1,4-dioxane focused mainly on product formation. Battin *et al.* [678,679] investigated the pyrolysis and oxidation of this CE in a static reactor. They detected  $\text{CO}$ ,  $\text{H}_2$ ,  $\text{C}_2\text{H}_4$ , and  $\text{CH}_2\text{O}$  as the main pyrolysis products. These species (plus  $\text{CO}_2$  and  $\text{H}_2\text{O}$ ) were also detected in abundance under oxidation conditions. More recently, Yang *et al.* [680] at Argonne National Laboratory investigated the pyrolysis of this CE in a ST and confirmed the results

from [678]. Under PLF conditions with MS analysis, Lin *et al.* [681] measured 20 C<sub>1</sub>-C<sub>4</sub> intermediates, six of those being radicals, and C<sub>2</sub>H<sub>2</sub>, C<sub>2</sub>H<sub>4</sub>, and CH<sub>2</sub>O are again the most abundant ones.

### 5.2.1.3. Comparison of the behavior of the non-substituted saturated cyclic ethers

The influence of the ring-size in non-substituted CEs containing one O-atom is discussed here. The chemical structure, the Bond Dissociation Energies (BDEs) and the ring strain energies of these CEs and their cycloalkane counterparts are presented in Table 17. The C–H BDE at the C<sub>2</sub> position decreases when going from oxirane to THF (103.6 to 92.3 kcal/mol calculated at the G4 level of theory) and then increases again from THF to THP (92.3 to 94.7 kcal/mol); indicating a clear ring size effect. This trend is also seen in the cycloalkane counterparts. Furthermore, the C–H BDE at the C<sub>2</sub> position is about 4-5 kcal/mol lower than those at other positions in the same CE or those of the cycloalkane counterparts, indicating a strong effect of the ether O-atom on the C–H BDE.

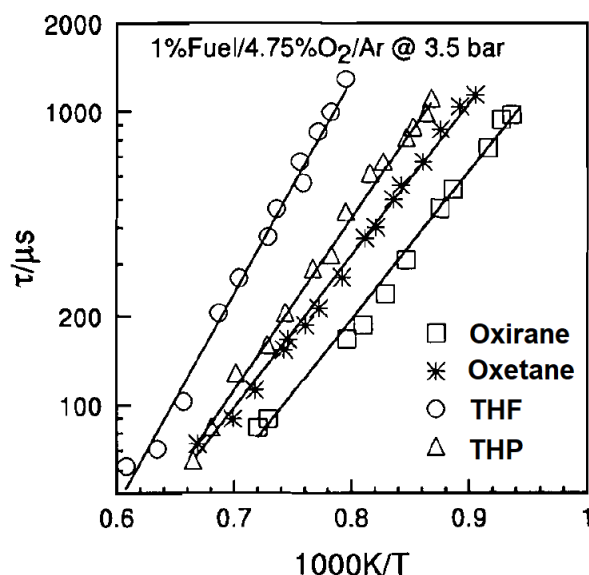
**Table 17.** Structures and ring strain energies of non-substituted saturated CEs and their cycloalkane counterparts. *Italic* numbers on CE structure: atom position. Other numbers on species structure: C–H BDE, in kcal/mol; those of CEs were calculated in the present work, at CBS-QB3 and at G4 (in parentheses); those of cycloalkanes were calculated at G3 by [692] and at G4 (in parentheses) by [693].

CEs	Ring strain energy (kcal/mol)	Cycloalkanes	Ring strain energy (kcal/mol)
Oxirane 	26.80 [141,187,200] 26.52 [694] 26.3-26.4 [695]	Cyclopropane 	27.60 [141,187,200] 27.5-27.7 [696]
Oxetane 	25.70 [141,187,200] 25.30 [694] 24.7-24.9 [695]	Cyclobutane 	26.20 [141,187,200] 26.80 [697] 25.8-26.5 [696]
THF 	5.90 [141,200] 5.96 [187] 5.4-5.7 [695]	Cyclopentane 	6.30 [141,187,200] 7.50 [697] 5.9-6.4 [696]
THP 	0.50 [141,200] 0.70 [187] 0 [696] 0-1.2 [695]	Cyclohexane 	0 (chair) [141,200,696] 0.08 (chair) [187] 1.0 (chair) [697]

As is shown in Table 17, the ring strain energy increases from THP (~0-1.2 kcal/mol) to oxirane (~26.3-26.8 kcal/mol); they are only slightly lower than those of their cycloalkane counterparts.

The differences in the chemical structures induce differences in the combustion chemistry/properties of these CEs. Leppard showed that THF has a significantly lower RON compared to cyclopentane (73 vs. 102), indicating that THF is more reactive under auto-ignition conditions [82]. Moreover, as described earlier, negative power dependences to fuel concentration were observed for the IDT of oxirane and oxetane [623,645] indicating a promoting effect of fuel concentration on the reactivity, while non-negative ones were seen for THF and THP [627,653]. Due to their high ring strain energies, oxirane and oxetane are mainly consumed by unimolecular initiation reactions under both pyrolysis and high-temperature oxidation conditions [594,610,623,644,647], whereas THF and THP mostly react via H-abstractions by small radicals (H-atom,  $\dot{\text{O}}\text{H}$ , etc.) [195,196,283,627,653]. Based on JSR experiments (800-1100 K,  $\phi=1$ , 10 bar, residence time of 0.5 s), Dagaut *et al.* [653] concluded that the fuel reactivity in their JSR increased from smaller to larger rings, *i.e.* oxirane < oxetane < THF < THP (the most reactive). In contrast, they found that the fuel ignition ability follows the order oxirane > oxetane > THP > THF based on IDTs (1100-1700 K, 1% fuel/4.75%O<sub>2</sub>/Ar, 3.5 bar) as shown in Fig. 60. The authors (Dagaut *et al.* [653]) explained this with the role of unimolecular decompositions, which are important under the studied ignition conditions but less important under the JSR oxidation conditions. Under the latter conditions, the reactivity increases with increasing the number of abstractable H-atoms in the fuels. IDTs are longer for THF than for THP, which is consistent with the ranking observed by Tran *et al.* [196] and with that observed for cyclopentane and cyclohexane [698]. Compared to cyclopropane, Lifshitz *et al.* [646] observed that oxirane has much lower IDTs (by an order of magnitude in the temperature range of 1200-1500 K), thus higher reactivity, which seems to be consistent with

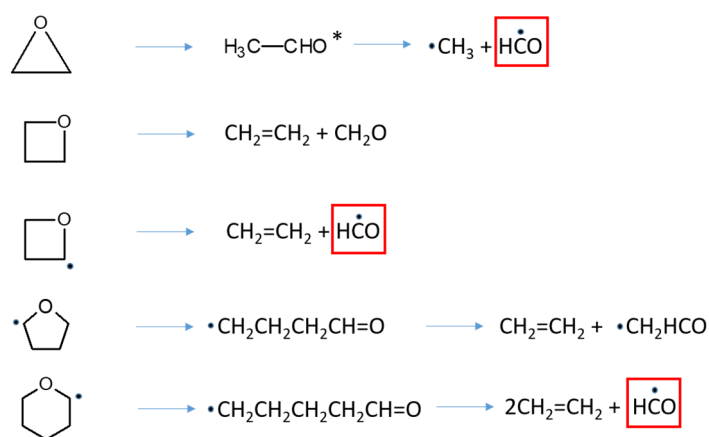
the lower C<sub>2</sub>-H BDE of oxirane as is shown in Table 17 and with the fact that the overall thermal decomposition rate of oxirane [617] is 3-10 times higher than those of cyclopropane [699]. To the best of our knowledge, there is no comparative study between oxetane and cyclobutane concerning their IDTs or unimolecular decomposition reactions.



**Fig. 60.** Comparison of the IDTs of non-substituted saturated CEs measured in ST. Symbols: experiments with constant initial and O<sub>2</sub> mole fractions. Lines: trendlines. Reproduced from Ref. [653] with permission of Taylor & Francis.

Dagaut *et al.* [653] explained the easier ignition of small CEs based on the order of ring strain energy that could strongly influence fuel unimolecular initiation steps. However, the study on the ignition of cyclopropane and cyclobutane (1200-1600 K,  $\phi=1$ ) by Slutsky *et al.* [700] does not find this ranking: they found cyclopropane to be more difficult to ignite than cyclobutane. A more convincing explanation of the IDT ranking might be found in the key chemical pathways, as displayed in Fig. 61. In oxirane and oxetane, fuel unimolecular initiation plays an important role. The unimolecular dissociation of oxirane leads to the formation of methyl and H $\dot{C}O$  radicals [617], while C<sub>2</sub>H<sub>4</sub> and CH<sub>2</sub>O are obtained from oxetane decomposition [619]. H $\dot{C}O$  radical is a source of H-atom, which promotes the H+O<sub>2</sub> branching step (the most promoting reaction in IDT studies). The unimolecular dissociation leading to two

radical, with one rapidly giving H-atom, explains the lowest IDTs observed for oxirane. Looking at the  $\beta$ - or  $\alpha$ -scission products of the dominant CE radical formed through H-abstraction, those are  $C_2H_4 + \dot{H}CO$  from oxetane,  $C_2H_4 + \dot{C}H_2CHO$  from THF (see flow rate analysis in Fig. 15 of Ref. [195]) and  $2 C_2H_4 + \dot{H}CO$  from THP (see flow rate analysis in Fig. 16 of Ref. [196]). The  $\dot{C}H_2CHO$  radical is not a direct source of H-atom as the  $\dot{H}CO$  radical; it can yield H-atom and ketene, but also CO and  $\dot{C}H_3$  radical and can combine with the  $\dot{C}H_3$  radical to give propanal. The CEs, which their radicals produce the  $\dot{H}CO$  radical (oxetane and THP) have similar IDTs, which are significantly lower than those of THF. In conclusion, although some first explanations about the relative reactivity of these saturated CEs could be offered based on the literature knowledge, more comparative investigations for these CEs will be useful.


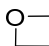
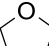
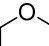
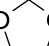
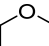


**Fig. 61.** Scheme of the major reactions providing a possible explanation for the IDT ranking of CE IDTs.

### 5.2.1.4. Detailed kinetic models of non-substituted saturated cyclic ethers

Table 18 summarizes the main detailed kinetic models for the non-substituted saturated CEs.

**Table 18.** Main detailed kinetic models for the combustion of non-substituted saturated CEs. For each CE, models are sorted by year of publication. Spe. N°: species number. Reac. N°: reaction number (forward). \* The conditions have been presented in previous rows of this table.

CE	Year & Ref.	Spe. N°	Reac. N°	Validation conditions (unit: T / K, P / bar)
Oxirane 	1990, Borisov <i>et al.</i> [701]	15	14	-IDT in ST and static reactor ( $T=770-1170$ , $P=0.3-1.5$ ) -ST pyrolysis species ( $T=900-1000$ , $P=0.25-1$ )
	1996, Kang <i>et al.</i> [644]	30	88	-IDT in ST ( $T=950-1220$ , $P=0.13^a$ , $\phi=0.5-2.0$ ) [644,645]
	1996, Würmel <i>et al.</i> [647]	30	60	-IDT in ST ( $T=1050-1400$ , $P=1.9-5$ , $\phi=0.5-2.0$ ) [647]
	1996, Dagaut <i>et al.</i> [610]	67	452	-JSR species ( $T=800-1150$ , $P=1-10.1$ , $\phi=0.5-2$ ) [610] -IDT in ST ( $T=1052-1315$ , $P=5.1$ , $\phi=0.4-3.2$ ) [643]
	2005, Joshi <i>et al.</i> [617]	45	332	-ST pyrolysis species ( $T=830-1200$ , $P=1.5-10.1$ ) [594]
Oxetane 	1997, Dagaut <i>et al.</i> [623]	63	423	-IDT in ST ( $T=1050-1780$ , $P=2-5.1$ , $\phi=0.5-2$ ) [623] -JSR species ( $T=800-1150$ , $P=1-10.1$ , $\phi=0.5-2$ ) [623]
THF 	1998, Dagaut <i>et al.</i> [653]	71	484	-IDT in ST ( $T=1000-1800$ , $P=2-5$ , $\phi=0.5-2$ ) [653] -JSR species ( $T=800-1100$ , $P=10$ , $\phi=0.5-1$ ) [653]
	2015, Tran <i>et al.</i> [195]	255	1723	-IDT in ST ( $T=1300-1700$ , $P=8.1-9.3$ , $\phi=0.5-2$ ) [195] -LBV ( $T_{initial}=298-398$ , $P=1$ , $\phi=0.55-1.6$ ) [195] -Species in PLF ( $P=0.07$ , $\phi=0.7-1.3$ ) [195]
	2018, Fenard <i>et al.</i> [283]	467	2390	-IDT in RCM ( $T=640-900$ , $P=5-10$ , $\phi=1$ ) [282] -IDT in ST ( $T=830-1100$ , $P=20-40$ , $\phi=1$ ) [281] -JSR species ( $T=500-1100$ , $P=1.1$ , $\phi=0.5-2$ ) [282] & [653]* -RCM species ( $T=711$ , $P=7.7$ ) [282] -Species in PLF [195]*
THP 	1997, Dagaut <i>et al.</i> [627]	72	507	-IDT in ST ( $T=1000-1700$ , $P=2-50$ , $\phi=0.5-2$ ) [627] -JSR species ( $T=800-1100$ , $P=10$ , $\phi=0.5-2$ ) [627]
	2013, Labbe <i>et al.</i> [626]	125	1046	-PLF species ( $P=0.03$ , $\phi=1.75$ ) [626]
	2015, Tran <i>et al.</i> [196]	273	2031	-LBV ( $T_{initial}=298-398$ , $P=1$ , $\phi=0.55-1.5$ ) [196] -IDT in ST ( $T=1350-1613$ , $P=8.9-9.1$ , $\phi=0.5-2$ ) [196] -FR pyrolysis species ( $T=913-1133$ , $P=1.7$ ) [196] & [626]*
1,3-Dioxolane 	2021, Wildenberg <i>et al.</i> [675]	601	3165	-IDT in ST ( $T=1032-1289$ , $P=20-40$ , $\phi=1$ ) [675] -IDT in RCM ( $T=662-911$ , $P=20-40$ , $\phi=1$ ) [675] -JSR species ( $T=700-1180$ , $P=10$ , $\phi=1$ ) [675]
1,4-Dioxane 	2011, Yang <i>et al.</i> [680]	--	83	-ST pyrolysis species ( $T=1550-2100$ , $P=0.07-0.16$ ) [680]

<sup>a</sup> Initial pressure ( $P_i$ ) of 0.13 bar, but final pressure ( $P_3$ ) was not provided in the original paper.

Five kinetic models were developed for **oxirane** with four in the 90s [610,644,647,701] and one in 2005 [617]. After the first proposition of Borisov *et al.* [701] based on literature or evaluated rate constants, the model by Kang *et al.* [644] was developed for oxirane oxidation with the part related to fuel decomposition calculated using *ab initio* methods (HF/6-31G\*). By determining transition states, four pathways to form acetaldehyde (1), vinyl alcohol (2), formaldehyde and carbene (3) and methoxy carbene (4) were confirmed. The first path is



energetically favorable as an initiation step. The model by Würmel *et al.* [647] developed in the same year was quite similar to that proposed by Kang *et al.* [644], but with rate constants exclusively taken from the literature, *e.g.* from [594]. Note that these models capture the ST high-temperature IDT of [644,645,647] (see conditions in Table 18) well. The more detailed model by Dagaut *et al.* [610] was developed by expanding that of Lifshitz and Ben-Hamou [594], with oxirane unimolecular initiation pathways adjusted to account for pressure dependence. The predictions of this model agreed reasonably well with the JSR experiments >800 K and the high-temperature IDT data of Burcat [643], showing nevertheless the need to better estimate the rate constants for oxirane decomposition at high temperatures. Later, Joshi *et al.* [617] proposed a kinetic model for oxirane pyrolysis by theoretically examining the unimolecular decomposition of oxirane and the fate of the oxiranyl radical (see Fig. Fig. 43 and Fig. 46 in Part 5.1). Compared to Lifshitz and Ben-Hamou [594], the computed rate constant for the oxirane-acetaldehyde isomerization was found to be in close agreement for  $T > 1000$  K, but lower by a factor of 2 at 800 K. The model was tested using the pyrolysis species profiles measured in ST by [594]. None of the models mentioned above consider low-temperature chemistry for oxirane oxidation.

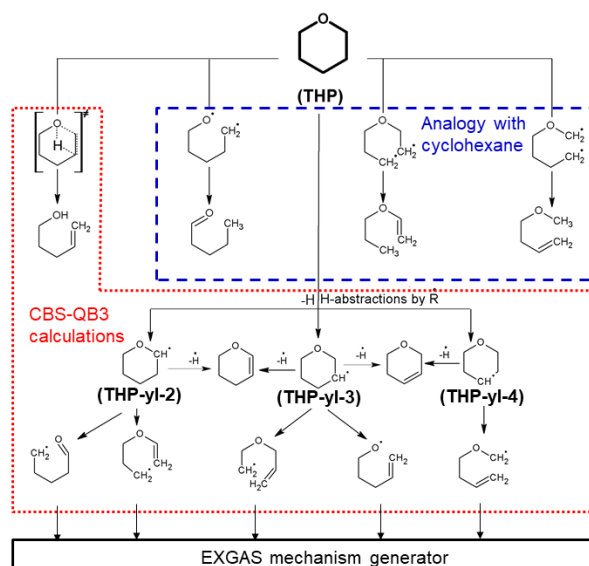
Regarding **oxetane**, the only available model is the oxidation model developed by Dagaut *et al.* [623] based on the oxirane model described above [610]. This model well predicts data for ST ignition and JSR oxidation (Table 18). The typical reaction classes for oxetane were implemented using mostly estimated rate constants, *e.g.* unimolecular initiation of the fuel to yield C<sub>2</sub>H<sub>4</sub> and CH<sub>2</sub>O, H-abstractions to yield oxetanyl radicals with their further  $\beta$ -scission decompositions.

Three main models are dedicated to **THF**. First, Dagaut *et al.* [653] developed a THF kinetic model starting from their oxirane and oxetane models [610,623]. This model includes both unimolecular initiation steps of THF suggested by Lifshitz *et al.* [613]

( $\text{THF} \rightarrow \text{C}_2\text{H}_4 + \text{C}_2\text{H}_4\text{O}$ ,  $\text{THF} \rightarrow \text{C}_3\text{H}_6 + \text{CH}_2\text{O}$ ). The rate coefficients for H-abstractions from THF and the reactions of the derived radicals were mostly estimated. The first  $\text{O}_2$  addition was globalized considering  $\dot{\text{O}}\text{H}$ ,  $\text{C}_2\text{H}_4$ , and  $\text{CHOCHO}$  as products and no second  $\text{O}_2$  addition chemistry was considered. Although, the model predicted IDTs in ST and JSR species profiles fairly well, the authors pointed out the need for more accurate rate coefficients for the  $\beta$ -scissions of the THF-yl radicals at temperatures above 800 K. Around 17 years later, the Nancy group developed a new model for the high-temperature THF oxidation [195] by combining reactions generated automatically by EXGAS with those calculated with CBS-QB3. The unimolecular initiations of THF, H-abstractions from THF and  $\beta$ -scissions of the fuel radicals were theoretically calculated by Verdicchio *et al.* [618] and by Tran *et al.* [195], respectively. A PES example is shown in Fig. 47. The model reproduced the high-temperature IDTs in ST, LBVs and species profiles in PLFs well, although a slight overprediction of LBVs was observed. In 2018, Fenard *et al.* [283] proposed the first detailed kinetic model for the low-temperature oxidation of THF with the high-temperature part taken mainly from [195]. The thermochemical and kinetic data of important reactions of the low-temperature part, especially those involved in the first  $\text{O}_2$  addition pathways, were derived from *ab initio* calculations at the CBS-QB3 level of theory (see PES in Fig. 49 for a comparison of results from different studies). The model predicted literature data measured in RCM, ST (IDTs), JSR and PLFs (species profiles) reasonably well despite a noted underprediction for the JSR mole fraction profiles of  $\text{CO}$ ,  $\text{CO}_2$  and those of some oxygenates below 800 K. This model was recently used by [590] for studying KHP formation, by [655] for studying low-temperature IDTs, and by [702,703] for developing reduced models. A recent theoretical study by Lockwood and Labbe [612] provided further insights into the second  $\text{O}_2$  addition pathways including KHP formation.

The three detailed models developed for **THP** (Table 18) apply only to high-temperature chemistry. The first one was developed by Dagaut *et al.* [627] with the rate coefficients for

unimolecular initiations assumed as those proposed by [613] for THF. Similar to the THF model, the first O<sub>2</sub> addition in the THP model was written as a globalized pathway yielding  $\dot{\text{O}}\text{H}$ ,  $\text{H}\dot{\text{C}}\text{O}$ , allyl, and CH<sub>2</sub>O, but neglecting the second O<sub>2</sub> addition chemistry. The model predictions showed fairly good agreement with IDTs measured in a ST and with JSR species profiles [627]. However, the authors pointed out the need of more accurate rate constants for the H-abstractions from THP by  $\dot{\text{O}}\text{H}$  and for the high-temperature decomposition of the THP-yl radicals (including THP-yl-2, THP-yl-3, THP-yl-4, see structures in Fig. 62). Later, Labbe *et al.* [626] proposed a model with the rate coefficients of unimolecular initiations taken from [627] and those of other reactions mainly based on analogies with cyclohexane [704]. The rate coefficients of H-abstractions from THP by H-atoms and  $\dot{\text{C}}\text{H}_3$  radicals and the fall-off for THP-yl decompositions were theoretically calculated. Simulations of species profiles in a fuel-rich PLFs (Table 18) showed good agreement with experimental data in terms of peak magnitudes, shapes, and positions of the mole fraction profiles of major species and several intermediates. However, CH<sub>2</sub>O mole fractions were over-predicted by a factor of 2.5 and H $\dot{\text{C}}\text{O}$  ones under-predicted by a factor of 4. This prompted Labbe *et al.* [626] to suggest that the decomposition chemistry of THP is more complex than thought. Later, Tran *et al.* [196] developed a model using EXGAS generation with key kinetic parameters for the primary mechanism updated using quantum-chemical calculation (CBS-QB3) and analogies with structurally similar species from cyclohexane. Fig. 62 summarizes the important primary reaction pathways and the methods used for determining their rate coefficients.



**Fig. 62.** Important reaction pathways and respective methods used for rate coefficient determinations in the high-temperature THP combustion model by Tran *et al.* [196].

One of the important differences between this last model and the previous ones [626,627] is the description of the initial unimolecular ring-opening reactions. Dagaut *et al.* and Labbe *et al.* [626,627] adopted the reaction steps proposed by Lifshitz *et al.* [613] for THF, in which the diradicals formed in the ring-opening bond scission step dominantly undergo subsequent  $\beta$ -scission reactions to create smaller species. In contrast, the model of Tran *et al.* [196] contains diradical chemistry that favors intramolecular H transfer over  $\beta$ -scissions. This model in general accurately predicted LBVs and IDTs measured in a ST, and species profiles measured in FRs and PLFs. Under flame conditions, the above-mentioned models showed that THP was largely consumed by H-abstractions followed by ring-opening of the formed fuel radicals. The model by [196] showed that THP pyrolysis is very sensitive to the unimolecular initiations involving C–C and C–O bond fissions (reactions 1-5 mentioned in Fig. 58), including (1)  $\text{THP} \rightarrow \text{CH}_2=\text{CHCH}_2\text{CH}_2\text{CH}_2\text{OH}$ , (2)  $\text{THP} \rightarrow \text{CH}_3\text{CH}_2\text{CH}_2\text{CH}_2\text{CHO}$ , (3)  $\text{THP} \rightarrow \text{CH}_3\text{CH}_2\text{CH}_2\text{OCH}=\text{CH}_2$ , (4)  $\text{THP} \rightarrow \text{CH}_2=\text{CHCH}_2\text{CH}_2\text{OCH}_3$ , (5)  $\text{THP} \rightarrow 1\text{-C}_4\text{H}_8 + \text{CH}_2\text{O}$ . However, once the radical pool is established, the product distribution and fuel consumption

are mainly controlled by H-abstraction reactions and not by the initial bond scission reactions [196].

A model was proposed for each of the two CEs containing two O-atoms in the ring, *i.e.* 1,3-dioxolane and 1,4-dioxane (Table 18). Wildenberg *et al.* [675] very recently developed a kinetic model for the low- and high-temperature oxidation of **1,3-dioxolane** with rate coefficients calculated theoretically for the  $\beta$ -scission reactions of the fuel radicals (1,3-dioxolan-2-yl and 1,3-dioxolan-4-yl) and estimated rate expression for other reactions using analogies, *e.g.* to 2-MTHF [658], diethoxy/dimethoxy methane [705,706], 1,4-dioxane [596], diethyl ether [707]. The model predictions agree well with high-pressure IDTs and species profiles. The authors pointed out that the 1,3-dioxolan-2-yl radical and the derived QOOH radical react faster by  $\beta$ -scission than by addition to O<sub>2</sub>, which explains the weak NTC behavior observed.

Yang *et al.* [680] proposed a model for the pyrolysis of **1,4-dioxane** including unimolecular initiation pathways that were theoretically investigated by these authors. The model predictions compared well with the ST pyrolysis species profiles measured in the same study. The authors pointed out that, in analogy to the THP chemistry proposed by Tran *et al.* [196], the dissociation/isomerization of 1,4-dioxane forms ethylene glycol vinyl ether and 2-ethoxyacetaldehyde, which rapidly dissociate to smaller species.

### 5.2.2. Substituted saturated cyclic ethers

As shown by Table 16, the investigated substituted saturated CEs include oxirane rings substituted by alkyl chains, and THF rings substituted by alkyl chains or an oxygenated group. A few studies were performed by Zalotai *et al.* [708,709] for the decomposition of methyloxetanes, but with the aim to determine reaction rates, thus they are not listed in Table 16. Except those by Zalotai *et al.* [708,709], no data can be found for substituted oxetanes and

substituted THPs. Moreover, no experimental study is available on the consumption chemistry of other substituted saturated CEs listed in Part 4.

#### **5.2.2.1. Oxirane rings substituted by alkyl chains**

The data concerning 2,3-dimethyloxirane and ethyloxirane are more limited than those about methyloxirane (Table 16).

*Flame velocities* were measured by Burluka *et al.* [648] in CVB for methyloxirane and its isomers, propanal and acetone. The following LBV order was observed: methyloxirane ( $\sim 70 \pm 1.5$  cm/s at  $\phi=1.1$ , 298 K, 1 bar) > acetone ( $\sim 47 \pm 1.5$  cm/s) > propanal ( $\sim 37 \pm 1.5$  cm/s). No other LBV data were published after 1980 for oxirane derivatives. However, Gibbs and Calcote [710] showed in 1959 using a Bunsen burner that methyloxirane had LBVs  $\sim 45\%$  lower than oxirane, indicating an important effect of the lateral methyl group.

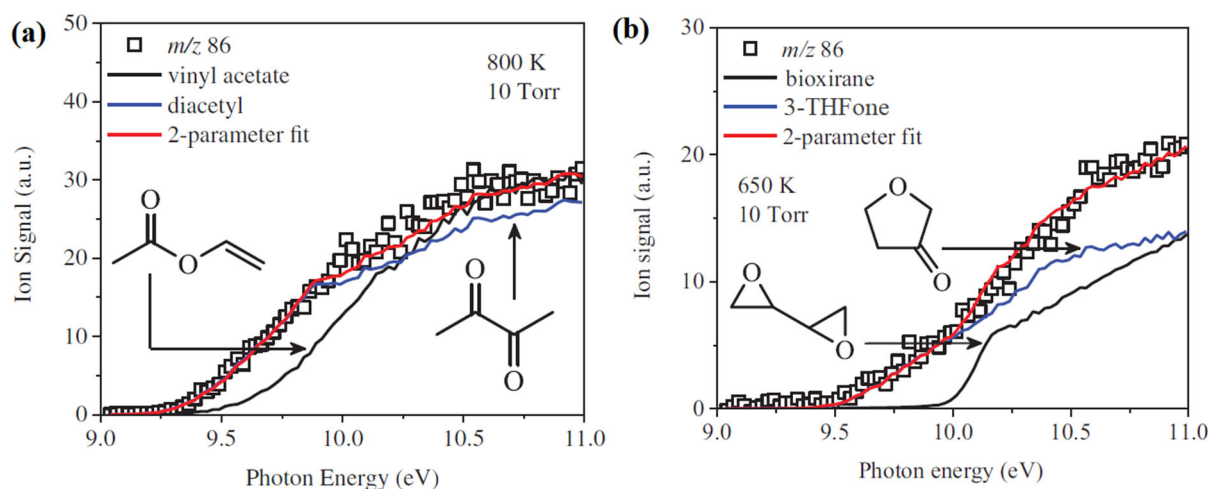
The earliest *ignition study* on the three substituted oxiranes (methyloxirane, 2,3-dimethyloxirane, ethyloxirane) was performed by the group of Lifshitz [646] in a ST at 900-1300 K (see Table 20). The IDTs can be ordered as follows: 2,3-dimethyloxirane  $\approx$  ethyloxirane > methyloxirane  $\approx$  oxirane. Similar to what was observed earlier for oxirane, the IDTs of the substituted oxiranes display a negative power dependence on fuel concentration, indicating a promoting effect by the fuel. Very recently, Ramalingam *et al.* [649] measured IDTs of methyloxirane in a RCM and a ST (870-1127 K, 10-40 bar). The authors did not observe NTC behavior for this fuel.

*High-temperature (> 900 K) product formation* was investigated for methyloxirane by Lifshitz *et al.* [614] and Ramalingam *et al.* [649] under ST pyrolysis conditions, and by Knyazkov *et al.* [650] in a PLF. The pyrolysis of 2,3-dimethyloxirane was studied by Flowers and Parker [711] in a static vessel and by Lifshitz and Tamburu [651] in a ST. The major products measured during the pyrolysis of both fuels are CO, C<sub>2</sub>H<sub>4</sub>, C<sub>2</sub>H<sub>6</sub>, and CH<sub>4</sub>. The fuel isomers, *i.e.* propanal and acetone for methyloxirane, and butanone and 2-methylpropanal for

2,3-dimethyloxirane, are early abundant products indicating the importance of isomerization in the initiation steps of both fuels. This is similar to what was observed for oxirane as discussed above. Using MBMS, Knyazkov *et al.* [650] only reported the formation of C<sub>1</sub>-C<sub>2</sub> oxygenated products and thus no fuel isomers.

*The product formation in low-temperature (< 800 K) was only very recently investigated for 2,3-dimethyloxirane and ethyloxirane by the group of Rotavera at the University of Georgia [395,511] focusing on the competition between the unimolecular decomposition reactions of fuel radicals and their reactions with O<sub>2</sub>. Products were probed using SVUV-MBMS during the Cl-initiated oxidation of both fuels in a FR. Several species were identified as being formed by the unimolecular decomposition of fuel radicals, such as C<sub>2</sub>H<sub>4</sub>, CH<sub>2</sub>O, ketene, and acrolein. Interestingly, reaction pathways prototypical for low-temperature chemistry of alkanes were experimentally observed for ethyloxirane oxidation but not for 2,3-dimethyloxirane, in which oxirane ring-opening dominated. In ethyloxirane oxidation, a conjugated alkene (ethenyloxirane) produced through 2-ethyloxirane-3-yl + O<sub>2</sub> combination followed by HO $\dot{O}$ -elimination was detected, whereas no conjugated alkene isomer was detected for 2,3-dimethyloxirane. As indicated by the PIE spectra in Fig. 63a, during the oxidation of 2,3-dimethyloxirane, vinyl acetate and diacetyl were detected but no CE typically involved in an  $\dot{O}H$ -elimination from  $\dot{Q}OOH$  radical decomposition even though Fig. 48 shows that pathways to CE exist, whereas two CE isomers (3-THFone and bioxirane) were detected during ethyloxirane oxidation (see Fig. 63b). Note that as displayed in Fig. 48, the radicals obtained by the isomerizations of the RO $\dot{O}$  radicals are resonance-stabilized KHP-type radicals, which from alkanes would be obtained by H-abstractions from KHPs. The formation of ketones and bicyclic ethers as shown in Fig. 63 indicates that the 2,3-dimethyloxirane/ethyloxirane consumption reactions are more complex than currently considered in chemical kinetics*

mechanisms and that reactions of substituted oxiranes may contribute to the radical pool more than what is currently considered.



**Fig. 63.** PIE spectrum of  $m/z$  86 signal from Cl-initiated oxidation of *cis*-2,3-dimethyloxirane (a) and ethyloxirane (b) in a FR. Reproduced from Refs. [395,511] with permission of John Wiley and Sons.

#### 5.2.2.2. THF substituted by alkyl chains

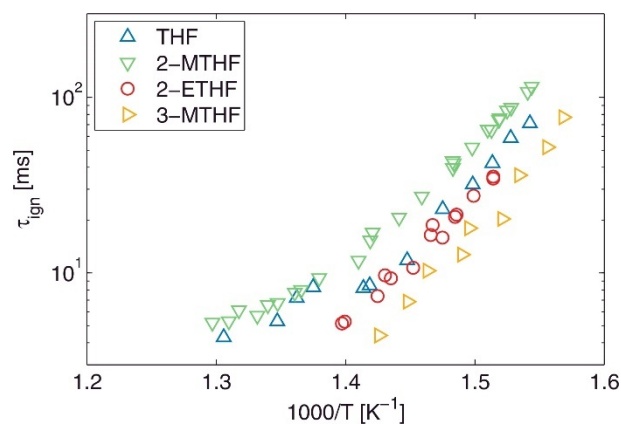
Among the THFs substituted by alkyl chains, 2-MTHF is the most often investigated fuel, with data reported for LBVs, IDTs, and species profiles, as shown in Table 16.

*Laminar burning velocities* of 2-MTHF were measured using PLF [658] and CVB [652,659,660] up to 10 bar. Those of 2,5-DMTHF and 2-BTHF were also investigated in CVB [652,672]. No LBV data has been reported for other alkyl substituted THFs. Wang *et al.* [652] observed LBV in the following order 2,5-DMTHF (*e.g.*  $47.65 \pm 2.2$  cm/s at  $\phi=1.1$ ,  $T_{\text{initial}}=373$  K) < 2-MTHF ( $53.32 \pm 1.89$  cm/s) < THF ( $59.06 \pm 1.79$  cm/s). De Bruycker *et al.* [658] obtained the same ranking between 2-MTHF and THF. While it is clear that methyl substitutions in THF fuels reduce LBVs, the explanation for this is less obvious. A variety of factors including adiabatic temperature, thermal diffusivities, and kinetics were considered to explain this ranking [652]. From a kinetic point of view, increasing the number of methyl substitutions increases the possibilities of formation of methyl radicals that remove H-atoms from the system through recombinations producing  $\text{CH}_4$ , thus reducing LBVs [658].



*High-temperature IDTs* of 2-MTHF were measured in STs by Wang *et al.* [661,662] and Jouzdani *et al.* [664,665]. Tripathi *et al.* [663,669], Fenard *et al.* [670], and Cai *et al.* [672] reported IDTs obtained in STs for 2-MTHF, 2,5-DMTHF, and 2-BTHF, respectively. In the temperature range above 1000 K, the IDTs of these CEs exhibit overall an Arrhenius behavior.

*Concerning low-temperature auto-ignition behavior* as described in Part 1 (Fig. 7), the group of Pitsch in Aachen [87] studied the DCN of a series of THF derivatives and found the following order: 2-BTHF(45.5) > 2-ETHF (28.1) > 2-MTHF (22.0)  $\approx$  THF (21.9). Thus, increasing the length of the alkane side chain facilitated, as expected, auto-ignition. In other studies, Pitsch and coworkers [654,663,669,672] and the group of Vanhove in Lille [666,670] reported IDTs measurements in RCM for these CEs, as well as for 2,5-DMTHF and 3-MTHF. Sudholt *et al.* [654] showed that for temperatures below 715 K the IDTs of the four THF derivatives presented in Fig. 64 followed an Arrhenius behavior with similar overall activation energies and suggested that the rate determining reaction steps for the ignition of these molecules are similar. Note that in the temperature range 750-850 K, Fenard *et al.* [666,670] noticed a deviation from Arrhenius behavior for the IDTs of 2-MTHF and 2,5-DMTHF, although not yet a NTC zone. Fig. 64 also shows that 3-MTHF is the easiest to ignite CE (shortest IDT), followed by 2-ETHF~THF, with 2-MTHF being the least ignitable one (longest IDT). The ranking between 2-MTHF and THF is consistent with that reported under engine conditions by Leppard [82]. The considerable difference in IDTs (*e.g.* a factor of 2.6 at 700 K) between 2-MTHF and 3-MTHF indicates a strong influence of the substituent position. An explanation for this trend is given in Part 5.2.2.4.



**Fig. 64.** IDTs of THF, 2-MTHF, 3-MTHF, 2-ETHF measured in RCM at  $\phi=1$  and 20 bar. Reproduced from Refs. [654] with permission of Elsevier.

*High-temperature (> 900 K) products*, as summarized in Table 16, were measured for 2-MTHF (FR and ST pyrolysis [658,664] and PLF [658,667,668]) and for 2,5-DMTHF (FR pyrolysis [671]). No speciation data was found for any other molecules of this class. In the 2-MTHF pyrolysis study of De Bruycker *et al.* [658] 16 species were detected among which 4-penten-1-ol was formed in significant amounts ( $\sim 2000$  ppm). The formation of this 2-MTHF isomer was explained with a concerted ring-opening reaction mechanism, which dominated over alternative ring-opening pathways.

Under flame conditions, a wide range of products ( $\sim 50$  hydrocarbons and oxygenated species from  $C_0$ - $C_7$ ) was experimentally detected [658,667,668]. 2-MTHF is classically consumed mainly by H-abstractions and decompositions of the resulting fuel radicals into small species by  $\beta$ -scissions. These species, such as 2-oxo-ethyl and 2-oxo-propyl radicals, may combine with hydrogen atoms and carbon-centered radicals to form several of the detected oxygenated products.

*Concerning low-temperature oxidation (< 800 K) products*, a few studies were performed, again only for 2-MTHF (in CFR engine [82] and RCM [666]) and 2,5-DMTHF (in RCM [670]). Under engine conditions, Leppard [82] indicated that in 2-MTHF oxidation the same general organic classes were formed as in THF oxidation: unsaturated cyclic ethers, cyclic

ketones, and bifunctional carbonyls. For instance, 2,3-DHF, tetrahydrofuran-3-one, and butanedial were detected in THF oxidation, while 5-methyl-2,3-DHF, 2-methyltetrahydrofuran-3-one, and 4-oxo-pentenal were identified in 2-MTHF oxidation. The latter three components simply differ from the former three by an additional CH<sub>3</sub> moiety. Fenard *et al.* [666] also detected 5-methyl-2,3-DHF and 2-methyltetrahydrofuran-3-one in RCM. 4-Oxo-pentenal (bifunctional carbonyl) was not reported, possibly due to the GC column used, instead its isomers (allyl acetate and 1-propen-2-ol acetate) were observed.

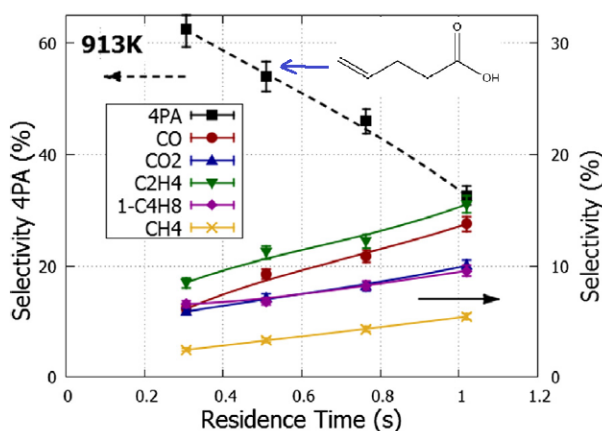
2,5-DMTHF, with two CH<sub>3</sub> moieties attached to the ring, produces fuel-specific intermediates different from those of THF. However, as shown in Fenard *et al.* [670], the reactions of this CE followed again the same pattern as that of THF with just adding two more CH<sub>3</sub> groups to the measured products. For example, 2,5-dimethylfuran was detected as the major unsaturated cyclic ether, and hexa-2,5-dione was identified as the important bifunctional carbonyl species. 2,5-Dimethyloxolan-3-one (an expected important cyclic ketone) was not reported, again possibly due to the GC column used by [670], suggesting that further measurements of fuel-specific species of 2,5-DMTHF low-temperature oxidation are needed.

### **5.2.2.3. THF substituted by an oxygenated group**

CEs substituted with a carbonyl (*e.g.*  $\gamma$ -valerolactone, GVL) or an alcohol (*e.g.* 2-THFFOH) function were recently investigated by studies [251,259,673,674] that exclusively focused on species detection (Table 16).

Concerning GVL, its pyrolysis was studied by De Bruycker *et al.* [259,673] in a FR. Among the 16 quantified species, 4-pentenoic acid (4PA), a GVL isomer, appears as an important oxygenated intermediate in the early stages of the pyrolysis as shown in Fig. 65. This indicates that the isomerization process is important for initiating GVL decomposition. The formation of unsaturated acids was also found for heavier lactones by Bailey and Bird in 1977 [712]. Under GVL/CH<sub>4</sub> flame conditions, Sudholt *et al.* [674] measured a wide range of species (40 species)

with the smaller ones such as formaldehyde, ethane, ethylene, and acetylene being produced with the largest amounts.



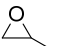

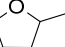

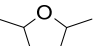
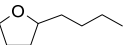
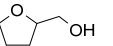
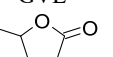
**Fig. 65.** GVL thermal decomposition in a FR: product selectivity as a function of residence time at 913 K, 4PA is 4-pentenoic acid). Lines indicate the observed trend. Reproduced from Ref. [673] with permission of Elsevier.

The flame chemistry of 2-THFFOH was recently investigated by Tran *et al.* [251,668]. More than 40 products were quantified in a CH<sub>4</sub> flame doped with 10-20% 2-THFFOH. Many of them, *i.e.* ethylene, formaldehyde, acrolein, allyl alcohol, 2,3-DHF, 3,4-dihydro-2H-pyran, 4-pentenal, and tetrahydrofuran-2-carbaldehyde were identified as important 2-THFFOH-specific decomposition products. The presence of an alcohol function favors the formation of allyl alcohol and acrolein. The detection of 3,4-dihydro-2H-pyran confirmed the possibility of ring enlargement in agreement with the theoretical calculations performed by the authors. A comparison of 2-THFFOH to 2-MTHF [668] demonstrates that the difference in their chemical structures does not have a notable impact on the mole fractions of CO, CO<sub>2</sub>, H<sub>2</sub>O, and H<sub>2</sub>, but significant differences exist for the yields of intermediate species. The doped 2-THFFOH flame produces more aldehydes, alcohols, and ethers but forms clearly less ketones and hydrocarbons.

#### 5.2.2.4. Detailed kinetic models of substituted saturated cyclic ethers

Table 19 summarizes the main detailed kinetic models for the substituted saturated CEs listed in Table 16. No models were found for ethyloxirane and 2-ETHF. The model (56 species, 183 reactions) developed by Wu *et al.* [702] for the oxidation of THF, 2-MTHF, and 2-BTHF is not listed in Table 19 because it is a reduced model based on the detailed models of Fenard *et al.* [283] (THF), Tripathi *et al.* [663] (2-MTHF), and Cai *et al.* [672] (2-BTHF).

**Table 19.** Main detailed kinetic models for the combustion of substituted saturated CEs. For each CE, the models are sorted by year of publication. Spe. N<sup>o</sup>: species number. Reac. N<sup>o</sup>: reaction number (forward). \* The conditions have been presented in previous rows of this table.

CE	Year & Ref.	Spe. N <sup>o</sup>	Reac. N <sup>o</sup>	Validation conditions (unit: T / K, P / bar)
Methyloxirane 	1994, Lifshitz <i>et al.</i> [614]	37	68	-ST pyrolysis species ( $T=850-1250, P=2$ ) [614]
	2010, Burluka <i>et al.</i> [648]	127	1200	-LBV ( $T_{initial}=298, P=1, \phi=0.7-2.1$ ) [648]
	2021, Ramalingam <i>et al.</i> [649]	573	3077	-LBV of [648]* -IDT in ST ( $T=962-1127, P=10-40, \phi=0.5-2$ ) [649] & ( $T=960-1300, P=2.5-7, \phi=0.5-1$ ) [646] -IDT in RCM ( $T=870-980, P=10-20, \phi=0.5-2$ ) [649] -ST pyrolysis species ( $T=900-1450, P=40$ ) [649] & [614]*
2,3-Dimethyloxirane 	1995, Lifshitz <i>et al.</i> [651]	41	65	-ST pyrolysis species ( $T=900-1150, P=2$ ) [651]
2-MTHF 	2013, Moshhammer <i>et al.</i> [667]	185	1412	-PLF species ( $P=0.04, \phi=1.7$ ) [667]
	2017, De Bruycker <i>et al.</i> [658]	412	2481	-LBV ( $T_{initial}=298-398, P=1, \phi=0.6-1.6$ ) [658] -FR pyrolysis species ( $T=900-1100, P=1.7$ ) [658] -PLF species ( $P=0.07, \phi=0.7-1.3$ ) [658] & [667]*
	2017, Tripathi <i>et al.</i> [663]	250	1247	-IDT in RCM ( $T=639-878, P=10-40, \phi=0.5-2$ ) [663] -IDT in ST ( $T=753-1349, P=10-20, \phi=0.5-2$ ) [663] -IDT in ST ( $T=1050-1800, P=10.1, \phi=1$ ) [661] -PLF species of [667]*
	2017, Fenard <i>et al.</i> [666]	507	2425	-IDT in RCM ( $T=640-900, P=30-21, \phi=1$ ) [666] -IDT in ST ( $T=1050-1800, P=1.2-10.1, \phi=0.5-2$ ) [661] -RCM species ( $T=719, P=7.6, \phi=1$ ) [666] -PLF species of [667]*
3-MTHF 	2019, Tripathi <i>et al.</i> [669]			-IDT in ST ( $T=715-1250, P=10-40, \phi=0.5-2$ ) [669] -IDT in RCM ( $T=615-900, P=10-40, \phi=0.5-2$ ) [654,669]
2,5-DMTHF 	2019, Fenard <i>et al.</i> [670]	664	3197	-IDT in ST ( $T=860-1320, P=10-40, \phi=1$ ) [670] -IDT in RCM ( $T=660-880, P=10-20, \phi=1$ ) [670] -RCM species ( $T=712, P=10, \phi=1$ ) [670]
2-BTHF 	2017, Cai <i>et al.</i> [672]	419	1588	-LBV ( $T_{initial}=448, P=1-3, \phi=0.7-1.35$ ) [672] -IDT in ST ( $T=705-1210, P=20, \phi=1$ ) [672] -IDT in RCM ( $T=650-900, P=10.1, \phi=0.5-1$ ) [672]
2-THFFOH 	2021, Tran <i>et al.</i> [251]	479	2914	-PLF species ( $P=0.05, \phi=1$ ) [251]
GVL 	2016, De Bruycker <i>et al.</i> [259]	520	3589	-FR pyrolysis species ( $T=900-1100, P=1.7$ ) [259]
	2017, Sudholt <i>et al.</i> [674]	347	1336	-PLF species ( $P=0.07, \phi=1$ ) [674]

For oxirane derivatives, Lifshitz and Tamburu [614,651] proposed the first kinetic model for the thermal decomposition of methyloxirane and 2,3-dimethyloxirane with the rate

coefficients for unimolecular initiation reactions of the fuel mainly derived from their experiments [614,651] and those of [711,713]. These models successfully reproduced the production rates and distribution of pyrolysis products measured in ST experiments (Table 19).

Later, Burluka *et al.* [648] developed a model for the high-temperature oxidation of methyloxirane combining pyrolysis reactions largely adopted from Lifshitz and Tamburu [614] with a mechanism for small hydrocarbons [714] and estimated kinetics of oxygenated species. The model predicted the LBVs of fuel-rich mixtures well but it significantly underpredicted those of fuel-lean and stoichiometric flames. The authors suggested to improve the ketene sub-mechanism.

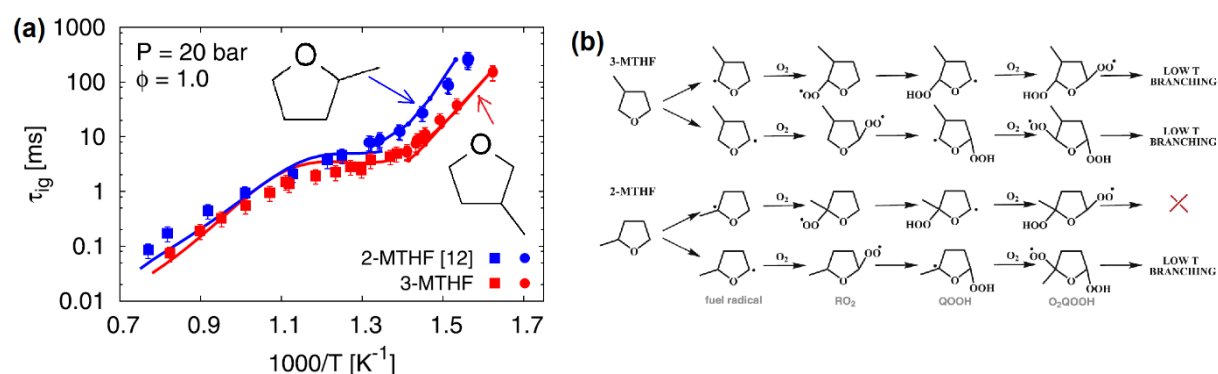
The Heufer group in Aachen [649] recently proposed a model for methyloxirane oxidation based on the Aramco Mech 3.0 model [496] that is more complete than earlier ones [614,648]. The reaction rates of fuel isomerizations to propanal, propanone, and methyl vinyl ether were obtained through fits to earlier data of [620,713]. Other unimolecular initiation reactions were adopted from Lifshitz and Tamburu [614]. H-abstraction reactions from the fuel and fuel radical decomposition kinetics were mainly estimated by analogy to other molecules such as oxirane, *iso*-butane, and the methoxymethyl radical. The model was tested against several data sets (Table 19) and was able to predict high-pressure IDTs and the profiles of pyrolysis product detected in a ST (up to 40 bar). Interestingly, despite the absence of a low-temperature oxidation reaction subset for the fuel radicals, the model also reproduces IDTs measured in a RCM (870-980 K) quite well. The authors pointed out that the conversion of methyloxirane to propanal is governed by isomerization channels even below 1000 K. This behavior is quite similar to the oxirane kinetic behavior discussed above. Note that the dominance of isomerization channels even at low-temperature has not yet been validated for more heavily substituted oxirane derivatives, for which no model is yet available.

Concerning THF rings substituted by alkyl chains, four main detailed models are known for 2-MTHF and one model was proposed for each of the other CEs (3-MTHF, 2,5-DMTHF, 2-BTHF) (Table 19). Moshhammer *et al.* [667] and De Bruycker *et al.* [658] proposed models for the high-temperature oxidation of **2-MTHF**. Both models reproduce flame speciation data well. The latter model also successfully predicts LBVs and pyrolysis species profiles. The description of primary 2-MTHF reactions, especially the decomposition of 2-MTHF derived radicals, is more detailed in the model by De Bruycker *et al.* than in that by Moshhammer *et al.* [667], since it also considered concerted ring-opening and favored intramolecular H transfer in diradical and carbene chemistry, for which rate coefficients were calculated at the CBS-QB3 level of theory. Furthermore, the model by De Bruycker *et al.* included reaction channels that aimed to explain experimentally detected oxygenated species, such as large aldehydes and ketones, as well as 4-penten-1-ol. These molecules were not considered by Moshhammer *et al.*

Tripathi *et al.* [663] in Aachen and Fenard *et al.* [666] in Lille proposed models for the low- and high-temperature chemistry of 2-MTHF. The Aachen model [663] adopted the high-temperature sub-model from Moshhammer *et al.* [667] with updates for H-abstractions by  $\dot{\text{O}}\text{H}$  and  $\text{HO}\dot{\text{O}}$  mainly taken from analogy to THF. The low-temperature sub-model contained 20 reaction classes and was developed systematically on the basis of rate rules and reaction classes [457,510] with updates based on the 2-BTHF model of Cai *et al.* [672]. A very similar methodology was used in the development of the Lille model [666], which also adopted the high-temperature sub-model from Moshhammer *et al.* [667] with updates using new rate constants for H-abstractions by  $\text{HO}\dot{\text{O}}$  based on the theoretical calculations of [608] and by  $\text{O}_2$  and  $\dot{\text{O}}\text{H}$  from analogy with methylcyclohexane [533]. The low-temperature sub-model was newly developed using rate coefficients from rate rules [470] and analogy to cycloalkanes [533]. The two 2-MTHF models [663,666] were tested against low- and high-temperature IDTs and species profiles (Table 19) and their predictions agreed overall well with the data. The

authors demonstrated the importance of the H-abstractions by  $\dot{\text{O}}\text{H}$  radicals and the need for theoretical studies of the corresponding rate coefficients in order to further improve the model performance.

Detailed models including low- and high-temperature chemistry were also developed in Aachen [669,672] for **3-MTHF** and **2-BTHF**. The high-temperature part was developed based on the current understanding of combustion chemistry for a variety of structurally similar molecules, *e.g.* THF and its derivatives, while the low-temperature part was developed using an approach based on rate rules [446,457,510]. The predictions of both models were compared to IDTs measured in a ST and a RCM, and those of 2-BTHF model were also compared to LBVs (Table 19). It was observed that the models generally reproduced the experimental data fairly well. The 3-MTHF model [669] predicts for 3-MTHF a considerably higher low-temperature reactivity compared to 2-MTHF, in agreement with experimental observations (Fig. 66a). The model demonstrated that 3-MTHF oxidation had more reaction pathways that create low-temperature branching (Fig. 66b).



**Fig. 66.** Ignition of 2-MTHF and 3-MTHF: **(a)** Experimental (symbols, measured in ST and RCM) and simulated (lines) IDTs; **(b)** Comparison of the low-temperature reaction pathways of both fuels. Reproduced from Ref. [669] with permission of Elsevier.

Extending their THF [283] and 2-MTHF [666] models, the group of Vanhove in Lille simulated **2,5-DMTHF** oxidation at low- and high-temperatures based on their experimental data for IDTs and species profiles obtained in a ST and a RCM. Their modelling analyses demonstrated the promoting influence of methyl radicals on IDTs above 1200 K due to the easy



C–C bond dissociation of 2,5-DMTHF producing methyl radical that is thus abundant. At lower temperatures, the reactivity is dominated by the classic branching pathways involving cyclic KHPs. 2,5-DMTHF was found to be consumed largely by H-abstractions at C<sub>2</sub> and C<sub>5</sub> positions because of their low C–H BDEs (see CE structure in Table 17), especially at low temperatures they accounted for more than 80% of 2,5-DMTHF consumption.

*Concerning THF rings substituted by an oxygenated group*, a model can be found for 2-THFFOH [251] and two models are available for GVL [673,674]. Tran *et al.* [251] recently proposed a detailed kinetic model for **2-THFFOH** high-temperature oxidation with the rate coefficients of important primary mechanism reactions derived from CBS-QB3 calculations. The model predicted experimental PLF species profiles reasonably well and showed that 2-THFFOH is mainly consumed by H-abstraction reactions, which is in agreement with other THF derivatives. Interestingly, the derived oxygenated species with *cis* configuration were found to be thermodynamically more stable than their corresponding *trans* configuration, which differs from usual observations for hydrocarbons. For example, the standard enthalpy of formation of (oxolan-2-ylidene)methanol (2-THFCHOH) is -61.0 and -64.7 kcal/mol for the *trans*- and *cis*-conformers, respectively, which was explained by Tran *et al.* [251] as due to the intramolecular hydrogen bond formed by the *cis*-isomer.

The group of Van Geem in Ghent [259] proposed a model for the thermal decomposition of **GVL**. The model considers the formation of 4PA via the concerted ring-opening of GVL. The reaction rates of this reaction and those of H-additions, H-abstractions, as well as fuel radical decomposition reactions were calculated at the CBS-QB3 level of theory. Model predictions were in good agreement with the FR pyrolysis species profiles and confirmed the importance of the isomerization of GVL to 4PA, which is similar to the formation mechanism of 4-penten-1-ol from 2-MTHF as presented above. 4PA is then mainly consumed by  $\dot{\text{C}}\text{H}_3$  and H-additions releasing other carboxylic acids. Later, Sudholt *et al.* [674] in Aachen developed a

model for GVL high-temperature oxidation by extending the pyrolysis sub-mechanism of [259]. The oxidation reaction part was established mainly based on the concept of reaction classes and rate rules [446,457] with some updates using analogies to 1- and 2-butanol [715] and 2-MTHF [667]. The model was tested against species profiles from a PLF study and showed good agreement with the species data in the pre-heat and reaction zones of the flame until the fuel is depleted. At larger heights above the burner, deviations between the model and the measurements were observed.

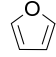
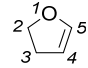
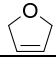
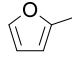
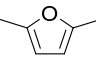
### **5.3. Experimental and modelling studies on the chemistry of unsaturated cyclic ethers**

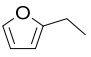
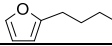
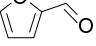
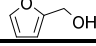

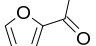
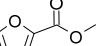
Unsaturated CEs have received similar interest from the scientific community as the saturated ones. Table 20 listed over 80 experimental studies related to the pyrolysis and combustion of unsaturated CEs. Each study contains different datasets that include several data points. These studies were performed experimental setups similar to those used for saturated CEs. There are more studies (we found about 30 of them) concerning the pyrolysis of unsaturated CEs than for saturated ones, because some unsaturated CEs are considered as model components in biomass pyrolysis studies. In contrast, far less studies were performed on the oxidation of unsaturated CEs below 1000 K (about 20 studies) than of saturated ones (about 40 studies) because they do not play a role in low-temperature oxidation. The largest number of studies concerns 2,5-DMF, with about 25 studies at temperatures ranging from 500 to 2500 K (because of its different nature, the initial temperatures of LBV or engine experiments are not considered),  $P$  from  $1.3 \times 10^{-6}$  bar to 80 bar,  $\phi$  from 0.03 to  $\infty$ . Apart from furfural, studies on other oxygen-substituted furans (*e.g.* 2-FFOH, 2-AF, 2-MOF) are still very limited with only pyrolysis data for the last two ones. Only very few studies involve diffusion flames and these only address soot formation. These studies are not listed in Table 20 because they are not dedicated to the investigation of the primary chemistry of CE during pyrolysis, oxidation or combustion.

The review paper by Xu *et al.* [716] very comprehensively analyzed the kinetic studies concerning furan, 2-MF and 2,5-DMF published before 2016. Therefore, even though for sake of consistency with Table 16 all the studies found in the literature are presented in Table 20, they are discussed in less detail in Part 5.3 than what has been done for saturated CEs in Part 5.2.

Part 5.3.1 describes the results concerning furan, 2-MF and 2,5-DMF, a group of three CEs often investigated together, briefly summarizing the data obtained before the review of [716] and with more emphasis on the work performed afterward. Then, the influence of the degree of unsaturation in furan derivatives and that of C<sub>1+</sub> alkylic substitutions are discussed in Part 5.3.2 while the impact of oxygenated substituents are discussed in Part 5.3.3. To conclude, the performance of the recent kinetics models concerning unsaturated CEs are discussed in Part 5.3.4.

**Table 20.** Main experimental studies on the pyrolysis and combustion of unsaturated CEs from 1980. The entries are sorted according to the experimental target, *i.e.* LBV, IDT, speciation data (spec. data). Entries within each target are sorted by the reactor type. “--” indicates that the information is not available. *Italic* numbers on 2,3-DHF structure are labels of the atom position, which are used in the main text.

Fuel	Exp. Target	Reactor	Operating conditions				Year, first author, ref.	
			<i>T</i> (K)	<i>P</i> (bar)	$\phi$	Fuel % (diluent)		
Furan 	LBV	CVB	363 <sup>a</sup>	1-5	0.8-1.4	3.6-6.2 (N <sub>2</sub> )	2021, Tanoue [717]	
	IDT	ST	1320-1880	1.2-10.5	0.5-2	0.25-1 (Ar)	2012, Wei [718]	
			977-1570	1-12	0.5-2.0	2.28-8.54 (Ar)	2014, Eldeeb [719]	
			1150-2010	1.2-16	1.0	0.5 (Ar)	2015, Xu [720]	
			870-950	20	1.0	4.46 ( <sup>b</sup> )	2016, Sudholt [654]	
			850-1050	18-33	0.5-2.0	1 (Ar)	2020, Wu [655]	
	Spec. data	ST	1050-1460	2.6-3.6	$\infty$	1 (Ar)	1986, Lifshitz [721]	
			1100-1700	20.3	$\infty$	0.2-2 (Ar)	1991, Organ [722]	
			500-3000	0.1-0.8	$\infty$	2-100 (Kr, Ne)	1998, Fulle [723]	
			1200-1900	0.7-1.6	$\infty$	5 $\times$ 10 <sup>-4</sup> , 9 $\times$ 10 <sup>-4</sup> (Ar)	2018, Weber [724]	
			1050-1920	1	$\infty$	1 (Ne)	2019, Weiser [297]	
		PLF	up to 1888	0.05	1.4-2.2	14-19 (Ar)	2011, Tian [226]	
			up to 2600	0.02-0.04	1.0-1.7	9-14 (Ar)	2014, Liu [273]	
		FR	1050-1270	1.3 $\times$ 10 <sup>-6</sup>	$\infty$	--	1985, Grela [725]	
			1250-1700	1-2	$\infty$	0.7-0.07 (He)	2009, Vasiliou [637]	
730-1170			1	0.5-2.0	0.93 (Ar)	2017, Tran [726]		
1100-1600	0.04	$\infty$	5 (Ar)	2017, Cheng [638]				
2,3-DHF 	IDT	ST	1100-1635	1.2-10.1	0.5-2.0	0.5 (Ar)	2016, Fan [633]	
		RCM	850-1050	18-33	0.5-2.0	1 ( <sup>b</sup> )	2020, Wu [655]	
	Spec. data	ST	900-1300	0.6	$\infty$	0.5 (Ar)	1989, Lifshitz [631]	
2,5-DHF 	IDT	ST	1100-1650	1.2-10.1	0.5-2.0	0.5 (Ar)	2016, Fan [633,727]	
	Spec. data	ST	980-1080	1.6-6.5	$\infty$	0.25-1 (Ar)	1986, Lifshitz [632]	
2-MF 	LBV	PLF	298-398 <sup>a</sup>	1	0.55-1.65	1.91-5.52 (N <sub>2</sub> )	2013, Somers [728]	
			CVB	333-393 <sup>a</sup>	1	0.6-1.4	2.08-4.73 <sup>c</sup> (N <sub>2</sub> )	2014, Ma [729]
				360 <sup>a</sup>	1-2	0.7-1.4	2.40-4.73 (N <sub>2</sub> )	2018, Zhongyang [730]
	IDT	ST	1200-1800	1	0.5-2	1 (Ar)	2013, Somers [728]	
			1120-1700	1.3-10.7	0.25-2.0	0.25-3.38 (Ar)	2013, Wei [731]	
			820-1215	40	1.0	3.32 (N <sub>2</sub> )	2014, Uygun [281]	
			977-1570	1-12	0.5-2.0	1-6.54 (Ar)	2014, 2015, Eldeeb [719,732]	
			1150-2010	1.2-16	1.0	0.5 (Ar)	2015, Xu [720]	
			830-910	20	1.0	3.38 ( <sup>b</sup> )	2016, Sudholt [654]	
		RCM	737-1143	16-30	0.5-2.0	1 (Ar)	2016, 2017, Xu [733,734]	
			861-912	20	1.0	3.38 <sup>d</sup> (Ar)	2018, Tripathi [735]	
			Spec. data	ST	1100-1400	1.7-2.9	$\infty$	0.5 (Ar)
		1200-1900			0.7-1.6	$\infty$	4 $\times$ 10 <sup>-4</sup> , 1 $\times$ 10 <sup>-3</sup> (Ar)	2018, Weber [724]
		1050-1920			1	$\infty$	1 (Ne)	2019, Weiser [297]
		PLF		--	0.04	0.8-1.5	21 (Ar)	2012, Wei [737]
up to 2500	0.02-0.04			1.0-1.7	7-11 (Ar)	2014, Tran [274]		
up to 2000	0.04			0.8-1.5	6.2 (Ar)	2017, Cheng [738]		
FR	600-925	1	0.5-2.0	1.5 (Ar)	2021, Wang [739]			
	1050-1270	1.3 $\times$ 10 <sup>-6</sup>	$\infty$	--	1985, Grela [725]			
	800-1400	1	0.02-3.33	0.01 ( <sup>e</sup> )	2016, Alexandrino [740]			
730-1170	1	0.5-2.0	1 (Ar)	2017, Tran [726]				
900-1530	0.04-1	$\infty$	2 (Ar)	2017, Cheng [741]				
2,5-DMF 	LBV	CVB	393 <sup>a</sup>	1	0.9-1.5	2.45-4.08 ( <sup>f</sup> )	2009, Wu [742]	
			323-373 <sup>a</sup>	1	0.6-2.0	1.67-5.37 (N <sub>2</sub> )	2010, Tian [270]	
			373-473 <sup>a</sup>	1-7.5	0.7-1.5	1.95-4.08 (N <sub>2</sub> )	2011, 2012 Wu [743-745]	
			PLF	298-358 <sup>a</sup>	1	0.6-1.6	1.67-4.34 (N <sub>2</sub> )	2013, Somers [746]
				IDT	ST	1300-1831	1-4	0.5-1.5
	820-1941	1-80	0.5-2			0.75-2.66 (N <sub>2</sub> /Ar)	2013, Somers [746]	
	977-1570	1-12	0.5-2.0			0.76-5.32 (N <sub>2</sub> /Ar)	2014, 2015, Eldeeb [719,732]	
	1150-2010	1.2-16	0.5-2.0			0.5 (Ar)	2015, Xu [720]	
	RCM	737-1143	16-30	0.5-2.0	0.5-2 ( <sup>b</sup> )	2016, Xu [733]		
		Spec. data	ST	1070-1370	2-3.7	$\infty$	0.5 (Ar)	1998, Lifshitz [748]

			1191-1328	2.3	$\infty$	3 (Ar)	2013, Somers [746]	
			1200-1900	0.7-1.6	$\infty$	$3.4 \times 10^{-1}$ , $4.4 \times 10^{-4}$ (Ar)	2018, Weber [724]	
			1050-1920	1	$\infty$	1 (Ne)	2019, Weiser [297]	
	PLF		--	0.04	2	--	2009, Wu [749]	
			up to 2500	0.02-0.04	1.0-1.7	5.9-9.2 (Ar)	2014, Togbé [275]	
			up to 2000	0.04	1.0-1.5	5.17 (Ar)	2015, Liu [750]	
	JSR		530-1190	10	0.5-2	0.1 (N <sub>2</sub> )	2013, Somers [746]	
	FR		1050-1270	$1.3 \times 10^{-6}$	$\infty$	--	1985, Grela [725]	
			873-1098	1.7	$\infty$	9 (N <sub>2</sub> )	2013, Djokic [641]	
			780-1470	0.04-1	$\infty$	2 (Ar)	2014, Cheng [751]	
			500-1400	1-40	0.03-3.33, $\infty$	0.01-0.45 <sup>§</sup> (N <sub>2</sub> )	2014, 2015, Alexandrino [752,753]	
			730-1170	1	0.5-2.0	1.5 (Ar)	2017, Tran [726]	
	LBV	CVB	373-433 <sup>a</sup>	1-4	0.7-1.4	1.95-3.77 (N <sub>2</sub> )	2021, Xu [754]	
		IDT	ST	1050-1290	5-12	1.0	2.72 (Ar)	2015, Eldeeb [732]
			RCM	780-870	20	1.0	2.72 (b)	2016, Sudholt [654]
				766-1013	16-30	0.5-2.0	1-2.7 (b)	2017, Xu [734]
	Spec. data	JSR		600-900	1	0.5-2.0	1 (Ar)	2022, Li [755]
		FR	846-1319	0.04-1	$\infty$	1 (Ar <sup>h</sup> )	2021, Song [756]	
	IDT	RCM	730-870	20	1.0	1.96 (b)	2016, Sudholt [654]	
	LBV	Conical flame	473 <sup>a</sup>	1	0.6-1.8	2.49-7.11 (N <sub>2</sub> )	2021, Jin [757]	
	Spec. data	JSR	1200-1800	0.1-0.2	$\infty$	0.2-0.6 (He/Ar)	2013, Vasiliou [758]	
			1023-1073	1	$\infty$	1 (Ar)	2019, Li [759]	
			900-1100	1.07	$\infty$	0.5 (He)	2019, Vermeire [423]	
			650-950	1	0.4-2	0.5 (Ar)	2021, Jin [757]	
	FR		1040	--	$\infty$	--	1986, Grela [760,761]	
			929-1365	0.04-1	$\infty$	1 (Ar)	2021, Wang [762]	
	Spec. data	FR	923-1223	0.04	$\infty$	0.5 (He <sup>i</sup> )	2021, Vermeire [640]	
	Spec. data	FR	973-1273	0.04	$\infty$	0.5 (He <sup>i</sup> )	2021, Vermeire [640]	
	Spec. data	JSR	770-1130	1	$\infty$	0.3 (Ar)	2022, He [763]	
	Spec. data	FR	879-1107	1	$\infty$	1 (Ar)	2019, Yan [764]	

<sup>a</sup> Initial temperature

<sup>b</sup> Mixture of N<sub>2</sub> and Ar

<sup>c</sup> Data for 2-MF and *iso*-octane mixtures are also available in [729].

<sup>d</sup> Data of 2-MF and *n*-heptane mixtures are also available in [735]

<sup>e</sup> Mixture of N<sub>2</sub> and H<sub>2</sub>O. Data with NO addition are also available in [740]

<sup>f</sup> 2-MF in air (thus N<sub>2</sub> was the diluent), and 2-MF in air plus additional N<sub>2</sub> or plus CO<sub>2</sub>.

<sup>§</sup> Mixtures with NO were also used.

<sup>h</sup> Ar plus 1% Kr

<sup>i</sup> 2% NO was also added used as a reference for quantification of the PICS

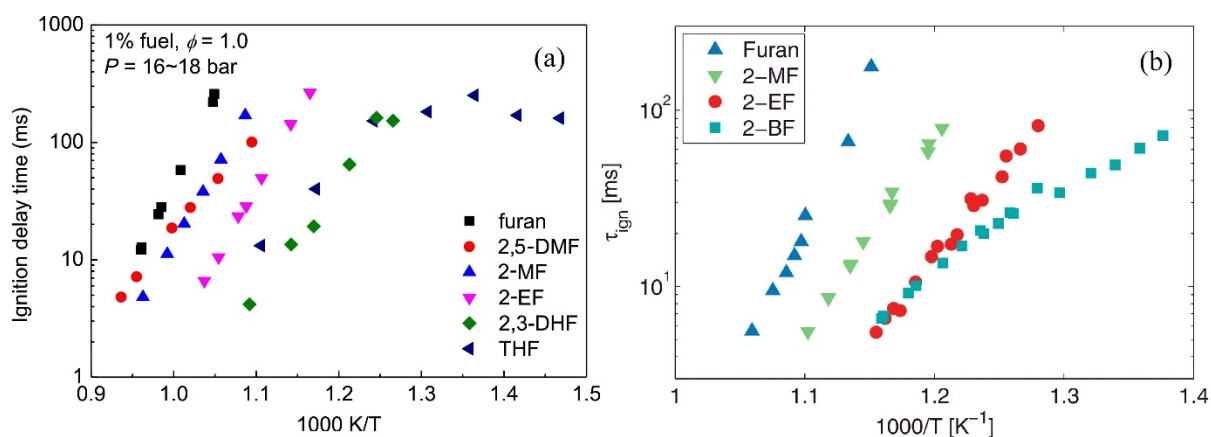
### 5.3.1. Furan, 2-MF and 2,5-DMF

The aromatic character of furan and alkyl furans has been noticed, among others, by Simmie and Curran [231] and by Sendt *et al.* [636]. The BDEs of the ring C–H in furan, 2-MF and 2,5-DMF are all close to 120 kcal/mol, while the corresponding BDE in benzene is only 112 kcal/mol. Therefore, H-abstraction reactions from furan, 2-MF and 2,5-DMF ring are very unlikely. The lack of a methyl group explains that the lowest reactivity is observed for unsubstituted furan, as shown by the DCN and IDT measurements and by the flow reactor studies described hereafter.

*The flame velocity* of furan has only recently been measured in 2021. Tanoue *et al.* [717] reported data for  $\phi=0.8, 1$  and  $1.4$  at atmospheric pressure. At  $363\text{ K}$  and  $\phi=1$ , the LBV of furan is  $\sim 21\%$  higher than that of 2-MF measured by Ma *et al.* [729]. The LBV of 2-MF reported by Zhongyang *et al.* [730] is even lower than that by Ma *et al.* [729]. The Nancy group also reported LBV data for some furans and THFs. For example, at  $1\text{ bar}$ ,  $298\text{ K}$ , and  $\phi=1.1$ , the LBV is found to be around  $46\pm 1.1\text{ cm/s}$  for 2-MF [728] and  $39\pm 1\text{ cm/s}$  for 2,5-DMF [746], compared to  $43\pm 1.7\text{ cm/s}$  for THF [195]. Tanoue *et al.* [717] showed a notable impact of pressure between  $1$  and  $5\text{ bar}$  at  $363\text{ K}$ , in agreement with Wu *et al.* [744], who observed a significant negative pressure dependence for 2,5-DMF at  $393\text{ K}$ .

*Concerning ignition behavior*, Fig. 7 in Part 1 indicates the following order for the DCNs reported by Sudholt *et al.* [87]: 2,5-DMF (10.9) > 2-MF (8.9) > furan (7.0). Measurements in STs (see studies listed in Table 20) show that the IDTs of the three compounds follow Arrhenius behavior. IDTs decrease with increasing pressure and with decreasing equivalence ratio. The highest values are found for furan, while those of 2-MF and 2,5-DMF are lower and close together. At the time of the review of Xu *et al.* [716], ignition studies in RCM for unsaturated CEs were missing. They became available with the work for 2-MF and 2,5-DMF by Xu *et al.*

[733] (the team at Xi'an Jiaotong University who noticed the lack of RCM data in their review [716]), and that for furan and C<sub>1+</sub> alkylated furan by Sudholt *et al.* in Aachen [654]. Furthermore, IDTs of 2-MF and 2-MF/*n*-heptane mixtures were measured by Tripathi *et al.* [735], who showed that both fuels compete for OH radical consumption. Finally, Wu *et al.* [655] studied the unsaturation effect as described in Part 5.3.2. As is shown in Fig. 67a, the IDTs of furan, 2-MF and 2,5-DMF in RCM follow also Arrhenius behavior. The IDT of 2-MF is about a factor 5 lower than that of furan at 970 K, but very close to that of 2,5-DMF indicating similar reaction channels during ignition of these CEs. According to the flow rate analysis by Xu *et al.* [733], the low-temperature IDT chemistry of 2-MF and 2,5-DMF does not proceed through the O<sub>2</sub> addition pathways as proposed by Simmie *et al.* [639] but instead the radicals obtained from H-abstraction on a methyl group react by combination/decomposition reactions with HO $\dot{O}$  or CH<sub>3</sub>O $\dot{O}$  radicals in a similar way as toluene [765] yielding ultimately furfural and 5-methylfurfural, respectively, as proposed by Somers *et al.* [746,766].



**Fig. 67.** Auto-ignition of furan derivatives in RCMs: IDTs ( $\phi=1$ ) of (a) furan [655], 2-MF, 2,5-DMF [733], 2-EF [734], 2,3-DHF and THF [655] at 16-18 bar plotted by [655] and (b) furan, 2-MF, 2-EF and 2-BF at 20 bar [654]. Reproduced from Ref. [654,655] with permission of Elsevier.

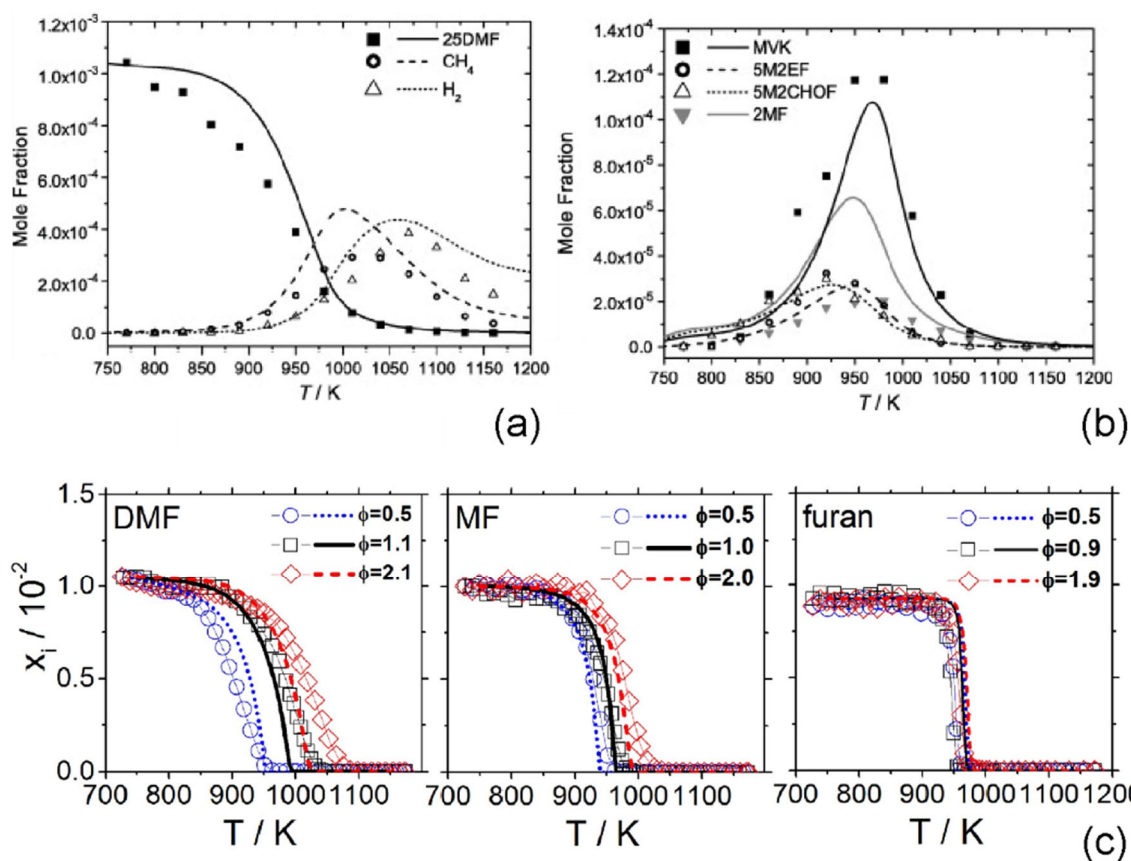
*Product quantifications during the pyrolysis* of furan, 2-MF, 2,5-DMF have been the topic of a large number of studies in STs and FRs, as is shown in Table 20. This was complemented by a significant theoretical effort as is described in Part 5.1.2. Again, these studies started with those performed in a single-pulse ST with GC analysis by the group of

Lifshitz [721,736,748], who first proposed rate constants for the initial decomposition steps of these three molecules. The understanding of these reactions steadily progressed until the most recent studies were made by the group of Olzmann in Karlsruhe in ST behind reflected shock wave with spectroscopic monitoring of H-atoms [724] and MS species detection (IE = 50 eV) [297]. According to [636,638,724], the thermal decomposition of furan proceeds through two parallel channels, (i) a molecular elimination step to form acetylene + ketene and (ii) a ring-opening reaction via 1,2-hydrogen migration and C–O bond fission to finally yield CO + propyne. For substituted furans H-ejection from the methyl groups needs to be considered in addition to ring-opening/H-shift reaction pathways. The major products obtained during the thermal decomposition in ST around 1400 K were CO, CH<sub>4</sub>, C<sub>2</sub>H<sub>2</sub>, C<sub>2</sub>H<sub>6</sub>, C<sub>2</sub>H<sub>4</sub>, C<sub>3</sub>H<sub>4</sub> isomers and benzene from 2-MF [297] and CO, CH<sub>4</sub>, C<sub>2</sub>H<sub>2</sub>, C<sub>2</sub>H<sub>4</sub>, C<sub>2</sub>H<sub>6</sub>, and cyclopentadiene from 2,5-DMF as agreed by [641] and [748]. The last studies also detected 1,3-C<sub>4</sub>H<sub>6</sub> and 2-MF in their GC analyses from single-pulse ST. It is now agreed that 2,5-DMF can produce cyclopentadiene as first shown by the PES calculated by Sirjean *et al.* [642] for (5-methylfuran-2-yl)methyl radical (R1C<sub>6</sub>H<sub>7</sub>O) decomposition displayed in Fig. 52 in Part 5.1.2. In their FR study below 1100 K using GC-2D, Djokic *et al.* [641] reported C<sub>2</sub>-C<sub>4</sub> product formation, as well as that of phenol at low conversion, and of benzene, toluene, indene and naphthalene at higher conversion. Phenol can be formed from cyclohexadienone, also a potential product according to the PES calculated by Sirjean *et al.* [642].

*Quantification of oxidation products* were performed in a JSR for 2-MF and 2,5-DMF and in a FR for the three CEs, which are mostly not reactive below 700 K in contrast to THF. Apart from furfural studies (see Part 5.3.3), the only two JSR studies concerning unsaturated CEs were performed by the groups of Dagaut [746] (for 2,5-DMF) and Wei [739] (for 2-MF). Fig. 68a displays an exemplary 2,5-DMF conversion profile. The formation of H<sub>2</sub>, H<sub>2</sub>O, CO, CO<sub>2</sub>, C<sub>1</sub>-C<sub>2</sub> hydrocarbons, formaldehyde, methyl vinyl ketone, 2-ethyl-5-methylfuran, 5-

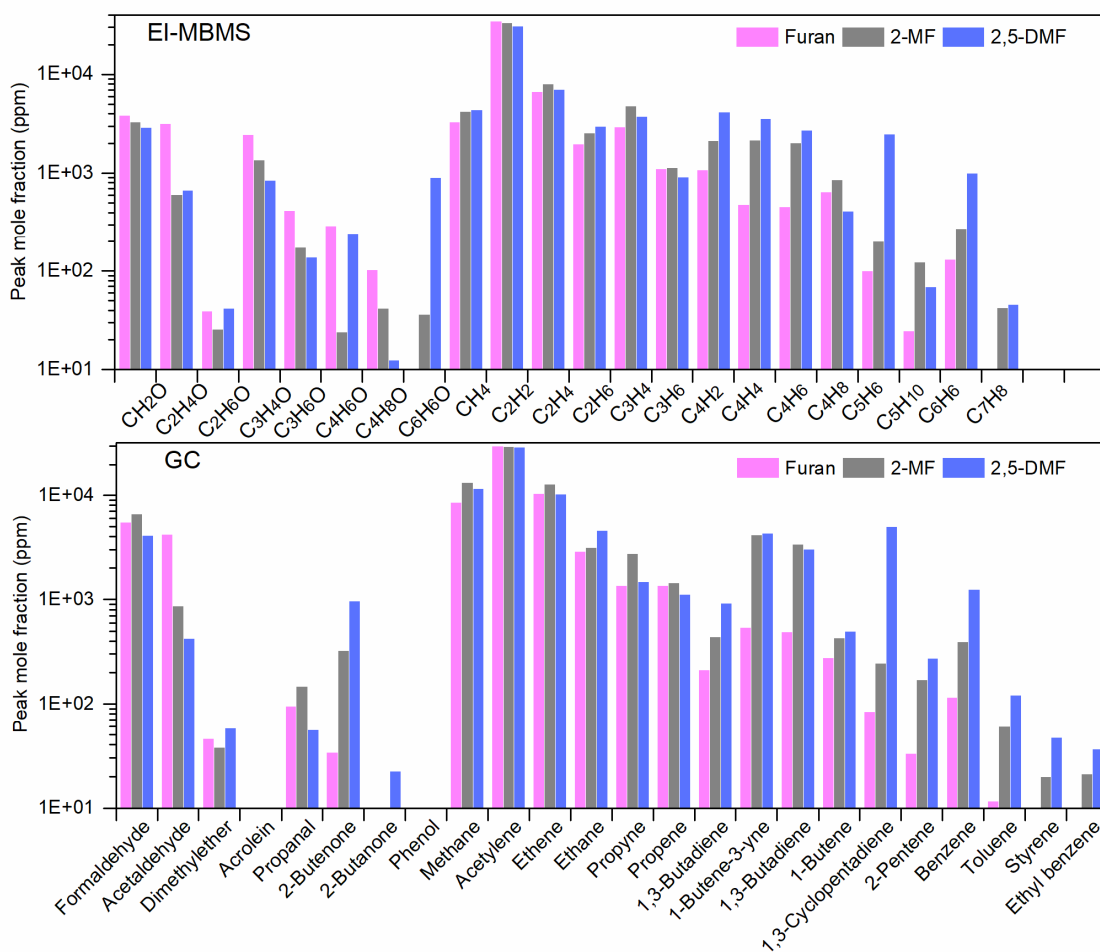


methylfurfural and 2-MF was reported (see Fig. 68b for the last four species). FR studies were carried out for 2-MF and 2,5-DMF by the group of Alzueta in Zaragoza [740,752,753] and for the three molecules by the group of Kohse-Höinghaus in Bielefeld [726]. Fig. 68c taken from the work in Bielefeld illustrates well the temperature shift for the start of reactivity between the three molecules with furan beginning to react at the highest temperature and 2,5-DMF at the lowest. Fig. 68c also shows that a decreasing of  $\phi$  has a more pronounced effect on fuel reactivity of 2,5-DMF than on that of the other two molecules. This trend that seems to be due to the number of lateral methyl groups in the fuel molecule. The strong impact of  $\phi$  on 2,5-DMF oxidation was confirmed by the work performed in Zaragoza [752], in which  $\phi$  was varied from 0.03-3.33. The Zaragoza study also observed a notable promoting impact of pressure on the fuel reactivity. As can be seen in Fig. 68 for  $\phi=1$ , the oxidation of 2,5-DMF in the JSR/FR studies at Orléans at 10 bar and at Bielefeld at 1 bar, both operating at similar residence times, starts at the same temperature close to 820 K, hence a pressure effect is not observable. In line with the reactions underlined by Xu *et al.* [733], significant yields of furfural and 5-methylfurfural were reported by Tran *et al.* [726] for the FR oxidation of 2-MF and 2,5-DMF, respectively. These results are consistent with the observations by [746] for 2,5-DMF oxidation (Fig. 68b). Acrolein and methyl vinyl ketone have been detected in large amounts in the oxidation of the three furanic fuels [726,746].



**Fig. 68.** Species mole fractions as a function of reactor temperature. **(a,b)** in 2,5-DMF oxidation ( $\tau=0.7$  s,  $P=10$  bar,  $\phi=1$ ) in a JSR [746]: fuel 2,5-DMF (2,5DMF), H<sub>2</sub>, CH<sub>4</sub> and C<sub>2+</sub> oxygenated products (methyl vinyl ketone (MVK), 2-ethyl-5-methylfuran (5M2EF), 5-methylfurfural (5M2CHO)); **(c)** oxidation ( $\tau=0.5-0.8$  s,  $P=1$  bar) in a FR [726]: the fuels are furan, 2-MF (MF) and 2,5-DMF (DMF). Symbols are experiments and lines simulations with the respective kinetic model of the study. Reproduced from Ref. [726,746] with permission of Elsevier.

*Product quantifications in flames fueled by furan, 2-MF, 2,5-DMF* (see 8 studies listed in Table 20) are described in detail in the review paper of Leitner *et al.* [8]. Fig. 69 displays product quantification by EI-MS in Bielefeld and GC in Nancy highlighting the good agreement between both techniques. Significant yields of C<sub>1</sub>-C<sub>2</sub> aldehydes are observed, with furan producing notably the highest amount of acetaldehyde. The reason for the latter trend is not clearly explained, leaving an interesting topic for future work. Fig. 69 also clearly demonstrates that all three CEs yield high amounts of acetylene but that 2,5-DMF leads to the highest formation of cyclopentadiene, benzene, and phenol, in agreement with PLF studies using SVUV-PIMS [750] and with the pyrolysis study by [641].



**Fig. 69.** Selected product quantitation in PLF of furan, 2-MF and 2,5-DMF under the same initial conditions and using GC and MBMS [103,273–275]. In the EI-MBMS data, the overall formula is presented and the cross section of the most abundant isomer measured by GC was used for calibration. In the GC data only the most abundant isomer is shown; the isomeric composition is available in their original papers. Acrolein and anisole were expected in GC, but cannot be detected since the first was hidden by furan and the second was lost in the transfer line.

The large production of possible soot precursors in 2,5-DMF combustion raises concerns about its potentially high tendency to form soot particulates. Conturso *et al.* [767] reported that the addition of 2,5-DMF in ethylene PLF reduces significantly the amount of large particles and the total mass of particles emitted, but not the number of particles smaller than 10 nm. Using an ethylene diffusion flame, Sirignano *et al.* [267] reported the lowest impact on particle production for furan whereas 2,5-DMF and 2-MF showed a higher propensity. Interestingly, 2-MF had a larger tendency to produce particles than 2,5-DMF.

### 5.3.2. Influence of the degree of unsaturation and of C<sub>1+</sub> alkyl substitutions

A comparison between the studies on furan, 2,3-DHF, 2,5-DHF, and THF provides hints about the influence of the degree of unsaturation and double bond location on their combustion. The DCN measurements of Sudholt *et al.* [87] showed the following order of DCN: THF (21.9) > 2,3-DHF (20.0) > 2,5-DHF (15.6) > furan (7.0) (see Fig. 7 of Part 1). Quantitative species yields can be found for ST measurements by the Lifshitz group [631,632], and for IDTs measured in two STs [633,727] and a RCM [655].

*Product quantifications during pyrolysis* in STs indicate that the major fate of 2,3-DHF is unimolecular isomerization yielding cyclopropane carboxaldehyde (c-C<sub>3</sub>H<sub>5</sub>CHO) [631] and that of 2,5-DHF is dehydrogenation to furan [632].

*Ignition studies* in a ST [633] indicated slightly longer IDTs for 2,5-DHF than for 2,3-DHF in agreement with DCN measurements. As shown in Fig. 67a, the IDTs of 2,3-DHF measured in RCM [655] follow a classical Arrhenius behavior above 850 K, with values close to those of THF, *i.e.* more than one magnitude order shorter than those of furan. However, in contrast to THF, no sign of low-temperature oxidation chemistry was reported for 2,3-DHF. No IDTs are reported for 2,5-DHF in a RCM.

In 2,3-DHF, the C<sub>3</sub>-H BDE (allylic H-atom, see carbon position in Table 20) is 11.4 kcal/mol lower than that of the C<sub>2</sub>-H in THF, but the obtained resonance stabilized dihydrofuranyl radical has no low energy consumption path other than that losing another H-atom to yield furan [655]. Therefore, the main 2,3-DHF degradation pathway in RCM is assumed to be through epoxidation with HO $\dot{O}$  radicals (similar to what is observed for alkenes (see Part 4.3.3) yielding 2,6-dioxabicyclo[3.1.0]hexane, which after H-abstraction from either CH<sub>2</sub> moiety produces acrolein and a  $\dot{H}CO$  radical [655]. Under ST conditions [633], molecular ring-opening isomerization of 2,3-DHF producing cyclopropane carboxaldehyde, and

furthermore crotonaldehyde, dominates. 2,5-DHF mostly dehydrogenates to furan explaining its lower reactivity [633].

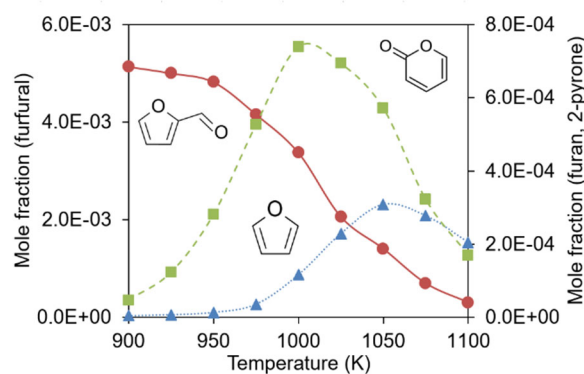
Apart from two very recent 2-EF studies in a JSR and a FR [755,756], studies on *C<sub>1+</sub> alkyl substituted furans* only consider global combustion parameters, e.g. LBVs [754], ignition behavior in a ST [732] and in two RCM studies [654,734]. In addition to DCN measurements [87] showing the following order: THF (21.9) > 2-BF (13.2) > 2-EF (10.2) > furan (7.0) (see Fig. 7 of Chapter 1), the team of Aachen reported IDTs in a RCM [654] for 2-MF, 2-EF and 2-BF as shown in Fig. 67b. This figure indicates similar IDT values for 2-EF and 2-BF above 830 K with a notably higher reactivity than that of 2-MF. At the lowest temperatures, IDTs of 2-BF deviate from the Arrhenius behavior suggesting the occurrence of low-temperature chemistry involving the alkyl chain. The results of Xu *et al.* [734] for 2-EF oxidation are in good agreement with those of Sudholt *et al.* [654] and explain the higher reactivity of 2-EF compared to that of 2-MF by the significant role of the reaction pathway yielding 2-vinylfuran, which resembles the formation of styrene from ethylbenzene [765]. 2-Vinylfuran was identified to be amongst the most important key products of 2-EF pyrolysis [756] and oxidation [755].

### **5.3.3. Influence of oxygenated substituents**

Only a limited number of furan derivatives including an oxygenated substituent were studied as is shown in Table 20. The previous reviews on furan derivatives [8,716] did not consider these compounds.

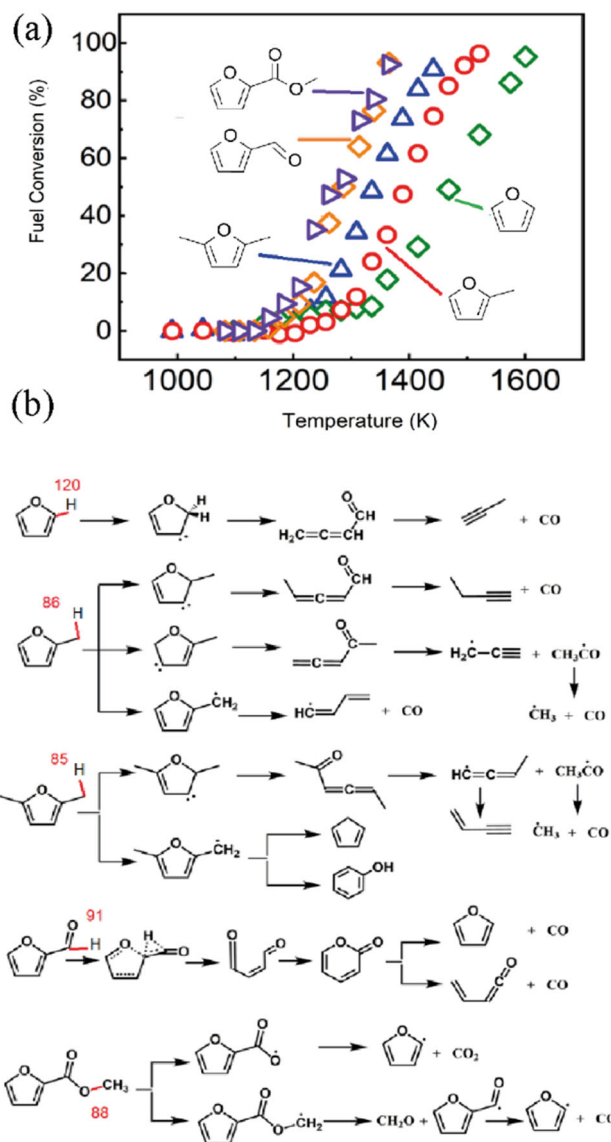
While a single study was found for any other CE, furfural was more intensively investigated with measurements of LBVs [757] and JSR/FR species profiles [423,757–762,768]. In their early studies of furfural pyrolysis using MS, Grela and Colussi [760,761] detected a species at *m/z* 68 (C<sub>4</sub>H<sub>4</sub>O), which was assigned to be vinylketene, and proposed that furfural decomposed into vinylketene + CO through ring-opening followed by H-atom transfer in the resulting biradical. Later, Li *et al.* [759] identified vinylketene and also furan as the

species detected at  $m/z$  68 using PI-MBMS at NSRL in Hefei. Recently, using the latter technique, Wang *et al.* [762] showed that furan was produced in amounts more than 100 times larger than those of vinylketene. The experimental and numerical studies of Vasiliou *et al.* [758], Vermeire *et al.* [423], and Jin *et al.* [757] showed that the most plausible decomposition pathway of furfural was by ring-opening isomerization with the formation of formylvinylketene ( $m/z$  96, the same mass as furfural), which decomposed into furan or 2-pyrone ( $m/z$  96). The latter species was experimentally measured using GC with even higher mole fractions than furan (see Fig. 70) [423]. Note however that under oxidation conditions, furfural was found to be consumed exclusively via radical chemistry (OH- and H-additions or H-abstractions) [757].



**Fig. 70.** Furfural pyrolysis (1.07 bar): fuel and the two key products, furan and 2-pyrone redrawn from the data of [423].

As shown in Fig. 71a, Wang *et al.* [762] observed a generally higher reactivity of furfural and 2-MOF (methyl furan-2-carboxylate) compared to the three unsaturated CEs discussed in Section 5.3.1, which is consistent with previous studies for furan and furfural [762,768]. Fig. 71b shows that the thermal decomposition pathways of furan derivatives strongly depend on the type of functional groups on the furan ring. The dominant decomposition pathways include carbene intermediates (furan), radical chemistry (2,5-DMF and 2-MOF) and H-transfer followed by ring-opening (furfural) [762].



**Fig. 71.** Pyrolysis of substituted furans in a FR: **(a)** fuel conversion profiles ( $P = 0.04$  bar), **(b)** major kinetic pathways. Adapted from Ref. [762] with permission of Elsevier. The bond with the lowest BDE (kcal/mol) in each fuel is highlighted in red.


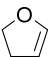
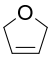
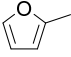
Recently, the group of Van Geem in Ghent investigated experimentally and theoretically the influence of the functional groups on the molecular and radical decomposition chemistry during the pyrolysis of 2-FFOH and 5-methylfurfural in a FR [640]. The authors found that the  $-CHO$  functional group of 5-methylfurfural accelerated the molecular ring-opening isomerization reaction and mostly suppressed carbene formation channels, which is somewhat consistent with previous studies on furfural [423,762]. The weaker C–H (79 kcal/mol) and C–O (77 kcal/mol) bonds in 2-FFOH and C–H bond (84 kcal/mol) in 5-methylfurfural compared

to furan (lowest C–H DBE: 119 kcal/mol) and furfural (lowest C–H DBE: 91 kcal/mol) respectively resulted in a higher importance of radical chemistry, which was proven by the detection of the fuel radicals using PI-MBMS at NSRL in Hefei [640].

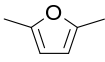
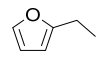
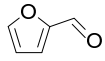
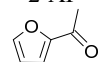
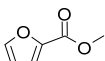
#### 5.3.4. Performance of kinetic models

Table 21 summarizes the main detailed kinetic models developed for the combustion of the furan derivatives listed in Table 20. Note that no models are available for 2-BF, 2-FFOH, and 5-methylfurfural. Only detailed models that contain a primary mechanism for furan derivatives, the development of which requested significant effort (more than only adjusting a few reactions or reusing available sub-models) are listed in Table 21. The models developed by Wu and coworkers [769,770] for furan, 2-MF, and 2,5-DMF or by Zhou *et al.* [771] for 2,5-DMF are not listed here because they were reduced from the detailed models of Somers *et al.* [728,746,766]. The models developed before 2016 for furan, 2-MF, and 2,5-DMF, which were already comprehensively analyzed in the review by Xu *et al.* [716], are presented in Table 21 for the sake of comprehensiveness, but only briefly described in the text hereafter. More details will be given for the newer models and those for other CEs.

**Table 21.** Main detailed kinetic models (they required a significant development effort on the primary mechanism) for the combustion of some unsaturated CEs. For each CE, the models are sorted by year of publication. Spe. N°: species number. Reac. N°: reaction number (forward). \*Conditions above presented in this table.

CE	Year & Ref.	Spe. N°	Reac. N°	Validation conditions (unit: T / K, P / bar)
 Furan	1991, Organ and Mackie [722]	-	-	-ST pyrolysis species (T=1100-1700, P=20.3) [722]
	2000, Sendt <i>et al.</i> [636]	-	82	-ST pyrolysis species of [722]*.
	2011, Tian <i>et al.</i> [226]	206	1368	-PLF species (P=0.05, $\phi$ =1.4-2.2) [226] -ST pyrolysis species (T=1533, P=0.26) [723], [722]*
	2014, Liu <i>et al.</i> [273]	305	1472	-PLF species (P=0.02-0.04, $\phi$ =1.0-1.7) [273], [226]*
	2017, Tran <i>et al.</i> [726]	524	3145	-FR species (T=730-1170, P=1, $\phi$ =0.5-2) [726] -JSR species (T=1000-1300, P=1) [768] -PLF species of [273]* -IDT in ST (T=1150-2010, P=1.2-16, $\phi$ =1) [720]
 2,3-DHF	2016, Fan <i>et al.</i> [633]	255	1723	-IDT in ST (T=1100-1635, P=1.2-10.1, $\phi$ =0.5-2) [633] -ST pyrolysis species (T=900-1300, P=0.6) [631]
	2020, Wu <i>et al.</i> [655] (used with the furan model of Tran <i>et al.</i> [726])	439	2434	-IDT in RCM (T=660-880, P=10-20, $\phi$ =1.0) [655] -IDT in ST of [633]*
 2,5-DHF	2016, Fan <i>et al.</i> [633]	255	1723	-IDT in ST (T=1100-1650, P=1.2-10.1, $\phi$ =0.5-2) [633] -ST pyrolysis species (T=900-1080, P=1.6-6.5) [632]
 2-MF	1997, Lifshitz <i>et al.</i> [736]	36	100	-ST pyrolysis species (T=1100-1400, P=1.7-2.9) [736]
	2013, 2014, Somers <i>et al.</i> [728,766]	567	2889	-IDT in ST (T=1120-1800, P=1-10.7, $\phi$ =0.5-2) [728,731] -LBV (T <sub>initial</sub> =298-398, P=1, $\phi$ =0.55-1.65) [728] -ST pyrolysis species of [736]*



				-PLF species ( $P=0.02-0.04$ , $\phi=1.0-1.7$ ) [274]
	2014, Tran <i>et al.</i> [274]	305	1472	-PLF species ( $P=0.02-0.04$ , $\phi=1.0-1.7$ ) [274]
	2017, Tran <i>et al.</i> [726]	524	3145	-IDT in RCM ( $T=737-1143$ , $P=16-30$ , $\phi=1$ ) [733] -IDT in ST ( $T=1150-2010$ , $P=1.2-16$ , $\phi=1$ ) [720] -FR species ( $T=730-1400$ , $P=1$ , $\phi=0.02-3.33$ ) [726,740] -PLF species ( $P=0.02-0.04$ , $\phi=1.0-1.7$ ) [274]
	2018, Tripathi <i>et al.</i> [735]	883	4221	-IDT in RCM ( $T=737-1143$ , $P=16-30$ , $\phi=1$ ) [654,720,735] -IDT in ST ( $T=820-2010$ , $P=1-40$ , $\phi=0.25-2$ ) [281,719,720,728,731] -LBV ( $T_{initial}=298-398$ , $P=1$ , $\phi=0.55-1.65$ ) [728,729] -PLF species ( $P=0.02-0.04$ , $\phi=0.8-1.7$ ) [274,738] -FR species ( $T=730-1400$ , $P=1$ , $\phi=0.02-3.33$ ) [726,740]
	2022, Wang <i>et al.</i> [739]	761	3498	-JSR species ( $T=600-925$ , $P=1.0$ , $\phi=0.5-2$ ) [739] -FR species of [726]* -IDT in ST ( $T=909-1820$ , $P=1-11$ , $\phi=0.5-2$ ) [719,728,731] -IDT in RCM ( $T=737-1143$ , $P=16-30$ , $\phi=1$ ) [733,735]
2,5-DMF 	1998, Lifshitz <i>et al.</i> [748]	50	180	-ST pyrolysis species ( $T=1070-1370$ , $P=2-3.7$ ) [748]
	2013, Sirjean <i>et al.</i> [747]	294	1459	-IDT in ST ( $T=1300-1831$ , $P=1-4$ , $\phi=0.5-1.5$ ) [747] -ST pyrolysis species of [748]*
	2013, Somers <i>et al.</i> [746]	545	2768	-IDT in ST ( $T=820-1800$ , $P=1-81.1$ , $\phi=0.5-2$ ) [746],[747]* -LBV ( $T_{initial}=298-473$ , $P=1-7.5$ , $\phi=0.6-1.6$ ) [270,742,746] -ST pyrolysis species ( $T=1200-1350$ , $P=1-2.5$ ) [746],[748]* -JSR species ( $T=770-1220$ , $P=10.1$ , $\phi=0.5-2$ ) [746] -FR pyrolysis species ( $T=873-1098$ , $P=1.7$ ) [641]
	2014, Togbé <i>et al.</i> [275]	305	1472	-PLF species ( $P=0.02-0.04$ , $\phi=1.0-1.7$ ) [275]
	2017, Tran <i>et al.</i> [726]	524	3145	-FR species ( $T=730-1170$ , $P=1$ , $\phi=0.5-2$ ) [726] -JSR species of [746]* -IDT in ST ( $T=1300-1900$ , $P=1.2-16$ , $\phi=0.5-2$ ) [720], [746]* -PLF species ( $P=0.02-0.04$ , $\phi=1.0-1.7$ ) [275]
	2017, Xu <i>et al.</i> [734]	568	2902	-IDT in RCM ( $T=766-1013$ , $P=16-30$ , $\phi=0.5-2$ ) [734]
2-EF 	2021, Song <i>et al.</i> [756]	659	3147	-FR pyrolysis species ( $T=846-1319$ , $P=0.04-1$ ) [756]
	2022, Li <i>et al.</i> [755]	723	3300	-JSR species ( $T=600-900$ , $P=1$ , $\phi=0.5-2$ ) [755] -IDT in RCM of [734]* -FR pyrolysis species of [756]*
Furfural 	2021, Wang <i>et al.</i> [762]	585	3018	-FR pyrolysis species ( $T=929-1365$ , $P=0.04-1$ ) [762] -JSR pyrolysis species ( $T=900-1100$ , $P=1.07$ ) [423]
	2021, Jin <i>et al.</i> [757]	382	2262	-LBV ( $T_{initial}=473$ , $P=1$ , $\phi=0.6-1.8$ ) [757] -JSR species ( $T=650-950$ , $P=1$ , $\phi=0.4-2$ ) [757] -JSR pyrolysis species ( $T=900-1100$ , $P=1.07$ ) [423]
2-AF 	2022, He <i>et al.</i> [763]	644	3134	-JSR pyrolysis species ( $T=770-1130$ , $P=1$ ) [763]
2-MOF 	2019, Yan <i>et al.</i> [764]	601	3086	-FR pyrolysis species ( $T=879-1107$ , $P=1$ ) [764]

### 5.3.4.1. Furan, 2-MF, 2,5-DMF

Before 2016, several detailed kinetic models were developed, such as those by Organ and Mackie [722], Sendt *et al.* [636], Lifshitz and coworkers [736,748], Curran, Simmie and coworkers [728,746,766] in Galway, and by the Nancy group [226,274,275,747,750]. The early models for furan pyrolysis [636,722] used rate coefficients of unimolecular initiations based on either ST experiments or *ab initio* calculations and considered biradical chemistry [722] or

carbene chemistry [636], respectively, as described in Part 5.1.2. These models were tested against the ST pyrolysis species profiles of [722]. Similarly, the early developments by the Lifshitz group [736,748] were dedicated to pyrolysis for 2-MF and 2,5-DMF using the kinetic data for unimolecular initiations based on ST experiments. Later, the Galway group proposed comprehensive models for the pyrolysis and oxidation of 2-MF and 2,5-DMF using theoretically calculated rate coefficients [728,746,766]. These models were tested using numerous experimental datasets including IDTs in STs, LBVs, and species profiles measured in STs, PLFs, JSRs, and FRs as is summarized in Table 21. In parallel, the Nancy group proposed kinetic models for the oxidation of these three furans using kinetic data from theoretical calculations for the key primary reactions [226,273–275,747]. The models were tested using PLF species profiles measured at Hefei, Nancy, and Bielefeld, and IDTs and pyrolysis products measured in STs (Table 21).

*After 2016*, together with the groups in Bielefeld and Ghent, the Nancy group continued to work on a model for these CEs by including important reactions for low/intermediate temperature oxidation [726]. This model distinguished itself from other literature models by including for the first time detailed reaction subsets for HO $\dot{O}$ - and O $_2$ -additions to the important resonance-stabilized fuel radicals, (furan-2-yl)methyl and (5-methylfuran-2-yl)methyl, with kinetic data computed using high-level theoretical calculations. The model was used to simulate a large number of experimental datasets measured in FRs, JSRs, RCMs, STs, and PLFs at temperatures from 730 K to 2600 K (Table 21). The model demonstrated that  $\dot{O}H$ -additions on the double bonds of furan, 2-MF, and 2,5-DMF forming acrolein and methyl vinyl ketone were very significant in the range of temperatures lower than 1000 K, which explained why these products were measured in large amounts as discussed in Part 3.3.1. Currently, this model and the above-mentioned models of the Galway group are the most used models in the combustion community for furan derivatives. One year later, the Aachen group proposed [735] a kinetic

model for the oxidation of 2-MF with the high-temperature part mainly adopted from Galway [746,766] and the low/intermediate temperature part from the latest model of Nancy [726], but adding some new reaction classes in the low-temperature 2-MF sub-model, such as O<sub>2</sub> addition reactions to the adducts formed in the  $\dot{\text{O}}\text{H}$  addition to the double bonds of 2-MF using kinetic data from Davis and Sarathy [772]. They also considered the co-oxidation reactions between 2-MF and *n*-heptane allowing to consider fuel mixtures. The model by Tripathi *et al.* [735] was tested using a large number of data (T from 730 K to 2400 K) as is summarized in Table 21. Very recently, Wang *et al.* [739] established a new model for 2-MF oxidation and validated it against the species profiles obtained in their JSR and in FR by Tran *et al.* [726] as well as IDT data from various studies of the literature. The model was developed mainly based on recent developments of Somers *et al.* [766], Davis and Sarathy [772], and Tran *et al.* [726], which are discussed above. Note that all of the above described models for furan, 2-MF, and 2,5-DMF do not contain second O<sub>2</sub> addition chemistry because such chemistry is insignificant for these CEs.

#### **5.3.4.2. Other furan derivatives**

Models concerning other furan derivatives, *e.g.* DHFs, 2-EF, furfural, 2-AF, and 2-MOF were proposed only from 2016 onwards.

*Concerning 2,3- and 2,5-DHFs*, Fan *et al.* [633] developed and tested a first detailed model starting from the THF model of Tran *et al.* [195] and considering new reactions for DHF unimolecular initiations. The model well reproduced IDTs measured in a ST [633] and pyrolysis species distributions [631,632]. More recently, Wu *et al.* [655] proposed a 2,3-DHF model based on the THF model of Fenard *et al.* [283] and using rate coefficients estimated from those of THF and from Fan *et al.* [633]. This 2,3-DHF model considers only a one-step lumped reaction of dihydrofuranyl radicals with O<sub>2</sub> forming  $\dot{\text{O}}\text{H}$ , formyl, and 3-oxoprop-1-en-1-yl radicals with the rate coefficients adjusted to get a better agreement between the model predictions and the experimental IDTs measured in a RCM.

*Concerning 2-EF*, three kinetic models were found, which were developed by Xu *et al.* [734], Song *et al.* [756], and Li *et al.* [755] using the 2,5-DMF model of Somers *et al.* [746], which already contains some 2-EF reactions. As the 2-EF sub-model of Somers *et al.* [746] was incomplete, Xu *et al.* [734] added reactions that are important under their RCM conditions, such as reactions between fuel radicals with HO $\dot{O}$  or O $_2$ . Later, Song *et al.* [756] performed quantum chemistry calculations and added important thermal decomposition reactions of 2-EF, such as unimolecular initiations via C-C bond scissions and carbene chemistry. These models were tested using IDTs measured in a RCM and pyrolysis species measured in a FR, respectively. The model predictions showed that 2-EF was consumed mainly via  $\dot{O}H$ -additions on double bonds under RCM conditions and rather by C-C bond scission of the lateral C $_2$ H $_5$  group, H-additions, and H-abstractions under FR pyrolysis conditions. The model predicted that 2-EF is the most reactive fuel among 2-EF, 2-MF, and 2,5-DMF, which is consistent with the experimental trend shown in Fig. 67a [734], and that 2-EF produces the lowest concentrations of aromatic compounds [756]. Very recently, Li *et al.* [755] expanded the model of Song *et al.* [756] by adding oxidation reactions with rate coefficients being obtained by new theoretical calculations or by analogy to similar reactions of 2-MF and ethylbenzene. The model reproduces very well the JSR species data obtained in the same study and the FR pyrolysis species profiles of [756] as well as the IDTs obtained in RCM of [734].

*Concerning furfural*, two kinetic models are available, which were very recently developed by Wang *et al.* [762] and Jin *et al.* [757] for pyrolysis and oxidation, respectively. The model by [762] was developed based on literature PES [423,758,759] and estimation of kinetic data. The model by [757] used theoretically calculated kinetic data for important oxidation reactions such as bimolecular initiations with O $_2$  or H-additions/abstractions on double bonds. These models reproduced the respective experimental data listed in Table 21 well and they helped with the interpretation of the experimentally observed trends discussed in

Section 5.3.3, *e.g.* the abundance of furan over vinylketene or the difference in the reactivity of furfural compared to other furan derivatives. Both models agree that furfural was consumed mainly by OH-additions and H-abstractions under oxidation conditions and by isomerization to formylvinylketene under pyrolysis conditions.

*Concerning 2-AF and 2-MOF*, one model was proposed for the thermal decomposition each of these CEs by the group of Wei at Guangxi University [763,764] using rate coefficients from new theoretical calculations and analogous reactions of acetone, methyl formate, dimethyl carbonate, methyl crotonate, furan, 2-MF, and 2,5-DMF. These models were tested using pyrolysis species measured in a JSR or a FR, respectively, and generally good agreement was observed. Modelling demonstrated that 2-AF consumption was mainly controlled by both unimolecular decomposition and H-addition reactions, and that 2-MOF was consumed largely via O–CH<sub>3</sub> bond scissions, which was consistent with the calculated BDEs for this CE.

Similarly to the models described in Section 5.3.4.1 for furan, 2-MF, and 2,5-DMF, the models for 2-EF, furfural, and 3-MOF do not contain second O<sub>2</sub> addition chemistry, which is insignificant for these CEs.

## 5.4. Conclusion

In order to better understand the consumption chemistry of CEs, Part 5 presented a systematic review of the experimental studies and of the detailed kinetic models related to the gas-phase pyrolysis and oxidation of saturated and unsaturated CEs, including substituted ones.

**Concerning the reviewed experimental work**, about 90 and 80 studies were identified for saturated and unsaturated CEs, respectively, with saturated CEs including compounds of the families of oxirane, oxetane, THF, THP, dioxolane, and dioxane, and unsaturated CEs consisting exclusively of furanic compounds. Each study contains different datasets that include several data points. A larger number of pyrolysis studies can be found for unsaturated (about 30 studies) than for saturated CEs (about 15 studies). On the other hand, the number of oxidation

studies below 1000 K for saturated CEs (about 40 studies) is higher than for unsaturated CEs (20 studies).

**Regarding global combustion property measurements**, the LBVs of CEs in air reach their maximum value at  $\phi=1.1$  and the LBVs decline with increasing of pressure. Note that the maximum LBV also occurs at  $\phi\sim 1.1$  for most carbon-based fuels [268,773]. No LBV measurements for CEs were found for pressures >10 bar. Under oxidation conditions above 1000 K, the IDTs of all the listed CEs follow classical Arrhenius behavior, increase as expected with increasing  $\phi$  and decrease with increasing pressure. Increasing the length of the lateral group or adding an oxygenated lateral group increases reactivity, while an increased level of unsaturation decreases it. The position of the lateral group is also of importance, as shown by the higher reactivity of 3-MTHF compared to 2-MTHF. Concerning the oxidation at temperatures below 800 K, cool flames were only detected for THF derivatives.

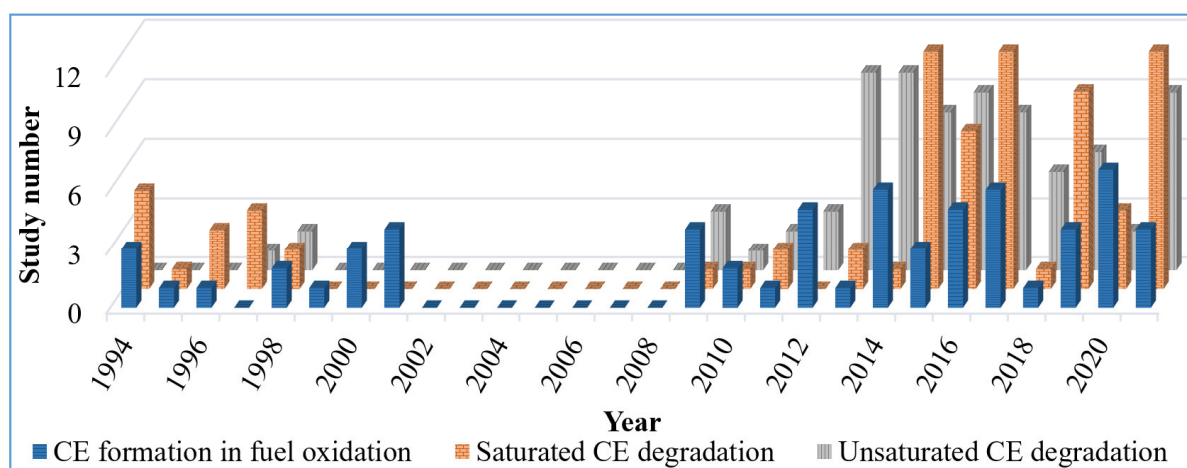
**Concerning the chemistry of saturated CEs**, oxirane, THF, 2-MTHF, and THP are the most intensively investigated species. Under pyrolysis conditions, both, carbene and biradical pathways play important roles, especially for oxetane and oxirane derivatives. The latter react to yield aldehydes. THF and THP derivatives are mainly consumed by H-abstractions. The reaction sequence of THF derivatives at low temperature follows the usual mechanism observed for alkanes. However, while cyclic-ether KHPs have been reported in THF oxidation, the formation of fused bicyclic ethers (as a result of the decomposition of cyclic-ether QOOH radical) have not been experimentally observed. The formation of bioxirane was recently reported from ethyloxirane oxidation [395], however, this is not a fused bicyclic ether. In this case oxidation started from the oxiranylalkyl radical meaning that the radical site was on the side chain and subsequently also the hydroperoxy group. For 2,3-dimethyloxirane, due to faster oxirane ring-opening, no bicyclic ether was observed [511].

**Concerning the chemistry of unsaturated CEs**, most of the available studies focused on furan, 2-MF, and 2,5-DMF. The carbene mechanism as well as biradical formation are important under pyrolysis conditions especially for aromatic furan derivatives. However, the presence of a long alkyl chain and/or of oxygenated substituents with relatively weak C–H bonds favors the formation of fuel radicals with their subsequent chemistry at the expense of unimolecular decomposition by ring-opening. Unsaturated CEs are also significantly consumed by H- and OH-additions to double bonds. Despite a significant effort made to study the ignition of unsaturated CEs in RCMs, the low-temperature chemistry via O<sub>2</sub> addition steps was pointed out to be insignificant for this type of CEs. Compared to saturated CEs, furan derivatives, especially 2,5-DMF, have a higher propensity to form soot precursors, indicating a strong influence of the degree of unsaturation and of the presence of lateral groups, which need to be investigated more.

**Detailed kinetic models** are available for 14 of the 16 saturated CEs listed in Table 16 and for 8 of the 11 unsaturated CEs listed in Table 20. No models were found for ethyloxirane, 2-ETHF, 2-BF, 2-FFOH, and 5-methylfurfural. In general, the models developed prior to 2000 were mainly based on estimated kinetic data, while newer models used theoretically calculated rates providing an improved predictive ability. In recent years, progress has been made in developing models for the low-temperature oxidation of THF derivatives by refining the rate constants involved in the O<sub>2</sub> addition sequence, and in those of furan derivatives by incorporating intermediate temperature reactions involving HO $\dot{O}$  or CH<sub>3</sub>O $\dot{O}$  radicals.

## 6. CONCLUSION AND PERSPECTIVES

To complete this paper, Part 6 aims to summarize the main conclusions, which can be drawn from the sum of the studies reviewed in Parts 4 and 5 and to present some emerging directions for research in CE reaction kinetics. Fig. 72 plots the time evolution of the number of studies that can be found in the literature related to CEs in the context of both their formation during fuel low-temperature oxidation and their own reactivity/degradation as fuels or as secondary products of the oxidation of other fuel components. Note that each study contains different datasets that include several data points.

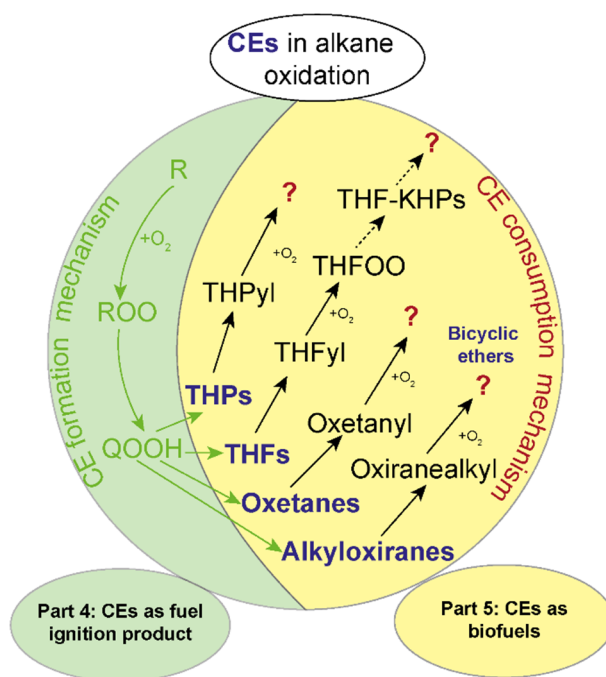


**Fig. 72.** Number of studies, which can be found in the literature over the years after from 1994 to 2021 related to CE formation during fuel low-temperature oxidation (as described in Part 4) and to the consumption of saturated and unsaturated CEs (as described in Part 5).

Fig. 72 shows that between 1994 and 2001, research mainly focused on the formation and the reactivity of saturated CEs, which are produced in competition to KHPs, while relatively few studies can be found on unsaturated CEs. This activity completely stopped between 2002 and 2007 when the focus switched to chemically activated HOO elimination and alkene formation. Interest in CEs rose again in 2008. Since then, the amount of CE formation studies is quite steady and at a slightly higher level than before 2001. Research on CE reactivity increased significantly after 2012 and can be divided almost equally in studies on saturated and on unsaturated CEs.



The text hereafter gives an assessment of the work reviewed in the previous parts and proposes a few potential research directions. The mechanisms of formation (as discussed in Part 4) and of consumption (as discussed in Part 5) of CEs are strongly connected, as is illustrated by Fig. 73 in the case of alkane low-temperature oxidation. This interconnection explains the need to keep this review paper as a single one despite its very large number of pages. More specifically, as described in this review, the CE yields in fuel low-temperature oxidation is determined by their rates of formation as part of the fuel oxidation chemistry, but also by their rates of consumption, which should not be discarded since H-abstraction reactions from most CEs are relatively fast due to the weak C–H bond in  $\alpha$ -position to the ether O-atom.



**Fig. 73.** Remaining unknowns related to CEs in the understanding of alkane low-temperature oxidation. Many aspects of the unimolecular decompositions of molecules and radicals are not shown. R is a  $C_{3+}$  alkyl radical and, except for “alkyloxiranes” and “oxiranealkyl”, which only relate to oxiranes substituted by a  $C_{2+}$  group, both substituted and unsubstituted CEs, are considered.

After this general chemical statement, let’s examine more closely the experimental kinetic studies related to CEs, the theoretical calculation procedures involved, and finally the ways that CEs are considered in kinetic models.

## 6.1. Experimental kinetic studies related to cyclic ethers

**On the point of view of the experimental reaction devices used**, the kinetic studies related to CEs were performed using the full set of what is available in combustion laboratories, as described in Part 3. While CE formation during fuel oxidation at low-temperature was mostly investigated in JSRs and RCMs, CE reactivity was followed using a wider variety of devices, including burners and STs. Part 4 shows that JSRs from different laboratories yield consistent data, which confirms that this set-up is very well suited for studying CE formation during low-temperature oxidation. As is described in Part 5, STs, especially when used in single pulse mode, have long been useful tools for studying CE pyrolysis and deriving data on their kinetics of decomposition. Burners with stabilized laminar flame at low pressures have allowed for the quantification of the wide range of products formed during the combustion of furan derivatives. While their formation levels are significant amongst the products formed in the low-temperature oxidation of fuel components under IC engine conditions, CEs are often omitted in the studies reporting quantitative specifications, especially in RCMs.

**Next:** Additional CE studies by a larger range of RCM laboratories would be helpful to increase the data sets and to test for their consistency. Similarly, since only two studies were found using a FR setup, more studies on CE kinetics with this device should be attempted, even if their unfavorable surface/volume ratio might favor wall effects, which could interfere with slow gas phase oxidation kinetics at low temperatures. It would be particularly interesting to use FR for investigations at higher pressures than currently achievable with JSR. For this to be helpful, it would be useful to first perform parallel JSR and FR studies at the same conditions in order to provide evidence that both setups provide consistent data. In addition, more JSR studies on THP and on CEs substituted by C<sub>1+</sub> alkyl chain would be of interest. For critical CE identification problems, the use of deuterated (or general isotope labelled) reactants could be

considered, if available. Also, photoinitiated oxidation studies, which have provided valuable mechanistic information in the past but mainly focused on time-resolved measurements of radicals, could be extended towards the quantification of CE yields, *e.g.* in cases in which unstable CEs are formed.

**On the point of view of used analytical techniques**, due to its ability to separate even chemically similar organic isomers from each other, GC has long been the technique of choice for CE analysis. When coupled to a quadrupole MS, CE species can easily be identified while the use of a FID allows their quantification with high accuracy within a wide range of concentrations. However, the ability of GCs to discriminate CE isomers deteriorates with increasing fuel size due to the increased number of chemically similar isomers. Drawbacks of the GC technique include possible decomposition of unstable species in the injection and column sections and the poor time resolution which prevents detection of highly reactive intermediates.

The latter issue is addressed with MBMS setups which are increasingly used in recent years [292,774–777]. In these devices time-of-flight MS is generally used, which allows for a full mass spectrum to be taken within milliseconds. When combined with soft ionization, *e.g.* photo-ionization with tunable narrow bandwidth light, the resulting PES can be used to identify the detected species. This method is particularly powerful when the usual ion detection is completed by additional diagnostics.

**Next:** Recently, 2D or GC×GC chromatographs using two columns of different affinity [778] have been used successfully to separate complex mixtures of species. It would be worth testing if such a setup is able to discriminate CE isomers formed by heavy fuels. The success of this technique mainly relies on being able to identify adequate pairs of columns for the separation.

For heavy fuels, the use of HPLC (high pressure liquid chromatography) to separate the CEs could also be tested. Belhadj [590] applied ultrahigh pressure liquid chromatography to separate KHP at  $m/z$  118 ( $C_4H_6O_4$ ) formed in THF oxidation at 590 K. Although the separation of five species was successful, these authors could not identify those.

In addition, future CE studies should take advantage of advanced multiplexed detection techniques, *e.g.* combining MS for ion detection with photo electron detectors, which is known as the PEPICO technique [392,437–440].

**On the point of view of the investigated reactant families**, CEs were detected in the oxidation of linear and cyclic hydrocarbons, as well as of linear oxygenated fuels. The chemistry of CE formation from aromatic species was found to be special as it involved a possible bridging between alkyl chains (*e.g.* in *o*-xylene [523] and cymene isomers [779]). Such cases have not yet been investigated much. The major part of the studies dealing with CE pyrolysis and oxidation focus on furan derivatives, but a small number of studies concerning  $C_2$ - $C_4$  hydrocarbons including an oxirane ring are also known. Recent work [511] indicates that the low-temperature oxidation of  $C_4$  oxiranes is more complex than assumed in current models. Concerning the reactivity of molecules including a 5-membered CE, 70% of the studies concern THF, 2-MTHF, furan, 2-MF and 2,5-DMF. Limited information (often only DCN numbers [87]) is available for molecules with a  $C_{2+}$  alkyl chain or an oxygenated substituent.

**Next:** Overall, more work is needed to address CE formation in the oxidation of branched and aromatic fuels. More experimental work is needed on substituted oxetanes and THPs, as well as of substituted saturated CEs that cannot be formed by alkane oxidation (*e.g.* bicyclic ethers...). Such studies *e.g.* in JSR would certainly be possible if these fuels can be purchased or easily synthesized. In addition, studies of substituted oxiranes might help to characterize the

chemistry of hydroperoxy oxiranes, the formation of which is found by up-to-date kinetic models to be significant [395,511]. Moreover, additional studies on the reactivity of oxygenated furan derivatives, such as 2-FFOH or 5-methyl furfural, could be of interest to improve the understanding of biomass pyrolysis and combustion [640].

**On the point of view of investigated experimental parameters,** CE studies were performed under the following conditions:

- Temperature range 400-1200 K for CE formation, 373-2300 K for the reactivity of saturated CEs, 500-3000 K for the reactivity of unsaturated ones,
- Pressure range 1-50 bar for CE formation, 0.01-40 bar for the reactivity of saturated CEs,  $1.3 \times 10^{-6}$ -80 bar for the reactivity of unsaturated ones,
- Equivalence ratio range 0.25-4 for CE formation, 0.2- $\infty$  for the reactivity of saturated CEs, 0.02- $\infty$  for the reactivity of unsaturated ones.

Amongst the 96 studies on saturated CE consumption, only about 19 were performed at pressure above 10 bar, all but one (a speciation in CFR engines [82]) concentrate on IDT measurements, and most of them were done in Aachen. Amongst the 89 studies on unsaturated CE consumption, about 15 were performed at pressure above 10 bar, all but one (speciation in a FR [752]) report on IDTs. RCM studies reporting CE formation were mostly done for stoichiometric mixtures. Moreover, while many studies address the pyrolysis of CEs ( $\phi = \infty$ ), less data are available for CE oxidation in lean mixtures.

**Next:** If seriously considered as transportation fuels, then studies on CE reactivity under more realistic conditions relevant to gasoline and HCCI type engines are needed, especially at high pressures with product quantification, or under lean to slightly rich conditions.

## 6.2. Theoretical calculation procedures in cyclic ether kinetic studies

**Concerning theoretical calculations about CE formation**, extensive studies on rate rules were performed with the CBS-QB3 method. However, the level of accuracy of this method has been questioned and newer coupled cluster based calculations (*e.g.* [463]) suggest that the recommended rate expressions overestimate the reactivity. While the structure of small species may be well defined, larger molecules exist as numerous conformers and isomers, which are often not taken into account. This large variety and complexity put limits on the accuracy of theoretical studies and thus on the thermochemical properties calculated. The description of pressure-dependence also leads to uncertainties caused by the energy transfer parameters and models used as well as possible numerical errors. Despite these uncertainties, theoretical calculations provide very valuable information and the results might be further improved by “multiscale informatics” optimization procedures [780].

**Next:** More work is needed to clarify if the activation energies from CBS-QB3 results are too low, the pre-exponential factors are too high, or both. Systematic studies with a higher-level method are needed to resolve this issue. The causes for deviating rate expressions obtained with seemingly the same *ab initio* method need to be analyzed and well-defined protocols to derive rate expressions but also thermodynamic properties (specifically entropies) would be helpful. The use of mathematical tools considering error propagation and uncertainties will likely increase to make kinetic models more predictive. Some inconsistencies revealed in the review between GA predicted and theoretically calculated thermodynamic data should be addressed.

**Concerning CE reactivity at high temperature**, the thermal decomposition of furan and some of its methyl derivatives were investigated thoroughly by high-level theoretical methods and the importance of pericyclic reactions and carbene intermediates was established.

Similarly, the understanding of the unimolecular decomposition of (substituted) THF and their radicals has been improved lately due to high-level studies of the corresponding PESs. More uncertainty exists for oxiranes and oxetanes, partly because the theory level was not very high and partly because of the multireference character of transition states. Rate coefficients for unimolecular CE decomposition reactions are generally available as a function of pressure. Systematic studies using isodesmic reactions provided accurate thermodynamic data for the most important CEs, which allows for the solution of the energy balance in high-temperature ignition tests. Unknown thermodynamic data can easily be estimated with web-based GA tools [187,188,781].

**Next:** Kinetic data for H-abstraction reactions by H- and O-atoms and  $\dot{\text{C}}\text{H}_3$  radicals, which are surprisingly still lacking, would improve high-temperature models that often use estimates to describe the CE decomposition chemistry. It is anticipated that algorithms designed to automatically explore possible reaction pathways (*e.g.* KINBOT [186]) will gain in importance in the future to address existing “mechanism truncation” problems [782].

**The low-temperature reactivity of CEs** is characterized by the competition of multiple reaction channels proceeding on complex PESs. These are nowadays routinely calculated, often at the CBS-QB3 or coupled cluster level of theory, and pressure-dependent rate expressions are derived. Compared to the oxidation of open-chain molecules,  $\text{O}_2$  addition to CE radicals competes with ring-opening and/or elimination reactions. In the case of THF, the theoretical treatment provided a kinetic model that predicted the formation of  $\alpha$ -KHP very well, which indicates the potential of current theoretical methods as an accurate source of thermochemical data. On the other hand, optimization tools based on “multiscale informatics” have been developed and applied to the oxidation of substituted oxiranes, which identify needed

adjustments of theoretical data within their uncertainty limits to improve the prediction of experimental data.

**Next:** H-abstraction reactions from CEs by  $\dot{\text{O}}\text{H}$  and  $\text{HO}\dot{\text{O}}$  proceeding through pre-reactive complexes have been identified as being crucial for predicting the oxidation products or intermediates in the low-temperature oxidation of CEs with good accuracy. The occurrence of equatorial and axial sites as well as syn- and anti- isomers (optical isomers) present challenges which have only sparingly been addressed in kinetic models. Existing lumped reactions should be reevaluated at a higher level of theory and replaced by elementary step reactions if needed. The identification of all the important pathways on the PES remains a challenge, which new algorithms will help to address in the future.

### **6.3. Ways cyclic ethers are considered in kinetic modelling**

**Concerning the consumption of furan derivatives**, thanks to the theoretical work here-before described, several models with fair prediction abilities are currently available to simulate IDTs in STs at high temperatures and/or the formation of species profiles of intermediate products in PLF for THF, 2-MTHF, furan, 2-MF and 2,5-DMF. In the last five years, progress has been made to extend these models towards low-temperature and intermediate temperature chemistry, which enabled the simulation of experimental data for saturated compounds (from 550 K onwards) and for unsaturated CEs from 730 K with satisfactory predictions of IDTs in RCMs. Thanks to available JSR data for THF and 2,5-DMF, as well as FR data for furan, 2-MF and 2,5-DMF, the newly developed models enabled detailed comparisons between experiments and predictions. In recent years, attempts have been made to model furfural pyrolysis and combustion with data for LBV and JSR species profiles, but not for IDTs. The number of models for other furan derivatives is much more limited.

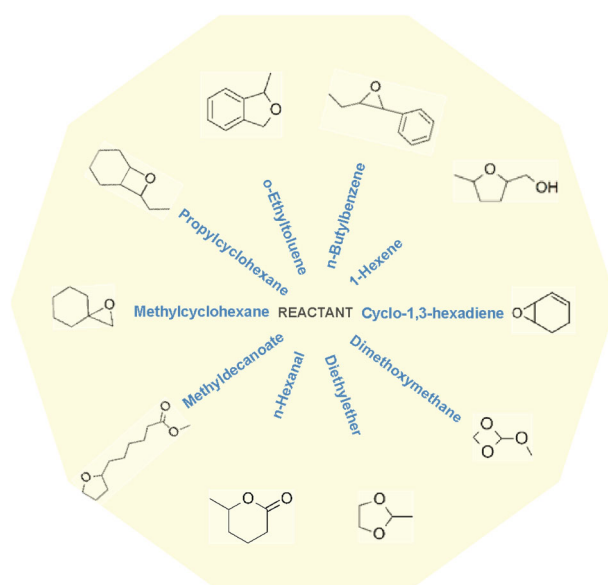


**Next:** As soon as new data in a JSR for furan derivatives substituted by C<sub>1+</sub> alkyl chain become available, there will be an incentive to update current models or develop new ones to predict those data. As mentioned in Part 5, for five alkyl substituted ethers there are currently no kinetic models available and should be developed to make use of the available experimental data. In the context of better using biomass and biofuels, the interest in modelling the reactions of furan derivatives substituted by oxygenated substituents will continue to increase.

**Concerning the simulated CE yields during fuel low-temperature oxidation,** Part 4 in this review describes the significant progress made over the years in predicting CE formation from a wide range of fuels, but with the highest accuracy achieved for linear alkanes. In contrast, Part 5 shows that the CE consumption chemistry is much more complex than what is prescribed in current chemical kinetics mechanisms. This is because the models contain only simplified reactions for the secondary chemistry of CEs in order to provide a sink for radicals. Often, only one or two reactions are included and with rather uncertain rate parameters. Furthermore, some rate expressions are generic and do not reflect the different reactivities of the abstracting radicals. Other kinetic models use experimental rate expressions that date back to the 1970s to 1990s. Moreover, modelling of the low-temperature oxidation of CEs is still in its infancy. As shown in Fig. 73, unknowns remain in the reaction pathways related to the consumption of all classes of CEs.

**Next:** A significant modelling effort is still needed concerning CE formation from branched alkanes, *e.g.* from hexane isomers, a challenging test for detailed kinetic models, and rate rules are still to be completed. This is even more true for cyclic, aromatic or oxygenated fuels. In addition, progress in the understanding of CE consumption chemistry over a wide temperature range should allow expanding the related sub-mechanisms considering additional

sources and sinks for radicals and consequently significantly improving the predictive capabilities of species profiles. Refining the CE secondary mechanism might increase modelling accuracy as much as considering the 3<sup>rd</sup> O<sub>2</sub> addition. The list of CEs to be studied does not only include alkyl oxiranes, oxetanes, THF and THP, which can be produced from the oxidation of linear and branched alkanes, but also all the types of molecules, which can be produced from various fuels as illustrated in Fig. 74. This model development should be done through the development of rate rules specific to CEs and the potential involvement of automatic generation algorithms.



**Fig. 74.** Examples of types of CEs different from those obtained from linear or branched alkanes that can be produced according to their reactant of origin.

## ACKNOWLEDGEMENTS

The authors wish to thank G. Vanhove, M. Ribaucour, H. Curran, Y. Fenard, Y. Li, J. Zou, and Z. Wang for their valuable assistance during the writing of this review. HHC acknowledges funding from the Aragón Government (Ref. T22\_20R), co-funded by FEDER 2014-2020 "Construyendo Europa desde Aragón".

## REFERENCES

- [1] Dec JE. Advanced compression-ignition engines—understanding the in-cylinder processes. *Proc Combust Inst* 2009;32:2727–42. <https://doi.org/10.1016/j.proci.2008.08.008>.
- [2] Musculus MPB, Miles PC, Pickett LM. Conceptual models for partially premixed low-temperature diesel combustion. *Prog Energy Combust Sci* 2013;39:246–83. <https://doi.org/10.1016/j.pecs.2012.09.001>.
- [3] Saxena S, Bedoya ID. Fundamental phenomena affecting low temperature combustion and HCCI engines, high load limits and strategies for extending these limits. *Prog Energy Combust Sci* 2013;39:457–88. <https://doi.org/10.1016/j.pecs.2013.05.002>.
- [4] Pollard R. Hydrocarbons. In *Comprehensive Chemical Kinetics: Gas-phase combustion*. Bamford CH, Tipper CFH Eds. vol. 17. Elsevier. Amsterdam: 1977.
- [5] Walker RW, Morley C. Basic chemistry of combustion. In *Comprehensive Chemical Kinetics: Low-temperature combustion and autoignition*. Pilling MJ Ed. vol. 35. Elsevier. Amsterdam: 1997.
- [6] Anca-Couce A, Hochenauer C, Scharler R. Bioenergy technologies, uses, market and future trends with Austria as a case study. *Renew Sust Energ Rev* 2021;135:110237. <https://doi.org/10.1016/j.rser.2020.110237>.
- [7] Lange J-P, van der Heide E, van Buijtenen J, Price R. Furfural - A promising platform for lignocellulosic biofuels. *ChemSusChem* 2012;5:150–66. <https://doi.org/10.1002/cssc.201100648>.
- [8] Leitner W, Klankermayer J, Pischinger S, Pitsch H, Kohse-Höinghaus K. Advanced biofuels and beyond: Chemistry solutions for propulsion and production. *Angew Chem-Int Edit* 2017;56:5412–52. <https://doi.org/10.1002/anie.201607257>.
- [9] Luterbacher JS, Alonso DM, Dumesic JA. Targeted chemical upgrading of lignocellulosic biomass to platform molecules. *Green Chem* 2014;16:4816–38. <https://doi.org/10.1039/C4GC01160K>.
- [10] Battin-Leclerc F. Detailed chemical kinetic models for the low-temperature combustion of hydrocarbons with application to gasoline and diesel fuel surrogates. *Prog Energy Combust Sci* 2008;34:440–98. <https://doi.org/10.1016/j.pecs.2007.10.002>.
- [11] Curran HJ. Developing detailed chemical kinetic mechanisms for fuel combustion. *Proc Combust Inst* 2019;37:57–81. <https://doi.org/10.1016/j.proci.2018.06.054>.
- [12] Westbrook CK, Mehl M, Pitz WJ, Kukkadapu G, Wagnon S, Zhang K. Multi-fuel surrogate chemical kinetic mechanisms for real world applications. *Phys Chem Chem Phys* 2018;20:10588–606. <https://doi.org/10.1039/C7CP07901J>.
- [13] Zádor J, Taatjes CA, Fernandes RX. Kinetics of elementary reactions in low-temperature autoignition chemistry. *Prog Energy Combust Sci* 2011;37:371–421. <https://doi.org/10.1016/j.pecs.2010.06.006>.
- [14] Sarathy SM, Osswald P, Hansen N, Kohse-Höinghaus K. Alcohol combustion chemistry. *Prog Energy Combust Sci* 2014;44:40–102. <https://doi.org/10.1016/j.pecs.2014.04.003>.
- [15] Glaude PA, Herbinet O, Bax S, Biet J, Warth V, Battin-Leclerc F. Modeling of the oxidation of methyl esters - Validation for methyl hexanoate, methyl heptanoate, and methyl decanoate in a jet-stirred reactor. *Combust Flame* 2010;157:2035–50. <https://doi.org/10.1016/j.combustflame.2010.03.012>.
- [16] Rotavera B, Taatjes CA. Influence of functional groups on low-temperature combustion chemistry of biofuels. *Prog Energy Combust Sci* 2021:100925. <https://doi.org/10.1016/j.pecs.2021.100925>.
- [17] Wang Z, Popolan-Vaida DM, Chen B, Moshhammer K, Mohamed SY, Wang H, et al. Unraveling the structure and chemical mechanisms of highly oxygenated intermediates in

- oxidation of organic compounds. *PNAS* 2017;114:13102–7. <https://doi.org/10.1073/pnas.1707564114>.
- [18] Savee JD, Papajak E, Rotavera B, Huang H, Eskola AJ, Welz O, et al. Direct observation and kinetics of a hydroperoxyalkyl radical (QOOH). *Science* 2015;347:643–6. <https://doi.org/10.1126/science.aaa1495>.
- [19] Hansen AS, Bhagde T, Moore III KB, Moberg DR, Jasper AW, Georgievskii Y, et al. Watching a hydroperoxyalkyl radical ( $\bullet$ QOOH) dissociate. *Science* 2021. <https://doi.org/10.1126/science.abj0412>.
- [20] Wang Z, Zhang L, Moshhammer K, Popolan-Vaida DM, Shankar VSB, Lucassen A, et al. Additional chain-branching pathways in the low-temperature oxidation of branched alkanes. *Combust Flame* 2016;164:386–96. <https://doi.org/10.1016/j.combustflame.2015.11.035>.
- [21] Luo Y-R. *Comprehensive handbook of chemical bond energies*. CRC Press. Boca Raton: 2007.
- [22] Tran L-S, Herbinet O, Li Y, Wullenkord J, Zeng M, Bräuer E, et al. Low-temperature gas-phase oxidation of diethyl ether: Fuel reactivity and fuel-specific products. *Proc Combust Inst* 2019;37:511–9. <https://doi.org/10.1016/j.proci.2018.05.135>.
- [23] Wang Z, Herbinet O, Hansen N, Battin-Leclerc F. Exploring hydroperoxides in combustion: History, recent advances and perspectives. *Prog Energy Combust Sci* 2019;73:132–81. <https://doi.org/10.1016/j.pecs.2019.02.003>.
- [24] Ju Y, Reuter CB, Yehia OR, Farouk TI, Won SH. Dynamics of cool flames. *Prog Energy Combust Sci* 2019;75:100787. <https://doi.org/10.1016/j.pecs.2019.100787>.
- [25] Ju Y. Understanding cool flames and warm flames. *Proceedings of the Combustion Institute* 2021;38:83–119. <https://doi.org/10.1016/j.proci.2020.09.019>.
- [26] Crochet M, Minetti R, Ribaucour M, Vanhove G. A detailed experimental study of n-propylcyclohexane autoignition in lean conditions. *Combust Flame* 2010;157:2078–85. <https://doi.org/10.1016/j.combustflame.2010.04.012>.
- [27] Barraza-Botet CL, Luecke J, Zigler BT, Wooldridge MS. The impact of physicochemical property interactions of iso-octane/ethanol blends on ignition timescales. *Fuel* 2018;224:401–11. <https://doi.org/10.1016/j.fuel.2018.03.105>.
- [28] Wang Z, Chen B, Moshhammer K, Popolan-Vaida DM, Sioud S, Shankar VSB, et al. n-Heptane cool flame chemistry: Unraveling intermediate species measured in a stirred reactor and motored engine. *Combust Flame* 2018;187:199–216. <https://doi.org/10.1016/j.combustflame.2017.09.003>.
- [29] Rodriguez A, Herbinet O, Meng X, Fittschen C, Wang Z, Xing L, et al. Hydroperoxide measurements during low-temperature gas-phase oxidation of n-heptane and n-decane. *J Phys Chem A* 2017;121:1861–76. <https://doi.org/10.1021/acs.jpca.6b10378>.
- [30] Herbinet O, Battin-Leclerc F. Progress in Understanding Low-Temperature Organic Compound Oxidation Using a Jet-Stirred Reactor. *Int J Chem Kinet* 2014;46:619–39. <https://doi.org/10.1002/kin.20871>.
- [31] Jalan A, Alecu IM, Meana-Paneda R, Aguilera-Iparraguirre J, Yang KR, Merchant SS, et al. New pathways for formation of acids and carbonyl products in low-temperature oxidation: The Korcek decomposition of gamma-ketohydroperoxides. *J Am Chem Soc* 2013;135:11100–14. <https://doi.org/10.1021/ja4034439>.
- [32] Herbinet O, Husson B, Serinyel Z, Cord M, Warth V, Fournet R, et al. Experimental and modeling investigation of the low-temperature oxidation of n-heptane. *Combust Flame* 2012;159:3455–71. <https://doi.org/10.1016/j.combustflame.2012.07.008>.
- [33] Zhang K, Banyon C, Bugler J, Curran HJ, Rodriguez A, Herbinet O, et al. An updated experimental and kinetic modeling study of n-heptane oxidation. *Combust Flame* 2016;172:116–35. <https://doi.org/10.1016/j.combustflame.2016.06.028>.

- [34] Pelucchi M, Bissoli M, Cavallotti C, Cuoci A, Faravelli T, Frassoldati A, et al. Improved kinetic model of the low-temperature oxidation of n-heptane. *Energy Fuels* 2014;28:7178–93. <https://doi.org/10.1021/ef501483f>.
- [35] BP Energy Outlook: 2020 Edition. Available under [Www.Bp.Com](http://www.bp.com), Accessed October 16, 2020: 2020.
- [36] EASAC policy report 37. Decarbonisation of transport: Options and challenges. Available under [Www.Easac.Eu](http://www.easac.eu): 2019.
- [37] Huber GW, Iborra S, Corma A. Synthesis of transportation fuels from biomass: Chemistry, catalysts, and engineering. *Chem Rev* 2006;106:4044–98. <https://doi.org/10.1021/cr068360d>.
- [38] Kohse-Höinghaus K, Oßwald P, Cool TA, Kasper T, Hansen N, Qi F, et al. Biofuel combustion chemistry: From ethanol to biodiesel. *Angew Chem-Int Edit* 2010;49:3572–97. <https://doi.org/10.1002/anie.200905335>.
- [39] Tran LS, Sirjean B, Glaude P-A, Fournet R, Battin-Leclerc F. Progress in detailed kinetic modeling of the combustion of oxygenated components of biofuels. *Energy* 2012;43:4–18. <https://doi.org/10.1016/j.energy.2011.11.013>.
- [40] Westbrook CK, Pitz WJ, Curran HJ. Chemical kinetic modeling study of the effects of oxygenated hydrocarbons on soot emissions from diesel engines. *J Phys Chem A* 2006;110:6912–22. <https://doi.org/10.1021/jp056362g>.
- [41] Grad P. Biofuelling Brazil: An overview of the bioethanol success story in Brazil. *Refocus* 2006;7:56–9. [https://doi.org/10.1016/S1471-0846\(06\)70576-5](https://doi.org/10.1016/S1471-0846(06)70576-5).
- [42] Agarwal AK. Biofuels (alcohols and biodiesel) applications as fuels for internal combustion engines. *Prog Energy Combust Sci* 2007;33:233–71. <https://doi.org/10.1016/j.pecs.2006.08.003>.
- [43] Sarathy SM, Farooq A, Kalghatgi GT. Recent progress in gasoline surrogate fuels. *Prog Energy Combust Sci* 2018;65:67–108. <https://doi.org/10.1016/j.pecs.2017.09.004>.
- [44] He B-Q, Shuai S-J, Wang J-X, He H. The effect of ethanol blended diesel fuels on emissions from a diesel engine. *Atmospheric Environ* 2003;37:4965–71. <https://doi.org/10.1016/j.atmosenv.2003.08.029>.
- [45] Knothe G, Razon LF. Biodiesel fuels. *Prog Energy Combust Sci* 2017;58:36–59. <https://doi.org/10.1016/j.pecs.2016.08.001>.
- [46] Abomohra AE-F, Elsayed M, Esakkimuthu S, El-Sheekh M, Hanelt D. Potential of fat, oil and grease (FOG) for biodiesel production: A critical review on the recent progress and future perspectives. *Prog Energy Combust Sci* 2020;81:100868. <https://doi.org/10.1016/j.pecs.2020.100868>.
- [47] Demirbas A. Biodiesel production from vegetable oils via catalytic and non-catalytic supercritical methanol transesterification methods. *Prog Energy Combust Sci* 2005;31:466–87. <https://doi.org/10.1016/j.pecs.2005.09.001>.
- [48] Cheah WY, Sankaran R, Show PL, Ibrahim TNBT, Chew KW, Culaba A, et al. Pretreatment methods for lignocellulosic biofuels production: Current advances, challenges and future prospects. *Biofuel Res J* 2020;7:1115. <https://doi.org/10.18331/BRJ2020.7.1.4>.
- [49] Yi Z, Xu H, Hu D, Yan K. Facile synthesis of supported Pd catalysts by chemical fluid deposition method for selective hydrogenation of biomass-derived furfural. *J Alloys Compd* 2019;799:59–65. <https://doi.org/10.1016/j.jallcom.2019.05.350>.
- [50] Hu D, Xu H, Yi Z, Chen Z, Ye C, Wu Z, et al. Green CO<sub>2</sub>-assisted synthesis of mono- and bimetallic Pd/Pt nanoparticles on porous carbon fabricated from sorghum for highly selective hydrogenation of furfural. *ACS Sustainable Chem Eng* 2019;7:15339–45. <https://doi.org/10.1021/acssuschemeng.9b02665>.

- [51] Boot MD, Tian M, Hensen EJM, Mani Sarathy S. Impact of fuel molecular structure on auto-ignition behavior – Design rules for future high performance gasolines. *Prog Energy Combust Sci* 2017;60:1–25. <https://doi.org/10.1016/j.pecs.2016.12.001>.
- [52] Thewes M, Muether M, Pischinger S, Budde M, Brunn A, Sehr A, et al. Analysis of the impact of 2-methylfuran on mixture formation and combustion in a direct-injection spark-ignition engine. *Energy Fuels* 2011;25:5549–61. <https://doi.org/10.1021/ef201021a>.
- [53] Brassat A, Thewes M, Müther M, Pischinger S, Lee C, Fernandes RX, et al. Analysis of the effects of certain alcohol and furan-based biofuels on controlled auto Ignition. *SAE Technical Papers* 2012;2012-01–1135.
- [54] Kumar A, Jones DD, Hanna MA. Thermochemical biomass gasification: A review of the current status of the technology. *Energies* 2009;2:556–81. <https://doi.org/10.3390/en20300556>.
- [55] Tijmensen MJA, Faaij APC, Hamelinck CN, van Hardeveld MRM. Exploration of the possibilities for production of Fischer Tropsch liquids and power via biomass gasification. *Biomass Bioenergy* 2002;23:129–52. [https://doi.org/10.1016/S0961-9534\(02\)00037-5](https://doi.org/10.1016/S0961-9534(02)00037-5).
- [56] Wang M, Dewil Raf, Maniatis K, Wheeldon J, Tan T, Baeyens J, et al. Biomass-derived aviation fuels: Challenges and perspective. *Prog Energy Combust Sci* 2019;74:31–49. <https://doi.org/10.1016/j.pecs.2019.04.004>.
- [57] Verhelst S, Turner JW, Sileghem L, Vancoillie J. Methanol as a fuel for internal combustion engines. *Prog Energy Combust Sci* 2019;70:43–88. <https://doi.org/10.1016/j.pecs.2018.10.001>.
- [58] Sikarwar VS, Zhao M, Fennell PS, Shah N, Anthony EJ. Progress in biofuel production from gasification. *Prog Energy Combust Sci* 2017;61:189–248. <https://doi.org/10.1016/j.pecs.2017.04.001>.
- [59] Azizi Z, Rezaeimanesh M, Tohidian T, Rahimpour MR. Dimethyl ether: A review of technologies and production challenges. *Chem Eng Process* 2014;82:150–72. <https://doi.org/10.1016/j.cep.2014.06.007>.
- [60] Xiu S, Shahbazi A. Bio-oil production and upgrading research: A review. *Renew Sust Energ Rev* 2012;16:4406–14. <https://doi.org/10.1016/j.rser.2012.04.028>.
- [61] Tekin K, Karagöz S, Bektaş S. A review of hydrothermal biomass processing. *Renew Sust Energ Rev* 2014;40:673–87. <https://doi.org/10.1016/j.rser.2014.07.216>.
- [62] Akhtar J, Amin NAS. A review on process conditions for optimum bio-oil yield in hydrothermal liquefaction of biomass. *Renew Sust Energ Rev* 2011;15:1615–24. <https://doi.org/10.1016/j.rser.2010.11.054>.
- [63] Lédé J. Biomass fast pyrolysis reactors: A review of a few scientific challenges and of related recommended research topics. *Oil Gas Sci Technol – Rev IFP Energies Nouvelles* 2013;68:801–14. <https://doi.org/10.2516/ogst/2013108>.
- [64] Kan T, Strezov V, Evans TJ. Lignocellulosic biomass pyrolysis: A review of product properties and effects of pyrolysis parameters. *Renew Sust Energ Rev* 2016;57:1126–40. <https://doi.org/10.1016/j.rser.2015.12.185>.
- [65] Negahdar L, Gonzalez-Quiroga A, Otyuskaya D, Toraman HE, Liu L, Jastrzebski JTBH, et al. Characterization and comparison of fast pyrolysis bio-oils from pinewood, rapeseed cake, and wheat straw using <sup>13</sup>C NMR and comprehensive GC×GC. *ACS Sustainable Chem Eng* 2016;4:4974–85. <https://doi.org/10.1021/acssuschemeng.6b01329>.
- [66] Djokic MR, Dijkmans T, Yildiz G, Prins W, Van Geem KM. Quantitative analysis of crude and stabilized bio-oils by comprehensive two-dimensional gas-chromatography. *J Chromatogr A* 2012;1257:131–40. <https://doi.org/10.1016/j.chroma.2012.07.035>.
- [67] Demirbas A. Biofuels sources, biofuel policy, biofuel economy and global biofuel projections. *Energy Convers Manag* 2008;49:2106–16. <https://doi.org/10.1016/j.enconman.2008.02.020>.

- [68] Sun Z, Fridrich B, de Santi A, Elangovan S, Barta K. Bright side of lignin depolymerization: Toward new platform chemicals. *Chem Rev* 2018;118:614–78. <https://doi.org/10.1021/acs.chemrev.7b00588>.
- [69] Ma R, Hao W, Ma X, Tian Y, Li Y. Catalytic Ethanolysis of Kraft Lignin into High-Value Small-Molecular Chemicals over a Nanostructured  $\alpha$ -Molybdenum Carbide Catalyst. *Angew Chem-Int Edit* 2014;126:7438–43. <https://doi.org/10.1002/ange.201402752>.
- [70] Tian M, McCormick RL, Luecke J, de Jong E, van der Waal JC, van Klink GPM, et al. Anti-knock quality of sugar derived levulinic esters and cyclic ethers. *Fuel* 2017;202:414–25. <https://doi.org/10.1016/j.fuel.2017.04.027>.
- [71] Climent MJ, Corma A, Iborra S. Conversion of biomass platform molecules into fuel additives and liquid hydrocarbon fuels. *Green Chem* 2014;16:516–47. <https://doi.org/10.1039/C3GC41492B>.
- [72] Dahmen M, Marquardt W. Model-based design of tailor-made biofuels. *Energy Fuels* 2016;30:1109–34. <https://doi.org/10.1021/acs.energyfuels.5b02674>.
- [73] Román-Leshkov Y, Barrett CJ, Liu ZY, Dumesic JA. Production of dimethylfuran for liquid fuels from biomass-derived carbohydrates. *Nature* 2007;447:982–5. <https://doi.org/10.1038/nature05923>.
- [74] De Jong E, Gruter G-J. *Furanics: a novel diesel fuel with superior characteristics*. Warrendale, PA: SAE International; 2009. <https://doi.org/10.4271/2009-01-2767>.
- [75] Gao Z, Li C, Fan G, Yang L, Li F. Nitrogen-doped carbon-decorated copper catalyst for highly efficient transfer hydrogenolysis of 5-hydroxymethylfurfural to convertibly produce 2,5-dimethylfuran or 2,5-dimethyltetrahydrofuran. *Appl Catal B: Environ* 2018;226:523–33. <https://doi.org/10.1016/j.apcatb.2018.01.006>.
- [76] Luterbacher JS, Rand JM, Alonso DM, Han J, Youngquist JT, Maravelias CT, et al. Nonenzymatic Sugar Production from Biomass Using Biomass-Derived  $\gamma$ -Valerolactone. *Science* 2014;343:277–80. <https://doi.org/10.1126/science.1246748>.
- [77] Geilen FMA, Engendahl B, Harwardt A, Marquardt W, Klankermayer J, Leitner W. Selective and flexible transformation of biomass-derived platform chemicals by a multifunctional catalytic system. *Angew Chem-Int Edit* 2010;49:5510–4. <https://doi.org/10.1002/anie.201002060>.
- [78] Liu C, Zhang C, Liu K, Wang Y, Fan G, Sun S, et al. Aqueous-phase hydrogenolysis of glucose to value-added chemicals and biofuels: A comparative study of active metals. *Biomass Bioenergy* 2015;72:189–99. <https://doi.org/10.1016/j.biombioe.2014.11.005>.
- [79] Marshall A-L, Alaimo PJ. Useful products from complex starting materials: Common chemicals from biomass feedstocks. *Chem Eur J* 2010;16:4970–80. <https://doi.org/10.1002/chem.200903028>.
- [80] Sandbrink L, Beckerle K, Meiners I, Liffmann R, Rahimi K, Okuda J, et al. Supported molybdenum catalysts for the deoxydehydration of 1,4-anhydroerythritol into 2,5-dihydrofuran. *ChemSusChem* 2017;10:1375–9. <https://doi.org/10.1002/cssc.201700010>.
- [81] Osmont A, Catoire L, Escot Bocanegra P, Gökalp I, Thollas B, Kozinski JA. Second generation biofuels: Thermochemistry of glucose and fructose. *Combust Flame* 2010;157:1230–4. <https://doi.org/10.1016/j.combustflame.2009.12.002>.
- [82] Leppard WR. Autoignition chemistries of octane-enhancing ethers and cyclic ethers: A motored engine study. *SAE Technical Paper* 912313 1991;100:589–604. <https://doi.org/10.4271/912313>.
- [83] Beydoun K, Klankermayer J. Ruthenium-catalyzed synthesis of cyclic and linear acetals by the combined utilization of CO<sub>2</sub>, H<sub>2</sub>, and biomass derived diols. *Chem Eur J* 2019;25:11412–5. <https://doi.org/10.1002/chem.201901660>.

- [84] Li H, Wu C, Zhang Q, Li X, Gao X. Synthesis of 1,3-dioxolane from aqueous formaldehyde solution and ethylene glycol: kinetics and reactive distillation. *Ind Eng Chem Res* 2019;58:7025–36. <https://doi.org/10.1021/acs.iecr.9b00331>.
- [85] Liu D, Liu C, Li H, Lei A. Direct functionalization of tetrahydrofuran and 1,4-dioxane: nickel-catalyzed oxidative c(sp<sup>3</sup>)-h arylation. *Angew Chem-Int Edit* 2013;52:4453–6. <https://doi.org/10.1002/anie.201300459>.
- [86] Ramalingam S, Rajendran S, Ganesan P. Improving the performance is better and emission reductions from Annona biodiesel operated diesel engine using 1,4-dioxane fuel additive. *Fuel* 2016;185:804–9. <https://doi.org/10.1016/j.fuel.2016.08.049>.
- [87] Sudholt A, Cai L, Heyne J, Haas FM, Pitsch H, Dryer FL. Ignition characteristics of a bio-derived class of saturated and unsaturated furans for engine applications. *Proc Combust Inst* 2015;35:2957–65. <https://doi.org/10.1016/j.proci.2014.06.147>.
- [88] Julis J, Leitner W. Synthesis of 1-octanol and 1,1-dioctyl ether from biomass-derived platform chemicals. *Angew Chem-Int Edit* 2012;51:8615–9. <https://doi.org/10.1002/anie.201203669>.
- [89] Shankar VSB, Li Y, Singh E, Sarathy SM. Understanding the synergistic blending octane behavior of 2-methylfuran. *Proc Combust Inst* 2021;38:5625–33. <https://doi.org/10.1016/j.proci.2020.06.277>.
- [90] Simmie JM. Kinetics and thermochemistry of 2,5-dimethyltetrahydrofuran and related oxolanes: next-generation biofuels. *J Phys Chem A* 2012;116:4528–38. <https://doi.org/10.1021/jp301870w>.
- [91] Wei H, Feng D, Shu G, Pan M, Guo Y, Gao D, et al. Experimental investigation on the combustion and emissions characteristics of 2-methylfuran gasoline blend fuel in spark-ignition engine. *Applied Energy* 2014;132:317–24. <https://doi.org/10.1016/j.apenergy.2014.07.009>.
- [92] Wu Y, Zhang X, Zhang Z, Wang X, Geng Z, Jin C, et al. Effects of diesel-ethanol-THF blend fuel on the performance and exhaust emissions on a heavy-duty diesel engine. *Fuel* 2020;271:117633. <https://doi.org/10.1016/j.fuel.2020.117633>.
- [93] Mathieu F, Reddemann M, Martin D, Kneer R. Experimental investigation of fuel influence on atomization and spray propagation using an outwardly opening GDI-injector. *SAE Technical Papers* 2010. <https://doi.org/10.4271/2010-01-2275>.
- [94] Yanowitz J, Christensen E, McCormick RL. Utilization of renewable oxygenates as gasoline blending components. Colorado: National Renewable Energy Laboratory, rapport N° NREL/TP-5400-50791; 2011.
- [95] Zeitsch KJ, editor. Properties of furan. In *Sugar Series*, vol. 13, Elsevier; 2000, p. 240–2. [https://doi.org/10.1016/S0167-7675\(00\)80036-6](https://doi.org/10.1016/S0167-7675(00)80036-6).
- [96] Song J, Zello V, Boehman AL, Waller FJ. Comparison of the impact of intake oxygen enrichment and fuel oxygenation on diesel combustion and emissions. *Energy Fuels* 2004;18:1282–90. <https://doi.org/10.1021/ef034103p>.
- [97] Bereczky Á, Lukács K, Farkas M, Dóbbé S. Effect of  $\gamma$ -valerolactone blending on engine performance, combustion characteristics and exhaust emissions in a diesel engine. *Nat Resour* 2014;5:177–91. <https://doi.org/10.4236/nr.2014.55017>.
- [98] Stickney JA, Sager SL, Clarkson JR, Smith LA, Locey BJ, Bock MJ, et al. An updated evaluation of the carcinogenic potential of 1,4-dioxane. *Regul Toxicol Pharmacol* 2003;38:183–95. [https://doi.org/10.1016/S0273-2300\(03\)00090-4](https://doi.org/10.1016/S0273-2300(03)00090-4).
- [99] Yuan Y, Zhao X, Wang S, Wang L. Atmospheric oxidation of furan and methyl-substituted furans Initiated by hydroxyl radicals. *J Phys Chem A* 2017;121:9306–19. <https://doi.org/10.1021/acs.jpca.7b09741>.
- [100] Wang C, Xu H, Daniel R, Ghafourian A, Martin Herreros J, Shuai S, et al. Combustion characteristics and emissions of 2-methylfuran compared to 2,5-dimethylfuran, gasoline



- and ethanol in a DISI engine. *Fuel* 2013;103:200–11. <https://doi.org/10.1016/j.fuel.2012.05.043>.
- [101] Daniel R, Wei L, Xu H, Wang C, Wyszynski ML, Shuai S. Speciation of hydrocarbon and carbonyl emissions of 2,5-dimethylfuran combustion in a DISI engine. *Energy Fuels* 2012;26:6661–8. <https://doi.org/10.1021/ef301236f>.
- [102] Xiao H, Yang X, Hou B, Wang R, Xue Q, Ju H. Combustion performance and pollutant emissions analysis of a diesel engine fueled with biodiesel and its blend with 2-methylfuran. *Fuel* 2019;237:1050–6. <https://doi.org/10.1016/j.fuel.2018.09.146>.
- [103] Tran L-S, Sirjean B, Glaude P-A, Kohse-Höinghaus K, Battin-Leclerc F. Influence of substituted furans on the formation of Polycyclic Aromatic Hydrocarbons in flames. *Proc Combust Inst* 2015;35:1735–43. <https://doi.org/10.1016/j.proci.2014.06.137>.
- [104] Huang H, Buekens A. On the mechanisms of dioxin formation in combustion processes. *Chemosphere* 1995;31:4099–117. [https://doi.org/10.1016/0045-6535\(95\)80011-9](https://doi.org/10.1016/0045-6535(95)80011-9).
- [105] Altarawneh M, Dlugogorski BZ, Kennedy EM, Mackie JC. Mechanisms for formation, chlorination, dechlorination and destruction of polychlorinated dibenzo-p-dioxins and dibenzofurans (PCDD/Fs). *Prog Energy Combust Sci* 2009;35:245–74. <https://doi.org/10.1016/j.pecs.2008.12.001>.
- [106] Pilling MJ. From elementary reactions to evaluated chemical mechanisms for combustion models. *Proc Combust Inst* 2009;32:27–44. <https://doi.org/10.1016/j.proci.2008.08.003>.
- [107] Zádor J, Klippenstein SJ, Miller JA. Pressure-dependent OH yields in alkene + HO<sub>2</sub> reactions: a theoretical study. *J Phys Chem A* 2011;115:10218–25. <https://doi.org/10.1021/jp2059276>.
- [108] Møller Chr, Plesset MS. Note on an approximation treatment for many-electron systems. *Phys Rev* 1934;46:618–22. <https://doi.org/10.1103/PhysRev.46.618>.
- [109] Roos BO, Linse P, Siegbahn PEM, Blomberg MRA. A simple method for the evaluation of the second-order-perturbation energy from external double-excitations with a CASSCF reference wavefunction. *Chemical Physics* 1982;66:197–207. [https://doi.org/10.1016/0301-0104\(82\)88019-1](https://doi.org/10.1016/0301-0104(82)88019-1).
- [110] Purvis GD, Bartlett RJ. A full coupled-cluster singles and doubles model: The inclusion of disconnected triples. *J Chem Phys* 1982;76:1910–8. <https://doi.org/10.1063/1.443164>.
- [111] Ross IG. Calculations of the energy levels of acetylene by the method of antisymmetric molecular orbitals, including  $\sigma$ - $\pi$  interaction. *Trans Faraday Soc* 1952;48:973–91. <https://doi.org/10.1039/TF9524800973>.
- [112] Ditchfield R, Hehre WJ, Pople JA. Self-consistent molecular-orbital methods. IX. an extended gaussian-type basis for molecular-orbital studies of organic molecules. *J Chem Phys* 1971;54:724–8. <https://doi.org/10.1063/1.1674902>.
- [113] Dunning TH. Gaussian basis sets for use in correlated molecular calculations. I. The atoms boron through neon and hydrogen. *J Chem Phys* 1989;90:1007–23. <https://doi.org/10.1063/1.456153>.
- [114] Lee TJ. Comparison of the T1 and D1 diagnostics for electronic structure theory: a new definition for the open-shell D1 diagnostic. *Chem Phys Lett* 2003;372:362–7. [https://doi.org/10.1016/S0009-2614\(03\)00435-4](https://doi.org/10.1016/S0009-2614(03)00435-4).
- [115] Harding LB, Klippenstein SJ, Jasper AW. Ab initio methods for reactive potential surfaces. *Phys Chem Chem Phys* 2007;9:4055–70. <https://doi.org/10.1039/B705390H>.
- [116] Stein CJ, Reiher M. Automated selection of active orbital spaces. *J Chem Theory Comput* 2016;12:1760–71. <https://doi.org/10.1021/acs.jctc.6b00156>.
- [117] Azizi Z, Roos BO, Veryazov V. How accurate is the CASPT2 method? *Phys Chem Chem Phys* 2006;8:2727–32. <https://doi.org/10.1039/B603046G>.

- [118] Bauer CA, Hansen A, Grimme S. The fractional occupation number weighted density as a versatile analysis tool for molecules with a complicated electronic structure. *Chem Eur J* 2017;23:6150–64. <https://doi.org/10.1002/chem.201604682>.
- [119] Stephens PJ, Devlin FJ, Chabalowski CF, Frisch MJ. Ab initio calculation of vibrational absorption and circular dichroism spectra using density functional force fields. *J Phys Chem* 1994;98:11623–7. <https://doi.org/10.1021/j100096a001>.
- [120] Zhao Y, Truhlar DG. The M06 suite of density functionals for main group thermochemistry, thermochemical kinetics, noncovalent interactions, excited states, and transition elements: two new functionals and systematic testing of four M06-class functionals and 12 other functionals. *Theor Chem Account* 2008;120:215–41. <https://doi.org/10.1007/s00214-007-0310-x>.
- [121] Sun H, Bozzelli JW. Structures, intramolecular rotation barriers, and thermochemical properties: ethanol,  $\alpha$ -monoethanols, dichloroethanols, and corresponding radicals derived from H atom loss. *J Phys Chem A* 2001;105:9543–52. <https://doi.org/10.1021/jp011949q>.
- [122] Curtiss LA, Raghavachari K, Redfern PC, Rassolov V, Pople JA. Gaussian-3 (G3) theory for molecules containing first and second-row atoms. *J Chem Phys* 1998;109:7764–76. <https://doi.org/10.1063/1.477422>.
- [123] Curtiss LA, Redfern PC, Raghavachari K. Gaussian-4 theory. *J Chem Phys* 2007;126:084108. <https://doi.org/10.1063/1.2436888>.
- [124] Montgomery JA, Frisch MJ, Ochterski JW, Petersson GA. A complete basis set model chemistry. VI. Use of density functional geometries and frequencies. *J Chem Phys* 1999;110:2822–7. <https://doi.org/10.1063/1.477924>.
- [125] Montgomery JA, Frisch MJ, Ochterski JW, Petersson GA. A complete basis set model chemistry. VII. Use of the minimum population localization method. *J Chem Phys* 2000;112:6532–42. <https://doi.org/10.1063/1.481224>.
- [126] Ochterski JW, Petersson GA, Montgomery JA. A complete basis set model chemistry. V. Extensions to six or more heavy atoms. *J Chem Phys* 1996;104:2598–619. <https://doi.org/10.1063/1.470985>.
- [127] Martin JML, de Oliveira G. Towards standard methods for benchmark quality ab initio thermochemistry - W1 and W2 theory. *J Chem Phys* 1999;111:1843–56. <https://doi.org/10.1063/1.479454>.
- [128] DeYonker NJ, Cundari TR, Wilson AK. The correlation consistent composite approach (ccCA): An alternative to the Gaussian-n methods. *J Chem Phys* 2006;124:114104. <https://doi.org/10.1063/1.2173988>.
- [129] Tajti A, Szalay PG, Császár AG, Kállay M, Gauss J, Valeev EF, et al. HEAT: High accuracy extrapolated ab initio thermochemistry. *J Chem Phys* 2004;121:11599–613. <https://doi.org/10.1063/1.1811608>.
- [130] Klippenstein SJ, Harding LB, Ruscic B. Ab initio computations and active thermochemical tables hand in hand: Heats of formation of core combustion species. *J Phys Chem A* 2017;121:6580–602. <https://doi.org/10.1021/acs.jpca.7b05945>.
- [131] Ruscic B. Uncertainty quantification in thermochemistry, benchmarking electronic structure computations, and Active Thermochemical Tables. *International Journal of Quantum Chemistry* 2014;114:1097–101. <https://doi.org/10.1002/qua.24605>.
- [132] Simmie JM, Somers KP. Benchmarking compound methods (CBS-QB3, CBS-APNO, G3, G4, W1BD) against the active thermochemical tables: A litmus test for cost-effective molecular formation enthalpies. *J Phys Chem A* 2015;119:7235–46. <https://doi.org/10.1021/jp511403a>.

- [133] Ruscic B, Pinzon RE, Morton ML, von Laszewski G, Bittner SJ, Nijssure SG, et al. Introduction to active thermochemical tables: several “key” enthalpies of formation revisited. *J Phys Chem A* 2004;108:9979–97. <https://doi.org/10.1021/jp047912y>.
- [134] Cagnina S, Nicolle A, de Bruin T, Georgievskii Y, Klippenstein SJ. First-principles chemical kinetic modeling of methyl trans-3-hexenoate epoxidation by HO<sub>2</sub>. *J Phys Chem A* 2017;121:1909–15. <https://doi.org/10.1021/acs.jpca.7b00519>.
- [135] Martin JML. Ab initio total atomization energies of small molecules - towards the basis set limit. *Chem Phys Lett* 1996;259:669–78. [https://doi.org/10.1016/0009-2614\(96\)00898-6](https://doi.org/10.1016/0009-2614(96)00898-6).
- [136] Feller D, Dixon DA. Extended benchmark studies of coupled cluster theory through triple excitations. *J Chem Phys* 2001;115:3484–96. <https://doi.org/10.1063/1.1388045>.
- [137] Feller D, Franz JA. A theoretical determination of the heats of formation of furan, tetrahydrofuran, THF-2-yl, and THF-3-yl. *J Phys Chem A* 2000;104:9017–25. <https://doi.org/10.1021/jp001972w>.
- [138] McQuarrie DA, Simon JD. *Molecular thermodynamics*. Sausalito, United States: University Science Books; 1999.
- [139] Keçeli M, Elliott SN, Li Y-P, Johnson MS, Cavallotti C, Georgievskii Y, et al. Automated computational thermochemistry for butane oxidation: A prelude to predictive automated combustion kinetics. *Proceedings of the Combustion Institute* 2019;37:363–71. <https://doi.org/10.1016/j.proci.2018.07.113>.
- [140] IUPAC: *Compendium of Chemical Terminology*. 2nd Edition. Compiled by A. D. McNaught and A. Wilkinson. (Online version (2019-) created by S. J. Chalk. ISBN 0-9678550-9-8). Oxford: Blackwell Scientific Publications; 1997.
- [141] Benson SW. *Thermochemical kinetics*, 2nd. Ed. New York: John Wiley&Sons. 1976.
- [142] Chen C-J, Bozzelli JW. Kinetic analysis for HO<sub>2</sub> addition to ethylene, propene, and isobutene, and thermochemical parameters of alkyl hydroperoxides and hydroperoxide alkyl radicals. *J Phys Chem A* 2000;104:4997–5012. <https://doi.org/10.1021/jp993111x>.
- [143] Bozzelli JW, Sheng C. Thermochemistry, reaction paths, and kinetics on the hydroperoxy-ethyl radical reaction with O<sub>2</sub>: New chain branching reactions in hydrocarbon oxidation. *J Phys Chem A* 2002;106:1113–21. <https://doi.org/10.1021/jp013604d>.
- [144] Hudzik JM, Bozzelli JW. Thermochemistry of hydroxyl and hydroperoxide substituted furan, methylfuran, and methoxyfuran. *J Phys Chem A* 2017;121:4523–44. <https://doi.org/10.1021/acs.jpca.7b02343>.
- [145] Sebban N, Bozzelli JW, Trimis D, Bockhorn H. Thermochemistry and kinetics of the 2-butanone-4-yl CH<sub>3</sub>C(=O)CH<sub>2</sub>CH<sub>2</sub>• + O<sub>2</sub> reaction system. *Int J Chem Kinet* 2019;51:541–62. <https://doi.org/10.1002/kin.21276>.
- [146] Petersson GA, Malick DK, Wilson WG, Ochterski JW, Montgomery Jr. JA, Frisch MJ. Calibration and comparison of the Gaussian-2, complete basis set, and density functional methods for computational thermochemistry. *J Chem Phys* 1998;109:10570–9. <https://doi.org/10.1063/1.477794>.
- [147] Wheeler SE, Houk KN, Schleyer P v. R, Allen WD. A hierarchy of homodesmotic reactions for thermochemistry. *J Am Chem Soc* 2009;131:2547–60. <https://doi.org/10.1021/ja805843n>.
- [148] Curtiss LA, Raghavachari K, Redfern PC, Pople JA. Assessment of Gaussian-2 and density functional theories for the computation of enthalpies of formation. *J Chem Phys* 1997;106:1063–79. <https://doi.org/10.1063/1.473182>.
- [149] Melius CF, Allendorf MD. Bond additivity corrections for quantum chemistry methods. *J Phys Chem A* 2000;104:2168–77. <https://doi.org/10.1021/jp9914370>.

- [150] Ince A, Carstensen H-H, Reyniers M-F, Marin GB. First-principles based group additivity values for thermochemical properties of substituted aromatic compounds. *AIChE Journal* 2015;61:3858–70. <https://doi.org/10.1002/aic.15008>.
- [151] Paraskevas PD, Sabbe MK, Reyniers M-F, Papayannakos N, Marin GB. Group additive values for the gas-phase standard enthalpy of formation, entropy and heat capacity of oxygenates. *Chem Eur J* 2013;19:16431–52. <https://doi.org/10.1002/chem.201301381>.
- [152] Pitzer KS, Gwinn WD. Energy levels and thermodynamic functions for molecules with internal rotation. I. Rigid frame with attached tops. *J Chem Phys* 1942;10:428–40. <https://doi.org/doi:10.1063/1.1723744>.
- [153] Pitzer KS, Kilpatrick JE. The entropies and related properties of branched paraffin hydrocarbons. *Chem Rev* 1946;39:435–47. <https://doi.org/10.1021/cr60124a005>.
- [154] Kilpatrick JE, Pitzer KS. Energy levels and thermodynamic functions for molecules with internal rotation. III. Compound rotation. *J Chem Phys* 1949;17:1064–75. <https://doi.org/10.1063/1.1747114>.
- [155] East ALL, Radom L. Ab initio statistical thermodynamical models for the computation of third-law entropies. *J Chem Phys* 1997;106:6655–74. <https://doi.org/10.1063/1.473958>.
- [156] Sharma S, Raman S, Green WH. Intramolecular hydrogen migration in alkylperoxy and hydroperoxyalkylperoxy radicals: accurate treatment of hindered rotors. *J Phys Chem A* 2010;114:5689–701. <https://doi.org/10.1021/jp9098792>.
- [157] Zheng J, Mielke SL, Clarkson KL, Truhlar DG. MSTor: A program for calculating partition functions, free energies, enthalpies, entropies, and heat capacities of complex molecules including torsional anharmonicity. *Comput Phys Commun* 2012;183:1803–12. <https://doi.org/10.1016/j.cpc.2012.03.007>.
- [158] Sumathi R, Carstensen H-H, Green WH. Reaction rate prediction via group additivity. Part 1: H abstraction from alkanes by H and CH<sub>3</sub>. *J Phys Chem A* 2001;105:6910–25. <https://doi.org/10.1021/jp010697q>.
- [159] Eyring H. The activated complex in chemical reactions. *J Chem Phys* 1935;3:107–15. <https://doi.org/10.1063/1.1749604>.
- [160] Evans MG, Polanyi M. Some applications of the transition state method to the calculation of reaction velocities, especially in solution. *Trans Faraday Soc* 1935;31:875–94. <https://doi.org/10.1039/TF9353100875>.
- [161] Pollak E, Pechukas P. Symmetry numbers, not statistical factors, should be used in absolute rate theory and in Broensted relations. *J Am Chem Soc* 1978;100:2984–91. <https://doi.org/10.1021/ja00478a009>.
- [162] Fernández-Ramos A, Ellingson BA, Meana-Pañeda R, Marques JMC, Truhlar DG. Symmetry numbers and chemical reaction rates. *Theor Chem Account* 2007;118:813–26. <https://doi.org/10.1007/s00214-007-0328-0>.
- [163] Eckart C. The penetration of a potential barrier by electrons. *Phys Rev* 1930;35:1303–9. <https://doi.org/10.1103/PhysRev.35.1303>.
- [164] Brown R. A method of calculating tunneling corrections for Eckart potential barriers. *J Res Natl Bur Stand* 1981;86:357–9. <https://doi.org/10.6028/JRES.086.014>.
- [165] Skodje RT, Truhlar DG, Garrett BC. A general small-curvature approximation for transition-state-theory transmission coefficients. *J Phys Chem* 1981;85:3019–23. <https://doi.org/10.1021/j150621a001>.
- [166] Marcus RA. Unimolecular dissociations and free radical recombination reactions. *J Chem Phys* 1952;20:359–64. <https://doi.org/10.1063/1.1700424>.
- [167] Beyer T, Swinehart DF. Algorithm 448: number of multiply-restricted partitions. *Commun ACM* 1973;16:379. <https://doi.org/10.1145/362248.362275>.

- [168] Stein SE, Rabinovitch BS. Accurate evaluation of internal energy level sums and densities including anharmonic oscillators and hindered rotors. *J Chem Phys* 1973;58:2438–45. <https://doi.org/10.1063/1.1679522>.
- [169] Klippenstein SJ. Variational optimizations in the Rice–Ramsperger–Kassel–Marcus theory calculations for unimolecular dissociations with no reverse barrier. *J Chem Phys* 1992;96:367–71. <https://doi.org/10.1063/1.462472>.
- [170] Georgievskii Y, Klippenstein SJ. Transition state theory for multichannel addition reactions: multifaceted dividing surfaces. *J Phys Chem A* 2003;107:9776–81. <https://doi.org/10.1021/jp034564b>.
- [171] Miller JA, Klippenstein SJ. Master equation methods in gas phase chemical kinetics. *J Phys Chem A* 2006;110:10528–44. <https://doi.org/10.1021/jp062693x>.
- [172] Robertson SH, Pilling MJ, Jitariu LC, Hillier IH. Master equation methods for multiple well systems: application to the 1-,2-pentyl system. *Phys Chem Chem Phys* 2007;9:4085–97. <https://doi.org/10.1039/B704736C>.
- [173] Jasper AW, Pelzer KM, Miller JA, Kamarchik E, Harding LB, Klippenstein SJ. Predictive a priori pressure-dependent kinetics. *Science* 2014;346:1212–5. <https://doi.org/10.1126/science.1260856>.
- [174] Glowacki DR, Liang C-H, Morley C, Pilling MJ, Robertson SH. MESMER: An open-source master equation solver for multi-energy well reactions. *J Phys Chem A* 2012;116:9545–60. <https://doi.org/10.1021/jp3051033>.
- [175] Georgievskii Y, Miller JA, Burke MP, Klippenstein SJ. Reformulation and solution of the master equation for multiple-well chemical reactions. *J Phys Chem A* 2013;117:12146–54. <https://doi.org/10.1021/jp4060704>.
- [176] Barker JR, Golden DM. Master equation analysis of pressure-dependent atmospheric reactions. *Chem Rev* 2003;103:4577–92. <https://doi.org/10.1021/cr020655d>.
- [177] Lindemann FA, Arrhenius S, Langmuir I, Dhar NR, Perrin J, Lewis WCM. Discussion on “the radiation theory of chemical action.” *Trans Faraday Soc* 1922;17:598–606. <https://doi.org/10.1039/TF9221700598>.
- [178] Troe J. Theory of thermal unimolecular reactions at low pressures. I. Solutions of the master equation. *J Chem Phys* 1977;66:4745–57. <https://doi.org/10.1063/1.433837>.
- [179] Bao JL, Zheng J, Truhlar DG. Kinetics of hydrogen radical reactions with toluene including chemical activation theory employing system-specific quantum rrk theory calibrated by variational transition state theory. *J Am Chem Soc* 2016;138:2690–704. <https://doi.org/10.1021/jacs.5b11938>.
- [180] Pratali Maffei L, Pelucchi M, Cavallotti C, Bertolino A, Faravelli T. Master equation lumping for multi-well potential energy surfaces: A bridge between ab initio based rate constant calculations and large kinetic mechanisms. *Chem Eng J* 2021;422:129954. <https://doi.org/10.1016/j.cej.2021.129954>.
- [181] DeSain JD, Klippenstein SJ, Miller JA, Taatjes CA. Measurements, theory, and modeling of OH formation in ethyl + O<sub>2</sub> and propyl + O<sub>2</sub> reactions. *J Phys Chem A* 2003;107:4415–27. <https://doi.org/10.1021/jp0221946>.
- [182] Burke MP, Klippenstein SJ, Harding LB. A quantitative explanation for the apparent anomalous temperature dependence of OH+HO<sub>2</sub>=H<sub>2</sub>O+O<sub>2</sub> through multi-scale modeling. *Proc Combust Inst* 2013;34:547–55. <https://doi.org/10.1016/j.proci.2012.05.041>.
- [183] Burke MP, Goldsmith CF, Klippenstein SJ, Welz O, Huang H, Antonov IO, et al. Multiscale informatics for low-temperature propane oxidation: further complexities in studies of complex reactions. *J Phys Chem A* 2015;119:7095–115. <https://doi.org/10.1021/acs.jpca.5b01003>.

- [184] Welz O, Burke MP, Antonov IO, Goldsmith CF, Savee JD, Osborn DL, et al. New insights into low-temperature oxidation of propane from synchrotron photoionization mass spectrometry and multiscale informatics modeling. *J Phys Chem A* 2015;119:7116–29. <https://doi.org/10.1021/acs.jpca.5b01008>.
- [185] Grambow CA, Jamal A, Li Y-P, Green WH, Zádor J, Suleimanov YV. Unimolecular reaction pathways of a  $\gamma$ -keto hydroperoxide from combined application of automated reaction discovery methods. *J Am Chem Soc* 2018;140:1035–48. <https://doi.org/10.1021/jacs.7b11009>.
- [186] Van de Vijver R, Zádor J. KinBot: Automated stationary point search on potential energy surfaces. *Comput Phys Commun* 2020;248:106947. <https://doi.org/10.1016/j.cpc.2019.106947>.
- [187] Gao CW, Allen JW, Green WH, West RH. Reaction mechanism generator: Automatic construction of chemical kinetic mechanisms. *Comput Phys Commun* 2016;203:212–25. <https://doi.org/10.1016/j.cpc.2016.02.013>.
- [188] Liu M, Grinberg Dana A, Johnson MS, Goldman MJ, Jocher A, Payne AM, et al. Reaction Mechanism Generator v3.0: Advances in Automatic Mechanism Generation. *J Chem Inf Model* 2021;61:2686–96. <https://doi.org/10.1021/acs.jcim.0c01480>.
- [189] Van de Vijver R, Van Geem KM, Marin GB. On-the-fly ab initio calculations toward accurate rate coefficients. *Proc Combust Inst* 2019;37:283–90. <https://doi.org/10.1016/j.proci.2018.05.056>.
- [190] Blurock ES. Reaction: System for modeling chemical reactions. *J Chem Inf Comput Sci* 1995;35:607–16. <https://doi.org/10.1021/ci00025a032>.
- [191] Moréac G, Blurock ES, Mauss F. Automatic generation of a detailed mechanism for the oxidation of n-decane. *Combust Sci Technol* 2006;178:2025–38. <https://doi.org/10.1080/00102200600793262>.
- [192] Ranzi E, Faravelli T, Gaffuri P, Sogaro A. Low-temperature combustion: Automatic generation of primary oxidation reactions and lumping procedures. *Combust Flame* 1995;102:179–92. [https://doi.org/10.1016/0010-2180\(94\)00253-O](https://doi.org/10.1016/0010-2180(94)00253-O).
- [193] Côme GM, Warth V, Glaude PA, Fournet R, Battin-Leclerc F, Scacchi G. Computer-aided design of gas-phase oxidation mechanisms - Application to the modeling of n-heptane and iso-octane oxidation. *Proc Combust Inst* 1996;26:755–62. [https://doi.org/10.1016/S0082-0784\(96\)80284-0](https://doi.org/10.1016/S0082-0784(96)80284-0).
- [194] Buda F, Bounaceur R, Warth V, Glaude P, Fournet R, Battin-Leclerc F. Progress toward a unified detailed kinetic model for the autoignition of alkanes from C4 to C10 between 600 and 1200 K. *Combust Flame* 2005;142:170–86. <https://doi.org/10.1016/j.combustflame.2005.03.005>.
- [195] Tran L-S, Verdicchio M, Monge F, Martin RC, Bounaceur R, Sirjean B, et al. An experimental and modeling study of the combustion of tetrahydrofuran. *Combust Flame* 2015;162:1899–918. <https://doi.org/10.1016/j.combustflame.2014.12.010>.
- [196] Tran L-S, De Bruycker R, Carstensen H-H, Glaude P-A, Monge F, Alzueta MU, et al. Pyrolysis and combustion chemistry of tetrahydropyran: Experimental and modeling study. *Combust Flame* 2015;162:4283–303. <https://doi.org/10.1016/j.combustflame.2015.07.030>.
- [197] Blurock E, Battin-Leclerc F, Faravelli T, Green WH. Chapter 3: Automatic generation of detailed mechanisms. *Cleaner combustion - Developing detailed chemical kinetic models*. Springer London Ltd, Editors: Battin-Leclerc F., Blurock E., Simmie J.M. Edition : Springer London Ltd; 2013.
- [198] Van de Vijver R, Vandewiele NM, Bhoorasingh PL, Slakman BL, Seyedzadeh Khanshan F, Carstensen H-H, et al. Automatic mechanism and kinetic model generation for gas- and solution-phase processes: a perspective on best practices, recent advances,

- and future challenges. *Int J Chem Kinet* 2015;47:199–231. <https://doi.org/10.1002/kin.20902>.
- [199] ACD/ChemSketch: Structure drawing software for academic and personal use. Advanced Chemistry Development, Inc., 8 King Street East, Suite 107 Toronto, ON, M5C 1B5 Canada: ACDLABS; 2020.
- [200] Poling EB, Prausnitz MJ, O’Connell PJ. The properties of gases and liquids. fifth edition, The McGraw-Hill Companies, 2001 ISBN: 0070116822. 2001.
- [201] Lay TH, Bozzelli JW, Dean AM, Ritter ER. Hydrogen atom bond increments for calculation of thermodynamic properties of hydrocarbon radical species. *J Phys Chem* 1995;99:14514–27. <https://doi.org/10.1021/j100039a045>.
- [202] NIST Chemistry WebBook, available at < <http://webbook.nist.gov/chemistry/> > 2021.
- [203] Chase Jr. MW. NIST-JANAF thermochemical tables, Fourth Edition. *J Phys Chem Ref Data* 1998;Monograph 9:1–1951.
- [204] Pell AS, Pilcher G. Measurements of heats of combustion by flame calorimetry. Part 3. Ethylene oxide, trimethylene oxide, tetrahydrofuran and tetrahydropy. *Trans Faraday Soc* 1965;61:71–7. <https://doi.org/10.1039/TF9656100071>.
- [205] Moureu H, Dode M. Chaleurs de formation de l’oxyde d’ethylene, de l’ethanediol et de quelques homologues. *Bull Soc Chim France* 1937;4:637–47.
- [206] Goldsmith CF, Magoon GR, Green WH. Database of small molecule thermochemistry for combustion. *J Phys Chem A* 2012;116:9033–57. <https://doi.org/10.1021/jp303819e>.
- [207] Wijaya CD, Sumathi R, Green WH. Thermodynamic properties and kinetic parameters for cyclic ether formation from hydroperoxyalkyl radicals. *J Phys Chem A* 2003;107:4908–20. <https://doi.org/10.1021/jp027471n>.
- [208] Auzmendi-Murua I, Bozzelli JW. Thermochemical properties and bond dissociation enthalpies of 3- to 5-member ring cyclic ether hydroperoxides, alcohols, and peroxy radicals: Cyclic ether radical + 3O<sub>2</sub> reaction thermochemistry. *J Phys Chem A* 2014;118:3147–67. <https://doi.org/10.1021/jp412590g>.
- [209] Chao J, Hall KR, Marsh KN, Wilhoit RC. Thermodynamic properties of key organic oxygen compounds in the carbon range C1 to C4. Part 2. Ideal gas properties. *J Phys Chem Ref Data* 1986;15:1369–436. <https://doi.org/10.1063/1.555769>.
- [210] Dorofeeva OV. Ideal gas thermodynamic properties of oxygen heterocyclic compounds. Part 1. Three-membered, four-membered and five-membered rings. *Thermochim Acta* 1992;194:9–46.
- [211] Sinke GC, Hildenbrand DL. Heat of formation of propylene oxide. *J Chem Eng Data* 1962;7:74–74. <https://doi.org/10.1021/jc60012a022>.
- [212] Cox JD, Pilcher G. Thermochemistry of organic and organometallic compounds. New York: Academic Press; 1970.
- [213] Auzmendi-Murua I, Charaya S, Bozzelli JW. Thermochemical properties of methyl-substituted cyclic alkyl ethers and radicals for oxiranes, oxetanes, and oxolanes: C–H bond dissociation enthalpy trends with ring size and ether site. *J Phys Chem A* 2013;117:378–92. <https://doi.org/10.1021/jp309775h>.
- [214] Oetting FL. Low-temperature heat capacity and related thermodynamic functions of propylene oxide. *J Chem Phys* 1964;41:149–53. <https://doi.org/10.1063/1.1725614>.
- [215] Beaumont RH, Clegg B, Gee G, Herbert JBM, Marks DJ, Roberts RC, et al. Heat capacities of propylene oxide and of some polymers of ethylene and propylene oxides. *Polymer* 1966;7:401–17. [https://doi.org/10.1016/0032-3861\(66\)90055-3](https://doi.org/10.1016/0032-3861(66)90055-3).
- [216] Podlogar BL, Raber DJ. Molecular mechanics calculations of epoxides. Extension of the MM2 force field. *J Org Chem* 1989;54:5032–5. <https://doi.org/10.1021/jo00282a016>.
- [217] Schönborn A, Le MD, Fournet R, Glaude P-A, Warth V, Sirjean B. Auto-ignition control using an additive with adaptable chemical structure. Part I: Development of a

- kinetic model for 1,3-cyclohexadiene and 1,3,5-hexatriene combustion. *Combust Flame* 2019;205:466–83. <https://doi.org/10.1016/j.combustflame.2019.04.020>.
- [218] Andruzzi F, Shaofeng L, Pilcher G, Heatley F. Enthalpy of polymerisation of 7-oxabicyclo[4.1.0]heptane. *Die Makromolekulare Chemie* 1987;188:2643–50. <https://doi.org/10.1002/macp.1987.021881115>.
- [219] Kozina MP, Timofeeva LP, Luk'Yanova VA, Pimenova SM, Kas'yan LI. Enthalpies of formation and some alicyclic epoxy compounds. *Russ J Phys Chem (Engl Transl)* 1988;62:609–12.
- [220] Sirjean B, Glaude PA, Ruiz-López MF, Fournet R. Theoretical kinetic study of the reactions of cycloalkylperoxy radicals. *J Phys Chem A* 2009;113:6924–35. <https://doi.org/10.1021/jp901492e>.
- [221] Douslin DR, Scott DW, Good WD, Osborn AG. Thermodynamic properties of organic compounds and thermodynamic properties of fluids. *Gov Rep Announce Index US* 76 1976;97.
- [222] Sun H, Bozzelli JW. Thermochemical and kinetic analysis on the reactions of neopentyl and hydroperoxy-neopentyl radicals with oxygen: Part I. OH and initial stable HC product formation. *J Phys Chem A* 2004;108:1694–711. <https://doi.org/10.1021/jp030667i>.
- [223] Zaheeruddin M, Lodhi ZH. Enthalpies of formation of some cyclic compounds. *Phys Chem (Peshawar Pak)* 1991;10:111–8.
- [224] Landrieu P, Baylocq F, Johnson JR. Etude thermochimique dans la serie furanique. *Bull Soc Chim France* 1929:36–49.
- [225] Guthrie GB, Scott DW, Hubbard WN, Katz C, McCullough JP, Gross ME, et al. Thermodynamic properties of furan. *J Am Chem Soc* 1952;74:4662–9. <https://doi.org/10.1021/ja01138a063>.
- [226] Tian Z, Yuan T, Fournet R, Glaude P-A, Sirjean B, Battin-Leclerc F, et al. An experimental and kinetic investigation of premixed furan/oxygen/argon flames. *Combust Flame* 2011;158:756–73. <https://doi.org/10.1016/j.combustflame.2010.12.022>.
- [227] Feller D, Simmie JM. High-level ab initio enthalpies of formation of 2,5-dimethylfuran, 2-methylfuran, and furan. *J Phys Chem A* 2012;116:11768–75. <https://doi.org/10.1021/jp3095984>.
- [228] Mai TVT, Chuang Y-Y, Giri BR, Huynh LK. Ab-initio studies of thermal unimolecular decomposition of furan: A complementary deterministic and stochastic master equation model. *Fuel* 2020;264:116492. <https://doi.org/10.1016/j.fuel.2019.116492>.
- [229] Denis PA. Coupled cluster, B2PLYP and M06-2X investigation of the thermochemistry of five-membered nitrogen containing heterocycles, furan, and thiophene. *Theor Chem Acc* 2011;129:219–27. <https://doi.org/10.1007/s00214-011-0922-z>.
- [230] Lo P-K, Lau K-C. High-level ab initio predictions for the ionization energies and heats of formation of five-membered-ring molecules: thiophene, furan, pyrrole, 1,3-cyclopentadiene, and borole, C<sub>4</sub>H<sub>4</sub>X/C<sub>4</sub>H<sub>4</sub>X<sup>+</sup> (X = S, O, NH, CH<sub>2</sub>, and BH). *J Phys Chem A* 2011;115:932–9. <https://doi.org/10.1021/jp110499c>.
- [231] Simmie JM, Curran HJ. Formation enthalpies and bond dissociation energies of alkylfurans. The strongest C-X bonds known? *J Phys Chem A* 2009;113:5128–37. <https://doi.org/10.1021/jp810315n>.
- [232] Sebbar N, Bozzelli JW, Bockhorn H. Enthalpy of formation and bond energies on unsaturated oxygenated hydrocarbons using G3MP2B3 calculation methods. *Int J Chem Kinet* 2005;37:633–48. <https://doi.org/10.1002/kin.20086>.
- [233] Steele WV, Chirico RD, Nguyen A, Hossenlopp IA, Smith NK. Determination of some pure compound ideal-gas enthalpies of formation. in *AICHE Symposium Series* 1989. United States: National Inst. for Petroleum and Energy Research, Bartlesville, OK (USA); 1989. <https://doi.org/10.2172/6020818>.



- [234] Miller P. The free energy of furfural and some of its derivatives. *Iowa State Coll J Sci* 1936;10:91–3. <https://doi.org/10.31274/rtd-180813-14020>.
- [235] Avramescu F, Isagescu DA. Heats of combustion of mono- and difurfurylidene acetone. *Rev Roum Chim* 1978;23:655–9.
- [236] Kudchadker SA, Kudchadker AP. Thermodynamic properties of oxygen compounds III. Benzaldehyde and furfural (2-furaldehyde). *Thermochimica Acta* 1975;12:432–7. [https://doi.org/10.1016/0040-6031\(75\)85074-X](https://doi.org/10.1016/0040-6031(75)85074-X).
- [237] Pedley JB. Thermochemical data and structures of organic compounds. vol. 1. Texas (USA): College Station: Thermodynamics Research Center: CRC Press; 1994.
- [238] Simmie JM, Somers KP, Metcalfe WK, Curran HJ. Substituent effects in the thermochemistry of furans: A theoretical (CBS-QB3, CBS-APNO and G3) study. *J Chem Thermodyn* 2013;58:117–28. <https://doi.org/10.1016/j.jct.2012.10.020>.
- [239] Ribeiro da Silva MAV, Amaral LMPF. Standard molar enthalpies of formation of 2-furancarbonitrile, 2-acetylfuran, and 3-furaldehyde. *J Chem Thermodyn* 2009;41:26–9. <https://doi.org/10.1016/j.jct.2008.08.004>.
- [240] Ribeiro da Silva MAV, Amaral LMPF. Standard molar enthalpies of formation of some methylfuran derivatives. *J Therm Anal Calorim* 2010;100:375–80. <https://doi.org/10.1007/s10973-009-0636-9>.
- [241] Chowdhury PK, Upadhyaya HP, Naik PD. ArF laser photodissociation dynamics of furfuryl alcohol: LIF observation of OH state distribution. *Chem Phys Lett* 2001;344:292–8. [https://doi.org/10.1016/S0009-2614\(01\)00783-7](https://doi.org/10.1016/S0009-2614(01)00783-7).
- [242] Parks GS, Mosley JR, Peterson PV. Heats of combustion and formation of some organic compounds containing oxygen. *J Chem Phys* 1950;18:152–3. <https://doi.org/10.1063/1.1747444>.
- [243] Verevkin SP, Welle FM. Thermochemical studies for determination of the standard molar enthalpies of formation of alkyl-substituted furans and some ethers. *Struct Chem* 1998;9:215–21. <https://doi.org/10.1023/A:1022475115296>.
- [244] Sirjean B, Fournet R. Unimolecular decomposition of 2,5-dimethylfuran: a theoretical chemical kinetic study. *Phys Chem Chem Phys* 2013;15:596–611. <https://doi.org/10.1039/c2cp41927k>.
- [245] Steele WV, Chirico RD. Thermodynamics and the hydrodeoxygenation of 2,3-benzofuran. National Inst. for Petroleum and Energy Research, Bartlesville, OK (USA); 1990. <https://doi.org/10.2172/5086490>.
- [246] Clegg GA, Gee DR, Melia TP, Tyson A. Thermodynamics of polymerization of heterocyclic compounds II—The heat capacity, entropy, enthalpy and free energy of polytetrahydrofuran. *Polymer* 1968;9:501–11. [https://doi.org/10.1016/0032-3861\(68\)90060-8](https://doi.org/10.1016/0032-3861(68)90060-8).
- [247] Lebedev BV, Rabinovich IB, Milov VI, Lityagov VY. Thermodynamic properties of tetrahydrofuran from 8 to 322 K. *J Chem Thermodyn* 1978;10:321–9. [https://doi.org/10.1016/0021-9614\(78\)90064-2](https://doi.org/10.1016/0021-9614(78)90064-2).
- [248] McMillen DF, Golden DM. Hydrocarbon bond dissociation energies. *Annu Rev Phys Chem* 1982;33:493–532. <https://doi.org/10.1146/annurev.pc.33.100182.002425>.
- [249] Muedas CA, Ferguson RR, Brown SH, Crabtree RH. Hydrogen atoms as convenient synthetic reagents: mercury-photosensitized dimerization of functionalized organic compounds in the presence of molecular hydrogen. *J Am Chem Soc* 1991;113:2233–42. <https://doi.org/10.1021/ja00006a048>.
- [250] Laarhoven LJJ, Mulder P.  $\alpha$ -C–H bond strengths in tetralin and THF: application of competition experiments in photoacoustic calorimetry. *J Phys Chem B* 1997;101:73–7. <https://doi.org/10.1021/jp960982n>.

- [251] Tran L-S, Carstensen H-H, Foo KK, Lamoureux N, Gosselin S, Gasnot L, et al. Experimental and modeling study of the high-temperature combustion chemistry of tetrahydrofurfuryl alcohol. *Proc Combust Inst* 2021;38:631–40. <https://doi.org/10.1016/j.proci.2020.07.057>.
- [252] Pihlaja K, Heikkilä J. Enthalpies of formation of cyclic acetals. 1,3-Dioxolane, 2-methyl-1,3-dioxolane, and 2,4-dimethyl-1,3-dioxolanes. *Acta Chem Scand* 1969;23:1053–5.
- [253] Clegg GA. Thermodynamics of polymerization of heterocyclic compounds. Part V. The heat capacity, entropy, enthalpy and free energy of 1,3-dioxolan and poly-1,3-dioxolan. *Polymer* 1969;10:912–22.
- [254] Pihlaja K, Heikkilä J. Heats of formation of cyclic vinyl ethers. A correction. *Suom Kemistilehti* 1972:148.
- [255] Wiberg KB, Waldron RF. Lactones. 2. Enthalpies of hydrolysis, reduction, and formation of the C4-C13 monocyclic lactones. Strain energies and conformations. *J Am Chem Soc* 1991;113:7697–705. <https://doi.org/10.1021/ja00020a036>.
- [256] Leitão MLP, Pilcher G, Meng-Yan Y, Brown JM, Conn AD. Enthalpies of combustion of  $\gamma$ -butyrolactone,  $\gamma$ -valerolactone, and  $\delta$ -valerolactone. *J Chem Thermodyn* 1990;22:885–91. [https://doi.org/10.1016/0021-9614\(90\)90176-Q](https://doi.org/10.1016/0021-9614(90)90176-Q).
- [257] Ismailov TS, Gabzalilova NR, Makhkamoov KhM. Complex study of physicochemical properties of  $\gamma$ -butyrolactone. *Uzb Khim Zh* 1988:48–50.
- [258] Yevstropov AA, Lebedev BV, Kiparisova YeG, Alekseyev VA, Stashina GA. Thermodynamic parameters of transformation of  $\gamma$ -butyrolactone into poly- $\gamma$ -butyrolactone at normal pressure in the range of 0-400°K. *Polym Sci USSR* 1980;22:2685–92.
- [259] De Bruycker R, Carstensen H-H, Reyniers M-F, Marin GB, Simmie JM, Van Geem KM. An experimental and kinetic modeling study of  $\gamma$ -valerolactone pyrolysis. *Combust Flame* 2016;164:183–200. <https://doi.org/10.1016/j.combustflame.2015.11.016>.
- [260] Cass RC, Fletcher SE, Mortimer CT, Springall HD, White TR. Heats of combustion and molecular structure. Part V. The mean bond energy term for the C–O bond in ethers, and the structures of some cyclic ethers. *J Chem Soc* 1958:1406–10. <https://doi.org/10.1039/JR9580001406>.
- [261] Snelson A, Skinner HA. Heats of combustion: sec-propanol, 1,4-dioxan, 1,3-dioxan and tetrahydropyran. *Trans Faraday Soc* 1961;57:2125–31. <https://doi.org/10.1039/TF9615702125>.
- [262] Dorofeeva OV. Ideal gas thermodynamic properties of oxygen heterocyclic compounds: Part 2. Six-membered, seven-membered and eight-membered rings. *Thermochimica Acta* 1992;200:121–50. [https://doi.org/10.1016/0040-6031\(92\)85111-8](https://doi.org/10.1016/0040-6031(92)85111-8).
- [263] Morais VMF. Ab initio energetics of nonsubstituted monocyclic pyrones. *J Chem Thermodyn* 2011;43:9–16. <https://doi.org/10.1016/j.jct.2010.07.009>.
- [264] Muller C, Michel V, Scacchi G, Côme GM. THERGAS: a computer program for the evaluation of thermochemical data of molecules and free radicals in the gas phase. *J Chim Phys* 1995;92:1154–78. <https://doi.org/10.1051/jcp/1995921154>.
- [265] Taatjes CA, Hansen N, Osborn DL, Kohse-Höinghaus K, Cool TA, Westmoreland PR. “Imaging” combustion chemistry via multiplexed synchrotron-photoionization mass spectrometry. *Phys Chem Chem Phys* 2007;10:20–34. <https://doi.org/10.1039/B713460F>.
- [266] Eskola AJ, Antonov IO, Sheps L, Savee JD, Osborn DL, Taatjes CA. Time-resolved measurements of product formation in the low-temperature (550–675 K) oxidation of neopentane: a probe to investigate chain-branching mechanism. *Phys Chem Chem Phys* 2017;19:13731–45. <https://doi.org/10.1039/C7CP01366C>.

- [267] Sirignano M, Conturso M, D'Anna A. Effect of furans on particle formation in diffusion flames: An experimental and modeling study. *Proc Combust Inst* 2015;35:525–32. <https://doi.org/10.1016/j.proci.2014.05.062>.
- [268] Konnov AA, Mohammad A, Kishore VR, Kim NI, Prathap C, Kumar S. A comprehensive review of measurements and data analysis of laminar burning velocities for various fuel+air mixtures. *Prog Energy Combust Sci* 2018;68:197–267. <https://doi.org/10.1016/j.pecs.2018.05.003>.
- [269] Egolfopoulos FN, Hansen N, Ju Y, Kohse-Höinghaus K, Law CK, Qi F. Advances and challenges in laminar flame experiments and implications for combustion chemistry. *Prog Energy Combust Sci* 2014;43:36–67. <https://doi.org/10.1016/j.pecs.2014.04.004>.
- [270] Tian G, Daniel R, Li H, Xu H, Shuai S, Richards P. Laminar burning velocities of 2,5-dimethylfuran compared with ethanol and gasoline. *Energy Fuels* 2010;24:3898–905. <https://doi.org/10.1021/ef100452c>.
- [271] GOEY LPH de, MAAREN A van, QUAX RM. Stabilization of Adiabatic Premixed Laminar Flames on a Flat Flame Burner. *Combust Sci Technol* 1993;92:201–7. <https://doi.org/10.1080/00102209308907668>.
- [272] Nilsson EJK, Konnov AA. Chapter 10: Flame studies of oxygenates. *Cleaner combustion - Developing detailed chemical kinetic models*. Springer London Ltd, Editors: Battin-Leclerc F., Blurock E., Simmie J.M. Edition : Springer London Ltd; 2013.
- [273] Liu D, Togbé C, Tran L-S, Felsmann D, Oßwald P, Nau P, et al. Combustion chemistry and flame structure of furan group biofuels using molecular-beam mass spectrometry and gas chromatography – Part I: Furan. *Combust Flame* 2014;161:748–65. <https://doi.org/10.1016/j.combustflame.2013.05.028>.
- [274] Tran L-S, Togbé C, Liu D, Felsmann D, Oßwald P, Glaude P-A, et al. Combustion chemistry and flame structure of furan group biofuels using molecular-beam mass spectrometry and gas chromatography – Part II: 2-Methylfuran. *Combust Flame* 2014;161:766–79. <https://doi.org/10.1016/j.combustflame.2013.05.027>.
- [275] Togbé C, Tran L-S, Liu D, Felsmann D, Oßwald P, Glaude P-A, et al. Combustion chemistry and flame structure of furan group biofuels using molecular-beam mass spectrometry and gas chromatography – Part III: 2,5-Dimethylfuran. *Combust Flame* 2014;161:780–97. <https://doi.org/10.1016/j.combustflame.2013.05.026>.
- [276] Gueniche HA, Glaude PA, Dayma G, Fournet R, Battin-Leclerc F. Rich methane premixed laminar flames doped with light unsaturated hydrocarbons: I. Allene and propyne. *Combust Flame* 2006;146:620–34. <https://doi.org/10.1016/j.combustflame.2006.07.004>.
- [277] Griffiths JF. Reduced kinetic models and their application to practical combustion systems. *Prog Energy Combust Sci* 1995;21:25–107. [https://doi.org/10.1016/0360-1285\(94\)00022-V](https://doi.org/10.1016/0360-1285(94)00022-V).
- [278] Goldsborough SS, Hochgreb S, Vanhove G, Wooldridge MS, Curran HJ, Sung C-J. Advances in rapid compression machine studies of low- and intermediate-temperature autoignition phenomena. *Prog Energy Combust Sci* 2017;63:1–78. <https://doi.org/10.1016/j.pecs.2017.05.002>.
- [279] Yasunaga K, Tranter RS. Chapter 6: Speciation in shock tubes. *Cleaner combustion - Developing detailed chemical kinetic models*. Springer London Ltd, Editors: Battin-Leclerc F., Blurock E., Simmie J.M. Edition : Springer London Ltd; 2013.
- [280] Gauthier BM, Davidson DF, Hanson RK. Shock tube determination of ignition delay times in full-blend and surrogate fuel mixtures. *Combust Flame* 2004;139:300–11. <https://doi.org/10.1016/j.combustflame.2004.08.015>.

- [281] Uygun Y, Ishihara S, Olivier H. A high pressure ignition delay time study of 2-methylfuran and tetrahydrofuran in shock tubes. *Combust Flame* 2014;161:2519–30. <https://doi.org/10.1016/j.combustflame.2014.04.004>.
- [282] Vanhove G, Yu Y, Boumehdi MA, Frottier O, Herbinet O, Glaude P-A, et al. Experimental study of tetrahydrofuran oxidation and ignition in low-temperature conditions. *Energy Fuels* 2015;29:6118–25. <https://doi.org/10.1021/acs.energyfuels.5b01057>.
- [283] Fenard Y, Gil A, Vanhove G, Carstensen H-H, Van G, Westmoreland PR, et al. A model of tetrahydrofuran low-temperature oxidation based on theoretically calculated rate constants. *Combust Flame* 2018;191:252–69. <https://doi.org/10.1016/j.combustflame.2018.01.006>.
- [284] Monge F, Aranda V, Millera A, Bilbao R, Alzueta MU. Chapter 9: Tubular flow reactors. *Cleaner combustion - Developing detailed chemical kinetic models*. Springer London Ltd, Editors: Battin-Leclerc F., Blurock E., Simmie J.M. Edition : Springer London Ltd; 2013.
- [285] Herbinet O, Dayma G. Chapter 8: Jet-stirred reactors. *Cleaner combustion - Developing detailed chemical kinetic models*. Springer London Ltd, Editors: Battin-Leclerc F., Blurock E., Simmie J.M. Edition : Springer London Ltd; 2013.
- [286] Zhao H, Souza MJ, Ju Y. A supercritical jet-stirred reactor. *Fusion - Journal of the American Scientific Glassblowers Society* 2018;66:19–24.
- [287] Chen W, Xu Q, Lou H, Di Q, Xie C, Liu B, et al. Variable pressure JSR study of low temperature oxidation chemistry of n-heptane by synchrotron photoionization mass spectrometry. *Combust Flame* 2022;240:111946. <https://doi.org/10.1016/j.combustflame.2021.111946>.
- [288] Rodriguez A. Étude de la combustion de composés organiques grâce au couplage d'un réacteur parfaitement agité avec des méthodes analytiques spectroscopiques et spectrométriques: application à la détection des hydroperoxydes. Thesis. Université de Lorraine, 2016.
- [289] Doner AC, Christianson MG, Davis JC, Koritzke AL, Larsson A, Frandsen K, et al. Vacuum-ultraviolet absorption cross-sections of functionalized cyclic hydrocarbons: Six-membered rings. *J Quant Spectrosc Radiat Transfer* 2019;236:106603. <https://doi.org/10.1016/j.jqsrt.2019.106603>.
- [290] Mamyrin BA. Time-of-flight mass spectrometry (concepts, achievements, and prospects). *Int J Mass Spectrom* 2001;206:251–66. [https://doi.org/10.1016/S1387-3806\(00\)00392-4](https://doi.org/10.1016/S1387-3806(00)00392-4).
- [291] Hoffmann E de. Mass spectrometry. *Kirk-Othmer Encyclopedia of Chemical Technology*, American Cancer Society; 2005. <https://doi.org/10.1002/0471238961.1301191913151518.a01.pub2>.
- [292] Qi F. Combustion chemistry probed by synchrotron VUV photoionization mass spectrometry. *Proc Combust Inst* 2013;34:33–63. <https://doi.org/10.1016/j.proci.2012.09.002>.
- [293] Rodriguez A, Herbinet O, Battin-Leclerc F. A study of the low-temperature oxidation of a long chain aldehyde: n-hexanal. *Proc Combust Inst* 2017;36:365–72. <https://doi.org/10.1016/j.proci.2016.05.047>.
- [294] Anderson JB. Molecular beams from nozzle sources. *Molecular Beams and Low Density Gasdynamics*. Wegener P.P., New York: Marcel Dekker, Inc.; 1974, p. 1–91. <https://doi.org/10.1002/0471238961.1301191913151518.a01.pub2>.
- [295] Dagaut P, Reuillon M, Cathonnet M. Experimental study of the oxidation of n-heptane in a jet stirred reactor from low to high temperature and pressures up to 40 atm. *Combust Flame* 1995;101:132–40. [https://doi.org/10.1016/0010-2180\(94\)00184-T](https://doi.org/10.1016/0010-2180(94)00184-T).

- [296] Belhadj N, Benoit R, Dagaut P, Lailliau M, Serinyel Z, Dayma G, et al. Oxidation of di-n-butyl ether: Experimental characterization of low-temperature products in JSR and RCM. *Combust Flame* 2020;222:133–44. <https://doi.org/10.1016/j.combustflame.2020.08.037>.
- [297] Weiser L, Weber I, Olzmann M. Pyrolysis of Furan and Its Methylated Derivatives: A Shock-Tube/TOF-MS and Modeling Study. *J Phys Chem A* 2019;123:9893–904. <https://doi.org/10.1021/acs.jpca.9b06967>.
- [298] Bradley JN, Kistiakowsky GB. Shock Wave Studies by Mass Spectrometry. I. Thermal Decomposition of Nitrous Oxide. *J Chem Phys* 1961;35:256–63. <https://doi.org/10.1063/1.1731897>.
- [299] Photonization Cross Section Database (Version 2.0). Edited by JiuZhong Yang and Combustion Team. <http://flame.nslr.ustc.edu.cn/database/>. National Synchrotron Radiation Laboratory, Hefei, China. (2017) n.d. <http://flame.nslr.ustc.edu.cn/database/?version=en> (accessed February 10, 2021).
- [300] Herbinet O, Battin-Leclerc F, Bax S, Le Gall H, Glaude P-A, Fournet R, et al. Detailed product analysis during the low temperature oxidation of n-butane. *Phys Chem Chem Phys* 2011;13:296–308. <https://doi.org/10.1039/c0cp00539h>.
- [301] Yang B, Wang J, Cool TA, Hansen N, Skeen S, Osborn DL. Absolute photoionization cross-sections of some combustion intermediates. *Int J Mass Spectrom* 2012;309:118–28. <https://doi.org/10.1016/j.ijms.2011.09.006>.
- [302] Holmes JL, Lossing FP. Ionization energies of homologous organic compounds and correlation with molecular size. *Org Mass Spectrom* 1991;26:537–41. <https://doi.org/10.1002/oms.1210260603>.
- [303] Aue DH, Webb HM, Davidson WR, Vidal M, Bowers MT, Goldwhite H, et al. Proton affinities and photoelectron spectra of three-membered-ring heterocycles. *J Am Chem Soc* 1980;102:5151–7. <https://doi.org/10.1021/ja00536a004>.
- [304] Aue DH, Bowers MT. Chapter 9 - Stabilities of positive ions from equilibrium gas-phase basicity measurements. In: Bowers MT, editor. *Gas Phase Ion Chemistry*, Academic Press; 1979, p. 1–51. <https://doi.org/10.1016/B978-0-12-120802-8.50007-2>.
- [305] Holmes J, Turlouw J, Lossing F. The Thermochemistry of C<sub>2</sub>H<sub>4</sub>O<sup>+</sup> Ions. *J Phys Chem* 1976;80:2860–2. <https://doi.org/10.1021/j100567a600>.
- [306] Corderman RR, LeBreton PR, Buttrill SE, Williamson AD, Beauchamp JL. Photoionization and ion cyclotron resonance studies of the ion chemistry of ethylene oxide. *J Chem Phys* 1976;65:4929–39. <https://doi.org/10.1063/1.432969>.
- [307] Kräßig R, Reinke D, Baumgärtel H. Photoreaktionen kleiner organischer Moleküle II. Die Photoionenspektren der Isomeren Propylen-Cyclopropan und Acetaldehyd-Äthylenoxyd. *Ber Bunsenges Phys Chem* 1974;78:425–36. <https://doi.org/10.1002/bbpc.19740780502>.
- [308] Basch H, Robin MB, Kuebler NA, Baker C, Turner DW. Optical and photoelectron spectra of small rings. III. The saturated three-membered rings. *J Chem Phys* 1969;51:52–66. <https://doi.org/10.1063/1.1671770>.
- [309] Lowrey A, Watanabe K. Absorption and ionization coefficients of ethylene oxide. *J Chem Phys* 1958;28:208–10. <https://doi.org/10.1063/1.1744093>.
- [310] Watanabe K, Nakayama T, Mottl J. Ionization potentials of some molecules. *J Quant Spectrosc Radiat Transfer* 1962;2:369–82. [https://doi.org/10.1016/0022-4073\(62\)90023-7](https://doi.org/10.1016/0022-4073(62)90023-7).
- [311] Vorob'ev AS, Furlei II, Sultanov ASh, Khvostenko VI, Leplyanin GV, Derzhinskii AR, et al. Mass spectrometry of resonance capture of electrons and photo-electron spectroscopy of molecules of ethylene oxide, ethylene sulfide, and their derivatives. *Russ Chem Bull* 1989;38:1388–94. <https://doi.org/10.1007/BF00978424>.

- [312] Johnson K, Powis I, Danby CJ. A photoelectron - photoion coincidence study of acetaldehyde and ethylene oxide molecular ions. *Chemical Physics* 1982;70:329–43. [https://doi.org/10.1016/0301-0104\(82\)88103-2](https://doi.org/10.1016/0301-0104(82)88103-2).
- [313] Bieri G, Åsbrink L, von Niessen W. 30.4-nm He (II) photoelectron spectra of organic molecules: Part VII. Miscellaneous compounds. *J Electron Spectros Relat Phenomena* 1982;27:129–78. [https://doi.org/10.1016/0368-2048\(82\)85059-7](https://doi.org/10.1016/0368-2048(82)85059-7).
- [314] Kimura K, Katsumata S, Achiba Y. Handbook of HeI photoelectron spectra of fundamental organic molecules ionization energies, Ab Initio assignments, and valence electronic structure for 200 molecules. Tokyo; New York: Japan scientific societies Press; Halsted Press; 1981.
- [315] Aue DH, Webb HM, Bowers MT. Proton affinities, ionization potentials, and hydrogen affinities of nitrogen and oxygen bases. Hybridization effects. *J Am Chem Soc* 1975;97:4137–9. <https://doi.org/10.1021/ja00847a050>.
- [316] McAlduff EJ, Houk KN. Photoelectron spectra of substituted oxiranes and thiiranes. Substituent effects on ionization potentials involving  $\sigma$  orbitals. *Can J Chem* 1977;55:318–32. <https://doi.org/10.1139/v77-048>.
- [317] Roszak S, Kaufman JJ, Koski WS, Barreto RD, Fehlner TP, Balasubramanian K. Experimental and theoretical studies of photoelectron spectra of oxetane and some of its halogenated methyl derivatives. *J Phys Chem* 1992;96:7226–30. <https://doi.org/10.1021/j100197a018>.
- [318] Mollere PD. The photoelectron spectrum of oxetane: Non-degenerate walsh orbitals in a four-membered heterocycle. *Tetrahedron Letters* 1973;14:2791–4. [https://doi.org/10.1016/S0040-4039\(01\)96140-4](https://doi.org/10.1016/S0040-4039(01)96140-4).
- [319] Hernandez GJ. Vacuum-ultraviolet absorption spectra of the cyclic ethers: trimethylene oxide, tetrahydrofuran, and tetrahydropyran. *J Chem Phys* 1963;38:2233–42. <https://doi.org/10.1063/1.1733955>.
- [320] Klapstein D, MacPherson CD, O'Brien RT. The photoelectron spectra and electronic structure of 2-carbonyl furans. *Can J Chem* 1990;68:747–54. <https://doi.org/10.1139/v90-118>.
- [321] Veszprémi T, Nyulászai L, Nagy J. Ultraviolet photoelectron spectroscopy and quantum-mechanical study of alkyl- and trimethylsilyl-furanes. *J Organomet Chem* 1987;331:175–80. [https://doi.org/10.1016/0022-328X\(87\)80019-0](https://doi.org/10.1016/0022-328X(87)80019-0).
- [322] Arimura M, Yoshikawa Y. Ionization efficiency and ionization energy of cyclic compounds by electron impact. *Shitsuryo Bunseki* 1984;32:375–80.
- [323] Klasinc L, Sabljic A, Kluge G, Rieger J, Scholz M. Chemistry of excited states. Part 13. Assignment of lowest  $\pi$ -ionizations in photoelectron spectra of thiophen, furan, and pyrrole. *J Chem Soc, Perkin Trans 2* 1982;539–43. <https://doi.org/10.1039/P29820000539>.
- [324] Galasso V, Klasinc L, Sabljic A, Trinajstić N, Pappalardo GC, Steglich W. Conformation and photoelectron spectra of 2-(2-furyl)pyrrole and 2-(2-thienyl)pyrrole. *J Chem Soc, Perkin Trans 2* 1981:127–31. <https://doi.org/10.1039/P29810000127>.
- [325] Willett G, Baer T. Thermochemistry and dissociation dynamics of state-selected C<sub>4</sub>H<sub>4</sub>X ions. 2. Furan and 3-butyn-2-one. *J Am Chem Soc* 1980;102:6769–73. <https://doi.org/10.1021/ja00542a017>.
- [326] Tedder JM, Vidaud PH. Charge-exchange mass spectra of thiophene, pyrrole and furan. *J Chem Soc, Faraday Trans 2* 1980;76:1516–22. <https://doi.org/10.1039/F29807601516>.
- [327] Holmes JL, Terlouw JK. Structures of [C<sub>4</sub>H<sub>4</sub>O]<sup>+</sup>. ions produced from 2- and 4-pyrone. *J Am Chem Soc* 1979;101:4973–5. <https://doi.org/10.1021/ja00511a029>.

- [328] Van Veen EH. Triplet  $\pi \rightarrow \pi^*$  transitions in thiophene, furan and pyrrole by low-energy electron-impact spectroscopy. *Chem Phys Lett* 1976;41:535–9. [https://doi.org/10.1016/0009-2614\(76\)85411-5](https://doi.org/10.1016/0009-2614(76)85411-5).
- [329] Aloisi GG, Santini S, Savelli G. Molecular complexes of heteroaromatic five membered ring compounds with tetracyanoethylene. Charge transfer spectra, equilibrium constants and ionization potentials of the donors. *J Chem Soc, Faraday Trans 1* 1975;71:2045–50. <https://doi.org/10.1039/F19757102045>.
- [330] Thorstad O, Undheim K. Mass spectrometry of onium compounds. XXIV. Ionisation potential in structure analysis of pyridodiazooxides. *Chem Scr* 1974;6:222–5.
- [331] Linda P, Marino G, Pignataro S. A comparison of sensitivities to substituent effects of five-membered heteroaromatic rings in gas phase ionization. *J Chem Soc B* 1971:1585–7. <https://doi.org/10.1039/J29710001585>.
- [332] Derrick PJ, Åsbrink L, Edqvist O, Jönsson B, Lindholm E. Rydberg series in small molecules. X. Photoelectron spectroscopy and electronic structure of furan. *Int J Mass Spectrom Ion Phys* 1971;6:161–75. [https://doi.org/10.1016/0020-7381\(71\)80001-3](https://doi.org/10.1016/0020-7381(71)80001-3).
- [333] Potapov VK, Bazhenov BA. The photionization of pyrrole, furan, and thiophene. *High Energy Chem* 1970;505:??-??
- [334] Johnstone RAW, Mellon FA, Ward SD. On-line acquisition of ionization efficiency data. *Int J Mass Spectrom Ion Phys* 1970;5:241–7. [https://doi.org/10.1016/0020-7381\(70\)80019-5](https://doi.org/10.1016/0020-7381(70)80019-5).
- [335] Baker ADavid, Betteridge David, Kemp NR, Kirby RE. Application of photoelectron spectrometry to pesticide analysis. Photoelectron spectra of five-membered heterocycles and related molecules. *Anal Chem* 1970;42:1064–73. <https://doi.org/10.1021/ac60291a042>.
- [336] Watanabe K. Ionization potentials of some molecules. *J Chem Phys* 1957;26:542–7. <https://doi.org/10.1063/1.1743340>.
- [337] Zykov BG, Erchak NP, Khvostenko VI, Lukevits E, Matorykina VF, Asfandiarov NL. Photoelectron spectra of furylsilanes and their carbon analogs. *J Organomet Chem* 1983;253:301–12. [https://doi.org/10.1016/S0022-328X\(00\)99225-8](https://doi.org/10.1016/S0022-328X(00)99225-8).
- [338] Bock H, Roth B. Radical ions 491 redox reactions of some thiophene derivatives. *Phosphorus Sulfur Silicon Relat Elem* 1983;14:211–23. <https://doi.org/10.1080/03086648308075943>.
- [339] Kobayashi T, Kubota T, Ezumi K, Utsunomiya C. Photoelectron angular distribution study of some isoxazoles combined with perturbation theoretic approach. *Bull Chem Soc Jpn* 1982;55:3915–9. <https://doi.org/10.1246/BCSJ.55.3915>.
- [340] Schweig A, Thiel W. Photoionization cross sections: He I- and He II-photoelectron spectra of homologous oxygen and sulphur compounds. *Mol Phys* 1974;27:265–8. <https://doi.org/10.1080/00268977400100241>.
- [341] Xie M, Zhou Z, Wang Z, Chen D, Qi F. Determination of absolute photoionization cross-sections of oxygenated hydrocarbons. *Int J Mass Spectrom* 2010;293:28–33. <https://doi.org/10.1016/j.ijms.2010.03.007>.
- [342] Czekner J, Taatjes CA, Osborn DL, Meloni G. Absolute photoionization cross-sections of selected furanic and lactonic potential biofuels. *Int J Mass Spectrom* 2013;348:39–46. <https://doi.org/10.1016/j.ijms.2013.04.020>.
- [343] Schmidt H, Schweig A, Anastassiou AG, Wetzel JC. The dominant role of hyperconjugation in the 9-oxabicyclo[4.2.1] nona-2,4,7-triene series. *Tetrahedron* 1976;32:2239–44. [https://doi.org/10.1016/0040-4020\(76\)85138-1](https://doi.org/10.1016/0040-4020(76)85138-1).
- [344] Schmidt H, Schweig A. Notiz zur transanularen  $n/\pi$ -Wechselwirkung in 2,5-Dihydrofuran. *Chem Ber* 1974;107:725–6. <https://doi.org/10.1002/cber.19741070249>.

- [345] Bain AD, Buenzli JC, Frost DC, Weiler Larry. Photoelectron spectra of cyclic ethers. *J Am Chem Soc* 1973;95:291–2. <https://doi.org/10.1021/ja00782a079>.
- [346] Holmes JL, Lossing FP. Title unavailable. Personal Communication to SG Lias 1986.
- [347] Wada Y, Kiser RW. Electron impact spectroscopy of some substituted oxiranes. *J Phys Chem* 1962;66:1652–7. <https://doi.org/10.1021/j100815a021>.
- [348] Pignataro S, Distefano G. n- $\sigma$  Mixing in pentatomic heterocyclic compounds of sixth group by photoelectron spectroscopy. *Chem Phys Lett* 1974;26:356–60. [https://doi.org/10.1016/0009-2614\(74\)89048-2](https://doi.org/10.1016/0009-2614(74)89048-2).
- [349] Gerson SH, Worley SD, Bodor N, Kaminski JJ, Flechtner TW. The photoelectron spectra of some heterocyclic compounds which contain N, O, Cl and Br. *J Electron Spectros Relat Phenomena* 1978;13:421–34. [https://doi.org/10.1016/0368-2048\(78\)85046-4](https://doi.org/10.1016/0368-2048(78)85046-4).
- [350] Doucet J, Sauvageau P, Sandorfy C. The vacuum ultraviolet spectrum of tetrahydrofuran. *Chem Phys Lett* 1972;17:316–9. [https://doi.org/10.1016/0009-2614\(72\)87085-4](https://doi.org/10.1016/0009-2614(72)87085-4).
- [351] Spilker R, Grützmacher H-F. Isomerization and fragmentation of methylfuran ions and pyran ions in the gas phase. *Org Mass Spectrom* 1986;21:459–66. <https://doi.org/10.1002/oms.1210210803>.
- [352] Lias SG, Ausloos P. Ionization energies of organic compounds by equilibrium measurements. *J Am Chem Soc* 1978;100:6027–34. <https://doi.org/10.1021/ja00487a009>.
- [353] Varsel CJ, Morrell FA, Resnik FE, Powell WA. Qualitative and quantitative analysis of organic compounds. Use of low-voltage mass spectrometry. *Anal Chem* 1960;32:182–6. <https://doi.org/10.1021/ac60158a011>.
- [354] Colonna FP, Distefano G, Guerra M, Jones D, Modelli A. Furyl- and thienyl-mercury derivatives studied by means of ultraviolet photoelectron spectroscopy. Evidence for the participation in bonding of the vacant  $6p\pi$  orbitals of mercury in bis-2-furyl- and bis-2-thienyl-mercury. *J Chem Soc, Dalton Trans* 1979:2037–41. <https://doi.org/10.1039/DT9790002037>.
- [355] Fringuelli F, Marino G, Taticchi A, Distefano G, Colonna FP, Pignataro S. Photoelectron spectra of the  $\alpha$ -substituted derivatives of furan, thiophen, selenophen, and tellurophen. A comparative study of the molecular orbital energies. *J Chem Soc, Perkin Trans 2* 1976:276–9. <https://doi.org/10.1039/P29760000276>.
- [356] Bloch M, Brogli F, Heilbronner E, Jones TB, Prinzbach H, Schweikert O. Photoelectron spectra of unsaturated oxides. I. 1,4-Dioxin and related systems. *Helv Chim Acta* 1978;61:1388–98. <https://doi.org/10.1002/hlca.19780610422>.
- [357] Planckaert AA, Doucet J, Sandorfy C. Comparative study of the vacuum ultraviolet absorption and photoelectron spectra of some simple ethers and thioethers. *J Chem Phys* 1974;60:4846–53. <https://doi.org/10.1063/1.1680992>.
- [358] Batich C, Heilbronner E, Quinn CB, Wiseman JR. The electronic structure of vinyl ethers and sulfides with interrupted conjugation examined by photoelectron spectroscopy. *Helv Chim Acta* 1976;59:512–22. <https://doi.org/10.1002/hlca.19760590217>.
- [359] Jinno M, Watanabe I, Yokoyama Y, Ikeda S. He I photoelectron spectra of ethylene carbonate and related compounds. *Bull Chem Soc Jpn* 1977;50:597–603. <https://doi.org/10.1246/bcsj.50.597>.
- [360] Behan JM, Dean FM, Johnstone RAW. Photoelectron spectra of cyclic aromatic ethers: The question of the mills-nixon effect. *Tetrahedron* 1976;32:167–71. [https://doi.org/10.1016/0040-4020\(76\)80038-5](https://doi.org/10.1016/0040-4020(76)80038-5).
- [361] Kobayashi T, Nagakura S. Photoelectron Spectra of Tetrahydropyran, 1,3-Dioxane, and 1,4-Dioxane. *Bull Chem Soc Jpn* 1973;46:1558–60. <https://doi.org/10.1246/BCSJ.46.1558>.



- [362] Sweigart DA, Turner DW. Lone pair orbitals and their interactions studied by photoelectron spectroscopy. II. Equivalent orbitals in saturated oxygen and sulfur heterocycles. *J Am Chem Soc* 1972;94:5599–603. <https://doi.org/10.1021/ja00771a012>.
- [363] Fraser-Monteiro ML, Fraser-Monteiro L, Butler JJ, Baer T, Hass JR. Thermochemistry and dissociation dynamics of state-selected C<sub>4</sub>H<sub>8</sub>O<sub>2</sub><sup>+</sup> ions. 1. 1,4-Dioxane. *J Phys Chem* 1982;86:739–47. <https://doi.org/10.1021/j100394a031>.
- [364] Gol'denfel'd IV, Korostyshevskii IZ, Mischanchuk BG, Pokrovskii VA. Determination of ionization potentials of atoms and molecules using a field mass spectrometer equipped with an energy analyzer. *Dokl Akad Nauk SSSR* 1973;213:626.
- [365] Collin J-E, Conde G. Spectrometrie de masse: l'ionisation et la dissociation des polyethers cycliques soumis a l'impact electronique. *Bull Cl Sci Acad R Belg* 1966;52:978–1009.
- [366] Asfandiarov NL, Zykov BG. Photoelectron spectra of methyl-substituted 1,3-dioxanes. *Russ Chem Bull* 1983;32:2069–72. <https://doi.org/10.1007/BF00955773>.
- [367] Coughlin DJ, Brown RS, Salomon RG. The prostaglandin endoperoxide nucleus and related bicyclic peroxides. Synthetic and spectroscopic studies. *J Am Chem Soc* 1979;101:1533–9. <https://doi.org/10.1021/ja00500a027>.
- [368] Rodin AA, Chistyakov AB, Sarkisov YS, Sergeev YL, V'yunov KA, Golovin AV. Electronic structure and geometric structure of three-member J. Heterocycl. Chem.. I. hotoelectron spectra of glycidyl and thioglycidyl ethers. *Russ J Phys Chem* 1985;59:444.
- [369] Yu M, Kim HS, LeBreton PR. UV photoelectron and theoretical characterization of 2'-deoxyguanosine-5'-phosphate valence electronic properties: Changes in structure associated with the B to Z-DNA conformational transition. *Biochem Biophys Res Commun* 1992;184:16–23. [https://doi.org/10.1016/0006-291X\(92\)91151-F](https://doi.org/10.1016/0006-291X(92)91151-F).
- [370] Kumakura M, Sugiura T, Okamura S. Characteristics of RPD ion source of time-of-flight mass spectrometer, and measurement of the ionization potential and the appearance potentials of trioxymethylene. *J Mass Spectrom Soc Jpn* 1968;16:16–22. <https://doi.org/10.5702/massspec1953.16.16>.
- [371] Dewar MJS, Worley SD. Photoelectron spectra of molecules. i. ionization potentials of some organic molecules and their interpretation. *J Chem Phys* 1969;50:654–67. <https://doi.org/10.1063/1.1671114>.
- [372] Smith AR, Meloni G. Absolute photoionization cross sections of furanic fuels: 2-ethylfuran, 2-acetylfuran and furfural. *J Mass Spectrom* 2015;50:1206–13. <https://doi.org/10.1002/jms.3638>.
- [373] Colonna FP, Distefano G, Guerra M, Jones D. Photoelectron (He(I), He(II) and X-ray) spectroscopy of  $\gamma$ -pyrone and its related sulphur derivatives: valence and core ionization energies and shake-up satellites. *J Electron Spectrosc Relat Phenom* 1980;18:309–28. [https://doi.org/10.1016/0368-2048\(80\)80019-3](https://doi.org/10.1016/0368-2048(80)80019-3).
- [374] Kreile J, Münzel N, Schweig A, Specht H. Uv photoelectron spectrum of cyclobutadiene. Free cyclobutadiene stable up to high temperatures. *Chem Phys Lett* 1986;124:140–6. [https://doi.org/10.1016/0009-2614\(86\)85133-8](https://doi.org/10.1016/0009-2614(86)85133-8).
- [375] Grützmacher H-F, Spilker R. Loss of CO from 4,6-dimethyl-2-pyrone and 2,6-dimethyl-4-prypne radical cations. *Org Mass Spectrom* 1985;20:258–61.
- [376] Thorstad O, Undheim K, Cederlund B, Hörnfeldt A-B, Servin R, Sternerup H. Ionisation potentials in tautomeric analysis of 2-hydroxy derivatives of thiophenes, selenophenes, and furans. *Acta Chem Scand* 1975;29b:647–51. <https://doi.org/10.3891/acta.chem.scand.29b-0647>.
- [377] Jørgensen FS, Gajhede M, Frei B. Cyclic acetals. structural analysis of 1,3-dioxepine and related compounds. *Helv Chim Acta* 1985;68:2148–57. <https://doi.org/10.1002/hlca.19850680809>.

- [378] Scharf H-D, Plum H, Fleischhauer J, Schleker W. Zur Diels-Alder-reaktivität s-cis-fixierter 1,3-diene. *Chem Ber* 1979;112:862–82. <https://doi.org/10.1002/cber.19791120312>.
- [379] Zverev VV, Villem YY, Villem NV, Klimovitskii EN, Arbuzov BA. Photoelectron spectra and intramolecular interactions of dimethoxymethane and 4,7-dihydro-1,3-dioxepin. *J Gen Chem USSR* 1982;52:1674.
- [380] Rotavera B, Zádor J, Welz O, Sheps L, Scheer AM, Savee JD, et al. Photoionization mass spectrometric measurements of initial reaction pathways in low-temperature oxidation of 2,5-dimethylhexane. *J Phys Chem A* 2014;118:10188–200. <https://doi.org/10.1021/jp507811d>.
- [381] Frisch MJ, Trucks GW, Schlegel HB, Scuseria GE, Robb MA, et al. Gaussian 16, Revision B. Gaussian, Inc., Wallingford, CT; 2019.
- [382] Rayne S, Forest K. Estimated adiabatic ionization energies for organic compounds using the Gaussian-4 (G4) and W1BD theoretical methods. *J Chem Eng Data* 2011;56:350–5. <https://doi.org/10.1021/je100913f>.
- [383] El-Nahas AM, Simmie JM, Mangood AH, Hirao K, Song J-W, Watson MA, et al. Assessment of hybrid, meta-hybrid-GGA, and long-range corrected density functionals for the estimation of enthalpies of formation, barrier heights, and ionisation potentials of selected C1–C5 oxygenates. *Molecular Physics* 2015;113:1630–5. <https://doi.org/10.1080/00268976.2014.1002552>.
- [384] Cord M, Husson B, Lizardo Huerta JC, Herbinet O, Glaude P-A, Fournet R, et al. Study of the low temperature oxidation of propane. *J Phys Chem A* 2012;116:12214–28. <https://doi.org/10.1021/jp309821z>.
- [385] Sun W, Lailliau M, Serinyel Z, Dayma G, Moshhammer K, Hansen N, et al. Insights into the oxidation kinetics of a cetane improver – 1,2-dimethoxyethane (1,2-DME) with experimental and modeling methods. *Proc Combust Inst* 2019;37:555–64. <https://doi.org/10.1016/j.proci.2018.06.077>.
- [386] Wang J, Yang B, Cool TA, Hansen N, Kasper T. Near-threshold absolute photoionization cross-sections of some reaction intermediates in combustion. *Int J Mass Spectrom* 2008;269:210–20. <https://doi.org/10.1016/j.ijms.2007.10.013>.
- [387] Baer T, Guyon PM. An historical introduction to threshold photoionization. High resolution laser photoionization and photoelectron studies. John Wiley&Sons Ltd, Chichester: Editors: Powis I., Baer T., Ng C.Y; 1995.
- [388] Osborn DL, Hayden CC, Hemberger P, Bodi A, Voronova K, Sztáray B. Breaking through the false coincidence barrier in electron–ion coincidence experiments. *J Chem Phys* 2016;145:164202. <https://doi.org/10.1063/1.4965428>.
- [389] Holzmeier F. Photoionization of reactive molecules – A powerful tool for understanding combustion processes. *Ber Bunsenges Phys Chem* 2020;2:27–34. <https://doi.org/10.26125/04EC-3M42>.
- [390] Eskola AJ, Welz O, Savee JD, Osborn DL, Taatjes CA. Synchrotron photoionization mass spectrometry measurements of product formation in low-temperature n-butane oxidation: Toward a fundamental understanding of autoignition chemistry and n-C<sub>4</sub>H<sub>9</sub> + O<sub>2</sub>/s-C<sub>4</sub>H<sub>9</sub> + O<sub>2</sub> reactions. *J Phys Chem A* 2013;117:12216–35. <https://doi.org/10.1021/jp408467g>.
- [391] Krüger J, Garcia GA, Felsmann D, Moshhammer K, Lackner A, Brockhinke A, et al. Photoelectron–photoion coincidence spectroscopy for multiplexed detection of intermediate species in a flame. *Phys Chem Chem Phys* 2014;16:22791–804. <https://doi.org/10.1039/C4CP02857K>.
- [392] Bourgalais J, Gouid Z, Herbinet O, Garcia GA, Arnoux P, Wang Z, et al. Isomer-sensitive characterization of low temperature oxidation reaction products by coupling a

- jet-stirred reactor to an electron/ion coincidence spectrometer: case of n-pentane. *Phys Chem Chem Phys* 2020;22:1222–41. <https://doi.org/10.1039/C9CP04992D>.
- [393] Oßwald P, Güldenberg H, Kohse-Höinghaus K, Yang B, Yuan T, Qi F. Combustion of butanol isomers – A detailed molecular beam mass spectrometry investigation of their flame chemistry. *Combust Flame* 2011;158:2–15. <https://doi.org/10.1016/j.combustflame.2010.06.003>.
- [394] Cool TA, Nakajima K, Taatjes CA, McIlroy A, Westmoreland PR, Law ME, et al. Studies of a fuel-rich propane flame with photoionization mass spectrometry. *Proc Combust Inst* 2005;30:1681–8. <https://doi.org/10.1016/j.proci.2004.08.103>.
- [395] Christianson MG, Doner AC, Davis MM, Koritzke AL, Turney JM, Schaefer HF, et al. Reaction mechanisms of a cyclic ether intermediate: Ethyloxirane. *Int J Chem Kinet* 2021;53:43–59. <https://doi.org/10.1002/kin.21423>.
- [396] Kanno N, Tonokura K. Vacuum ultraviolet photoionization mass spectra and cross-sections for volatile organic compounds at 10.5 eV. *Appl Spectrosc* 2007;61:896–902. <https://doi.org/10.1366/000370207781540033>.
- [397] Davis JC, Koritzke AL, Caravan RL, Antonov IO, Christianson MG, Doner AC, et al. Influence of the ether functional group on ketohydroperoxide formation in cyclic hydrocarbons: tetrahydropyran and cyclohexane. *J Phys Chem A* 2019;123:3634–46. <https://doi.org/10.1021/acs.jpca.8b12510>.
- [398] Rotavera B, Savee JD, Antonov IO, Caravan RL, Sheps L, Osborn DL, et al. Influence of oxygenation in cyclic hydrocarbons on chain-termination reactions from R+O<sub>2</sub>: tetrahydropyran and cyclohexane. *Proc Combust Inst* 2017;36:597–606. <https://doi.org/10.1016/j.proci.2016.05.020>.
- [399] Koritzke AL, Davis JC, Caravan RL, Christianson MG, Osborn DL, Taatjes CA, et al. QOOH-mediated reactions in cyclohexene oxidation. *Proc Combust Inst* 2019;37:323–35. <https://doi.org/10.1016/j.proci.2018.05.029>.
- [400] Schenk M, Leon L, Moshhammer K, Oßwald P, Zeuch T, Seidel L, et al. Detailed mass spectrometric and modeling study of isomeric butene flames. *Combust Flame* 2013;160:487–503. <https://doi.org/10.1016/j.combustflame.2012.10.023>.
- [401] Tran L-S, Pieper J, Zeng M, Li Y, Zhang X, Li W, et al. Influence of the biofuel isomers diethyl ether and n-butanol on flame structure and pollutant formation in premixed n-butane flames. *Combust Flame* 2017;175:47–59. <https://doi.org/10.1016/j.combustflame.2016.06.031>.
- [402] Biordi JC. Molecular beam mass spectrometry for studying the fundamental chemistry of flames. *Prog Energy Combust Sci* 1977;3:151–73. [https://doi.org/10.1016/0360-1285\(77\)90002-8](https://doi.org/10.1016/0360-1285(77)90002-8).
- [403] Zhou Z, Du X, Yang J, Wang Y, Li C, Wei S, et al. The vacuum ultraviolet beamline/endstations at NSRL dedicated to combustion research. *J Synchrotron Rad, J Synchrotron Radiat* 2016;23:1035–45. <https://doi.org/10.1107/S1600577516005816>.
- [404] Li Y, Zhang L, Tian Z, Yuan T, Wang J, Yang B, et al. Experimental Study of a Fuel-Rich Premixed Toluene Flame at Low Pressure. *Energy Fuels* 2009;23:1473–85. <https://doi.org/10.1021/ef800902t>.
- [405] Bierkandt T, Oßwald P, Gaiser N, Krüger D, Köhler M, Hoener M, et al. Observation of low-temperature chemistry products in laminar premixed low-pressure flames by molecular-beam mass spectrometry. *International Journal of Chemical Kinetics* 2021;53:1063–81. <https://doi.org/10.1002/kin.21503>.
- [406] Bartle KD, Myers P. History of gas chromatography. *Trends Analyt Chem* 2002;21:547–57.

- [407] Minetti R, Ribaucour M, Carlier M, Fittschen C, Sochet LR. Experimental and modeling study of oxidation and autoignition of butane at high pressure. *Combust Flame* 1994;96:201–11. [https://doi.org/10.1016/0010-2180\(94\)90009-4](https://doi.org/10.1016/0010-2180(94)90009-4).
- [408] Minetti R, Carlier M, Ribaucour M, Therssen E, Sochet LR. A rapid compression machine investigation of oxidation and auto-ignition of n-Heptane: Measurements and modeling. *Combust Flame* 1995;102:298–309. [https://doi.org/10.1016/0010-2180\(94\)00236-L](https://doi.org/10.1016/0010-2180(94)00236-L).
- [409] Minetti R, Roubaud A, Therssen E, Ribaucour M, Sochet LR. The chemistry of pre-ignition of n-pentane and 1-pentene. *Combust Flame* 1999;118:213–20. [https://doi.org/10.1016/S0010-2180\(98\)00151-5](https://doi.org/10.1016/S0010-2180(98)00151-5).
- [410] Minetti R, Carlier M, Ribaucour M, Therssen E, Sochet LR. Comparison of oxidation and autoignition of the two primary reference fuels by rapid compression. *Proc Combust Inst* 1996;26:747–53. [https://doi.org/10.1016/S0082-0784\(96\)80283-9](https://doi.org/10.1016/S0082-0784(96)80283-9).
- [411] Ribaucour M, Minetti R, Sochet LR. Autoignition of n-pentane and 1-pentene: Experimental data and kinetic modeling. *Proc Combust Inst* 1998;27:345–51. [https://doi.org/10.1016/S0082-0784\(98\)80422-0](https://doi.org/10.1016/S0082-0784(98)80422-0).
- [412] Dagaut P, Reuillon M, Cathonnet M. High pressure oxidation of liquid fuels from low to high temperature. 1. n-Heptane and iso-octane. *Combust Sci Technol* 1993;95:233–60. <https://doi.org/10.1080/00102209408935336>.
- [413] Dagaut P, Reuillon M, Cathonnet M. High-pressure oxidation of liquid fuels from low to high-temperature. 2. Mixtures of n-heptane and isooctane. *Combust Sci Technol* 1994;103:315–36. <https://doi.org/10.1080/00102209408907701>.
- [414] Dagaut P, Reuillon M, Cathonnet M. High pressure oxidation of liquid fuels from low to high temperature. 3. n-Decane. *Combust Sci Technol* 1994;103:349–59. <https://doi.org/10.1080/00102209408907703>.
- [415] Hakka MH, Glaude P-A, Herbinet O, Battin-Leclerc F. Experimental study of the oxidation of large surrogates for diesel and biodiesel fuels. *Combust Flame* 2009;156:2129–44. <https://doi.org/10.1016/j.combustflame.2009.06.003>.
- [416] Bax S, Hakka MH, Glaude P-A, Herbinet O, Battin-Leclerc F. Experimental study of the oxidation of methyl oleate in a jet-stirred reactor. *Combust Flame* 2010;157:1220–9. <https://doi.org/10.1016/j.combustflame.2009.12.008>.
- [417] Husson B, Herbinet O, Glaude PA, Ahmed SS, Battin-Leclerc F. Detailed product analysis during low- and intermediate-temperature oxidation of ethylcyclohexane. *J Phys Chem A* 2012;116:5100–11. <https://doi.org/10.1021/jp301043r>.
- [418] Serinyel Z, Herbinet O, Frottier O, Dirrenberger P, Warth V, Glaude PA, et al. An experimental and modeling study of the low- and high-temperature oxidation of cyclohexane. *Combust Flame* 2013;160:2319–32. <https://doi.org/10.1016/j.combustflame.2013.05.016>.
- [419] Wang Z, Herbinet O, Cheng Z, Husson B, Fournet R, Qi F, et al. Experimental investigation of the low temperature oxidation of the five isomers of hexane. *J Phys Chem A* 2014;118:5573–94. <https://doi.org/10.1021/jp503772h>.
- [420] Battin-Leclerc F, Rodriguez A, Husson B, Herbinet O, Glaude P-A, Wang Z, et al. Products from the oxidation of linear isomers of hexene. *J Phys Chem A* 2014;118:673–83. <https://doi.org/10.1021/jp4107102>.
- [421] Meng X, Herbinet O, Wang T, Battin-Leclerc F. Experimental and modeling study of 1-octene jet-stirred reactor oxidation. *Fuel* 2017;207:763–75. <https://doi.org/10.1016/j.fuel.2017.06.128>.
- [422] Tran L-S, Wullenkord J, Li Y, Herbinet O, Zeng M, Qi F, et al. Probing the low-temperature chemistry of di-n-butyl ether: Detection of previously unobserved

- intermediates. *Combust Flame* 2019;210:9–24. <https://doi.org/10.1016/j.combustflame.2019.08.022>.
- [423] Vermeire FH, Carstensen H-H, Herbinet O, Battin-Leclerc F, Marin GB, Van Geem KM. The thermal decomposition of furfural: molecular chemistry unraveled. *Proc Combust Inst* 2019;37:445–52. <https://doi.org/10.1016/j.proci.2018.05.119>.
- [424] Bissoonauth T, Wang Z, Mohamed SY, Wang J, Chen B, Rodriguez A, et al. Methylcyclohexane pyrolysis and oxidation in a jet-stirred reactor. *Proc Combust Inst* 2019;37:409–17. <https://doi.org/10.1016/j.proci.2018.05.086>.
- [425] NIST Standard Reference Database. NIST/EPA/NIH Mass Spectral Library. Available at <<https://www.nist.gov/srd/nist-standard-reference-database-1a>> n.d.
- [426] Dagaut P, Reuillon M, Cathonnet M, Presvots D. Gas chromatography and mass spectrometry identification of cyclic ethers formed from reference fuels combustion. *Chromatographia* 1995;40:147–54. <https://doi.org/10.1007/BF02272163>.
- [427] Herbinet O, Bax S, Glaude P-A, Carre V, Battin-Leclerc F. Mass spectra of cyclic ethers formed in the low-temperature oxidation of a series of n-alkanes. *Fuel* 2011;90:528–35. <https://doi.org/10.1016/j.fuel.2010.09.047>.
- [428] Koritzke AL, Frandsen KM, Christianson MG, Davis JC, Doner AC, Larsson A, et al. Fragmentation mechanisms from electron-impact of complex cyclic ethers formed in combustion. *Int J Mass Spectrom* 2020;454:116342. <https://doi.org/10.1016/j.ijms.2020.116342>.
- [429] Bugler J, Rodriguez A, Herbinet O, Battin-Leclerc F, Togbe C, Dayma G, et al. An experimental and modelling study of n-pentane oxidation in two jet-stirred reactors: The importance of pressure-dependent kinetics and new reaction pathways. *Proc Combust Inst* 2017;36:441–8. <https://doi.org/10.1016/j.proci.2016.05.048>.
- [430] McWilliam IG, Dewar RA. Flame ionization detector for gas chromatography. *Nature* 1958;181:760–760. <https://doi.org/10.1038/181760a0>.
- [431] Tranchant J, Gardais JF, Gorin P, Serpinet J, Untz G. Manuel pratique de chromatographie en phase gazeuse. Paris: Masson; 1982.
- [432] Zhu G, Zhao F, Wang D, Xia C. Extended effective carbon number concept in the quantitative analysis of multi-ethers using predicted response factors. *J Chromatogr A* 2017;1513:194–200. <https://doi.org/10.1016/j.chroma.2017.07.036>.
- [433] Vermeire FH, Carstensen H-H, Herbinet O, Battin-Leclerc F, Marin GB, Van Geem KM. Experimental and modeling study of the pyrolysis and combustion of dimethoxymethane. *Combust Flame* 2018;190:270–83. <https://doi.org/10.1016/j.combustflame.2017.12.001>.
- [434] Porter K, Volman DH. Flame ionization detection of carbon monoxide for gas chromatographic analysis. *Anal Chem* 1962;34:748–9. <https://doi.org/10.1021/ac60187a009>.
- [435] Tran LS. Étude de la formation de polluants lors de la combustion de carburants oxygénés. Thesis. Université de Lorraine, 2013.
- [436] Wang Z, Mohamed SY, Zhang L, Moshhammer K, Popolan-Vaida DM, Shankar VSB, et al. New insights into the low-temperature oxidation of 2-methylhexane. *Proc Combust Inst* 2017;36:373–82. <https://doi.org/10.1016/j.proci.2016.06.085>.
- [437] Hoener M, Kaczmarek D, Bierkandt T, Bodi A, Hemberger P, Kasper T. A pressurized flow reactor combustion experiment interfaced with synchrotron double imaging photoelectron photoion coincidence spectroscopy. *Rev Sci Instrum* 2020;91:045115. <https://doi.org/10.1063/1.5141168>.
- [438] Felsmann D, Moshhammer K, Krüger J, Lackner A, Brockhinke A, Kasper T, et al. Electron ionization, photoionization and photoelectron/photoion coincidence

- spectroscopy in mass-spectrometric investigations of a low-pressure ethylene/oxygen flame. *Proc Combust Inst* 2015;35:779–86. <https://doi.org/10.1016/j.proci.2014.05.151>.
- [439] Sztáray B, Voronova K, Torma KG, Covert KJ, Bodi A, Hemberger P, et al. CRF-PEPICO: Double velocity map imaging photoelectron photoion coincidence spectroscopy for reaction kinetics studies. *J Chem Phys* 2017;147:013944. <https://doi.org/10.1063/1.4984304>.
- [440] Battin-Leclerc F, Bourgalais J, Gouid Z, Herbinet O, Garcia G, Arnoux P, et al. Chemistry deriving from OOQOOH radicals in alkane low-temperature oxidation: A first combined theoretical and electron-ion coincidence mass spectrometry study. *Proc Combust Inst* 2021;38:309–19. <https://doi.org/10.1016/j.proci.2020.06.159>.
- [441] Knox JH. A new mechanism for the low temperature oxidation of hydrocarbons in the gas phase. *Combust Flame* 1965;9:297–310. [https://doi.org/10.1016/0010-2180\(65\)90095-7](https://doi.org/10.1016/0010-2180(65)90095-7).
- [442] Fish A. The non-isothermal oxidation of neopentane. *Combust Flame* 1969;13:23–32. [https://doi.org/10.1016/0010-2180\(69\)90024-8](https://doi.org/10.1016/0010-2180(69)90024-8).
- [443] Fish A. The non-isothermal oxidation of 2-methylpentane. II. The chemistry of cool flames. *Proc R Soc Lond A* 1967;298:204–37. <https://doi.org/10.1098/rspa.1967.0100>.
- [444] Hughes KJ, Halford-Maw PA, Lightfoot PD, Turányi T, Pilling MJ. Direct measurements of the neopentyl peroxy-hydroperoxy radical isomerisation over the temperature range 660–750 K. *Proc Combust Inst* 1992;24:645–52. [https://doi.org/10.1016/S0082-0784\(06\)80079-2](https://doi.org/10.1016/S0082-0784(06)80079-2).
- [445] Baldwin RR, Hisham MWM, Walker RW. Arrhenius parameters of elementary reactions involved in the oxidation of neopentane. *J Chem Soc, Faraday Trans 1* 1982;78:1615–27. <https://doi.org/10.1039/F19827801615>.
- [446] Curran HJ, Gaffuri P, Pitz WJ, Westbrook CK. A comprehensive modeling study of n-heptane oxidation. *Combust Flame* 1998;114:149–77. [https://doi.org/10.1016/S0010-2180\(97\)00282-4](https://doi.org/10.1016/S0010-2180(97)00282-4).
- [447] Ranzi E, Gaffuri P, Faravelli T, Dagaut P. A wide-range modeling study of n-heptane oxidation. *Combust Flame* 1995;103:91–106. [https://doi.org/10.1016/0010-2180\(95\)00091-J](https://doi.org/10.1016/0010-2180(95)00091-J).
- [448] Glaude PA, Warth V, Fournet R, Battin-Leclerc F, Scacchi G, Côme GM. Modelling of normal-heptane and iso-octane gas-phase oxidation at low temperature by using computer aided designed mechanisms. *Bull Soc Chim Belg* 1997;106:343–8.
- [449] Koert DN, Miller DL, Cernansky NP. Experimental studies of propane oxidation through the negative temperature coefficient region at 10 and 15 atmospheres. *Combust Flame* 1994;96:34–49. [https://doi.org/10.1016/0010-2180\(94\)90156-2](https://doi.org/10.1016/0010-2180(94)90156-2).
- [450] Wang S, Miller DL, Cernansky NP, Curran HJ, Pitz WJ, Westbrook CK. A flow reactor study of neopentane oxidation at 8 atmospheres: experiments and modeling. *Combust Flame* 1999;118:415–30. [https://doi.org/10.1016/S0010-2180\(99\)00014-0](https://doi.org/10.1016/S0010-2180(99)00014-0).
- [451] Bourgalais J, Herbinet O, Carstensen H-H, Debleza J, Garcia GA, Arnoux P, et al. Jet-stirred reactor study of low-temperature neopentane oxidation: a combined theoretical, chromatographic, mass spectrometric, and PEPICO analysis. *Energy Fuels* 2021;35:19689–704. <https://doi.org/10.1021/acs.energyfuels.1c02080>.
- [452] Ramalingam A, Fenard Y, Heufer A. Ignition delay time and species measurement in a rapid compression machine: A case study on high-pressure oxidation of propane. *Combust Flame* 2020;211:392–405. <https://doi.org/10.1016/j.combustflame.2019.10.015>.
- [453] Tran L-S, Li Y, Zeng M, Pieper J, Qi F, Battin-Leclerc F, et al. Elevated pressure low-temperature oxidation of linear five-heavy-atom fuels: diethyl ether, n-pentane, and their mixture. *Z Physik Chem* 2020;234:1269–93. <https://doi.org/10.1515/zpch-2020-1613>.

- [454] Zhang K, Banyon C, Togbé C, Dagaut P, Bugler J, Curran HJ. An experimental and kinetic modeling study of n-hexane oxidation. *Combust Flame* 2015;162:4194–207. <https://doi.org/10.1016/j.combustflame.2015.08.001>.
- [455] Hakka HM, Cracknell RF, Pekalski A, Glaude P-A, Battin-Leclerc F. Experimental and modeling study of ultra-rich oxidation of n-heptane. *Fuel* 2015;144:358–68. <https://doi.org/10.1016/j.fuel.2014.12.058>.
- [456] Herbinet O, Husson B, Gall HL, Battin-Leclerc F. An experimental and modeling study of the oxidation of n-heptane, ethylbenzene, n-butylbenzene in a jet-stirred reactor at pressures up to 10 bar. *Int J Chem Kinet* 2020;52:1006–21. <https://doi.org/10.1002/kin.21417>.
- [457] Sarathy SM, Westbrook CK, Mehl M, Pitz WJ, Togbe C, Dagaut P, et al. Comprehensive chemical kinetic modeling of the oxidation of 2-methylalkanes from C7 to C20. *Combust Flame* 2011;158:2338–57. <https://doi.org/10.1016/j.combustflame.2011.05.007>.
- [458] Sarathy SM, Javed T, Karsenty F, Heufer A, Wang W, Park S, et al. A comprehensive combustion chemistry study of 2,5-dimethylhexane. *Combust Flame* 2014;161:1444–59. <https://doi.org/10.1016/j.combustflame.2013.12.010>.
- [459] Mergulhão CS, Carstensen H-H, Song H, Wagnon SW, Pitz WJ, Vanhove G. Probing the antiknock effect of anisole through an ignition, speciation and modeling study of its blends with isooctane. *Proc Combust Inst* 2021;38:739–48. <https://doi.org/10.1016/j.proci.2020.08.013>.
- [460] Kukkadapu G, Wagnon SW, Mehl M, Zhang K, Westbrook CK, Pitz WJ, et al. An updated comprehensive chemical kinetic model of C8-C20 n-alkanes. 10th US National Combustion Meeting 2017.
- [461] Chen W, Rodriguez A, Xie C, Li Y, Xu Q, Wang H, et al. Exploring low temperature oxidation of iso-octane under atmospheric pressure. *Combust Flame* 2022;(in press).
- [462] Ranzi E, Cavallotti C, Cuoci A, Frassoldati A, Pelucchi M, Faravelli T. New reaction classes in the kinetic modeling of low temperature oxidation of n-alkanes. *Combust Flame* 2015;162:1679–91. <https://doi.org/10.1016/j.combustflame.2014.11.030>.
- [463] Bugler J, Power J, Curran HJ. A theoretical study of cyclic ether formation reactions. *Proc Combust Inst* 2017;36:161–7. <https://doi.org/10.1016/j.proci.2016.05.006>.
- [464] Biet J, Hakka MH, Warth V, Glaude P-A, Battin-Leclerc F. Experimental and modeling study of the low-temperature oxidation of large alkanes. *Energy Fuels* 2008;22:2258–69. <https://doi.org/10.1021/ef8000746>.
- [465] Hakka MH. Étude de l'oxydation en phase gazeuse de composants des gazoles et des biocarburants diesel. These de doctorat. Vandoeuvre-les-Nancy, INPL, 2010.
- [466] Bugler J, Marks B, Mathieu O, Archuleta R, Camou A, Grégoire C, et al. An ignition delay time and chemical kinetic modeling study of the pentane isomers. *Combust Flame* 2016;163:138–56. <https://doi.org/10.1016/j.combustflame.2015.09.014>.
- [467] Atef N, Kukkadapu G, Mohamed SY, Rashidi MA, Banyon C, Mehl M, et al. A comprehensive iso-octane combustion model with improved thermochemistry and chemical kinetics. *Combust Flame* 2017;178:111–34. <https://doi.org/10.1016/j.combustflame.2016.12.029>.
- [468] Liao H, Chen H, Liu Z, Zhang R, Zhang F, Yang B. MBMS study on plasma-assisted low-temperature oxidation of n-heptane and iso-octane in a flow reactor. *Int J Chem Kinet* 2021;53:428–39. <https://doi.org/10.1002/kin.21454>.
- [469] Warth V, Stef N, Glaude PA, Battin-Leclerc F, Scacchi G, Côme GM. Computer-aided derivation of gas-phase oxidation mechanisms: application to the modeling of the oxidation of n-butane. *Combust Flame* 1998;114:81–102. [https://doi.org/10.1016/S0010-2180\(97\)00273-3](https://doi.org/10.1016/S0010-2180(97)00273-3).

- [470] Villano SM, Huynh LK, Carstensen H-H, Dean AM. High-pressure rate rules for alkyl + O<sub>2</sub> reactions. 1. The dissociation, concerted elimination, and isomerization channels of the alkyl peroxy radical. *J Phys Chem A* 2011;115:13425–42. <https://doi.org/10.1021/jp2079204>.
- [471] Duan J, Ji J, Ye L, Meng Q, Zhai Y, Zhang L. Theoretical calculation of low-temperature oxidation of heptyl radicals and O<sub>2</sub>. *Combustion and Flame* 2020;217:274–84. <https://doi.org/10.1016/j.combustflame.2020.03.021>.
- [472] Battin-Leclerc F, Herbinet O, Glaude P-A, Fournet R, Zhou Z, Deng L, et al. New experimental evidences about the formation and consumption of ketohydroperoxides. *Proc Combust Inst* 2011;33:325–31. <https://doi.org/10.1016/j.proci.2010.05.001>.
- [473] Taatjes CA. Uncovering the fundamental chemistry of alkyl + O<sub>2</sub> reactions via measurements of product formation. *J Phys Chem A* 2006;110:4299–312. <https://doi.org/10.1021/jp056997f>.
- [474] Pilling MJ. Interactions between theory and experiment in the investigation of elementary reactions of importance in combustion. *Chem Soc Rev* 2008;37:676–85. <https://doi.org/10.1039/B715767C>.
- [475] Klippenstein SJ, Pande VS, Truhlar DG. Chemical kinetics and mechanisms of complex systems: a perspective on recent theoretical advances. *J Am Chem Soc* 2014;136:528–46. <https://doi.org/10.1021/ja408723a>.
- [476] Klippenstein SJ. From theoretical reaction dynamics to chemical modeling of combustion. *Proc Combust Inst* 2017;36:77–111. <https://doi.org/10.1016/j.proci.2016.07.100>.
- [477] Miller JA, Sivaramakrishnan R, Tao Y, Goldsmith CF, Burke MP, Jasper AW, et al. Combustion chemistry in the twenty-first century: Developing theory-informed chemical kinetics models. *Prog Energy Combust Sci* 2021;83:100886. <https://doi.org/10.1016/j.peccs.2020.100886>.
- [478] Quelch GE, Gallo MM, Shen M, Xie Y, Schaefer HF, Moncrieff D. Aspects of the reaction mechanism of ethane combustion. 2. Nature of the intramolecular hydrogen transfer. *J Am Chem Soc* 1994;116:4953–62. <https://doi.org/10.1021/ja00090a046>.
- [479] Ignatyev IS, Xie Y, Allen WD, Schaefer HF. Mechanism of the C<sub>2</sub>H<sub>5</sub>+O<sub>2</sub> reaction. *J Chem Phys* 1997;107:141–55. <https://doi.org/10.1063/1.474610>.
- [480] Rienstra-Kiracofe JC, Allen WD, Schaefer HF. The C<sub>2</sub>H<sub>5</sub> + O<sub>2</sub> reaction mechanism: high-level ab initio characterizations. *J Phys Chem A* 2000;104:9823–40. <https://doi.org/10.1021/jp001041k>.
- [481] Wilke JJ, Allen WD, Schaefer HF. Establishment of the C<sub>2</sub>H<sub>5</sub>+O<sub>2</sub> reaction mechanism: A combustion archetype. *J Chem Phys* 2008;128:074308. <https://doi.org/10.1063/1.2827133>.
- [482] Miller JA, Klippenstein SJ. The reaction between ethyl and molecular oxygen II: Further analysis. *Int J Chem Kinet* 2001;33:654–68. <https://doi.org/10.1002/kin.1063>.
- [483] Clifford EP, Farrell JT, DeSain JD, Taatjes CA. Infrared Frequency-Modulation Probing of Product Formation in Alkyl + O<sub>2</sub> Reactions: I. The Reaction of C<sub>2</sub>H<sub>5</sub> with O<sub>2</sub> between 295 and 698 K. *J Phys Chem A* 2000;104:11549–60. <https://doi.org/10.1021/jp0024874>.
- [484] Carstensen H-H, Naik CV, Dean AM. Detailed Modeling of the Reaction of C<sub>2</sub>H<sub>5</sub> + O<sub>2</sub>. *J Phys Chem A* 2005;109:2264–81. <https://doi.org/10.1021/jp0451142>.
- [485] DeSain JD, Klippenstein SJ, Miller JA, Taatjes CA. Measurements, theory, and modeling of OH formation in ethyl + O<sub>2</sub> and propyl + O<sub>2</sub> reactions. (This is a correction for the original article with the same title). *J Phys Chem A* 2004;108:7127–8. <https://doi.org/10.1021/jp040467m>.



- [486] Launder AM, Turney JM, Agarwal J, Schaefer HF. Ethylperoxy radical: approaching spectroscopic accuracy via coupled-cluster theory. *Phys Chem Chem Phys* 2017;19:15715–23. <https://doi.org/10.1039/C7CP02795H>.
- [487] Villano SM, Huynh LK, Carstensen H-H, Dean AM. High-Pressure Rate Rules for Alkyl + O<sub>2</sub> Reactions. 2. The Isomerization, Cyclic Ether Formation, and  $\beta$ -Scission Reactions of Hydroperoxy Alkyl Radicals. *J Phys Chem A* 2012;116:5068–89. <https://doi.org/10.1021/jp3023887>.
- [488] Villano SM, Carstensen H-H, Dean AM. Rate rules, branching ratios, and pressure dependence of the HO<sub>2</sub> + olefin addition channels. *J Phys Chem A* 2013;117:6458–73. <https://doi.org/10.1021/jp405262r>.
- [489] Ranzi E, Frassoldati A, Granata S, Faravelli T. Wide-range kinetic modeling study of the pyrolysis, partial oxidation, and combustion of heavy n-alkanes. *Ind Eng Chem Res* 2005;44:5170–83. <https://doi.org/10.1021/ie049318g>.
- [490] Ranzi E, Faravelli T, Gaffuri P, Sogaro A, D'Anna A, Ciajolo A. A wide-range modeling study of iso-octane oxidation. *Combust Flame* 1997;108:24–42. [https://doi.org/10.1016/S0010-2180\(95\)00274-X](https://doi.org/10.1016/S0010-2180(95)00274-X).
- [491] Westbrook CK, Pitz WJ, Herbinet O, Curran HJ, Silke EJ. A comprehensive detailed chemical kinetic reaction mechanism for combustion of n-alkane hydrocarbons from n-octane to n-hexadecane. *Combust Flame* 2009;156:181–99. <https://doi.org/10.1016/j.combustflame.2008.07.014>.
- [492] Muharam Y, Warnatz J. Kinetic modelling of the oxidation of large aliphatic hydrocarbons using an automatic mechanism generation. *Phys Chem Chem Phys* 2007;9:4218–29. <https://doi.org/10.1039/B703415F>.
- [493] Wang Z, Sarathy SM. Third O<sub>2</sub> addition reactions promote the low-temperature auto-ignition of n-alkanes. *Combust Flame* 2016;165:364–72. <https://doi.org/10.1016/j.combustflame.2015.12.020>.
- [494] Miyoshi A. Systematic computational study on the unimolecular reactions of alkylperoxy (RO<sub>2</sub>), hydroperoxyalkyl (QOOH), and hydroperoxyalkylperoxy (O<sub>2</sub>QOOH) radicals. *J Phys Chem A* 2011;115:3301–25. <https://doi.org/10.1021/jp112152n>.
- [495] Pfaendtner J, Yu X, Broadbelt LJ. Quantum chemical investigation of low-temperature intramolecular hydrogen transfer reactions of hydrocarbons. *J Phys Chem A* 2006;110:10863–71. <https://doi.org/10.1021/jp061649e>.
- [496] Zhou C-W, Li Y, Burke U, Banyon C, Somers KP, Ding S, et al. An experimental and chemical kinetic modeling study of 1,3-butadiene combustion: Ignition delay time and laminar flame speed measurements. *Combust Flame* 2018;197:423–38. <https://doi.org/10.1016/j.combustflame.2018.08.006>.
- [497] Chan W-T, Pritchard HO, Hamilton IP. Dissociative ring-closure in aliphatic hydroperoxyl radicals. *Phys Chem Chem Phys* 1999;1:3715–9. <https://doi.org/10.1039/A901134J>.
- [498] Cord M, Sirjean B, Fournet R, Tomlin A, Ruiz-Lopez M, Battin-Leclerc F. Improvement of the modeling of the low-temperature oxidation of n-butane: Study of the primary reactions. *J Phys Chem A* 2012;116:6142–58. <https://doi.org/10.1021/jp211434f>.
- [499] Bugler J, Somers KP, Silke EJ, Curran HJ. Revisiting the kinetics and thermodynamics of the low-temperature oxidation pathways of alkanes: A case study of the three pentane isomers. *J Phys Chem A* 2015;119:7510–27. <https://doi.org/10.1021/acs.jpca.5b00837>.
- [500] DeSain JD, Taatjes CA, Miller JA, Klippenstein SJ, Hahn DK. Infrared frequency-modulation probing of product formation in alkyl + O<sub>2</sub> reactions. Part IV. Reactions of propyl and butyl radicals with O<sub>2</sub>. *Faraday Discuss* 2002;119:101–20. <https://doi.org/10.1039/B102237G>.

- [501] Sheng CY, Bozzelli JW, Dean AM, Chang AY. Detailed kinetics and thermochemistry of  $C_2H_5 + O_2$ : Reaction kinetics of the chemically-activated and stabilized  $CH_3CH_2OO\bullet$  adduct. *J Phys Chem A* 2002;106:7276–93. <https://doi.org/10.1021/jp014540+>.
- [502] Oakley LH, Casadio F, Shull KR, Broadbelt LJ. Theoretical study of epoxidation reactions relevant to hydrocarbon oxidation. *Ind Eng Chem Res* 2017;56:7454–61. <https://doi.org/10.1021/acs.iecr.7b01443>.
- [503] Hashemi H, Jacobsen JG, Rasmussen CT, Christensen JM, Glarborg P, Gersen S, et al. High-pressure oxidation of ethane. *Combust Flame* 2017;182:150–66. <https://doi.org/10.1016/j.combustflame.2017.03.028>.
- [504] Xu Y, Xi S, Wang F, Li X. Theoretical study on reactions of alkylperoxy radicals. *J Phys Chem A* 2019;123:3949–58. <https://doi.org/10.1021/acs.jpca.9b01496>.
- [505] Duan J, Ji J, Ye L, Zhai Y, Zhang L. A theoretical kinetics study on low-temperature oxidation of n-C<sub>4</sub>H<sub>9</sub> radicals. *Proc Combust Inst* 2021;38:681–9. <https://doi.org/10.1016/j.proci.2020.07.120>.
- [506] Wood GPF, Henry DJ, Radom L. Performance of the RB3-LYP, RMP2, and UCCSD(T) Procedures in Calculating Radical Stabilization Energies for  $\bullet$ NHX Radicals. *J Phys Chem A* 2003;107:7985–90. <https://doi.org/10.1021/jp035945s>.
- [507] Wilk RD, Green RM, Pitz WJ, Westbrook CK, Addagarla S, Miller DL, et al. An experimental and kinetic modeling study of the combustion of n-butane and isobutane in an internal combustion engine. Warrendale, PA: SAE International; 1990. <https://doi.org/10.4271/900028>.
- [508] Curran HJ, Gaffuri P, Pitz WJ, Westbrook CK. A comprehensive modeling study of iso-octane oxidation. *Combust Flame* 2002;129:253–80. [https://doi.org/10.1016/S0010-2180\(01\)00373-X](https://doi.org/10.1016/S0010-2180(01)00373-X).
- [509] Fang R, Kukkadapu G, Wang M, Wagnon SW, Zhang K, Mehl M, et al. Fuel molecular structure effect on autoignition of highly branched iso-alkanes at low-to-intermediate temperatures: Iso-octane versus iso-dodecane. *Combust Flame* 2020;214:152–66. <https://doi.org/10.1016/j.combustflame.2019.12.037>.
- [510] Cai L, Pitsch H, Mohamed SY, Raman V, Bugler J, Curran H, et al. Optimized reaction mechanism rate rules for ignition of normal alkanes. *Combust Flame* 2016;173:468–82. <https://doi.org/10.1016/j.combustflame.2016.04.022>.
- [511] Doner AC, Davis MM, Koritzke AL, Christianson MG, Turney JM, Schaefer HF, et al. Isomer-dependent reaction mechanisms of cyclic ether intermediates: cis-2,3-dimethyloxirane and trans-2,3-dimethyloxirane. *Int J Chem Kinet* 2021;53:127–45. <https://doi.org/10.1002/kin.21429>.
- [512] Fridlyand A, Goldsborough SS, Al Rashidi M, Sarathy SM, Mehl M, Pitz WJ. Low temperature autoignition of 5-membered ring naphthenes: Effects of substitution. *Combustion and Flame* 2019;200:387–404. <https://doi.org/10.1016/j.combustflame.2018.10.028>.
- [513] Al Rashidi MJ, Mármol JC, Banyon C, Sajid MB, Mehl M, Pitz WJ, et al. Cyclopentane combustion. Part II. Ignition delay measurements and mechanism validation. *Combust Flame* 2017;183:372–85. <https://doi.org/10.1016/j.combustflame.2017.05.017>.
- [514] Lokachari N, Wagnon SW, Kukkadapu G, Pitz WJ, Curran HJ. An experimental and kinetic modeling study of cyclopentane and dimethyl ether blends. *Combustion and Flame* 2021;225:255–71. <https://doi.org/10.1016/j.combustflame.2020.10.017>.
- [515] Silke EJ, Pitz WJ, Westbrook CK, Ribaucour M. Detailed chemical kinetic modeling of cyclohexane oxidation. *J Phys Chem A* 2007;111:3761–75. <https://doi.org/10.1021/jp067592d>.

- [516] Buda F, Heyberger B, Fournet R, Glaude P-A, Warth V, Battin-Leclerc F. Modeling of the gas-phase oxidation of cyclohexane. *Energy Fuels* 2006;20:1450–9. <https://doi.org/10.1021/ef060090e>.
- [517] Voisin D, Marchal A, Reuillon M, Boettner J-C, Cathonnet M. Experimental and kinetic modeling study of cyclohexane oxidation in a jsr at high pressure. *Combust Sci Technol* 1998;138:137–58. <https://doi.org/10.1080/00102209808952066>.
- [518] Dagaut P. On the kinetics of hydrocarbons oxidation from natural gas to kerosene and diesel fuel. *Phys Chem Chem Phys* 2002;4:2079–94. <https://doi.org/10.1039/B110787A>.
- [519] Ristori A, Dagaut P, El Bakali A, Cathonnet M. The oxidation of n-propylcyclohexane: experimental results and kinetic modeling. *Combust Sci Technol* 2001;165:197–228. <https://doi.org/10.1080/00102200108935832>.
- [520] Sheps L, Dewyer AL, Demireva M, Zádor J. Quantitative detection of products and radical intermediates in low-temperature oxidation of cyclopentane. *J Phys Chem A* 2021;125:4467–79. <https://doi.org/10.1021/acs.jpca.1c02001>.
- [521] Lemaire O, Ribaucour M, Carlier M, Minetti R. The production of benzene in the low-temperature oxidation of cyclohexane, cyclohexene, and cyclohexa-1,3-diene. *Combust Flame* 2001;127:1971–80. [https://doi.org/10.1016/S0010-2180\(01\)00301-7](https://doi.org/10.1016/S0010-2180(01)00301-7).
- [522] Zou J, Jin H, Liu D, Zhang X, Su H, Yang J, et al. A comprehensive study on low-temperature oxidation chemistry of cyclohexane. II. Experimental and kinetic modeling investigation. *Combust Flame* 2022;235:111550. <https://doi.org/10.1016/j.combustflame.2021.111550>.
- [523] Roubaud A, Lemaire O, Minetti R, Sochet LR. High pressure auto-ignition and oxidation mechanisms of o-xylene, o-ethyltoluene, and n-butylbenzene between 600 and 900 K. *Combust Flame* 2000;123:561–71. [https://doi.org/10.1016/S0010-2180\(00\)00174-7](https://doi.org/10.1016/S0010-2180(00)00174-7).
- [524] Ribaucour M, Roubaud A, Minetti R, Sochet LR. The low-temperature autoignition of alkylaromatics: Experimental study and modeling of the oxidation of n-butylbenzene. *Proceedings of the Combustion Institute* 2000;28:1701–7. [https://doi.org/10.1016/S0082-0784\(00\)80570-6](https://doi.org/10.1016/S0082-0784(00)80570-6).
- [525] Husson B, Bounaceur R, Tanaka K, Ferrari M, Herbinet O, Glaude PA, et al. Experimental and modeling study of the oxidation of n-butylbenzene. *Combust Flame* 2012;159:1399–416. <https://doi.org/10.1016/j.combustflame.2011.12.006>.
- [526] Granata S, Faravelli T, Ranzi E. A wide range kinetic modeling study of the pyrolysis and combustion of naphthenes. *Combust Flame* 2003;132:533–44. [https://doi.org/10.1016/S0010-2180\(02\)00465-0](https://doi.org/10.1016/S0010-2180(02)00465-0).
- [527] Gulati SK, Walker RW. Addition of cyclohexane to slowly reacting H<sub>2</sub>-O<sub>2</sub> mixtures at 480°C. *J Chem Soc, Faraday Trans 2* 1989;85:1799–812. <https://doi.org/10.1039/F29898501799>.
- [528] Zou J, Li W, Ye L, Zhang X, Li Y, Yang J, et al. Exploring the low-temperature oxidation chemistry of cyclohexane in a jet-stirred reactor: An experimental and kinetic modeling study. *Chin J Chem Phys* 2018;31:537–46. <https://doi.org/10.1063/1674-0068/31/CJCP1806135>.
- [529] Zou J, Li Y, Ye L, Jin H. A comprehensive study on low-temperature oxidation chemistry of cyclohexane. I. Conformational analysis and theoretical study of first and second oxygen addition. *Combust Flame* 2022;235:111658. <https://doi.org/10.1016/j.combustflame.2021.111658>.
- [530] Sirjean B, Glaude PA, Ruiz-Lopèz MF, Fournet R. Theoretical kinetic study of thermal unimolecular decomposition of cyclic alkyl radicals. *J Phys Chem A* 2008;112:11598–610. <https://doi.org/10.1021/jp805640s>.

- [531] Cavallotti C, Rota R, Faravelli T, Ranzi E. Ab initio evaluation of primary cyclo-hexane oxidation reaction rates. *Proc Combust Inst* 2007;31:201–9. <https://doi.org/10.1016/j.proci.2006.07.195>.
- [532] Pitz WJ, Mueller CJ. Recent progress in the development of diesel surrogate fuels. *Prog Energy Combust Sci* 2011;37:330–50. <https://doi.org/10.1016/j.pecs.2010.06.004>.
- [533] Pitz WJ, Naik CV, Mhaolduin TN, Westbrook CK, Curran HJ, Orme JP, et al. Modeling and experimental investigation of methylcyclohexane ignition in a rapid compression machine. *Proc Combust Inst* 2007;31:267–75. <https://doi.org/10.1016/j.proci.2006.08.041>.
- [534] Mittal G, Sung C-J. Autoignition of methylcyclohexane at elevated pressures. *Combust Flame* 2009;156:1852–5. <https://doi.org/10.1016/j.combustflame.2009.05.009>.
- [535] Weber BW, Pitz WJ, Mehl M, Silke EJ, Davis AC, Sung C-J. Experiments and modeling of the autoignition of methylcyclohexane at high pressure. *Combust Flame* 2014;161:1972–83. <https://doi.org/10.1016/j.combustflame.2014.01.018>.
- [536] Yang Y, Boehman AL, Simmie JM. Effects of molecular structure on oxidation reactivity of cyclic hydrocarbons: Experimental observations and conformational analysis. *Combust Flame* 2010;157:2369–79. <https://doi.org/10.1016/j.combustflame.2010.04.015>.
- [537] Zou J, Zhang X, Li Y, Ye L, Xing L, Li W, et al. Experimental and kinetic modeling investigation on ethylcyclohexane low-temperature oxidation in a jet-stirred reactor. *Combust Flame* 2020;214:211–23. <https://doi.org/10.1016/j.combustflame.2019.12.038>.
- [538] Wang Z, Zhao L, Wang Y, Bian H, Zhang L, Zhang F, et al. Kinetics of ethylcyclohexane pyrolysis and oxidation: An experimental and detailed kinetic modeling study. *Combust Flame* 2015;162:2873–92. <https://doi.org/10.1016/j.combustflame.2015.03.017>.
- [539] Battin-Leclerc F, Warth V, Bounaceur R, Husson B, Herbinet O, Glaude P-A. The oxidation of large alkylbenzenes: An experimental and modeling study. *Proc Combust Inst* 2015;35:349–56. <https://doi.org/10.1016/j.proci.2014.05.087>.
- [540] Husson B. Étude en réacteur auto-agité par jets gazeux de l'oxydation d'hydrocarbures naphténiques et aromatiques présents dans les gazoles. These de doctorat. Université de Lorraine, 2013.
- [541] Diévert P, Dagaut P. The oxidation of n-butylbenzene: Experimental study in a JSR at 10atm and detailed chemical kinetic modeling. *Proc Combust Inst* 2011;33:209–16. <https://doi.org/10.1016/j.proci.2010.05.013>.
- [542] Roubaud A, Minetti R, Sochet LR. Oxidation and combustion of low alkylbenzenes at high pressure: comparative reactivity and auto-ignition. *Combust Flame* 2000;121:535–41. [https://doi.org/10.1016/S0010-2180\(99\)00169-8](https://doi.org/10.1016/S0010-2180(99)00169-8).
- [543] Ye L, Wang D, Bian H, Li B, Gao W, Bi M. Exploring the chemical kinetics on oxygen addition reactions of o-xylyl radical at the low temperature. *Combust Flame* 2021;227:95–105. <https://doi.org/10.1016/j.combustflame.2021.01.002>.
- [544] Zhou C-W, Farooq A, Yang L, Mebel AM. Combustion chemistry of alkenes and alkadienes. *Prog Energy Combust Sci* 2022;90:100983. <https://doi.org/10.1016/j.pecs.2021.100983>.
- [545] Baldwin RR, Lodhi ZH, Stothard N, Walker RW. The oxidation chemistry of allyl radicals and related “stable” radicals. *Proc Combust Inst* 1991;23:123–30. [https://doi.org/10.1016/S0082-0784\(06\)80250-X](https://doi.org/10.1016/S0082-0784(06)80250-X).
- [546] Stark MS, Waddington DJ. Oxidation of propene in the gas phase. *Int J Chem Kinet* 1995;27:123–51. <https://doi.org/10.1002/kin.550270205>.
- [547] Stark MS. Epoxidation of Alkenes by Peroxyl Radicals in the Gas Phase: Structure–Activity Relationships. *J Phys Chem A* 1997;101:8296–301. <https://doi.org/10.1021/jp972054+>.

- [548] Meng X, Rodriguez A, Herbinet O, Wang T, Battin-Leclerc F. Revisiting 1-hexene low-temperature oxidation. *Combust Flame* 2017;181:283–99. <https://doi.org/10.1016/j.combustflame.2017.03.031>.
- [549] Burke SM, Metcalfe W, Herbinet O, Battin-Leclerc F, Haas FM, Santner J, et al. An experimental and modeling study of propene oxidation. Part 1: Speciation measurements in jet-stirred and flow reactors. *Combust Flame* 2014;161:2765–84. <https://doi.org/10.1016/j.combustflame.2014.05.010>.
- [550] Westbrook CK, Pitz WJ, Mehl M, Glaude P-A, Herbinet O, Bax S, et al. Experimental and kinetic modeling study of 2-methyl-2-butene: allylic hydrocarbon kinetics. *J Phys Chem A* 2015;119:7462–80. <https://doi.org/10.1021/acs.jpca.5b00687>.
- [551] Vermeire FH, De Bruycker R, Herbinet O, Carstensen H-H, Battin-Leclerc F, Marin GB, et al. Experimental and kinetic modeling study of the pyrolysis and oxidation of 1,5-hexadiene: The reactivity of allylic radicals and their role in the formation of aromatics. *Fuel* 2017;208:779–90. <https://doi.org/10.1016/j.fuel.2017.07.042>.
- [552] Ribaucour M, Lemaire O, Minetti R. Low-temperature oxidation and autoignition of cyclohexene: A modeling study. *Proc Combust Inst* 2002;29:1303–10. [https://doi.org/10.1016/S1540-7489\(02\)80160-2](https://doi.org/10.1016/S1540-7489(02)80160-2).
- [553] Zádor J, Jasper AW, Miller JA. The reaction between propene and hydroxyl. *Phys Chem Chem Phys* 2009;11:11040–53. <https://doi.org/10.1039/B915707G>.
- [554] Lizardo-Huerta JC, Sirjean B, Bounaceur R, Fournet R. Intramolecular effects on the kinetics of unimolecular reactions of  $\beta$ -HORO $\cdot$  and HOQ $\cdot$ OOH radicals. *Phys Chem Chem Phys* 2016;18:12231–51. <https://doi.org/10.1039/C6CP00111D>.
- [555] Goldsmith CF, Klippenstein SJ, Green WH. Theoretical rate coefficients for allyl+HO $_2$  and allyloxy decomposition. *Proc Combust Inst* 2011;33:273–82. <https://doi.org/10.1016/j.proci.2010.05.054>.
- [556] Cao C, Zhang X, Zhang Y, Zou J, Li Y, Yang J, et al. Probing the fuel-specific intermediates in the low-temperature oxidation of 1-heptene and modeling interpretation. *Proc Combust Inst* 2021;38:385–94. <https://doi.org/10.1016/j.proci.2020.06.025>.
- [557] Lee J, Bozzelli JW. Thermochemical and kinetic analysis of the allyl radical with O $_2$  reaction system. *Proc Combust Inst* 2005;30:1015–22. <https://doi.org/10.1016/j.proci.2004.08.092>.
- [558] Döntgen M, Pekkanen TT, Joshi SP, Timonen RS, Eskola AJ. Oxidation kinetics and thermodynamics of resonance-stabilized radicals: the pent-1-en-3-yl + O $_2$  reaction. *J Phys Chem A* 2019;123:7897–910. <https://doi.org/10.1021/acs.jpca.9b03923>.
- [559] Baldwin RR, Stout DR, Walker RW. Arrhenius parameters for the addition of HO $_2$  radicals to ethene between 400 and 500 °C. *J Chem Soc, Faraday Trans* 1991;87:2147–50. <https://doi.org/10.1039/FT9918702147>.
- [560] Guo J, Xu J, Li Z, Tan N, Li X. Temperature and Pressure Dependent Rate Coefficients for the Reaction of C $_2$ H $_4$  + HO $_2$  on the C $_2$ H $_4$ O $_2$ H Potential Energy Surface. *J Phys Chem A* 2015;119:3161–70. <https://doi.org/10.1021/jp511991n>.
- [561] Kohse-Höinghaus K. Combustion in the future: The importance of chemistry. *Proc Combust Inst* 2021;38:1–56. <https://doi.org/10.1016/j.proci.2020.06.375>.
- [562] Herbinet O, Pitz WJ, Westbrook CK. Detailed chemical kinetic oxidation mechanism for a biodiesel surrogate. *Combust Flame* 2008;154:507–28. <https://doi.org/10.1016/j.combustflame.2008.03.003>.
- [563] Rogers CO, Kaczmarek D, Kasper T, Labbe NJ. Probing the low-temperature chemistry of methyl hexanoate: Insights from oxygenate intermediates. *Proc Combust Inst* 2021;38:621–9. <https://doi.org/10.1016/j.proci.2020.07.056>.

- [564] Togbé C, May-Carle J-B, Dayma G, Dagaut P. Chemical kinetic study of the oxidation of a biodiesel–bioethanol surrogate fuel: methyl octanoate–ethanol mixtures. *J Phys Chem A* 2010;114:3896–908. <https://doi.org/10.1021/jp906882h>.
- [565] Dayma G, Togbé C, Dagaut P. Detailed kinetic mechanism for the oxidation of vegetable oil methyl esters: new evidence from methyl heptanoate. *Energy Fuels* 2009;23:4254–68. <https://doi.org/10.1021/ef900184y>.
- [566] Rouso AC, Jasper AW, Ju Y, Hansen N. Extreme low-temperature combustion chemistry: ozone-initiated oxidation of methyl hexanoate. *J Phys Chem A* 2020;124:9897–914. <https://doi.org/10.1021/acs.jpca.0c07584>.
- [567] Zhai Y, Feng B, Zhang Y, Mei B, Zou J, Yang J, et al. Experimental and kinetic modeling study of methyl heptanoate low-temperature oxidation in a jet-stirred reactor. *Fuel* 2021;283:118885. <https://doi.org/10.1016/j.fuel.2020.118885>.
- [568] Meng X, Herbinet O, Coniglio L, Wang T, Battin-Leclerc F. Gas-phase oxidation of methyl-10-undecenoate in a jet-stirred reactor. *Int J Chem Kinet* 2017;49:711–28. <https://doi.org/10.1002/kin.21109>.
- [569] Pelucchi M, Namysl S, Ranzi E, Frassoldati A, Herbinet O, Battin-Leclerc F, et al. An experimental and kinetic modelling study of n-C4–C6 aldehydes oxidation in a jet-stirred reactor. *Proc Combust Inst* 2019;37:389–97. <https://doi.org/10.1016/j.proci.2018.07.087>.
- [570] Serinyel Z, Lailliau M, Thion S, Dayma G, Dagaut P. An experimental chemical kinetic study of the oxidation of diethyl ether in a jet-stirred reactor and comprehensive modeling. *Combust Flame* 2018;193:453–62. <https://doi.org/10.1016/j.combustflame.2018.04.002>.
- [571] Belhadj N, Benoit R, Dagaut P, Lailliau M, Serinyel Z, Dayma G. Oxidation of di-n-propyl ether: Characterization of low-temperature products. *Proc Combust Inst* 2021;38:337–44. <https://doi.org/10.1016/j.proci.2020.06.350>.
- [572] Pelucchi M, Namysl S, Ranzi E, Rodriguez A, Rizzo C, Somers KP, et al. Combustion of n-C3–C6 linear alcohols: an experimental and kinetic modeling study. Part II: Speciation measurements in a jet-stirred reactor, ignition delay time measurements in a rapid compression machine, model validation, and kinetic analysis. *Energy Fuels* 2020;34:14708–25. <https://doi.org/10.1021/acs.energyfuels.0c02252>.
- [573] De Bruycker R, Herbinet O, Carstensen H-H, Battin-Leclerc F, Van Geem KM. Understanding the reactivity of unsaturated alcohols: Experimental and kinetic modeling study of the pyrolysis and oxidation of 3-methyl-2-butenol and 3-methyl-3-butenol. *Combust Flame* 2016;171:237–51. <https://doi.org/10.1016/j.combustflame.2016.06.009>.
- [574] Pelucchi M, Ranzi E, Frassoldati A, Faravelli T. Alkyl radicals rule the low temperature oxidation of long chain aldehydes. *Proc Combust Inst* 2017;36:393–401. <https://doi.org/10.1016/j.proci.2016.05.051>.
- [575] Namysl S. Experimental study of the formation of pollutants during the combustion of bio-oil surrogate molecules. These de doctorat. Université de Lorraine, 2019.
- [576] Ranzi E, Frassoldati A, Stagni A, Pelucchi M, Cuoci A, Faravelli T. Reduced kinetic schemes of complex reaction systems: Fossil and biomass-derived transportation fuels. *Int J Chem Kinet* 2014;46:512–42.
- [577] Togbé C, Dagaut P, Mzé-Ahmed A, Diévar P, Halter F, Foucher F. Experimental and detailed kinetic modeling study of 1-hexanol oxidation in a pressurized jet-stirred reactor and a combustion bomb. *Energy Fuels* 2010;24:5859–75. <https://doi.org/10.1021/ef101255w>.
- [578] Welz O, Zádor J, Savee JD, Sheps L, Osborn DL, Taatjes CA. Low-temperature combustion chemistry of n-butanol: principal oxidation pathways of hydroxybutyl radicals. *J Phys Chem A* 2013;117:11983–2001. <https://doi.org/10.1021/jp403792t>.

- [579] Hartness SW, Rotavera B. Dependence of Biofuel Ignition Chemistry on OH-Initiated Branching Fractions. *Frontiers in Mechanical Engineering* 2021;7:76. <https://doi.org/10.3389/fmech.2021.718598>.
- [580] Cai L, Uygun Y, Togbé C, Pitsch H, Olivier H, Dagaut P, et al. An experimental and modeling study of n-octanol combustion. *Proc Combust Inst* 2015;35:419–27. <https://doi.org/10.1016/j.proci.2014.05.088>.
- [581] Serinyel Z, Togbé C, Dayma G, Dagaut P. An experimental and modeling study of 2-methyl-1-butanol oxidation in a jet-stirred reactor. *Combust Flame* 2014;161:3003–13. <https://doi.org/10.1016/j.combustflame.2014.06.004>.
- [582] Welz O, Savee JD, Osborn DL, Taatjes CA. Chlorine atom-initiated low-temperature oxidation of prenol and isoprenol: The effect of CC double bonds on the peroxy radical chemistry in alcohol oxidation. *Proc Combust Inst* 2015;35:401–8. <https://doi.org/10.1016/j.proci.2014.05.004>.
- [583] Cai L, vom Lehn F, Pitsch H. Higher alcohol and ether biofuels for compression-ignition engine application: A review with emphasis on combustion kinetics. *Energy Fuels* 2021;35:1890–917. <https://doi.org/10.1021/acs.energyfuels.0c03590>.
- [584] Thion S, Togbé C, Serinyel Z, Dayma G, Dagaut P. A chemical kinetic study of the oxidation of dibutyl-ether in a jet-stirred reactor. *Combust Flame* 2017;185:4–15. <https://doi.org/10.1016/j.combustflame.2017.06.019>.
- [585] Fan X, Sun W, Liu Z, Gao Y, Yang J, Yang B, et al. Exploring the oxidation chemistry of diisopropyl ether: Jet-stirred reactor experiments and kinetic modeling. *Proc Combust Inst* 2021;38:321–8. <https://doi.org/10.1016/j.proci.2020.06.242>.
- [586] Serinyel Z, Lailliau M, Dayma G, Dagaut P. A high pressure oxidation study of di-n-propyl ether. *Fuel* 2020;263:116554. <https://doi.org/10.1016/j.fuel.2019.116554>.
- [587] Fan X, Sun W, Gao Y, Hansen N, Chen B, Pitsch H, et al. Chemical insights into the multi-regime low-temperature oxidation of di-n-propyl ether: Jet-stirred reactor experiments and kinetic modeling. *Combustion and Flame* 2021;233:111592. <https://doi.org/10.1016/j.combustflame.2021.111592>.
- [588] Cai L, Sudholt A, Lee DJ, Egolfopoulos FN, Pitsch H, Westbrook CK, et al. Chemical kinetic study of a novel lignocellulosic biofuel: Di-n-butyl ether oxidation in a laminar flow reactor and flames. *Combust Flame* 2014;161:798–809. <https://doi.org/10.1016/j.combustflame.2013.10.003>.
- [589] Marrodán L, Royo E, Millera Á, Bilbao R, Alzueta MU. High pressure oxidation of dimethoxymethane. *Energy Fuels* 2015;29:3507–17. <https://doi.org/10.1021/acs.energyfuels.5b00459>.
- [590] Belhadj N, Benoit R, Dagaut P, Lailliau M. Experimental characterization of tetrahydrofuran low-temperature oxidation products including ketohydroperoxides and highly oxygenated molecules. *Energy Fuels* 2021;35:7242–52. <https://doi.org/10.1021/acs.energyfuels.0c03291>.
- [591] Bogan DJ, Hand CW. Absolute rate constant, kinetic isotope effect and mechanism of the reaction of ethylene oxide with oxygen(3P) atoms. *J Phys Chem* 1978;82:2067–73. <https://doi.org/10.1021/j100508a006>.
- [592] Ravishankara AR, Davis DD. Kinetic rate constants for the reaction of hydroxyl with methanol, ethanol, and tetrahydrofuran at 298 K. *J Phys Chem* 1978;82:2852–3. <https://doi.org/10.1021/j100515a022>.
- [593] Duke MG, Holbrook KA. Reactions of methyl radicals with oxetan, 2-methyloxetan and 2,4-dimethyloxetan. *J Chem Soc, Faraday Trans 1* 1980;76:1232–9. <https://doi.org/10.1039/F19807601232>.

- [594] Lifshitz A, Ben-Hamou H. Thermal reactions of cyclic ethers at high temperatures. 1. Pyrolysis of ethylene oxide behind reflected shocks. *J Phys Chem* 1983;87:1782–7. <https://doi.org/10.1021/j100233a026>.
- [595] Schliephake V, Mix K-H, Wagner HG. Investigations of the kinetics of the reactions of tetrahydrofuran, tetrahydropyran, cyclopentanone and cyclohexanone with atomic oxygen. *Z Physik Chem* 1986;150:1–15. <https://doi.org/10.1524/zpch.1986.150.1.001>.
- [596] Dagaut Philippe, Liu Renzhang, Wallington TJ, Kurylo MJ. Flash photolysis resonance fluorescence investigation of the gas-phase reactions of hydroxyl radicals with cyclic ethers. *J Phys Chem* 1990;94:1881–3. <https://doi.org/10.1021/j100368a030>.
- [597] Atkinson R. A structure-activity relationship for the estimation of rate constants for the gas-phase reactions of OH radicals with organic compounds. *Int J Chem Kinet* 1987;19:799–828. <https://doi.org/10.1002/kin.550190903>.
- [598] Wallington TJ, Liu R, Dagaut P, Kurylo MJ. The gas phase reactions of hydroxyl radicals with a series of aliphatic ethers over the temperature range 240–440 K. *Int J Chem Kinet* 1988;20:41–9. <https://doi.org/10.1002/kin.550200106>.
- [599] Wallington TJ, Dagaut P, Kurylo MJ. Correlation between gas-phase and solution-phase reactivities of hydroxyl radicals towards saturated organic compounds. *J Phys Chem* 1988;92:5024–8. <https://doi.org/10.1021/j100328a039>.
- [600] Liu R, Dagaut P, Huie RE, Kurylo MJ. A flash photolysis resonance fluorescence investigation of the reactions of Oxygen O(3P) atoms with aliphatic ethers and diethers in the gas phase. *Int J Chem Kinet* 1990;22:711–7. <https://doi.org/10.1002/kin.550220707>.
- [601] Winer AM, Lloyd AC, Darnall KR, Atkinson R, Pitts JN. Rate constants for the reaction of OH radicals with n-propyl acetate, sec-butyl acetate, tetrahydrofuran and peroxyacetyl nitrate. *Chem Phys Lett* 1977;51:221–6. [https://doi.org/10.1016/0009-2614\(77\)80388-6](https://doi.org/10.1016/0009-2614(77)80388-6).
- [602] Moriarty J, Sidebottom H, Wenger J, Mellouki A, Le Bras G. Kinetic studies on the reactions of hydroxyl radicals with cyclic ethers and aliphatic diethers. *J Phys Chem A* 2003;107:1499–505. <https://doi.org/10.1021/jp021267i>.
- [603] Middala S, Campbell S, Olea C, Scruggs A, Hasson AS. Kinetics and mechanism of the reaction of propylene oxide with chlorine atoms and hydroxy radicals. *Int J Chem Kinet* 2011;43:507–21. <https://doi.org/10.1002/kin.20580>.
- [604] Barnes I, Kirschbaum S, Simmie JM. Combined experimental and theoretical study of the reactivity of  $\gamma$ -butyro- and related lactones, with the OH radical at room temperature. *J Phys Chem A* 2014;118:5013–9. <https://doi.org/10.1021/jp502489k>.
- [605] Illés Á, Farkas M, Zügner GL, Novodárszki G, Mihályi M, Dóbé S. Direct and relative rate coefficients for the gas-phase reaction of OH radicals with 2-methyltetrahydrofuran at room temperature. *Reac Kinet Mech Cat* 2016;119:5–18. <https://doi.org/10.1007/s11144-016-1037-2>.
- [606] Giri BR, Khaled F, Szőri M, Viskolcz B, Farooq A. An experimental and theoretical kinetic study of the reaction of OH radicals with tetrahydrofuran. *Proc Combust Inst* 2017;36:143–50. <https://doi.org/10.1016/j.proci.2016.06.016>.
- [607] Illés Á, Rózsa ZB, Thangaraj R, Décsiné Gombos E, Dóbé S, Giri BR, et al. An experimental and theoretical kinetic study of the reactions of hydroxyl radicals with tetrahydrofuran and two deuterated tetrahydrofurans. *Chem Phys Lett* 2021;776:138698. <https://doi.org/10.1016/j.cplett.2021.138698>.
- [608] Chakravarty HK, Fernandes RX. Reaction kinetics of hydrogen abstraction reactions by hydroperoxyl radical from 2-methyltetrahydrofuran and 2,5-dimethyltetrahydrofuran. *J Phys Chem A* 2013;117:5028–41. <https://doi.org/10.1021/jp402801c>.
- [609] Saheb V, Bahadori A. Theoretical studies on the kinetics of the hydrogen-abstraction reactions from 1,3,5-trioxane and 1,4-dioxane by OH radicals. *Prog React Kinet Mech* 2020;45:1468678319899252. <https://doi.org/10.1177/1468678319899252>.



- [610] Dagaut P, Voisin D, Cathonnet M, McGuinness M, Simmie J. The oxidation of ethylene oxide in a jet-stirred reactor and its ignition in shock waves. *Combust Flame* 1996;106:62–8. [https://doi.org/10.1016/0010-2180\(95\)00229-4](https://doi.org/10.1016/0010-2180(95)00229-4).
- [611] Lopez JG, Rasmussen CL, Alzueta MU, Gao Y, Marshall P, Glarborg P. Experimental and kinetic modeling study of C<sub>2</sub>H<sub>4</sub> oxidation at high pressure. *Proc Combust Inst* 2009;32:367–75. <https://doi.org/10.1016/j.proci.2008.06.188>.
- [612] Lockwood KS, Labbe NJ. Insights on keto-hydroperoxide formation from O<sub>2</sub> addition to the beta-tetrahydrofuran radical. *Proc Combust Inst* 2021;38:533–41. <https://doi.org/10.1016/j.proci.2020.06.357>.
- [613] Lifshitz A, Bidani M, Bidani S. Thermal reactions of cyclic ethers at high temperatures. 2. Pyrolysis of tetrahydrofuran behind reflected shocks. *J Phys Chem* 1986;90:3422–9.
- [614] Lifshitz A, Tamburu C. Isomerization and decomposition of propylene oxide. Studies with a single-pulse shock tube. *J Phys Chem* 1994;98:1161–70. <https://doi.org/10.1021/j100055a020>.
- [615] Holbrook KA, Scott RA. Gas-phase thermal unimolecular decomposition of oxetan. *J Chem Soc, Faraday Trans 1* 1975;71:1849–56. <https://doi.org/10.1039/F19757101849>.
- [616] Baldwin RR, Keen A, Walker RW. Studies of the decomposition of oxirane and of its addition to slowly reacting mixtures of hydrogen and oxygen at 480 °C. *J Chem Soc, Faraday Trans 1* 1984;80:435–56. <https://doi.org/10.1039/F19848000435>.
- [617] Joshi A, You X, Barckholtz TA, Wang H. Thermal decomposition of ethylene oxide: potential energy surface, master equation analysis, and detailed kinetic modeling. *J Phys Chem A* 2005;109:8016–27. <https://doi.org/10.1021/jp0516442>.
- [618] Verdicchio M, Sirjean B, Tran LS, Glaude P-A, Battin-Leclerc F. Unimolecular decomposition of tetrahydrofuran: Carbene vs. diradical pathways. *Proc Combust Inst* 2015;35:533–41. <https://doi.org/10.1016/j.proci.2014.08.015>.
- [619] Shiroudi A, Tahan A, Zahedi E. The unimolecular thermal decomposition of oxetane and its methyl derivatives: An Ab initio and RRKM calculations. *Russ J Phys Chem* 2012;86:1245–9. <https://doi.org/10.1134/S0036024412060246>.
- [620] Dubnikova F, Lifshitz A. Isomerization of propylene oxide. quantum chemical calculations and kinetic modeling. *J Phys Chem A* 2000;104:4489–96. <https://doi.org/10.1021/jp994485t>.
- [621] Lizardo-Huerta J-C, Sirjean B, Glaude P-A, Fournet R. Pericyclic reactions in ether biofuels. *Proc Combust Inst* 2017;36:569–76. <https://doi.org/10.1016/j.proci.2016.07.035>.
- [622] Wang H, Bozzelli JW. Thermochemistry and Kinetic Analysis of the Unimolecular Oxiranyl Radical Dissociation Reaction: A Theoretical Study. *ChemPhysChem* 2016;17:1983–92. <https://doi.org/10.1002/cphc.201600152>.
- [623] Dagaut P, Cathonnet M, McGuinness M, Simmie JM. The ignition of oxetane in shock waves and oxidation in a jet-stirred reactor: An experimental and kinetic modeling study. *Combust Flame* 1997;110:409–17. [https://doi.org/10.1016/S0010-2180\(97\)00075-8](https://doi.org/10.1016/S0010-2180(97)00075-8).
- [624] Antonov IO, Zádor J, Rotavera B, Papajak E, Osborn DL, Taatjes CA, et al. Pressure-Dependent Competition among Reaction Pathways from First- and Second-O<sub>2</sub> Additions in the Low-Temperature Oxidation of Tetrahydrofuran. *J Phys Chem A* 2016;120:6582–95. <https://doi.org/10.1021/acs.jpca.6b05411>.
- [625] Hansen N, Moshhammer K, Jasper AW. Isomer-selective detection of keto-hydroperoxides in the low-temperature oxidation of tetrahydrofuran. *J Phys Chem A* 2019;123:8274–84. <https://doi.org/10.1021/acs.jpca.9b07017>.
- [626] Labbe NJ, Seshadri V, Kasper T, Hansen N, Oßwald P, Westmoreland PR. Flame chemistry of tetrahydropyran as a model heteroatomic biofuel. *Proc Combust Inst* 2013;34:259–67. <https://doi.org/10.1016/j.proci.2012.07.027>.

- [627] Dagaut P, McGuinness M, Simmie JM, Cathonnet M. The ignition and oxidation of tetrahydropyran : experiments and kinetic modeling. *Combust Sci Technol* 1997;129:1–16. <https://doi.org/10.1080/00102209708935717>.
- [628] Telfah H, Reza MA, Alam J, Paul AC, Liu J. Direct observation of tetrahydrofuran and tetrahydropyran peroxy radicals via cavity ring-down spectroscopy. *J Phys Chem Lett* 2018;9:4475–80. <https://doi.org/10.1021/acs.jpcclett.8b01721>.
- [629] Chen M-W, Rotavera B, Chao W, Zádor J, Taatjes CA. Direct measurement of  $\cdot\text{OH}$  and  $\text{HO}_2\cdot$  formation in  $\cdot\text{R} + \text{O}_2$  reactions of cyclohexane and tetrahydropyran. *Phys Chem Chem Phys* 2018;20:10815–25. <https://doi.org/10.1039/C7CP08164B>.
- [630] Dubnikova F, Lifshitz A. Isomerization of 2,3-dihydrofuran and 5-methyl-2,3-dihydrofuran: quantum chemical and kinetics calculations. *J Phys Chem A* 2002;106:1026–34. <https://doi.org/10.1021/jp012714h>.
- [631] Lifshitz A, Bidani M. Thermal reactions of cyclic ethers at high temperatures. 5. Pyrolysis of 2,3-dihydrofuran behind reflected shocks. *J Phys Chem* 1989;93:1139–44. <https://doi.org/10.1021/j100340a024>.
- [632] Lifshitz A, Bidani M, Bidani S. Thermal reactions of cyclic ethers at high temperatures. 4. Pyrolysis of 2,5-dihydrofuran behind reflected shocks. *J Phys Chem* 1986;90:6011–4.
- [633] Fan X, Wang X, Wang J, Yang K. Comparative shock tube and kinetic study on high-temperature ignition of 2,3-dihydrofuran and 2,5-dihydrofuran. *Energy Fuels* 2016;30:8727–36. <https://doi.org/10.1021/acs.energyfuels.6b01332>.
- [634] Dubnikova F, Lifshitz A. Molecular hydrogen elimination from 2,5-dihydrofuran, 2,3-dihydrofuran, and 2-methyl-2,5-dihydrofuran: Quantum chemical and kinetics calculations. *Int J Chem Kinet* 2001;33:685–97. <https://doi.org/10.1002/kin.1065>.
- [635] Westbrook CK, Curran HJ. Chapter 7 - Detailed kinetics of fossil and renewable fuel combustion. In: Faravelli T, Manenti F, Ranzi E, editors. *Computer Aided Chemical Engineering*, vol. 45, Elsevier; 2019, p. 363–443. <https://doi.org/10.1016/B978-0-444-64087-1.00007-3>.
- [636] Sendt K, Bacskay GB, Mackie JC. Pyrolysis of furan : ab initio quantum chemical and kinetic modeling studies. *J Phys Chem A* 2000;104:1861–75. <https://doi.org/10.1021/jp993537b>.
- [637] Vasiliou A, Nimlos MR, Daily JW, Ellison GB. Thermal decomposition of furan generates propargyl radicals. *J Phys Chem A* 2009;113:8540–7. <https://doi.org/10.1021/jp903401h>.
- [638] Cheng Z, Tan Y, Wei L, Xing L, Yang J, Zhang L, et al. Experimental and kinetic modeling studies of furan pyrolysis: Fuel decomposition and aromatic ring formation. *Fuel* 2017;206:239–47. <https://doi.org/10.1016/j.fuel.2017.05.090>.
- [639] Simmie JM, Metcalfe WK. Ab initio study of the decomposition of 2,5-dimethylfuran. *J Phys Chem A* 2011;115:8877–88. <https://doi.org/10.1021/jp2039477>.
- [640] Vermeire FH, Yang J, Cao C, Liu Z, Marin GB, Van Geem KM. Thermal decomposition of furans with oxygenated substituents: A combined experimental and quantum chemical study. *Proc Combust Inst* 2021;38:699–707. <https://doi.org/10.1016/j.proci.2020.07.124>.
- [641] Djokic M, Carstensen H-H, Van Geem KM, Marin GB. The thermal decomposition of 2,5-dimethylfuran. *Proc Combust Inst* 2013;34:251–8. <https://doi.org/10.1016/j.proci.2012.05.066>.
- [642] Sirjean B, Fournet R. Theoretical study of the thermal decomposition of the 5-methyl-2-furanylmethyl radical. *J Phys Chem A* 2012;116:6675–84. <https://doi.org/10.1021/jp303680h>.
- [643] Burcat A. Kinetics of the ignition of fuels in artificial air mixtures. I. The oxidation of ethylene oxide. *Combust Sci Technol* 1980;21:169–74. <https://doi.org/10.1080/00102208008946930>.

- [644] Kang J-G, Ryu J-C, Choi ES, Kang SK, Yeo H-G. Determination of ignition delay times in mixtures of ethylene oxide, oxygen, and argon behind a reflected shock. *Combust Flame* 1996;106:81–8. [https://doi.org/10.1016/0010-2180\(95\)00244-8](https://doi.org/10.1016/0010-2180(95)00244-8).
- [645] Yoon H, Yeo H, Yun SS, Kim C, Kang J-G. Ignition delay times in ethylene oxide-oxygen-argon mixtures behind a reflected shock. *Combust Flame* 1993;92:481–4. [https://doi.org/10.1016/0010-2180\(93\)90160-5](https://doi.org/10.1016/0010-2180(93)90160-5).
- [646] Lifshitz A, Suslensky A. Shock-initiated ignition in ethylene oxide, propylene oxide, 1,2-epoxybutane, and 2,3-epoxybutane. *Proc Combust Inst* 1994;25:1571–7. [https://doi.org/10.1016/S0082-0784\(06\)80802-7](https://doi.org/10.1016/S0082-0784(06)80802-7).
- [647] Würmel J, McGuinness M, Simmie J. High-temperature oxidation of ethylene oxide in shock waves. *J Chem Soc, Faraday Trans* 1996;92:715–21. <https://doi.org/10.1039/FT9969200715>.
- [648] Burluka AA, Harker M, Osman H, Sheppard CGW, Konnov AA. Laminar burning velocities of three C<sub>3</sub>H<sub>6</sub>O isomers at atmospheric pressure. *Fuel* 2010;89:2864–72. <https://doi.org/10.1016/j.fuel.2010.02.004>.
- [649] Ramalingam A, Minwegen H, Fenard Y, Heufer KA. Insights into the oxidation of propylene oxide through the analysis of experiments and kinetic modeling. *Proc Combust Inst* 2021;38:459–67. <https://doi.org/10.1016/j.proci.2020.06.290>.
- [650] Knyazkov DA, Dmitriev AM, Korobeinichev OP, Osipova KN, Pio G, Shmakov AG, et al. Structure of premixed flames of propylene oxide: Molecular beam mass spectrometric study and numerical simulation. *Proc Combust Inst* 2021;38:2467–75. <https://doi.org/10.1016/j.proci.2020.06.336>.
- [651] Lifshitz A, Tamburu C. Isomerization and decomposition of 2,3-dimethyloxirane. studies with a single-pulse shock tube. *J Phys Chem* 1995;99:10251–60. <https://doi.org/10.1021/j100025a028>.
- [652] Wang X, Chen R, He B, Li D, Qin M, Fan X. Laminar flame characteristics of THF family fuels at elevated temperatures and pressures. *Fuel* 2020;273:117721. <https://doi.org/10.1016/j.fuel.2020.117721>.
- [653] Dagaut P, McGuinness M, Simmie JM, Cathonnet M. The ignition and oxidation of tetrahydrofuran: experiments and kinetic modeling. *Combust Sci Technol* 1998;135:3–29. <https://doi.org/10.1080/00102209808924147>.
- [654] Sudholt A, Lee C, Klankermayer J, Fernandes RX, Pitsch H. Ignition characteristics of saturated and unsaturated furans. *Combust Flame* 2016;171:133–6. <https://doi.org/10.1016/j.combustflame.2016.05.016>.
- [655] Wu Y, Xu N, Yang M, Liu Y, Tang C, Huang Z. Ignition delay time measurement and kinetic modeling of furan, and comparative studies of 2,3-dihydrofuran and tetrahydrofuran at low to intermediate temperatures by using a rapid compression machine. *Combust Flame* 2020;213:226–36. <https://doi.org/10.1016/j.combustflame.2019.12.010>.
- [656] Kasper T, Lucassen A, Jasper AW, Li W, Westmoreland PR, Kohse-Höinghaus K, et al. Identification of tetrahydrofuran reaction pathways in premixed flames. *Z Physik Chem* 2011;225:1237–70. <https://doi.org/10.1524/zpch.2011.0163>.
- [657] Molera MJ, Couto A, Garcia-Dominguez JA. Gas phase oxidation of tetrahydrofuran. *Int J Chem Kinet* 1988;20:673–85. <https://doi.org/10.1002/kin.550200902>.
- [658] De Bruycker R, Tran L-S, Carstensen H-H, Glaude P-A, Monge F, Alzueta MU, et al. Experimental and modeling study of the pyrolysis and combustion of 2-methyl-tetrahydrofuran. *Combust Flame* 2017;176:409–28. <https://doi.org/10.1016/j.combustflame.2016.11.017>.

- [659] Wang X, Fan X, Yang K, Wang J, Jiao X, Guo Z. Laminar flame characteristics and chemical kinetics of 2-methyltetrahydrofuran and the effect of blending with isooctane. *Combust Flame* 2018;191:213–25. <https://doi.org/10.1016/j.combustflame.2017.12.028>.
- [660] Li Y, Xu W, Jiang Y, Liew KM, Qiu R. Laminar burning velocities of 2-methyltetrahydrofuran at elevated pressures. *Proc Combust Inst* 2021;38:2175–83. <https://doi.org/10.1016/j.proci.2020.06.253>.
- [661] Wang J, Wang X, Fan X, Yang K. Shock tube experimental and modeling study of MTHF ignition characteristics at high temperatures. Warrendale, PA: SAE International; 2015. <https://doi.org/10.4271/2015-01-1807>.
- [662] Wang J, Wang X, Fan X, Yang K, Zhang Y. An ignition delay time and kinetic study of 2-methyltetrahydrofuran at high temperatures. *Fuel* 2016;186:758–69. <https://doi.org/10.1016/j.fuel.2016.08.104>.
- [663] Tripathi R, Lee C, Fernandes RX, Olivier H, Curran HJ, Mani Sarathy S, et al. Ignition characteristics of 2-methyltetrahydrofuran: An experimental and kinetic study. *Proc Combust Inst* 2017;36:587–95. <https://doi.org/10.1016/j.proci.2016.07.103>.
- [664] Jouzdani S, Zheng X, Zhou A, Akih-Kumgeh B. Shock tube investigation of methyl tert butyl ether and methyl tetrahydrofuran high-temperature kinetics. *Int J Chem Kinet* 2019;51:848–60. <https://doi.org/10.1002/kin.21314>.
- [665] Jouzdani S, Eldeeb MA, Zhang L, Akih-Kumgeh B. High-temperature study of 2-methyl furan and 2-methyl tetrahydrofuran combustion. *Int J Chem Kinet* 2016;48:491–503. <https://doi.org/10.1002/kin.21008>.
- [666] Fenard Y, Boumechdi MA, Vanhove G. Experimental and kinetic modeling study of 2-methyltetrahydrofuran oxidation under engine-relevant conditions. *Combust Flame* 2017;178:168–81. <https://doi.org/10.1016/j.combustflame.2017.01.008>.
- [667] Moshhammer K, Vranckx S, Chakravarty HK, Parab P, Fernandes RX, Kohse-Höinghaus K. An experimental and kinetic modeling study of 2-methyltetrahydrofuran flames. *Combust Flame*, 2013;160:2729–43. <https://doi.org/10.1016/j.combustflame.2013.07.006>.
- [668] Tran L-S, Carstensen H-H, Lamoureux N, Foo KK, Gosselin S, El Bakali A, et al. Exploring the flame chemistry of C5 tetrahydrofuranic biofuels: tetrahydrofurfuryl alcohol and 2-methyltetrahydrofuran. *Energy Fuels* 2021;35:18699–715. <https://doi.org/10.1021/acs.energyfuels.1c01949>.
- [669] Tripathi R, Ramalingam AK, Minwegen H, Alqaity ABS, Heufer KA, Pitsch H. Unraveling the high reactivity of 3-methyltetrahydrofuran over 2-methyltetrahydrofuran through kinetic modeling and experiments. *Proc Combust Inst* 2019;37:221–30. <https://doi.org/10.1016/j.proci.2018.05.129>.
- [670] Fenard Y, Song H, Minwegen H, Parab P, Sampaio Mergulhão C, Vanhove G, et al. 2,5-Dimethyltetrahydrofuran combustion: Ignition delay times at high and low temperatures, speciation measurements and detailed kinetic modeling. *Combust Flame* 2019;203:341–51. <https://doi.org/10.1016/j.combustflame.2019.02.022>.
- [671] Wang Q-P, Tang X-Y, Yang J-Z, Zhang Y, Cao C-C, Zhai Y-T, et al. Low pressure pyrolysis experiment and kinetic modeling study of 2,5-dimethyltetrahydrofuran. *K Cheng Je Wu Li Hsueh Pao/J Eng Thermophys* 2019;40:2928–37.
- [672] Cai L, Minwegen H, Beeckmann J, Burke U, Tripathi R, Ramalingam A, et al. Experimental and numerical study of a novel biofuel: 2-Butyltetrahydrofuran. *Combust Flame* 2017;178:257–67. <https://doi.org/10.1016/j.combustflame.2016.12.021>.
- [673] De Bruycker R, Carstensen H-H, Simmie JM, Van Geem KM, Marin GB. Experimental and computational study of the initial decomposition of gamma-valerolactone. *Proc Combust Inst* 2015;35:515–23. <https://doi.org/10.1016/j.proci.2014.04.001>.

- [674] Sudholt A, Tripathi R, Mayer D, Glaude P-A, Battin-Leclerc F, Pitsch H. The oxidation of the novel lignocellulosic biofuel  $\gamma$ -valerolactone in a low pressure flame. *Proc Combust Inst* 2017;36:577–85. <https://doi.org/10.1016/j.proci.2016.05.025>.
- [675] Wildenberg A, Fenard Y, Carbonnier M, Kéromnès A, Lefort B, Serinyel Z, et al. An experimental and kinetic modeling study on the oxidation of 1,3-dioxolane. *Proc Combust Inst* 2021;38:543–53. <https://doi.org/10.1016/j.proci.2020.06.362>.
- [676] Cutler AH, Antal MJ, Jones M. Kinetics and mechanism of the vapor phase pyrolysis of 1,3-dioxolane in steam. *J Anal Appl Pyrolysis* 1987;12:223–42. [https://doi.org/10.1016/0165-2370\(87\)85003-9](https://doi.org/10.1016/0165-2370(87)85003-9).
- [677] Fernández-Sánchez E, García-Domínguez JA, De la Iglesia-Gayá B. Radical-sensitized thermal decomposition of 1,3-dioxolane in the gas phase. *J Anal Appl Pyrolysis* 1991;18:219–32. [https://doi.org/10.1016/0165-2370\(91\)87003-5](https://doi.org/10.1016/0165-2370(91)87003-5).
- [678] Battin F, Marquaire PM, Baronnet F, Côme GM. Products of the gas-phase pyrolysis of 1,4-dioxane. *J Anal Appl Pyrolysis* 1989;16:345–54. [https://doi.org/10.1016/0165-2370\(89\)80017-8](https://doi.org/10.1016/0165-2370(89)80017-8).
- [679] Battin F, Scacchi G, Baronnet F. Gas-phase oxidation of 1,4-dioxane. *Int J Chem Kinet* 1991;23:861–79. <https://doi.org/10.1002/kin.550231003>.
- [680] Yang X, Jasper AW, Giri BR, Kiefer JH, Tranter RS. A shock tube and theoretical study on the pyrolysis of 1,4-dioxane. *Phys Chem Chem Phys* 2011;13:3686–700. <https://doi.org/10.1039/C0CP01541E>.
- [681] Lin Z, Han D, Li S, Li Y, Yuan T. Combustion intermediates in fuel-rich 1,4-dioxane flame studied by tunable synchrotron vacuum ultraviolet photoionization. *J Phys Chem A* 2009;113:1800–6. <https://doi.org/10.1021/jp8098895>.
- [682] Klute CH, Walters WD. The thermal decomposition of tetrahydrofuran. *J Am Chem Soc* 1946;68:506–11. <https://doi.org/10.1021/ja01207a045>.
- [683] McDonald G, Lodge NM, Walters WD. The effect of added gases upon the thermal decomposition of tetrahydrofuran. *J Am Chem Soc* 1951;73:1757–60.
- [684] Burden FA, Burgoyne JH. The ignition and flame reactions of ethylene oxide. *Proc R Soc Lond A* 1949;199:328–51. <https://doi.org/10.1098/rspa.1949.0141>.
- [685] Wesdemiotis C, Leyh B, Fura A, McLafferty FW. The isomerization of oxirane. Stable  $\cdot\text{CH}_2\text{OCH}_2\cdot$ ,  $\cdot\text{CH}_2\text{CH}_2\text{O}\cdot$ , and  $\cdot\text{CHOCH}_3$ , and their counterpart ions. *J Am Chem Soc* 1990;112:8655–60. <https://doi.org/10.1021/ja00180a004>.
- [686] Burgoyne JH, Kapur PK. The oxidation of ethylene oxide in the vapour phase. *Trans Faraday Soc* 1952;48:234–43. <https://doi.org/10.1039/TF9524800234>.
- [687] Zalotai L, Hunyadi-zoltán Z, Bérces T, Márta F. Kinetics of gas-phase decomposition of oxetan and oxetan-2,2-d<sub>2</sub>. *Int J Chem Kinet* 1983;15:505–19. <https://doi.org/10.1002/kin.550150602>.
- [688] Zalotai L, Bérces T, Márta F. Collisional energy transfer in the thermal decomposition of oxetane. *React Kinet Catal Lett* 1989;40:35–40. <https://doi.org/10.1007/BF02235135>.
- [689] Guenther WB, Walters WD. The thermal decomposition of dioxolane. *J Am Chem Soc* 1951;73:2127–31. <https://doi.org/10.1021/ja01149a064>.
- [690] Roquette BC. The photochemistry of 1,3-dioxolane. *J Phys Chem* 1966;70:2863–8. <https://doi.org/10.1021/j100881a023>.
- [691] Molera MJ, Domínguez JAG, Acuña AU. Gas-phase oxidation of 1,3-dioxolan. *J Chem Soc B* 1971:1916–23. <https://doi.org/10.1039/J29710001916>.
- [692] Tian Z, Fattahi A, Lis L, Kass SR. Cycloalkane and cycloalkene C–H bond dissociation energies. *J Am Chem Soc* 2006;128:17087–92. <https://doi.org/10.1021/ja065348u>.
- [693] Wiberg KB, Rablen PR. Re-examination of some carbocations. structures, energies, and charge distributions. *J Org Chem* 2020;85:11741–9. <https://doi.org/10.1021/acs.joc.0c01469>.

- [694] Stedjan MK, Augspurger JD. Ring strain energy in ether- and lactone-containing spiro compounds. *J Phys Org Chem* 2015;28:298–303. <https://doi.org/10.1002/poc.3410>.
- [695] Bach RD, Dmitrenko O. Effect of geminal substitution on the strain energy of dioxiranes. origin of the low ring strain of dimethyldioxirane. *J Org Chem* 2002;67:3884–96. <https://doi.org/10.1021/jo025743c>.
- [696] Dudev T, Lim C. Ring strain energies from ab initio calculations. *J Am Chem Soc* 1998;120:4450–8. <https://doi.org/10.1021/ja973895x>.
- [697] Sirjean B, Glaude PA, Ruiz-Lopez MF, Fournet R. Detailed kinetic study of the ring opening of cycloalkanes by CBS-QB3 calculations. *J Phys Chem A* 2006;110:12693–704. <https://doi.org/10.1021/jp0651081>.
- [698] Sirjean B, Buda F, Hakka H, Glaude PA, Fournet R, Warth V, et al. The autoignition of cyclopentane and cyclohexane in a shock tube. *Proc Combust Inst* 2007;31:277–84. <https://doi.org/10.1016/j.proci.2006.07.247>.
- [699] Barnard JA, Cocks AT, Lee RK-Y. Kinetics of the thermal unimolecular reactions of cyclopropane and cyclobutane behind reflected shock waves. *J Chem Soc, Faraday Trans 1* 1974;70:1782–92. <https://doi.org/10.1039/F19747001782>.
- [700] Slutsky VG, Kazakov OD, Severin ES, Bepalov EV, Tsyganov SA. Self-ignition of small-ring hydrocarbons behind reflected shock waves. *Combust Flame* 1993;94:108–12. [https://doi.org/10.1016/0010-2180\(93\)90023-V](https://doi.org/10.1016/0010-2180(93)90023-V).
- [701] Borisov AA, Zamanskii VM, Konnov AA, Lisyanskii VV, Shachkov GL. Pyrolysis and combustion of ethylene-oxide. *Sov J Chem Phys* 1990;6:2181–95.
- [702] Wu S, Tay KL, Yu W, Lin Q, Li H, Zhao F, et al. Development of a highly compact and robust chemical reaction mechanism for the oxidation of tetrahydrofurans under engine relevant conditions. *Fuel* 2020;276. <https://doi.org/10.1016/j.fuel.2020.118034>.
- [703] Eldeeb MA, Wadugurunnehilage M. Chemical kinetic model reduction and analysis of tetrahydrofuran combustion using stochastic species elimination. vol. 2020- August, 2020. <https://doi.org/10.1115/POWER2020-16583>.
- [704] Li W, Law ME, Westmoreland PR, Kasper T, Hansen N, Kohse-Höinghaus K. Multiple benzene-formation paths in a fuel-rich cyclohexane flame. *Combust Flame* 2011;158:2077–89. <https://doi.org/10.1016/j.combustflame.2011.03.014>.
- [705] Kröger LC, Döntgen M, Firaha D, Kopp WA, Leonhard K. Ab initio kinetics predictions for H-atom abstraction from diethoxymethane by hydrogen, methyl, and ethyl radicals and the subsequent unimolecular reactions. *Proc Combust Inst* 2019;37:275–82. <https://doi.org/10.1016/j.proci.2018.06.056>.
- [706] Jacobs S, Döntgen M, Alqaity ABS, Kopp WA, Kröger LC, Burke U, et al. Detailed kinetic modeling of dimethoxymethane. Part II: Experimental and theoretical study of the kinetics and reaction mechanism. *Combust Flame* 2019;205:522–33. <https://doi.org/10.1016/j.combustflame.2018.12.026>.
- [707] Mendes J, Zhou C-W, Curran HJ. Rate constant calculations of H-atom abstraction reactions from ethers by HO<sub>2</sub> radicals. *J Phys Chem A* 2014;118:1300–8. <https://doi.org/10.1021/jp412496g>.
- [708] Zalotai L, Bérces T, Márta F. Kinetics and energy transfer in the thermal decomposition of 2-methyloxetane and 3-methyloxetane. *J Chem Soc, Faraday Trans* 1990;86:21–5. <https://doi.org/10.1039/FT9908600021>.
- [709] Zalotai L, Bérces T, Márta F. Collisional energy transfer in the decomposition of 2-methyloxetane and 3-methyloxetane, I. Gas/gas collisions. *React Kinet Catal Lett* 1990;42:79–86. <https://doi.org/10.1007/BF02137621>.
- [710] Gibbs GJ, Calcote HF. Effect of molecular structure on burning velocity. *J Chem Eng Data* 1959;4:226–37. <https://doi.org/10.1021/je60003a011>.

- [711] Flowers MC, Parker RM. Kinetics of the thermal gas phase reactions of cis- and trans-2,3-epoxybutane. *J Chem Soc B* 1971;1980–8. <https://doi.org/10.1039/J29710001980>.
- [712] Bailey WJ, Bird CN. Pyrolysis of esters. 27. Pyrolysis of lactones. *J Org Chem* 1977;42:3895–9. <https://doi.org/10.1021/jo00444a021>.
- [713] Flowers MC. Kinetics of the thermal gas-phase decomposition of 1,2-epoxypropane. *J Chem Soc, Faraday Trans 1* 1977;73:1927–35. <https://doi.org/10.1039/F19777301927>.
- [714] Coppens FHV, De Ruyck J, Konnov AA. The effects of composition on burning velocity and nitric oxide formation in laminar premixed flames of CH<sub>4</sub> + H<sub>2</sub> + O<sub>2</sub> + N<sub>2</sub>. *Combust Flame* 2007;149:409–17. <https://doi.org/10.1016/j.combustflame.2007.02.004>.
- [715] Sarathy SM, Vranckx S, Yasunaga K, Mehl M, Oßwald P, Metcalfe WK, et al. A comprehensive chemical kinetic combustion model for the four butanol isomers. *Combust Flame* 2012;159:2028–55. <https://doi.org/10.1016/j.combustflame.2011.12.017>.
- [716] Xu N, Gong J, Huang Z. Review on the production methods and fundamental combustion characteristics of furan derivatives. *Renew Sust Energ Rev* 2016;54:1189–211. <https://doi.org/10.1016/j.rser.2015.10.118>.
- [717] Tanoue K, Takayama T, Ueno S, Mieno T, Irikura K, Kiritani T, et al. Study on the combustion characteristics of furan- and nitromethane-added hydrocarbon fuels. *Fuel* 2021;287:119550. <https://doi.org/10.1016/j.fuel.2020.119550>.
- [718] Wei L, Tang C, Man X, Jiang X, Huang Z. High-temperature ignition delay times and kinetic study of furan. *Energy Fuels* 2012;26:2075–81. <https://doi.org/10.1021/ef300336y>.
- [719] Eldeeb MA, Akih-Kumgeh B. Reactivity trends in furan and alkyl furan combustion. *Energy Fuels* 2014;28:6618–26. <https://doi.org/10.1021/ef501181z>.
- [720] Xu N, Tang C, Meng X, Fan X, Tian Z, Huang Z. Experimental and kinetic study on the ignition delay times of 2,5-dimethylfuran and the comparison to 2-methylfuran and furan. *Energy Fuels* 2015;29:5372–81. <https://doi.org/10.1021/acs.energyfuels.5b00906>.
- [721] Lifshitz A, Bidani M, Bidani S. Thermal reactions of cyclic ethers at high temperatures. 3. Pyrolysis of furan behind reflected shocks. *J Phys Chem* 1986;90:5373–7.
- [722] Organ PP, Mackie JC. Kinetics of pyrolysis of furan. *J Chem Soc, Faraday Trans* 1991;87:815–23. <https://doi.org/10.1039/FT9918700815>.
- [723] Fulle D, Dib A, Kiefer JH, Zhang Q, Yao J, Kern RD. Pyrolysis of furan at low pressures : vibrational relaxation, unimolecular dissociation, and incubation times. *J Phys Chem A* 1998;102:7480–6. <https://doi.org/10.1021/jp9823042>.
- [724] Weber I, Friese P, Olzmann M. H-atom-forming reaction pathways in the pyrolysis of furan, 2-methylfuran, and 2,5-dimethylfuran: A shock-tube and modeling study. *J Phys Chem A* 2018;122:6500–8. <https://doi.org/10.1021/acs.jpca.8b05346>.
- [725] Grela MA, Amorebieta VT, Colussi AJ. Very low pressure pyrolysis of furan, 2-methylfuran and 2,5-dimethylfuran. The stability of the furan ring. *J Phys Chem* 1985;89:38–41. <https://doi.org/10.1021/j100247a011>.
- [726] Tran L-S, Wang Z, Carstensen H-H, Hemken C, Battin-Leclerc F, Kohse-Höinghaus K. Comparative experimental and modeling study of the low- to moderate-temperature oxidation chemistry of 2,5-dimethylfuran, 2-methylfuran, and furan. *Combust Flame* 2017;181:251–69. <https://doi.org/10.1016/j.combustflame.2017.03.030>.
- [727] Fan X, Wang X, Yang K, Li Y, Wu C, Li Z. Experimental and modeling study on ignition characteristics of 2,5-dihydrofuran. *SAE Int J Fuels Lubr* 2016;9:315–21. <https://doi.org/10.4271/2016-01-1270>.
- [728] Somers KP, Simmie JM, Gillespie F, Burke U, Connolly J, Metcalfe WK, et al. A high temperature and atmospheric pressure experimental and detailed chemical kinetic modelling study of 2-methyl furan oxidation. *Proc Combust Inst* 2013;34:225–32. <https://doi.org/10.1016/j.proci.2012.06.113>.

- [729] Ma X, Jiang C, Xu H, Ding H, Shuai S. Laminar burning characteristics of 2-methylfuran and isooctane blend fuels. *Fuel* 2014;116:281–91. <https://doi.org/10.1016/j.fuel.2013.08.018>.
- [730] Zhongyang L, Oppong F, Wang H, Li X, Xu C, Wang C. Investigating the laminar burning velocity of 2-methylfuran. *Fuel* 2018;234:1469–80. <https://doi.org/10.1016/j.fuel.2018.07.005>.
- [731] Wei L, Tang C, Man X, Huang Z. Shock-tube experiments and kinetic modeling of 2-methylfuran ignition at elevated pressure. *Energy Fuels* 2013;27:7809–16. <https://doi.org/10.1021/ef401809y>.
- [732] Eldeeb MA, Akih-Kumgeh B. Investigation of 2,5-dimethyl furan and iso-octane ignition. *Combust Flame* 2015;162:2454–65. <https://doi.org/10.1016/j.combustflame.2015.02.013>.
- [733] Xu N, Wu Y, Tang C, Zhang P, He X, Wang Z, et al. Experimental study of 2,5-dimethylfuran and 2-methylfuran in a rapid compression machine: Comparison of the ignition delay times and reactivity at low to intermediate temperature. *Combust Flame* 2016;168:216–27. <https://doi.org/10.1016/j.combustflame.2016.03.016>.
- [734] Xu N, Wu Y, Tang C, Zhang P, He X, Wang Z, et al. Ignition delay times of low alkylfurans at high pressures using a rapid compression machine. *Proc Combust Inst* 2017;36:323–32. <https://doi.org/10.1016/j.proci.2016.07.075>.
- [735] Tripathi R, Burke U, Ramalingam AK, Lee C, Davis AC, Cai L, et al. Oxidation of 2-methylfuran and 2-methylfuran/n-heptane blends: An experimental and modeling study. *Combust Flame* 2018;196:54–70. <https://doi.org/10.1016/j.combustflame.2018.05.032>.
- [736] Lifshitz A, Tamburu C, Shashua R. Decomposition of 2-methylfuran. Experimental and modeling study. *J Phys Chem A* 1997;101:1018–29. <https://doi.org/10.1021/jp962646c>.
- [737] Wei L, Li Z, Tong L, Wang Z, Jin H, Yao M, et al. Primary combustion intermediates in lean and rich low-pressure premixed laminar 2-methylfuran/oxygen/argon flames. *Energy Fuels* 2012;26:6651–60. <https://doi.org/10.1021/ef301173z>.
- [738] Cheng Z, Niu Q, Wang Z, Jin H, Chen G, Yao M, et al. Experimental and kinetic modeling studies of low-pressure premixed laminar 2-methylfuran flames. *Proc Combust Inst* 2017;36:1295–302. <https://doi.org/10.1016/j.proci.2016.07.032>.
- [739] Wang J, He S, Wang H, Cheng Z, Wei L, Wang J, et al. Experimental and kinetic modeling studies of the low-temperature oxidation of 2-methylfuran in a jet-stirred reactor. *Combust Flame* 2021;233:111588. <https://doi.org/10.1016/j.combustflame.2021.111588>.
- [740] Alexandrino K, Millera A, Bilbao R, Alzueta MU. 2-Methylfuran oxidation in the absence and presence of NO. *Flow Turbul Combust* 2016;96:343–62. <https://doi.org/10.1007/s10494-015-9635-z>.
- [741] Cheng Z, He S, Xing L, Wei L, Li W, Li T, et al. Experimental and kinetic modeling study of 2-methylfuran pyrolysis at low and atmospheric pressures. *Energy Fuels* 2017;31:896–903. <https://doi.org/10.1021/acs.energyfuels.6b02399>.
- [742] Wu X, Huang Z, Jin C, Wang X, Zheng B, Zhang Y, et al. Measurements of laminar burning velocities and markstein lengths of 2,5-dimethylfuran-air-diluent premixed flames. *Energy Fuels* 2009;23:4355–62. <https://doi.org/10.1021/ef900454v>.
- [743] Wu X, Huang Z, Jin C, Wang X, Wei L. Laminar burning velocities and markstein lengths of 2,5-dimethylfuran-air premixed flames at elevated temperatures. *Combust Sci Technol* 2011;183:220–37. <https://doi.org/10.1080/00102202.2010.516037>.
- [744] Wu X, Huang Z, Wang X, Jin C, Tang C, Wei L, et al. Laminar burning velocities and flame instabilities of 2,5-dimethylfuran-air mixtures at elevated pressures. *Combust Flame* 2011;158:539–46. <https://doi.org/10.1016/j.combustflame.2010.10.006>.



- [745] Wu X, Li Q, Fu J, Tang C, Huang Z, Daniel R, et al. Laminar burning characteristics of 2,5-dimethylfuran and iso-octane blend at elevated temperatures and pressures. *Fuel* 2012;95:234–40. <https://doi.org/10.1016/j.fuel.2011.11.057>.
- [746] Somers KP, Simmie JM, Gillespie F, Conroy C, Black G, Metcalfe WK, et al. A comprehensive experimental and detailed chemical kinetic modelling study of 2,5-dimethylfuran pyrolysis and oxidation. *Combust Flame* 2013;160:2291–318. <https://doi.org/10.1016/j.combustflame.2013.06.007>.
- [747] Sirjean B, Fournet R, Glaude P-A, Battin-Leclerc F, Wang W, Oehlschlaeger MA. Shock tube and chemical kinetic modeling study of the oxidation of 2,5-dimethylfuran. *J Phys Chem A* 2013;117:1371–92. <https://doi.org/10.1021/jp308901q>.
- [748] Lifshitz A, Tamburu C, Shashua R. Thermal decomposition of 2,5-dimethylfuran. Experimental results and computer modeling. *J Phys Chem A* 1998;102:10655–70. <https://doi.org/10.1021/jp982772b>.
- [749] Wu X, Huang Z, Yuan T, Zhang K, Wei L. Identification of combustion intermediates in a low-pressure premixed laminar 2,5-dimethylfuran/oxygen/argon flame with tunable synchrotron photoionization. *Combust Flame* 2009;156:1365–76. <https://doi.org/10.1016/j.combustflame.2009.04.002>.
- [750] Liu X, Yao M, Wang Y, Wang Z, Jin H, Wei L. Experimental and kinetic modeling study of a rich and a stoichiometric low-pressure premixed laminar 2,5-dimethylfuran/oxygen/argon flames. *Combust Flame* 2015;162:4586–97. <https://doi.org/10.1016/j.combustflame.2015.09.017>.
- [751] Cheng Z, Xing L, Zeng M, Dong W, Zhang F, Qi F, et al. Experimental and kinetic modeling study of 2,5-dimethylfuran pyrolysis at various pressures. *Combust Flame* 2014;161:2496–511. <https://doi.org/10.1016/j.combustflame.2014.03.022>.
- [752] Alexandrino K, Millera Á, Bilbao R, Alzueta MU. Novel aspects in the pyrolysis and oxidation of 2,5-dimethylfuran. *Proc Combust Inst* 2015;35:1717–25. <https://doi.org/10.1016/j.proci.2014.06.002>.
- [753] Alexandrino K, Millera Á, Bilbao R, Alzueta MU. Interaction between 2,5-Dimethylfuran and Nitric Oxide: Experimental and Modeling Study. *Energy Fuels* 2014;28:4193–8. <https://doi.org/10.1021/ef5005573>.
- [754] Xu C, Liu W, Zhang B, Liao H, He W, Wei L. Experimental and numerical study on laminar premixed flame characteristics of 2-ethylfuran. *Combust Flame* 2021;234:111631. <https://doi.org/10.1016/j.combustflame.2021.111631>.
- [755] Li P, He W, Wang J, Song S, Wang J, Lv T, et al. Experimental and kinetic modeling investigations on low-temperature oxidation of 2-ethylfuran in a jet-stirred reactor. *Combust Flame* 2022;241:112098. <https://doi.org/10.1016/j.combustflame.2022.112098>.
- [756] Song S, Wang J, He W, Lu J, Su H, Xu Q, et al. Experimental and kinetic modeling studies of 2-ethylfuran pyrolysis at low and atmospheric pressures. *Combust Flame* 2021;226:430–44. <https://doi.org/10.1016/j.combustflame.2020.12.029>.
- [757] Jin Z-H, Yu D, Liu Y-X, Tian Z-Y, Richter S, Braun-Unkloff M, et al. An experimental investigation of furfural oxidation and the development of a comprehensive combustion model. *Combust Flame* 2021;226:200–10. <https://doi.org/10.1016/j.combustflame.2020.12.015>.
- [758] Vasiliou AK, Kim JH, Ormond TK, Piech KM, Urness KN, Scheer AM, et al. Biomass pyrolysis: Thermal decomposition mechanisms of furfural and benzaldehyde. *J Chem Phys* 2013;139:104310. <https://doi.org/10.1063/1.4819788>.
- [759] Li Y, Meng Q, Wang J, Zhang Y, Cao C, Cheng Z, et al. Experimental and theoretical investigation of the pyrolysis of furfural. *J Phys Chem A* 2019;123:103–10. <https://doi.org/10.1021/acs.jpca.8b06261>.

- [760] Grela MA, Colussi AJ. Kinetics and mechanism of the thermal decomposition of unsaturated aldehydes: benzaldehyde, 2-butenal, and 2-furaldehyde. *J Phys Chem* 1986;90:434–7. <https://doi.org/10.1021/j100275a016>.
- [761] Grela M, Colussi A. Vacuum pyrolysis of furfural: a facile synthesis of vinylketene. *Anales de La Asociación Química Argentina* 1987;75:111–5.
- [762] Wang J, Tian J, Xing L, He S, Cheng Z, Wei L, et al. Experimental and kinetic modeling studies of furfural pyrolysis at low and atmospheric pressures. *J Anal Appl Pyrolysis* 2021;157:105161. <https://doi.org/10.1016/j.jaap.2021.105161>.
- [763] He W, Xu Q, Xie C, Yin J, Li P, Wang Z, et al. Experimental and kinetic modeling studies of 2-acetylfuran pyrolysis at atmospheric pressure. *Combust Flame* 2022;236:111824. <https://doi.org/10.1016/j.combustflame.2021.111824>.
- [764] Yan B, Wang J, Meng Q, Cheng Z, Wei L, Zhang Y, et al. Experimental and kinetic modeling studies of methyl 2-furoate pyrolysis at atmospheric pressure. *Energy Fuels* 2019;33:4611–20. <https://doi.org/10.1021/acs.energyfuels.9b00367>.
- [765] Bounaceur R, Da Costa I, Fournet R, Billaud F, Battin-Leclerc F. Experimental and modeling study of the oxidation of toluene. *Int J Chem Kinet* 2005;37:25–49. <https://doi.org/10.1002/kin.20047>.
- [766] Somers KP, Simmie JM, Metcalfe WK, Curran HJ. The pyrolysis of 2-methylfuran: A quantum chemical, statistical rate theory and kinetic modelling study. *Phys Chem Chem Phys* 2014;16:5349–67. <https://doi.org/10.1039/c3cp54915a>.
- [767] Conturso M, Sirignano M, D'Anna A. Effect of 2,5-dimethylfuran doping on particle size distributions measured in premixed ethylene/air flames. *Proc Combust Inst* 2017;36:985–92. <https://doi.org/10.1016/j.proci.2016.06.048>.
- [768] Thornton MM, Malte PC, Crittenden AL. Oxidation of furan and furfural in a well-stirred reactor. *Proc Combust Inst* 1988;21:979–89. [https://doi.org/10.1016/S0082-0784\(88\)80329-1](https://doi.org/10.1016/S0082-0784(88)80329-1).
- [769] Tay KL, Yang W, Zhao F, Lin Q, Wu S. Development of a highly compact and robust chemical reaction mechanism for unsaturated furan oxidation in internal combustion engines via a multiobjective genetic algorithm and generalized polynomial chaos. *Energy Fuels* 2020;34:936–48. <https://doi.org/10.1021/acs.energyfuels.9b03272>.
- [770] Wu S, Tay KL, Li J, Yang W, Yang S. Development of a compact and robust kinetic mechanism for furan group biofuels combustion in internal combustion engines. *Fuel* 2021;298:120824. <https://doi.org/10.1016/j.fuel.2021.120824>.
- [771] Zhou C, Chang Y, Wang P, Niu B, Jia M. Construction of a skeletal oxidation mechanism for 2,5-dimethylfuran using decoupling methodology and reaction class-based global sensitivity analysis. *Energy Fuels* 2020;34:16654–65. <https://doi.org/10.1021/acs.energyfuels.0c03086>.
- [772] Davis AC, Sarathy SM. Computational study of the combustion and atmospheric decomposition of 2-methylfuran. *J Phys Chem A* 2013;117:7670–85. <https://doi.org/10.1021/jp403085u>.
- [773] Chu H, Xiang L, Nie X, Ya Y, Gu M, E J. Laminar burning velocity and pollutant emissions of the gasoline components and its surrogate fuels: A review. *Fuel* 2020;269:117451. <https://doi.org/10.1016/j.fuel.2020.117451>.
- [774] Osborn DL, Zou P, Johnsen H, Hayden CC, Taatjes CA, Knyazev VD, et al. The multiplexed chemical kinetic photoionization mass spectrometer: A new approach to isomer-resolved chemical kinetics. *Rev Sci Instrum* 2008;79:104103. <https://doi.org/10.1063/1.3000004>.
- [775] Sheps L, Antonov I, Au K. Sensitive mass spectrometer for time-resolved gas-phase chemistry studies at high pressures. *J Phys Chem A* 2019;123:10804–14. <https://doi.org/10.1021/acs.jpca.9b08393>.

- [776] Li Y, Qi F. Recent applications of synchrotron VUV photoionization mass spectrometry: insight into combustion chemistry. *Acc Chem Res* 2010;43:68–78. <https://doi.org/10.1021/ar900130b>.
- [777] Struckmeier U, Oßwald P, Kasper T, Boehling L, Heusing M, Koehler M, et al. Sampling probe influences on temperature and species concentrations in molecular beam mass spectroscopic investigations of flat premixed low-pressure flames. *Z Physik Chem* 2009;223:503–37. <https://doi.org/10.1524/zpch.2009.6049>.
- [778] Liu Z, Phillips JB. Comprehensive two-dimensional gas chromatography using an on-column thermal modulator interface. *J Chromatogr Sci* 1991;29:227–31. <https://doi.org/10.1093/chromsci/29.6.227>.
- [779] Rotavera B, Scheer AM, Huang H, Osborn DL, Taatjes CA. Influence of temperature and resonance-stabilization on the ortho-effect in cymene oxidation. *Proc Combust Inst* 2015;35:543–52. <https://doi.org/10.1016/j.proci.2014.05.012>.
- [780] Burke MP. Harnessing the combined power of theoretical and experimental data through multiscale informatics. *Int J Chem Kinet* 2016;48:212–35. <https://doi.org/10.1002/kin.20984>.
- [781] RMG: Molecule Search n.d. [https://rmg.mit.edu/molecule\\_search](https://rmg.mit.edu/molecule_search) (accessed January 27, 2022).
- [782] Green WH. Chapter 5 - Automatic generation of reaction mechanisms. In: Faravelli T, Manenti F, Ranzi E, editors. *Computer Aided Chemical Engineering*, vol. 45, Elsevier; 2019, p. 259–94. <https://doi.org/10.1016/B978-0-444-64087-1.00005-X>.